ÇUKUROVA UNIVERSITY
INSTITUTE OF NATURAL AND APPLIED SCIENCES

MSc THESIS

Gül TURĞUT

A COMPARISON OF APPROACHES TO INVOLUTE BEVEL GEAR DESIGN

DEPARTMENT OF MECHANICAL ENGINEERING

ADANA-2019

ÇUKUROVA UNIVERSITY
INSTITUTE OF NATURAL AND APPLIED SCIENCES

> A COMPARISON OF APPROACHES TO INVOLUTE BEVEL GEAR
> DESIGN

Gül TURĞUT

MSc. THESIS

DEPARTMENT OF MECHANICAL ENGINEERING

We certified that the thesis titled above was reviewed and approved for the award degree of the master of mechanical engineering by the board of jury on 24/10/2019

....
Prof. Dr. Necdet GEREN   Prof. Dr. Melih BAYRAMOĞLU   Prof. Dr. Uğur EŞME
SUPERVISOR   MEMBER   MEMBER

This M Sc. Thesis is performed in Department of Mechanical Engineering of the Institute of Natural and Applied Sciences of Çukurova University.
Registration No:

Prof. Dr. Mustafa GÖK
Director
Institute of Natural and Applied Science

Note: The use of tables, figures and photographs (original or referenced) from this thesis, without proper reference, is subject to provisions of Law 5846 concerning Intellectual Property and Artistic Creations.

ABSTRACT

MSc THESIS

A COMPARISON OF APPROACHES TO INVOLUTE BEVEL GEAR DESIGN

Gül Turğut

ÇUKUROVA UNIVERSITY
INSTITUTE OF NATURAL AND APPLIED SCIENCES
DEPARTMENT OF MECHANICAL ENGINEERING

This thesis meets a need of selecting and using appropriate involute bevel gear design approaches for all designers from the expert to novice learners who are practicing a straight bevel gear design. Four straight bevel gear design approaches with different level of difficulty, including the ones available in the most commonly used machine elements textbooks, national and international standards were selected for comparison of design results. The results of each approach were analysed by using a finite element method, ANSYS. And the variations on the design results of each of the approach were determined, and the results were given comparatively considering the gear failures criteria, speed ratios and power transmission ranges. The outputs, practical curves and charts were introduced to select the appropriate design approach. In addition to this, the study provides conversion factors which may be used to translate the results of simple gear design approaches into ANSI/AGMA international standards or in any of the four selected one by multiplying with the appropriate conversion factors. It also offers the best approach for students and designers who aim to optimize the bevel gear design.

Key Words: Straight bevel gear design, Design approaches, Design outputs, Comparison

ÖZ

YÜKSEK LİSANS TEZİ

EVOLVENT BEVEL DİŞLİ TASARIM YAKLAŞIMLARININ KIYASLANMASI

Gül Turğut

ÇUKUROVA ÜNİVERSİTESİ
FEN BİLİMLERİ ENSTİTÜSÜ
MAKİNE MÜHENDİSLİĞİ ANABİLİM DALI

Danışman	: Prof. Dr. Necdet GEREN
	Yıl: 2019, Sayfa: 331
Juri	: Prof. Dr. Necdet GEREN
	: Prof. Dr. Melih BAYRAMOĞLU
	: Prof. Dr. Uğur EŞME

Bu tez konik düz dişli tasarımı ile uğraşan uzman tasarımcılar ve öğrenciler dahil tüm tasarımcılar için farklı zorluk seviyelerindeki en uygun evolvent konik düz dişli tasarım yaklaşımlarını seçme ve kullanma ihtiyacını karşılar. Tasarım sonuçlarının karşılaştırılması için en yaygın kullanılan makine elemanları ders kitaplarında yer alan tasarım metotları ile birlikte, ulusal ve uluslararası konik düz dişli standartları içeren dört farklı tasarım yaklaşımı seçilmiştir. Her yaklaşımın sonuçları bir sonlu elemanlar metodu, ANSYS kullanılarak analiz edildi. Her bir yaklaşımın verdiği tasarım sonuçları arasındaki farklılıklar belirlendi ve sonuçlar dişli hasar kriterleri, hız oranları ve güç aktarma aralıkları göz önünde bulundurularak karşılaştırmalı olarak verildi. Uygun tasarım yaklaşımını seçmek için çıktılar, pratik eğriler ve çizelgelerde sunuldu. Buna ilaveten, çalışma, basit dişli tasarım yaklaşımlarının sonuçlarının ya da dört farklı yaklaşımdan seçilen herhangi birinin ANSI/AGMA Standardına dönüştürmek için kullanılabilen dönüşüm faktörleri sağlar. Ayrıca dişli tasarımını optimize etmeyi amaçlayan tasarımcılar ve öğrenciler için en iyi yaklaşımı önerir.

Anahtar Kelimeler: Konik düz dişli tasarımı, dişli tasarım yaklaşımları, Tasarım çıktıları, karşılaştırma

EXTENDED ABSTRACT

There are many design parameters in the design of bevel gears that are module (m) or diametral pitch (P), cone distance (A_0) and face width (F or b). The proper values of these are searched in the gear design before material is pre-selected. After defining the pinion and gear materials, module is estimated, and calculations are carried out to determine the suitable face width. The diametral pitch P is the ratio of the number of teeth on the gear to the pitch diameter. So, it is the reciprocal of the module. Since the diametral pitch is used only with U.S. units, it is expressed as teeth per inch. The cone distance A_0 shown in Figure 1.9, is that the distance along with a reference cone generator, from the cone apex to the specified cone. A suitable module is to be selected and the face width calculations is to be performed using the $F = 0.3A_0$ or $F = 10/P$. Various design approaches each of which provides different formulas are available in the machine elements or machine design textbooks for the design or finding "m" or "F". This is also the case when the dictated technical standards are used. However, the results of using different approaches have not been compared so far. Thus the designer does not aware of the success or loss gained using each of the approaches. Therefore, there is a need to compare the results of each of the most accepted design approach for bevel gear design. Hence, this study aims to compare the design results (F and m) obtained using the different design approaches to determine loss or gain obtained using each of the approaches.

In this study, design of an involute bevel gear has been performed based on both bending fatigue failure and surface contact failure theories. Defining the pinion and gear material depending on the working conditions, the allowable minimum number of teeth for the pinion and gear will be the initial requirements to determine. And then a suitable module is selected and the face width calculations will be performed using the $F = 0.3A_0$ or $F = 10/P$, whichever is smaller, then the face width (F) is chosen as an output of the design. The results obtained in each of the approaches under the different speed ratios will be compared with each other and all of these theoretical calculations will be executed using the Microsoft Excel pages.

To verify the results and to use a base as a solid reference, a finite element method (FEM) will be used to analyse the results obtained using the theoretical approaches. For this, 3-D models of bevel gears, which are created in SOLIDWORKS, will be imported into ANSYS Workbench 16.1. Then, the module and face widths found using each approach will be compared with the results of FEM. This approach will be used to verify each of the design approaches used in this study against ANSYS, and then more solid comparisons will be obtained.

The module (m) and face width (b) that are obtained from four of the approaches (ANSI/AGMA 2003-B97 standards, Fundamentals of Machine Component Design 5th Edition, K.Gopinath & M.M.Mayuram 4th Edition) are different from each other, even under the same input parameters. These are leading to different gear designs that are associated with cost. So, gear designers require detailed knowledge of the relative comparison of design outputs.

For this reason, the differences in the results obtained from different gear standards have significantly been the subject of investigations for many types of researches. And a translation technique using conversion factors in between the standards are demanded as a stated need in the literature. Thus, this paper firstly obtains dimensionless gear rating numbers (GRi) to rate the design results of bevel gears determined from the four approaches, and then it derives correlation equations to generate dimensionless conversion factors (CFs) to convert the design results obtained from the four gear design approaches. The CFs allow designers to easily move from one standard to another. This enables engineering students and designers to meet the ever-changing needs of the global market fast.

Finally, the study will allow comparing the design results of the most approaches given in the most commonly used textbooks and international and national standards.

The main intention is to compare the design results given by the most commonly used gear design approaches. Hence, the designer can be aware of the success or loss gained using each of the approaches. The results of the study may also help to select the proper gear design approach depending on the requirements of the particular design.

Two design parameters are module (m) and face width (F) are searched in the gear design before material is pre-selected. After defining the pinion and gear materials, module is estimated, and design calculations are carried out to determine the face width a suitable module. Number of design approaches providing differing design formulas are available in the machine elements or

machine design textbooks for the design or finding "m" or "F". This situation is further complicated by the available gear design standards which suggest differing design expressions. But, the results of using different approaches have not been compared so far. Thus, the designer does not aware of the success or loss gained using each of the approaches. Because of that, there is a need to compare the results of each of the most accepted design formula or design approach for bevel gear design.

This thesis meets a need of selecting and using appropriate involute bevel gear design approaches for all designers including the expert designers and novice learners who are practicing a bevel gear design. This was made by comparing the most commonly used involute bevel gear design approaches available in the literature. The selected approaches are given as follow;

1- ANSI/AGMA 2003-B97 Standards
2- Fundamental of Machine Component Design 5th Edition, Juvinall R.C. and Marshek K.M., 2011
3- ISO Standards 10300-(Part 1-2-3), 2001
4- K.Gopinath & M.M.Mayuram 4th Edition, 2009

This study proposes to use the easier and the most appropriate approach provided in the common text books considering the verified results of FEA, if there is no obligation to use ISO or ANSI/AGMA Standards. Because these standards are more challenging, time consuming and include complicated equations. Conversion factors for the conversion of text books results to the verified results were developed. And now, the results obtained by text books can be converted to the standards with the aid of conversion factors developed in this study. As a result of these, gear designers do not have to deal with the computational load of the standards. This does not only allow saving time and resources, but also provides safer and reliable designs.

A systematic methodology which relies on dimensionless numbers called as GRi and CFs, has been described and proposed to rate most common design

approaches with ANSI/AGMA 2003-B97 based on bending fatigue failure for bevel gears. Although the results of four design approaches differ from each other, good similarity and continuity of the charts were found out. This allowed obtaining CFs between the standards. Now, these two approaches can be converted to each other with min of error. Beyond the investigations already available in the literature, following conclusions can be drawn in this study.

Dimensionless conversion factors (CFs) were generated for bevel gears to convert the design results, module (m) and face width (F) of ISO Standard, K&M textbook and J&M textbook into AGMA with a minor error. Radar charts presented to make a relative comparison between design approaches. The results showed that gear design approaches have similar trends in all power ranges.

Two methods are now available to obtain CFs. One can be made by linear interpolation from Table 4.11 for pressure angle of 20° and Table 4.14 for pressure angle of 25°. Secondly, Cp expressions can be used for any desired speed ratio from Table 4.12 for pressure angle of 20° and Table 4.15 for pressure angle of 25°.Universality of CFs were verified by case studies and worked reasonably well. The maximum total Gear Volume error (GVe) was found as 7,29% for pressure angle of 20° in Table 4.13 and 9.45% for pressure angle of 25° in Table 4.16 with the aid of CFs.And for verifying our studies we used the design values of the bending fatigue failure as an input in the surface contact fatigue failure equations (at speed ratio 2:1) and the results for pressure angle of 20° and material type 1 are given in Table 4.23, Table 4.24, Table 4.25 and Table 4.26.

In short, this study may serve as a guideline for a designer who deals with the design of an involute bevel gear. If a designer concerns with light weighted applications, the overall size of a gear is important as well as material usage that are objectives of optimization. On the other hand bevel gear design is the subject of almost all machine design courses. And it is important to introduce clear, easy to understand and reliable design approach for learners and students. Consequently, the results of this work interests both expert and novice designers and learners.

GENİŞLETİLMİŞ ÖZET

Konik dişlilerin tasarımında modül (m) ve çap aralığı (P), konik mesafesi (A_0) ve yüz genişliği (F veya b) olan birçok tasarım parametresi vardır. Bunların uygun değerleri, malzeme seçilmeden önce dişli tasarımında aranır. Pinyon ve dişli malzemelerinin tanımlanmasından sonra, modül tahmin edilir ve uygun yüz genişliğini belirlemek için hesaplamalar yapılır. Çap aralığı P, dişlideki diş sayısının adım çapına oranıdır. Yani, modülün tersidir. Çap aralığı sadece ABD birimlerinde kullanıldığından, inç başına diş olarak ifade edilir. Şekil 1.9'da gösterilen koni mesafesi A_0, bir koni apeksinden belirtilen koniye kadar bir referans koni oluşturucu ile birlikte olan mesafedir. Uygun bir modül seçilecek ve yüz genişliği hesaplamaları $F = 0.3A_0$ veya $F = 10 / P$ kullanılarak yapılmalıdır. Her biri farklı formüller sağlayan çeşitli tasarım yaklaşımları, makine elemanları veya makine tasarımı ders kitaplarında, tasarım veya "m" veya "F" yi bulmak için mevcuttur. Dikte edilen teknik standartlar kullanıldığında da durum budur. Ancak, farklı yaklaşımlar kullanmanın sonuçları şu ana kadar karşılaştırılmamıştır. Böylece tasarımcı, yaklaşımların her birini kullanarak kazanılan başarı veya kaybın farkında değildir. Bu nedenle, konik dişli tasarımı için en çok kabul edilen tasarım yaklaşımının sonuçlarını karşılaştırmaya ihtiyaç vardır. Bu nedenle, bu çalışma, farklı yaklaşımlardan yararlanarak elde edilen tasarım sonuçlarını (F ve m), yaklaşımların her birini kullanarak elde edilen kayıp veya kazancı belirlemek için karşılaştırmayı amaçlamaktadır.

Bu çalışmada, hem eğilmeli yorulma arızası hem de yüzey temas arızası teorilerine dayanarak, konvansiyonel bir konik dişlinin tasarımı yapılmıştır. Çalışma koşullarına bağlı olarak pinyon ve dişli malzemesinin tanımlanması, pinyon ve dişli için izin verilen minimum diş sayısını belirlemek için ilk gereksinimler olacaktır. Ve sonra uygun bir modül seçilir ve yüz genişliği hesaplamaları, $F = 0.3A_0$ veya $F = 10 / P$ (hangisi daha küçükse) kullanılarak gerçekleştirilir, ardından yüz genişliği (F) tasarımın bir çıktısı olarak seçilir. Farklı hız oranlarındaki yaklaşımların her birinde elde edilen sonuçlar birbirleriyle karşılaştırılacak ve bu teorik hesaplamaların tümü Microsoft Excel sayfaları kullanılarak gerçekleştirilecektir.

Sonuçları doğrulamak ve bir tabanı katı referans olarak kullanmak için, teorik yaklaşımlar kullanılarak elde edilen sonuçları analiz etmek için sonlu elemanlar

yöntemi (FEM) kullanılacaktır. Bunun için, SOLIDWORKS'te oluşturulan 3 boyutlu konik dişli modelleri ANSYS Workbench 16.1'e aktarılacak. Ardından, her bir yaklaşımı kullanarak bulunan modül ve yüz genişlikleri FEM'in sonuçlarıyla karşılaştırılacaktır. Bu yaklaşım, bu çalışmada kullanılan tasarım yaklaşımlarının her birini ANSYS'e karşı doğrulamak için kullanılacak ve daha sonra daha sağlam karşılaştırmalar elde edilecektir.

Dört yaklaşımdan elde edilen modül (m) ve yüz genişliği (b) (ANSI/AGMA 2003-B97 standards, ISO Standards, Fundamentals of Machine Component Design 5th Edition, K.Gopinath & M.M.Mayuram 4th Edition) aynı giriş parametreleri altında bile, birbirinden farklıdır,. Bunlar, maliyetle ilişkili farklı dişli tasarımına yol açmaktadır. Bu nedenle, dişli tasarımcıları, tasarım çıktılarının nispi karşılaştırması hakkında ayrıntılı bilgi gerektirir.

Bu nedenle, farklı dişli standartlarından elde edilen sonuçlardaki farklılıklar, birçok araştırma türüne yönelik araştırmalara konu olmuştur. Ve literatürde belirtilen bir ihtiyaç olarak standartlar arasında dönüşüm faktörlerini kullanan bir çeviri tekniği talep edilmektedir. Bu nedenle, bu makale ilk olarak dört yaklaşımdan belirlenen konik dişlilerin tasarım sonuçlarını derecelendirmek için boyutsuz dişli derecelendirme numaralarını (GRi) alır ve ardından dört dişli tasarımı yaklaşımından elde edilen tasarım sonuçlarını dönüştürmek için boyutsuz dönüştürme faktörlerini (CF'ler) üretmek için korelasyon denklemlerini türetir.. CF'ler tasarımcıların bir standarttan diğerine kolayca geçmesini sağlar. Bu, mühendislik öğrencilerinin ve tasarımcıların küresel pazarın sürekli değişen ihtiyaçlarını hızlı bir şekilde karşılamalarını sağlar.

Son olarak, çalışma en çok kullanılan ders kitaplarında ve uluslararası ve ulusal standartlarda verilen yaklaşımların tasarım sonuçlarının karşılaştırılmasına olanak sağlayacaktır.

Temel amaç, en yaygın kullanılan dişli tasarım yaklaşımları tarafından verilen tasarım sonuçlarını karşılaştırmaktır. Dolayısıyla tasarımcı, yaklaşımların her birini kullanarak kazanılan başarı veya kaybın farkında olabilir. Çalışmanın sonuçları ayrıca, belirli tasarımın gerekliliklerine bağlı olarak uygun dişli tasarım yaklaşımının seçilmesine de yardımcı olabilir.

Malzeme seçilmeden önce iki tasarım parametresi modül (m) ve yüz genişliği (F) dişli tasarımında aranır. Pinyon ve dişli malzemelerinin tanımlanmasından sonra,

modül tahmin edilir ve yüz genişliğini uygun bir modül belirlemek için tasarım hesaplamaları yapılır. Farklı tasarım formülleri sağlayan tasarım yaklaşımlarının sayısı, makine elemanlarında veya makine tasarımı ders kitaplarını tasarlama "m" veya "F" bulmak için mevcuttur. Bu durum, farklı tasarım ifadeleri öneren mevcut dişli tasarım standartları ile daha da karmaşıklaşır. Ancak, farklı yaklaşımlar kullanmanın sonuçları şu ana kadar karşılaştırılmamıştır. Böylece tasarımcı, yaklaşımların her birini kullanarak kazanılan başarı veya kaybın farkında değildir. Bu nedenle, konik dişli tasarımı için en çok kabul edilen tasarım formülünün veya tasarım yaklaşımının sonuçlarını karşılaştırmaya ihtiyaç vardır.

Bu tez, konik dişli tasarımı kullanan uzman tasarımcı ve acemi öğrenciler de dahil olmak üzere tüm tasarımcılar için uygun konik dişli tasarım yaklaşımlarını seçme ve kullanma ihtiyacını karşılar. Bu, literatürde bulunan en yaygın kullanılan konik dişli tasarım yaklaşımlarını karşılaştırarak yapıldı. Seçilen yaklaşımlar aşağıdaki gibi verilmiştir;

1- ANSI/AGMA 2003-B97 Standards
2- Fundamental of Machine Component Design 5th Edition, Juvinall R.C. and Marshek K.M., 2011
3- ISO Standards 10300-(Part 1-2-3), 2001
4- K.Gopinath & M.M.Mayuram 4th Edition, 2009

Bu çalışma, ISO veya ANSI / AGMA Standartlarını kullanma zorunluluğu yoksa, FEA'nın doğrulanmış sonuçlarını dikkate alarak, ortak kitaplarda sağlanan en kolay ve en uygun yaklaşımı kullanmayı önermektedir. Çünkü bu standartlar daha zor, zaman alıcı ve karmaşık denklemler içeriyor. Ders kitaplarının sonuçlarının doğrulanmış sonuçlara dönüştürülmesi için dönüşüm faktörleri geliştirilmiştir. Ve şimdi, ders kitaplarında elde edilen sonuçlar, bu çalışmada geliştirilen dönüşüm faktörleri ile standartlara dönüştürülebilir. Bunun bir sonucu olarak, dişli tasarımcılarının standartların hesaplamalı yüküyle uğraşması gerekmez. Bu sadece zamandan ve kaynaklardan tasarruf sağlamaz, aynı zamanda daha güvenli ve güvenilir tasarımlar sunar.

GRi ve CF olarak adlandırılan boyutsuz sayılara dayanan sistematik bir metodoloji, konik dişlilerin eğilme yorulmalarına dayanarak, ANSI / AGMA 2003-B97

ile en yaygın tasarım yaklaşımlarını değerlendirmek için tanımlanmış ve önerilmiştir. Dört tasarım yaklaşımının sonuçları birbirinden farklı olsa da, grafiklerin iyi benzerliği ve sürekliliği tespit edildi. Bu, standartlar arasında CF'lerin elde edilmesine izin verdi. Şimdi, bu iki yaklaşım minimum hatayla birbirlerine dönüştürülebilir. Literatürde zaten mevcut olan araştırmaların ötesinde, bu çalışmada şu sonuçlar çıkarılabilir;

ISO Standard, K.Gopinath & M.M.Mayuram 4th Edition, 2009 ders kitabı ve Juvinall R.C. and Marshek K.M., 2011 ders kitabının tasarım sonuçlarını, modülünü (m) ve yüz genişliğini (F) küçük hatalarla dönüştürmek için konik dişliler için boyutsuz dönüştürme faktörleri (CF'ler) oluşturulmuştur.

Tasarım yaklaşımları arasında göreceli bir karşılaştırma yapmak için radar grafikleri sunulmuştur. Sonuçlar, dişli tasarımı yaklaşımlarının tüm güç aralıklarında benzer eğilimlere sahip olduğunu göstermiştir.

CF'leri elde etmek için iki yöntem mevcuttur. Biri, 20° 'lik basınç açısı için Tablo 4.11'den ve 25° ' lik basınç açısı için Tablo 4.14'den doğrusal enterpolasyon ile yapılabilir. İkincisi, Cp ifadeleri, 20° 'lik basınç açısı için Tablo 4.12'den 25° ' lik basınç açısı için Tablo 4.15'ten istenen herhangi bir hız oranı için kullanılabilir.

CF'lerin evrenselliği vaka çalışmaları ile doğrulanmış ve oldukça iyi çalışmıştır. Maksimum toplam Dişli Hacmi hatası (GVe), CF'lerin yardımıyla Tablo 4.13'te 20° basınç açısı için% 7,29 ve Tablo 4.16'da 25° basınç açısı için% 9,45 olarak bulundu.

Ve çalışmalarımızı doğrulamak için, eğri yorulma arızasının tasarım değerlerini, yüzey temas yorulma arızası denklemlerine (hız oranı 2: 1) bir girdi olarak kullandık ve 20° basınç açısı ve malzeme tipi 1 için sonuçlar Tablo 4.23'te verilmiştir. , Tablo 4.24, Tablo 4.25 ve Tablo 4.26.

Kısacası, bu çalışma, konvansiyonel bir konik dişli tasarımıyla ilgilenen bir tasarımcı için bir rehber niteliğinde olabilir. Bir tasarımcı hafif ağırlıklı uygulamalarla ilgileniyorsa, genel olarak bir dişli boyutu, optimizasyonun amacı olan malzeme kullanımı kadar önemlidir. Öte yandan, konik dişli tasarımı hemen hemen tüm makine tasarım kurslarının konusudur. Öğrenenler ve öğrenciler için açık, anlaşılması kolay ve güvenilir bir tasarım yaklaşımı sunmak önemlidir. Sonuç olarak, bu çalışmanın sonuçları hem uzman hem de acemi tasarımcıları ve öğrencileri ilgilendirir.

ACKNOWLEDGEMENT

CONTENTS   **PAGE**

XIII

XIV

LIST OF TABLES   **PAGE**

XVI

XVII

XVIII

XXII

XXIII

XXIV

XXVII

1. INTRODUCTION

1.1. History of Gears

Gears are toothed members which transmit power or motion between two shafts by meshing without any slip. Due to this, gear drives are also called positive drives. In any pair of gears, the smaller one is called pinion and the larger one is called gear immaterial of which is driving the other. When the pinion is the driver, it results in step down drive in which the output speed decreases and the torque increases. On the other hand, when the gear is the driver, it results in step-up drive in which the output speed increases and the torque decreases. When we look at Indian history, as per our mythological stories is more than 12,000 years old. The knowledge of gears has gone from India to China as back as 2600 years BC. They have used the gears ingeniously in chariots for measuring the speed and other mechanisms. Primitive gears shown in Figure 1.1, were first used in door drive mechanism in temples and caves, and water lifting mechanisms 2600 B.C. in India and elsewhere. Aristotle in the fourth century B.C. mentions in his writings that gears were being used very commonly in many applications. Classical origin of worm gearing was made by Archimedes 287-212 B.C. (K.Gopinath & M.M.Mayuram, 2009
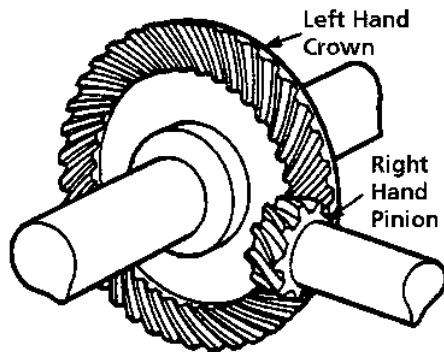
Figure 1.1. Primitive gears made of wood (K.Gopinath & M.M.Mayuram, 2009)

Vitruvius, who is a military engineer, in his writing in 28 B.C. has described many gear applications, typical ones are shown in figure 1.2.
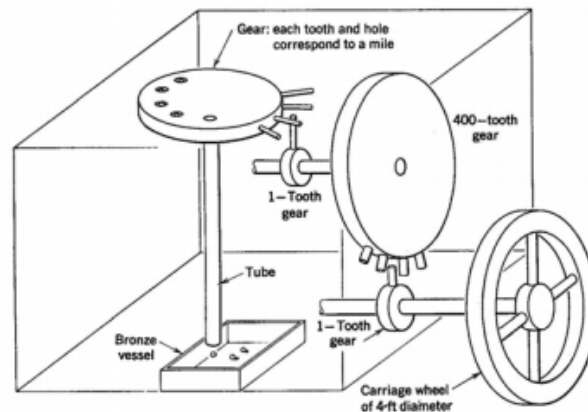
Figure 1.2. Schematic diagram of an odometer for a carriage described by
          Vitruvius 28 BC (K.Gopinath & M.M.Mayuram, 2009)

Leonard da Vinci used multitudes of gears in various mechanisms developed by him 500 A.D. Greek and Roman literatures show extensive usage of gears for forwarding motion. Toothed gears are used for the clocks of Cathedrals

2

and other ecclesiastical buildings during the middle ages. These are still preserved in many places. Salisbury cathedral still possesses the oldest clock in England made in 1386. The Wells Cathedral clock, made in 1392, is preserved in the Science museum, South Kensington. Though the iron gears have worn out to some extent, they still keep good timings. German artist Albrecht Durer's engravings show a vehicle designed for Emperor Maximilian I during the 15th century. That vehicle was driven by worm gears on all four wheels. This clearly shows that he knew the concept of gearing which helped him in sketching them accurately. In the 18th century, the Industrial Revolution in England led to the usage of cycloidal gears for clocks, irrigation devices, water mills, and powered machines. Figure 1.3 gives the glimpses of their contribution to engine application.

The industrialization of the west made a big impact on gear technology which is the key to modern development and the gear technology is advancing rapidly. It is most unlikely that gears are going to be replaced by any other component for their function shortly (K.Gopinath & M.M.Mayuram. 2009).
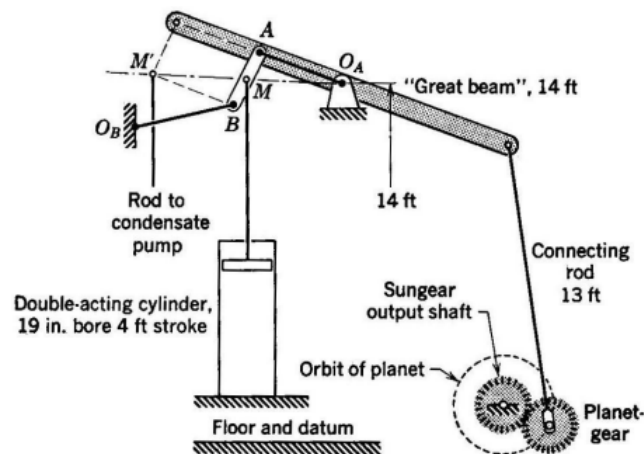
Figure 1.3. Schematic diagram of Watt's rotating Engine, 1784, the first engine to produce power directly on a shaft (K.Gopinath & M.M.Mayuram, 2009)

3

1.2. Gear Transmission

Gear transmissions are commonly used in various industries and their efficiency and reliability are critical in the final product performance evaluation. Gear transmissions affect energy consumption during usage, vibrations, noise, and warranty costs among other factors. These factors are very critical in modern competitive manufacturing, especially in the aviation industry which demands exceptional operational requirements concerning high reliability and strength, low weight and energy consumption, low vibrations and noise. Thinking their reliability and efficiency are some of the most important factors, problems of distribution of loads and, as a result, distribution of stresses in the whole gear transmission, particularly in teeth of mating gears, need to be thoroughly analysed (Kawalec A. et al.,2006).

In this study, an involute bevel gear design has been performed at different speed ratios of 1:1, 2:1, 3:1, 4:1, 5:1, 6:1, 7:1, and 8:1. And these speed reductions have been carried out at the different amounts of power transmissions. When we compare module (m) and face width (F) results obtained at power transmission values starting from 0,5 kW to 1000 kW with the increments of 50 kW but for all other studies for the designs are carried out for the power transmissions values starting from 0,5 kW to 1000 kW with the increments of 20 kW. And have been used module table that in below Table 1.1;

Table 1.1. Metric/American Gear module and Equivalents (SDP/SI)

Diametral Pitch, P	Module, m	Circular Pitch		Circular Tooth Thickness		Addendum	
		in	mm	in	mm	in	mm
203.2000	0.125	0.0155	0.393	0.0077	0.196	0.0049	0.125
200	0.12700	0.0157	0.399	0.0079	0.199	0.0050	0.127
180	0.14111	0.0175	0.443	0.0087	0.222	0.0056	0.141
169.333	0.15	0.0186	0.471	0.0093	0.236	0.0059	0.150
150	0.16933	0.0209	0.532	0.0105	0.266	0.0067	0.169
127.000	0.2	0.0247	0.628	0.0124	0.314	0.0079	0.200
125	0.20320	0.0251	0.638	0.0126	0.319	0.0080	0.203
120	0.21167	0.0262	0.665	0.0131	0.332	0.0083	0.212
101.600	0.25	0.0309	0.785	0.0155	0.393	0.0098	0.250
96	0.26458	0.0327	0.831	0.0164	0.416	0.0104	0.265
92.3636	0.275	0.0340	0.864	0.0170	0.432	0.0108	0.275
84.6667	0.3	0.0371	0.942	0.0186	0.471	0.0118	0.300
80	0.31750	0.0393	0.997	0.0196	0.499	0.0125	0.318
78.1538	0.325	0.0402	1.021	0.0201	0.511	0.0128	0.325
72.5714	0.35	0.0433	1.100	0.0216	0.550	0.0138	0.350
72	0.35278	0.0436	1.108	0.0218	0.554	0.0139	0.353
67.733	0.375	0.0464	1.178	0.0232	0.589	0.0148	0.375
64	0.39688	0.0491	1.247	0.0245	0.623	0.0156	0.397
63.500	0.4	0.0495	1.257	0.0247	0.628	0.0157	0.400
50.800	0.5	0.0618	1.571	0.0309	0.785	0.0197	0.500
50	0.50800	0.0628	1.596	0.0314	0.798	0.0200	0.508
48	0.52917	0.0655	1.662	0.0327	0.831	0.0208	0.529
44	0.57727	0.0714	1.814	0.0357	0.907	0.0227	0.577
42.333	0.6	0.0742	1.885	0.0371	0.942	0.0236	0.600
40	0.63500	0.0785	1.995	0.0393	0.997	0.0250	0.635
36.2857	0.7	0.0866	2.199	0.0433	1.100	0.0276	0.700
36	0.70556	0.0873	2.217	0.0436	1.108	0.0278	0.706

Table 1.1.(continue)

33.8667	0.75	0.0928	2.356	0.0464	1.178	0.0295	0.750
32	0.79375	0.0982	2.494	0.0491	1.247	0.0313	0.794
31.7500	0.8	0.0989	2.513	0.0495	1.257	0.0315	0.800
30	0.84667	0.1047	2.660	0.0524	1.330	0.0333	0.847
28.2222	0.9	0.1113	2.827	0.0557	1.414	0.0354	0.900
28	0.90714	0.1122	2.850	0.0561	1.425	0.0357	0.907
25.4000	1	0.1237	3.142	0.0618	1.571	0.0394	1.000
24	1.0583	0.1309	3.325	0.0654	1.662	0.0417	1.058
22	1.1545	0.1428	3.627	0.0714	1.813	0.0455	1.155
20.3200	1.25	0.1546	3.927	0.0773	1.963	0.0492	1.250
20	1.2700	0.1571	3.990	0.0785	1.995	0.0500	1.270
18	1.4111	0.1745	4.433	0.0873	2.217	0.0556	1.411
16.9333	1.5	0.1855	4.712	0.0928	2.356	0.0591	1.500
16	1.5875	0.1963	4.987	0.0982	2.494	0.0625	1.588
15	1.6933	0.2094	5.320	0.1047	2.660	0.0667	1.693
14.5143	1.75	0.2164	5.498	0.1082	2.749	0.0689	1.750
14	1.8143	0.2244	5.700	0.1122	2.850	0.0714	1.814
13	1.9538	0.2417	6.138	0.1208	3.069	0.0769	1.954
12.7000	2	0.2474	6.283	0.1237	3.142	0.0787	2.000
12	2.1167	0.2618	6.650	0.1309	3.325	0.0833	2.117
11.2889	2.25	0.2783	7.069	0.1391	3.534	0.0886	2.250
11	2.3091	0.2856	7.254	0.1428	3.627	0.0909	2.309
10.1600	2.50	0.3092	7.854	0.1546	3.927	0.0984	2.500
10	2.5400	0.3142	7.980	0.1571	3.990	0.1000	2.540

9.2364	2.75	0.3401	8.639	0.1701	4.320	0.1083	2.750
9	2.8222	0.3491	8.866	0.1745	4.433	0.1111	2.822
8.4667	3	0.3711	9.425	0.1855	4.712	0.1181	3.000
8	3.1750	0.3927	9.975	0.1963	4.987	0.1250	3.175
7.8154	3.25	0.4020	10.210	0.2010	5.105	0.1280	3.250
7.2571	3.5	0.4329	10.996	0.2164	5.498	0.1378	3.500
7	3.6286	0.4488	11.400	0.2244	5.700	0.1429	3.629
6.7733	3.75	0.4638	11.781	0.2319	5.890	0.1476	3.750
6.3500	4	0.4947	12.566	0.2474	6.283	0.1575	4.000
6	4.2333	0.5236	13.299	0.2618	6.650	0.1667	4.233
5.6444	4.5	0.5566	14.137	0.2783	7.069	0.1772	4.500
5.3474	4.75	0.5875	14.923	0.2938	7.461	0.1870	4.750
5.0800	5	0.6184	15.708	0.3092	7.854	0.1969	5.000
5	5.0800	0.6283	15.959	0.3142	7.980	0.2000	5.080
4.6182	5.5000	0.6803	17.279	0.3401	8.639	0.2165	5.500
4.2333	6	0.7421	18.850	0.3711	9.425	0.2362	6.000
4	6.3500	0.7854	19.949	0.3927	9.975	0.2500	6.350
3.9077	6.5000	0.8040	20.420	0.4020	10.210	0.2559	6.500
3.6286	7	0.8658	21.991	0.4329	10.996	0.2756	7.000
3.5000	7.2571	0.8976	22.799	0.4488	11.399	0.2857	7.257
3.1750	8	0.9895	25.133	0.4947	12.566	0.3150	8.000
3.1416	8.0851	1.0000	25.400	0.5000	12.700	0.3183	8.085
3	8.4667	1.0472	26.599	0.5236	13.299	0.3333	8.467
2.8222	9	1.1132	28.274	0.5566	14.137	0.3543	9.000

6

Table 1.1. (continue)

2.5400	10	1.2368	31.416	0.6184	15.708	0.3937	10.000
2.5000	10.160	1.2566	31.919	0.6283	15.959	0.4000	10.160
2.3091	11	1.3605	34.558	0.6803	17.279	0.4331	11.000
2.1167	12	1.4842	37.699	0.7421	18.850	0.4724	12.000
2	12.700	1.5708	39.898	0.7854	19.949	0.5000	12.700
1.8143	14	1.7316	43.982	0.8658	21.991	0.5512	14.000
1.5875	16	1.9790	50.265	0.9895	25.133	0.6299	16.000
1.5000	16.933	2.0944	53.198	1.0472	26.599	0.6667	16.933
1.4111	18	2.2263	56.549	1.1132	28.274	0.7087	18.000
1.2700	20	2.4737	62.832	1.2368	31.416	0.7874	20.000
1.1545	22	2.7211	69.115	1.3605	34.558	0.8661	22.000
1.0583	24	2.9684	75.398	1.4842	37.699	0.9449	24.000
1.0160	25	3.0921	78.540	1.5461	39.270	0.9843	25.000
1	25.400	3.1416	79.796	1.5708	39.898	1.0000	25.400
0.9407	27	3.3395	84.823	1.6697	42.412	1.0630	27.000
0.9071	28	3.4632	87.965	1.7316	43.982	1.1024	28.000
0.8467	30	3.7105	94.248	1.8553	47.124	1.1811	30.000
0.7938	32	3.9579	100.531	1.9790	50.265	1.2598	32.000
0.7697	33	4.0816	103.673	2.0408	51.836	1.2992	33.000
0.7500	33.867	4.1888	106.395	2.0944	53.198	1.3333	33.867
0.7056	36	4.4527	113.097	2.2263	56.549	1.4173	36.000
0.6513	39	4.8237	122.522	2.4119	61.261	1.5354	39.000
0.6350	40	4.9474	125.664	2.4737	62.832	1.5748	40.000
0.6048	42	5.1948	131.947	2.5974	65.973	1.6535	42.000
0.5644	45	5.5658	141.372	2.7829	70.686	1.7717	45.000
0.5080	50	6.1842	157.080	3.0921	78.540	1.9685	50.000
0.5000	50.800	6.2832	159.593	3.1416	79.796	2.0000	50.800

1.3. Conjugate Action

To obtain the expected velocity ratio of two tooth profiles, the normal line of their profiles must pass through the corresponding pitch point, which is decided by the velocity ratio. The two profiles which satisfy this requirement are called conjugate profiles. Sometimes, we simply termed the tooth profiles which satisfy the fundamental law of gear-tooth action the conjugate profiles.

Although many tooth shapes are possible for which a mating tooth could be designed to satisfy the fundamental law, only two are in general use: the cycloidal and involute profiles. Involute has important advantages. It is easy to manufacture and the center distance between a pair of involute gears can be varied without changing the velocity ratio. Thus close tolerances between shaft locations are not required when using the involute profile. The most commonly used conjugate tooth curve is the involute curve (Erdman & Sandor 84).

7

In detail, the law of conjugate gear tooth action states that as the gears rotate, the common normal to the surfaces at the point of contact must always intersect the line of centers at the same point P, called the pitch point. The law of conjugate gear tooth action can be satisfied by various tooth shapes (Juvinall R.C., Marshek K.M., 2011). Figure 1.4 as shown below;
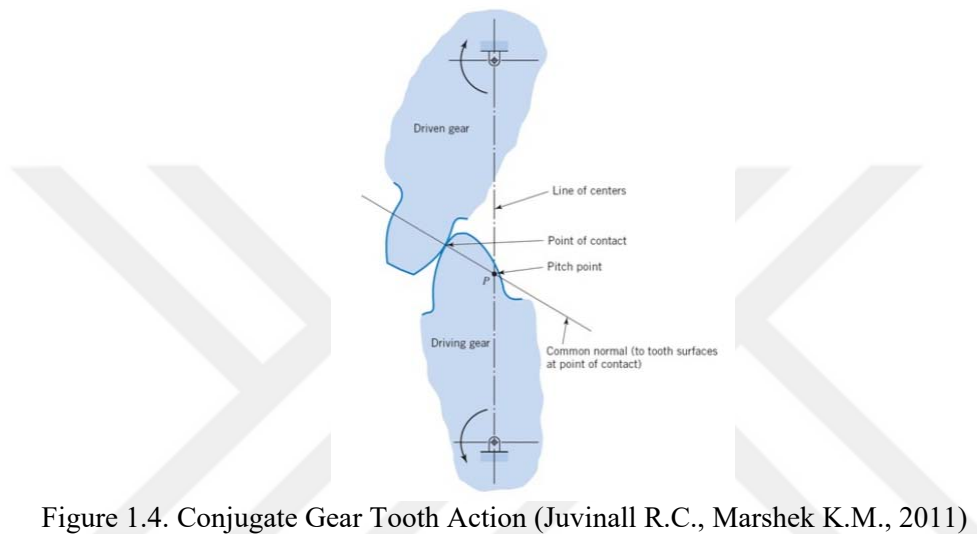
Figure 1.4. Conjugate Gear Tooth Action (Juvinall R.C., Marshek K.M., 2011)

1.4. Involute Profile

Simple teeth on a cylindrical wheel have some disadvantages that the speed ratio is not constant and the speed reduction causes noise and vibration problems especially at elevated speeds while a pair of gear is in a mesh. For this goal, different kinds of geometrical forms can be used but the full depth involute profile is currently used in most engineering practices (Juvinall R.C., Marshek K.M., 2011).

In theory, it is possible arbitrarily to select any profile for one tooth and then to find a profile for the meshing tooth that will give conjugate action. One of these solutions is the involute profile, which, with few exceptions, is in universal use for gear teeth, and is the only one with which we will be concerned (Budynas R.G. and Nisbett J.K., 2011).

An involute of the circle is the curve generated by any point on a taut thread as it unwinds from a circle, called the base circle. The generation of two involutes is shown in Figure 1.5. Most gears use involute profiles, so it is good to understand how to draw an involute profile.
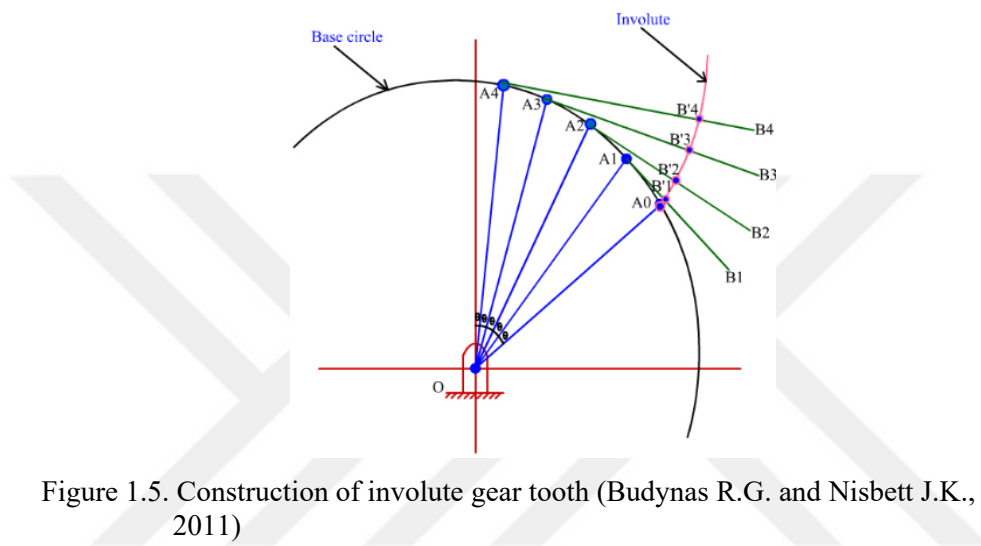
Figure 1.5. Construction of involute gear tooth (Budynas R.G. and Nisbett J.K., 2011)

1.5. Gear Classification

Gears can be divided into a several classifications based on the arrangement of the axes of the gear pair and generally categorized as spur gears, helical gears, bevel gears and worm gears. Within these gears there are sub-classification based on designs. Gears are made of ferrous (steel, cast iron), non-ferrous metals (bronze based) and non-metallic materials (Nylon, fibre reinforced in phenolic resin etc.). Steel is the most widely used material for gears.

1.5.1. Spur Gears

Gears have specially constructed toothed profile, and are extensively used to transmit power in machines. Spur gears are the simplest and most common types of gears, having the maximum precision and high power transmission efficiency

9

compared to any other gears. Hence, they are preferred as the first choice in industrial machines, except high speed and high load applications. In spur gears, two meshing gears are mounted on parallel shafts. The teeth are cut parallel to the axis of gear. In a normal or external spur gear, the teeth are cut on the outside of the rim of gear Figure 1.6.

Figure 1.6. Normal or external spur gears on ring spinning machine

Generally, the input gear is smaller in size and the output gear is larger in size to get speed reduction. The driver and the driven gears are called 'pinion', and 'gear', respectively.

As shown in Figure 1.7, they are used to transfer motion between parallel shafts and their teeth are parallel to the shaft axes.
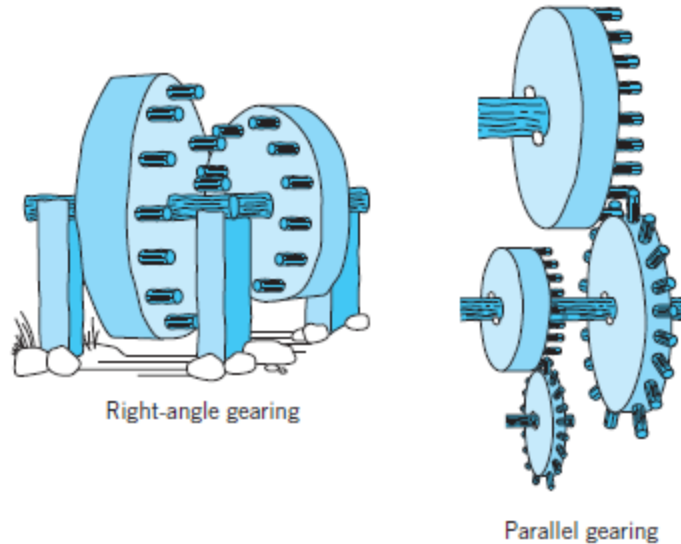
Figure 1.7. Primitive gears (Juvinall R.C., Marshek K.M., 2011)

The spur gears are ordinarily thought of slow-speed gears, as helical gears are thought of as high-speed gears. If noise is not an important design problem, spur gears can be used at almost any speed that can be handled by other types of gears.

1.5.2. Helical Gears

Helical gears offer a refinement over spur gears. The leading edges of the teeth are not parallel to the axis of rotation but are set at an angle. Since the gear is curved, this angling causes the tooth shape to be a segment of a helix. The angled teeth engage more gradually than the spur gear teeth. This causes helical gears to run more smoothly and quietly than spur gears. Helical gears also offer the possibility of using non-parallel shafts. A pair of helical gears can be meshed in two ways: with shafts oriented at either the sum or the difference of the helix angles of the gears. These configurations are referred to as parallel or crossed, respectively. The parallel configuration is the more mechanically sound. In it, the

11

helices of a pair of meshing teeth meet at a common tangent, and the contact between the tooth surfaces will, generally, be a curve extending some distance across their face widths. In the crossed configuration, the helices do not meet tangentially, and only point contact is achieved between tooth surfaces. Because of the small area of contact, crossed helical gears can only be used with light loads (Dudley, Darle W. 1994. Handbook of Practical Gear Design, Boca Raton, FL: CRC Press).

Quite commonly, helical gears come in pairs where the helix angle of one is the negative of the helix angle of the other; such a pair might also be referred to as having a right-handed helix and a left-handed helix of equal angles. If such a pair has meshed in the 'parallel' mode, the two equal but opposite angles add to zero: the angle between shafts is zero. This means that the shafts are parallel. If the pair has meshed in the 'crossed' mode, the angle between shafts will be twice the absolute value of either helix angle.

Note that 'parallel' helical gears need not have parallel shafts. This only occurs if their helix angles are equal but opposite. The 'parallel' in 'parallel helical gears' must refer, if anything, to the (quasi) parallelism of the teeth, not to the shaft orientation.

As mentioned above, helical gears operate more smoothly than the spur gears. With parallel helical gears, each pair of teeth first make contact at a single point at one side of the gear wheel; a moving curve of contact then grows gradually across the tooth face. It may span the entire width of the tooth for a time.

Finally, it recedes until the teeth break contact at a single point on the opposite side of the wheel. Thus force is taken up and released gradually. With spur gears, the situation is quite different. When a pair of teeth meets, they immediately make line contact across their entire width. This causes impact stress and noise. Noise levels are lower than spur gears. This is because helical teeth enter the meshing zone progressively and make point contact in mesh rather than line contact. Therefore, it tends to be quieter.

12

Besides, the load transmitted may be somewhat larger, or the life of the gears may be greater for the same loading, than with an equivalent pair of spur gears. In some cases, the smaller size of helical gears may be used to transmit the same amount of loading when compared with spur gears (Stephen P. R.,2012).

1.5.3. Bevel Gears

Bevel gear is a type of all gears. Bevel gears are used to transmit motion between two non-parallel, usually orthogonal, co-planar intersecting shafts.

The gears generally fail when tooth stress exceeds the safe limit. When failure occurs, they are expensive not only in terms of the cost of replacement or repair but also the cost associated with the downtime of the system of which they are a part. So, it is important to understand various problems that can occur in gears. The three most common failure modes are bending fatigue, contact fatigue, wear and scuffing. Bending fatigue of failure, caused by repeated loading, starts as a crack that grows until the part fractures. As a fatigue crack propagates, it leaves "beach marks" that correspond to positions where the crack stopped. Most fatigue failures occur in the tooth root fillet. Whereas surface contact stresses are on the side of tooth may causes scoring wear, pitting fatigue failure (K.Gopinath & M.M.Mayuram, 2009).

Bevel gears have teeth formed on conical surfaces. Bevel gears are used for motor transmission differential drives, valve control, and mechanical instruments. A variety of tooth forms are possible, including straight bevel gears, spiral bevel gears, and zerol bevel gears. Straight bevel gears have a straight tooth form cut parallel to the cone axis, which if extended would pass through a point of intersection on the shaft axis. Straight bevel gears are usually only suitable for speeds up to 5 m/s. Spiral bevel gears have curved teeth that are formed along a spiral angle to the cone axis. The advantage of spiral bevel gears over straight teeth is that the gears engage more gradually. This supplies a smoother transmission of power and reduces the risk of tooth breakage. Spiral bevel gears are recommended

for pitch line speeds in the range from 5 to 40 m/s. Zerol bevel gears have a tooth form that is curved. They represent an intermediate category between straight and spiral bevel gears (Childs. Peter R. N., 2013).

1.5.4. Worm Gears

Worm gears are used for transmitting power between two non-parallel, non-intersecting shafts. High gear ratios of 200:1 can be obtained.

(a)   (b)
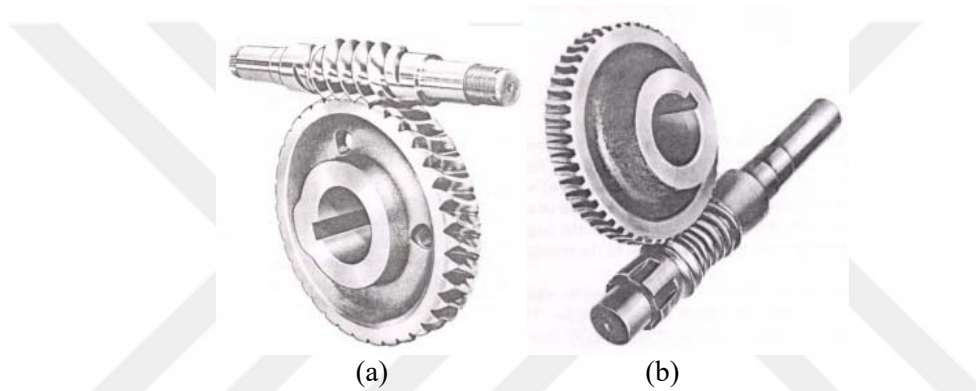
Figure 1.8. (a) Single enveloping worm gear, (b) Double enveloping worm gear

Originally, worm gearing was used to secure, by compact means, a large reduction of speed between the driving and driven shafts with a proportionate increase (except for frictional loss) in the torque of the driven shaft. Worm gearing is still used for this purpose, and frequently the wheel is driven by a single-thread worm of such low helix angle that the drive cannot be reversed; that is the wheel cannot drive the worm as the gearing automatically locks itself against backward rotation. Although a multiple-threaded worm, when applied under like conditions, is much more efficient than a single-threaded worm, it does not follow that the multiple-threaded worm should always be used. A single-threaded worm might be preferable when the most important requirement is to obtain a high ratio and especially if the worm must be self-locking. When power is the primary factor,

multiple-threaded worms should be used. Lubrication is an important factor when using worm gearing. An increase in heat generated means a decrease in efficiency. (Martin- Sprocket-Worm-Gears).

1.6. Aim of Study

There are many design parameters in the design of bevel gears that are module (m) or diametral pitch (P), cone distance (A_0) and face width (F or b). The proper values of these are searched in the gear design before material is pre-selected. After defining the pinion and gear materials, module is estimated, and calculations are carried out to determine the suitable face width. The diametral pitch P is the ratio of the number of teeth on the gear to the pitch diameter. So, it is the reciprocal of the module. Since the diametral pitch is used only with U.S. units, it is expressed as teeth per inch. The cone distance A_0 shown in Figure 1.9, is that the distance along with a reference cone generator, from the cone apex to the specified cone. A suitable module is to be selected and the face width calculations is to be performed using the $F = 0.3A_0$ or $F = 10/P$. Various design approaches each of which provides different formulas are available in the machine elements or machine design textbooks for the design or finding "m" or "F". This is also the case when the dictated technical standards are used. However, the results of using different approaches have not been compared so far. Thus the designer does not aware of the success or loss gained using each of the approaches. Therefore, there is a need to compare the results of each of the most accepted design approach for bevel gear design. Hence, this study aims to compare the design results (F and m) obtained using the different design approaches to determine loss or gain obtained using each of the approaches.

In this study, design of an involute bevel gear has been performed based on both bending fatigue failure and surface contact failure theories. Defining the pinion and gear material depending on the working conditions, the allowable minimum number of teeth for the pinion and gear will be the initial requirements to

determine. And then a suitable module is selected and the face width calculations will be performed using the $F = 0.3A_0$ or $F = 10/P$, whichever is smaller, then the face width (F) is chosen as an output of the design. The results obtained in each of the approaches under the different speed ratios will be compared with each other and all of these theoretical calculations will be executed using the Microsoft Excel pages.

To verify the results and to use a base as a solid reference, a finite element method (FEM) will be used to analyse the results obtained using the theoretical approaches. For this, 3-D models of bevel gears, which are created in SOLIDWORKS, will be imported into ANSYS Workbench 16.1. Then, the module and face widths found using each approach will be compared with the results of FEM. This approach will be used to verify each of the design approaches used in this study against ANSYS, and then more solid comparisons will be obtained.

The module (m) and face width (b) that are obtained from four of the approaches (ANSI/AGMA 2003-B97 standards, ISO Standards, Fundamentals of Machine Component Design 5th Edition, K.Gopinath & M.M.Mayuram 4th Edition) are different from each other, even under the same input parameters. These are leading to different gear designs that are associated with cost. So, gear designers require detailed knowledge of the relative comparison of design outputs.

For this reason, the differences in the results obtained from different gear standards have significantly been the subject of investigations for many types of researches. And a translation technique using conversion factors in between the standards are demanded as a stated need in the literature. Thus, this paper firstly obtains dimensionless gear rating numbers (GRi) to rate the design results of bevel gears determined from the four approaches, and then it derives correlation equations to generate dimensionless conversion factors (CFs) to convert the design results obtained from the four gear design approaches. The CFs allow designers to easily move from one standard to another. This enables engineering students and designers to meet the ever-changing needs of the global market fast.

Finally, the study will allow comparing the design results of the most approaches given in the most commonly used textbooks and international and national standards.

The main intention is to compare the design results given by the most commonly used gear design approaches. Hence, the designer can be aware of the success or loss gained using each of the approaches. The results of the study may also help to select the proper gear design approach depending on the requirements of the particular design.

2. PREVIOUS STUDIES

Various studies are available for the design of an involute spur and helical gears in literature. But there is not many study related to design an involute straight bevel gear in the literature. Mostly all works are related to decreasing bending and surface contact stresses, few developed computer programs to parametrically draw and model the gear wheels and gear wheel pairs in a CAD (Computer Aided Design) environment and some carried out failure analyses. To decrease gear stresses, researches put efforts improving gear profile and optimization of dimensions by using different kinds of methods mentioned in the following sections.

2.1. Most Commonly Used Gear Design Approaches

The design of an involute bevel gear design requires a number of determinations that require different design factors. In order to perform a bevel gear design, national and international standards and/or machine elements textbooks have been provided to designers. Available straight bevel gear design approaches and their basis of origins are searched and given in Table 2.1. In this study, the most commonly used machine element textbooks and the design procedures available in international design standards have been searched and four of them have been considered. Two of them are from machine design textbooks (Fundamentals of Machine Component Design 5th Edition, Machine Design II, K.Gopinath & M.M.Mayuram 4th Edition). The remaining one is selected from international standards. These are ANSI/AGMA 2003-B97 standards. Which is most commonly used and introducing a design of bevel gear clearly? Standards and design approaches that are not considered given Table 2.1.

Table 2.1.Available straight bevel gear design approaches and their basis of origins

Available Design Approaches	The main Basis of Design approach
Mechanical Engineering Design 1st Metric Edition (Shigley's J.E., 1985)	ANSI/AGMA Standards**
Fundamentals of Machine Component Design 5th Edition (Juvinall R.C., Marshek K.M., 2011)	Similar to ANSI/AGMA**
Shigley's Mechanical Engineering Design 9th Edition (Budynas R.G. and Nisbett J.K., 2011)	Lewis and Hertzian Theory and includes ANSI/AGMA Standards**
ANSI/AGMA Standards	ANSI/AGMA Standards*
Makine Elemanları ve Konstrüksiyon Örnekleri (Babalık F.C., 2010)	DIN Standards
Machine Design II, K.Gopinath & M.M.Mayuram 4th Edition Standards 4th Edition	ANSI/AGMA Standards**

*Most commonly used
** Introduces the design of a bevel gear clearly

2.2. Gear Design using Computer Aided Engineering (CAE)

The term computer aided engineering (CAE) usually applies to all computer related engineering applications. With this definition, CAD can be considered as a subset of CAE (Budynas R.G. and Nisbett J.K.,2011).

The CAE systems make sophisticated mathematical algorithms to perform calculations. Information about the process to be simulated must be attributed to the CAE system to make the calculations. This information is called entrance variables. Both variables are specifically defined in the function of the process and/or the product studied. To carry out the simulation calculations, CAE uses finite technical elements. The working procedures to carry out simulations with

CAE systems can be divided into three main phases: pre-processing (generation of the sweater of finite elements and variables of entrance), processing (calculation of the demands) and post-processing (evaluation and interpretation of the answer of the software) approached with more property in the sequence (Adriano Fagali De Souza and Sabrina Bodziak Adriano Fagali De Souza and Sabrina Bodziak, 2013). There are various software programs available for modelling. Some of them are Cad Key, Pro Engineer, Solid works, Inventor, Mechanical Desktop, Unigraphics, Catia V5, etc.

The finite element method is a numerical analysis technique for obtaining approximate solutions to a wide variety of engineering problems. Thus due to its diversity and flexibility as an analysis tool, it is receiving much attention in almost every industry. Since it is not possible to obtain theoretical mathematical solutions for many engineering problems, it is necessary to obtain approximate solutions to the problem rather than an exact closed-form solution. The finite element method has become a powerful tool for the numerical solutions of a wide range of engineering problems. Various commercial software products are available for finite element analysis (FEA) such as Ansys, Nastran, Cosmos, LS-Dyna (Parthiban A.et al, 2013).

Geren N. and Baysal M. (2000) developed an expert system which is a branch of Artificial Intelligence. They used this system for gearbox design by operating Delphi from Borland for an expert system development tool. And the American Gear Manufacturers Association (AGMA) methods and its recommendations were used for designing the spur gear. The developed program by Geren N. and Baysal M. has a user-friendly interface that allows to the dealer to select the type of gear, material etc. The program includes the recommended module size list box which is the result of estimating gear size procedure. It is stated that the developed software reduced the design duration to 2 minutes for an experienced designers and few minutes for an inexperienced designers, allowing the user to try different design alternatives in a short time, eliminating the errors made during the manual design process.

Al-Qrimli HF, Almurib HA, Kumar N, Mahdi FA (2015) used orthotropic materials are selected to be used as a straight bevel gear. These materials have the advantage of being light, are durable at high speeds, require the minimum need for oil, high strength, and extra loading capacities. Due to these properties, it is highly preferable compared to conventional materials. This work demonstrates a standard form of the straight bevel gear, to focus on the study of the behaviour of the material. It used the complex proportional assessment method to determine the optimum material to be used for the gear. This method is one of the most common methods in determining the best designs. The first step of the methodology is the numerical procedure by using the finite element method. After that, they used this method to select which material is the best to be used as a straight bevel gear. Figure 2.1 summarizes the whole procedure that was used in this work to realize the orthotropic straight bevel gear. This type of approach was decided as it is adequate to wide categories of dynamic gear problems under sophisticated design considerations. The concept and reality flowchart for straight bevel gear design was given in Figure 2.1. Boundary conditions are shown in Figure 2.2.
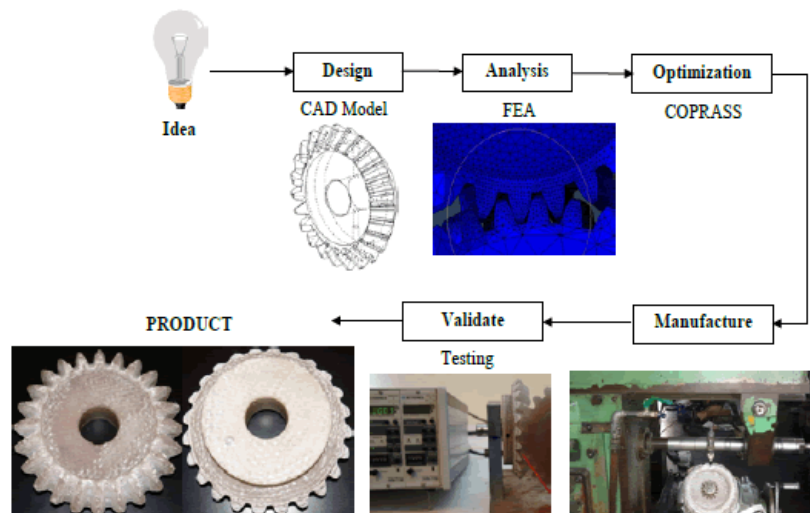
Figure 2.1. Concept and reality flowchart for straight bevel gear design (Al-Qrimli HF, Almurib HA, Kumar N, Mahdi FA 2015)
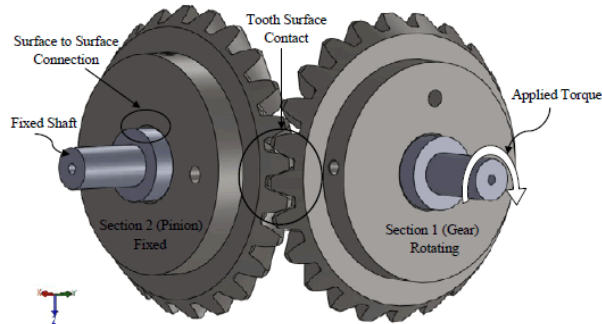
Figure 2.2. Boundary conditions of the straight bevel gear (Al-Qrimli HF, Almurib
           HA, Kumar N, Mahdi FA 2015)

The magnitude of the applied torque used in the work was (17640 N.m),
which resulted in the tangential force of the gear's tooth surface of (245N). All the
standard parameter used to construct the straight bevel gear is shown in Table 2.2.

Table 2.2. Standard gear parameters (Al-Qrimli HF, Almurib HA, Kumar N, Mahdi
           FA 2015)

NO.	Design Parameter	Value	Options
1.	Pressure angle	20o	
2.	Module	6	Material model
3.	Face width	28.5m	Glasses/Epoxy
4.	Addendum	1m	Carbon/Epoxy
5.	Dedendum	1.25m	Jute/Epoxy
6.	Shaft angle	90o	Chopped/Epoxy
7.	Root fillet radius	0.3m	Steel
8.	Number of teeth	24	

Haidar Fadhil AL-Qrimlia, Ahmed M. Abdelrhman and Karam S. Khiled.
et al, (2016) studied the model numerically by running the straight bevel gear
generation built using a commercial software to create points that describe the
whole gear body, these points with composite mechanical properties are the input
data for ABAQUS program to draw the bevel gear domain and contour the
principle stresses inhabited in its teeth made of composite material, and draw the
mode shape present due to the same load conditions. They derived an theoretical

23

model based on the AGMA standard. The gear is modelled using CAD commercial software to generate the whole gear in three dimension coordinates, and then analysis begins with a calculation of the gear loads generated by the bevel mesh. This theoretical calculation was constructed to allow them to calculate the straight bevel gear profile points, which are crucial for modelling and fabricating the composite gear model, and to numerically analyse the stresses and deflection in a single point in the midpoint of the gear tooth surface. This is found to be useful to verify the stresses and deflections that they determined and measured the work carried out using the finite element method. The results were extensively compared with each other. This comparison attempted to study the composite bevel gear teeth problem. During design, it is assumed that the direction of the material is one direction in the finite element model. After running the simulation in the ABAQUS solver stage, the stress-strain behaviour of the models was compared to the analytical calculation shown in Table 2.3 below.

Table 2.3. Numerical and analytical results of the straight bevel gear for a different type of materials (Haidar Fadhil AL-Qrimlia, Ahmed M. Abdelrhman and Karam S. Khiled 2016)

Stress/Material	Steel		Glass/Epoxy		Carbon/Epoxy		Jute/Epoxy	
	FEA	AGMA	FEA	AGMA	FEA	AGMA	FEA	AGMA
$\sigma1$ (Mpa)	236.497	263.34	347.367	261.652	361.712	358.219	233.809	184.025
$\sigma2$ (Mpa)				295.527		343.125		285.516
$\sigma3$ (Mpa)				253.991		266.981		221.724

The validity of the FEM achieved by comparing its results (ABAQUS) for (steel, glass/epoxy, carbon/epoxy, and jute/epoxy) with one analytical calculation load applied at the midpoint of the gear tooth surface. The comparison shows that there is a good agreement; therefore, the validity of the FEM is satisfied. Static stress analysis of these glass/epoxy, carbon/epoxy, jute/epoxy, and mild steel materials gears are performed and their normal stresses in X, Y, Z directions are obtained. The same load of 245.25 N per mm length of face width of gear tooth was applied in all the cases.

2.3. Verification of Gear Design Results with Finite Element Analysis

Gear design is realized considering the fatigue bending stress (bending fatigue) and contact stress (surface contact fatigue). Surface contact fatigue is the most common cause of gear failure. It results in fatigue failure to contacting surfaces which can significantly reduce the load-carrying capacity of gears, and may ultimately lead to complete failure of a gear. Tooth bending fatigue is one of the most common modes of fatigue failure in gears. It results in progressive damage to gear teeth and ultimately leads to complete failure of the gear. The tooth root is subjected to fatigue bending stress and the tooth surfaces are subjected to fatigue contact stresses. Gear stresses have significant importance because the failure of gear due to bending causes tooth breakage whereas due to surface contact causes pitting, scoring and/or wear.

Jingtao Han, Zhengyi Jiang and Sihai Jiao (2010) have analysed solid modelling and dynamic simulation of spur bevel gear. Based on 3D solid modelling software, Solid Works, a drawing method of spherical involute has been achieved, and the solid modelling accuracy of spur bevel gear was improved. After solid modelling, bevel gear analysis has carried out with ANSYS/LS-DYNA software, and the contact stress and acceleration change of driven wheel during the meshing process have been calculated, which is to be used to guide the modification of spur bevel gear.

Wenzhe Chen, Pinqiang Dai, Yonglu Chen, Qianting Wang and Zhengyi Jiang (2012) have studied meshing performance analysis of new non-zero-positive modification spiral bevel gear. They claimed that for non-zero-modification of spiral bevel gear, its machining parameters could be designed with big contact ratio by Local Synthesis. This design method could make up the shortage of low coincidence degree resulted in increasing mesh angle in the non-zero-positive transmission designing. Taking an example, according to comparing the new with conventional design simulation results, the max root tensile stress of pinion was reduced by 28.36%, and the max root compressive stress was reduced by 23.31%,

and the max tooth surface contact stress was reduced by 3.5%, and the root stress of gear decreased slightly under the same load conditions. The conclusions showed that the pinion bending strength was improved. As a result, the tooth profile of a new design and its parameters for machining made gear pair possess higher reliability and life.

Xipeng Xu, Chuanzhen Huang, Dunwen Zuo and Ming Chen (2013) have analysed Modelling of Error Analysis Simulation of Normal Circular Arc Bevel Gear Transmission. The normal circular arc bevel gears are used in industrial areas of high speed, high bearing and high strength widely. A mathematical simulation model is built and the built model was used to analyse transmission error and contact zone of normal circular arc bevel gears. In this model, the instantaneous engaging points of gear pair are transformed into the least-values of rotary angles of corresponding points between two gears along with the final motion, so this method was found to be very simple and effective. Under the condition of existing helix angle error, transmission error and contact zone of a pair of normal circular arc bevel gears simulating analysed. Finally, they concluded that the operation test of contact zone of gears indicates that gears provide stable transmission and the gears contact zones are largely in line with the simulation results.

Nalluveettil and Muthuveerappan (1993) carried out a finite element analysis of a straight bevel gear tooth for evaluation of bending stresses wherein iso-parametric brick element was selected for FEA. Stress distribution results at the root of the tooth were compared with the experimental results. The tooth behaviour at the root was studied by altering different parameters like pressure angle, rim thickness, etc.

Vijayarangan and Ganesan (1994) investigated the results of static load distribution analysed by 3D finite element method on composite bevel gears. Comparative studies on the performance of composite gear showed that the static strength of glass epoxy bevel gear was nearly closer to that of carbon steel bevel gear than that of boron/epoxy bevel gear. The displacement of glass/epoxy showed

more deviation as compared to carbon steel which was even more for the boron/epoxy case. It was concluded that boron/epoxy is better than steel.

2.3.1. The studies on the Effect of Profile Modification

As the gear stresses have to be taken into consideration for design, various investigations on the tooth profile have been done to reduce gear stresses.

Seung-Bok Choi, Prasad Yarlagadda and Mohammad Abdullah-Al-Wadud (2014) have studied the influence of technical parameters on contact pressure in straight bevel gear meshing. Wear is one of the main failure modes of gears in the meshing performance, and the contact pressure is the key factor to determine the wear of gears. The main purpose of this paper is to investigate the contact pressure distribution and evolution laws in straight bevel gear meshing. Based on a 3D finite element model of the specific loaded assembling straight bevel gear pair, the influence of friction coefficient f, torque T and elastic modulus E on the contact pressure of straight bevel gear in a meshing circle is studied. The results show that the contact area and contact pressure increase dramatically with the increase of the torque. The contact area decreases and the contact pressure increases with the increase of elastic modulus. Friction coefficient almost does not effect on the contact area and contact pressure. This research has great theoretical significance to reveal the wear mechanism and improve the meshing performance of straight bevel gears. Boundary conditions of straight bevel gear are seen at Figure 2.3;
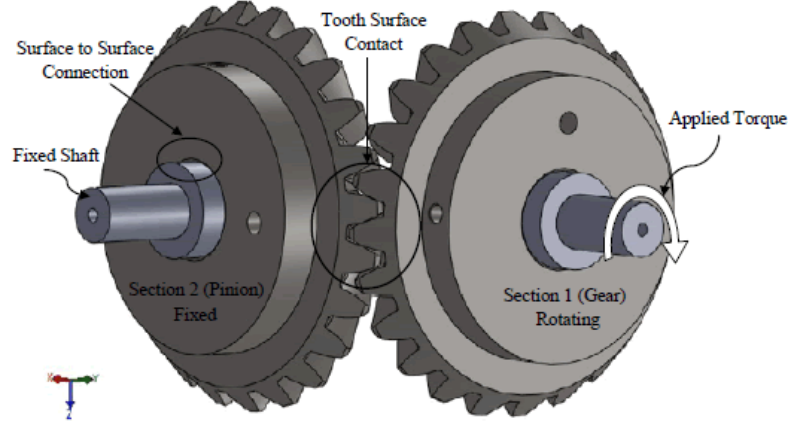
Figure 2.3. Boundary conditions of the straight bevel gear (Al-Qrimli HF, Almurib HA, Kumar N, Mahdi FA 2015)

Liangchi Zhang, Chunliang Zhang and Zichen Chen (2011) have studied on contact force of tooth profile modification. Linear, conic, cubic, and sine relief curves are compiled and established in MATLAB, on which gear models are built in UG and a new method of establishing relief gear models is proposed in their paper. Based on the theory of the elastic contact method is used on the proposed finite element models of gears by LS-DYNA software. The total contact force of teeth face, contact force of single tooth and equivalent stress on relief gears in different cases are obtained. The results show that contact impact existing in meshing between teeth of gears is ameliorated. As a result of this, contact force of tooth face and equivalent stress were reduced. The effect of cubic and the sine relief curve was found to be the best. So dynamic simulation on sine relief curve has found to have great significance to reduce contact force between teeth faces of gears.

Vilmos V.Simon (2011) has shown the influence of tooth modifications on tooth contact in face-hobbed spiral bevel gears. In this study, the influence of tooth modifications induced by machine tool setting and head-cutter profile variations on tooth contact characteristics in face-hobbed spiral bevel gears was investigated. The concept of face-hobbed spiral bevel gear generation by an imaginary

generating crown gear was applied. The modifications of tooth surfaces were introduced into the teeth of both members. The lengthwise crowning of teeth was achieved by applying a slightly bigger radius of lengthwise tooth flank curvature of the crown gear generating the concave side of pinion/gear tooth-surfaces, and by the variety of machine tool settings in the generation of pinion/gear teeth. The ease-off in the tooth height direction of meshing tooth surfaces was achieved by applying a head-cutter whose profile consists of two circular arcs, instead of a straight-line. The method of tooth contact analysis applied determines the path of contact, the potential contact lines, the separations along these lines, and the transmission errors. A computer program implemented to use the method. By using this program, the influence of the variation of machine tool settings and of head-cutter geometry on tooth contact was investigated and discussed in detail. Tooth contact points which are provided by Vilmos V.Simon (2011) are given in Figures 2.4 and 2.5;
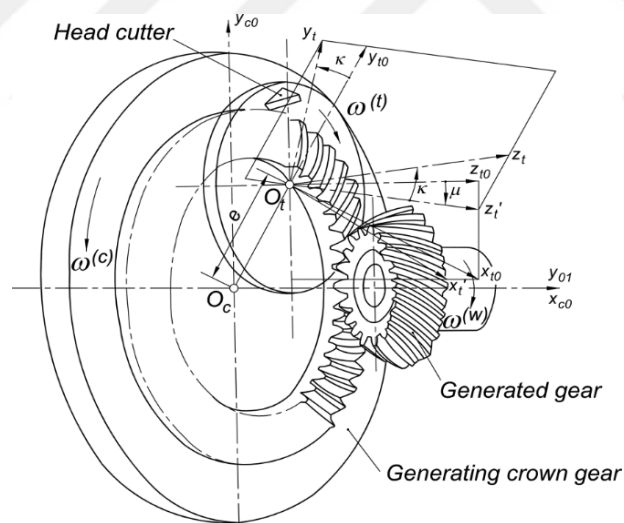

Figure 2.4. Tooth contact points (Vilmos V.Simon 2011)

29
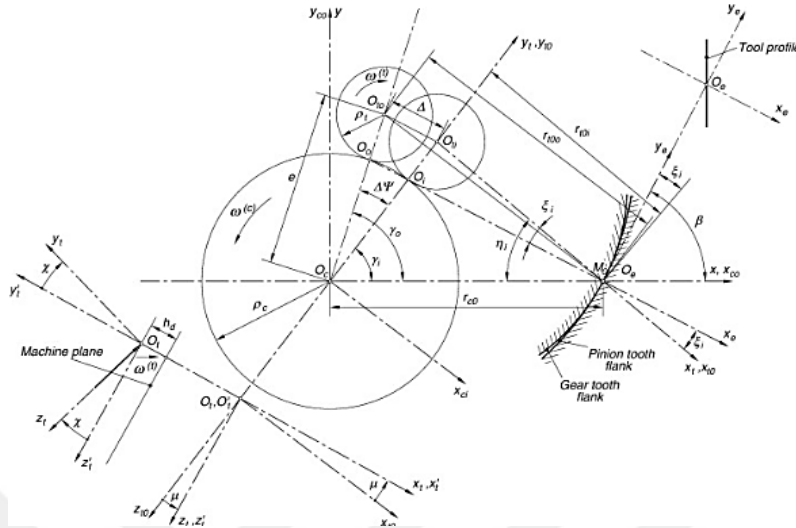
Figure 2.5. Tooth contact points (Vilmos V.Simon 2011)

Chen-Hsiang Lin and Zhang-Hua Fong (2014) investigated numerical tooth contact analysis of a bevel gear set by using measured tooth geometry data. A numerical tooth contact analysis (NTCA) technique was developed to simulate the single flank test by the gear geometry data measured on a gear measuring center. The proposed NTCA uses only the position vector to calculate continuous transmission error (CTE) and the corresponding contact pattern. The proposed NTCA is very flexible since the tooth surface is measured from real gear and reconstructed as a B-spline free form surface; no mathematical model for specified gear type is required. The calculation speed of NTCA was fast for the multiple tooth contact since the structure of the proposed numerical algorithm was suitable for the parallel computing. The least rotation angle (LRA) method and the improved quad-tree (QT) search algorithm were used to determine the CTE and the tooth contact pattern. The validation of the proposed NTCA was verified by comparing the contact pattern and TE of test gear to the theoretical TCA results generated by the commercial TCA software. Tooth contact analyses are given in Figure 2.6 and 2.7 which gives more detailed views of Figure 2.6.

30

Figure 2.6. Tooth contact analysis (Chen-Hsiang Lin and Zhang-Hua Fong, 2014)

Figure 2.7. Tooth contact analysis, detailed (Chen-Hsiang Lin and Zhang-Hua Fong, 2014)

3. MATERIAL AND METHOD

3.1. Material

Before starting to deal with a gear design problem, gear materials are selected to provide the optimum combination of properties, at the lowest possible cost consistent with satisfying other requirements. Some of the important physical properties of gears are wear resistance, toughness, static compression strength, shear strength, fatigue strength, and strength at elevated temperatures. In the design of straight bevel gear, the properties of pinion and gear materials must be in a good agreement for good design.

Because of widely varying requirements, gears are produced from a wide variety of materials. These materials are cast iron, steel, bronze, and phenolic resins.The combination of a steel pinion and cast iron gears represent a well-balanced design. Because cast iron has low cost, ease of casting, good machinability, good wear resistance.

In this study, three different materials for pinion, which are AISI 4130 oil quenched and tempered at 425°C, AISI 1030 Q&T 650°C and AISI 4140 OIL Q&T 207°C, have been selected. And ASTM Ductile iron quenched to bainite, Grade 120-90-02 has been selected for the gear. The properties of materials for both pinion and gear have been given in Table 3.1.

Table 3.1. Material Properties of Selected Pinion and Gear

Material Types for Pinion and Gear and Mechanical Properties	Pinion			Gear
	Type 1 : AISI 1030 Q&T @650 ℃	Type 2 : AISI 4130 oil Q&T @425 ℃	Type 3 : AISI 4140 oil Q&T @207 ℃	ASTM Ductile iron HT and OQ&T and ground, GR.120-90-02
Yield strength (Mpa)	441	1190	1640	621
Ultimate tensile strength (Mpa)	586	1280	1770	827
Brinell hardness number (HB)	207	380	510	300
Density (kg/m3)	7850	7850	7850	7850
Poisson's Ratio	0,3	0,3	0,3	0,3
Modulus of Elasticity (Gpa)	200	200	200	170

3.2. Method

Lots of design formulas are available in the machine elements for the design or finding "m" or "F". However, the results of using different approaches have not been compared so far. Thus the designer does not aware of the success or loss gained using each of the approaches. Hence, there is a need to compare the results of each of the most accepted design formula or design approach for straight bevel gear design. Hence, in this study comparison has been made between four types of design approaches results (F and m) and obtained using the design formula and design approaches to indicate loss or gain taken in each of the approaches as shown in Figure 3.1.

```
┌─────────────────────────────────────┐
│         BEVEL GEAR DESIGN            │
└─────────────────────────────────────┘
                  │
                  ▼
   ╭─────────────────────────────────────────╮
   │  Carry out the design process iteratively│
   │  considering the all input parameters    │
   │  and design variables                     │
   ╰─────────────────────────────────────────╯
                  │
                  ▼
        ╱─────────────────────╱
       ╱      DATA            ╱
      ╱   COLLECTION         ╱
     ╱─────────────────────╱
                  │
                  ▼
```

Repeat to obtain design results (module (m) and face width (F)) for all combinations of gear speed reduction ratios (from 1:1 to 8:1 with increment of 1:1) and power transmissions (from 0,5 to 1000kW)

Obtain GR_i NUMBERS

Generate GR_{AGMA} numbers to show the similarities between the standards and to draw a useful charts for comparison

Obtain CONVERSION FACTORS

Derive correlation equations for obtaining CFs to convert the design results (m and b) from AGMA to ISO, Mayuram and Juvinal

Figure 3.1. Design process for bevel gears

The designs of bevel gears using the expressions of Table 3.1 are performed based on selecting the module (m), and determining the face width. This iterative process starts with an initial estimation of a module and repeated until the face width reaches in an accepted range as given in Figure 3.1.

And now, when we look at this thesis work, design of an involute straight bevel gear has been performed based on both bending fatigue failure and surface contact failure theories according to the four most common design approaches and standards. These are;

1. ANSI/AGMA 2003-B97 standards (Shigley's Mechanical Engineering Design 9th Edition),
2. Fundamentals of Machine Component Design 5th Edition (Juvinall R.C., Marshek K.M., 2011),
3. Machine Design II, K.Gopinath & M.M.Mayuram 4th Edition   (Indian Institute of Technology Madras)
4. ISO Standards 10300- (Part 1-2-3), 2001

When we examine the ANSI/AGMA 2003-B97 standards and Shigley's approach, we saw all formulas and results are exactly same, because of that we choose the using ANSI/AGMA 2003-B97 standards.

And now, the computational load of the approaches considering the number of relevant pages and design variables with its sub variables based on bending fatigue and surface contact fatigue failure are presented in Table 3.2.

Table 3.2. Computational load of the approaches for bending and surface contact
         fatigue failure for bevel gear design

DESIGN APPROACHES	Number of relevant pages	Number of Design Variables+Sub Design Variables	
		Bending fatigue failure	Surface contact fatigue failure
ANSI/AGMA 2003-B97 standards	23	9+13	4+9
Fundamental of Machine Component Design 5th Edition	11	8+11	5+8
Machine Design II, K.Gopinath & M.M.Mayuram 4th Edition	33	8+9	13+8
ISO Standards 10300-(Part 1-2-3), 2001	43	3+13	

Two design parameters, module (m) and face width (F) calculations have been carried out with the four most common design approaches three mentioned above and ISO Standards. In each of the above approaches, bending fatigue failure and surface contact failure have depended on design variables that affect the material strength and failure stresses. But different kinds of design approaches have shown that the design variables have been tackled in some different ways in each of the approaches.

Two design parameters are module (m) and face width (F) are searched in the gear design, before the material is pre-selected. In this study, these two important parameters have been estimated based on "bending stress" and "surface contact stress". "Bending stress" occurs in the tooth root, and "surface contact stress" occurs on tooth surfaces while a pair of gear is in a mesh. After defining the pinion and gear materials, the module is estimated and calculations are carried out to determine the face width. A suitable module is selected and the face width calculations are performed using the $F = 0.3A_0$ or $F = 10/P$, whichever is smaller, face width is chosen. This procedure has been made for all types of design approaches.

After the calculations have been carried out for each of the design approaches, the reliability of results has been verified by using ANSYS Workbench 16.1. Design of an involute straight bevel gear has been achieved analytically using the most common design approaches mentioned above, then bevel gears have been modelled on SOLIDWORKS, 2018 with the aid of design results (module and face width). Finally, 3D models of bevel gears have been subjected to gear stresses on ANSYS Workbench 16.1, and numerically obtained results have been compared with analytical calculations.

```
┌─────────────────────────────────────┐
│      Obtain inputs from statements of │
│           design problems             │
└─────────────────────────────────────┘
                  │
                  ▼
┌─────────────────────────────────────┐
│   Selection of material for a pair of gear │
│   considerating the operating conditions │
└─────────────────────────────────────┘
                  │
                  ▼
┌─────────────────────────────────────┐
│       Selection of design approach;   │
│      ANSI/AGMA 2003-B97 standarts     │
│    Fundamentals of Machine Component  │
│                Design                 │
│     Machine Design II, K.Gopinath &   │
│      M.M.Mayuram 4th Edition          │
│             ISO Standards             │
└─────────────────────────────────────┘
                  │
                  ▼
┌─────────────────────────────────────┐
│      Carry out the design for the selected │
└─────────────────────────────────────┘
                  │
                  ▼
┌─────────────────────────────────────┐
│    Development of Microsoft Excel pages │
│              systematically           │
└─────────────────────────────────────┘
                  │
                  ▼
┌─────────────────────────────────────┐
│    Obtain results and compare m₁, F₁, │
│         m₁F₁/m₀F₀, etc.approach        │
└─────────────────────────────────────┘
                  │
                  ▼
┌─────────────────────────────────────┐
│    Valiadation of results by Finite Element │
│               Analysis                │
└─────────────────────────────────────┘
                  │
                  ▼
┌─────────────────────────────────────┐
│           Recommentations             │
└─────────────────────────────────────┘
```

Figure 3.2. General systematic approach used for obtaining the results for the comparison of gear design approaches

39
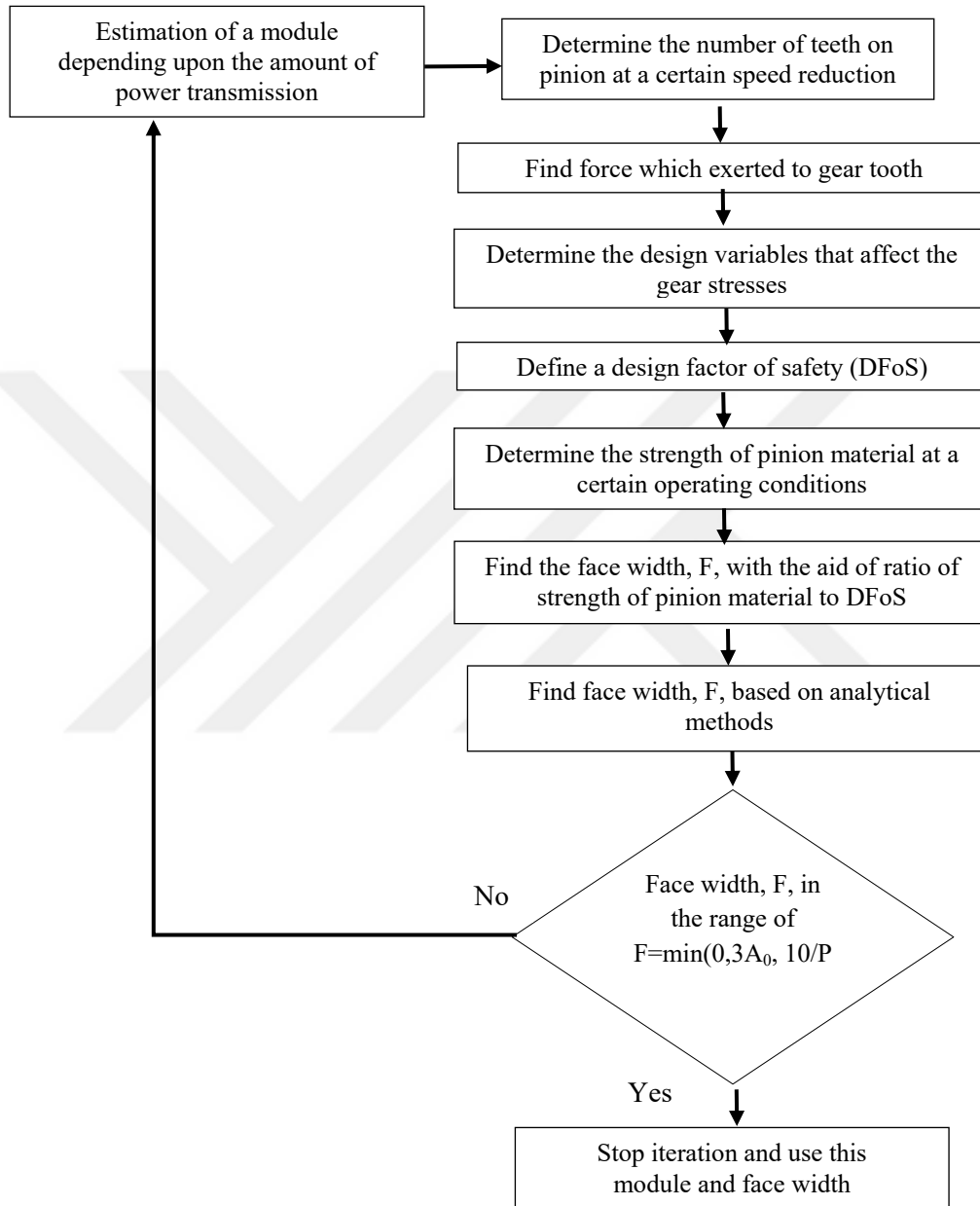
Figure 3.3. Flow chart for the design of an involute bevel gear

In each type of design approach, the operating conditions such as a number of cycles, gear speed ratio, gear transmission accuracy, the input speed of a power source, design factor of safety, reliability, etc. have been kept identical throughout the study. This provides a fair comparison of the results.

Different design approaches recommend different value of design factor. Design approaches given in ANSI/AGMA 2003-B97 standards and Machine Element textbooks recommend using design factor of safety equal or greater than 2,0 (ANSI/AGMA 2003-B97 standards / (Shigley's Mechanical Engineering Design 9th Ed.). In 5th Edition of Fundamentals of Machine Component Design, value of about 1,5 is recommended. In 4th Edition of Machine Design II, (K.Gopinath & M.M.Mayuram 4th Edition, 2009) suggests to select a design factor of safety by deciding between both manufacturer and user, however, 1th Edition of Fundamentals of Machine Design recommends a minimum safety factor of 2,0. Also ANSI/AGMA 2003-B97 Standard does not specify a certain value for a design factor of safety. Instead of defining a certain value for safety, ANSI/AGMA 2003-B97 Standard recommends using a factor by using some analysis of service experiences according to the type of industrial applications. Considering the above and providing the same conditions for the comparison of the results obtained from each approaches a safety factor of 2,1 has been taken. These are also tabulated in Table 3.3. Finding module and face width have been made by equating gear stress equation with strength of material by considering a certain design factor of safety. Design of involute bevel gear has been defined for a life cycle of 10^8.

Table 3.3.Recommended values for design factor of safety

Design Approaches	Recommended Design Factor of Safety
ANSI/AGMA 2003-B97 standards	~ 2,0
Fundamentals of Machine Component Design	1,3 ~ 1,5
Machine Design II, K.Gopinath & M.M.Mayuram 4th Edition	depends on both manufacturer and user decision

In Shigley's books (Shigley J.E., 1985, Budynas R.G. and Nisbett J.K., 2011), ANSI/AGMA 2003-B97 standards and Fundamentals of Machine Component Design 5th Edition (Juvinall R.C., Marshek K.M., 2011) gear quality has been classified as machined, shaved or ground. But, there is a difference between two books, in Fundamentals of Machine Component Design 5th Edition gear qualities described by symbols A to E in descending order. Symbol B meets number 6 for a gear quality level for ANSI/AGMA Standards. The gear transmission quality for AGMA and ISO there has been some of the notable differences between the AGMA and ISO standards. The AGMA system of numbering for different classes of quality is from Q3 through Q15 in order of increasing precision. In other words, the higher the number, the higher the quality of accuracy (smaller tolerance). The ISO system is just the opposite. It consists of 13 accuracy grades of which 0 is the smallest tolerance and grade 12 is the lowest accuracy or largest tolerance (FTM 1 by R. E. Smith, MITSUBISHI Machine Tools), see Table 3.4.

42

Table 3.4. Approximate equivalence of gear precision quality classes numbers for
International ISO, Germany DIN, Japan JIS, USA AGMA
Standards(Mott, R. L. 2004)

International ISO	Germany DIN	Japan JIS	U.S.A. AGMA
4	4	0	13
5	5	1	12
6	6	2	11
7	7	3	10
8	8	4	9
9	9	5	8

Since gears are compact, positive-engagement, power transmission elements that determine the speed, torque, and direction of rotation of driven machine elements, also used as good speed reducers all calculations have been done at a gear speed ratio of 1:1, 2:1, 3:1, 4:1, 5:1, 6:1, 7:1 and 8:1 respectively and when we compare module (m) and face width (F) results obtained at power transmission values starting from 0,5 kW to 1000 kW with the increments of 50 kW but for all other studies for the designs are carried out for the power transmissions values starting from 0,5 kW to 1000 kW with the increments of 20 kW for each of the speed ratio. All results have been plotted and tabulated on the same diagram for the ease of comparison. All of the calculations have been indicated on Microsoft Excel pages. The results obtained from excel pages were also verified for only 1:1 gear speed ratio and at 10 kW power transmissions by using a numerical finite element method, ANSYS Workbench 16.1.

In this study, only the design of pinion has been considered for the comparison of the results of the different approaches. This is because pinion is the smallest and weakest member in meshing couple and rotates more than the gear itself for the speed ratios greater than 1:1. This approach is also used very commonly for the design of gears. The work aims to determine the effect of speed ratio, because of that, gear speed ratios of 1:1, 2:1, 3:1, 4:1, 5:1, 6:1, 7:1 and 8:1 were considered and for these speed ratios the minimum number of teeth on pinion

has been selected to be the same and determined at the following section considering the interference-free involute profile.

3.2.1. Determination of Interference-Free Pinion Gear Teeth Number

Bevel gears, whose pitch surfaces are cones, are used to drive intersecting axes. Bevel gears are classified according to their type of the tooth forms into Straight Bevel Gear, Spiral Bevel Gear, Zerol Bevel Gear, Skew Bevel Gear etc. The meshing of bevel gears means the pitch cone of two gears contact and roll with each other. Let Z_1 and Z_2 be pinion and gear tooth numbers; shaft angle Σ; and reference cone angles $\delta 1$ and $\delta 2$;

$$\tan\delta_1 = \frac{\sin\Sigma}{\frac{Z_2}{Z_1}+\cos\Sigma}$$

$$\tan\delta_2 = \frac{\sin\Sigma}{\frac{Z_1}{Z_2}+\cos\Sigma}$$

(3.1)

Generally, a shaft angle $\Sigma=90°$ is most used. Table 3.5 shows the minimum number of the teeth to prevent undercut at the shaft angle $\Sigma=90°$.

Table 3.5. Minimum number of teeth on pinion for various speed ratios and combination of number of teeth

Speed ratio	Minimum number of teeth on Pinion ($\phi_n = 25°$)	Minimum number of teeth on Pinion ($\phi_n = 20°$)
1 : 1	13	16
2 : 1	13	14
3 : 1	13	13
4 : 1	13	13
5 : 1	13	13
6 : 1	13	13
7 : 1	13	13
8 : 1	13	13

Literature research has been shown that bevel gears are also used as a

speed reducer till 8:1 (Berg Manufacturing, Gear Reference Guide). To this respect, calculations have been carried out with a range from 1:1 to 8:1 speed reduction.

Now in the following sections, design of an involute bevel pinion gear has been described for each of the design approaches.

3.2.2. Bevel Gear Design Based on Bending Fatigue Failure

3.2.2.1. Design Approach Using ANSI/AGMA 2003-B97 standards

In this design approach, failure by bending will occur when the significant tooth stress equals or exceeds either the yield strength or the bending endurance strength. Allowable bending stress has been equalized to fully corrected endurance strength of gear tooth by considering the selected design factor of safety.

Bending stress;

$$\sigma_F = \frac{1000 Wt}{b} \frac{K_A K_V}{m_{et}} \frac{Y_X K_{H\beta}}{Y_B Y_J} \tag{3.2}$$

where

σ_F: Calculated bending stress number, N/mm^2

Wt: Tangential transmitted load, N

K_A: Overload factor

K_V: Dynamic factor

Y_X: Size factor for bending strength

$K_{H\beta}$: Load-Distribution factor

b : Face width, mm

m_{et}: Outer transverse module, mm

Y_B: Lengthwise curvature factor for bending strength

Y_J: Geometry factor for bending strength

In determining shaft and bearing loads for bevel-gear applications, the usual practice is to use the tangential or transmitted load that would occur if all the forces were concentrated at the midpoint of the tooth. While the actual resultant occurs somewhere between the midpoint and the large end of the tooth, there is only a small error in making this assumption. For the transmitted load, this gives;

$$W_t = \frac{60000H}{\pi d n} \tag{3.3}$$

H : Power, kW
d : Gear diameter, mm
n : speed, rev/min

For gears designed for long or infinite life at nominal rated torque, K_A is defined as the ratio between the maximum repetitive cyclic torque applied to the gear set and nominal rated torque (see Table 3.6).

Table 3.6. Overload Factors K_A (ANSI/AGMA 2003-B97 standards)

Character of Prime Mover	Character of Load on Driven Machine			
	Uniform	Light Shock	Medium Shock	Heavy Shock
Uniform	1.00	1.25	1.50	1.75 or higher
Light shock	1.10	1.35	1.60	1.85 or higher
Medium shock	1.25	1.50	1.75	2.00 or higher
Heavy shock	1.50	1.75	2.00	2.25 or higher

AGMA uses a transmission accuracy number Q_V to describe the precision with which tooth profiles are spaced along the pitch circle. Figure 3.4 shows graphically how pitch-line velocity and transmission accuracy numbers are related to the dynamic factor K_v.
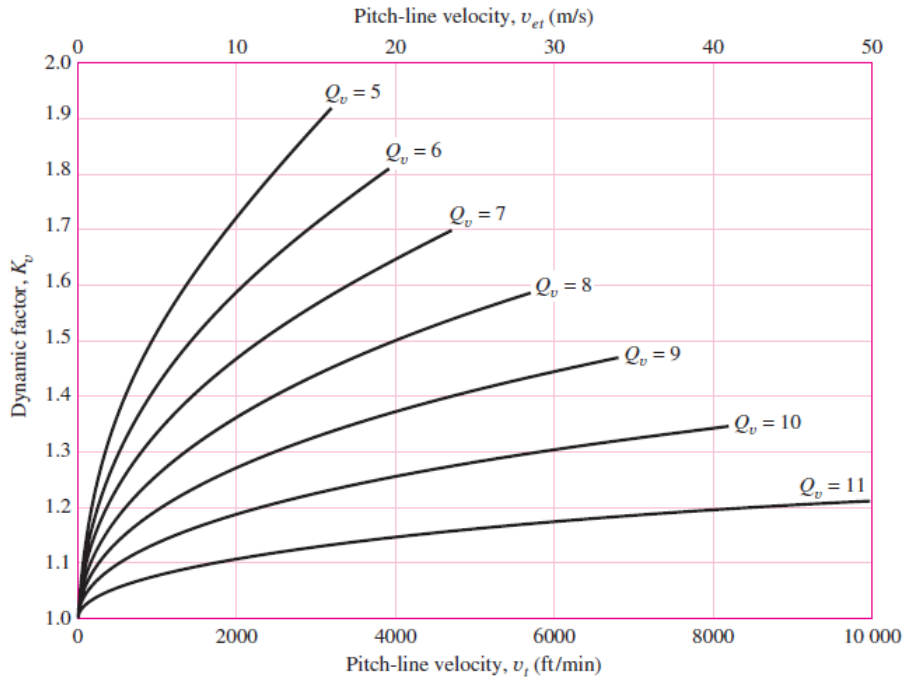
Figure 3.4. Dynamic factor Kv (ANSI/AGMA 2003-B97 standards)

The dynamic factor is given by equation 3.2 and is determined by the parameters A and B, which are given by equation 3.5 and 3.6 respectively, and the pitch line velocity at the operating pitch diameter, which can be seen in equation 3.4.

$$K_v = \left(\frac{A + \sqrt{200 V_{et}}}{A} \right) B \tag{3.4}$$

where

A = 50 + 56(1 − B)   (3.5)

B = 0.25(12 –Qv) 2/3   (3.6)

(v_{et}) is the pitch-line velocity at outside pitch diameter (m/s) :

v_{et}=5.236(10−5)$d_1 n_1$ (3.7.)

47

The size factor , Y_X, is accounts for statistics indicating that the stress levels at which fatigue damage occurs decrease with an increase of component size, as a consequence of the influence on subsurface defects combined with small stress gradients, and of the influence of size on material quality.

$$Y_X = \begin{cases} 0,5 & m_{et} < 16\,mm \\ 0,4867 + 0,008339 m_{et} & 1,6 \leq m_{et} \leq 50mm \end{cases} \qquad (3.8)$$

$K_{H\beta}$ is defined as the load distribution factor and equals to the ratio between the maximum load per unit face width and the mean load per unit face width. $K_{H\beta}$ may be evaluated by observed contact patterns on various defined load levels.

$$K_{H\beta} = K_{mb} + 5,6(10^{-6})b^2 \qquad (3.9)$$

where

$$K_{mb} = \begin{cases} 1.00 & \text{both members straddle mounted} \\ 1.10 & \text{one member straddle mounted} \\ 1.25 & \text{neither member straddle mounted} \end{cases}$$

Figure 3.5 shows the geometry factor J for straight-bevel gears with a 20° pressure angle and 90° shaft angle.
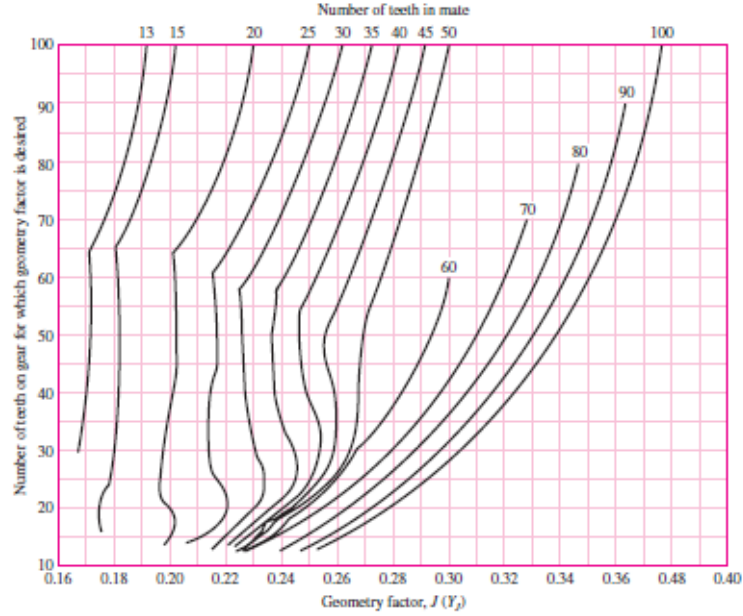
Figure 3.5. Geometry factor J for straight-bevel gears with a 20° pressure
           angle and 90° shaft angle (ANSI/AGMA 2003-B97 standards)

The relation of calculated bending stress number to allowable bending stress
number is;

$$\sigma_{FP} = \frac{\sigma_{Flim} Y_{NT}}{S_F K_\theta Y_Z}$$ (3.10)

where

σ_{Flim} : Bending stress number (allowable) (N/mm²)

Y_{NT} :   Stress cycle factor for bending strength

S_F :   Bending safety factor

K_θ :   Temperature factor

Y_Z :   Reliability factor for bending strength

The allowable stress numbers, σ_{FP}, for gear materials vary with items such as material composition, cleanliness, residual stress, microstructure, quality, heat treatment, and processing practices (ANSI/AGMA 2101-D04, 2004).

Stress-Cycle Factor for Bending Strength (Y_{NT});
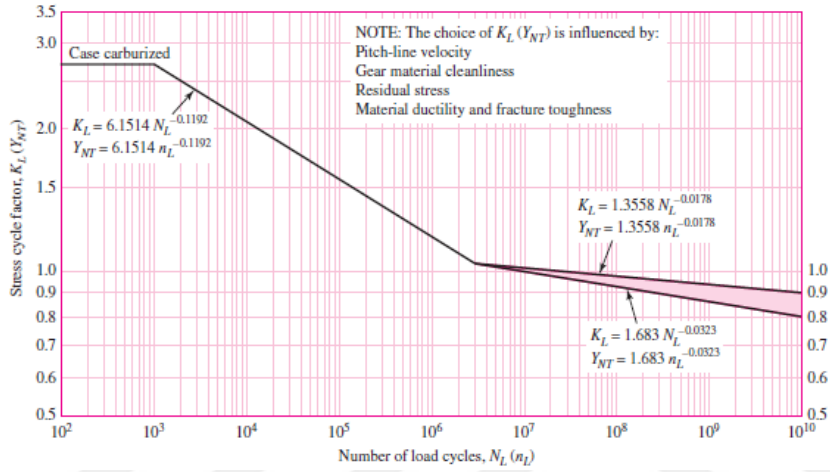
Figure 3.6. Stress cycle factor for bending strength K_L (Y_{NT}) for carburized case-hardened steel bevel gears (ANSI/AGMA 2003-B97.)

$$Y_{NT} = \begin{Bmatrix} 2.7 & 10^2 \leq nL < 10^3 \\ 6.1514 n_L^{-0.1182} & 10^3 \leq nL < 3(10^6) \\ 1.6831 n_L^{-0.0323} & 3(10^6) \leq nL \leq 10^{10} \\ 1.3558 n_L^{-0.0323} & 3(10^6 \leq nL \leq 10^{10} \end{Bmatrix} \tag{3.11}$$

Temperature Factor (K_θ);

$$K_\theta - \begin{Bmatrix} 1 & 0°C \leq \theta \leq 120°C \\ (273 + \theta)/393 & \theta > 120°C \end{Bmatrix} \tag{3.12}$$

Safety Factors S_F;

The factors of safety S_H and S_F as defined in 2003-B97 are adjustments to strength, not load, and consequently cannot be used as is to assess (by comparison) whether the threat is from wear fatigue or bending fatigue. Since W_t is the same for the pinion and gear, the comparison of $\sqrt{S_H}$ to S_F allows direct comparison.

Reliability Factors Y_Z;

Requirements of Application	Reliability Factors for Steel*	
	C_R (Z_Z)	K_R (Y_Z)[†]
Fewer than one failure in 10 000	1.22	1.50
Fewer than one failure in 1000	1.12	1.25
Fewer than one failure in 100	1.00	1.00
Fewer than one failure in 10	0.92	0.85[‡]
Fewer than one failure in 2	0.84	0.70[§]

Figure 3.7. Reliability Factors (ANSI/AGMA 2003-B97)

$$Y_Z = \begin{cases} 0.5 - 0.25 \log(1 - R) & 0.99 \leq R \leq 0.999 \\ 0.7 - 0.15 \log(1 - R) & 0.9 \leq R \leq 0.99 \end{cases} \tag{3.13}$$

3.2.2.2. Design Approach Using Fundamentals of Machine Component Design 5th Edition

The design approach is given by Juvinall and Marshek slightly differs from the previous ones for bending fatigue failure. The design calculations of bevel gear-tooth-bending and surface fatigue strengths are even more complex than for spur and helical gears. The treatment given here is very brief. This approach mostly recommends that in the absence of more specific information, the factors affecting gear tooth bending stress;

The equation for bevel gear-bending stress is the same as for spur gears:

51

$$\sigma = \frac{F_t P}{b J} K_v K_o K_m \qquad\qquad (3.14)$$

where

σ : Bending fatigue stress,

b : Face width, mm

F_t : Tangential load

P : Diametral pitch at the large end of the tooth

J: Bevel gear geometry factor, determined from Figure 3.7 (straight bevel)

K_v : Velocity or dynamic factor that indicating the severity of impact as successive pairs of teeth engage. This is a function of pitch line velocity and manufacturing accuracy (When better information is not available, use a value between unity and curve C of Figure 15.24, depending on the degree of manufacturing precision)

K_o : Overload factor that reflecting the degree of non-uniformity of driving and load torques. In the absence of better information, the values in Table 3.7 have long been used as a basis for rough estimates.

K_m : Mounting factor, depending on whether gears are straddle-mounted (between two bearings) or overhung (outboard of both bearings), and on the degree of mounting rigidity (see Table 3.6)
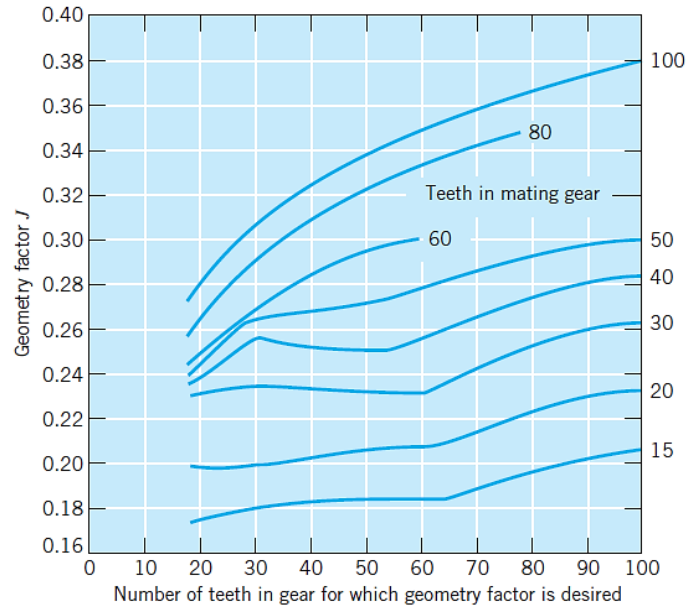
Figure 3.8. Geometry factors J for straight bevel gears. Pressure angle = 20°, shaft angle = 90° (From AGMA Information Sheet 226.01; also see ANSI/AGMA 2003-A86.)

Table 3.7. Mounting Correction Factor K_m for Bevel Gears (Juvinall R.C., Marshek K.M., 2011)

	Driven Machinery		
Source of Power	Uniform	Moderate Shock	Heavy Shock
Uniform	1.00	1.25	1.75
Light shock	1.25	1.50	2.00
Medium shock	1.50	1.75	2.25

Table 3.8. Overload Correction Factor Ko (Juvinall R.C., Marshek K.M., 2011)

	Driven Machinery		
Source of Power	Uniform	Moderate Shock	Heavy Shock
Uniform	1.00	1.25	1.75
Light shock	1.25	1.50	2.00
Medium shock	1.50	1.75	2.25
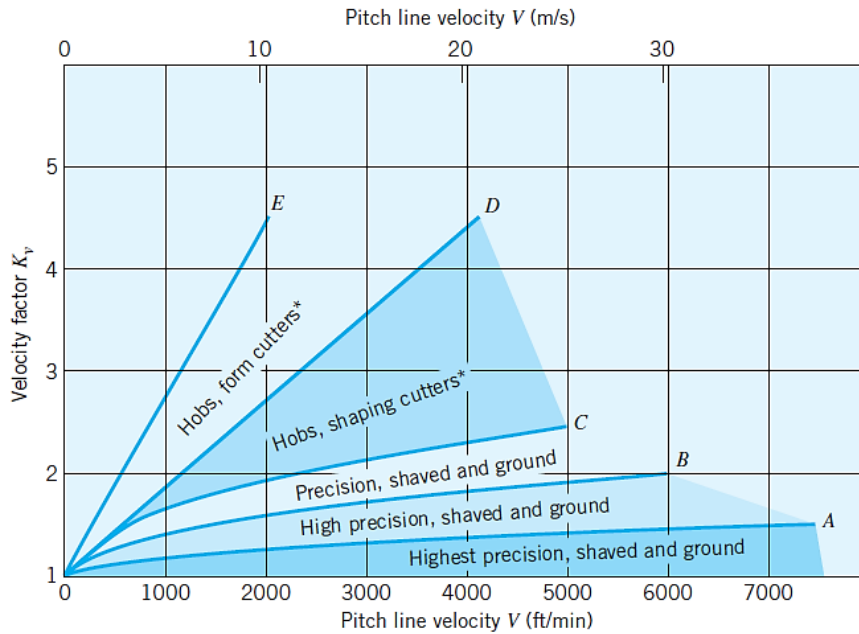
Figure 3.9. Velocity factor K_v (Note: This figure, in a very rough way, is intended to account for the effects of tooth spacing and profile errors, tooth stiffness and the velocity, inertia, and stiffness of the rotating parts.)

The effective fatigue stress from below equation must be compared with the corresponding fatigue strength. For infinite life, the appropriate endurance limit is estimated from the following equation. Five of factors are involved in the estimate for this endurance limit;

$$S_n = S_n' C_L C_G C_S C_T C_R \tag{3.15}$$

Which, for these steel members are usually;

$$S_n = (0.5 S_u) C_L C_G C_S C_T C_R \tag{3.16}$$

where

S_n' : Standard R. R. Moore endurance limit

For steel $S_n' = (0,5)$. S_{ut} and

for other ductile materials $S_n' = (0,7)$. S_{ut}

C_L : Load factor = 1,0 for bending loads

C_G : Gradient factor = 1,0 for P>5 (m<0,2), and 0,85 for P≤5 (m≥0,2)

54

C_S: Surface factor, Figure 3.8. Be sure that this pertains to the surface in the fillet, where a fatigue crack would likely start. (In the absence of specific information, assume this to be equivalent to a machined surface)
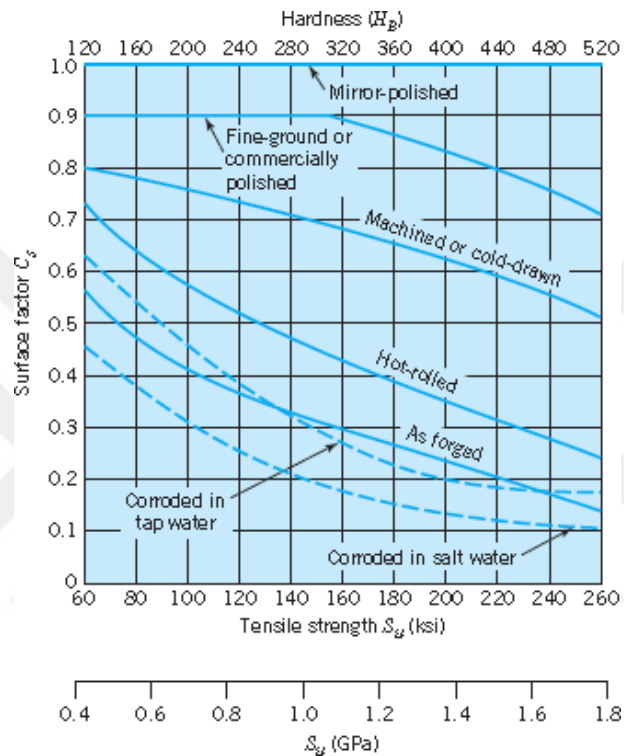
Figure 3.10. Surface factor C_S (Juvinall R.C., Marshek K.M., 2011)

C_T : Temperature factor, see in following table;

Table 3.9. Temperature factor, Juvinall R.C., Marshek K.M., 2011

C_T	(temperature factor)	Values are only for steel		
	T ≤ 840 °F	1.0	1.0	1.0
	840 °F < T ≤ 1020 °F		1 - (0.0032T − 2.688)	

C_R : Reliability factor, see in following Table 3.9;

Table 3.10. Reliability factor C_R, Juvinall R.C., Marshek K.M., 2011

C_R	(reliability factor):[d]			
	50% reliability	1.000	"	"
	90% "	0.897	"	"
	95% "	0.868	"	"
	99% "	0.814	"	"
	99.9% "	0.753	"	"

The temperature factor, C_T, accounts for the fact that the strength of a material decreases with increased temperature, and the reliability factor, CR, acknowledges that a more reliable (above 50%) estimate of endurance limit requires using a lower value of endurance limit (Juvinall R.C., Marshek K.M., 2011).

This approach recommends that the design factor of safety for bending fatigue can be taken as the ratio of fatigue strength to fatigue stress. The design factor of safety does not be as large as it would otherwise be necessary. Typically, a safety factor of 1,5 might be selected, together with a reliability factor corresponding to 99,9 percent reliability (Juvinall R.C., Marshek K.M., 2011). But in this study, it is aimed to use a design factor as 2,1 for all the design approaches in order to compare the approaches at the same conditions.

3.2.2.3. Design Approach Using Machine Design II, K.Gopinath & M.M.Mayuram 4th Edition

When we look at Machine Design II, K.Gopinath & M.M.Mayuram 4th Edition book approaches the maximum tensile stress at the tooth root may not exceed the permissible bending stress for the material. This is the basis for rating the bending strength of gear teeth. The actual tooth root stress σ_b and the permissible tooth root bending stress σ_p shall be calculated separately for pinion and wheel; σ_b shall be less than σ_p. The equation for bevel gear bending stress is the same as for spur gears as shown below:

$$\sigma_b = \frac{F_t}{mbJ} K_v K_o K_m \qquad (3.17)$$

where,

F_t : Tangential load, N

m :   module at the large end of the tooth, mm

b :   Face width, mm

J :   Geometry form factor based on virtual number of teeth from Figure 3.10 and 3.11.

K_v : Velocity factor, from Figure.3.12.

K_o : Overload factor, Table 3.10.

K_m : Mounting factor, depending on whether gears are straddle mounted (between two bearings) or overhung (outboard of both bearings), and on the degree of mounting rigidity as shown in Table 3.11.
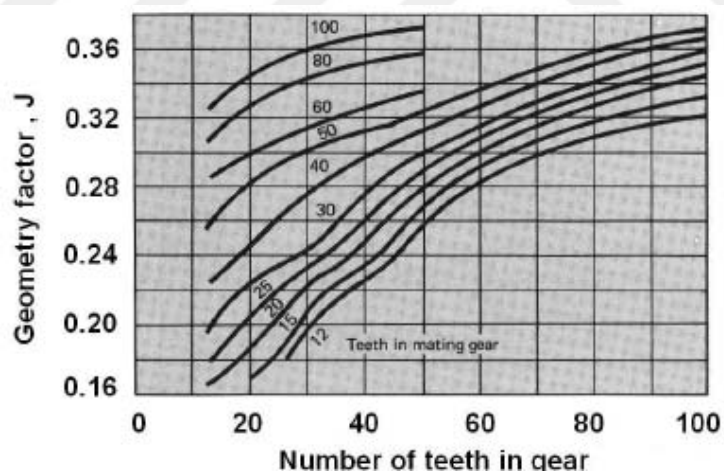
Figure 3.11. Number of teeth in gear for which geometry factor J is desired,
            pressure angle 20°, and shaft angle 90°, (K.Gopinath &
            M.M.Mayuram, IIT-Madras, 2009)
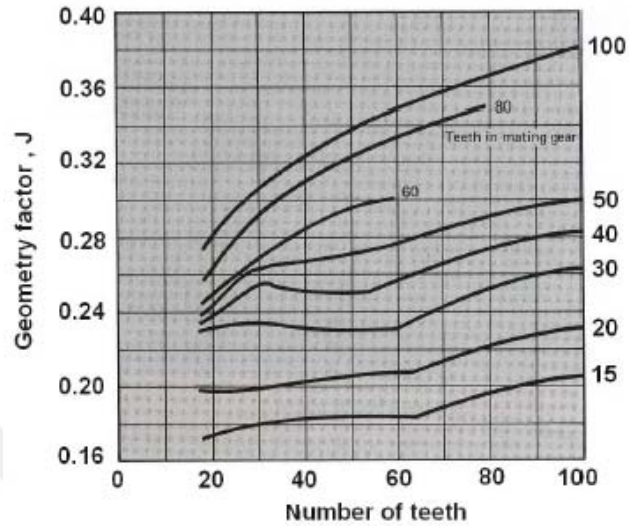
Figure 3.12. Number of teeth in gear for which geometry factor J is desired,
            pressure angle 20°, spiral angle 35° and shaft angle 90° (From AGMA
            Information Sheet 226.01; also see ANSI/AGMA 2003-A86)
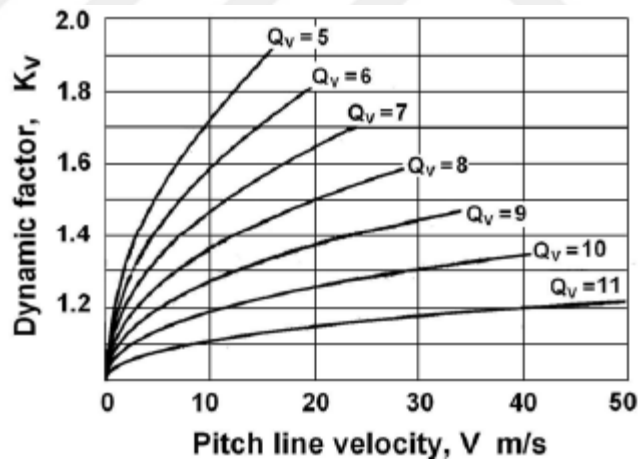
Figure 3.13. Velocity factor K_v (Note: This figure, in a very rough way, is intended
            to account for the effects of tooth spacing and profile errors, tooth
            stiffness, and the velocity, inertia, and stiffness of the rotating parts.)

K_o: Overload factor K_O, from Table 3.11 (K.Gopinath & M.M.Mayuram, IIT-Madras, 2009)

58

Table 3.11. Overload factor K_O (K.Gopinath & M.M.Mayuram, IIT-Madras, 2009)

	Driven Machinery		
Source of power	Uniform	Moderate Shock	Heavy Shock
Uniform	1.00	1.25	1.75
Light shock	1.25	1.50	2.00
Medium shock	1.50	1.75	2.25

The overload factor K_O, makes allowance for the externally applied loads which are more than nominal tangential load, Wt. Overload factors can only be established after considerable field experience is gained in a particular application. For an overload factor of unity, this rating method includes the capacity to sustain a limited number of up to 200% momentary overload cycles (typically less than four starts 8 hours, with a peak not exceeding one second duration).

Examples of operating characteristics of driving machines:

➢ Uniform – Electric motor, steam turbine, gas turbine.
➢ Light shock – Multi-cylinder internal combustion engine with many cylinders.
➢ Medium shock – Multi-cylinder internal combustion engine with few cylinders.
➢ Heavy shock – Single-cylinder internal combustion engine.

Table 3.12. Mounting Factor K_m for Bevel Gears, (K.Gopinath & M.M.Mayuram, IIT-Madras, 2009)

Mounting Type		Mounting Rigidity Maximum to Questionable
Both gears are straddle-mounted		1.0 to 1.25
One gear straddle-mounted; the other overhung		1.1 to 1.4
Both gear overhung		1.25 to 1.5
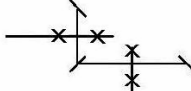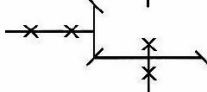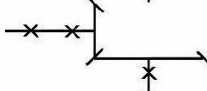
$$F_t = \frac{W}{V_{av}} \tag{3.18}$$

W = Watt

$V_{av} = \pi dn/60000$

$$\sigma_b = \frac{F_t}{mbJ}K_v K_o K_m = \frac{W}{mbJV_{av}}K_v K_o K_m = \frac{60000W}{mbJ\pi dn}K_v K_o K_m = \frac{60000W}{mbJ\pi dn}K_v K_o K_m \tag{3.19.}$$

We will first determine the permissible stresses for the pinion and gear materials.

$$\sigma_e = \sigma_e' k_L k_v k_o k_T k_f k_m \tag{3.20}$$

where

σ_e' endurance limit of rotating-beam specimen

k_L : Load factor, = 1.0 for bending loads

k_v : Size factor, = 1.0 for m < 5 mm and

  = 0.85 for m > 5 mm

k_s : Surface factor, taken from Figure 3.13 based on the ultimate strength of the material and for cut, shaved, and ground gears.

k_r : Reliability factor given in Table 3.13.

k_T : Temperature factor, $= 1$ for T$\leq 120\,^{o}$C and more than $120\,^{o}$C, $k_T < 1$ to be taken from AGMA standards
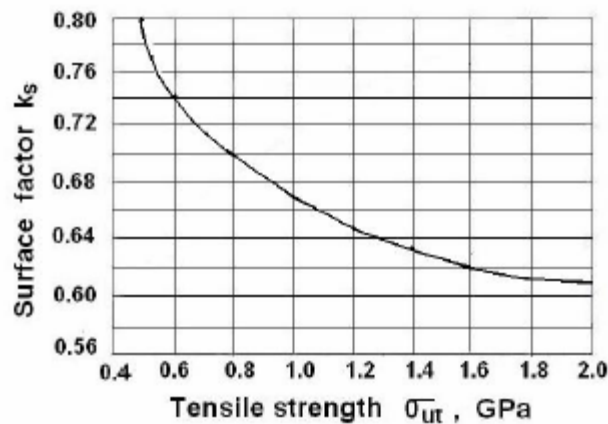
Figure 3.14. Surface factor, K_s (K.Gopinath & M.M.Mayuram, IIT-Madras, 2009)

Table 3.13. Reliability Correction Factor k_r.

Reliability (%)	50	90	99	99,9	99,99	99,999
Factor k_r	1	0,897	0,814	0,753	0,702	0,659

k_f : Fatigue stress concentration factor. Since this factor is included in J factor its value is 1.

k_m : Factor for miscellaneous effects. For idler gears subjected to two way bending, k_m : 1. For other gears subjected to one way bending, the value is taken from Figure 3.14. Use $k_m = 1.33$ for σ_{ut} less than 1.4 GP.
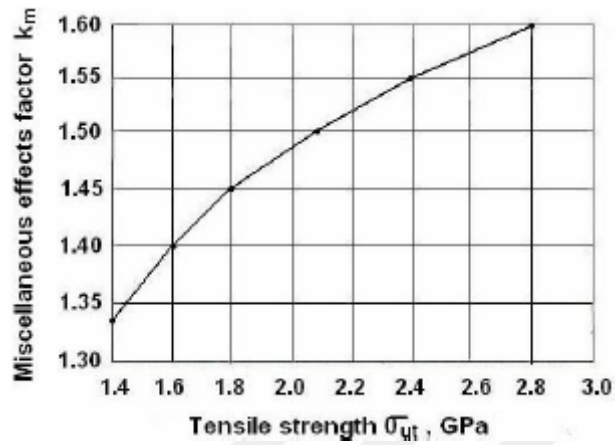
Figure 3.15. Miscellaneous effects factor Km, (K.Gopinath & M.M.Mayuram, IIT-Madras, 2009)

Permissible bending stress is given by

$$[\sigma_b] = \frac{\sigma_b}{s}$$

(3.21)

Hence the design equation from bending consideration is,

$$\sigma_b \leq [\sigma_b]$$

3.2.2.4. Design Approach Using ISO Standards 10300 - Part 3

ISO Standard provides gear design standards with standard number of 10300. In IS0 10300-3 part specifies the fundamental formulae for use in the tooth-bending stress calculation of straight, helical, zerol and spiral-bevel gears with a minimum rim thickness under the root ≥3,5 mm. All load influences on tooth stress are included, in so far as they are the result of load transmitted by the gearing and able to be evaluated quantitatively. (Stresses such as those caused by the shrink-fitting of gear rims, which are superposed on stresses due to tooth loading, are to be taken into consideration in the calculation of the tooth root stress CTF or the permissible tooth root stress OFP.)

The formulae in this part of IS0 10300 are valid for bevel gears with teeth with a transverse contact ratio of while the results are valid within the range of the applied factors given in IS0 10300-1 and IS0 6336-3.,

ISO Standard 10300-3 is related to calculation of tooth bending strength, but some modifying factors to determine the bending stress are included in ISO Standards 10300 - Part 1, -Part 2, and -Part 3.

These ISO Standards give two methods to calculate these factors included in parts. These methods are mentioned as B1 and B2 in decreasing order of accuracy.

Tooth root stress σF is the maximum tensile stress at the surface in the root.

The tooth root stress is determined separately for pinion and gear;

$$\sigma_F = \sigma_{FO} K_A K_v K_{F\beta} K_{F\alpha} \leq \sigma_{FP} \tag{3.22}$$

where

σ_{FO}: Nominal tooth root stress, which is the maximum local principal stress produced at the tooth root

σ_F: Permissible bending stress

K_A: External force and application factor, is given by Table 3.14

K_v: Dynamic factor

$K_{F\beta}$: Face load factor

$K_{F\alpha}$: Transverse load factor

σ_{FP}: The permissible tooth root stress is given by equation 3.30;

Table 3.14. Application factor K_A values

Working characteristics of the driving machine	Working characteristics of the driven machine			
	Uniform	Light shocks	Medium shocks	Heavy shocks
Uniform	1,00	1,25	1,50	1,75 or higher
Light shocks	1,10	1,35	1,60	1,85 or higher
Medium shocks	1,25	1,50	1,75	2,00 or higher
Heavy shocks	1,50	1,75	2,00	2,25 or higher

The dynamic factor K_V is given by equation 3.23 and is determined by the parameters A and B, which are given by equation 3.24 and 3.25 respectively, and the pitch line velocity at the operating pitch diameter, which can be seen in equation 3.4.

$$K_V = \left[\frac{A}{A+\sqrt{200 V_{et}}}\right]^{-B} \qquad (3.23)$$

For $6 \leq C \leq 9$,

A= 50+56(1.0-B)   (3.24)

$B = 0.25(C-5)^{0.667}$ (3.25)

C: the transmission accuracy level number

$$V_{et} = v_{mt}\frac{d_{et,a}}{d_{m,a}}$$

$$V_{etmax} = \frac{[A+(14-C)]^2}{200}$$

$K_{F\beta}$ is defined as the ratio between the maximum tooth root stress and the mean tooth root stress over the face width and is given by equation 3.26;

$K_{H\beta}$ is defined as the ratio between the maximum load per unit face width and the mean load per unit face width, and is given by Table 3.15;

$$K_{F\beta} = K_{H\beta}/K_{F0} \tag{3.26}$$

We assume $K_{F0} = 1$

Table 3.15. Mounting factor $K_{H\beta-be}$

Verification of contact pattern	Mounting conditions of pinion and gear		
Contact pattern is checked:	Neither member cantilever mounted	One member cantilever mounted	Both members cantilever mounted
for each gear set in its housing under full load	1,00	1,00	1,00
for each gear set under light test load	1,05	1,10	1,25
for a sample gear set and estimated for full load	1,20	1,32	1,50
NOTE Based on optimum tooth contact pattern under maximum operating load as evidenced by results of a deflection test on the gears in their mountings.			

In order to compensate for an effective face width under full load b_e less than 85% of the face width b, the face load factor are to be corrected. Because of that, the decisive load distribution factor $K_{H\beta-c}$ is given by equation 3.27;

$K_{H\beta-c}$: Face load factor

$$K_{H\beta-c} = 1,5K_{H\beta-be} \quad \text{for } b_e \geq 0,85b \tag{3.27}$$

$$K_{H\beta-c} = 1,5K_{H\beta-be} \cdot \frac{0,85}{b_e/b} \qquad \text{for } b_e < 0,85b$$

And the table $K_{H\alpha-c}$ and $K_{F\alpha-c}$ shall be taken from Table 3.16;

65

Table 3.16. Transverse load distribution factors, $K_{H\alpha-C}$ and $K_{F\alpha-C}$

Specific loading $K_A F_{mt}/b_e$			6 and better	7	8	9	10	11	12	< 100 N/mm all accuracy grades
Gear accuracy grade according to ISO 1328-1 (using d_m and m_{mn}) (see 5.3.2)							≥ 100 N/mm			
Surface hardened	Straight bevel gears	$K_{H\alpha}$	1,0		1,1	1,2	$1/Z_{LS}^2$ or 1,2, whichever is greater			
		$K_{F\alpha}$					$1/Y_\varepsilon$ or 1,2, whichever is greater			
	Helical and spiral bevel gears	$K_{H\alpha}$	1,0	1,1	1,2	1,4	ε_{van} or 1,4, whichever is greater			
		$K_{F\alpha}$								
Not surface hardened	Straight bevel gears	$K_{H\alpha}$	1,0			1,1	1,2	$1/Z_{LS}^2$ or 1,2 whichever is greater		
		$K_{F\alpha}$						$1/Y_\varepsilon$ or 1,2 whichever is greater		
	Helical and spiral bevel gears	$K_{H\alpha}$	1,0	1,1	1,2	1,4		ε_{van} or 1,4 whichever is greater		
		$K_{F\alpha}$								
NOTE	For Z_{LS} see ISO 10300-2, for Y_ε see ISO 10300-3.									

$$\sigma_{F0} = \frac{F_{mt}}{bm_{mn}} Y_{Fa} Y_{Sa} Y_\varepsilon Y_K Y_{LS} \tag{3.28}$$

σ_{F0} is the local tooth root stress defined as the maximum tensile stress arising at the tooth root due to the nominal torque when a perfect gear is loaded is given by equation 3.28,

F_{mt} is the nominal tangential force at the reference cone at mid-face width, Y_{Fa} is the tooth form factor, which accounts for the influence of the tooth form on the nominal bending stress for load application at the tooth tip,

Y_{Sa} is the stress correction factor which accounts for the conversion of the nominal bending stress for load application at tooth tip to the corresponding local tooth root stress. Because of that Y_{Sa} accounts for the stress-increasing effect of the notch, as well as for the fact that the stress condition in the critical root section is complex, but not for the influence of the bending moment arm,

Yε is the contact-ratio factor, which accounts for the conversion of the local stress determined for the load application at the tooth tip to the determinant position is given by equation 3.29,

Y_K is the bevel-gear factor, which accounts for smaller values for I_b compared to total face width b and the inclined lines of contact,

Y_{LS} is the load sharing factor, which accounts for load distribution between two or more pairs of teeth.

$$Y_\varepsilon = 0{,}25 + \frac{0{,}75}{\varepsilon_{v\alpha}} \geq 0{,}625 \qquad (\varepsilon_{v\beta} = 0) \qquad (3.29)$$

$$Y_\varepsilon = 0{,}25 + \frac{0{,}75}{\varepsilon_{v\alpha}} \geq 0{,}625 \qquad (\varepsilon_{v\beta} = 0)$$

$$Y_\varepsilon = 0{,}625 \qquad (\varepsilon_{v\beta} > 1)$$

$$Y_K = (\frac{1}{2} + \frac{1}{2}\frac{l^t{}_{bm}}{b})^2 \frac{b}{l^t{}_{bm}}$$

$$Y_{LS} = Z_{LS}{}^2$$

$$\sigma_{FP} = \frac{\sigma_{F\,lim}Y_{ST}Y_{NT}}{S_{F\,min}}Y_{\delta\,relT}Y_{R\,relT}Y_N \qquad (3.30)$$

$$\sigma_{F\,lim} = A * x + B \qquad (3.31)$$

This method is generally sufficiently exact for industrial gears. In the case of gears with $q_s \geq 1{,}5$ it is set as:

$$Y_{\delta\,relT} = 1{,}0$$

For $q_s \geq 2{,}5$ the calculation is on the safe side.

The reduction of the allowable tooth root stress expected in case of $q_s < 13$ is accounted for by:

$$Y_{\delta\,relT} = 0{,}95$$

The relative surface condition factor, Y_{RrelT}, determined by tests with test specimens and is given by equation 3.32, 3.33 and 3.34.

Range $R_z < 1$ µm:

For through-hardened and case-hardened steels:

$Y_{RrelT} = 1,12$

For soft steels:

$Y_{RrelT} = 1,07$

For grey cast iron, nitrided, and nitro-carburized steels:

$Y_{RrelT} = 1,025$

Range 1 µm $< R_z < 40$ µm:

For through-hardened and case-hardened steels:

$$Y_{RrelT} = \frac{Y_R}{Y_{RT}} = 1,674 - 0,529(R_z + 1)^{1/10} \tag{3.32}$$

For soft steels:

$$Y_{RrelT} = \frac{Y_R}{Y_{RT}} = 5,306 - 4,203(R_z + 1)^{1/100} \tag{3.33}$$

For grey cast iron, nitrided, and nitro-carburized steels:

$$Y_{RrelT} = \frac{Y_R}{Y_{RT}} = 4,299 - 3,259(R_z + 1)^{1/200} \tag{3.34}$$

The size factor, Y_X,

For structural and through-hardened steels, spheroidal cast iron, perlitic malleable cast iron and is given by eq.3.35, 3.36 and 3.37;

$$Y_X = 1,03 - 0,006 m_{mn} \tag{3.35}$$

with the restriction $0,85 \leq Y_X \leq 1,0$

For case, flame, induction-hardened steels, nitrided or nitro-carburized steels

$$Y_X = 1,05 - 0,01 m_{mn} \tag{3.36}$$

With the restriction $0,80 \leq Y_X \leq 1,0$

For grey cast iron

$$Y_X = 1,075 - 0,015 m_{mn} \tag{3.37}$$

with the restriction $0,70 \leq Y_X \leq 1,0$

3.2.3. Bevel Gear Design Based on Surface Contact Failure

3.2.3.1. Design Approach Using ANSI/AGMA 2003-B97 standards

Surface fatigue is the failure of a material as a result of repeated surface or sub-surface stresses beyond the endurance limit of the material. Different modes of failure may occur on a gear surface, and sometimes may different failure modes occur in combination which might make it hard to determine which type of failure that originally caused the damage (Dudley, 1994). For example; Pitting is a surface fatigue failure due to many repetitions of high contact stresses. Failure of the surfaces of gear teeth generally called as wear. Wear as the process when layers of metal are removed from the surfaces that are in contact. Calculation of face width relies on the same procedure as in bending fatigue failure, surface compressive stress should be equal or less than the surface fatigue stress (Shigley J.E., 1985).

In this approach, a surface failure occurs when the significant contact stress equals or exceeds the surface endurance strength.

$$\sigma_H = Z_E \sqrt{\left(\frac{1000W^t}{bdZ_1}K_A K_v K_{H\beta} Z_x Z_{xc}\right)} \tag{3.38}$$

where

Z_E: Elastic coefficient for pitting resistance

$$Z_E = \sqrt{\frac{1}{\pi\left[\frac{(1-v_1^2)}{E_1}+(1-v_2^2)/E_2\right]}} \tag{3.39}$$

Z_E = elastic coefficient, $190 \sqrt{N/mm^2}$ for steel

W^t: Tangential component of load, in N

Z_1 : Number of pinion teeth

b : Net face width, in mm

K_A : Overload Factor Table 3.14

Table 3.17. Overload Factors, K_A Source: ANSI/AGMA 2003-B97.

Character of Prime Mover	Character of Load on Driven Machine			
	Uniform	Light Shock	Medium Shock	Heavy Shock
Uniform	1.00	1.25	1.50	1.75 or higher
Light shock	1.10	1.35	1.60	1.85 or higher
Medium shock	1.25	1.50	1.75	2.00 or higher
Heavy shock	1.50	1.75	2.00	2.25 or higher

Kv: Dynamic Factor
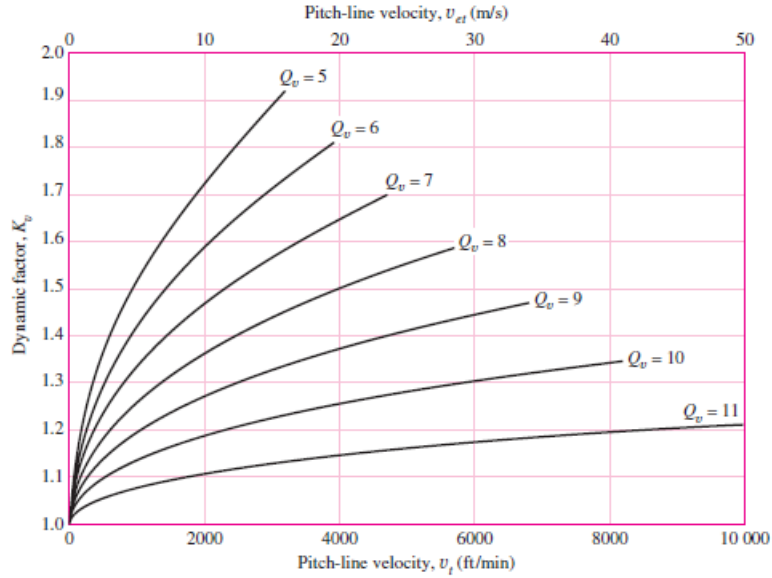
Figure 3.16. Dynamic factor Kv (Source: ANSI/AGMA 2003-B97.)

$K_{H\beta}$: Load-Distribution Factor

$$K_{H\beta} = K_{mb} + 5.6(10^{-6})b^2 \tag{3.40}$$

where

$$K_{mb} = \begin{cases} 1.00 \ both \ members \ straddle - mounted \\ 1.10 \ one \ member \ straddle - \ mounted \\ 1.25 \ neither \ member \ straddle - mounted \end{cases}$$

Z_x : Size Factor for Pitting Resistance

$$Z_X = \begin{cases} 0.5 & b < 12.7 \ mm \\ 0.00492b + 0.4375 & 12.7 \leq b \leq 114.2 \ mm \\ 1 & b > 114.3 \ mm \end{cases} \tag{3.41}$$

Z_{xc} : Crowning Factor for Pitting

The teeth of most bevel gears are crowned in the lengthwise direction during manufacture to accommodate the deflection of the mountings.

71

$$Z_{xc} = \begin{Bmatrix} 1.5 & \text{properly crowned teeth} \\ 2 & \text{or larger uncrowned teeth} \end{Bmatrix}$$

Permissible Contact Stress Number (Strength) equation 3.42;

$$\sigma_{HP} = \frac{\sigma_{Hlim} Z_{NT} Z_W}{S_H K_\theta Z_Z} \tag{3.42}$$

According to ANSI/AGMA 2003-B97 standards, the equation above is used when the allowable contact stress number is given for a specific load case and a certain number of cycles and with a specific percentage of reliability. The other parameters are then used for modifying the allowable contact stress such that it will represent other scenarios, e.g. using the stress cycle factor in order to calculate stresses for another number of lives such that a stress rating curve can be established. The factors can be derived by using the ANSI/AGMA 2101-D04 standard (AGMA, 2004).

S_H: Safety Factors

The factors of safety S_H as defined in 2003-B97 are adjustments to strength, not load, and consequently cannot be used as is to assess (by comparison) whether the threat is from wear fatigue or bending fatigue. Since W_t is the same for the pinion and gear, the comparison of $\sqrt{SH}$ to allows direct comparison (Shigley J.E., 1985).

Z_{NT} : Stress-Cycle Factor for Pitting Resistance

$$Z_{NT} = \begin{Bmatrix} 2 & 10^3 \leq n_L < 10^4 \\ 3.4822 n_L^{-0.602} & 10^4 \leq n_L \leq 10^{10} \end{Bmatrix} \tag{3.43}$$
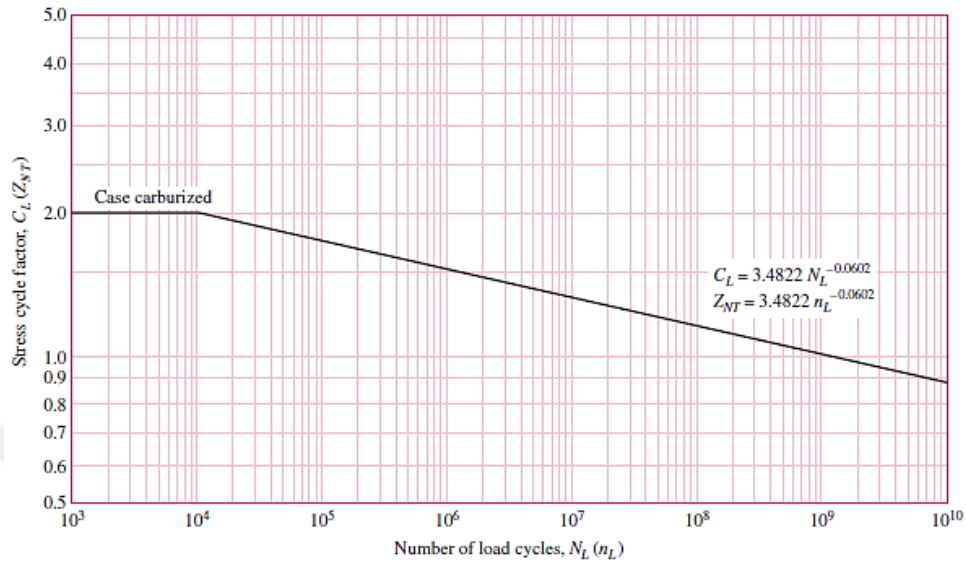
Figure 3.17. Contact stress cycle factor for pitting resistance C_L (Z_{NT}) for carburized case-hardened steel bevel gears (Source: ANSI/AGMA 2003-B97.)

Z_W: Hardness-Ratio Factor

$$Z_W = 1 + B_1(z_1/z_2 - 1) \quad B_1 = 0.008\ 98(H_{B1}/H_{B2}) - 0.008\ 29 \tag{3.44}$$

The preceding equations are valid when $1.2 \leq H_{BP}/H_{BG} \leq 1.7$ ($1.2 \leq H_{B1}/H_{B2} \leq 1.7$). Figure 3.17 graphically displays.

73
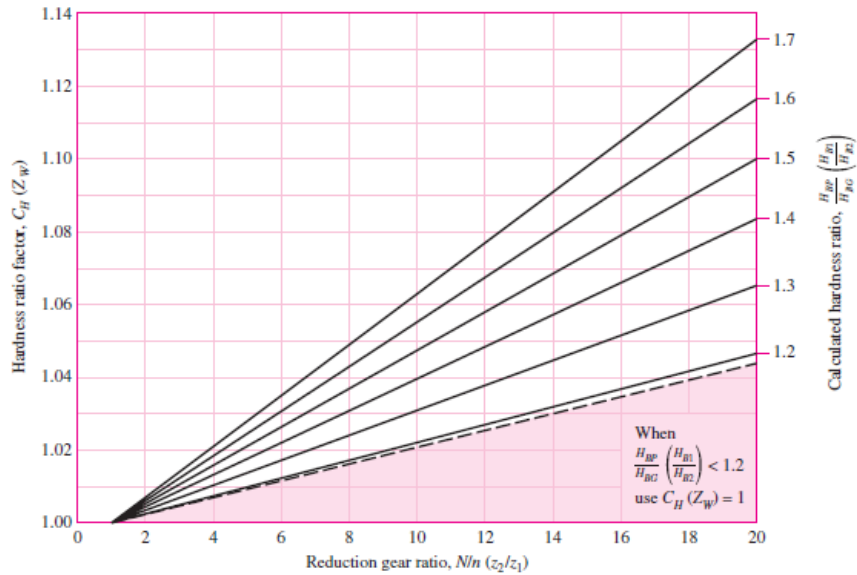
Figure 3.18. Hardness-ratio factor, Z_W for through-hardened pinion and gear (Source: ANSI/AGMA 2003-B97.)

Z_Z: Reliability Factors

Table 3.18 displays the reliability factors. Note that $C_R = \sqrt{K_R}$ and $Z_Z = \sqrt{Y_Z}$. Logarithmic interpolation equations are;

$$Y_Z = K_R = 0.50 - 0.25 log(1 - R)(1 - R)(1 - R)$$ (3.45)

Table 3.18. Reliability Factors Z_Z (Source: ANSI/AGMA 2003-B97.)

Requirements of Application	Reliability Factors for Steel*	
	C_R (Z_Z)	K_R (Y_Z)[†]
Fewer than one failure in 10 000	1.22	1.50
Fewer than one failure in 1000	1.12	1.25
Fewer than one failure in 100	1.00	1.00
Fewer than one failure in 10	0.92	0.85[‡]
Fewer than one failure in 2	0.84	0.70[§]

K_θ: Temperature Factor

$$K_\theta - \begin{Bmatrix} 1 & 0°C \le \theta \le 120°C \\ (273 + \theta)/393 & \theta > 120°C \end{Bmatrix}$$
(3.46)

Table 3.19. Allowable Contact Stress Number for Steel Gears, σ_{Hlim} Source: ANSI/AGMA 2003-B97.

Material Designation	Heat Treatment	Minimum Surface* Hardness	Allowable Contact Stress Number, s_{ac} ($\sigma_{H\,lim}$) lbf/in² (N/mm²)		
			Grade 1[†]	Grade 2[†]	Grade 3[†]
Steel	Through-hardened[‡]	Fig. 15–12	Fig. 15–12	Fig. 15–12	
	Flame or induction hardened[§]	50 HRC	175 000 (1210)	190 000 (1310)	
	Carburized and case hardened[§]	2003-B97 Table 8	200 000 (1380)	225 000 (1550)	250 000 (1720)
AISI 4140	Nitrided[§]	84.5 HR15N		145 000 (1000)	
Nitralloy 135M	Nitrided[§]	90.0 HR15N		160 000 (1100)	

3.2.3.2. Design Approach Using Fundamentals of Machine Component Design 5th Edition

The approach given by Juvinall and Marshek recommends that gear tooth surface fatigue stress has to be equal or less than gear tooth surface fatigue strength by considering a certain value of design factor of safety. Bevel gear surface fatigue stresses can be calculated as;

$$\sigma_H = C_p \sqrt{\frac{F_t}{b d_p} K_v K_o K_m}$$
(3.47)

C_p: Commonly called the elastic coefficient in the unit of $\sqrt{MPa}$ and its value is read from Table 3.20 below.

Table 3.20. Values of Elastic Coefficient C_p for Bevel Gears in $\sqrt{MPa}$ (Juvinall R.C., Marshek K.M., 2011)

Pinion Material	Gear Material			
	Steel	Cast Iron	Aluminum Bronze	Tin Bronze
Steel, E = 207 GPa	191	166	162	158
Cast iron, E = 131 GPa	166	149	149	145
Aluminum bronze, E = 121 GPa	162	149	145	141
Tin bronze, E = 110 GPa	158	145	141	137

I: Commonly called the geometry factor;
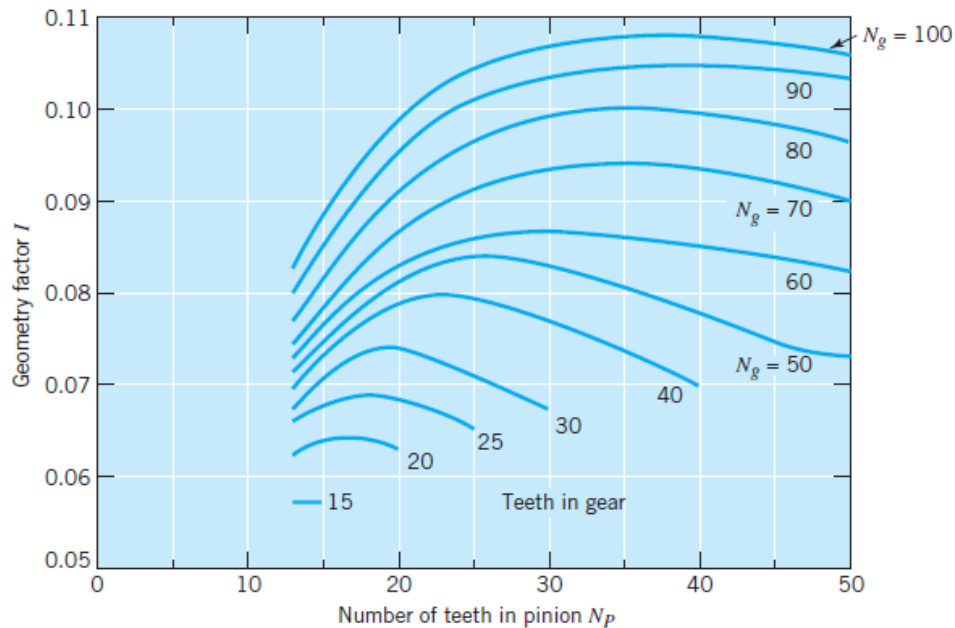
Figure 3.19. Geometry factors I for straight bevel gears. Pressure angle = 20°, shaft angle = 90° (From AGMA Information Sheet 215.91; also see ANSI/AGMA 2003-A86.)

With only two modifications: (1) the values of Cp are 1.23 times the values given in Table 3.16. This modification reflects a somewhat more localized contact area than for bevel gears. (2) Values of geometry factor I are taken from Figure

76

3.18. (Straight teeth) (See AGMA 215.01 for calculation of I values for other tooth shapes.)

The effective fatigue stress from equation 3.47 must be compared with the corresponding fatigue strength. The surface endurance strength is estimated from equation 3.48 as;

$$S_H = S_{fe} C_{Li} C_R \qquad (3.48)$$

$$S_H = S_{fe} C_{Li} C_R \qquad (3.49)$$

where

S_{fe}: Surface fatigue strength determined from Table 3.21.

Table 3.21. Surface Fatigue Strength S_{fe} (Juvinall R.C., Marshek K.M., 2011)

Material	S_{fe} (ksi)	S_{fe} (MPa)
Steel	0.4 (Bhn)–10 ksi	28 (Bhn)–69 MPA
Nodular iron	0.95[0.4 (Bhn)–10 ksi]	0.95[28 (Bhn)–69 MPa]
Cast iron, grade 20	55	379
grade 30	70	482
grade 40	80	551
Tin bronze AGMA 2C (11 percent tin)	30	207
Aluminum bronze (ASTM B 148—52) (Alloy 9C—H.T.)	65	448

C_{Li} : Life factor
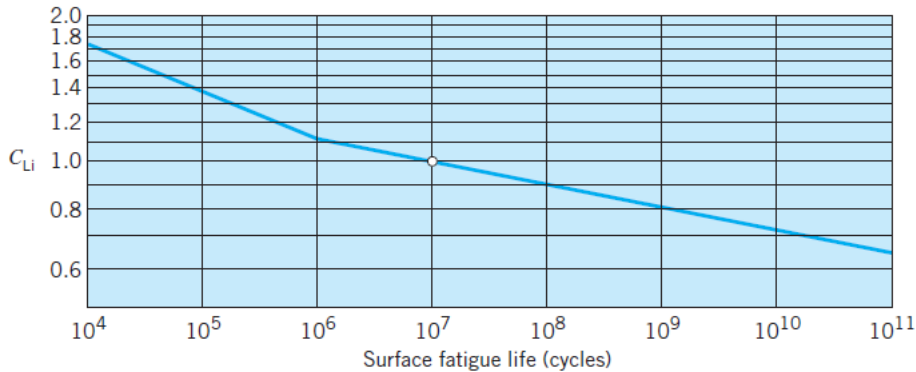
Figure 3.20. Values of C_{Li} for steel gears (general shape of surface fatigue S–N curve) (Juvinall R.C., Marshek K.M., 2011)

C_R : Reliability factor, C_R, is given in Table 3.22.

Table 3.22. Reliability Correction Factor, kr (Juvinall R.C., Marshek K.M., 2011)

Reliability (%)	50	90	99	99.9	99.99	99.999
Factor k_r	1.000	0.897	0.814	0.753	0.702	0.659

Now, the safety factor for bending fatigue can be taken as the ratio of fatigue strength to fatigue stress. Typically, a safety factor of 1.5 might be selected, together with a reliability factor corresponding to 99.9 percent reliability (Juvinall R.C., Marshek K.M., 2011).

3.2.3.3. Design Approach Using Machine Design II, K.Gopinath & M.M.Mayuram 4th Edition

Gear failure can occur in various modes. Surface contact fatigue is the most common cause of gear failure. It results in damage to contacting surfaces which can significantly reduce the load-carrying capacity of components, and may ultimately lead to complete failure of a gear (P.J.L.Fernandes C.Mc Duling).

Failure of the surfaces of gear teeth generally called as wear. Three most common causes of gear tooth wear are metal-to-metal contact due to lack of oil

78

film, ingress of abrasive particles in the oil and chemical wear due to the composition of oil and its additives. Calculation of face width relies on the same procedure as in bending fatigue failure, surface compressive stress should be equal or less than the surface fatigue stress (Shigley's J.E., 1985).

In this approach, a surface failure occurs when the significant contact stress equals or exceeds the surface endurance strength. The gear failure is explained by means of the flow diagram in Figure 3.21.
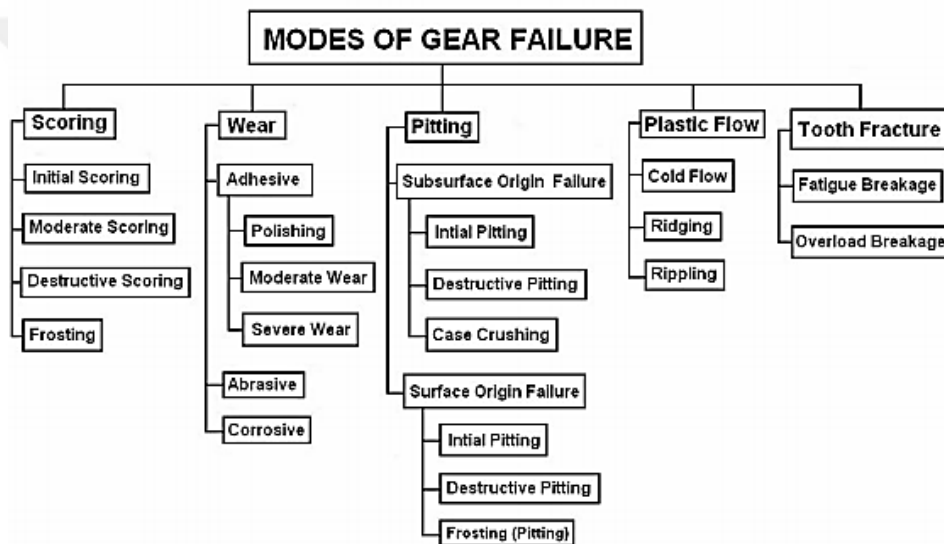
Figure 3.21. Different modes of failure (K.Gopinath & M.M.Mayuram, IIT-Madras, 2009)

Bevel gear surface fatigue stress can be calculated as for bevel gears, with only two modifications.

$$\sigma_H = C_p \sqrt{\frac{F_t}{bdI} K_v K_o K_m}$$ (3.50)

1.23 times the Cp values given in Table 3.23 are taken to account for a somewhat more localized contact area than bevel gears.

79

Table 3.23. Elastic Coefficient, Cp for bevel gears, in $(MPa)^{0.5}$

Pinion Material	Gear material			
(μ = 0.3 in all cases)	Steel	Cast iron	Al Bronze	Tin Bronze
Steel, E=307GPa	191	166	162	158
Cast iron, E = 131GPa	166	149	149	145
Al Bronze, E = 121GPa	162	149	145	142
Tin Bronze, E = 110GPa	158	145	141	137

I: Geometry factor, given in Figure 3.22.
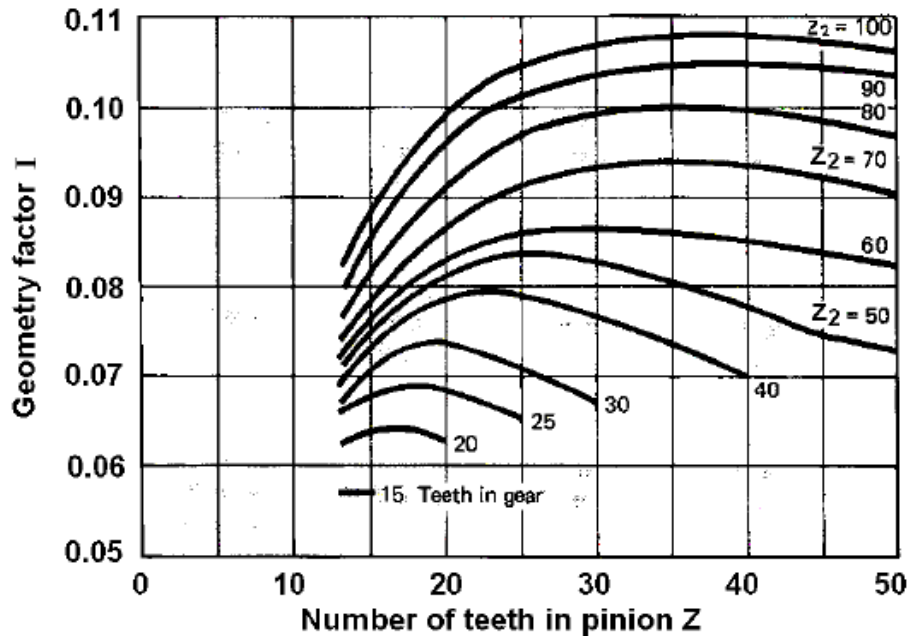
Figure 3.22. Geometry factor I for straight bevel gear pressure angle 20° and shaft angle 90°

Surface fatigue strength is given as;

$$\sigma_{sf} = \sigma_{sf}' \, K_L K_H K_R K_T \tag{3.51}$$

where

σ_{sf}' = surface fatigue strength of the material given in Table 3.21.

80

Table 3.24. Surface fatigue strength, σ_{sf} (MPa) (K.Gopinath & M.M.Mayuram, 2009)

Material	σsf (MPa)
Steel	2.8 (Bhn) – 69 MPa
Nodular iron	0.95 [2.8 (Bhn) – 69 MPa]
Cast iron, grade 20	379
Cast iron, grade 30	482
Cast iron, grade 40	551
Tin Bronze, AGMA 2C (11% Sn)	207
Aluminium Bronze (ASTM b 148 – 52) (Alloy 9C – H.T)	448

K_L = Life factor given in Figure 3.23.
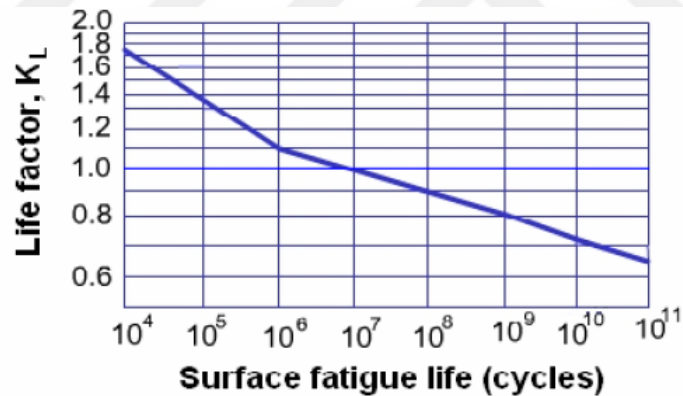
Figure 3.23. Life factor K_L (K.Gopinath & M.M.Mayuram, IIT-Madras, 2009)

K_H is hardness ratio factor, K the Brinell hardness of the pinion by Brinell hardness of the gear as given in Figure 3.24.

K_H = 1.0 for K < 1.2
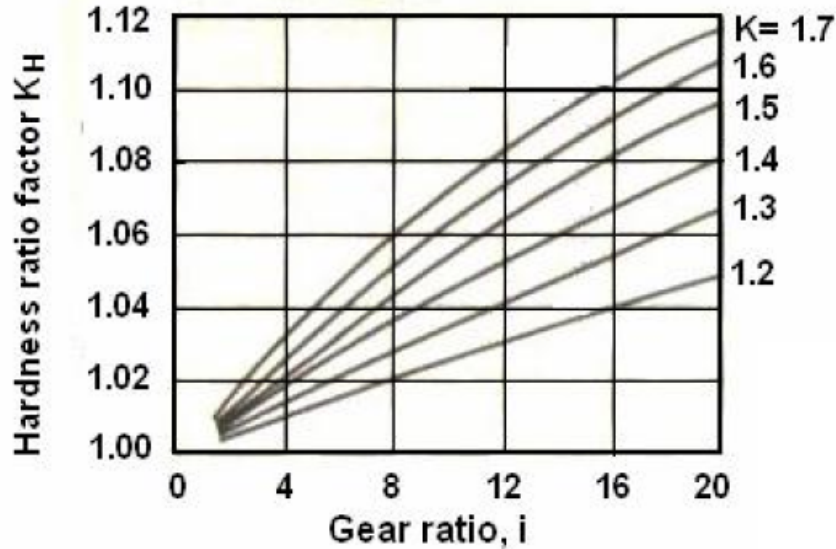
Figure 3.24. Hardness ratio factor, K_H (K.Gopinath & M.M.Mayuram, IIT-Madras, 2009)

K_R : Reliability factor, given in Table 3.25.

Table 3.25. Reliability factor, K_R (K.Gopinath & M.M.Mayuram, IIT-Madras, 2009)

Reliability factor R	0.50	0.90	0.95	0.99	0.999	0.9999
Factor Kr	1.000	0.897	0.868	0.814	0.753	0.702

K_T = temperature factor, = 1 for T≤ 120°C based on lubricant temperature. Above 120°C, it is less than 1 to be taken from AGMA standards. Allowable surface fatigue stress for design is given by,

$$[\sigma_H] = \sigma_{Sf} / s \qquad\qquad (3.52)$$

Factor of safety s = $\sqrt{2,1}$

Hence Design equation is: $\sigma_H \leq [\sigma_H]$

82

3.2.3.4. Design Approach Using ISO Standards 10300 - Part 2

ISO Standards 10300 provides gear design formula based on the surface contact. The calculation of surface durability is based on surface contact stress, σ_H, at the pitch point or at the lowest point of single pair tooth contact. The higher of the two values obtained is used to determine capacity.

The values of σ_H and the permissible contact stress, σ_{HP}, shall be calculated separately for wheel and pinion; σ_H shall be less than or equal to σ_{HP} (ISO 10300). σ_H is contact stress and is given by equation 3.53;

$$\sigma_H = \sigma_{H0}\sqrt{K_A K_V K_{H\beta} K_{H\alpha}} \leq \sigma_{HP} \tag{3.53}$$

$K_{H\beta}$ is defined as the ratio between the maximum load per unit face width and the mean load per unit face width;

$K_{H\beta} = K_{F\beta}$: Face load factor.

$K_{H\alpha}$: Transverse load factor and is given by Figure 3.25;
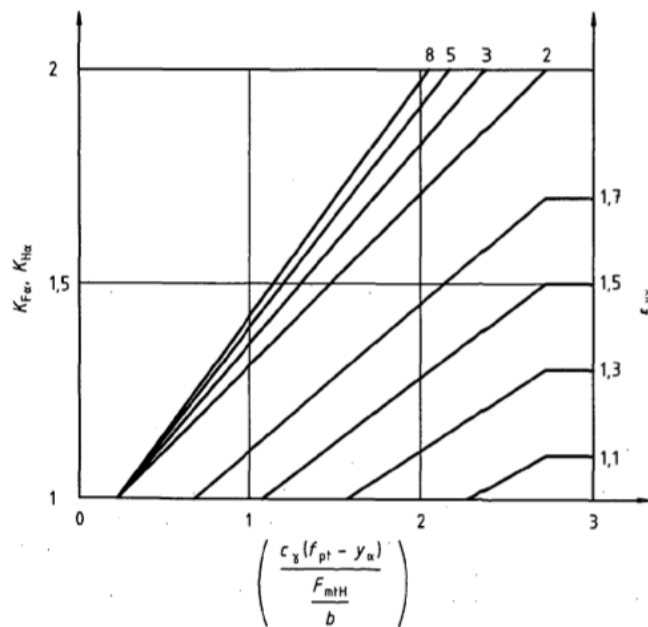
Figure 3.25. Transverse load factor, $K_{H\alpha}$

83

$$\sigma_{H0} = \sqrt{\frac{F_{mt}}{d_{m1}l_{bm}}\frac{\sqrt{u^2+1}}{u}}\,Z_{M-B}Z_H Z_E Z_{LS} Z_\beta Z_K \tag{3.54}$$

σ_H: Contact stress

σ_{H0}: Nominal contact stress at the pitch point and given by equation 3.54;

σ_{HP}: Permissible contact stress

u :   Gear ratio

d_{m1}: Mean pitch diameter,

l_{bm}: The length of the middle line contact

Z_{M-B}: Mid zone factor and given by equation 3.56,

Z_H: The zone factor and given by equation 3.55,

Z_E: Elasticity factor and given by equation 3.57,

Z_{LS}: Load sharing factor and given by equation 3.58,

Z_β: Spiral-angle factor and given by equation 3.59,

Z_K: Empirical factor, $Z_K = 0.8$

$$Z_H = 2\sqrt{\frac{\cos\beta_{vb}}{\sin(2\alpha_{vt})}} \tag{3.55}$$

$$Z_{M-B} = \frac{\tan\alpha_{vt}}{\sqrt{\left[\sqrt{\left(\frac{d_{vaa}}{d_{vba}}\right)^2 - 1 - F_1\frac{\pi}{z_{v1}}}\right]\left[\sqrt{\left(\frac{d_{vaa}}{d_{vba}}\right)^2 - 1 - F_2\frac{\pi}{z_{v2}}}\right]}} \tag{3.56}$$

Table. 3.25. Factors for calculation of mid-zone factor, Z_{M-B}

	F_1	F_2
$\varepsilon_{v\beta} = 0$	2	$2\,(\varepsilon_{v\alpha} - 1)$
$0 < \varepsilon_{v\beta} < 1$	$2 + (\varepsilon_{v\alpha} - 2)\,\varepsilon_{v\beta}$	$2\,\varepsilon_{v\alpha} - 2 + (2 - \varepsilon_{v\alpha})\,\varepsilon_{v\beta}$
$\varepsilon_{v\beta} > 1$	$\varepsilon_{v\alpha}$	$\varepsilon_{v\alpha}$

$\varepsilon_{v\alpha}$:Transverse contact ratio

$\varepsilon_{v\beta}$:Overlap ratio

$$Z_E = \sqrt{\frac{1}{\pi\left(\frac{1-v_1^2}{E_1}+\frac{1-v_2^2}{E_2}\right)}} \qquad (3.57)$$

v_1, v_2: Poisson's ratios for materials of pinion and gear, respectively (use a value of 0.3 for materials defined in this standard);

E_1, E_2: Young's moduli of elasticity for materials of pinion and gear, respectively, N/mm^2 .

$Z_{LS} = 1$ for $\varepsilon_{v\gamma} \leq 2$

$$Z_{LS} = \left\{1 + 2\left[1 - \left(\frac{2}{\varepsilon_{v\beta}}\right)^{1.5}\right]\sqrt{1 - \frac{4}{\varepsilon_{v\gamma}^2}}\right\}^{-0.5} \qquad \text{for } \varepsilon_{v\gamma} > 2 \text{ and } \varepsilon_{v\beta} > 1 \qquad (3.58)$$

$\varepsilon_{v\gamma}$: Modified contact ratio

$$Z_\beta = \sqrt{\cos\beta_m} \qquad (3.59.)$$

$$l_{bm} = \frac{b\varepsilon_{v\alpha}}{\cos\beta_{vb}}\sqrt{\frac{\varepsilon_{v\gamma}^2 - [(2-\varepsilon_{v\alpha})(1-\varepsilon_{v\beta})]^2}{\varepsilon_{v\gamma}^2}} \qquad \text{for } \varepsilon_{v\beta} < 1 \qquad (3.60)$$

$$l_{bm} = \frac{b\varepsilon_{v\alpha}}{\cos\beta_{vb}\varepsilon_{v\gamma}} \quad \text{for } \varepsilon_{v\beta} \geq 1 \qquad (3.61)$$

$$d_{m1,2} = m_{mn}z_{1,2}/\cos\beta_m \qquad (3.62.)$$

m_{mn}:Mean normal module

$$m_{mn} = m_{mt}\cos\beta_m \qquad (3.63.)$$

m_{mt}: Mean transverse module

$$m_{mt} = \frac{R_m}{R_e}m_{et} \qquad (3.64)$$

R_m: Mean cone distance

R_e: Outer cone distance

m_{et}: Outer transverse module

$$R_e = 0.5d_{e1}/\sin\delta_1 = 0.5d_{e2}/\sin\delta_2 \tag{3.65}$$

$$\tan\delta_1 = 1/u, \ \tan\delta_2 = u \text{ for } \Sigma=90° \tag{3.66}$$

$$R_m = R_e - \left(\frac{b}{2}\right) \quad m_{et} = d_{e2}/z_2 = d_{e1}/z_1 = 25.4/P_d \tag{3.67}$$

$$\sigma_{HP} = \frac{\sigma_{Hlim}Z_{NT}}{S_{Hlim}}Z_X Z_L Z_R Z_v Z_W \tag{3.68}$$

σ_{Hlim}: The endurance limit for contact stress,

Size factor, Z_X, is affected from material quality, heat treatment, depth of hardening, distribution of hardening, radius of flank curvature and module in the case of surface hardening, depth of hardened layer relative to the size of teeth.

For through hardened gears and for surface hardened gears with adequate case depth relative to tooth size and radius of relative curvature, Z_X, is taken to be 1,0.

Z_X: Size factor, $Z_X = 1$

In ISO 10300-2 standard, influences on lubrication film formation has been taken by using following factors; Z_L, accounts for the influence of nominal viscosity of the lubricant, Z_V, for the influence of tooth flank velocities and Z_R, for the influence of surface roughness on the formation of the lubricant film in the contact zone.

Z_L: Lubricant factor

Z_v: Speed factor

Z_R: Roughness factor

Z_W: Work-hardening factor

The work hardening factor, Z_W takes into account the increased surface durability due to meshing a steel wheel (structural steel, through - hardened steel) with a pinion which is significantly (~200 HB or more) harder than the wheel and with smooth tooth flanks. ISO 10300-2 is applied, as follows;

$$Z_W = 1.2 - \frac{HB-180}{1700} \tag{3.69}$$

HB: the Brinell hardness of tooth flanks of the softer gear of the pair;

$Z_W = 1.2$ for HB<130 and 1,0 for HB>470

$Z_L Z_R Z_v = 1$ for $Rz_{10} \leq 4\,\mu m$

$Z_L Z_R Z_v = 0.92$ for $Rz_{10} > 4\,\mu m$

Rz_{10}: *mean relative roughness* and is given by equation 3.70;

$$Rz_{10} = \frac{Rz_1 + Rz_2}{2} \cdot \sqrt[3]{\frac{10}{\rho_{red}}} \tag{3.70}$$

$$\rho_{red} = \frac{a_p sin\alpha_{vt}}{cos\beta_{vb}} \frac{u_v}{(1+u_v)^2} \tag{3.71}$$

$$R_a = \frac{Rz}{6} \tag{3.72}$$

R_a: *roughness* of pinion or gear and is given by equation 3.72.

3.3. Development of Microsoft Excel Pages

Module selection and face width determination require iterations as described in Figure 3.2. And depending on the experiences of designer, iterations takes considerable calculation time. Because of that, all the determinations that referred to in Section 3.2.2 and 3.2.3, have been performed by using Microsoft Excel pages. This method has allowed simplicity for designing a bevel gear iteratively since it needs complicated determinations. Therefore loss or gain in

volume or the selection of material type or stress related performance has been seen easily on excel pages by changing the parameters.

The excel pages have been carried out in a systematic way. A gear design includes input parameters and design variables to find the design outputs that are the suitable module (m) and the appropriate face width (F). Both m and F are the most important design parameters.

Input parameters have been defined before starting the gear design as it is given in Table 3.26 and specified in excel pages. These input parameters can then be changed according to the requirements of users or operating conditions if it is needed.

Table 3.26. Selected input parameters for the design

Input Parameters
Type of gear profile
Pressure angle,
Input speed of a power source, rpm
Number of life cycles, N
Design factor of safety, n_d
Material properties of gear pair
Operating temperature, T
Quality number for gear
Reliability, %
Working characteristics of driving and driven machines
Selected transmitted power range, Kw
Selected Gear speed ratio range, m_G

Defined input parameters cover the operating conditions, material properties of a pair of gear. It also gives information about gear tooth profile. Figure 3.26 shows the input parameters that are entered into the excel pages prepared for the ANSI/AGMA 2003-B97 standards. Though these input parameters

have been kept identical for the design approaches, there have been slight differences for the values of input parameters. This is because design variables are taken into account in different ways for each of the design approaches.

input parameters that affect speed ratio					
input parameter for power transmission					
input parameters for service conditions					

Figure 3.26. Input parameters that represented on excel pages

The approach of using Excel pages enabled to obtain the results in a very short time for the various selected speed ratios and for the selected power transmission ranges.

And now I will explain the geometric rating numbers (GRi) and conversion factors (CFs). After finding the design outputs (m&b), m times b (m.b) results were obtained. The results of m times b which will allow to see the all effect of both m and b on the results of K.Gopinath & M.M.Mayuram, Juvinall and AGMA gear designs, were carried out for the allowable range of speed ratio (1:1 to 8:1) and

wide range of power (0,5-1000 kW) and for the lowest and highest strengths of materials. Because of that, a new dimensionless quantity occurs and which may be called as "Geometric Rating Number GRi, are defined specifically in equation 3. 73 to rate the standards

$$GRi = \frac{m_i x b_i}{m_o x b_o} \tag{3.73}$$

Where m_i and F_i are the module and face width obtained for the target gear design approach respectively, and where m_0 and F_0 are the module and face width obtained from ANSI/AGMA 2003-B97 standards respectively.

For explaining the differences between the four design approaches, conversion factors were generated to convert the module and face width obtained from ISO Standard to AGMA standards and Juvinall to AGMA Standard or from K.Gopinath & M.M.Mayuram to AGMA, etc. Equations 3.40 to 3.43 give the conversion approach to obtain the mean values of conversion factors for module ($\overline{CF}$m) and face width ($\overline{CF}$b) together with their standard deviations. $\overline{CF}$m and $\overline{CF}$b are the mean $\overline{CF}$j for Juvinal, and m*juvinal and b*juvinal are defined as;

$$m^* juvinal = \frac{m_{juvinal}}{m_{AGMA}} \tag{3.74}$$

$$b^* juvinal = \frac{b_{juvinal}}{b_{AGMA}} \tag{3.75}$$

$$\overline{CF_m} = \frac{1}{N} \cdot \sum_{j=1}^{N} m^*_{juvinal} \tag{3.76}$$

$$\sigma_{\overline{CF}mi} = \sqrt{\frac{1}{N} \sum_{j=1}^{N} (m^*_{juvinal,j} - \overline{CF_{m,juvinal}})} \tag{3.77}$$

$$\overline{CF_b} = \frac{1}{N} \cdot \sum_{j=1}^{N} b^*_{juvinal} \tag{3.78}$$

$$\sigma_{\overline{CF}bi} = \sqrt{\frac{1}{N} \sum_{j=1}^{N} (b^*_{juvinal,j} - \overline{CF_{b,juvinal}})} \tag{3.79}$$

3.4. Development of Finite Element Method (FEM)

The Finite Element Method (FEM) is a numerical analysis technique for obtaining approximate solutions to a wide variety of engineering problems. For most engineering problems which consist of complex mathematical models such as designing a gear, it is not always possible to obtain analytical solutions. Because of that reason, numerical methods provide approximate but acceptable solutions. As mentioned in Chapter 2, in this work, the numerical results of FEM are compared with the analytical results of the selected gear design approaches. This is mainly used to verify the analytical results, and to select the best gear design approach which is used for various comparisons to obtain more refined results.

In this thesis work, module and face width have been found by analytical methods iteratively with the aid of excel pages and a numerical "Analysis System" (ANSYS) Workbench 16.1 has been used to compare the analytical results with numerical solutions. The software ANSYS needs a structural model to execute the analysis. So by using the design parameters, and the obtained module and face width through the iterations, a 3D model of pinion was created on SOLIDWORKS, 2018.

Structural analysis requires three steps generally: pre-processing, solver and post-processing. In pre-processing, the geometry of the structure is made and creating mesh elements, solver is the definition of boundary conditions and lastly in post-processing analysis results are obtained.

In the following chapter, the use of SOLIDWORKS, 2018 and ANSYS software's have been given including the design results.

Since the ANSYS software analyses the gear stresses, gear bending stress has been determined numerically considering the final design results of module and face width. Bevel gears that have been designed for 1:1 speed ratio at 10 kW power transmissions have been modelled using the same design input parameters. The results obtained and provided in the following section gave the highest module values at 1:1 speed ratio. As a result of this 1:1 speed ratio was selected as the most

critical ratio for the module. The selection of power is not as straight forward as speed ratio. The most common power range in many industrial applications is 1 to 10 kW. Therefore 10 kW is selected as the power input. It is believed that these input values may allow obtaining suitable conclusions. The FEM results have been obtained for the four gear design approaches based on bending fatigue failure criteria.

3.5. Summary

The formulas in the gear design approach given in the previous sections were rewritten to obtain the face width (F). The obtained face width equations for each type of design approaches have been represented in Table 3.27 based on bending stress and in Table 3.28 based on surface contact stress. As it is seen from the tables, there are significant differences when comparing the different types of design approaches. Each face width equation depends on some design variables that are completly differ to each other. These equations are then used in the Excel pages together with all inputs.

Table 3.27.Face width equations of the design approaches based on bending fatigue stress failure criteria

Design Approaches	Face Width
ANSI/AGMA 2003-B97 standards (Shigley's Mechanical Engineering Design 9th Ed.)	$b = \dfrac{1000 Wt}{\sigma_F} \dfrac{K_A K_V}{m_{et}} \dfrac{Y_X K_{H\beta}}{Y_B Y_J}$
Fundamental Of Machine Component Design 5th Ed.	$b = \dfrac{F_t P}{\sigma J} K_v K_O K_m$
Machine Design II, K.Gopinath & M.M.Mayuram 4th Ed.	$b = \dfrac{F_t}{\sigma_b m J} K_v K_o K_m$

Table 3.28.Face width equations of the design approaches based on surface contact
fatigue stress failure criteria

Design Approaches	Face Width
ANSI/AGMA 2003-B97 Standards (Shigley's Mechanical Engineering Design 9th Ed)	$b = Z_E^2 \dfrac{1000 W^t}{\sigma_H^2 d Z_I} K_A K_v K_{H\beta} Z_R Z_{NC}$
Fundamental Of Machine Component Design 5th Ed.	$b = C_P^2 \dfrac{P_t}{\sigma_H^2 d_P I} K_v K_o K_m$
Machine Design II, K.Gopinath & M.M.Mayuram 4th Ed.	$b = C_P^2 \dfrac{P_t}{\sigma_H^2 d_P I} K_v K_o K_m$

4. RESULTS AND DISCUSSIONS

When designing gears, the most important design parameters are module and face width. As mentioned in Chapter 3, these have been determined considering "the bending stress" and "surface contact stress" by using four different types of design approaches, given by ANSI/AGMA 2003-B97 standards, Juvinall R.C., Marshek K.M. (2011), K.Gopinath & M.M.Mayuram, IIT-Madras, 2009 and ISO Standards 10300-(Part 1-2-3), 2001.

For the selected 4 approaches, equations for face width "F" based on bending stress and face width "F" based on surface contact stress have been obtained considering the four types of gear design approaches or formulations and given in Table 3.23 and 3.24 respectively.

Figure 3.3 in Chapter 3 has also described the iterations needed for proper module selection and face width determination. Before starting the iterations, geometrical criterions, operating conditions and material properties for a pair of gear have been defined as input parameters. While the iterations are carried out, all the input parameters have been kept constant. Table 4.1 shows the input parameters with their values that are considered in this study, and they have been kept identical for the four types of design approaches. A fair comparison between the design approaches was obtained by keeping input parameters identical throughout the study. After determining the input parameters that are kept constant for all of the gear designs, iterations for proper module selection were made by determining design variables that affect the failure stresses of material strength. The calculations were carried out and the face width calculations were performed using the $F = 0.3A_0$ or $F = 10/P$, whichever is smaller, then face width and the module were obtained. . Module "m" and face width "F" is obtained for 4 design approaches with different power transmissions and speed ratios. 51 different power transmission values are used for 1 speed ratio for each design approach. Each design approaches have 8 different speed ratios which give 816 design results for just one. 3264 design results for 4 different design approaches is calculated for only

type 1 material. Since 3 different type of material for 20° and 25° are used, 19584 design results are calculated, in total.

Table 4.1.Values of the selected Input parameters for the design

Input Parameters	Value
Pressure angle, Ø	20° and 25°
Type of gear profile	Involute
Input speed of a power source, rpm	1200
Number of life cycles, N	10^8
Design factor of safety, n_d	2,1
Reliability, %	99,9
Operating temperature, T	Moderate or low (~120°C)
Quality number for gear	K.Gopinath & M.M.Mayuram, IIT-Madras, 2009: 9; ANSI/AGMA 2003-B97 standards; Juvinall R.C., Marshek K.M.,2011: shaved or ground
Material properties of gear pair	see Table 3.1
Working characteristics of driving and driven Machines	Uniform
Selected transmitted power range, kW	0,5 kW - 1000 kW
Selected Gear speed ratio range, m_G	1:1, 2:1, 3:1, 4:1, 5:1, 6:1, 7:1, 8:1

4.1. Design Results

As mentioned in Section 3.3, loss or gain in volume or in selection of material type or stress related performance has been also seen easily on excel pages by changing the parameters. Because of that, this provided to determine the loss or the gain between different types of design approaches by obtaining useful charts and/or practical curves using the design results. Figure 4.1 shows an example for the excel page that prepared for bevel gear design based on bending fatigue failure by using ANSI/AGMA 2003-B97 standards.

It consists of input parameters, design variables and the most important design parameters that are module and face width. Design results are directly dependent on the input parameters as mentioned above. And design variables are provided in the form of equations, table and/or figure readings depending on the design approach.

Traditionally, gear-box design has always initiated with the selection of the module, which makes the whole design process iterative, time-consuming and costly. Also, the design work requires experience, which is lacking for an inexperienced designer. Thus excel program pages were arranged to carry out the design calculations.
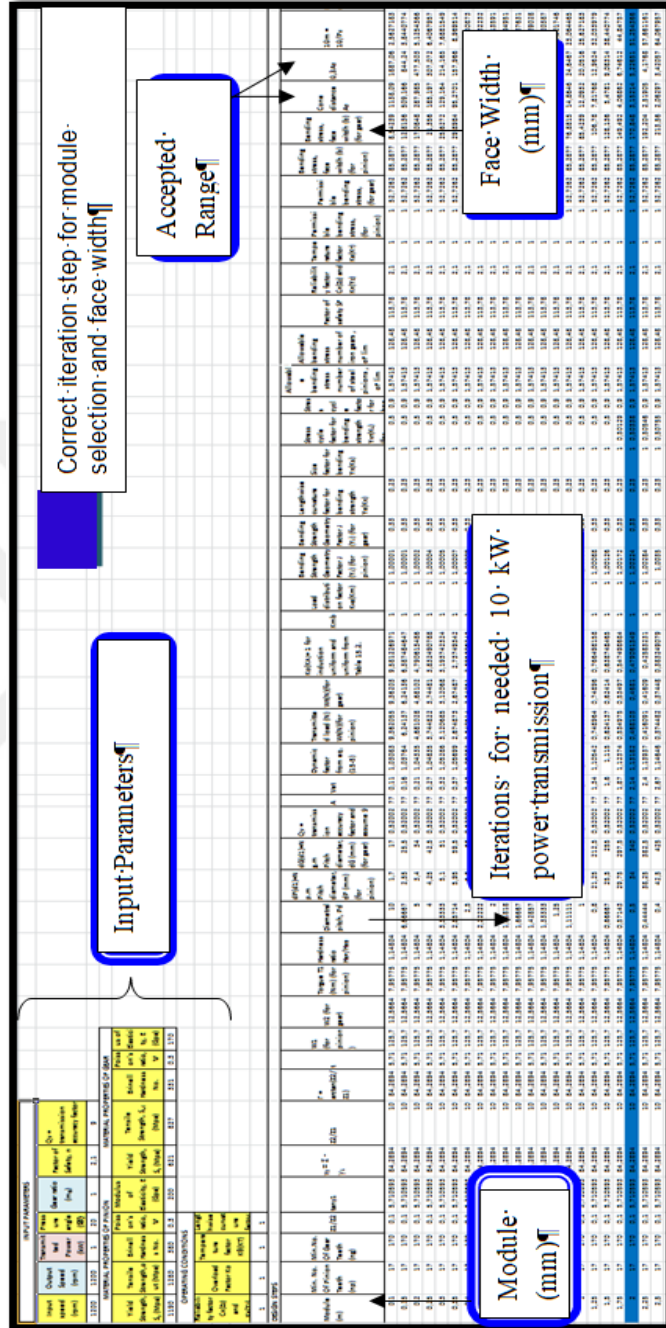
Figure 4.1. A general view of Microsoft Excel page used in iterations for needed 10 kW power transmission

As mentioned before, speed reduction by using a bevel gear can be achieved up to a gear ratio of 8:1 in a single stage. Thus gear designs are carried out for the gear speed ratio of 1:1, 2:1, 3:1, 4:1, 5:1, 6:1, 7:1 and 8:1. This range may allow plotting results in a curve. Similarly, the power range is selected to cover a wider range. Hence, when we compare module (m) and face width (F) results obtained at power transmission values starting from 0,5 kW to 1000 kW with the increments of 50 kW but for all other studies for the designs are carried out for the power transmissions values starting from 0,5 kW to 1000 kW with the increments of 20 kW. Figure 4.2 displays speed ratio and power combinations used in this study except comparing module and face width results. The designs and their results were carried out for the four types of design approaches considering the bending fatigue and surface contact fatigue separately. This means that for the speed ratio of 1:1, 51 design results are obtained for the bending fatigue and 51 for the surface contact fatigue. This gives a total of 51x2=102 design results for each of the design approach. The excel pages have provided to obtain these results accurately in a short time.
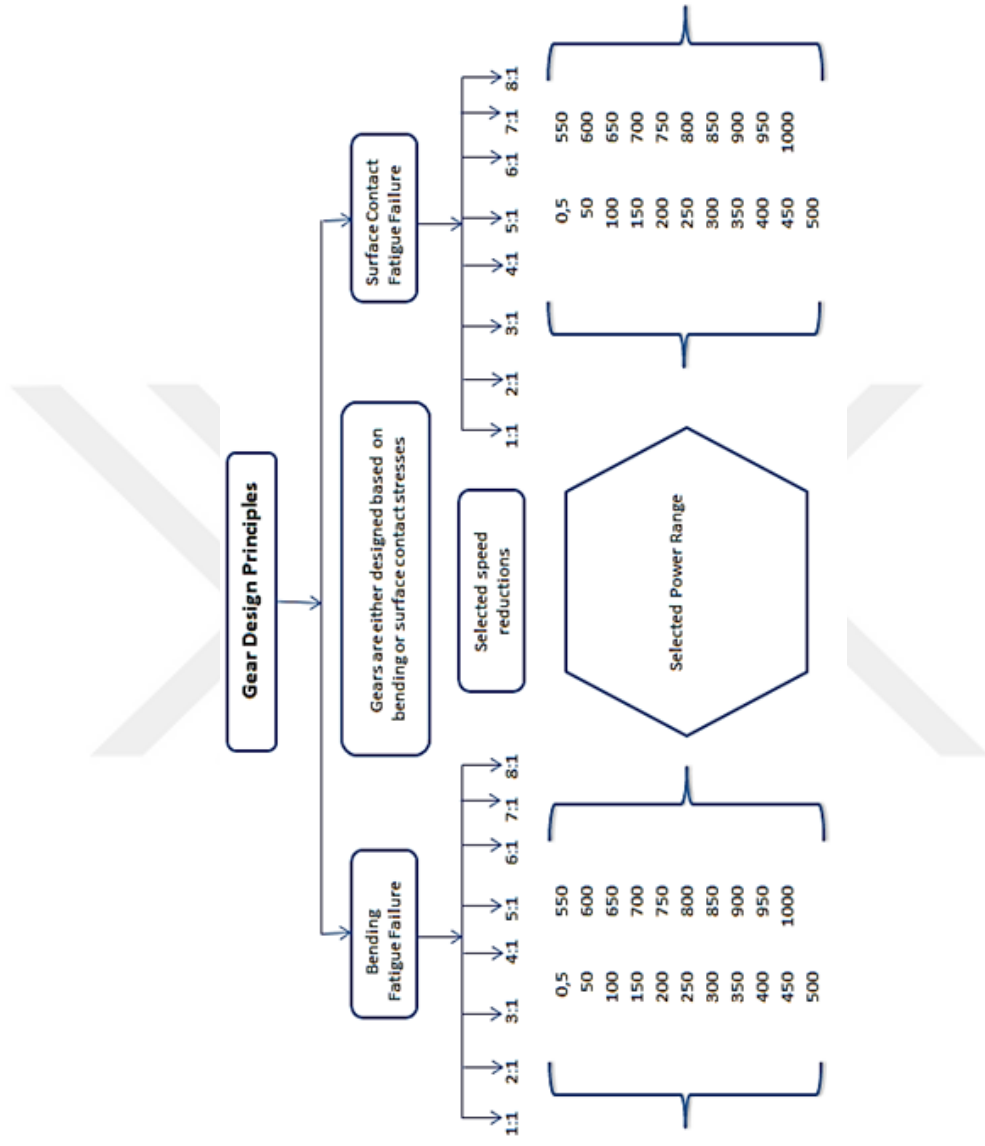
Figure 4.2. Speed ratio and power combinations used in the study for four different types of design approaches (except comparing module and face width results)

4.2. Comparison of Module Selection and Face Width Results of the Design Approaches

As described in Figure 4.2, design results were obtained in a wider range (speed ratio from 1:1 to 8:1 and transmitted power from 0,5 kW to 1000 kW for the design approaches). Therefore the results have been compared considering the power transmission ranges and gear speed ratios respectively.

4.3. Comparison of Results Considering Power Transmission

Curves from Figure 4.3 to Figure 4.12 have been shown for module selection and face width for the four design approaches. These figures allow selecting module and facing width for selected speed ratios at any desired power transmission ranges for the design approaches.

In this study, FEA has been also used to analyse bending stress of 3D bevel gears that were modelled with the assist of using the same inputs and using the obtained results of the design approaches. These are discussed in detail in Section 4.4. And considering Table 4.8 and Table 4.9, ANSI/AGMA 2003-B97 design approach that has already been used as the most common standard for the design of a bevel gear, gives a closer result to FEA results. As a result of this, the following figures are discussed by using Tables from 4.2. The ratio of module given by the design approaches to the module given by ANSI/AGMA 2003-B97 standards ($m_{\text{design approach}}/m_{\text{AGMA}}$) has obtained and represented in tabular form. The formation of these tables has been explained in Table 4.2.

Table 4.2. The ratio of modules with respect to ANSI/AGMA 2003-B97   standards

Ratio of modules	Abbreviations
$\dfrac{m\ AGMA}{m\ AGMA}$	m_{AGMA} : the module obtained by the approach has given by ANSI/AGMA 2003-B97 standards
$\dfrac{m_{J\&M}}{m\ AGMA}$	$m_{J\&M}$: the module obtained by the approach has given by Juvinall R.C., Marshek K.M. (2011)
$\dfrac{m_{K\&M}}{m\ AGMA}$	$m_{K\&M}$: the module obtained by the approach has given by K.Gopinath & M.M.Mayuram, IIT-Madras (2009)
$\dfrac{m_{ISO}}{m\ AGMA}$	m_{ISO} : the module obtained by the approach has given by ISO Standards 10300-(Part 1-2-3), 2001

The differences between modules have been investigated in order to have an idea of whether the same behaviours are available or not to mention general trends. For this reason, a novel method has been developed as explained in Table 4.2. The method normalizes the modules obtained by the design approaches. In here normalization was made with respect to ANSI/AGMA 2003-B97 standards by dividing the module obtained from the design approaches to the module obtained by ANSI/AGMA 2003-B97 standards, for instance, $m_{J\&M}/m_{AGMA}$ is used.

Practical curves have been represented based on both bending fatigue failure and surface contact fatigue failure respectively and discussions on module have been provided in tabular form.

4.3.1. Comparison of Results Based on Bending Fatigue Failure

The following figures and tables provide a comparison of results based on bending fatigue failure for pressure angle of 20° and material type 1. Figures have shown the general trends of module and face width with the increment of transmitted power for each design approaches. However, comparisons are also represented in tabular form but only considering the differences in modules.

Comparisons of results based on bending fatigue failure for pressure angle of 20° are given in the appendices;

➢ for material type 2, see Appendix A.1.

➢ for material type 3, see Appendix B.1.

Comparisons of results based on bending fatigue failure for pressure angle of 25° are given in the appendices;

➢ for material type 1, see Appendix C.1.

➢ for material type 2, see Appendix D.1.

➢ for material type 3, see Appendix E.1.
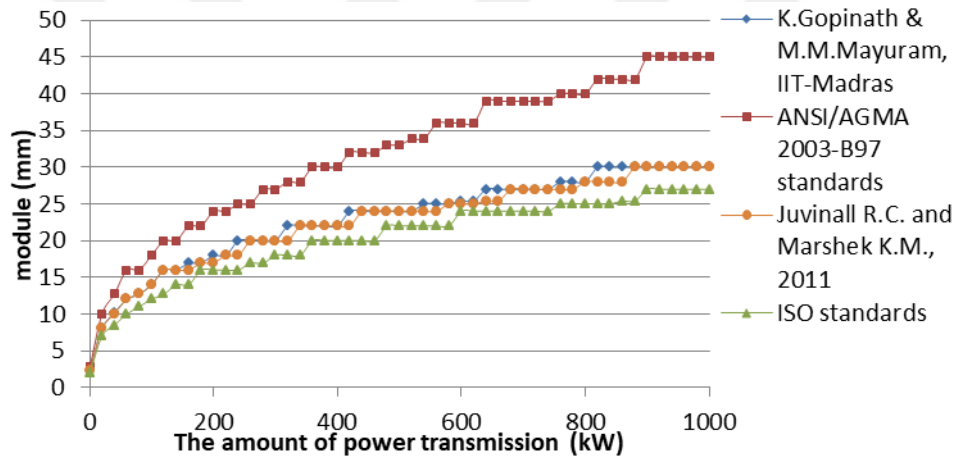
Figure 4.3. Module variation considering bending fatigue failure under
increasing power at 1:1 speed ratio (for Ø=20°, Material type 1)
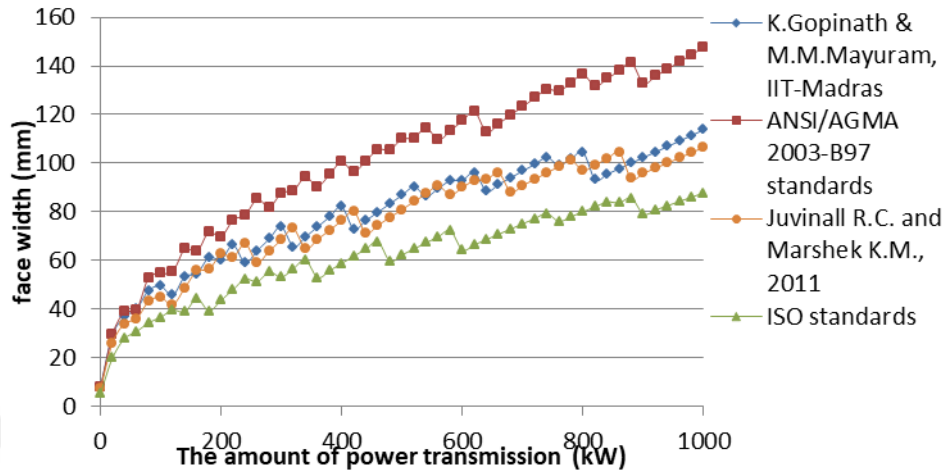
Figure 4.4. Face width variation considering bending fatigue failure under
              increasing power at 1:1 speed ratio (for Ø=20°, Material type 1)

Figure 4.3 shows that the approach given by ISO Standards 10300-(Part 1-2-3), 2001 gives the minimum design results for the module and the face width when speed ratio is 1:1.
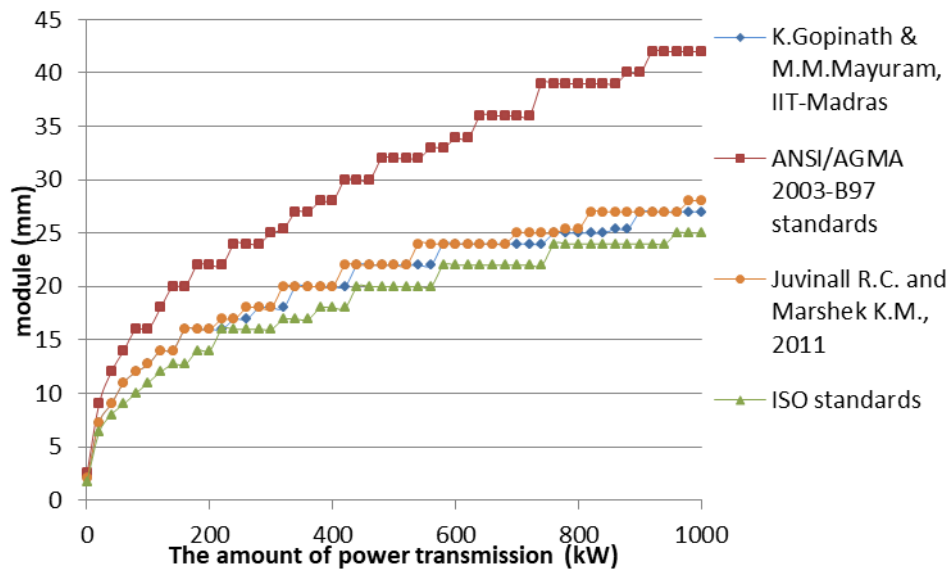
Figure 4.5. Module variation considering bending fatigue failure under
              increasing power at 2:1 speed ratio (for Ø=20°, Material type 1)
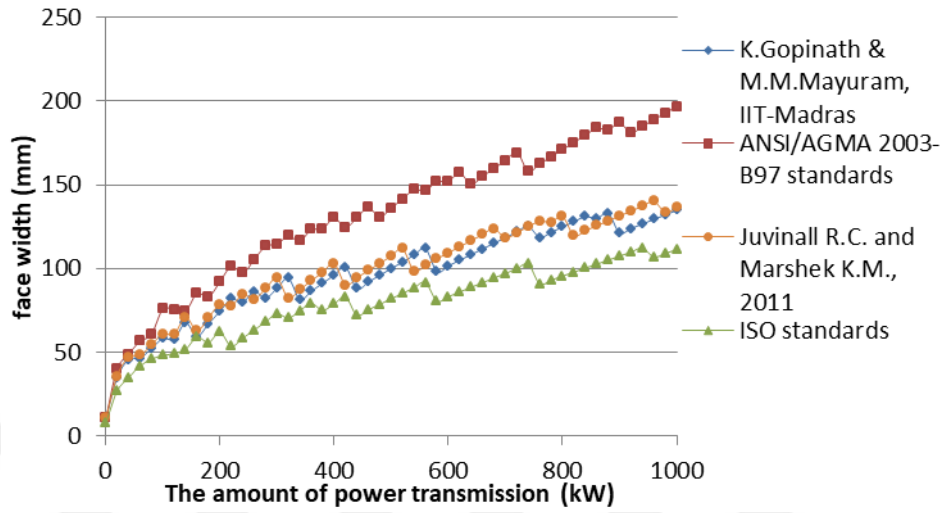
Figure 4.6. Face width variation considering bending fatigue failure under
increasing power at 2:1 speed ratio (for Ø=20°, Material type 1)
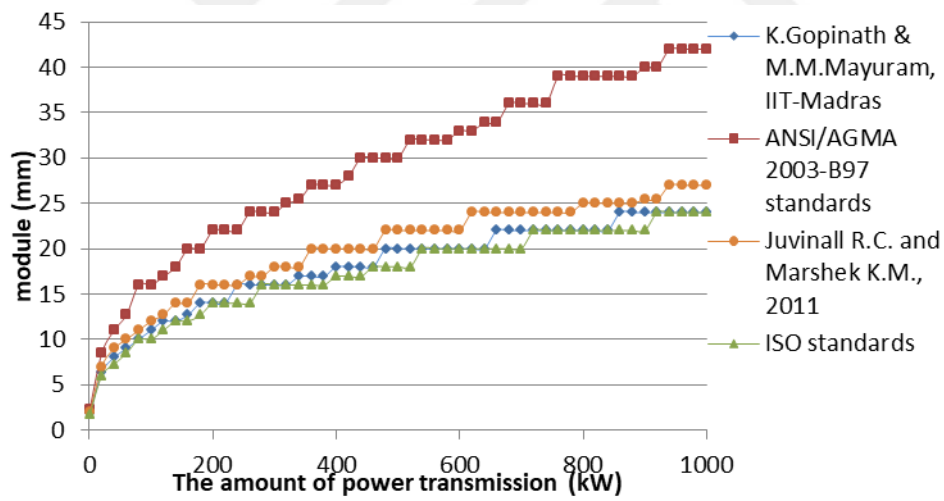
Figure 4.7. Module variation considering bending fatigue failure under
increasing power at 3:1 speed ratio (for Ø=20°, Material type 1)

105
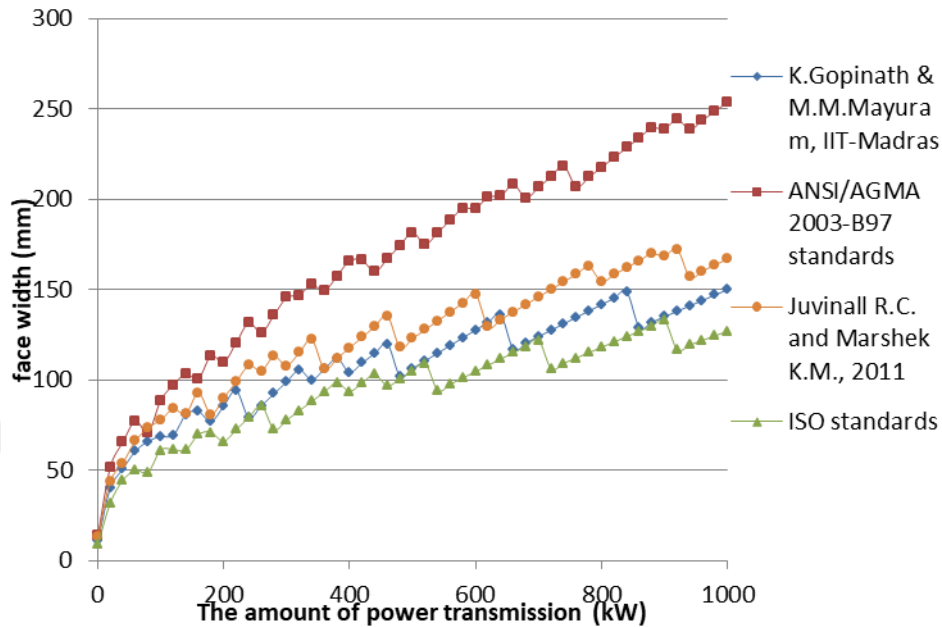
Figure 4.8. Face width variation considering bending fatigue failure under
increasing power at 3:1 speed ratio (for Ø=20°, Material type 1)

In these figures four different approaches and standards given by
ANSI/AGMA 2003-B97 standards, Fundamentals of Machine Component Design
5th Edition (Juvinall R.C., Marshek K.M., 2011), ISO Standards 10300-(Part 1-2-
3), 2001 and Machine Design II, K.Gopinath & M.M.Mayuram 4th Edition have
given the maximum results (module and face width). And grater module means
bigger gear size, more material usage, less cost effective design and etc.
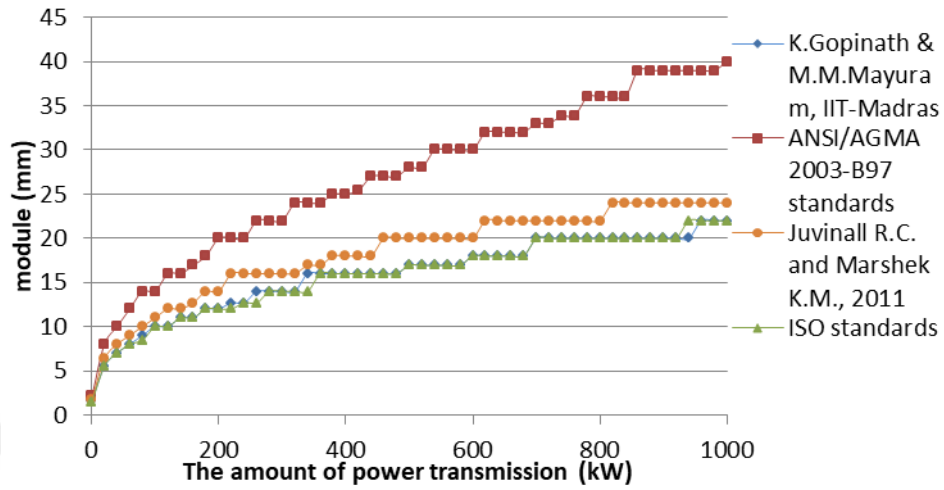
Figure 4.9. Module variation considering bending fatigue failure under
increasing power at 4:1 speed ratio (for Ø=20°, Material type 1)
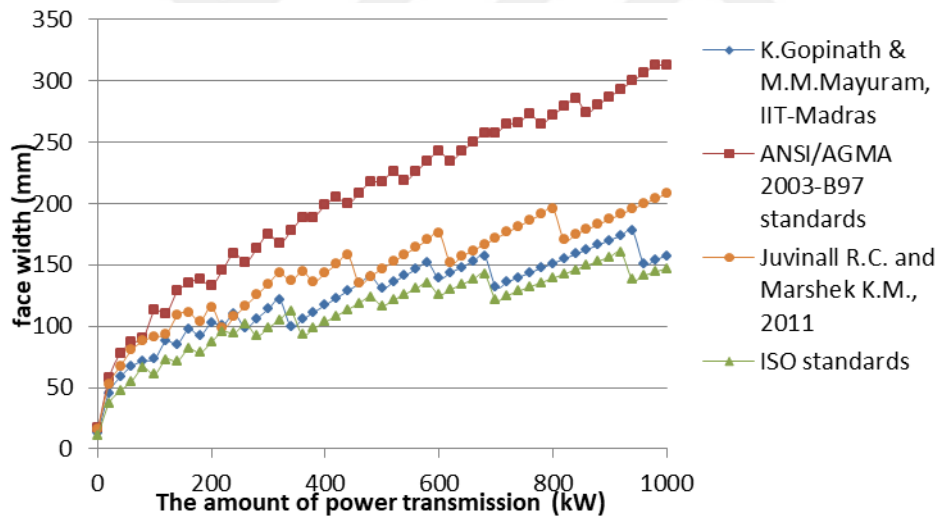
Figure 4.10. Face width variation considering bending fatigue failure under
increasing power at 4:1 speed ratio (for Ø=20°, Material type 1)

107
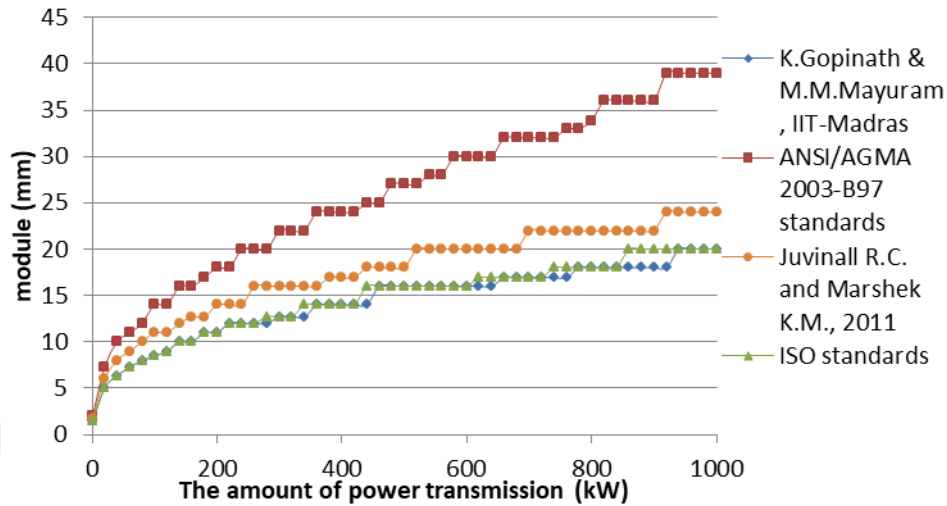
Figure 4.11. Module variation considering bending fatigue failure under
increasing power at 5:1 speed ratio (for Ø=20°, Material type 1)
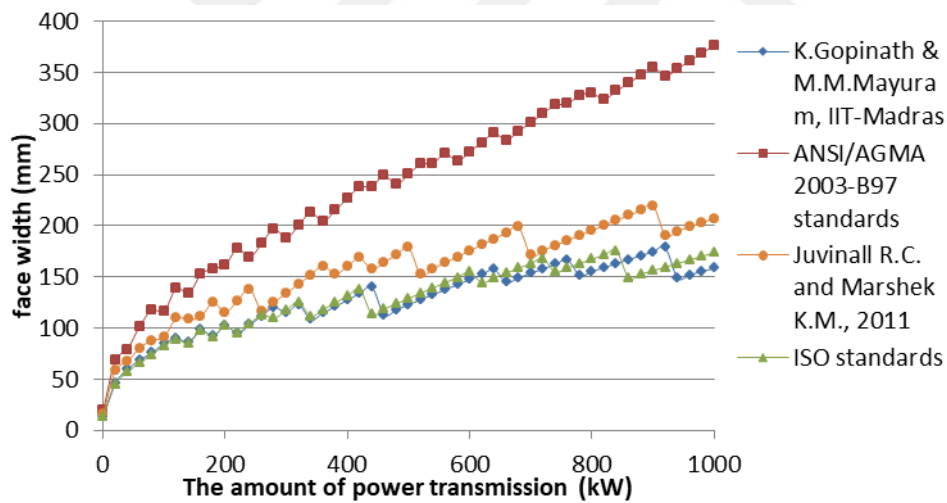
Figure 4.12. Face width variation considering bending fatigue failure under
increasing power at 5:1 speed ratio (for Ø=20°, Material type 1)

In Figure 4.7 also four different approaches and standards given by
ANSI/AGMA 2003-B97 standards, Fundamentals of Machine Component Design
5th Edition (Juvinall R.C., Marshek K.M., 2011), ISO Standards 10300-(Part 1-2-

3), 2001 and Machine Design II, K.Gopinath & M.M.Mayuram 4th Edition have given the same modules. And trend is the same as the before speed ratio. Because of that, a designer can select one of these approaches which provide ease of use.
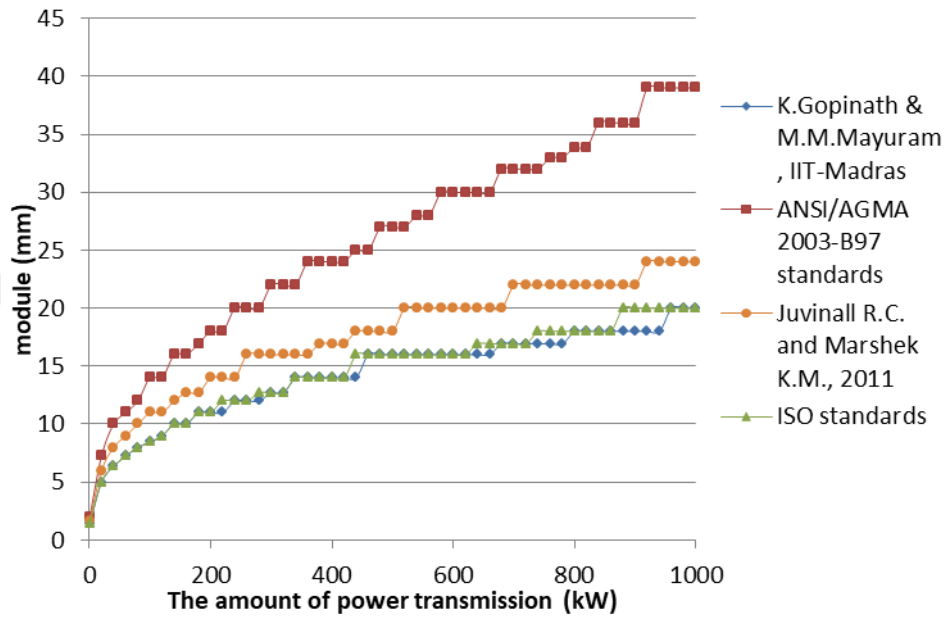
Figure 4.13. Module variation considering bending fatigue failure under increasing power at 6:1 speed ratio (for $\varnothing=20^{o}$, Material type 1)
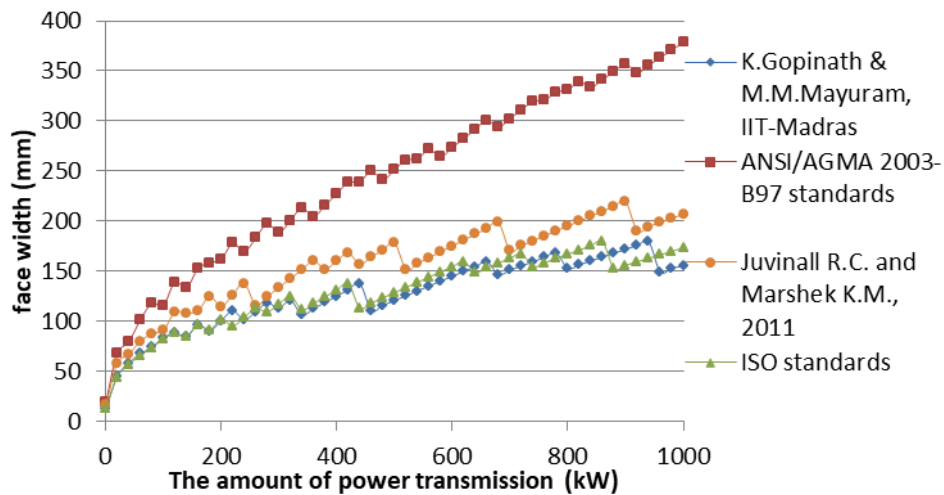
Figure 4.14. Face width variation considering bending fatigue failure under increasing power at 6:1 speed ratio (for $\varnothing=20^{o}$, Material type 1)

109
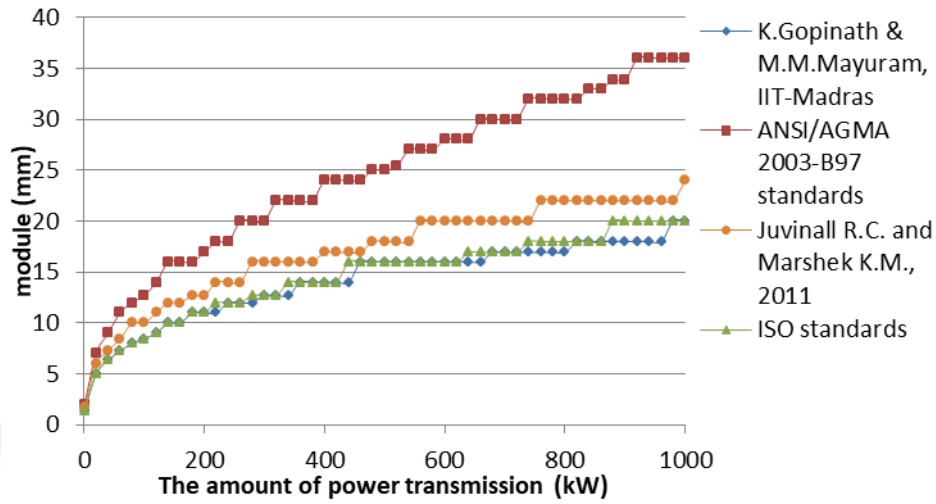
Figure 4.15. Module variation considering bending fatigue failure under
increasing power at 7:1 speed ratio (for Ø=20°, Material type 1)
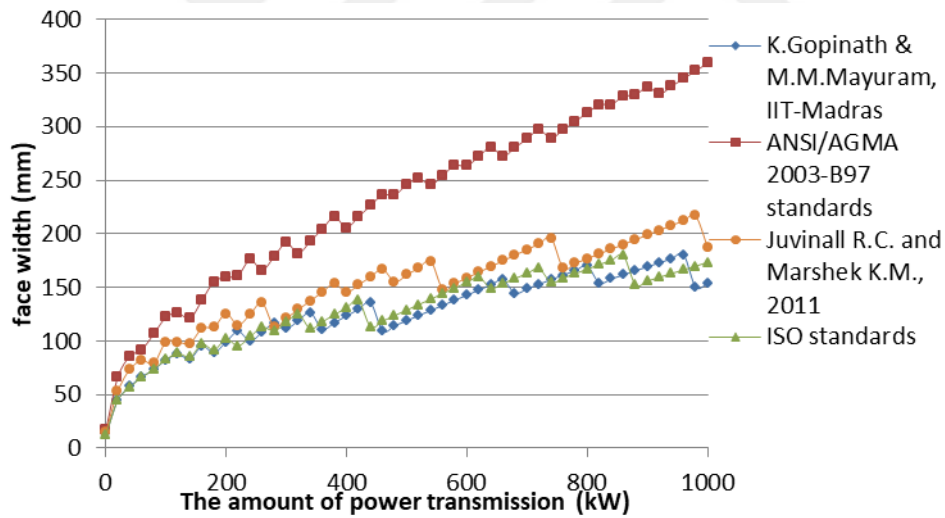
Figure 4.16. Face width variation considering bending fatigue failure under
increasing power at 7:1 speed ratio (for Ø=20°, Material type 1)
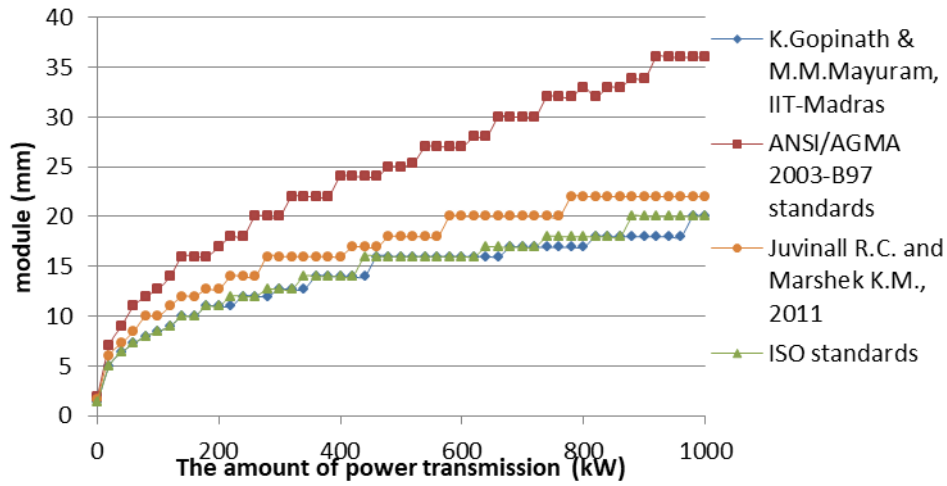
Figure 4.17. Module variation considering bending fatigue failure under
increasing power at 8:1 speed ratio (for Ø=20°, Material type 1)
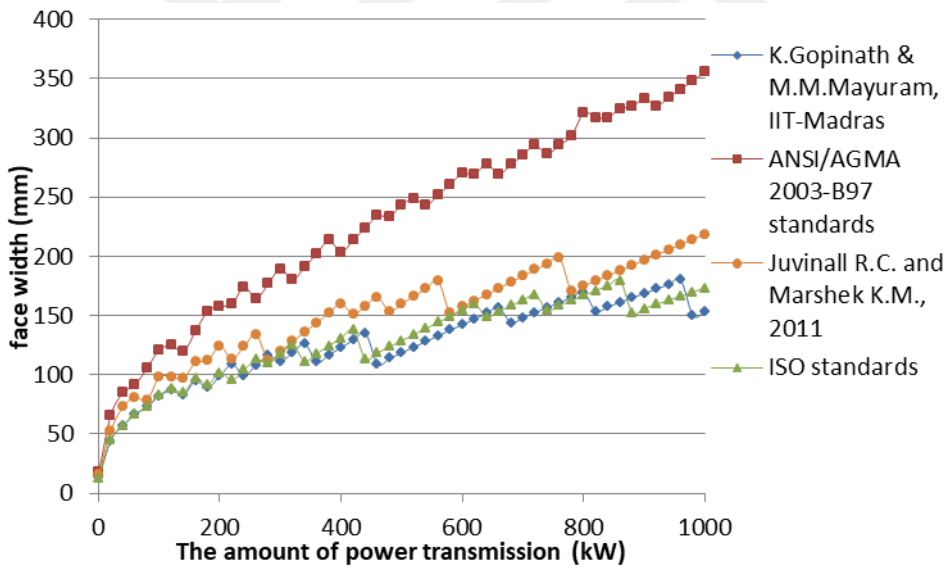
Figure 4.18. Face width variation considering bending fatigue failure under
increasing power at 8:1 speed ratio (for Ø=20°, Material type 1)

And the almost same trend has still been maintained in Figures 4.3 to 4.18.
In these igures, the maximum results have been given by ANSI/AGMA 2003-B97
standards.

111

These figures and tables have indicated that it is usually possible to mention similar trends considering the Tables from 4.26 to 4.33. Because when the modules are inversely normalized to ANSI/AGMA 2003-B97 standards, almost the same coefficients have been obtained for the selected speed ratios and power transmission ranges.

But there is another trend that can be seen between the approach of Juvinall R.C., Marshek K.M., 2011) and ANSI/AGMA 2003-B97 standards.

4.3.2. Comparison of Results Based on Surface Contact Fatigue Failure

The following figures and tables provide comparison of results based on surface contact fatigue failure for pressure angle of 20° and material type 1. Comparison of results between the designs approaches have been made considering the differences between modules.

Comparisons of results based on surface contact fatigue failure for pressure angle of 20° are given in the appendices;

➢ for material type 2, see Appendix F.1.
➢ for material type 3, see Appendix G.1.

Comparisons of results based on surface contact fatigue failure for pressure angle of 25° are given in the appendices;

➢ for material type 1, see Appendix H.1.
➢ for material type 2, see Appendix J.1.
➢ for material type 3, see Appendix K.1.
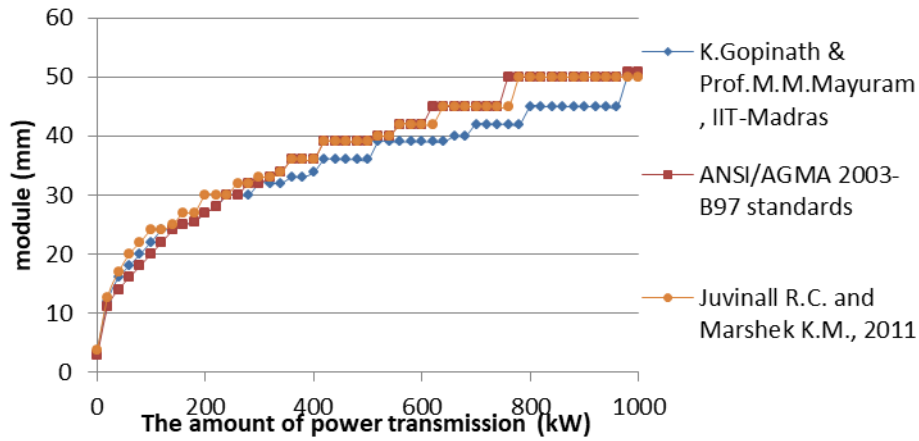
Figure 4.19. Module variation considering surface contact fatigue failure under increasing power at 1:1 speed ratio (for Ø=20°, Material type 1)
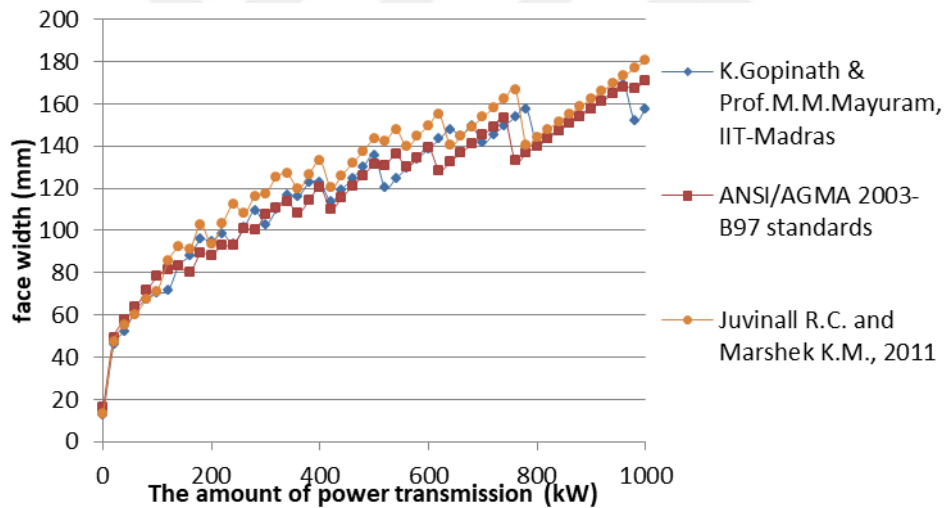
Figure 4.20. Face width variation considering surface contact fatigue failure under increasing power at 1:1 speed ratio (for Ø=20°, Material type 1)

For the design criteria of surface contact fatigue failure, Juvinall R.C., Marshek K.M., 2011) has given the maximum results at 1:1 speed ratio. And the minimum results are obtained by ANSI/AGMA 2003-B97 standards.

113
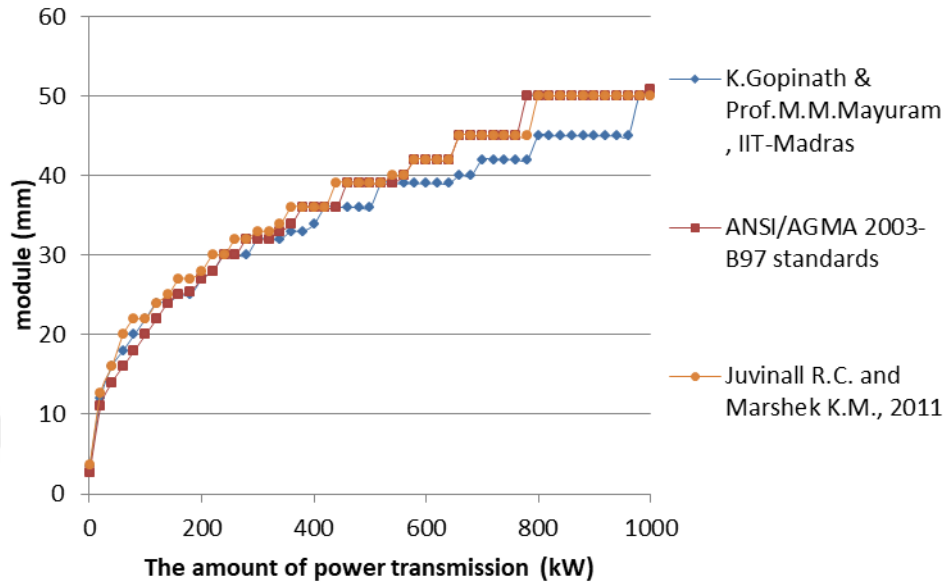
Figure 4.21. Module variation considering surface contact fatigue failure under increasing power at 2:1 speed ratio (for Ø=20°, Material type 1)
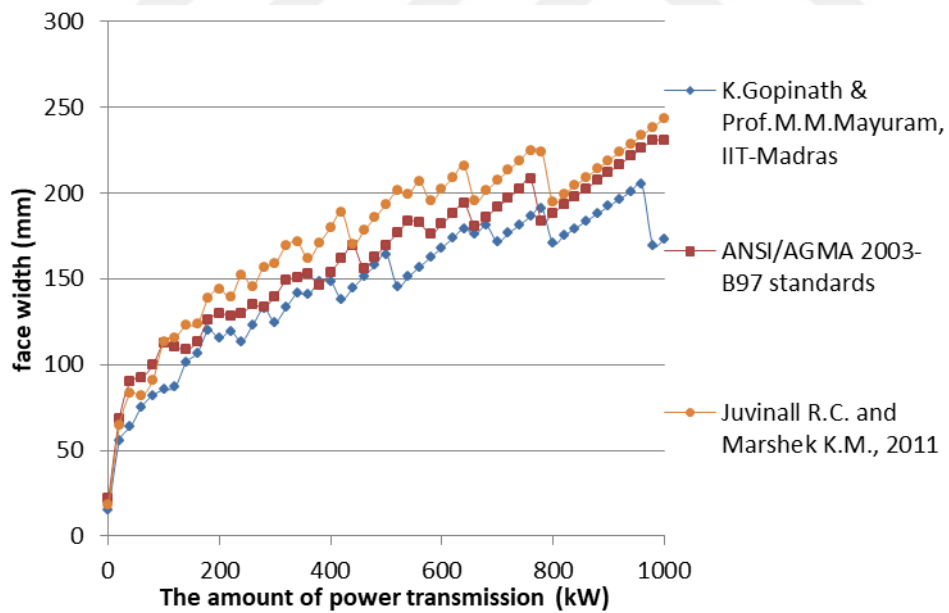
Figure 4.22. Face width variation considering surface contact fatigue failure under increasing power at 2:1 speed ratio (for Ø=20°, Material type 1)

114

It is also possible to mention about that similar trends prevail in these results, Figures 4.19 to 4.34.
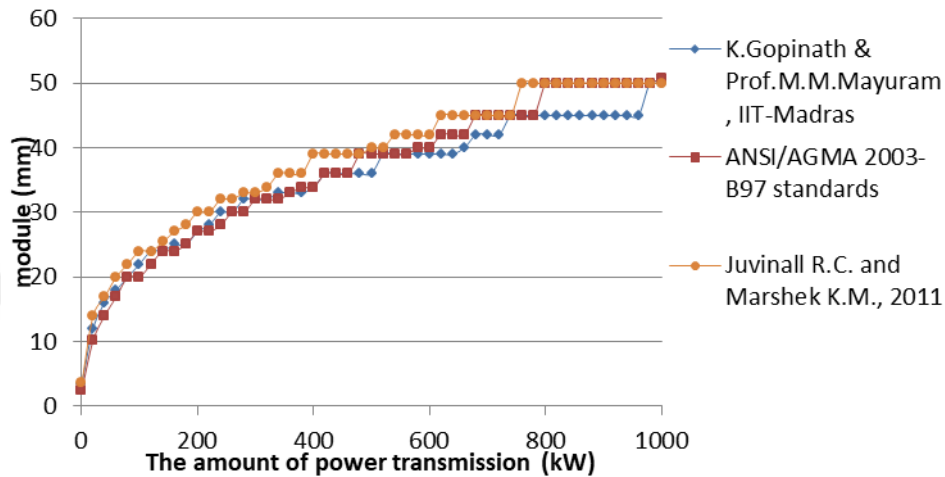
Figure 4.23. Module variation considering surface contact fatigue failure under increasing power at 3:1 speed ratio (for Ø=20°, Material type 1)
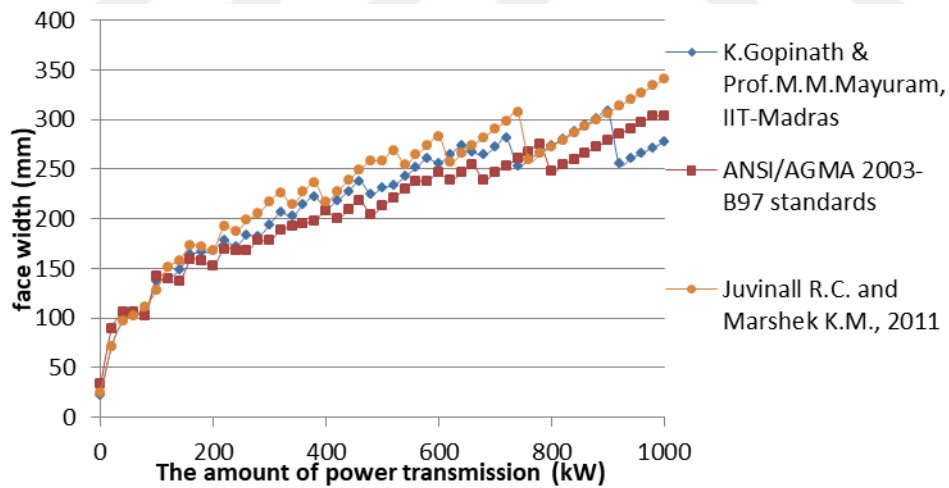
Figure 4.24. Face width variation considering surface contact fatigue failure under increasing power at 3:1 speed ratio (for Ø=20°, Material type 1)

115
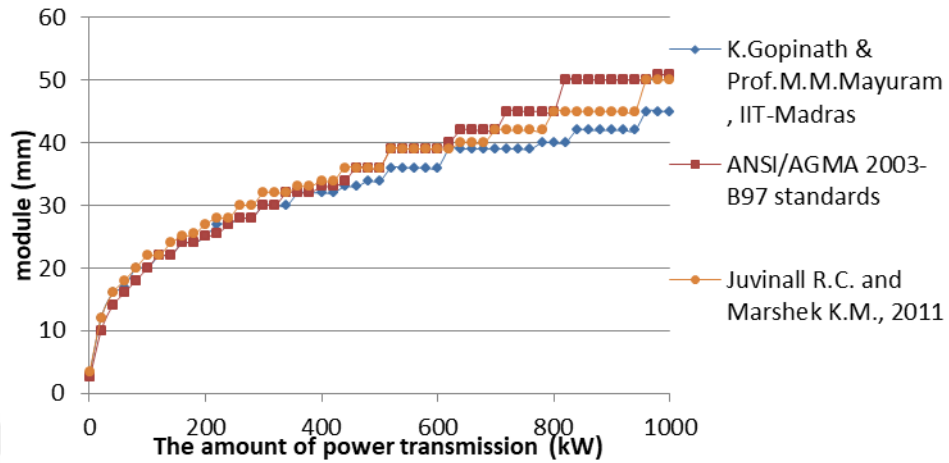
Figure 4.25. Module variation considering surface contact fatigue failure under increasing power at 4:1 speed ratio (for Ø=20°, Material type 1)
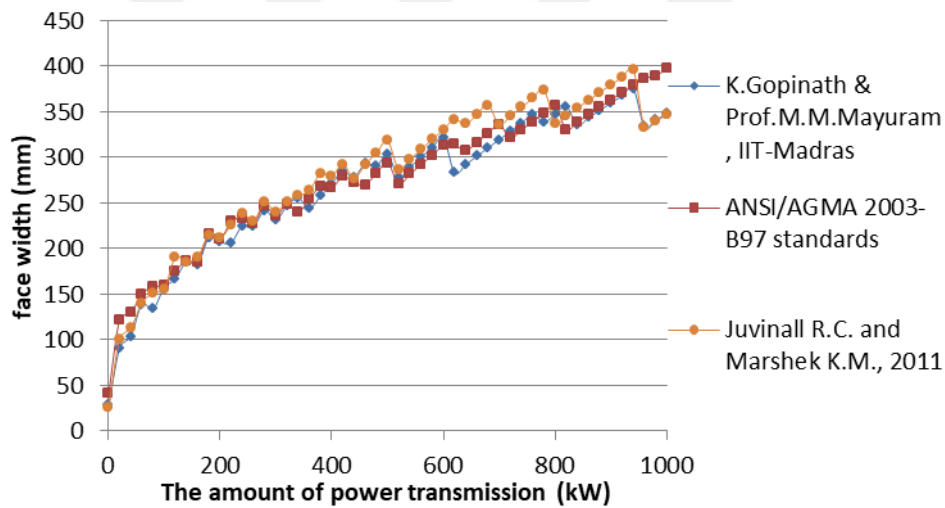
Figure 4.26. Face width variation considering surface contact fatigue failure under increasing power at 4:1 speed ratio (for Ø=20°, Material type 1)

116
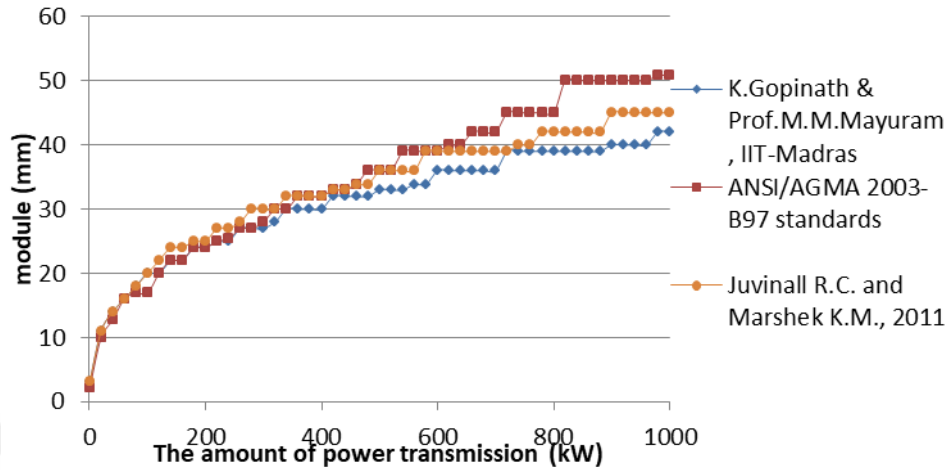
Figure 4.27. Module variation considering surface contact fatigue failure under increasing power at 5:1 speed ratio (for Ø=20°, Material type 1)
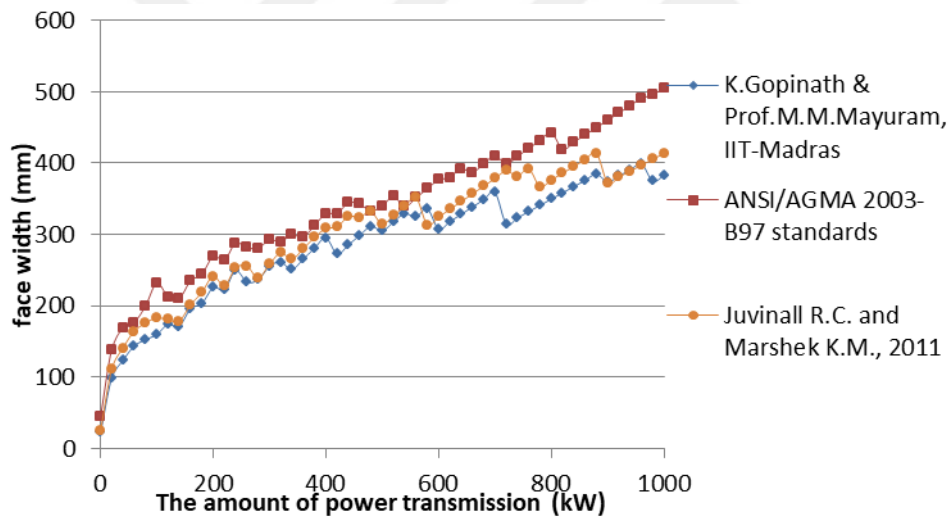
Figure 4.28. Face width variation considering surface contact fatigue failure under increasing power at 5:1 speed ratio (for Ø=20°, Material type 1)

117
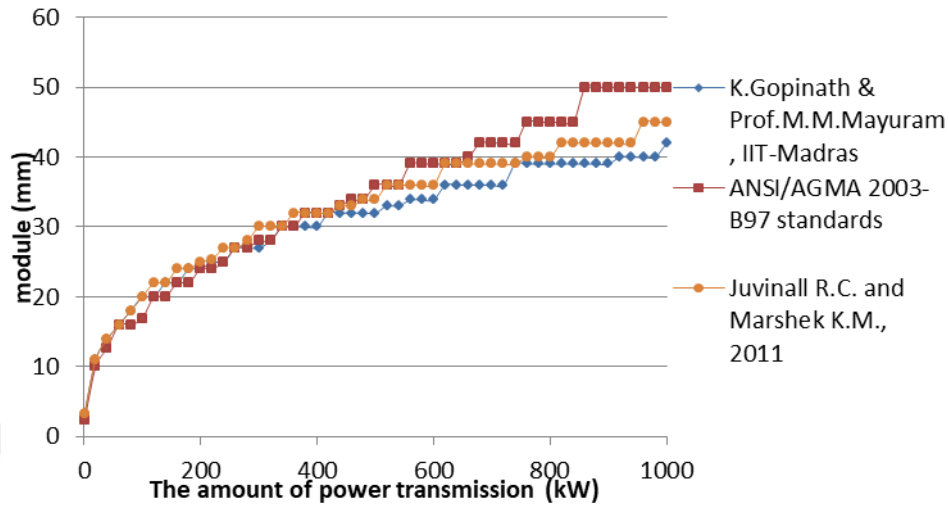
Figure 4.29. Module variation considering surface contact fatigue failure under increasing power at 6:1 speed ratio (for Ø=20°, Material type 1)
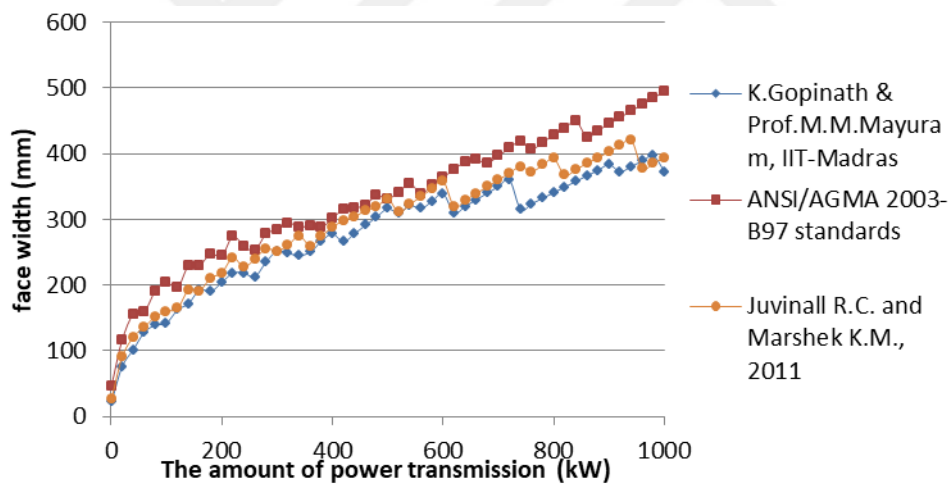
Figure 4.30. Face width variation considering surface contact fatigue failure under increasing power at 6:1 speed ratio (for Ø=20°, Material type 1)

118
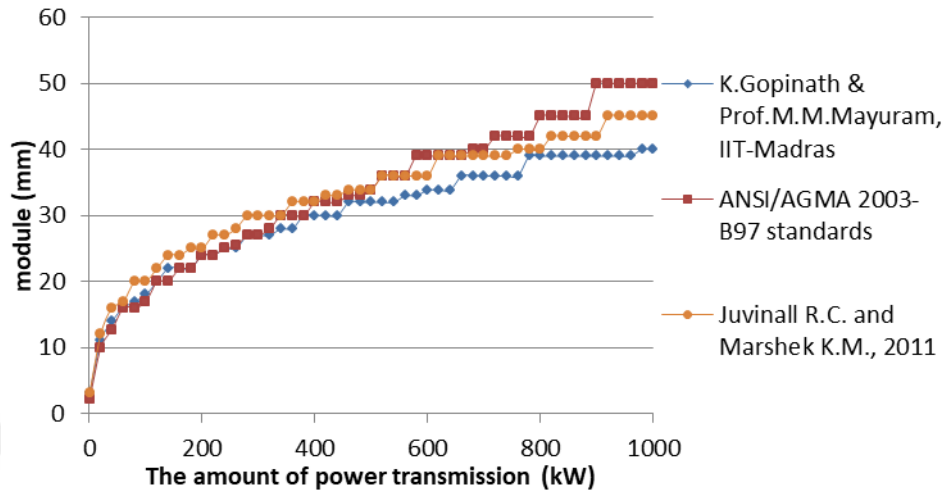
Figure 4.31. Module variation considering surface contact fatigue failure under increasing power at 7:1 speed ratio (for Ø=20°, Material type 1)
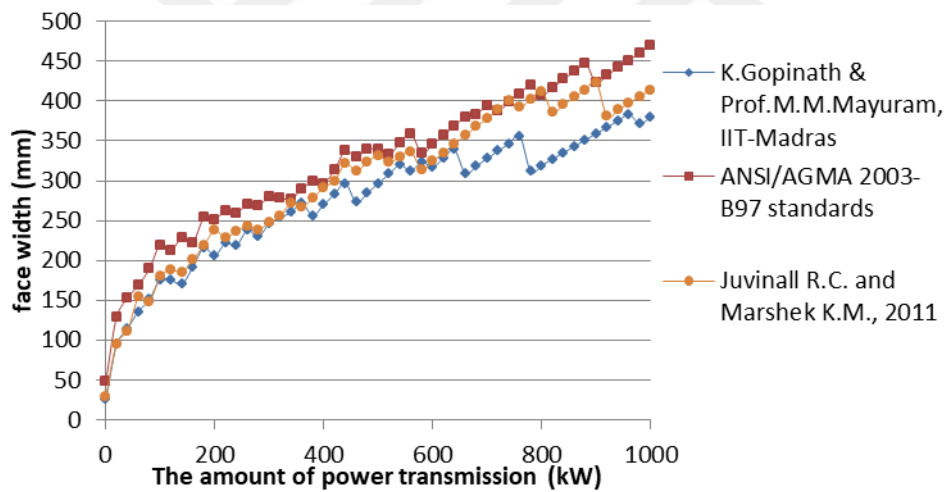
Figure 4.32. Face width variation considering surface contact fatigue failure under increasing power at 7:1 speed ratio (for Ø=20°, Material type 1)

119
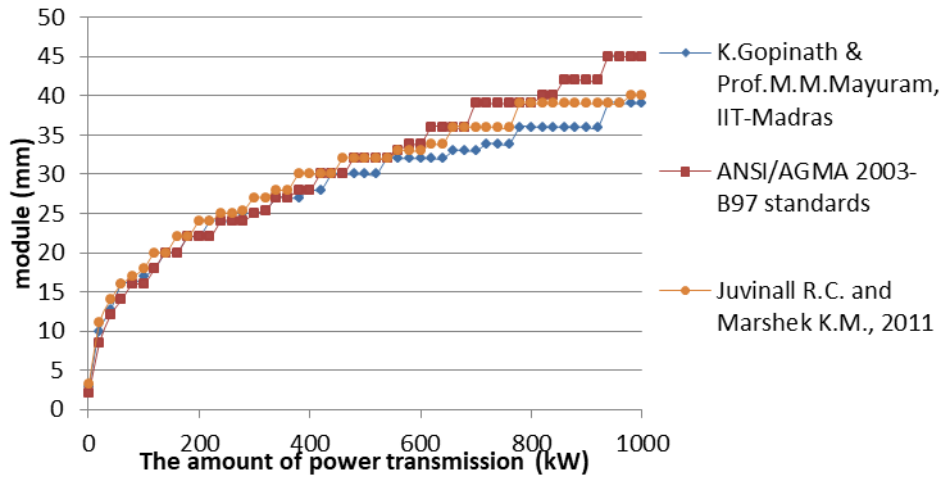
Figure 4.33.Module variation considering surface contact fatigue failure under increasing power at 8:1 speed ratio (for Ø=20°, Material type 1)
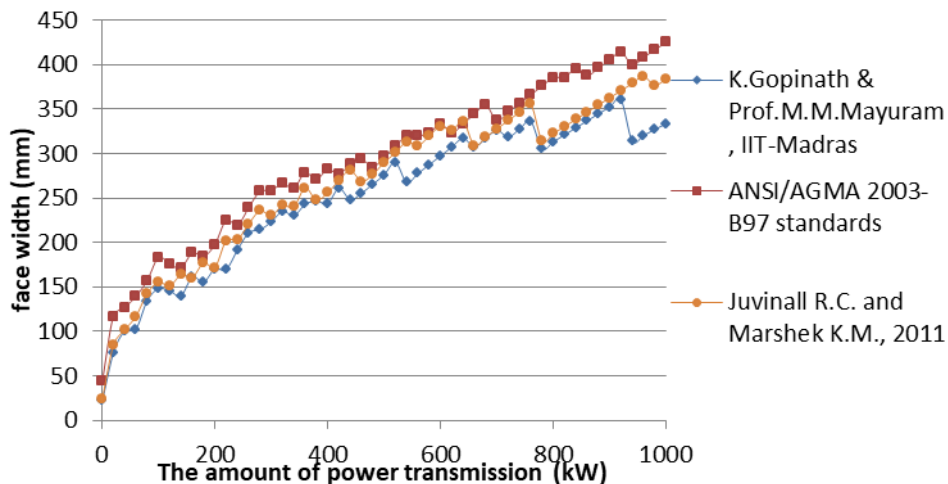
Figure 4.34. Face width variation considering surface contact fatigue failure under increasing power at 8:1 speed ratio (for Ø=20°, Material type 1)

When the curves are analysed, nearly the same trends are obtained at power transmission ratios of 0,5 kW and 10 kW. And it is seen that the general trend is similar for all range of gear speed ratios. But, the design approaches provided different trends above 100 kW of the transmitted power. This is because of the varying design variables and inherited features of each of design approaches.

120

4.4. Comparison of Results Considering Speed Ratio

Speed ratio can be affected by the tooth addendum, the pressure angle, the tooth size and to simplify the analysis, the torque and other parameters were held the center distance. For low-speed-ratio gears (speed ratio less than 2.0), increasing the speed ratio reduced the gear dynamic load. For high-speed-ratio gears (speed ratio equal to or greater than 2.0), the selection of speed ratio should be taken into consideration the intended operating speeds. In general, high-speed-ratio gears minimized dynamic load better than low-speed-ratio gears. (NASA, Technical Memorandum, Chuen-Huei Liou and Hsiang Hsi Lin and Fred B. Oswald and Dennis P. Townsend)

Speed ratio also affects the number of teeth on gear when meshing with a pinion. As it is shown by tables in Section 4.2, the selection of proper module for an involute bevel gear decreases if the gear speed ratio is desired to be higher. This is because of the number of teeth on gear increases which is in a mesh while running with a pinion. Thus gear stresses decreases and the module can be selected smaller for a better design.

The effect of speed ratio on the selection of module has varied for the design approaches too. At a certain amount of power transmission, comparison of module selections is given on bar charts. The charts of Figure 4.35 to 4.39 were obtained for the bending fatigue failure criterion. The charts of Figure 4.40 to 4.44 were obtained for surface contact fatigue failure criteria.

4.4.1. Comparison of Results Based on Bending Fatigue Failure

Straight bevel gears can operate under high speeds and high loads. Their precision rating is fair to good. They are suitable for 1:1 and higher velocity ratios and for right-angle meshes to any other angles. When straight bevel gears are designed according to bending fatigue failure it is seen that the differences between the design approaches are larger at a speed ratio of 1:1 for the selected power transmission ranges. When the speed ratio decreases these differences are getting bigger, and the results given by the design approaches are getting farther to each other. When the speed ratio increases these differences are getting smaller, and the

121

results given by the design approaches are getting closer to each other. Comparison of results are shown in following figures below based on bending fatigue failure for pressure angle of 20° and material type 1.
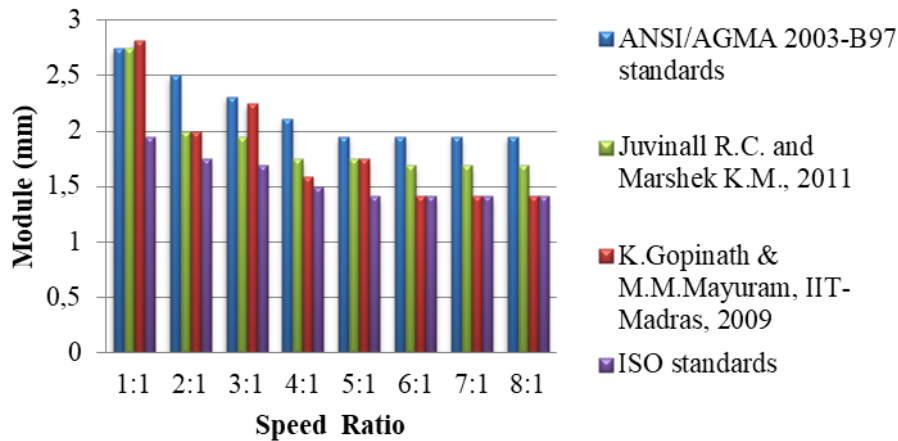
Figure 4.35. The effect of speed ratio on module selection based on bending fatigue failure at 0,5 kW power transmission (for Ø=20°, Material type 1)
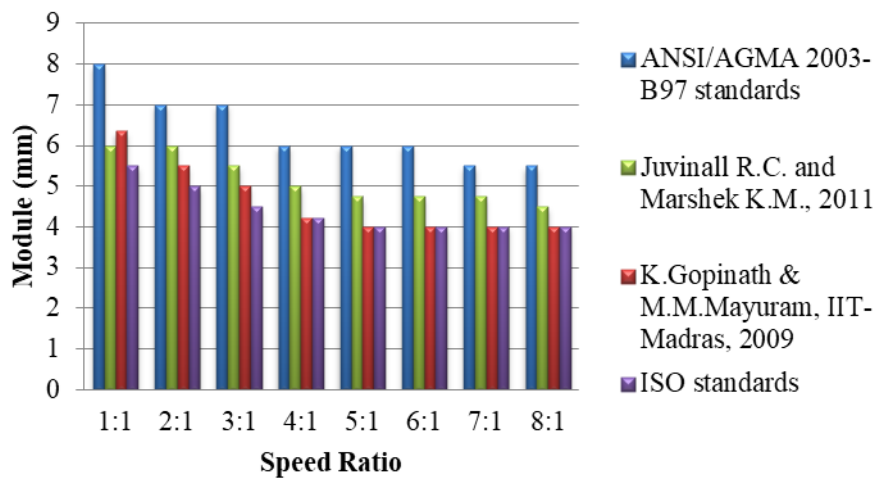
Figure 4.36. The effect of speed ratio on module selection based on bending fatigue failure at 10 kW power transmission (for Ø=20°, Material type 1)
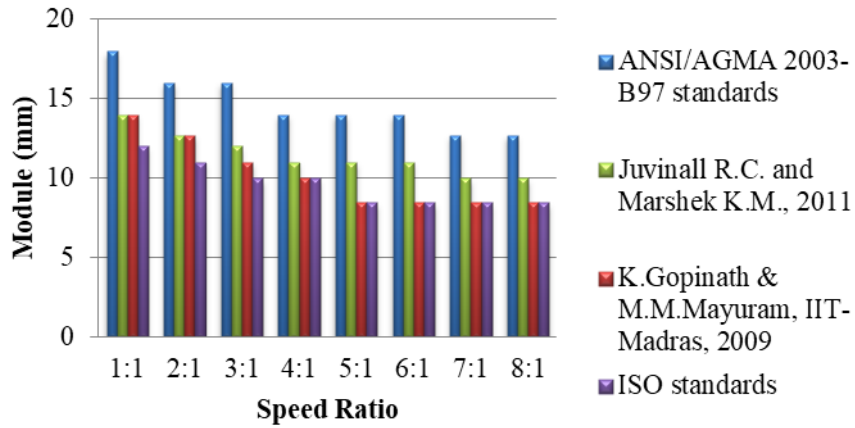
Figure 4.37. The effect of speed ratio on module selection based on bending fatigue failure at 100 kW power transmission (for Ø=20°, Material type 1)
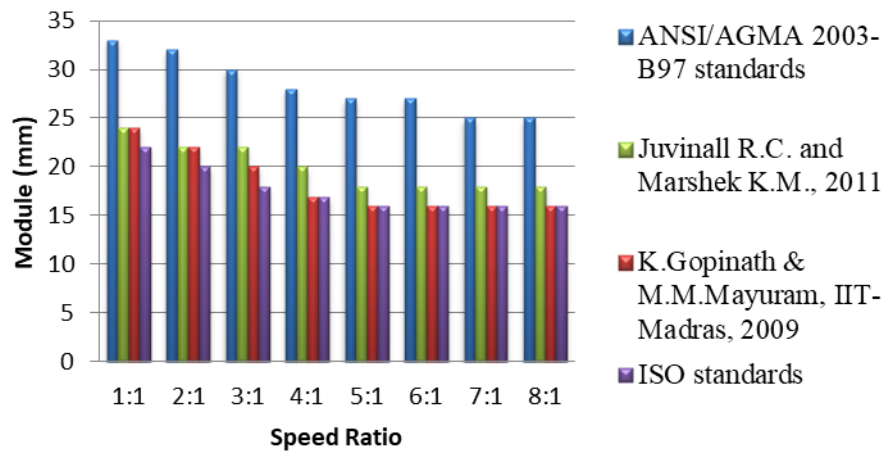
Figure 4.38. The effect of speed ratio on module selection based on bending fatigue failure at 500 kW power transmission (for Ø=20°, Material type 1)

123
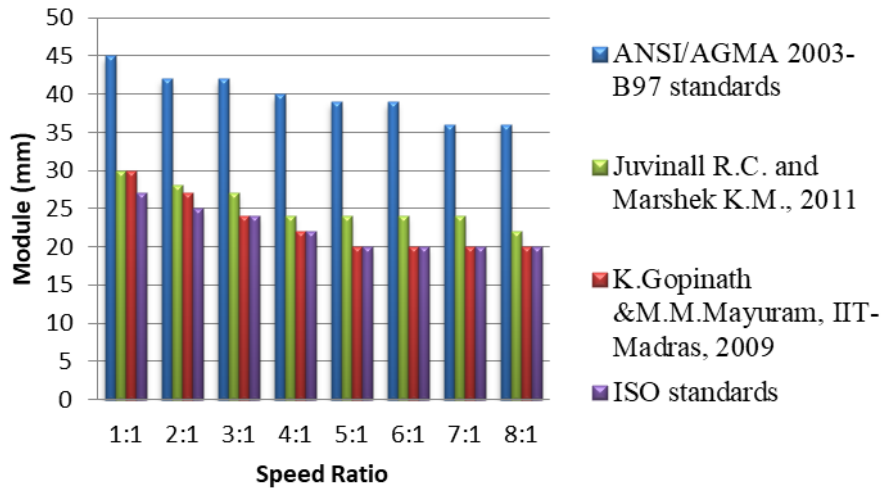
Figure 4.39. The effect of speed ratio on module selection based on bending fatigue failure at 1000 kW power transmission (for Ø=20°, Material type 1)

When all above diagrams are examined, the general trend is that modules decrease for almost all power transmission ranges as the speed ratio increases. And when power increases for almost all approaches module increases, too.

Comparison of the results based on bending fatigue failure considering speed ratio for the selected power transmissions for pressure angle of 20° are given in the appendices;

➢ for material type 2, see Appendix A.2.
➢ for material type 3, see Appendix B.2.

Comparison of the results based on bending fatigue failure considering speed ratio for the selected power transmissions for pressure angle of 25° are given in the appendices;

➢ for material type 1, see Appendix C.2.
➢ for material type 2, see Appendix D.2.
➢ for material type 3, see Appendix E.2.

124

4.4.2. Comparison of Results Based on Surface Contact Fatigue Failure

When straight bevel gears are designed based on surface contact fatigue, the design factor of safety is applied to tangential force by its square except the design approach given by ANSI/AGMA 2003-B97 standards. As a result of this, ANSI/AGMA 2003-B97 standards gear design approach gives the lowest module selection when compared to another type of design approaches as shown in figures below. But in this case, the differences between the design approaches have become greater. Comparison of results are shown in following figures below based on surface contact fatigue failure for pressure angle of 20° and material type 1.
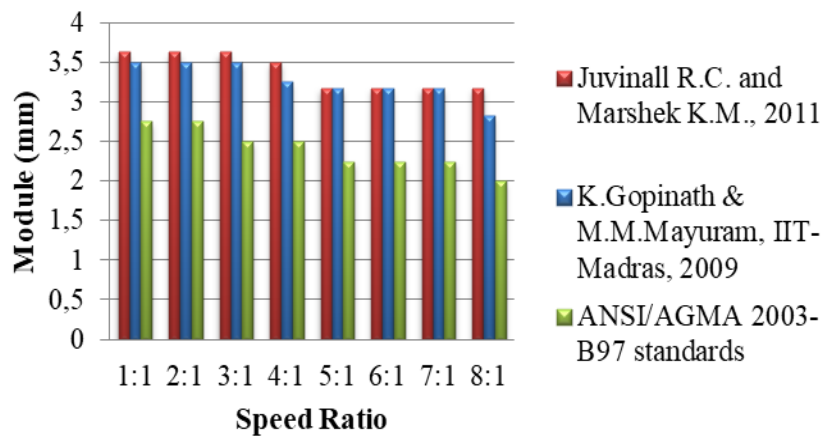
Figure 4.40. The effect of speed ratio on module selection based on surface contact fatigue failure at 0,5 kW power transmission (for Ø=20°, Material type 1)
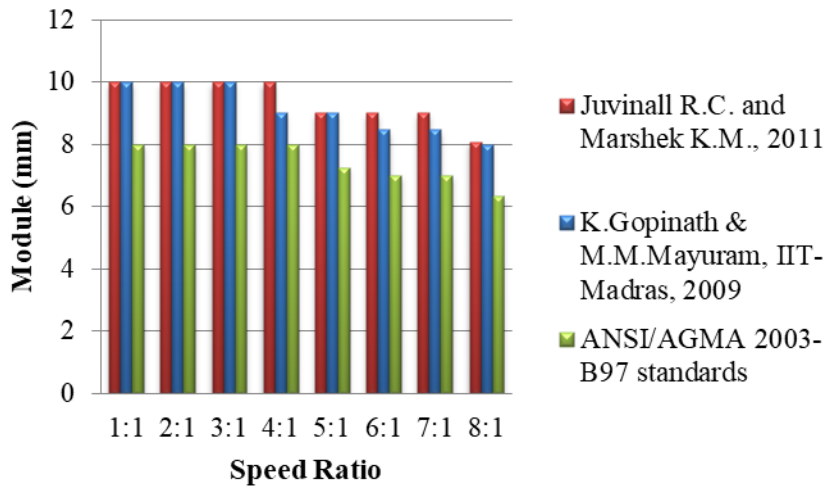
Figure 4.41. The effect of speed ratio on module selection based on surface contact fatigue failure at 10 kW power transmission (for Ø=20°, Material type 1)
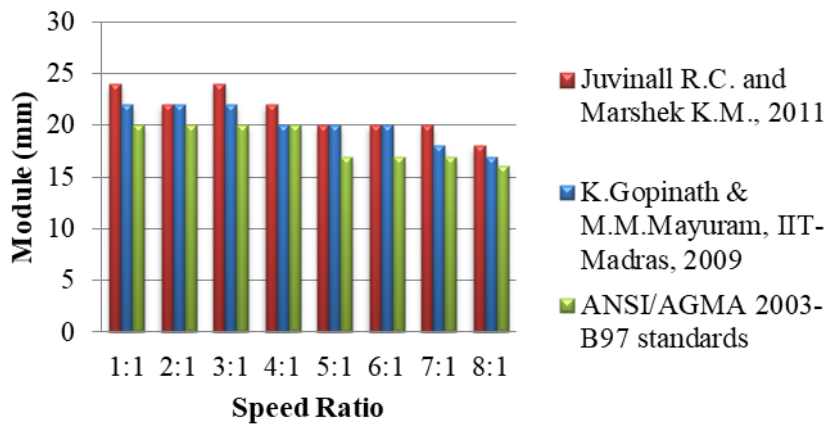
Figure 4.42. The effect of speed ratio on module selection based on surface contact fatigue failure at 100 kW power transmission (for Ø=20°, Material type 1)
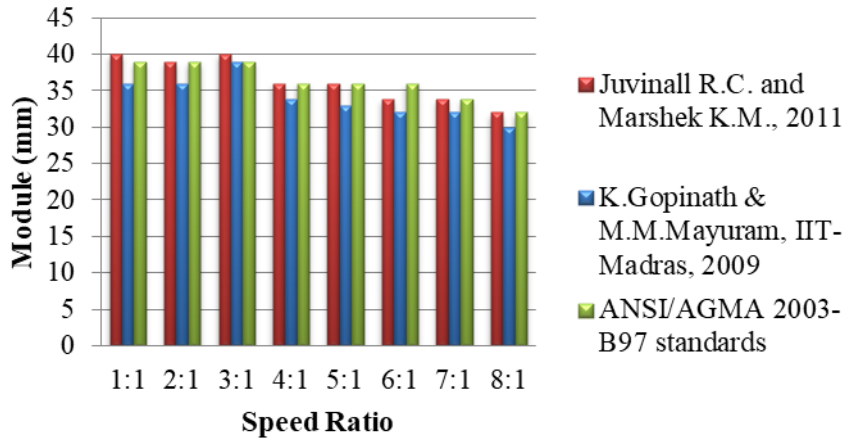
Figure 4.43. The effect of speed ratio on module selection based on surface contact fatigue failure at 500 kW power transmission (for Ø=20°, Material type 1)
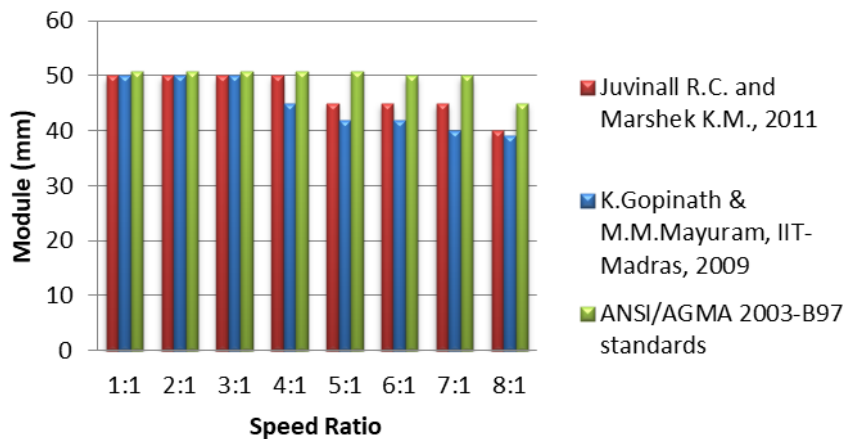
Figure 4.44. The effect of speed ratio on module selection based on surface contact fatigue failure at 1000 kW power transmission (for Ø=20°,Material type 1)

As a result, when designing the gear based on surface contact fatigue failure, it is possible to mention a general trend for the design approaches. In here, the trends between design approaches are different and the results are not converging between each other. Another trend is also was found to exist for all the speed ratios in all the selected power ranges.

127

The trend is that all the gear design approaches were found to be in the same way (except for the power of 1 kW). The gear design approaches were ranked for the increasing modules as in approaches of;

1. K.Gopinath & M.M.Mayuram,2009
2. Juvinall R.C., Marshek K.M., 2011
3. ANSI/AGMA 2003-B97 standards
4. ISO Standards 10300-(Part 1-2-3), 2001

Comparison of the results based on surface contact fatigue failure considering speed ratio for the selected power transmissions for pressure angle of 20° are given in the appendices;

➢ for material type 2, see Appendix F.2.
➢ for material type 3, see Appendix G.2.

Comparison of the results based on surface contact fatigue failure considering speed ratio for the selected power transmissions for pressure angle of 25° are given in the appendices;

➢ for material type 1, see Appendix H.2.
➢ for material type 2, see Appendix J.2.
➢ for material type 3, see Appendix K.2.

4.5. Comparison of Gear Stress by Using a Finite Element Method (FEM)

Using the FEM was mentioned in Section 3.4. Now, in here the creation of a geometrical form of a bevel gear and the setup of analysis problem has been indicated in figures respectively. Figure 4.45 shows the creation of a gear by using

128

an involute curve; represents the involute curve of a bevel gear that is created considering the module, number of teeth and pressure angle, and are the formation of gear tooth profile, is the 2D model of an involute bevel gear and is the 3D model of an involute bevel gear that is analysed in ANSYS Workbench 16.1.
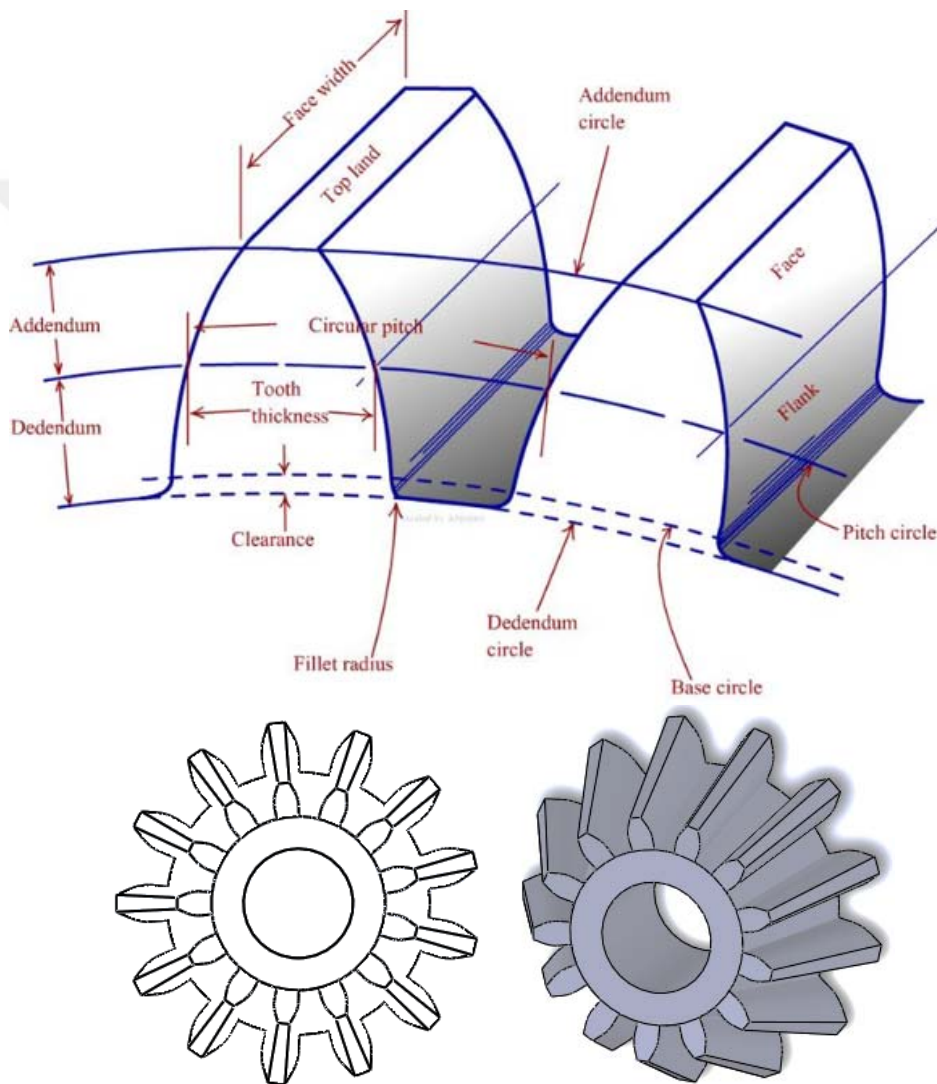
Figure 4.45.Generating an involute bevel gear by using the design parameters

129

After the geometry was created it was transferred to ANSYS as a file format of "Standard for the Exchange of Product" (STP). And then material properties mentioned in Table 3.1 were defined in the window of engineering data in ANSYS Workbench 16.1. Boundary conditions for the structure of bevel gear were defined as pinion that is taken to tangential load to the pitch diameter along its axis with frictionless support as seen in Figure 4.46. In this figure, (a) shows the mesh elements, which is the subject of pre-processing in ANSYS Workbench 16.1. Figure 4.46 (b) shows the boundary conditions, and the tangential load is applied along the pitch line as represented in (c) and in (d) shows the post-processing in which the results are obtained.
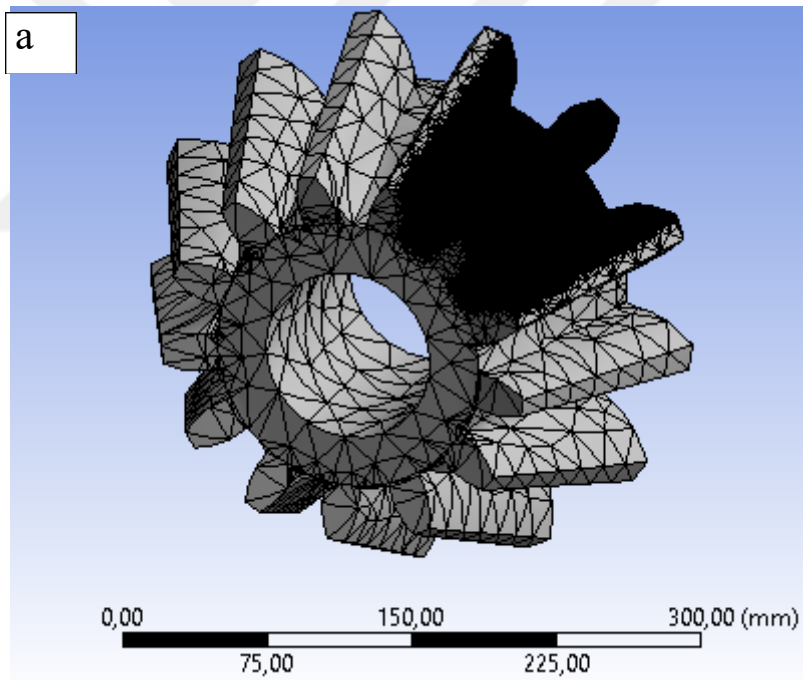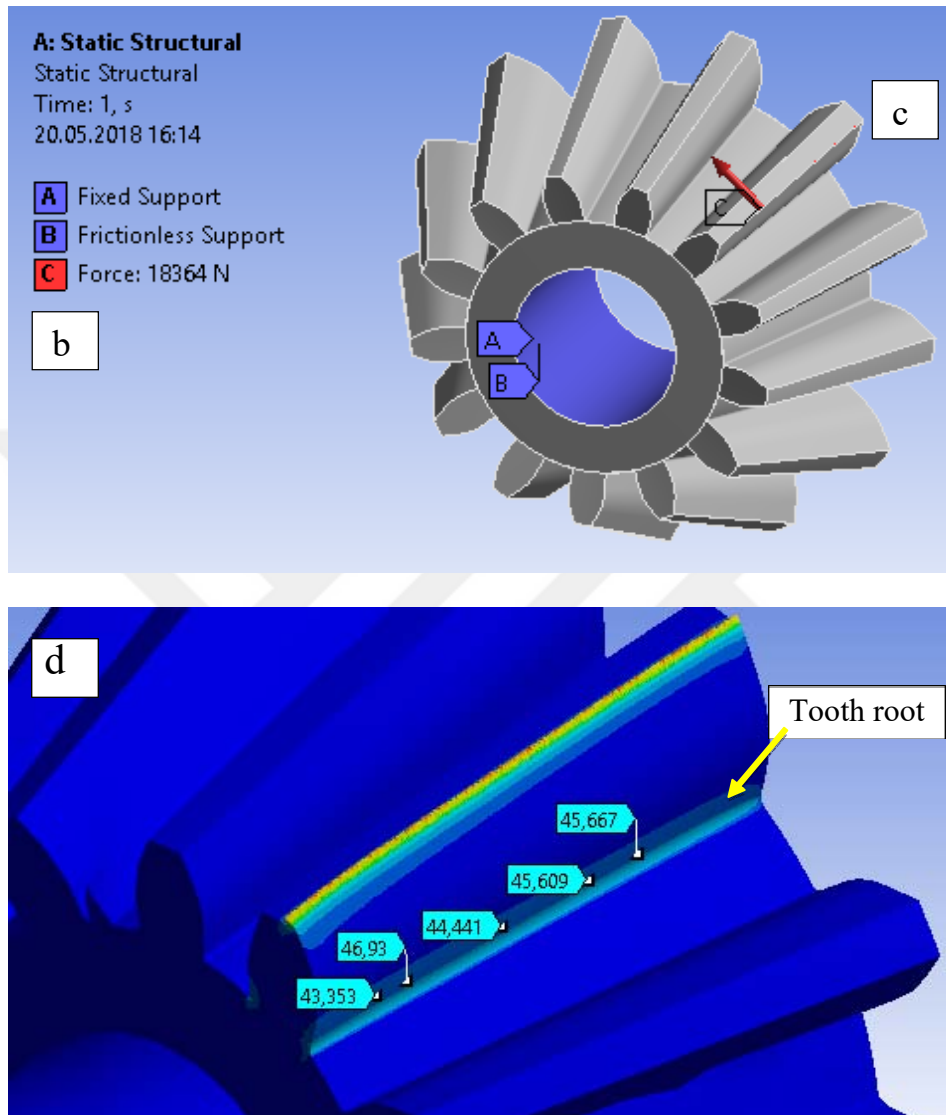
Figure 4.46. Pre-processing, solver and post-processing steps in ANSYS
           Workbench 16.1

By using the final design results, m and F, gear bending stress has been determined numerically on the software of ANSYS Workbench 16.1. Bevel gears were modelled for the design approaches using the same design input parameters. According to ANSI/AGMA 2003-B97 standards, Ansys results are shown in

131

Figure 4.47. And then the results of finite element analysis (FEA) have been given comparatively with theoretical results in Table 4.3.
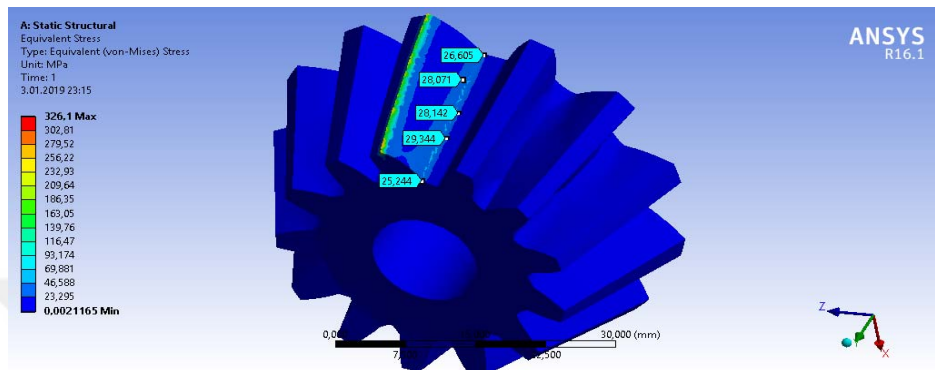
Figure 4.47. ANSYS Results according to ANSI/AGMA 2003-B97 standards

Table 4.3. Comparison of bending stresses according to ANSI/AGMA 2003-
B97 standards obtained from the theoretical approaches and a
numerical (FEA) method for pressure angle of 20° and material type 1

ANSI/AGMA 2003-B97 standards				
Power, Kw	Module, mm	Theoretical Bending Stress	Numerical Bending Stress	% Difference
1	3,175	27,08295039	28,2584	4,34
50	12	27,08295039	27,7688	2,53
200	22	27,08295039	29,8846	10,34
600	33	27,08295039	27,7086	2,31
1000	42	27,08295039	24,876	-8,15

According to Juvinall R.C., Marshek K.M., 2011, Ansys results are shown in Figure 4.48. And then the results of finite element analysis (FEA) have been given comparatively with theoretical results in Table 4.4.
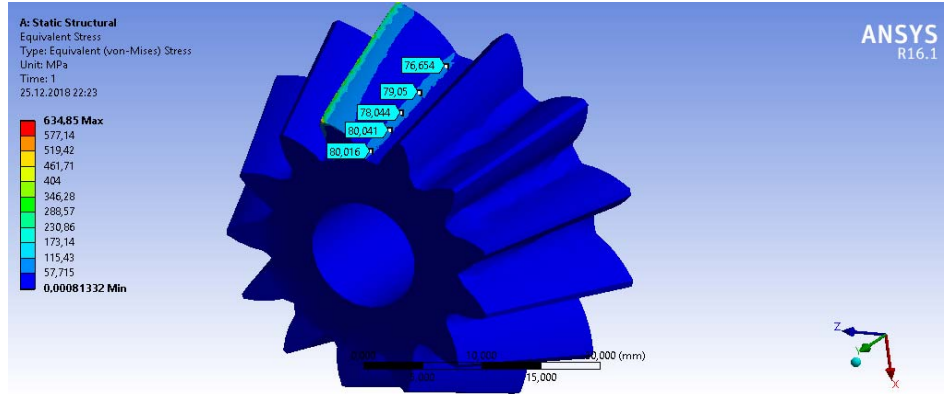
Figure 4.48. ANSYS Results according to Juvinall R.C., Marshek K.M., 2011

Table 4.4. Comparison of bending stresses according to Juvinall R.C., Marshek
         K.M., 2011 obtained from the theoretical approaches and a numerical
         (FEA) method for pressure angle of 20° and material type 1

Juvinall R.C., Marshek K.M., 2011				
Power, Kw	Module, mm	Theoretical Bending Stress	Numerical Bending Stress	% Difference
1	2,5	80,3719928	86,746	7,93
50	10	80,3719928	91,503	13,85
200	16	80,3719928	75,473	-6,10
600	22	80,3719928	77,216	-3,93
1000	27	80,3719928	85,613	6,52

According to K.Gopinath & M.M.Mayuram, 2009, Ansys results are shown in Figure 4.49. And then the results of finite element analysis (FEA) have been given comparatively with theoretical results in Table 4.5.
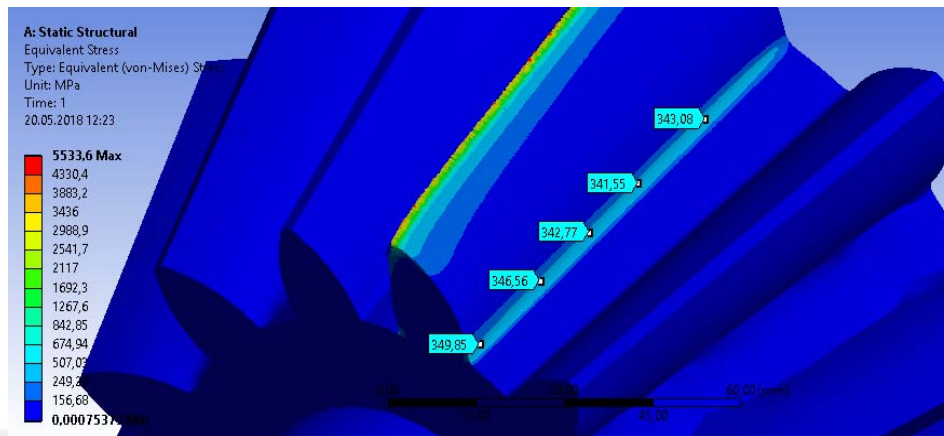
Figure 4.49. ANSYS Results according to K.Gopinath& M.M.Mayuram, 2009

Table 4.5. Comparison of bending stresses according to K.Gopinath & M.M.Mayuram, 2009 obtained from the theoretical approaches and a numerical (FEA) method for pressure angle of 20° and material type 1

K.Gopinath & M.M.Mayuram,2009				
Power, Kw	Module, mm	Theoretical Bending Stress	Numerical Bending Stress	% Difference
1	2,25	88,010011245	82,329	-6,45
50	8,4667	88,010011245	96,842	10,04
200	14	88,010011245	84,699	-3,76
600	20	88,010011245	86,001	-2,28
1000	24	88,010011245	83,416	-5,22

According to ISO Standards, Ansys results are shown in Figure 4.50. And then the results of finite element analysis (FEA) have been given comparatively with theoretical results in Table 4.6.

134
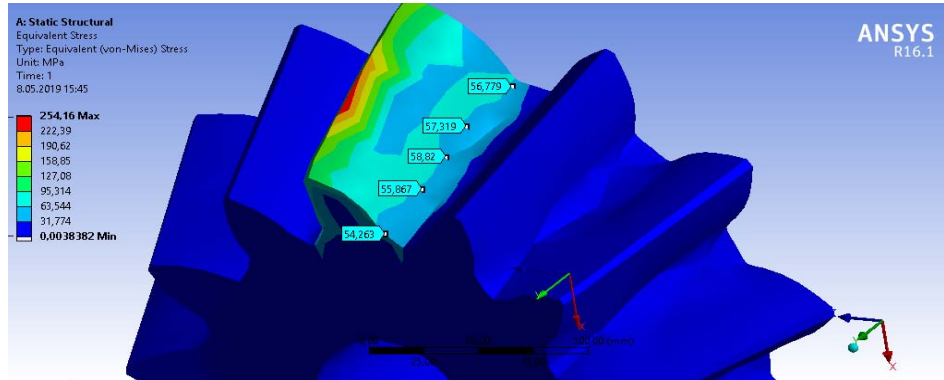
Figure 4.50. ANSYS Results according to ISO Standards

Table 4.6. Comparison of bending stresses according to ISO Standards obtained
        from the theoretical approaches and a numerical (FEA) method for
        pressure angle of 20° and material type 1

ISO Standards				
Power, Kw	Module, mm	Theoratical Bending Stress	Numerical Bending Stress	% Difference
1	2,1167	80,0792	83,315	4,04
50	8	70,80452	72,46	-2,34
200	14	64,81055	60,8	6,19
600	20	60,04684	64,548	-7,50
1000	24	57,26277	54,263	5,24

Table 4.3, 4.4, 4.5 and 4.6 have shown that the design approach given the four approaches have given the closest results when we compare to the theoretical approaches and a numerical (FEA) method. Comparison of bending stresses obtained from the four theoretical approaches and numerical (FEA) method for pressure angle 25° and material 1 ise given in Table 4.7.

135

Table 4.7. Comparison of bending stresses obtained from the four theoretical approaches and numerical (FEA) method for pressure angle 25º and material 1.

Results for Bending Stress (for 1 kW)				
Design Approaches	Juvinall R.C., Marshek K.M., 2011	K.Gopinath & M.M.Mayuram ,2009	ISO Standards 10300-(Part 1-2-3), 2001	ANSI/AGMA 2003-B97 Standards
Module (mm)	2,500	2,500	2,117	2,822
Diametral pitch (mm)	0,400	0,400	0,472	0,354
Face Width (mm)	14,232	14,471	12,236	17,173
Number of Pinion	13	13	13	13
Force (kN)	489,708	480,758	578	433,799
Theoratical (MPa)	80,372	88,010	80,079	27,083
Numerical (MPa)	85,228	90,965	75,483	29,289
Difference (%)	-6,04	-3,36	5,74	-8,15

4.6. Comparison of Combined Module and Face width for Design Approaches

In this section, it is seen the combination of module and face width is given altogether. Because both face width and module have to be taken into consideration for making a geometrical optimization. Thus it is going to be very useful to see all effect of both face width and module on the gear design results. For this, mxF results are combined to obtain a more like a geometrical value.

The results (m, F) of ANSI/AGMA 2003-B97 standards have been taken as a reference because the most reliable solution is obtained by FEA. And now, the following ratio has been defined to compare the results of design approaches;

$$GRi = \frac{m_i \times F_i}{m_0 \times F_0}$$

(3.80)

Where m_i and F_i are the module and face width obtained for the target gear design approach respectively, and where m_0 and F_0 are the module and face width obtained from ANSI/AGMA 2003-B97 standards respectively.

The ratio results to indicate the most or worst design. The smaller ratios will be a good indicator of better or cost-effective design approaches and the opposite ratio results will be the bad indicator. Results were made below for fatigue failure criteria.

4.6.1. Obtaining Geometric Rating Number (GRi) for Design Approaches, Bending Fatigue Failure

In this section we will be interested in the design results of m times F (mxF), which were obtained based on bending fatigue failure. The values of m and F were multiplied and divided into the product of results (m_0xF_0) obtained from ANSI/AGMA 2003-B97 standards. Comparison of m_ixF_i/m_0xF_0 (that means Geometric rating numbers, (GRi)) results that are obtained by using the design approaches are presented by preparing radar charts. The charts are occurred and presented for the selected range of speed ratio for the selected power range.

The results presented in the radar charts allow comparing each of the gear design approaches for the overall size.

Figures between 4.51 and 4.58 show that the general trend is very similar with good continuity of the results for the design approaches 20° and material type 1. As a result of this, ranking can be achieved for ANSI/AGMA 2003-B97 standards, Juvinall R.C., Marshek K.M., 2011, ISO Standards 10300-(Part 1-2-3), 2001 and K.Gopinath & M.M.Mayuram, 2009 approaches ratings.

Remaining results for geometric rating number (GR_i) of design approaches for pressure angle of 20° are given in the appendices;

➢ for material type 2, see Appendix A.3.

➢ for material type 3, see Appendix B.3.

Remaining results for geometric rating number (GR_i) of design approaches for pressure angle of 25° are given in the appendices;

➢ for material type 1, see Appendix C.3.

➢ for material type 2, see Appendix D.3.

➢ for material type 3, see Appendix E.3.

Figures show that results are very similar because of relative comparison provided by GR_i. As a result of this, ranking can be achieved for the different approaches.

Mean GR_i numbers for various design approaches for each speed ratio with 20° pressure angle are shown in Table 4.8 and with 25° pressure angle are shown in Table 4.9.

Table 4.8. Mean GR_i numbers for the various design approaches for each speed ratio with 20° pressure angle

Ø=20°	Material Type 1			Material Type 2			Material Type 3		
Speed ratio	ISO	J&M	K&M	ISO	J&M	K&M	ISO	J&M	K&M
1	0,390	0,565	0,552	0,567	0,701	0,691	0,647	0,775	0,769
2	0,377	0,538	0,512	0,334	0,671	0,658	0,406	0,695	0,676
3	0,346	0,516	0,416	0,308	0,645	0,634	0,374	0,696	0,687
4	0,329	0,496	0,373	0,303	0,631	0,590	0,373	0,703	0,691
5	0,312	0,461	0,317	0,297	0,598	0,503	0,366	0,638	0,593
6	0,315	0,459	0,320	0,295	0,592	0,494	0,362	0,632	0,583
7	0,348	0,471	0,354	0,323	0,606	0,530	0,400	0,661	0,634
8	0,349	0,477	0,355	0,330	0,621	0,546	0,401	0,658	0,635
Average	0,346	0,498	0,400	0,345	0,633	0,581	0,416	0,682	0,659
Std.	0,026	0,036	0,082	0,085	0,035	0,069	0,089	0,043	0,056

139

Table 4. 9. Mean GR$_i$ numbers for the various design approaches for each speed ratio with 25° pressure angle

Ø=25°	Material Type 1			Material Type 2			Material Type 3		
Speed ratio	ISO	J&M	K&M	ISO	J&M	K&M	ISO	J&M	K&M
1	0,416	0,535	0,537	0,550	0,645	0,804	0,678	0,669	0,915
2	0,408	0,542	0,545	0,357	0,661	0,825	0,433	0,696	0,934
3	0,402	0,527	0,536	0,355	0,656	0,807	0,434	0,700	0,934
4	0,389	0,513	0,528	0,350	0,652	0,796	0,426	0,695	0,933
5	0,370	0,479	0,492	0,334	0,611	0,757	0,415	0,664	0,895
6	0,386	0,487	0,498	0,348	0,613	0,747	0,431	0,665	0,890
7	0,402	0,494	0,500	0,361	0,617	0,761	0,445	0,667	0,900
8	0,398	0,490	0,502	0,373	0,629	0,771	0,453	0,668	0,902
Average	0,396	0,508	0,517	0,379	0,635	0,784	0,464	0,678	0,913
Std.	0,014	0,023	0,020	0,066	0,019	0,026	0,081	0,015	0,017

The mean GR_i numbers are obtained for each design approach by taking average of values of GR_i at each speed ratio. The approaches are then ranked by GR_i numbers and given in Table 4.10. Results show that general trend for GR_i with 20° pressure angle are the same, as well. If the design methods are ranked from highest to lowest, it will be as follow,

- ✓ Material Type 1: J&M > K&M >ISO;
- ✓ Material Type 2: J&M > K&M >ISO;
- ✓ Material Type 3: J&M > K&M >ISO.

The same study has been done for 25° pressure angle. Results indicate that general trend for GR_i with 25° pressure angle are same, as well. If the design methods are ranked from highest to lowest, it will be as follow,

- ✓ Material Type 1: K&M > J&M >ISO;
- ✓ Material Type 2: K&M > J&M >ISO;
- ✓ Material Type 3: K&M > J&M >ISO.

As a result, ISO gives the lowest GR_i regardless of pressure angle when considering 3 types of material.

Table 4.10. Mean GR_i numbers for the various design approaches

Geometric rating numbers for the approaches with three types of material	GR_i					
	Ø=20°			Ø=25°		
	Type 1	Type 2	Type 3	Type 1	Type 2	Type 3
K&M	0,400	0,581	0,659	0,517	0,784	0,913
ISO	0,346	0,345	0,416	0,396	0,379	0,464
J&M	0,498	0,633	0,682	0,508	0,635	0,678
ANSI/AGMA	1.000	1.000	1.000	1.000	1.000	1.000
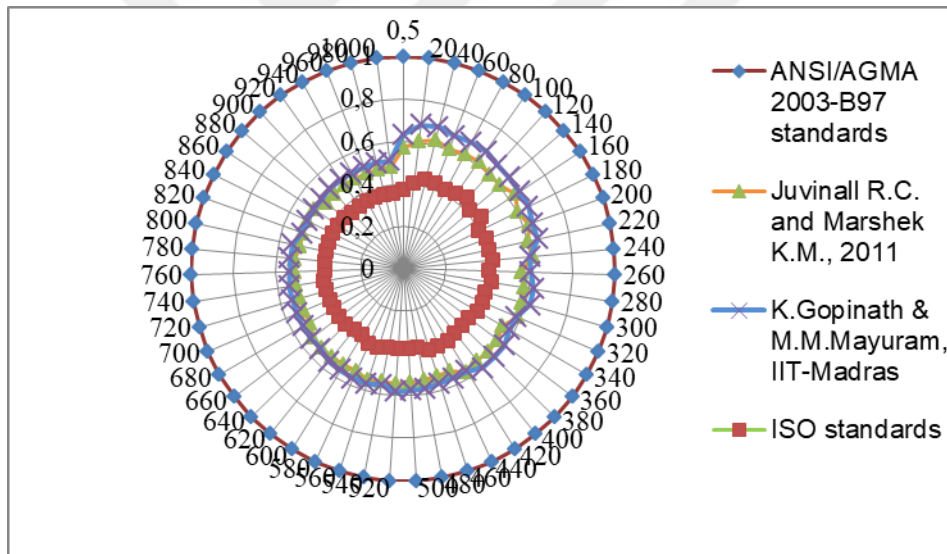
Figure 4.51. Comparison of mxF/m_0xF_0 ratios for the design approaches at 1:1 speed ratio (for Ø=20°, Material type 1)
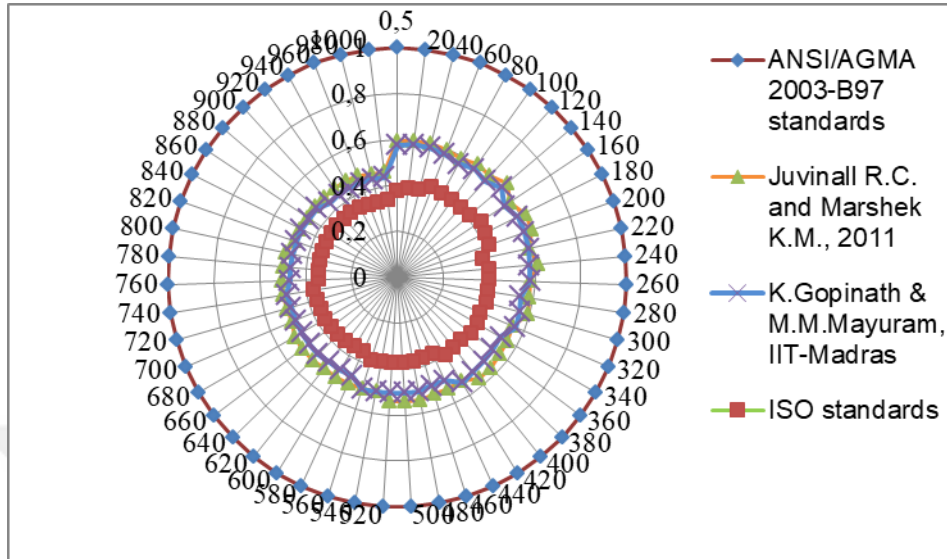
Figure 4.52. Comparison of mxF/m_0xF_0 ratios for the design approaches at 2:1 speed ratio (for Ø=20°, Material type 1)
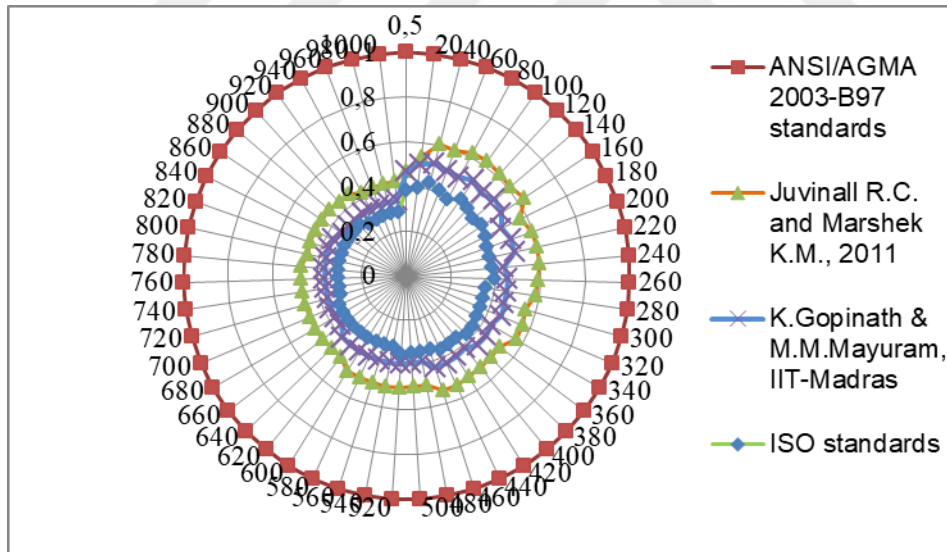
Figure 4.53. Comparison of mxF/m_0xF_0 ratios for the design approaches at 3:1 speed ratio(for Ø=20°, Material type 1)

143
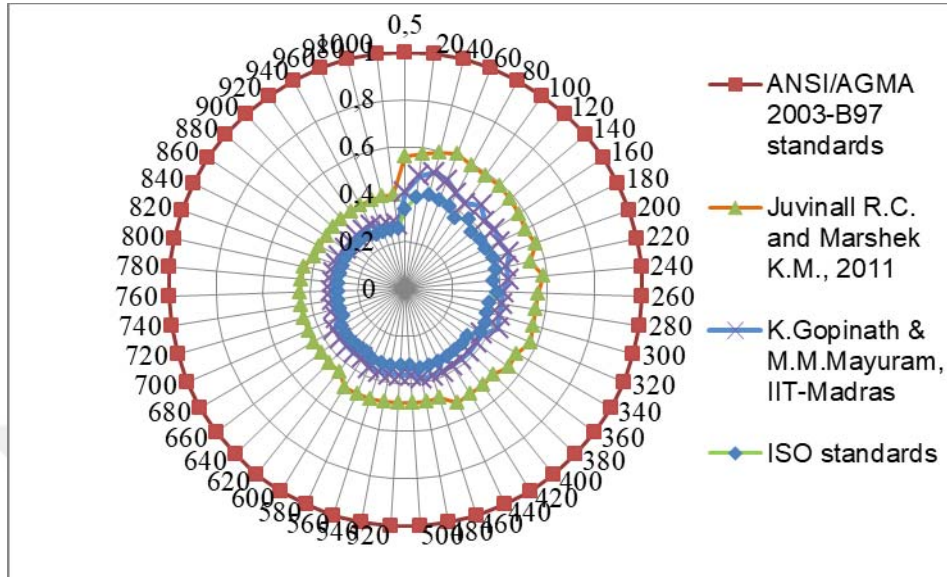
Figure 4.54. Comparison of mxF/m_0xF_0 ratios for the design approaches at 4:1 speed ratio(for Ø=20°, Material type 1)
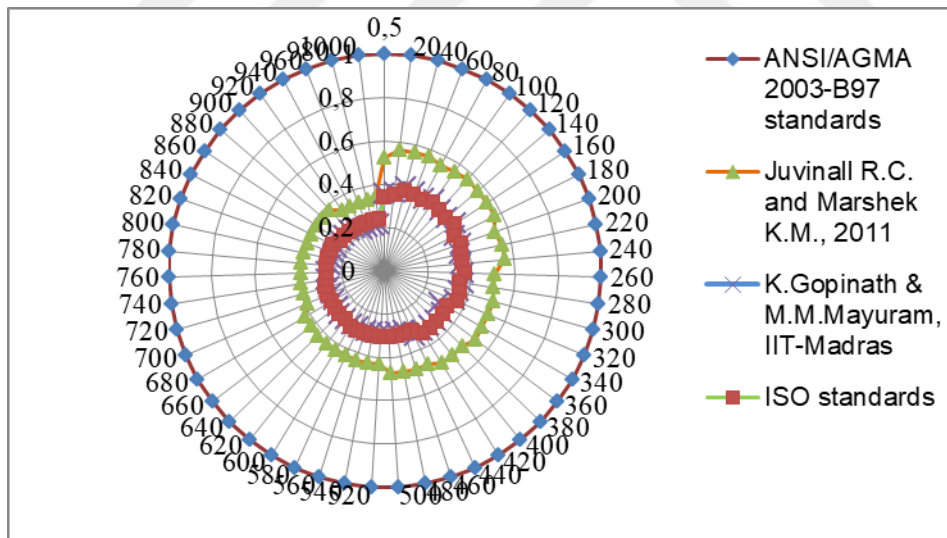
Figure 4.55. Comparison of mxF/m_0xF_0 ratios for the design approaches at 5:1 speed ratio (for Ø=20°, Material type 1)
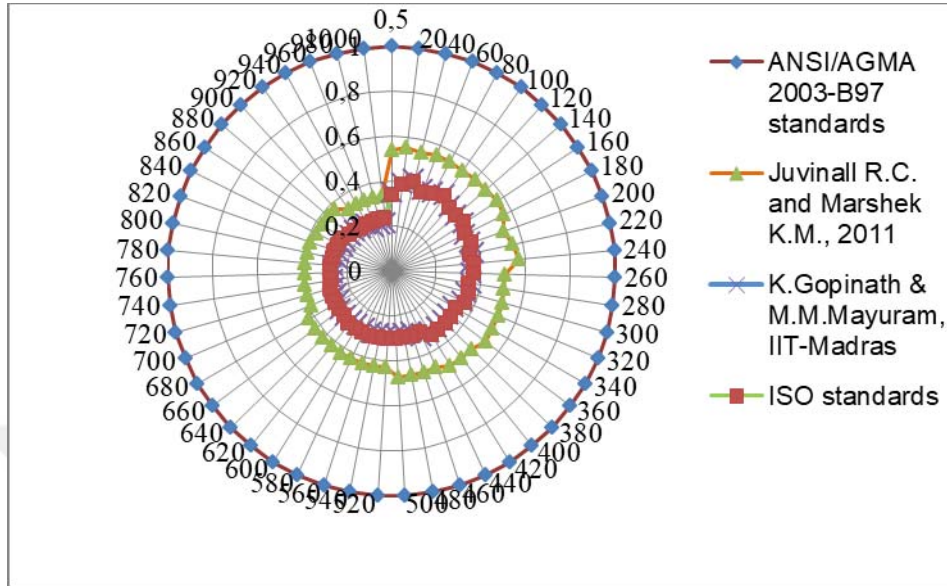
Figure 4.56. Comparison of mxF/m_0xF_0 ratios for the design approaches at 6:1 speed ratio (for Ø=20°, Material type 1)
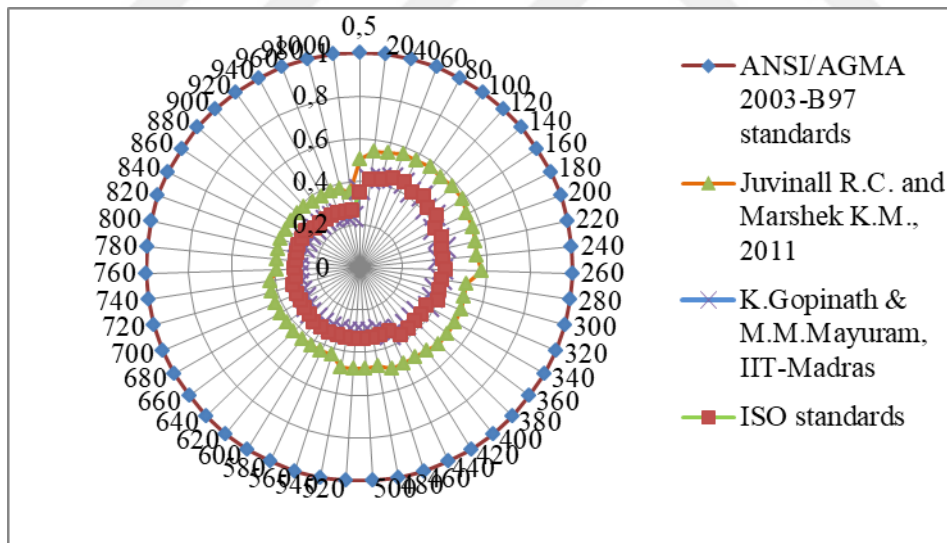
Figure 4.57. Comparison of mxF/m_0xF_0 ratios for the design approaches at 7:1 speed ratio (for Ø=20°, Material type 1)
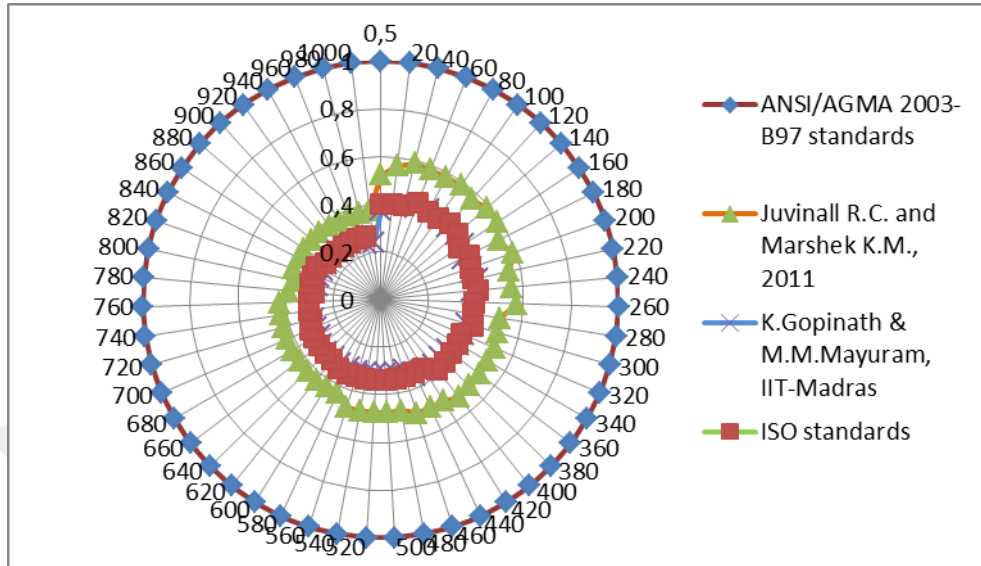
Figure 4.58. Comparison of mxF/m_0xF_0 ratios for the design approaches at 8:1 speed ratio (for $\varnothing=20^{\circ}$, Material type 1)

When the figures are analysed, it is seen that the design of bevel gear by using ANSI/AGMA 2003-B97 standards gives the largest size for the selected speed ratios for the selected power transmission ranges (except 1:1 speed ratio and 0,5 kW). And the approach is given by Juvinall R.C., Marshek K.M., 2011 gives the smallest size for a bevel gear considering the same conditions with ANSI/AGMA 2003-B97 standards. And optimum values are obtained in K.Gopinath & M.M.Mayuram, 2009 and ISO Standards 10300-(Part 1-2-3), 2001 (except 1:1 speed ratio and 0,5 kW).

4.6.2. Obtaining Geometric Rating Number (GRi) for Design Approaches, Surface Contact Fatigue Failure

In this section, the design results of m times F (mxF), were acquired based on surface contact fatigue failure. The values of m and F were multiplied and divided into the product of results (m_0xF_0) obtained from ANSI/AGMA 2003-B97

146

standards. And the results of gear design approaches for 20º and material type 1 have been represented comparatively in Figures 4.59 ton 4.66.

Remaining results for geometric rating number (GR_i) of design approaches for pressure angle of 20º are given in the appendices;

➢ for material type 2, see Appendix F.3.
➢ for material type 3, see Appendix G.3.

Remaining results for geometric rating number (GR_i) of design approaches for pressure angle of 25º are given in the appendices;

➢ for material type 1, see Appendix H.3.
➢ for material type 2, see Appendix J.3.
➢ for material type 3, see Appendix K.3.
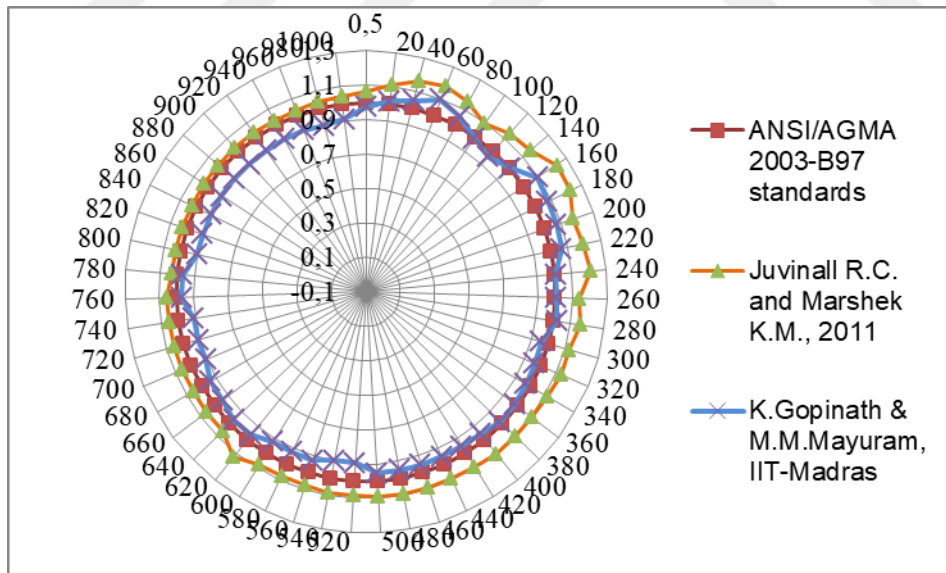
Figure 4.59. Comparison of mxF/m_0xF_0 ratios for the design approaches at 1:1 speed ratio (for Ø=20º, Material type 1)

When the Figures from 4.59 to 4.62 are examined, at 1:1 speed ratio Juvinall R.C., Marshek K.M., 2011 and K.Gopinath & M.M.Mayuram, 2009 results are near each other. And except 1:1 speed ratio for all power transmission ranges, the results from the biggest to the smallest is ranked as;

1) Juvinall R.C., Marshek K.M., 2011
2) ANSI/AGMA 2003-B97 standards
3) K.Gopinath & M.M.Mayuram,2009
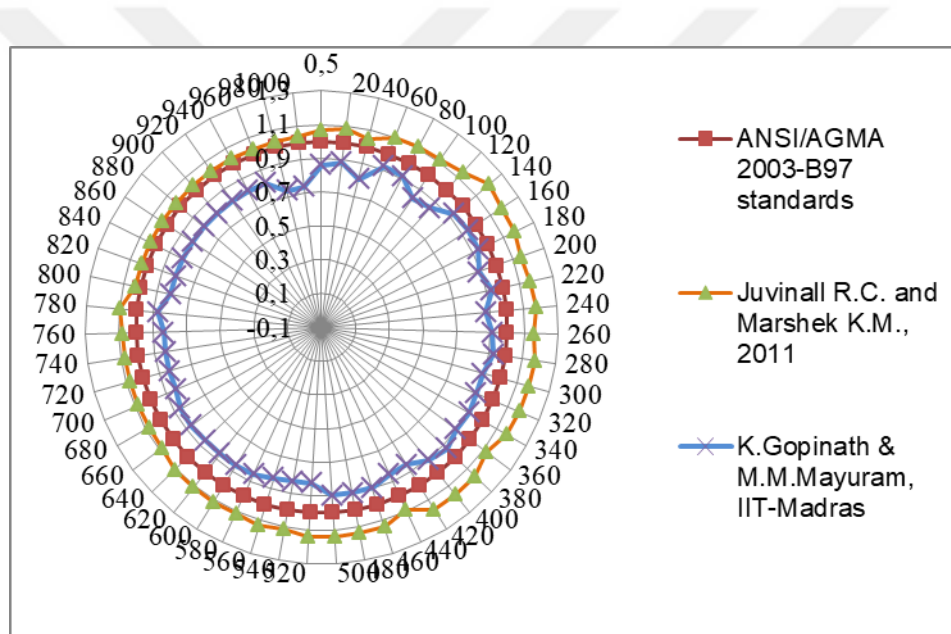
Figure 4.60. Comparison of mxF/m_0xF$_0$ ratios for the design approaches at 2:1 speed ratio (for Ø=20°, Material type 1)
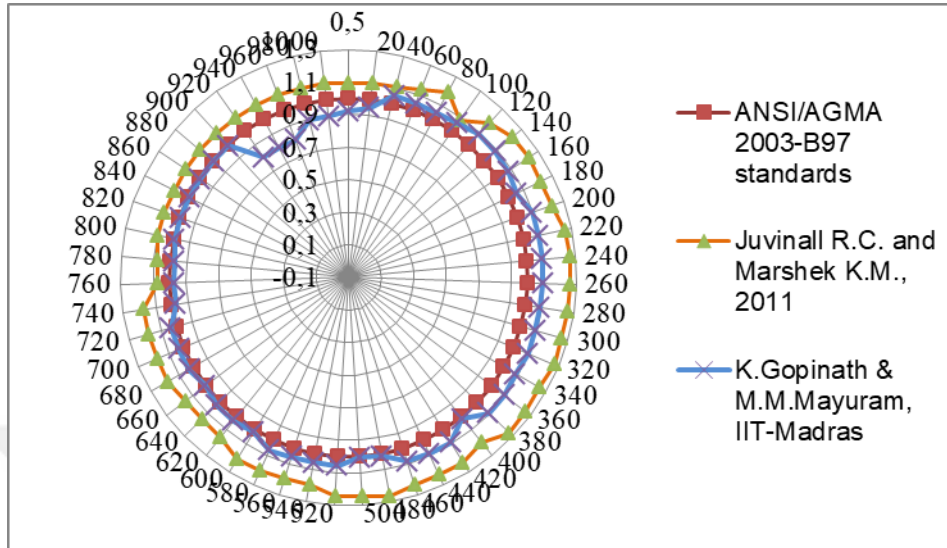
Figure 4.61. Comparison of mxF/m_0xF$_0$ ratios for the design approaches at 3:1 speed ratio (for Ø=20°, Material type 1)
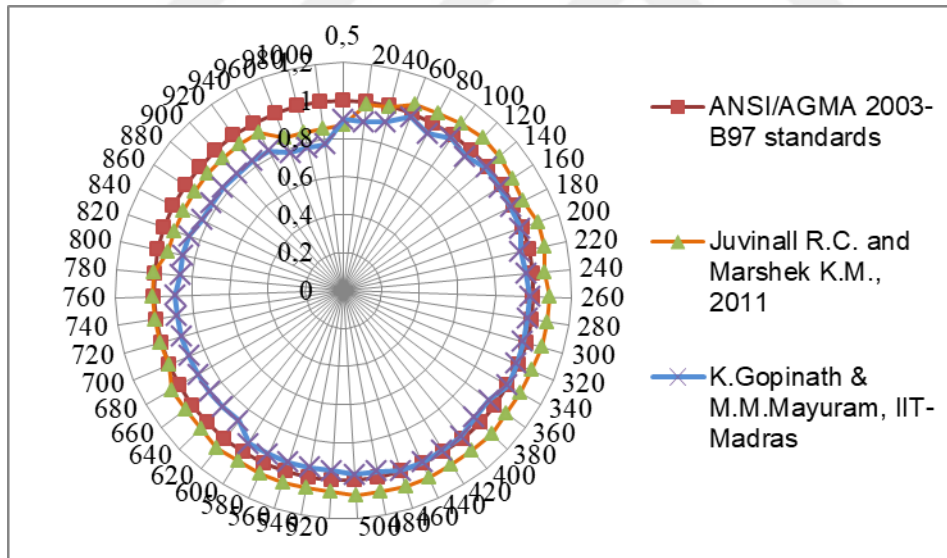
Figure 4.62. Comparison of mxF/m_0xF$_0$ ratios for the design approaches at 4:1 speed ratio (for Ø=20°, Material type 1)
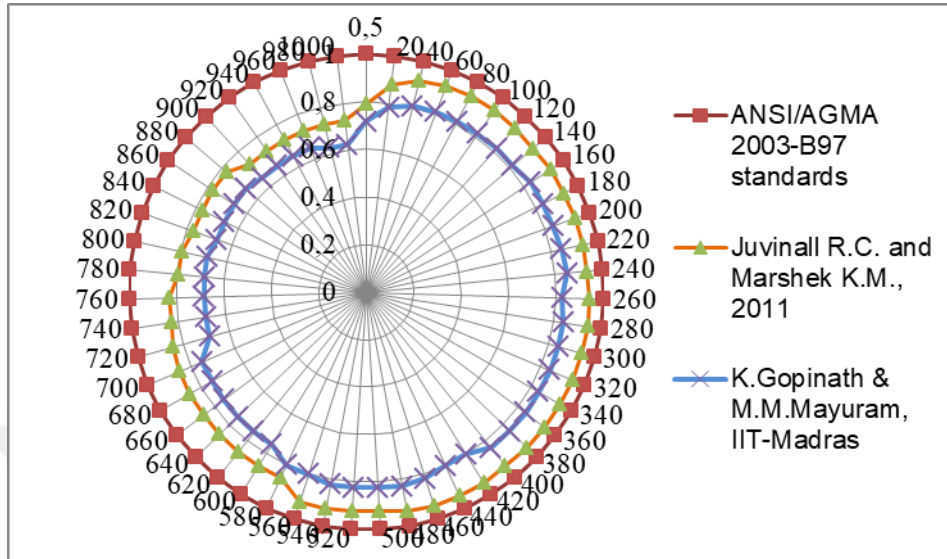
Figure 4.63. Comparison of mxF/m_0xF_0 ratios for the design approaches at 5:1 speed ratio (for $\emptyset$=20°, Material type 1)
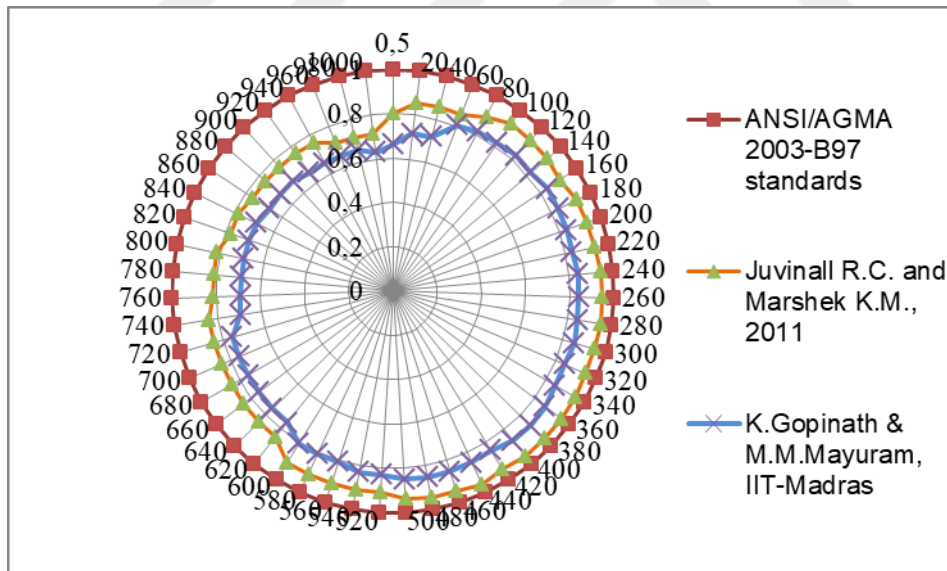
Figure 4.64. Comparison of mxF/m_0xF_0 ratios for the design approaches at 6:1 speed ratio (for $\emptyset$=20°, Material type 1)
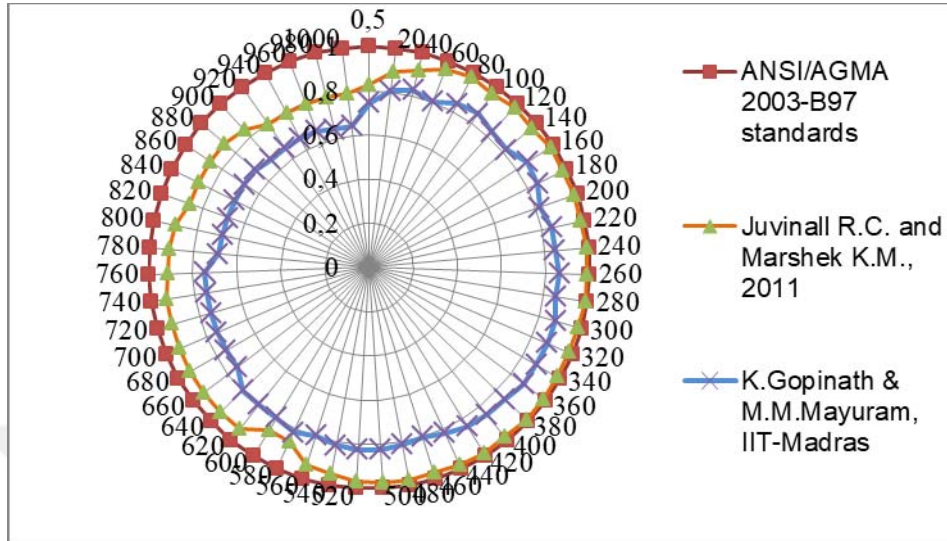
Figure 4.65.Comparison of mxF/m_0xF_0 ratios for the design approaches at 7:1 speed ratio (for Ø=20°, Material type 1)
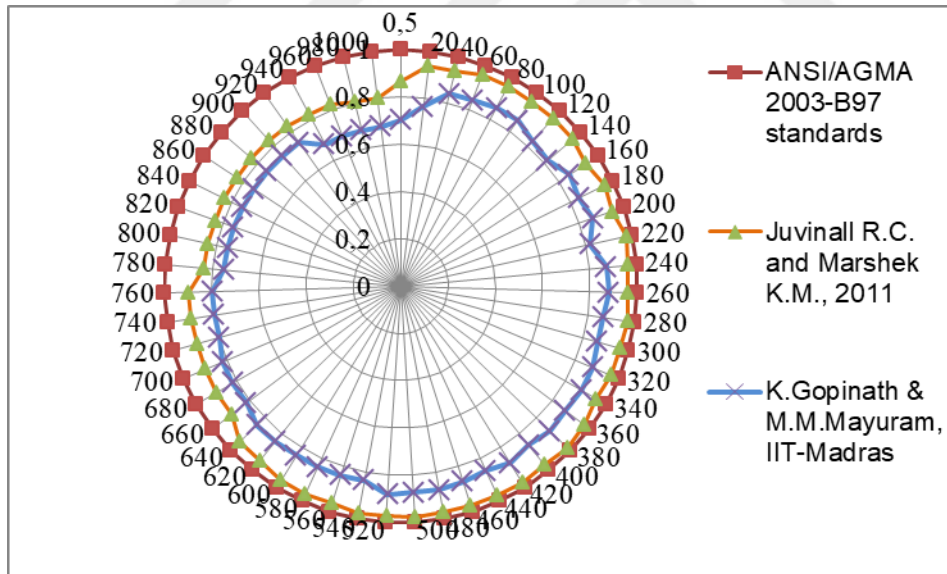
Figure 4.66. Comparison of mxF/m_0xF_0 ratios for the design approaches at 8:1 speed ratio (for Ø=20°, Material type 1)

151

Conversely to the bending fatigue failure, ANSI/AGMA 2003-B97 standards and the approach given by Juvinall R.C., Marshek K.M., 2011 have given the largest size for a straight bevel gear that is designed based on surface contact fatigue failure. And the approach given by ANSI/AGMA 2003-B97 standards has given the smallest size, explained in Section 4.3.2.2.

Therefore all these radar charts except for the speed ratio of 1:1 have also shown that design approaches have maintained general trends even the effect of face width has included. To sum up, these charts have indicated the design approaches that provide a straight bevel gear with the minimum size. This allows to the designer to estimate the amount of material as well as the overall cost of gearbox. And if the optimum material selection using proper material selection approaches and the optimization of a gearbox design can be achieved completely.

4.6.3. Obtaining AGMA Conversion Factors (CFs) for Module and Face Width

Conversion factors for module ($\overline{CF}_{ml}$) and face width ($\overline{CF}_{Fl}$) can be calculated by using the equations given in equation in 3.76, 3.77, 3.78 and 3.79 together with their standard deviation, for module ($\sigma_{\overline{CF}_{ml}}$) and for face width ($\sigma_{\overline{CF}_{Fl}}$), respectively. The results are found and tabulated in Table 4.11 (for pressure angle 20° and material 1) and a fourth order correlation polynomial (C_p) expressions were obtained and given in Table 4.12 (for pressure angle 20° and material 1).

Table 4.11. Conversion factors for module and face width for pressure angle 20°, material type 1

Design approaches		From K&M to AGMA				From ISO to AGMA				From J&M to AGMA			
m_G	N_p	$\overline{CF_m}$	$\sigma_{\overline{CF_m}}$	$\overline{CF_F}$	$\sigma_{\overline{CF_F}}$	$\overline{CF_m}$	$\sigma_{\overline{CF_m}}$	$\overline{CF_F}$	$\sigma_{\overline{CF_F}}$	$\overline{CF_m}$	$\sigma_{\overline{CF_m}}$	$\overline{CF_F}$	$\sigma_{\overline{CF_F}}$
1:1	13	0,732	0,044	0,792	0,046	0,640	0,033	0,611	0,037	0,718	0,046	0,762	0,047
2:1	14	0,699	0,050	0,732	0,047	0,632	0,034	0,596	0,040	0,713	0,046	0,754	0,050
3:1	16	0,634	0,051	0,655	0,066	0,608	0,041	0,569	0,050	0,699	0,051	0,738	0,065
4:1	16	0,604	0,055	0,615	0,069	0,600	0,051	0,549	0,054	0,696	0,059	0,710	0,060
5:1	16	0,572	0,057	0,532	0,058	0,582	0,053	0,535	0,054	0,704	0,071	0,652	0,065
6:1	16	0,571	0,058	0,532	0,062	0,582	0,053	0,539	0,058	0,705	0,069	0,648	0,065
7:1	16	0,596	0,057	0,559	0,068	0,610	0,048	0,570	0,064	0,717	0,062	0,656	0,065
8:1	16	0,596	0,057	0,558	0,063	0,610	0,048	0,570	0,059	0,712	0,065	0,667	0,067

Table 4.12. Conversion factors for face width and module at any speed ratio for pressure angle 20°, material

Design approach (from)		C_p Expressions for Module (m_i) (to AGMA) regressions for	R^2
0,5kW - 500kW	K&M to AGMA (K-A)	$\overline{CF_{m,K-A}} = -0,0005m_G^4 + 0,0091m_G^3 - 0,0496m_G^2 + 0,0551m_G + 0,7546$	0,9901
	ISO to AGMA (I-A)	$\overline{CF_{m,I-A}} = -0,0002m_G^4 + 0,0033m_G^3 - 0,018m_G^2 + 0,0251m_G + 0,651$	0,8635
	J&M to AGMA (J-A)	$\overline{CF_{m,J-A}} = 1E{-}05m_G^4 - 0,0007m_G^3 + 0,0093m_G^2 - 0,0363m_G + 0,7834$	0,8892
500kW - 1000kW	K&M to AGMA (K-A)	$\overline{CF_{m,K-A}} = -0,0006m_G^4 + 0,0112m_G^3 - 0,0643m_G^2 + 0,0893m_G + 0,6584$	0,9943
	ISO to AGMA (I-A)	$\overline{CF_{m,I-A}} = -0,0005m_G^4 + 0,0091m_G^3 - 0,056m_G^2 + 0,1084m_G + 0,5547$	0,9648
	J&M to AGMA (J-A)	$\overline{CF_{m,J-A}} = -0,0004m_G^4 + 0,0066m_G^3 - 0,0371m_G^2 + 0,0685m_G + 0,6427$	0,9706
		C_p Expressions for Face Width (F) (to AGMA) regressions for	
0,5kW - 500kW	K&M to AGMA (K-A)	$\overline{CF_{F,K-A}} = -0,0009m_G^4 + 0,0188m_G^3 - 0,1222m_G^2 + 0,2595m_G + 0,5906$	0,9765
	ISO to AGMA (I-A)	$\overline{CF_{F,I-A}} = -0,0005m_G^4 + 0,0093m_G^3 - 0,0558m_G^2 + 0,1101m_G + 0,5565$	0,9405
	J&M to AGMA (J-A)	$\overline{CF_{F,J-A}} = -9E{-}05m_G^4 + 0,0029m_G^3 - 0,0252m_G^2 + 0,0574m_G + 0,7505$	0,9635
500kW - 1000kW	K&M to AGMA (K-A)	$\overline{CF_{F,K-A}} = -0,0005m_G^4 + 0,0105m_G^3 - 0,0609m_G^2 + 0,0643m_G + 0,7768$	0,9842
	ISO to AGMA (I-A)	$\overline{CF_{F,I-A}} = -0,0004m_G^4 + 0,0081m_G^3 - 0,0468m_G^2 + 0,0786m_G + 0,5705$	0,9799
	J&M to AGMA (J-A)	$\overline{CF_{F,J-A}} = -0,0002m_G^4 + 0,0053m_G^3 - 0,0416m_G^2 + 0,0933m_G + 0,7025$	0,9719

154

Table 4.13. Validating and proving conversion factors with the percentage errors in the range of 0,5 kW to 1000 kW (Ø=20°, Material type 1)

Case: Design approach, m(speed ratio), Power (kW)	m_i	F_i	m_{AGMA}	F_{AGMA}	$(mxF)_{AGMA}$	$\overline{CF_{mi}}$	$m_{c,AGMA}$	m_i Error (%)	$\overline{CF_{Fi}}$	$F_{c,AGMA}$	F_i Error (%)	$(mxF)_{c,AGMA}$	GV_e (%)
J&M (2.5:1) 580 kW	24	120,93	33,867	173,08	5861,67	0,67	+35,84	5,84	0,75	-161,08	6,93	5773,63	-1,50
J&M (6.3:1) 80 kW	10	87,59	12,000	127,97	1535,67	0,76	+13,08	9,00	0,70	-125,97	1,56	1647,64	7,29
K&M (3.4:1) 135 kW	12	68,13	16,933	110,99	1879,46	0,66	+18,20	7,47	0,68	-100,36	9,58	1826,29	-2,83
K&M (5.6:1) 600 kW	16	145,07	30	273,49	8204,79	0,51	+31,41	4,69	0,58	-250,42	8,44	7864,84	-4,14
ISO (3.6:1) 630 kW	20	117,44	28	263,46	7377,00	0,56	+35,73	27,60	0,56	-210,59	20,07	7524,19	2,00
ISO (7.5:1) 675 kW	17	153,79	30	275,46	8263,85	0,47	+35,67	18,90	0,68	-226,47	17,79	8077,75	-2,25

155

And then, conversion factors for module ($\overline{CF}_{mt}$) and face width ($\overline{CF}_{Ft}$) are found and tabulated in Table 4.14 for pressure angle of $25^{°}$ and material type 1.

Standard deviations for module ($\sigma_{\overline{CF}_{mt}}$) and for face widths ($\sigma_{\overline{CF}_{Ft}}$) given in Table 4.14 show that the module and face width results obtained from the design approaches (ISO, K&M, J&M) can be converted to AGMA with reasonable error at the selected speed ratios from 1:1 to 8:1. In addition to constant conversion factors at certain speed ratios, correlation equations were derived in order to obtain a conversion factor at any speed ratio. Fourth order correlation polynomial (Cp) expressions were obtained and given in Table 4.15.

The second case study has been carried out to prove and validate the universality of conversion factors by using C_p expressions for pressure angle of $25^{°}$ as seen in Table 4.16. The design results (module and face width) selection is same as first case study (see Table 4.13) for each design approaches. Since the both module (m) and face width (F) values affect the design, converted m_i times F_i values are considered to validate the success of expressions of $\overline{CF}_{mt}$ and $\overline{CF}_{Ft}$. Then total error considering converted m times F $((mxF)_{AGMA})$ values of AGMA is obtained using a gear volume error (GV_e) equation and the results are given in the last column of Table 4.16. The maximum total GV_e is below 9.45%.

Table 4.14. Conversion factors for module and face width for pressure angle 25°. material type 1

Design approaches		From K&M to AGMA				From ISO to AGMA				From J&M to AGMA			
m_G	N_p	$\overline{CF_m}$	$\sigma_{\overline{CF_m}}$	$\overline{CF_F}$	$\sigma_{\overline{CF_F}}$	$\overline{CF_m}$	$\sigma_{\overline{CF_m}}$	$\overline{CF_F}$	$\sigma_{\overline{CF_F}}$	$\overline{CF_m}$	$\sigma_{\overline{CF_m}}$	$\overline{CF_F}$	$\sigma_{\overline{CF_F}}$
1:1	13	0,700	0,049	0,768	0,055	0,654	0,034	0,636	0,041	0,703	0,047	0,761	0,046
2:1	13	0,713	0,058	0,763	0,047	0,657	0,042	0,621	0,040	0,715	0,056	0,758	0,044
3:1	13	0,712	0,059	0,751	0,062	0,653	0,042	0,615	0,056	0,713	0,054	0,740	0,053
4:1	13	0,701	0,057	0,752	0,067	0,640	0,043	0,605	0,062	0,702	0,057	0,730	0,071
5:1	13	0,712	0,065	0,689	0,058	0,622	0,047	0,592	0,073	0,711	0,063	0,671	0,066
6:1	13	0,719	0,065	0,690	0,068	0,638	0,046	0,603	0,064	0,722	0,063	0,673	0,061
7:1	13	0,727	0,065	0,686	0,071	0,652	0,047	0,615	0,066	0,723	0,059	0,682	0,063
8:1	13	0,727	0,060	0,688	0,068	0,650	0,048	0,612	0,069	0,726	0,057	0,673	0,067

Table 4.15. Conversion factors for face width and module at any speed ratio for pressure angle 25°, material type 1

	Design approach (from)	C_p Expressions for Module (m_i) (to AGMA) regressions for	R^2
0,5kW - 500kW	K&M to AGMA (K-A)	$\overline{CF}_{m,K-A} = -0,0003m_G^4 + 0,0056m_G^3 - 0,0337m_G^2 + 0,0798m_G + 0,6488$	0,9349
	ISO to AGMA (I-A)	$\overline{CF}_{m,I-A} = -0,0004m_G^4 + 0,0072m_G^3 - 0,0452m_G^2 + 0,1004m_G + 0,5902$	0,8455
	J&M to AGMA (J-A)	$\overline{CF}_{m,J-A} = -0,0003m_G^4 + 0,0047m_G^3 - 0,0288m_G^2 + 0,0673m_G + 0,661$	0,8748
500kW - 1000kW	K&M to AGMA (K-A)	$\overline{CF}_{m,K-A} = -0,0002m_G^4 + 0,0034m_G^3 - 0,0204m_G^2 + 0,0455m_G + 0,6358$	0,9753
	ISO to AGMA (I-A)	$\overline{CF}_{m,I-A} = -0,0002m_G^5 + 0,0052m_G^4 - 0,0397m_G^3 + 0,1321m_G^2 - 0,1938m_G + 0,7274$	0,9353
	J&M to AGMA (J-A)	$\overline{CF}_{m,J-A} = -0,0002m_G^4 + 0,0035m_G^3 - 0,0207m_G^2 + 0,0453m_G + 0,6424$	0,8651
		C_p Expressions for Face Width (F) (to AGMA) regressions for	
0,5kW - 500kW	K&M to AGMA (K-A)	$\overline{CF}_{F,K-A} = 0,0001m_G^4 - 0,0013m_G^3 + 0,0006m_G^2 + 0,0082m_G + 0,7791$	0,7748
	ISO to AGMA (I-A)	$\overline{CF}_{F,I-A} = -0,0002m_G^5 + 0,0057m_G^4 - 0,0478m_G^3 + 0,1828m_G^2 - 0,3093m_G + 0,822$	0,9105
	J&M to AGMA (J-A)	$\overline{CF}_{F,J-A} = 0,0001m_G^4 - 0,0011m_G^3 + 0,0007m_G^2 + 0,0016m_G + 0,7794$	0,8042
500kW - 1000kW	K&M to AGMA (K-A)	$\overline{CF}_{F,K-A} = -0,0001m_G^4 + 0,0035m_G^3 - 0,0299m_G^2 + 0,0683m_G + 0,7019$	0,9707
	ISO to AGMA (I-A)	$\overline{CF}_{F,I-A} = -0,0005m_G^4 + 0,0083m_G^3 - 0,0474m_G^2 + 0,0807m_G + 0,5768$	0,9818
	J&M to AGMA (J-A)	$\overline{CF}_{F,J-A} = -0,0007m_G^4 + 0,014m_G^3 - 0,091m_G^2 + 0,1983m_G + 0,6157$	0,9810

Table 4.16. Validating and proving conversion factors with the percentage errors in the range of 0,5 kW to 1000 kW (Ø=25°, Material type 1)

Case: Design approach, m(speed ratio), Power (kW)	m_i	F_i	m_{AGMA}	F_{AGMA}	$(mxF)_{AGMA}$	$\overline{CF_{mi}}$	$m_{c, AGMA}$	m_i Error (%)	$\overline{CF_{Fi}}$	$F_{c, AGMA}$	F_i Error (%)	$(mxF)_{c, AGMA}$	GV_e (%)
J&M (2.5:1) 580 kW	22	126,22	32	164,28	5256,86	0,67	+32,68	2,13	0,73	+172,08	4,75	5623,95	6,98
J&M (6.3:1) 80 kW	10	74,60	12	125,93	1511,21	0,64	+15,51	29,29	0,70	-106,61	15,34	1654,04	9,45
K&M (3.4:1) 135 kW	12	85,58	16	107,24	1715,83	0,71	+16,89	5,55	0,78	+110,26	2,82	1862,09	8,52
K&M (5.6:1) 600 kW	18	164,05	27	256,51	6925,66	0,65	+27,64	2,37	0,66	-247,42	3,54	6838,35	-1,26
ISO (7.5:1) 675 kW	17	161,93	27	269,78	7284,02	0,92	-18,45	31,67	0,44	+371,98	37,88	6862,75	-5,78
ISO (3.6:1) 630 kW	20	123,10	30	214,43	6432,93	0,80	-25,09	16,38	0,46	+265,36	23,75	6656,61	3,48

The header spanning columns: m_i and F_i converted to $m_{c, AGMA}$ and $F_{c, AGMA}$

The percentage differences of conversion factors concerning different pressure angles are tabulated in following Table 4.17 for module and Table 4.18 for face width to find out the correlation in between. Consequently, the highest difference observed with K&M design approach while the lowest difference is with J&M design approach. This is valid for both module and face width.

Table 4.17. Conversion factor differences considering pressure angle of 20° and 25° for module

Speed ratio	From K&M to AGMA			From ISO to AGMA			From J&M to AGMA		
	$\overline{CF_m}$, Ø=20°	$\overline{CF_m}$, Ø=25°	Difference (%)	$\overline{CF_m}$, Ø=20°	$\overline{CF_m}$, Ø=25°	Difference (%)	$\overline{CF_m}$, Ø=20°	$\overline{CF_m}$, Ø=25°	Difference (%)
1:1	0,732	0,700	4,597	0,640	0,654	2,118	0,718	0,703	2,068
2:1	0,699	0,713	2,029	0,632	0,657	3,789	0,713	0,715	0,348
3:1	0,634	0,712	10,919	0,608	0,653	6,820	0,699	0,713	1,914
4:1	0,604	0,701	13,779	0,600	0,640	6,322	0,696	0,702	0,897
5:1	0,572	0,712	19,705	0,582	0,622	6,358	0,704	0,711	1,027
6:1	0,571	0,719	20,568	0,582	0,638	8,714	0,705	0,722	2,404
7:1	0,596	0,727	18,072	0,610	0,652	6,433	0,717	0,723	0,837
8:1	0,596	0,727	18,010	0,610	0,650	6,115	0,712	0,726	1,987

Table 4.18. Conversion factor differences considering pressure angle of 20° and 25° for face width

Speed ratio	From K&M to AGMA			From ISO to AGMA			From J&M to AGMA		
	$\overline{CF_{F}}$, Ø=20°	$\overline{CF_{F}}$, Ø=25°	Difference (%)	$\overline{CF_{F}}$, Ø=20°	$\overline{CF_{F}}$, Ø=25°	Difference (%)	$\overline{CF_{F}}$, Ø=20°	$\overline{CF_{F}}$, Ø=25°	Difference (%)
1:1	0,792	0,768	3,178	0,611	0,636	3,960	0,762	0,761	0,093
2:1	0,732	0,763	4,089	0,596	0,621	4,011	0,754	0,758	0,498
3:1	0,655	0,751	12,783	0,569	0,615	7,535	0,738	0,740	0,205
4:1	0,615	0,752	18,272	0,549	0,605	9,313	0,710	0,730	2,746
5:1	0,532	0,689	22,746	0,535	0,592	9,644	0,652	0,671	2,766
6:1	0,532	0,690	22,914	0,539	0,603	10,563	0,648	0,673	3,722
7:1	0,559	0,686	18,460	0,570	0,615	7,289	0,656	0,682	3,841
8:1	0,558	0,688	18,909	0,570	0,612	6,804	0,667	0,673	0,945

And for verifying our studies we used the design values of the bending fatigue failure as an input in the surface contact fatigue failure equations (at speed ratio 2:1), and the results for pressure angle of 20° and material type 1 are given in Table 4.19, Table 4.20, Table 4.21 and Table 4.22 below;

Table 4.19. Factor of safety results according to AGMA Standards

Power (kW)	AGMA Standards		SH (factor of safety)	Result
	Module (m)	Face width (F)		
0,5	2,5	14,62433	1,332	The design is safe
20	9	48,13641	1,152	The design is safe
100	16	79,7181	1,014	The design is safe
200	22	92,12924	0,949	The design is not safe
300	25	114,5563	0,940	The design is not safe
400	28	130,2378	0,956	The design is not safe
500	32	136,2155	0,978	The design is not safe
600	33,867	152,0675	0,988	The design is not safe
700	36	164,5459	1,000	The design is safe
800	39	171,1072	1,003	The design is safe
900	40	187,0283	1,021	The design is safe
1000	42	196,8801	1,031	The design is safe

Table 4.20. Factor of safety results according to Juvinal R.C.,Marshek K.M.

Power (kW)	Juvinall R.C. and Marshek K.M., 2011		SH (factor of safety)	Result
	Module (m)	Face width (F)		
0,5	2	10,81157	1,382	The design is safe
20	7,2571	35,59366	1,363	The design is safe
100	12,7	60,97239	1,287	The design is safe
200	16	78,576	1,192	The design is safe
300	18	94,25831	1,097	The design is safe
400	20	102,9411	1,002	The design is safe
500	22	107,4544	0,907	The design is not safe
600	24	109,4088	0,957	The design is not safe
700	25	118,1839	0,972	The design is not safe
800	25,4	131,085	0,987	The design is not safe
900	27	131,4373	1,002	The design is safe
1000	28	136,3769	1,017	The design is safe

Table 4.21. Factor of safety results according to K.Gopinath & M.M.Mayuram

Power (kW)	K.Gopinath & M.M.Mayuram 4th Edition		SH (factor of safety)	Result
	Module (m)	Face width (F)		
0,5	2	10,51518	1,352	The design is safe
20	7,2571	34,77259	1,342	The design is safe
100	12,7	58,15556	1,302	The design is safe
200	16	74,44373	1,252	The design is safe
300	18	88,22961	1,202	The design is safe
400	20	96,03241	1,152	The design is safe
500	22	99,97608	1,102	The design is safe
600	24	101,5847	1,054	The design is safe
700	24	118,5155	1,022	The design is safe
800	25	124,8272	0,952	The design is not safe
900	27	121,3157	1,212	The design is safe
1000	27	134,7952	1,162	The design is safe

Table 4.22. Factor of safety results according to ISO Standards

Power (kW)	ISO Standards		SH (factor of safety)	Result
	Module (m)	Face width (F)		
0,5	1,75	7,896124	1,253	The design is safe
20	6,35	26,73143	0,925	The design is not safe
100	11	48,06257	0,918	The design is not safe
200	14	61,92237	0,947	The design is not safe
300	16	73,03567	0,940	The design is not safe
400	18	78,94242	0,967	The design is not safe
500	20	81,94073	0,994	The design is not safe
600	22	83,25519	0,974	The design is not safe
700	22	97,13105	0,980	The design is not safe
800	24	95,51315	0,988	The design is not safe
900	24	107,4523	0,976	The design is not safe
1000	25	111,3243	1,009	The design is safe

And for verifying our studies we used the design values of the bending fatigue failure as an input in the surface contact fatigue failure equations. And the results for pressure angle of 25° and material type 1 are given in Table 4.23, Table 4.24, Table 4.25 and Table 4.26 below;

Table 4.23. Factor of safety results according to AGMA Standards

Power (kW)	AGMA Standards		SH (factor of safety)	Result
	Module (m)	Face width (F)		
0,5	2,5	12,85702	1,463	The design is safe
20	10	33,97292	1,248	The design is safe
100	16,933	70,04087	1,182	The design is safe
200	22	93,00975	1,145	The design is safe
300	27	103,2803	1,126	The design is safe
400	30	118,9351	1,145	The design is safe
500	32	136,3285	1,156	The design is safe
600	36	140,6089	1,184	The design is safe
700	39	148,8105	1,202	The design is safe
800	39	170,0692	1,203	The design is safe
900	42	175,5714	1,221	The design is safe
1000	45	180,7979	1,239	The design is safe

Table 4.24. Factor of safety results according to Juvinal R.C.,Marshek K.M.

Power (kW)	Juvinall R.C. and Marshek K.M., 2011		SH (factor of safety)	Result
	Module (m)	Face width (F)		
0,5	2,1167	9,896698	1,303	The design is safe
20	8	30,11182	1,344	The design is safe
100	14	51,60152	1,340	The design is safe
200	16,933	71,86611	1,336	The design is safe
300	20	78,60485	1,331	The design is safe
400	22	87,50225	1,326	The design is safe
500	24	92,78756	1,322	The design is safe
600	24	111,3451	1,317	The design is safe
700	25	120,2642	1,312	The design is safe
800	27	118,8686	1,308	The design is safe
900	28	124,8672	1,303	The design is safe
1000	30	121,8359	1,298	The design is safe

Table 4.25. Factor of safety results according to K.Gopinath & M.M.Mayuram

Power (kW)	K.Gopinath & M.M.Mayuram 4th Edition		SH (factor of safety)	Result
	Module (m)	Face width (F)		
0,5	2,1167	10,14586956	1,186	The design is safe
20	8	30,6540719	1,184	The design is safe
100	14	51,67502414	1,179	The design is safe
200	16,933	71,20413044	1,173	The design is safe
300	20	77,15854194	1,167	The design is safe
400	22	85,68228119	1,161	The design is safe
500	24	90,68842408	1,161	The design is safe
600	24	108,8261089	1,165	The design is safe
700	25	117,0098323	1,169	The design is safe
800	27	115,523258	1,173	The design is safe
900	27	129,9636653	1,177	The design is safe
1000	30	118,7395305	1,186	The design is safe

Table 4.26. Factor of safety results according to ISO Standards

Power (kW)	ISO Standards		SH (factor of safety)	Result
	Module (m)	Face width (F)		
0,5	1,9538	7,111831	1,104842	The design is safe
20	7	24,76595	0,922558	The design is not safe
100	12	45,54504	0,927344	The design is not safe
200	16	54,07947	0,945478	The design is not safe
300	16,933	73,29673	0,953883	The design is not safe
400	20	72,76985	0,959042	The design is not safe
500	22	77,00052	0,986277	The design is not safe
600	22	92,40062	0,98694	The design is not safe
700	24	92,73524	0,995656	The design is not safe
800	25	98,81231	0,981484	The design is not safe
900	25,4	108,1876	1,012511	The design is safe
1000	27	108,3485	1,000812	The design is safe

5. CONCLUSION

Two design parameters are module (m) and face width (F) are searched in the gear design before material is pre-selected. After defining the pinion and gear materials, module is estimated, and design calculations are carried out to determine the face width a suitable module. Number of design approaches providing differing design formulas are available in the machine elements or machine design textbooks for the design or finding "m" or "F". This situation is further complicated by the available gear design standards which suggest differing design expressions. But, the results of using different approaches have not been compared so far. Thus, the designer does not aware of the success or loss gained using each of the approaches. Because of that, there is a need to compare the results of each of the most accepted design formula or design approach for bevel gear design.

This thesis meets a need of selecting and using appropriate involute bevel gear design approaches for all designers including the expert designers and novice learners who are practicing a bevel gear design. This was made by comparing the most commonly used involute bevel gear design approaches available in the literature. The selected approaches are given as follow;

5- ANSI/AGMA 2003-B97 Standards
6- Fundamental of Machine Component Design 5th Edition, Juvinall R.C. and Marshek K.M., 2011
7- ISO Standards 10300-(Part 1-2-3), 2001
8- K.Gopinath & M.M.Mayuram 4th Edition, 2009

This study proposes to use the easier and the most appropriate approach provided in the common text books considering the verified results of FEA, if there is no obligation to use ISO or ANSI/AGMA Standards. Because these

standards are more challenging, time consuming and include complicated equations. Conversion factors for the conversion of text books results to the verified results were developed. And now, the results obtained by text books can be converted to the standards with the aid of conversion factors developed in this study. As a result of these, gear designers do not have to deal with the computational load of the standards. This does not only allow saving time and resources, but also provides safer and reliable designs.

A systematic methodology which relies on dimensionless numbers called as GRi and CFs, has been described and proposed to rate most common design approaches with ANSI/AGMA 2003-B97 based on bending fatigue failure for bevel gears. Although the results of four design approaches differ from each other, good similarity and continuity of the charts were found out. This allowed obtaining CFs between the standards. Now, these two approaches can be converted to each other with min of error. Beyond the investigations already available in the literature, following conclusions can be drawn in this study;

- Differences of GRi numbers provide a relative comparison between each approach (for 20° and material type 1). For example, mean values of
  - GR_{AGMA} minus $GR_{J\&M}$ (1.00-0,5=-0.50)
  - GR_{AGMA} minus GR_{ISO} (1.00-0,35=-0.65)
  - GR_{AGMA} minus $GR_{K\&M}$ (1.00-0.4=0.60)

provides relative gear tooth volume differences for pressure angle of 20° and material type 1. Under this comparison, m times F values of the simple approach J&M are approximately 50% outside of the verified AGMA as the ISO Standard is outside by 65%.

- Likewise for pressure angle of 25° and material type 1, mean values of
    - GR_{AGMA} minus $GR_{J\&M}$ (1.00-0,51=-0.0,49)
    - GR_{AGMA} minus GR_{ISO} (1.00-0,4=-0,6)
    - GR_{AGMA} minus $GR_{K\&M}$ (1.00-0,52=-0.48)

provides relative gear tooth volume differences. Under this comparison, m times F values of the simple approach J&M are approximately 49% outside of the verified AGMA as the ISO Standard is outside by 60%.

- Dimensionless conversion factors (CFs) were generated for bevel gears to convert the design results, module (m) and face width (F) of ISO Standard, K&M textbook and J&M textbook into AGMA with a minor error.
- Radar charts presented to make a relative comparison between design approaches. The results showed that gear design approaches have similar trends in all power ranges.
- Two methods are now available to obtain CFs. One can be made by linear interpolation from Table 4.11 for pressure angle of 20° and Table 4.14 for pressure angle of 25°. Secondly, Cp expressions can be used for any desired speed ratio from Table 4.12 for pressure angle of 20° and Table 4.15 for pressure angle of 25°.
- Universality of CFs were verified by case studies and worked reasonably well. The maximum total Gear Volume error (GVe) was found as 7,29% for pressure angle of 20° in Table 4.13 and 9.45% for pressure angle of 25° in Table 4.16 with the aid of CFs.
- And for verifying our studies we used the design values of the bending fatigue failure as an input in the surface contact fatigue failure equations (at speed ratio 2:1) and the results for pressure angle of 20° and material type 1 are given in Table 4.23, Table 4.24, Table 4.25 and Table 4.26.

In short, this study may serve as a guideline for a designer who deals with the design of an involute bevel gear. If a designer concerns with light weighted applications, the overall size of a gear is important as well as material usage that are objectives of optimization. On the other hand bevel gear design is the subject of almost all machine design courses. And it is important to introduce clear, easy to understand and reliable design approach for learners and students. Consequently, the results of this work interests both expert and novice designers and learners.

As future work, conversion factors between spur and bevel gear could investigated. Spur gear design is relatively easy when it is compared with bevel gear design. If this is studied as future work, it would be even easier to design bevel gears. Secondly, a future study can be done for different speed ratios which is bigger than 8:1.

REFERENCES

Ansi/Agma 2003-B97 Standards, 2004. Fundamental rating factors and calculation methods for involute bevel gear teeth. 59 pages, Virginia, USA.

Ambade V.V., Vanalkar A.V. and Gajbhiye P.R., 2013. Involute Gear Tooth Contact and Bending Stress Analysis, International Journal of Computational Engineering Research, Vol.03, Issue, 8: 30-36.

Ashby M.F., 2010. Material Selection in Mechanical Design. Butterworth-Heinemann 4th Edition, 640 pages.

Babalik F.C., 2010, Makine Elemanları ve Konstrüksiyon Örnekleri. Dora BasımYayınevi, 4. Baskı, 860 sayfa.

Budynas R.G. and Nisbett J.K., 2011. Shigley's Mechanical Engineering Design. Ninth Edition, McGraw-Hill, 1120 pages.

Chala, G., 1999. ISO 6336 Vs Agma 2001 Gear Rating Comparison for Industrial Gear Applications, Rexnord Industries, LLC.

Childs P.R.N., 2013. Mechanical Design Engineering Handbook. First Edition, Butterworth-Heinemann Ltd, 856 pages. Elements of metric gear technology, WWW.SDP-SI.COM,2014.

Faydor L. Litvin, Alfonso Fuentes; Gear Geometry and Applied Geometry, 2nd edition, Cambridge University Press, 2004.

Fetvaci M.C. and İmrak C.E., 2004. Düz Dişli Çarkların Sonlu Elemanlar Metodu ile Modellenmesi. Sigma Journal of engineering and natural sciences, Vol. 19, 2, 199-203.

Geren N. and Baysal M.M., 2000. Expert System Development for Spur Gear Design. 9. International Conference on Machine Design and Production.

Gökçek M., 2012, Mechanical Engineering. First Published by In Tech, 670 pages. Kapelevich A.L., 2013. Direct Gear Design. CRC Press, Taylor & Francis Group. 324 pages.

Hwang S.C., Lee J.H., Lee D.H., Han S.H. and Lee K.H., 2013. Contact Stress Analysis for a Pair of Mating Gears. Mathematical and Computer Modelling 57, p. 40–49.

Jelaska D.T, 2012, Gears and Gear Drives. 1st Edition, Wiley, 462 pages.

Juvinall R.C., Marshek K.M., 2011. Fundamentals of Machine Component Design. Wiley 5th Edition, 928 pages.

ISO 10300-1, Calculation of load capacity of bevel gears - Part 1: Introduction and general influence factors

ISO 10300-2, Calculation of load capacity of bevel gears - Part 2: Calculation of surface durability (pitting)

ISO 10300-3, Calculation of load capacity of bevel gears - Part 3: Calculation of tooth root strength

Li C., Chiou H., Hung C., Chang Y. and Yen C., 2002. Integration of Finite Element Analysis and Optimum Design on Gear Systems. Finite Elements in Analysis and Design 38, p. 179-192.

LI S., 2007. Finite Element Analyses For Contact Strength and Bending Strength of A Pair of Spur Gears With Machining Errors, Assembly Errors and Tooth Modifications. Mechanism and Machine Theory 42, 88–114.

Litvin F. L., Fuentes A., Hayasaka K. (2006), Design, manufacture, stress analysis, and experimental tests of low-noise high endurance spiral bevel gears, Mechanism and Machine Theory, 41, 83-118.

Marciniec A., Pisula J., Płocica M., Sobolewski B. (2011), Design of bevel gears using mathematical modelling and simulation in the CAD environment, Mechanic, 7, 602-605 (in Polish).

Mott R.L., 2003. Machine Elements in Mechanical Design. 4th Edition, Prentice Hall, 944 pages.

Pedersen N.L., Raju P.R., Sreenivasulu V., Rao P.D. and Kiran C.U.,2010. Improving Bending Stress in Spur Gears Using Asymmetric Gears and Shape Optimization. Mechanism and Machine Theory 45, p.1707–1720.

176

K.Gopinath & M.M.Mayuram, Machine Design II, Indian Institute of
Technology Madras.

Radzevich S.P., 2012. Dudley's Handbook of Practical Gear Design and
Manufacture. Second Edition, CRC Press, Taylor & Francis Group, 878
pages.

Sgihley J.E., 1985. Mechanical Engineering Design: First Metric Edition. Mcgraw-
Hill, 698 pages.

Shiferaw Damtie Beyene 2014, Contact Stress Analysis and Surface   Fatigue Life
Estimation of Involute Spur Gear by Finite Element Method (FEM), 65
pages.

Tiwari S.K. and Joshi U.K., 2012, Stress Analysis of Mating Involute Spur Gear
teeth. International Journal of Engineering Research and Technology,
Volume 1, Issue 9.

Ugural A.C., 2003. Mechanical Design an Integrated Approach 1st Edition.
McGraw Hill, 864 pages.

Url : http://machinedesign.com/
BERG MANUFACTURING, Gear Reference Guide.

V. V. Simon, "Optimal machine-tool settings for the manufacture of face-hobbed
spiral bevel gears," Journal of Mechanical Design, Transactions of the
ASME, vol.136, no.8, Article ID 081004,2014.

BIOGRAPHY

Gül TURĞUT was born in 10.10.1989 in Ömerli/MARDİN. She had lived in Mardin, Adana, Mersin, İzmir, Gaziantep. She has lived in Adana since 2014. She graduated from Pozcu High School in 2007 and enrolled at Automotive Engineering Department of Çukurova University in 2008. She graduated with his Bachelor of Science degree in Automotive Engineering Department with the 4th degree in 2013. She also completed the undergraduate program of Mechanical Engineering with double major in the same year. She started to work in HDM ÇELİK BORU San. ve Tic.Ltd.Şti as an Planning Engineer on May, 2014. In 2015 on September she began her Master of Science education at Mechanical Engineering Department of Çukurova University. She had worked for about three months in HDM ÇELİK BORU San. ve Tic.Ltd.Şti and leaved on August, and in the same month starts the working SANKO MAKİNA as an Assembly Engineer. Since 2014, she has been working at SANKO MAKİNA and now working as a Responsible Engineer.

APPENDIX

A.1. Comparison of Module Selection and Face Width Results of the Design Approaches for Ø=20°, Material type 2
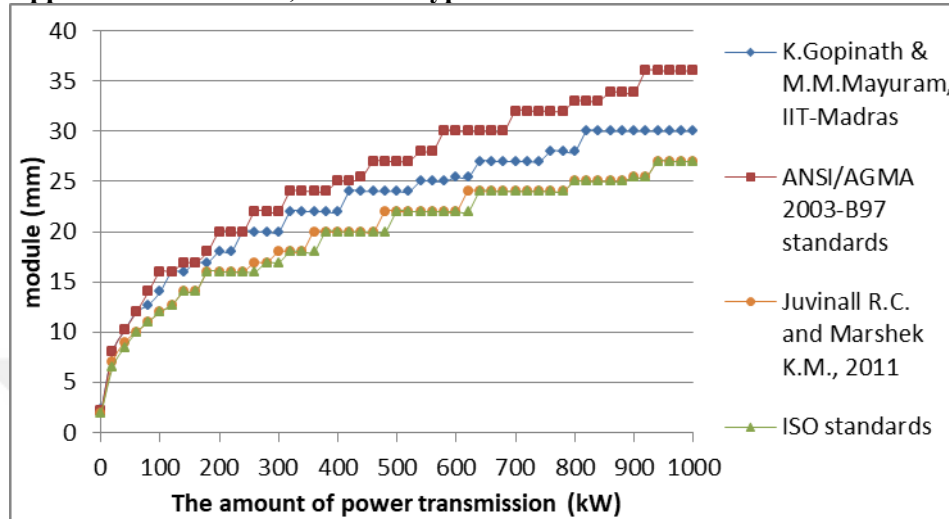
Figure A.1. Module variation considering bending fatigue failure under increasing power at 1:1 speed ratio (for Ø=20°, Material type 2)
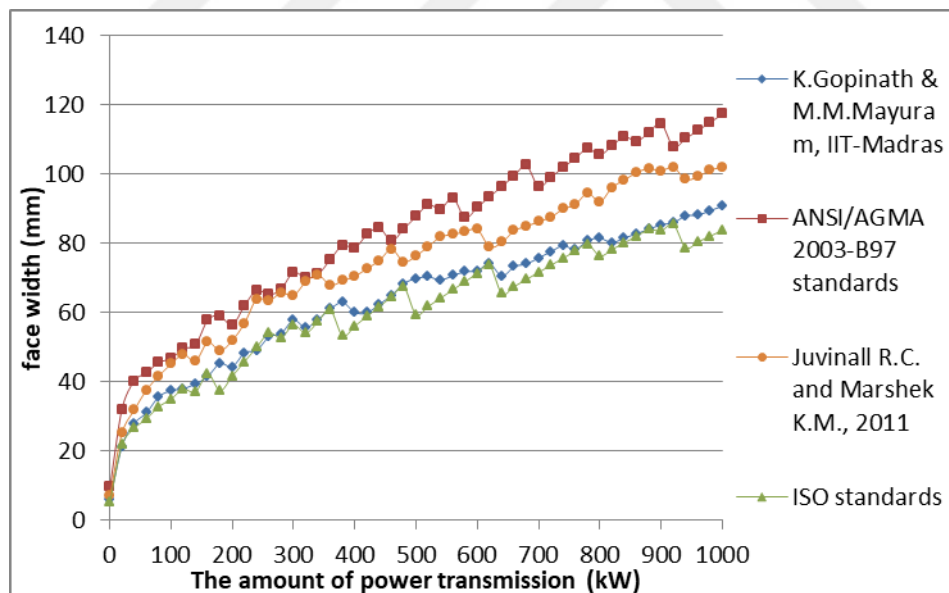
Figure A.2. Face width variation considering bending fatigue failure under increasing power at 1:1 speed ratio (for Ø=20°, Material type 2)
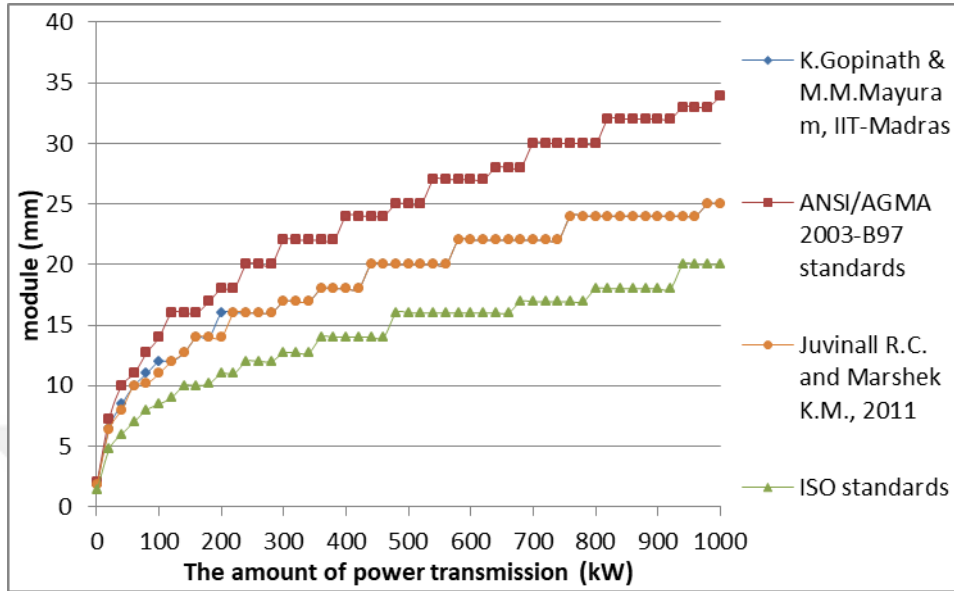
Figure A.3. Module variation considering bending fatigue failure under increasing power at 2:1 speed ratio (for Ø=20°, Material type 2)
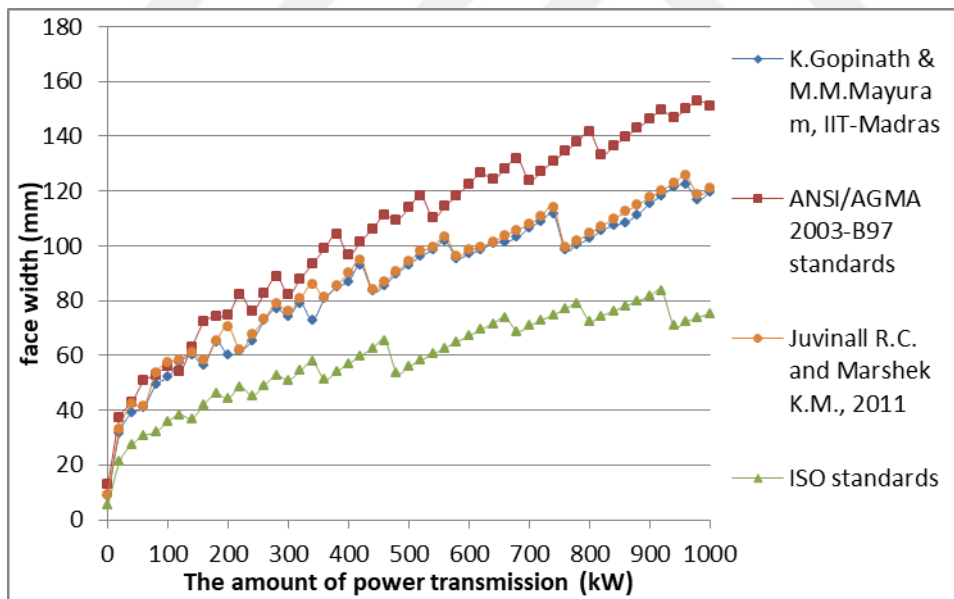
Figure A.4. Face width variation considering bending fatigue failure under increasing power at 2:1 speed ratio (for Ø=20°, Material type 2)
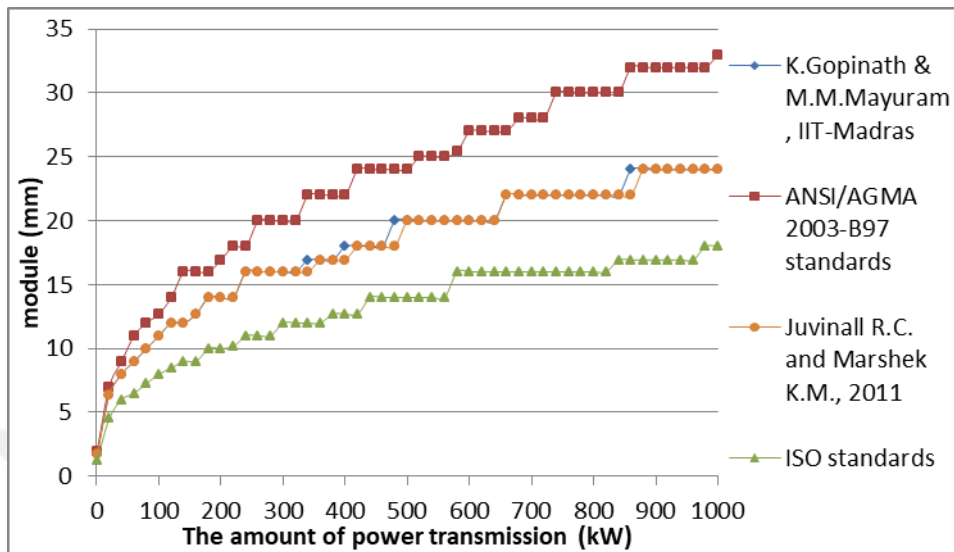
Figure A.5. Module variation considering bending fatigue failure under increasing power at 3:1 speed ratio (for Ø=20°, Material type 2)
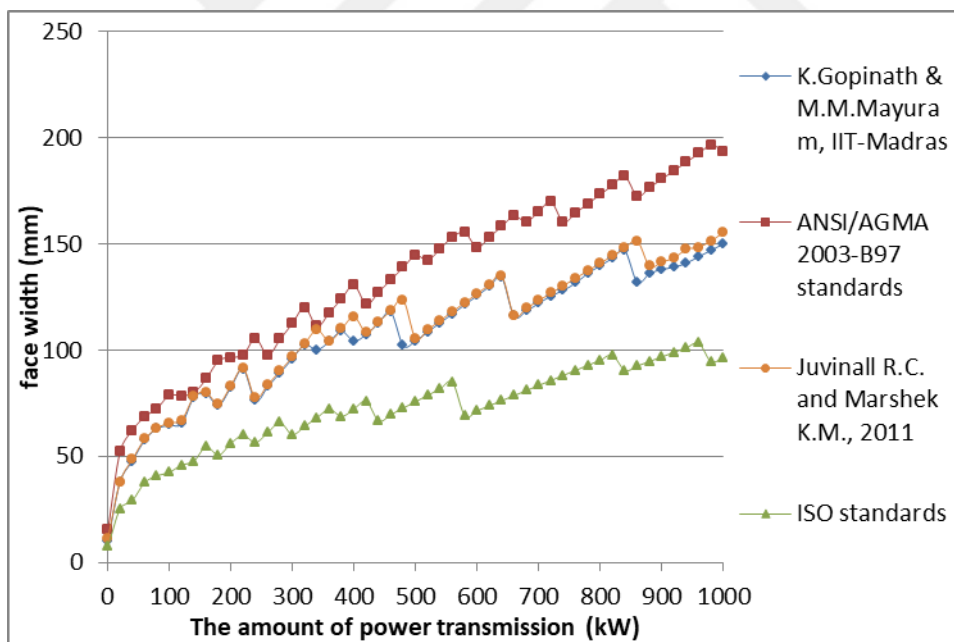
Figure A.6. Face width variation considering bending fatigue failure under increasing power at 3:1 speed ratio (for Ø=20°, Material type 2)
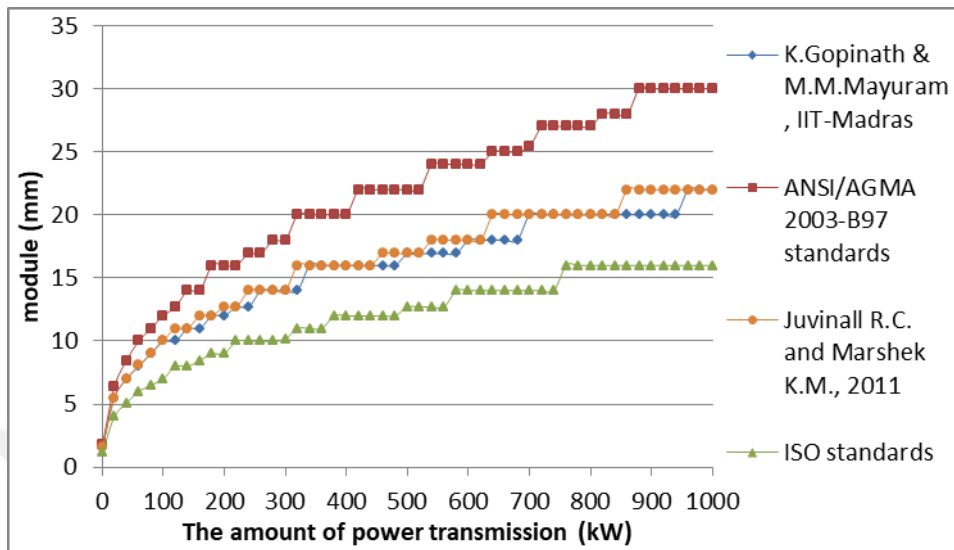
Figure A.7. Module variation considering bending fatigue failure under increasing power at 4:1 speed ratio (for Ø=20$^{\text{o}}$, Material type 2)
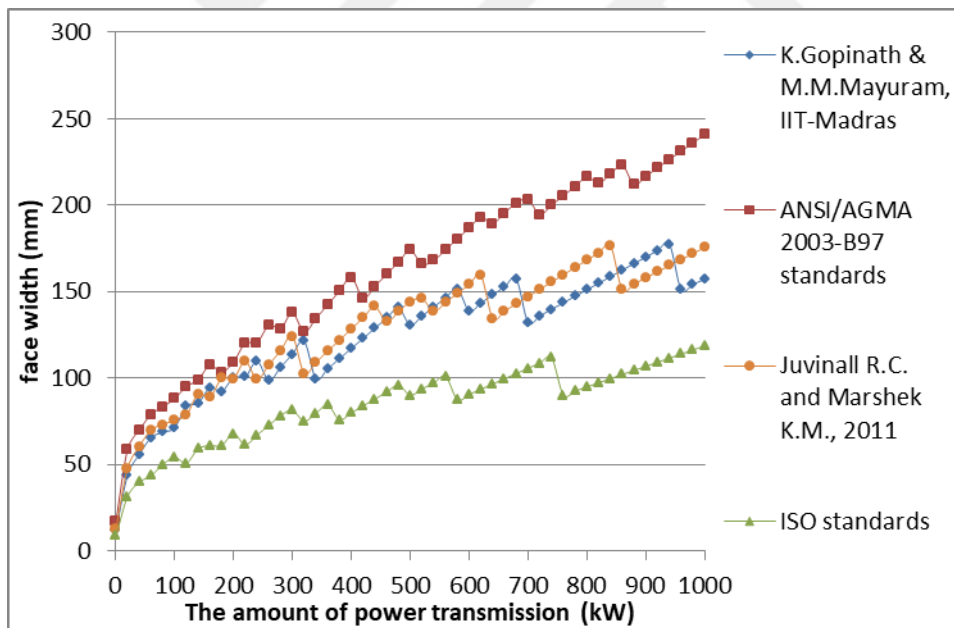
Figure A.8. Face width variation considering bending fatigue failure under increasing power at 4:1 speed ratio (for Ø=20$^{\text{o}}$, Material type 2)
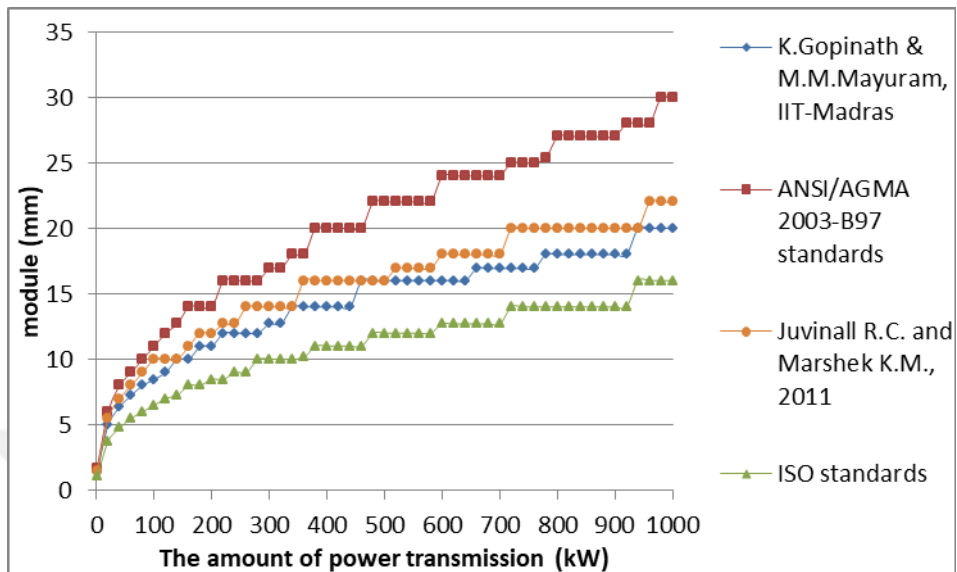
Figure A.9. Module variation considering bending fatigue failure under increasing power at 5:1 speed ratio (for Ø=20°, Material type 2)
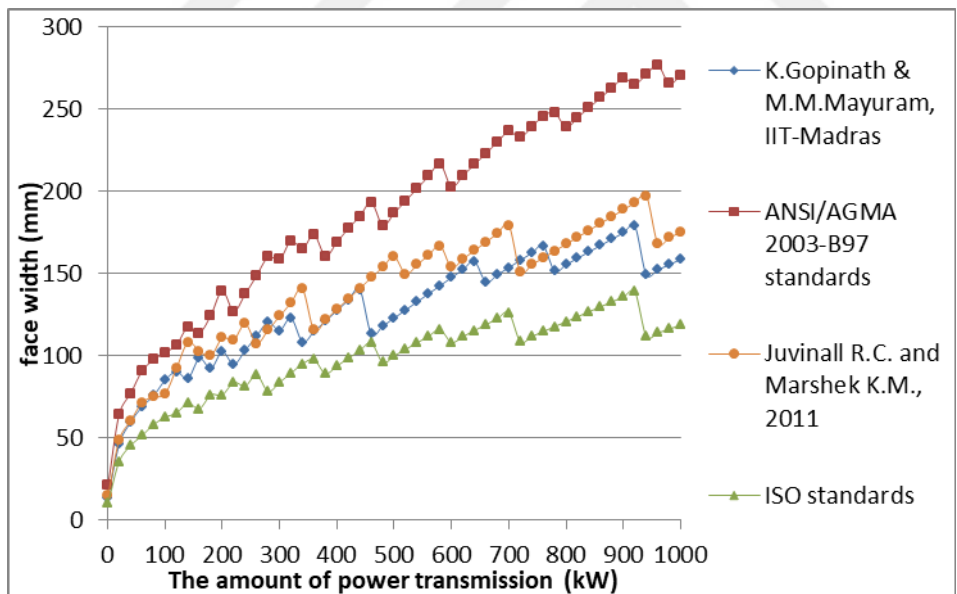

Figure A.10. Face width variation considering bending fatigue failure under increasing power at 5:1 speed ratio (for Ø=20°, Material type 2)
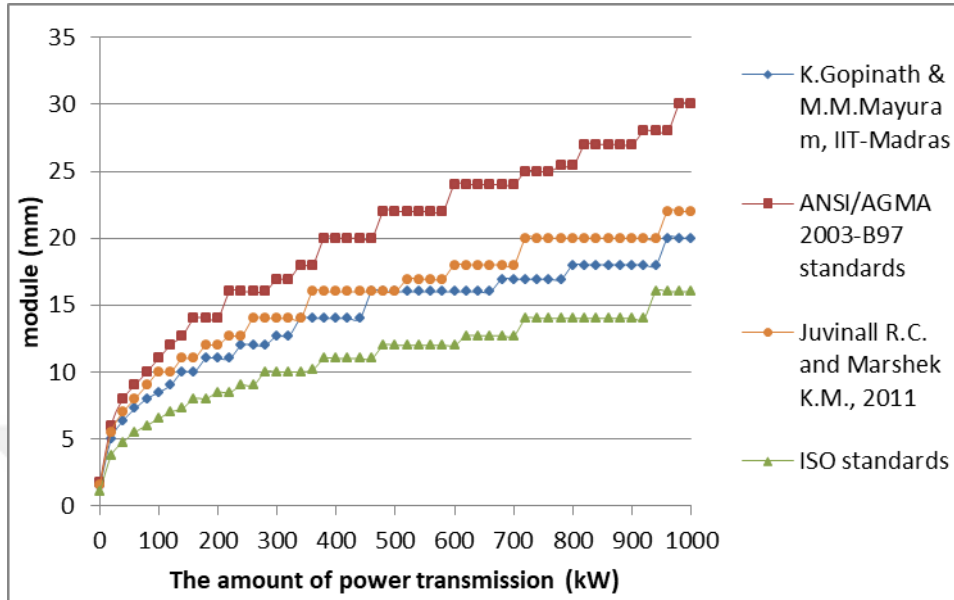
Figure A.11. Module variation considering bending fatigue failure under increasing power at 6:1 speed ratio (for Ø=20°, Material type 2)
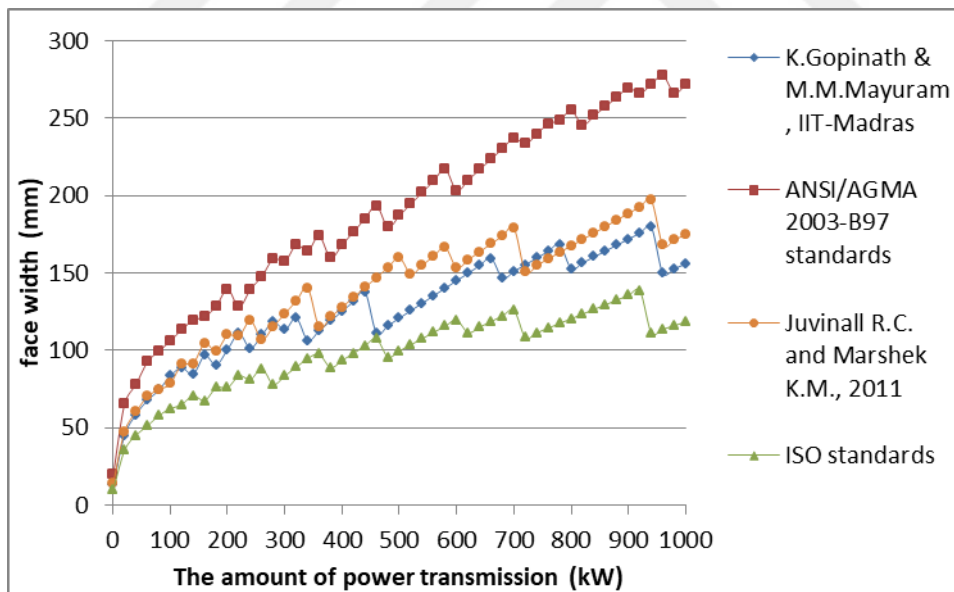
Figure A.12. Face width variation considering bending fatigue failure under increasing power at 6:1 speed ratio (for Ø=20°, Material type 2)
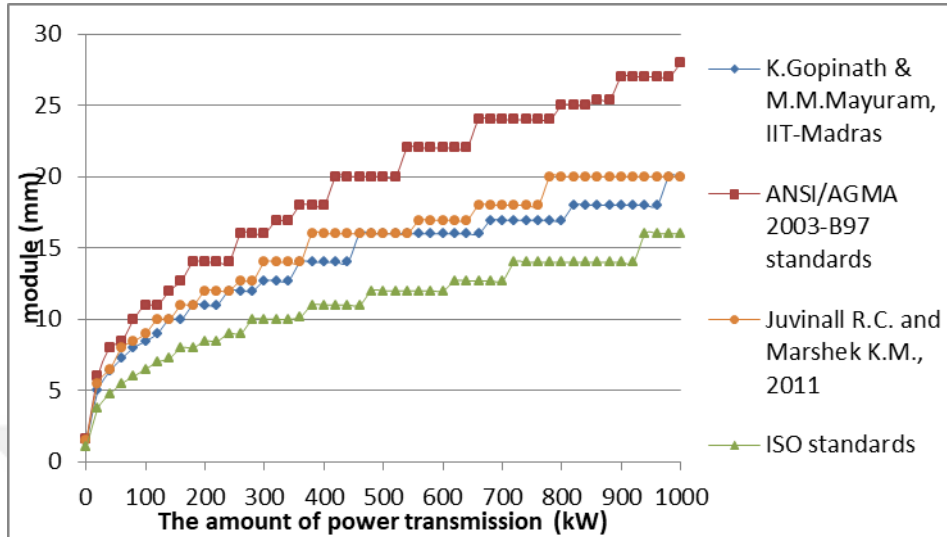
Figure A.13. Module variation considering bending fatigue failure under increasing
power at 7:1 speed ratio (for Ø=20°, Material type 2)
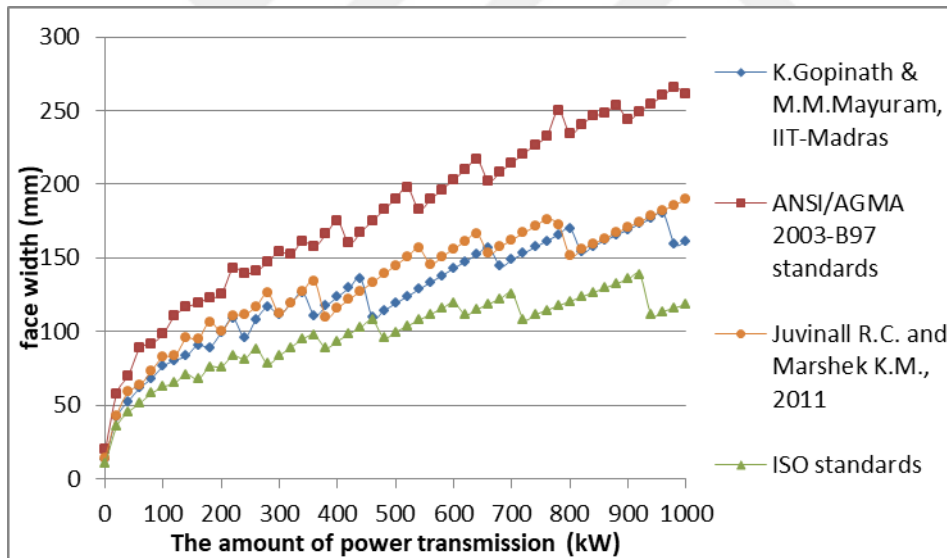
Figure A.14. Face width variation considering bending fatigue failure under
increasing power at 7:1 speed ratio (for Ø=20°, Material type 2)
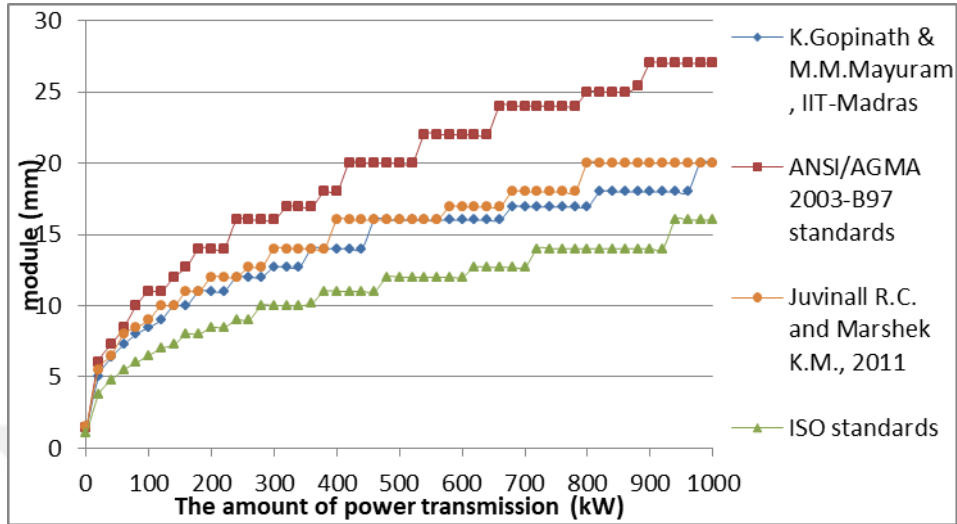
Figure A.15. Module variation considering bending fatigue failure under increasing power at 8:1 speed ratio (for Ø=20°, Material type 2)
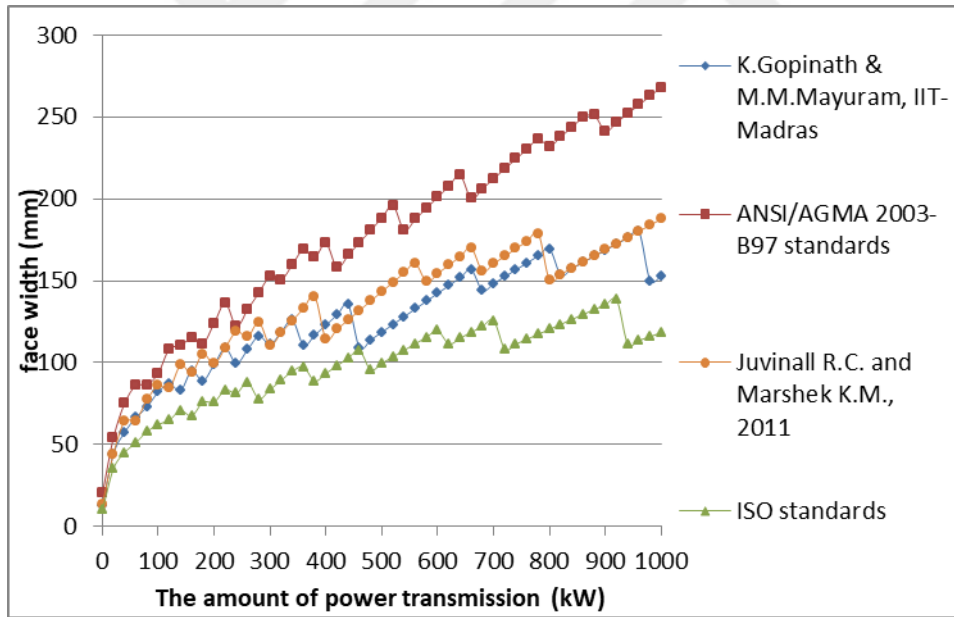
Figure A.16. Face width variation considering bending fatigue failure under increasing power at 8:1 speed ratio (for Ø=20°, Material type 2)

A.2. Comparison of the Results Based on Bending Fatigue Failure Considering Speed Ratio for the Selected Power Transmissions for Ø=20°, Material type 2
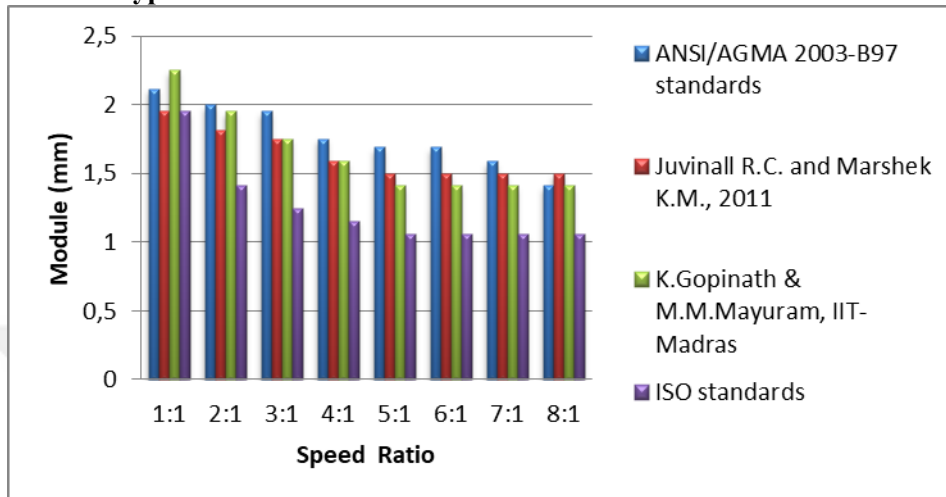
Figure A.17. The effect of speed ratio on module selection based on bending fatigue failure at 0,5 kW power transmission (for Ø=20°, Material type 2)
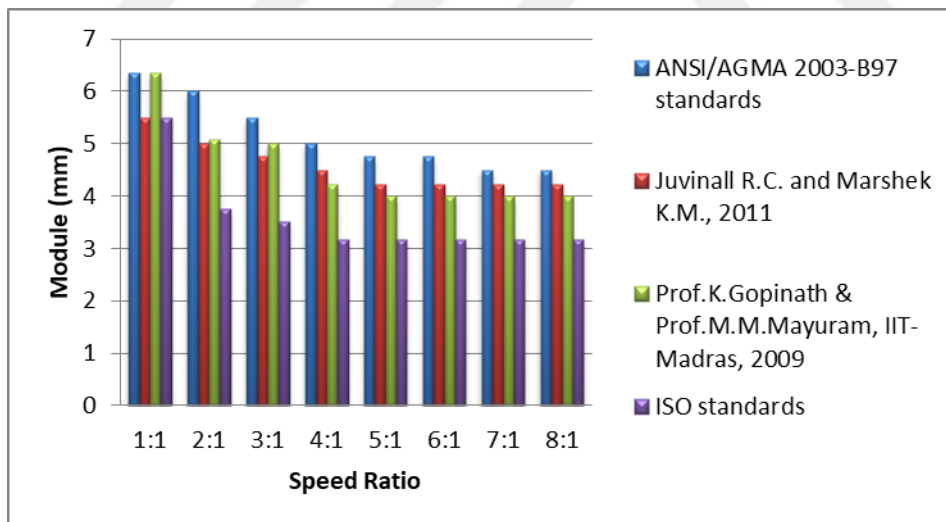
Figure A.18. The effect of speed ratio on module selection based on bending fatigue failure at 10 kW power transmission (for Ø=20°, Material type 2)
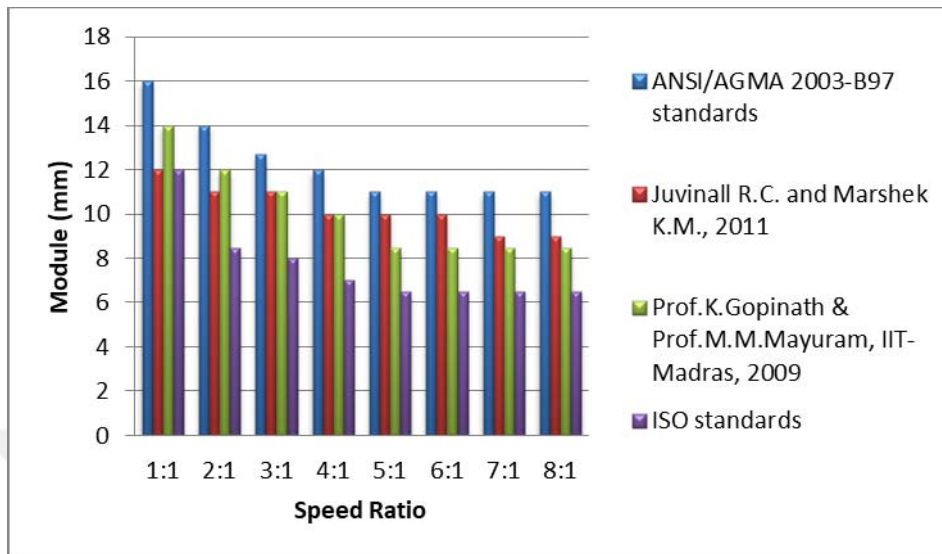
Figure A.19. The effect of speed ratio on module selection based on bending fatigue failure at 100 kW power transmission (for Ø=20°, Material type 2)
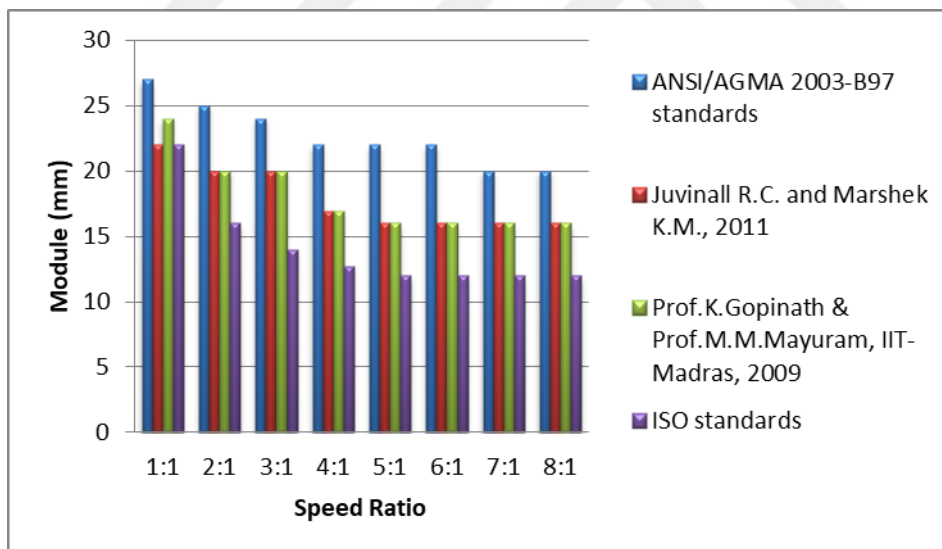
Figure A.20. The effect of speed ratio on module selection based on bending fatigue failure at 500 kW power transmission (for Ø=20°, Material type 2)
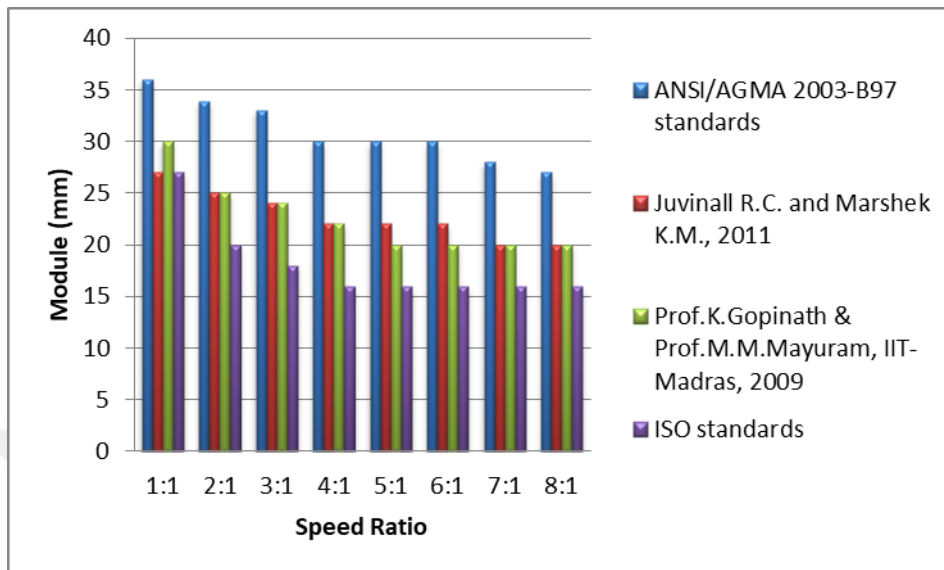
Figure A.21. The effect of speed ratio on module selection based on bending fatigue failure at 1000 kW power transmission (for $\emptyset=20^{o}$, Material type 2)

A.3. Obtaining Geometric Rating Number (GRi) for Design Approaches for Ø=20⁰, Material type 2
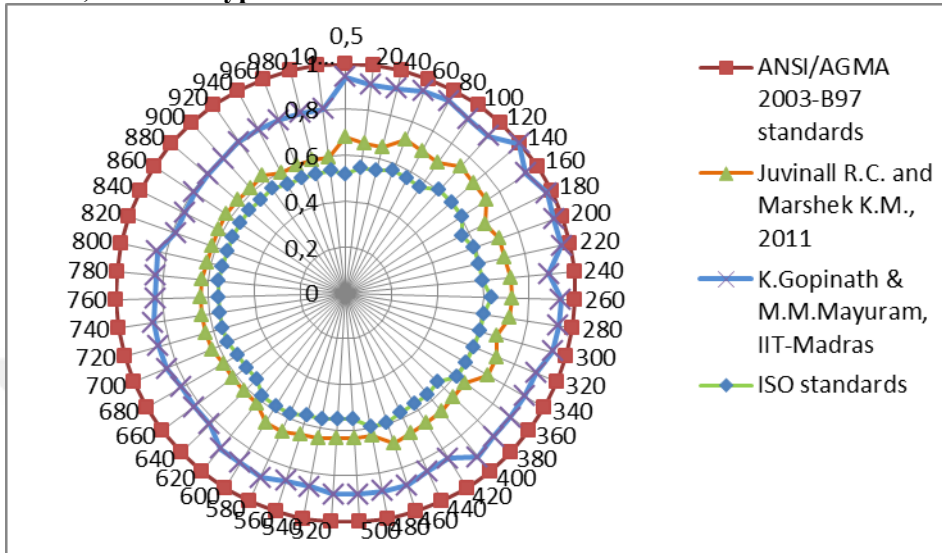
Figure A.22. Comparison of mxF/m_0xF_0 ratios for the design approaches at 1:1 speed ratio (for Ø=20°, Material type 2)
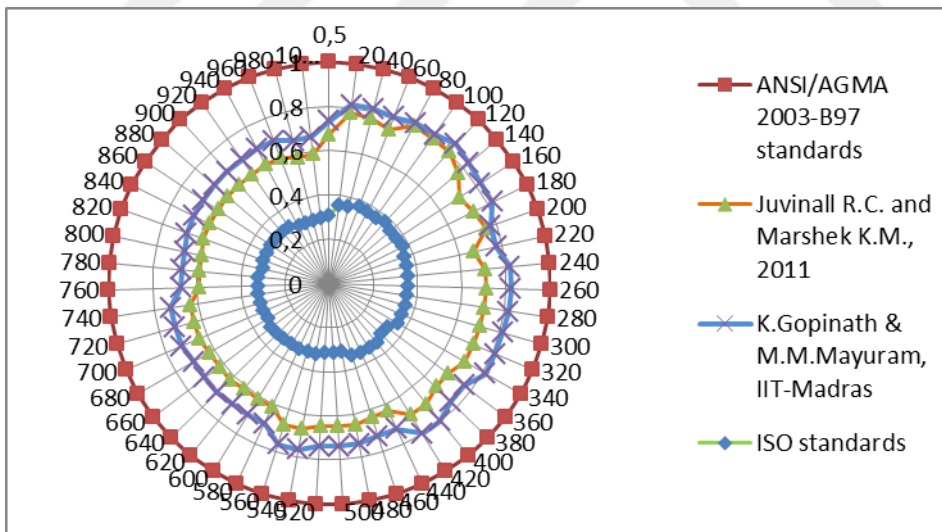
Figure A.23. Comparison of mxF/m_0xF_0 ratios for the design approaches at 2:1 speed ratio (for Ø=20°, Material type 2)
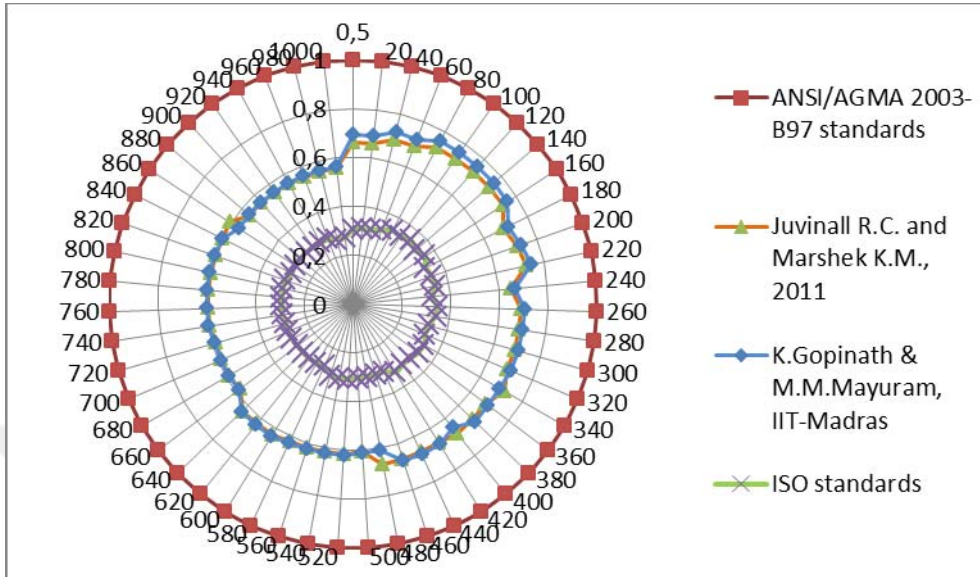
Figure A.24. Comparison of mxF/m_0xF_0 ratios for the design approaches at 3:1 speed ratio (for Ø=20°, Material type 2)
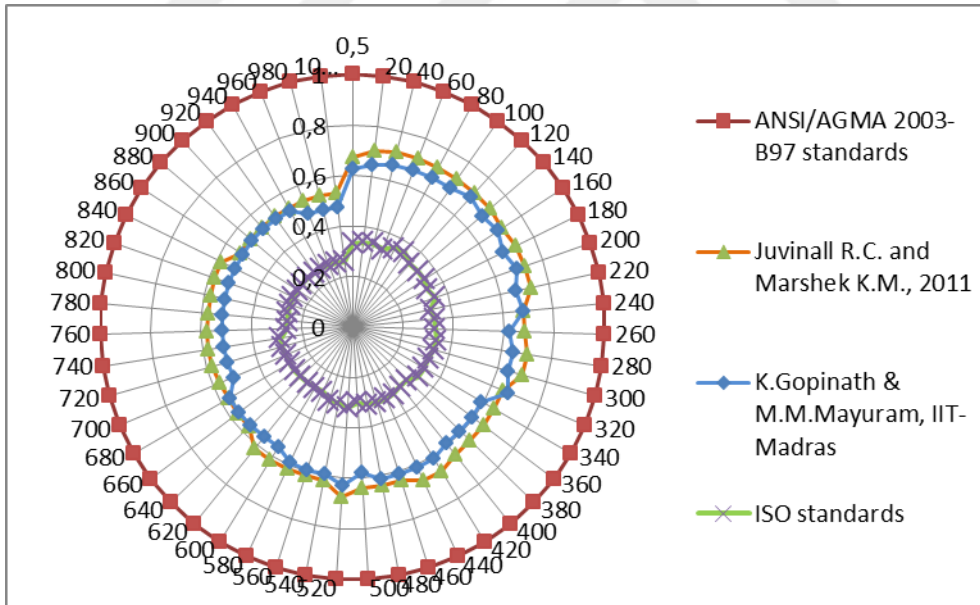
Figure A.25. Comparison of mxF/m_0xF_0 ratios for the design approaches at 4:1 speed ratio (for Ø=20°, Material type 2)
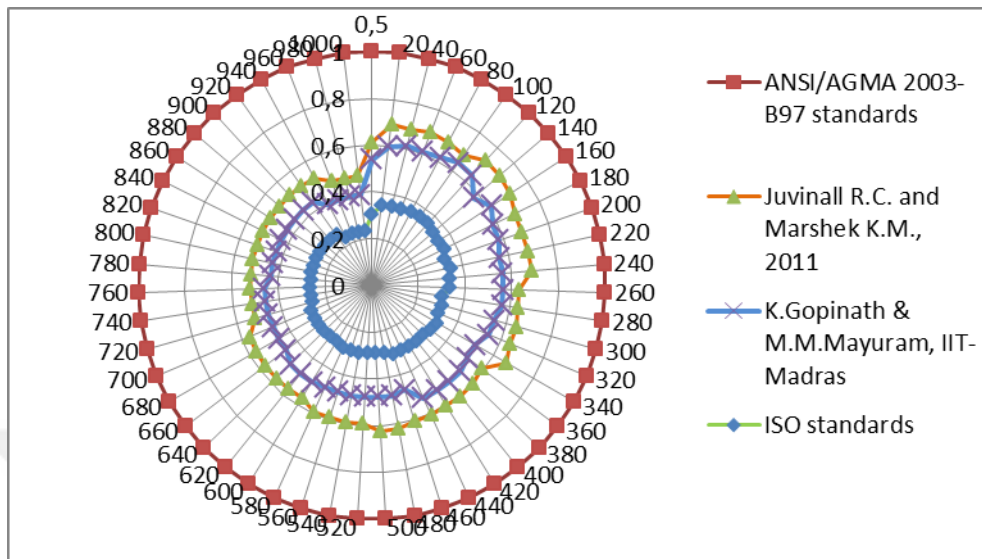
Figure A.26. Comparison of mxF/m_0xF_0 ratios for the design approaches at 5:1 speed ratio (for $\varnothing=20^o$, Material type 2)
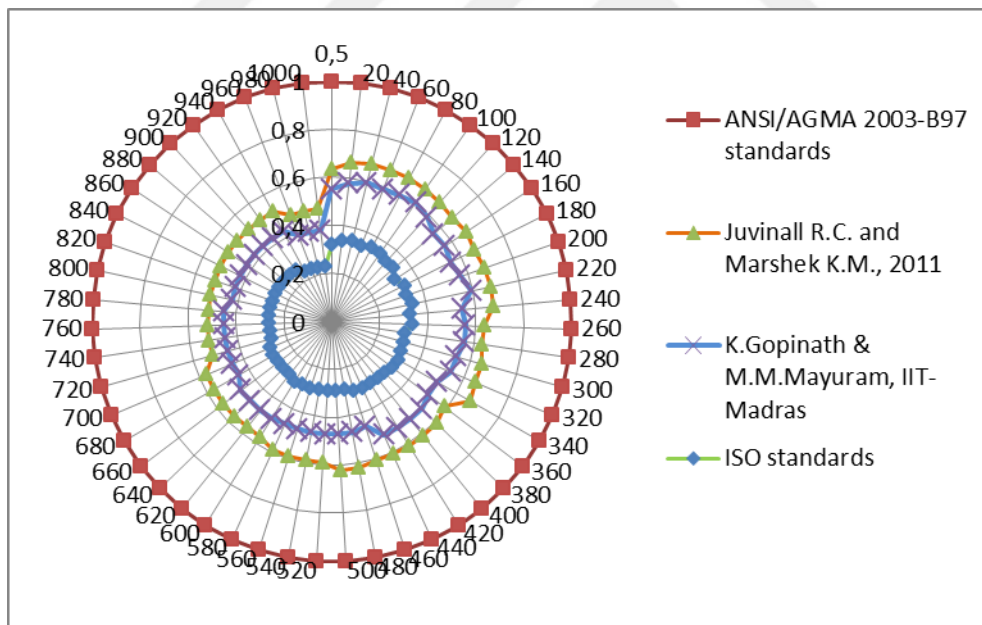
Figure A.27. Comparison of mxF/m_0xF_0 ratios for the design approaches at 6:1 speed ratio (for $\varnothing=20^o$, Material type 2)
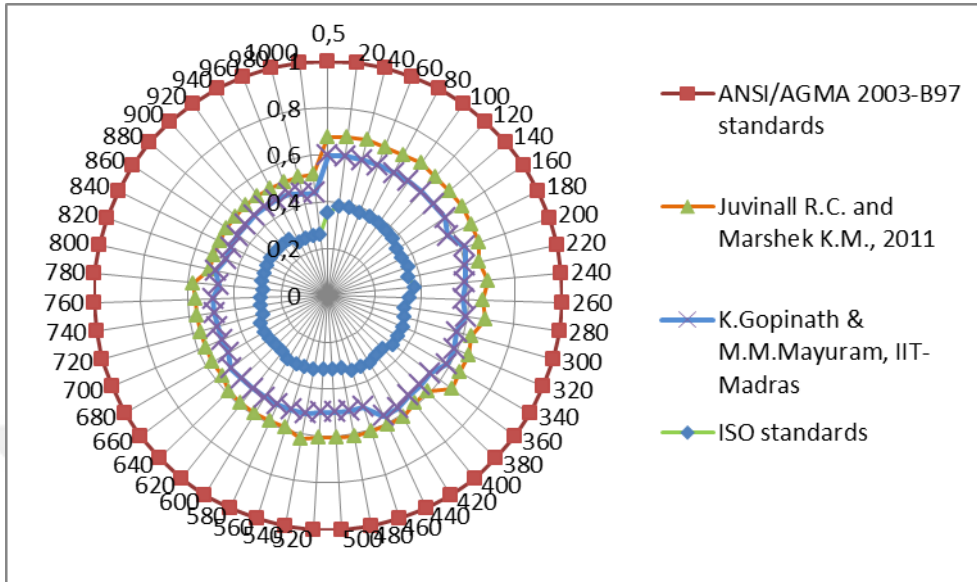
Figure A.28. Comparison of mxF/m_0xF_0 ratios for the design approaches at 7:1 speed ratio (for $\emptyset=20^o$, Material type 2)
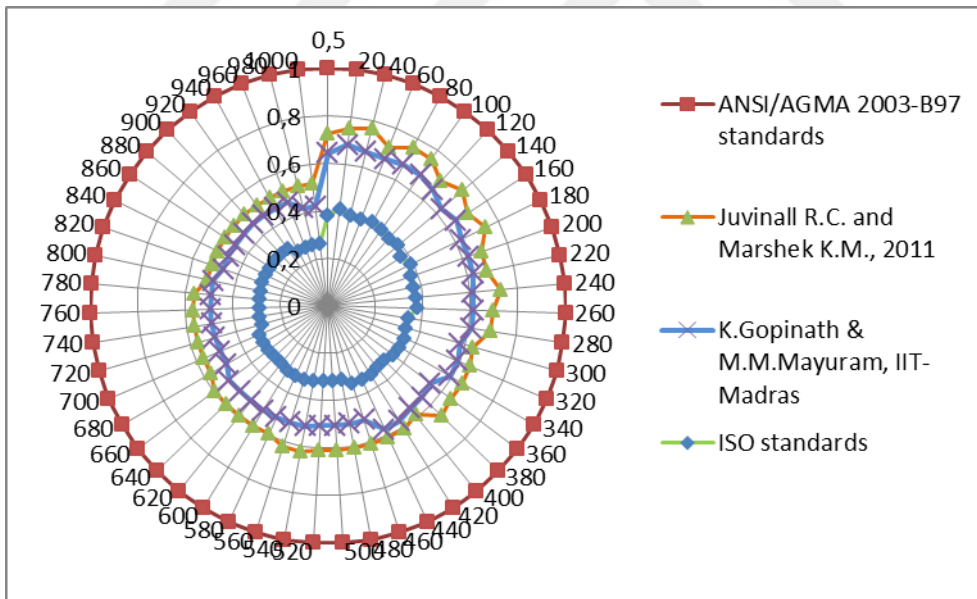
Figure A.29. Comparison of mxF/m_0xF_0 ratios for the design approaches at 8:1 speed ratio (for $\emptyset=20^o$, Material type 2)

APPENDIX B

B.1. Comparison of Module Selection and Face Width Results of the Design Approaches for Ø=20°, Material type 3
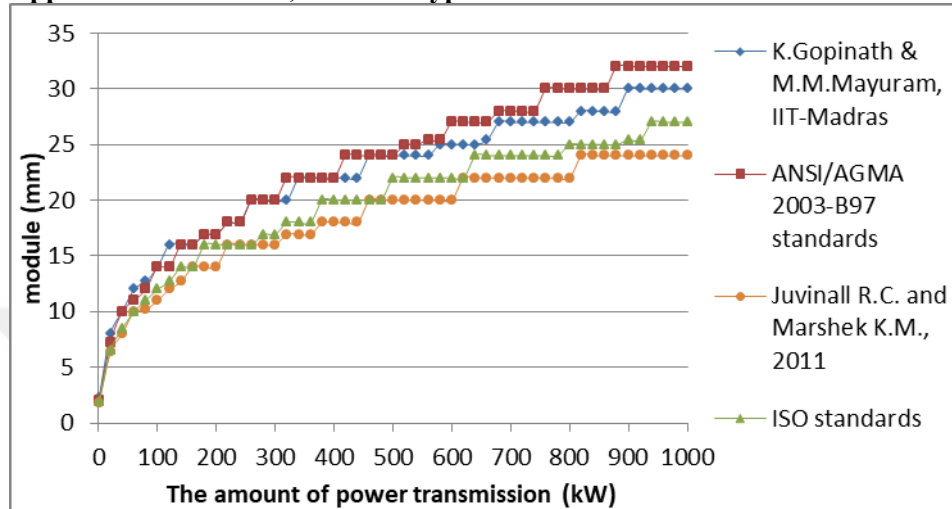

Figure B.1. Module variation considering bending fatigue failure under increasing power at 1:1 speed ratio (for Ø=20°, Material type 3)
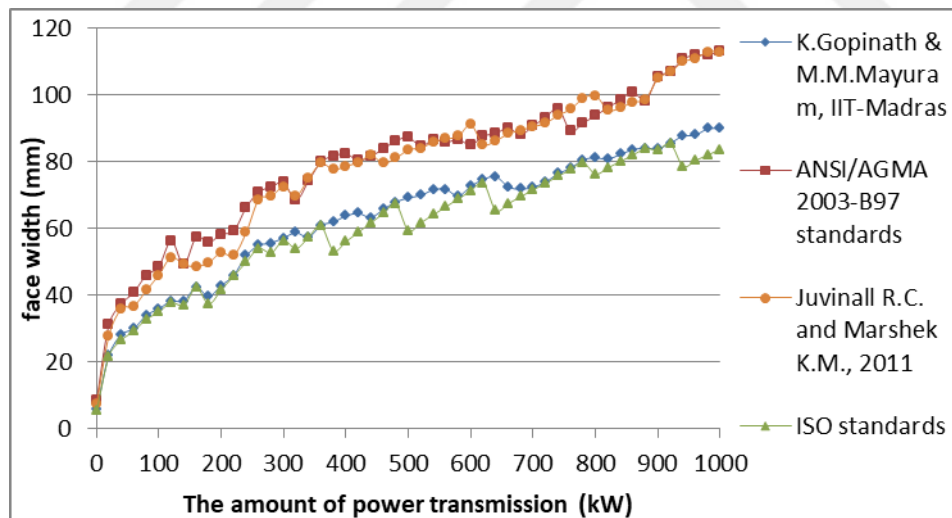

Figure B.2. Face width variation considering bending fatigue failure under increasing power at 1:1 speed ratio (for Ø=20°, Material type 3)

197
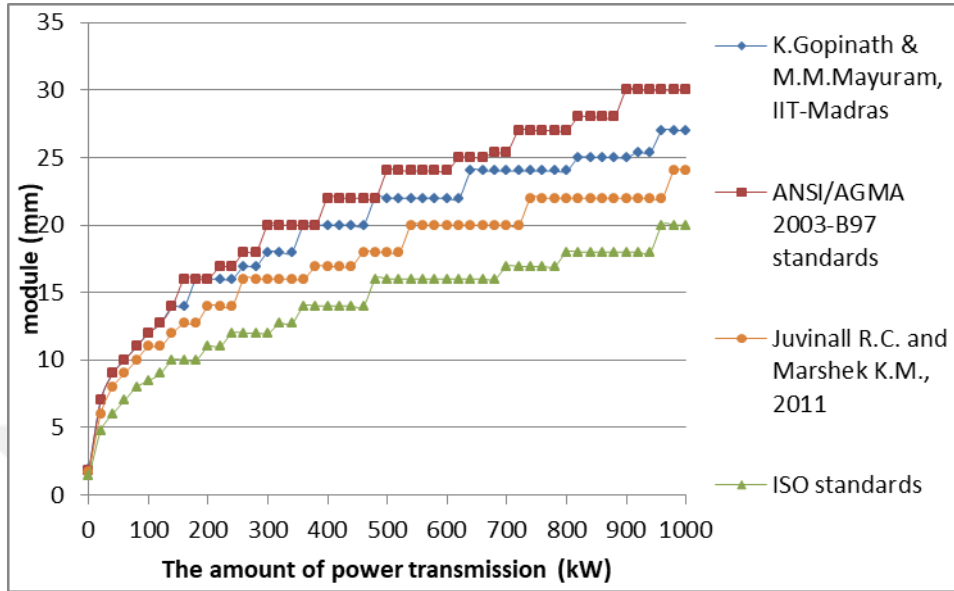
Figure B.3. Module variation considering bending fatigue failure under increasing power at 2:1 speed ratio (for Ø=20°, Material type 3)
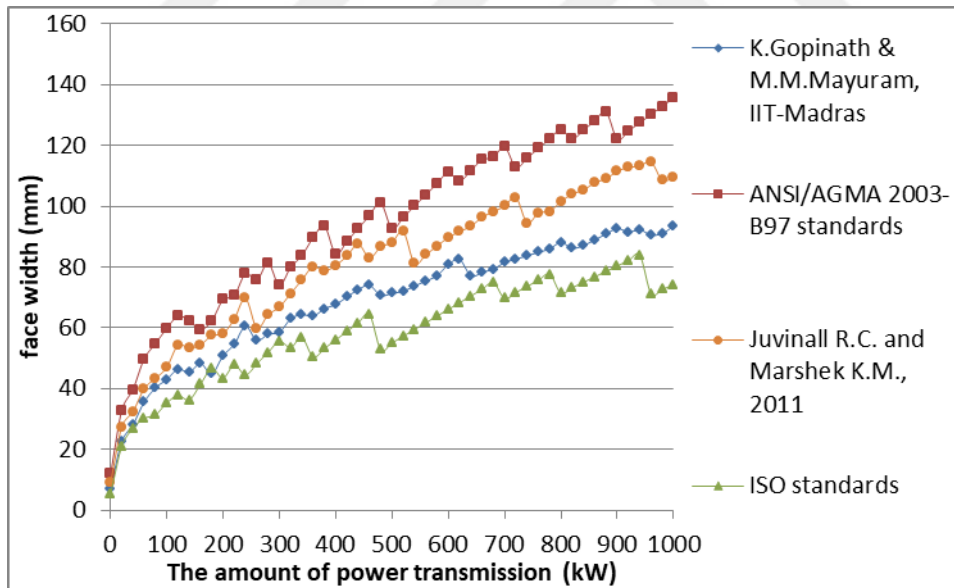
Figure B.4. Face width variation considering bending fatigue failure under increasing power at 2:1 speed ratio (for Ø=20°, Material type 3)
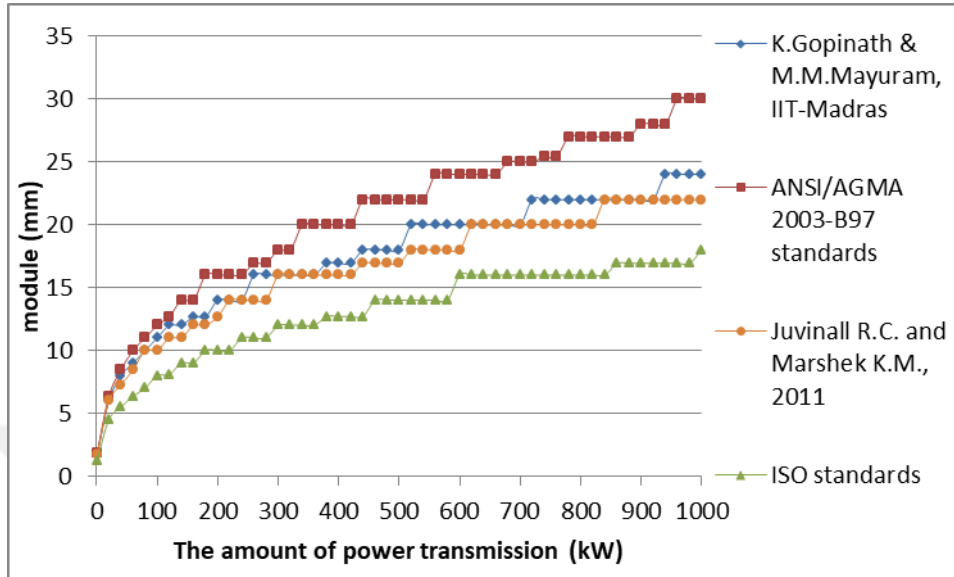
Figure B.5. Module variation considering bending fatigue failure under increasing power at 3:1 speed ratio (for Ø=20°, Material type 3)
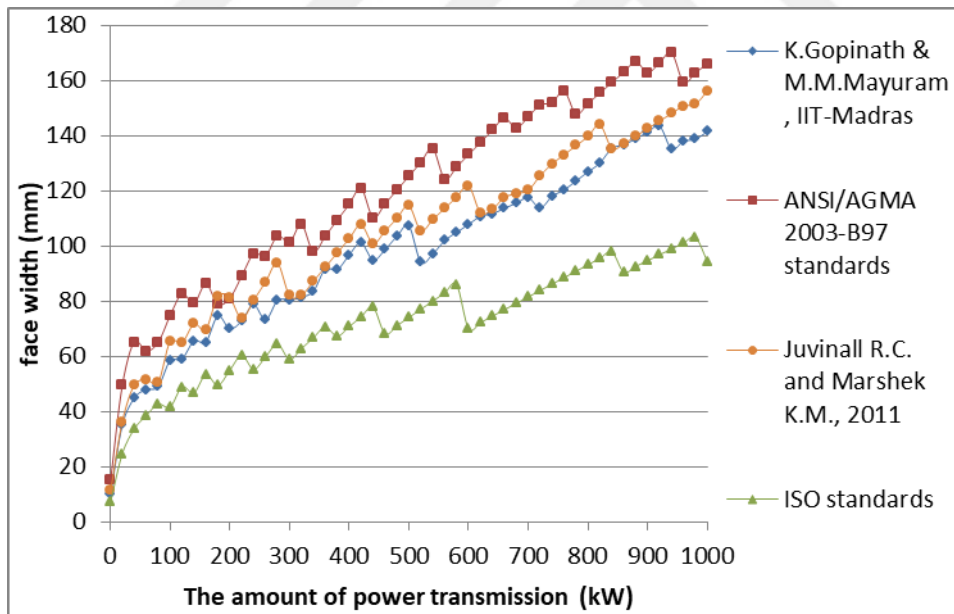
Figure B.6. Face width variation considering bending fatigue failure under increasing power at 3:1 speed ratio (for Ø=20°, Material type 3)
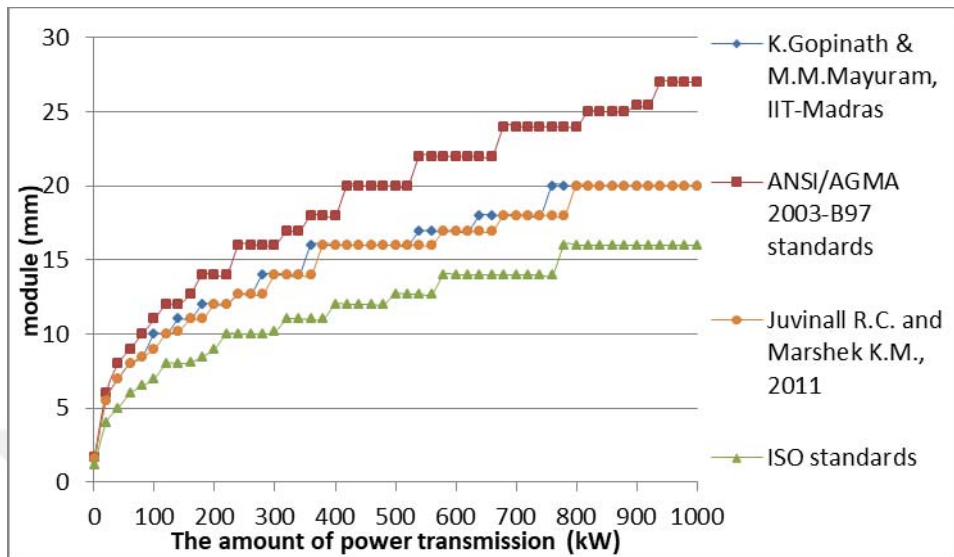
Figure B.7. Module variation considering bending fatigue failure under increasing power at 4:1 speed ratio (for Ø=20°, Material type 3)
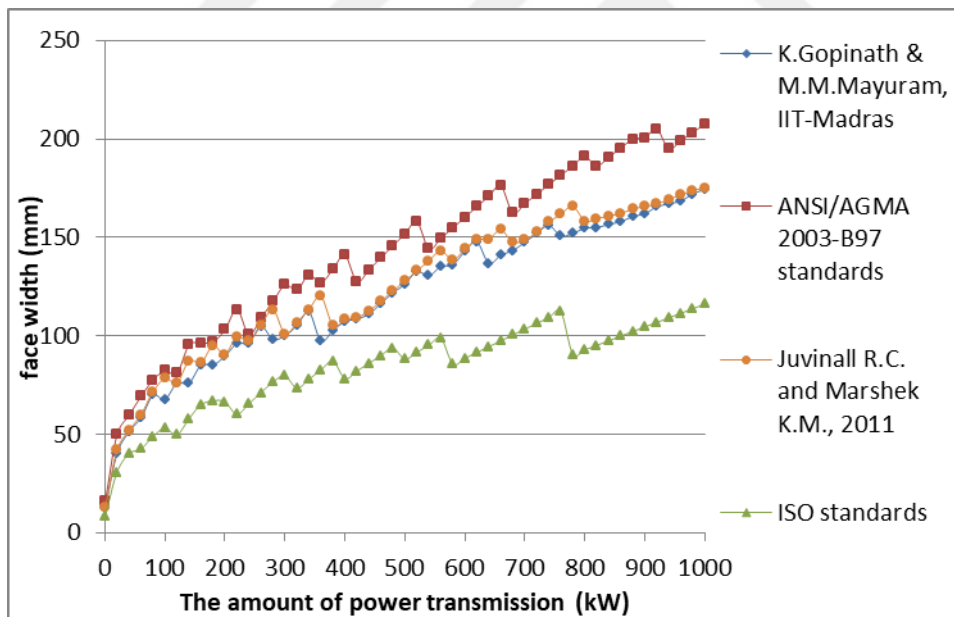
Figure B.8. Face width variation considering bending fatigue failure under increasing power at 4:1 speed ratio (for Ø=20°, Material type 3)
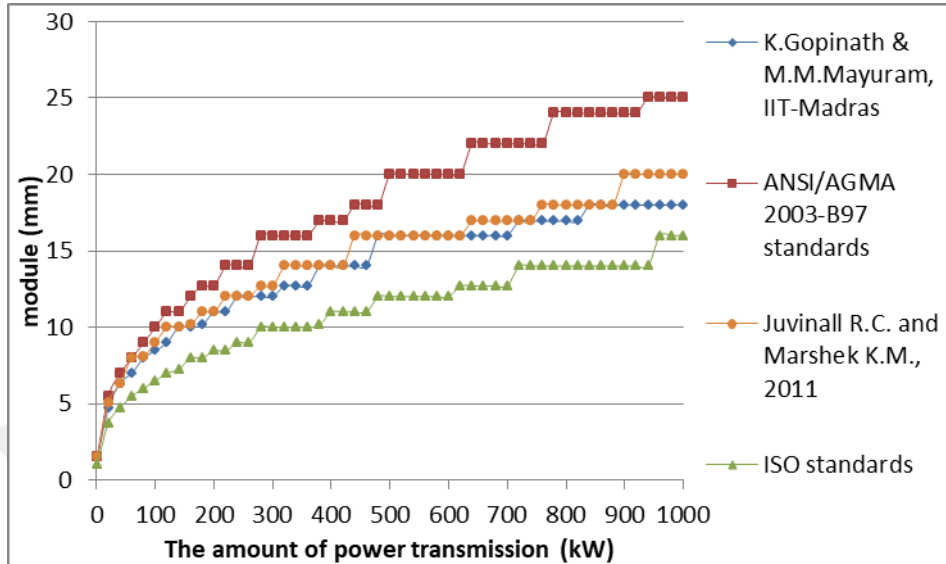
Figure B.9. Module variation considering bending fatigue failure under increasing power at 5:1 speed ratio (for Ø=20°, Material type 3)
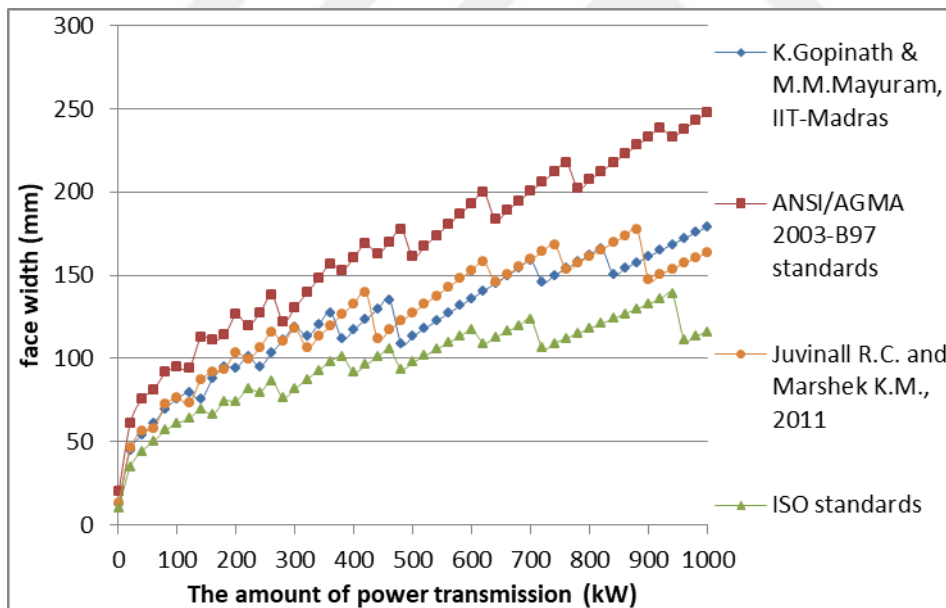
Figure B.10. Face width variation considering bending fatigue failure under increasing power at 5:1 speed ratio (for Ø=20°, Material type 3)
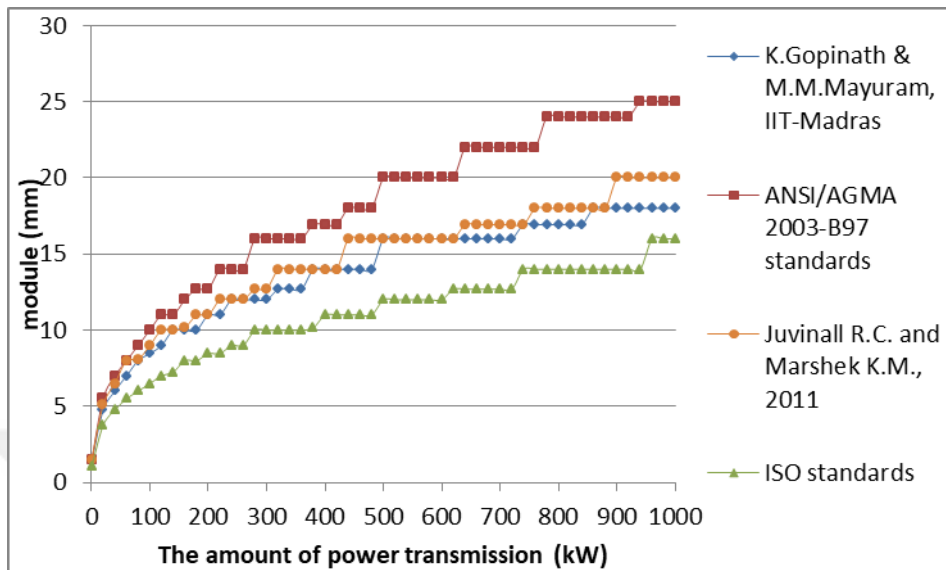
Figure B.11. Module variation considering bending fatigue failure under increasing power at 6:1 speed ratio (for Ø=20°, Material type 3)
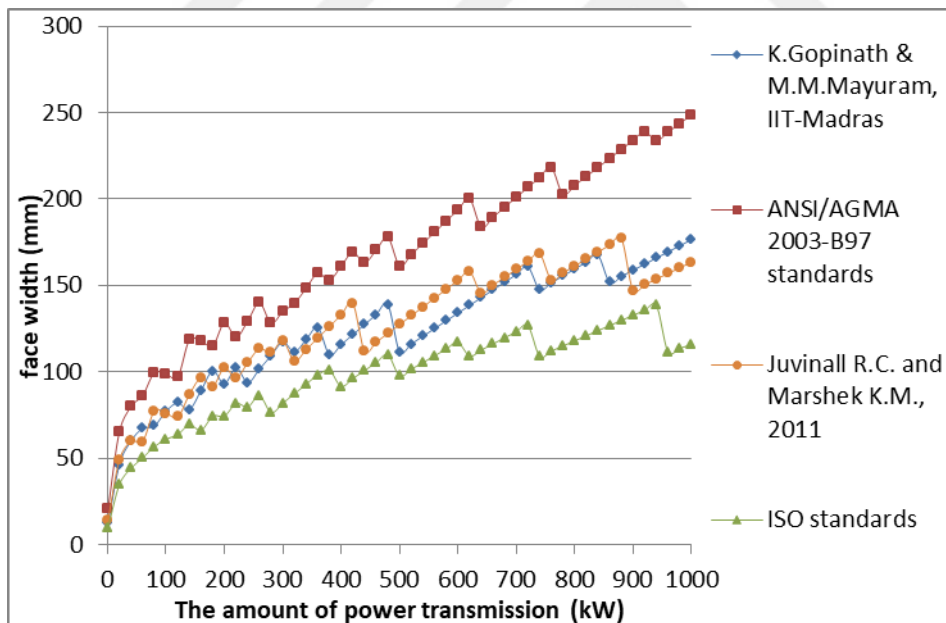
Figure B.12. Face width variation considering bending fatigue failure under increasing power at 6:1 speed ratio (for Ø=20°, Material type 3)
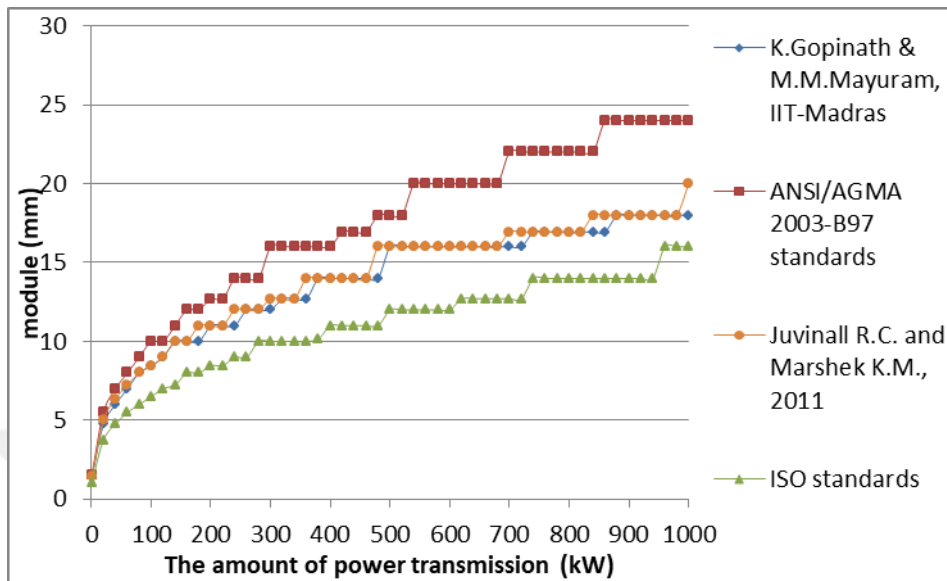
Figure B.13. Module variation considering bending fatigue failure under increasing power at 7:1 speed ratio (for Ø=20°, Material type 3)
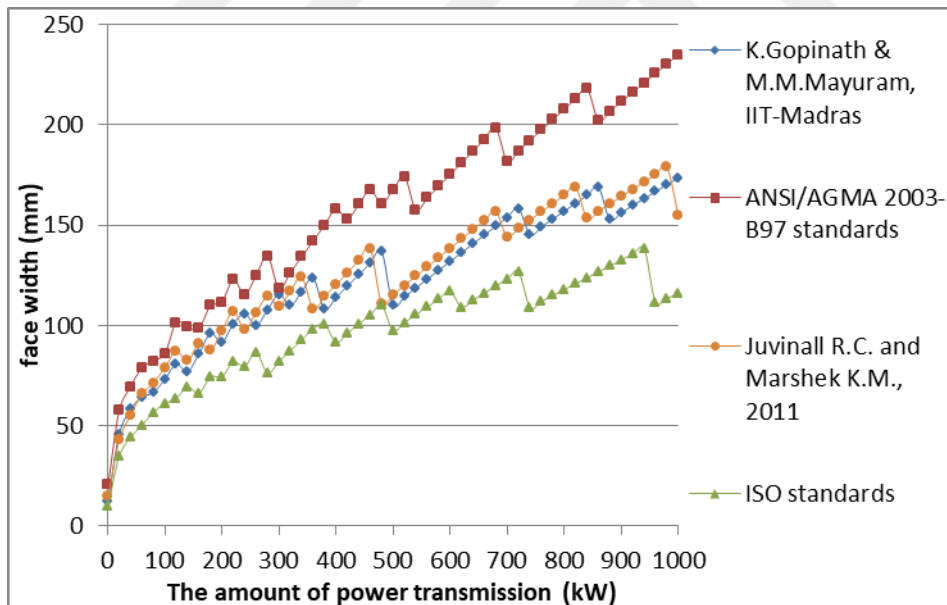
Figure B.14. Face width variation considering bending fatigue failure under increasing power at 7:1 speed ratio (for Ø=20°, Material type 3)
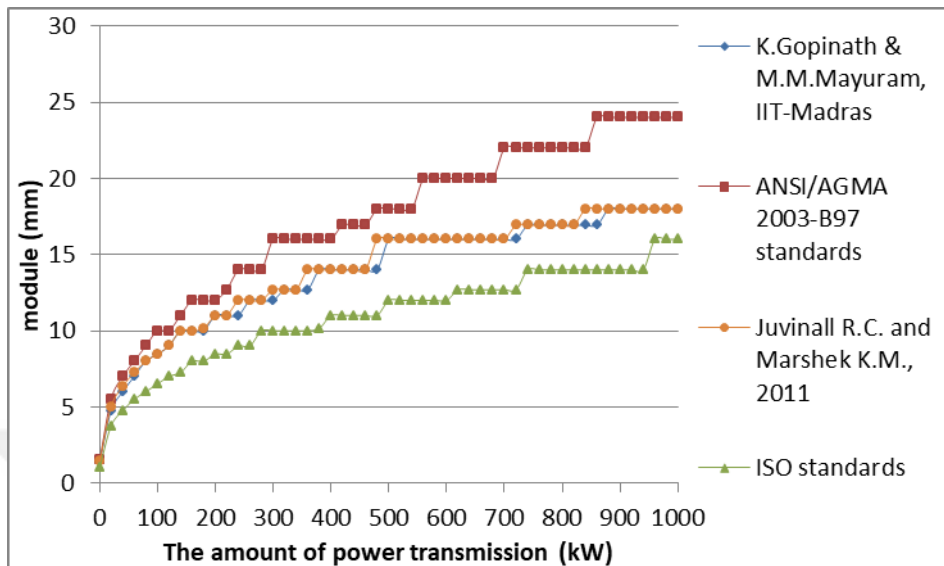
Figure B.15. Module variation considering bending fatigue failure under increasing power at 8:1 speed ratio (for Ø=20°, Material type 3)
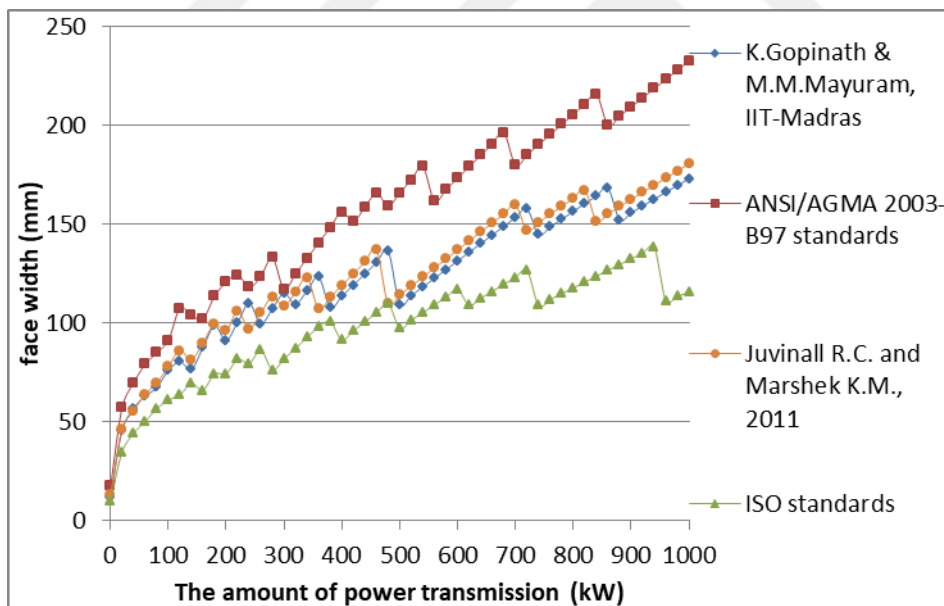
Figure B.16. Face width variation considering bending fatigue failure under increasing power at 8:1 speed ratio (for Ø=20°, Material type 3)

B.2. Comparison of the Results Based on Bending Fatigue Failure Considering Speed Ratio for the Selected Power Transmissions for Ø=20°, Material type 3
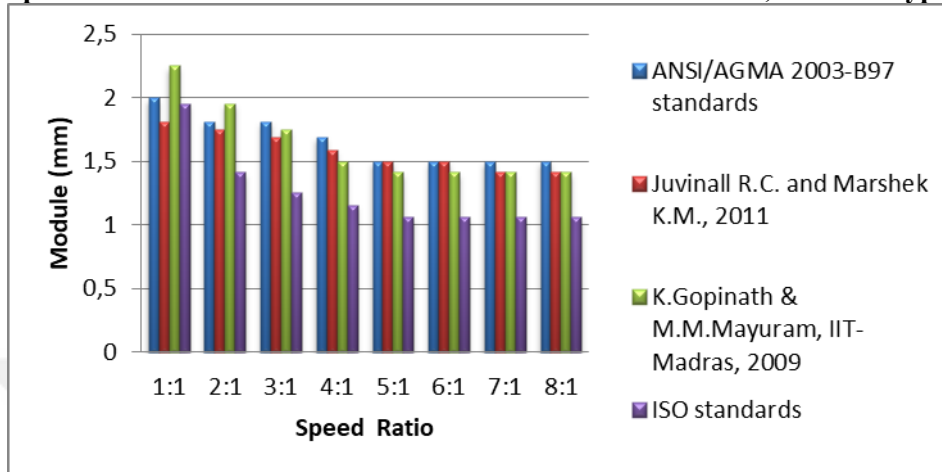
Figure B.17. The effect of speed ratio on module selection based on bending fatigue failure at 0,5 kW power transmission (for Ø=20°, Material type 3)
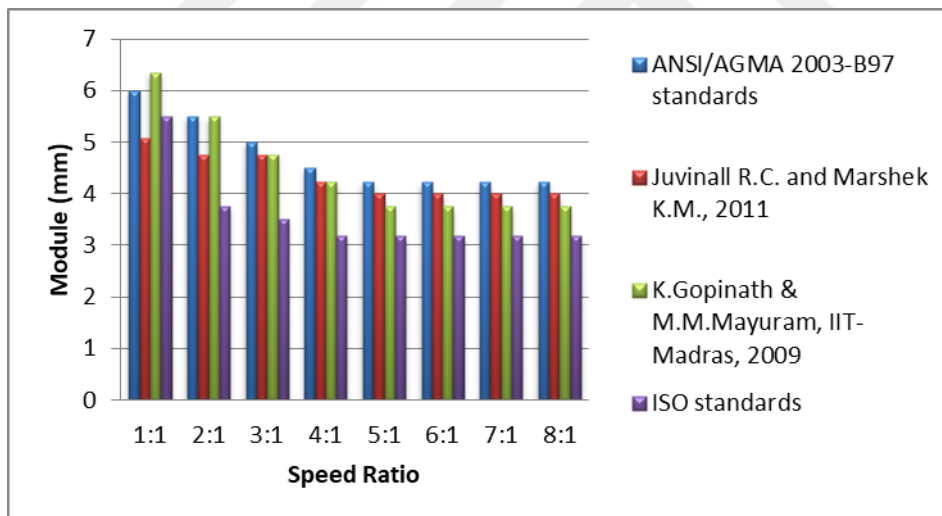
Figure B.18. The effect of speed ratio on module selection based on bending fatigue failure at 10 kW power transmission (for Ø=20°, Material type 3)
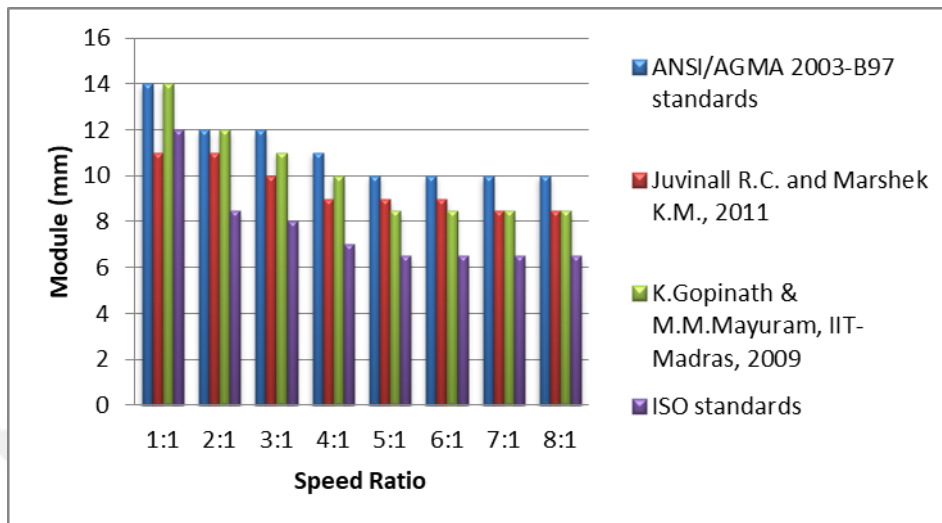
Figure B.19. The effect of speed ratio on module selection based on bending fatigue failure at 100 kW power transmission (for Ø=20°, Material type 3)
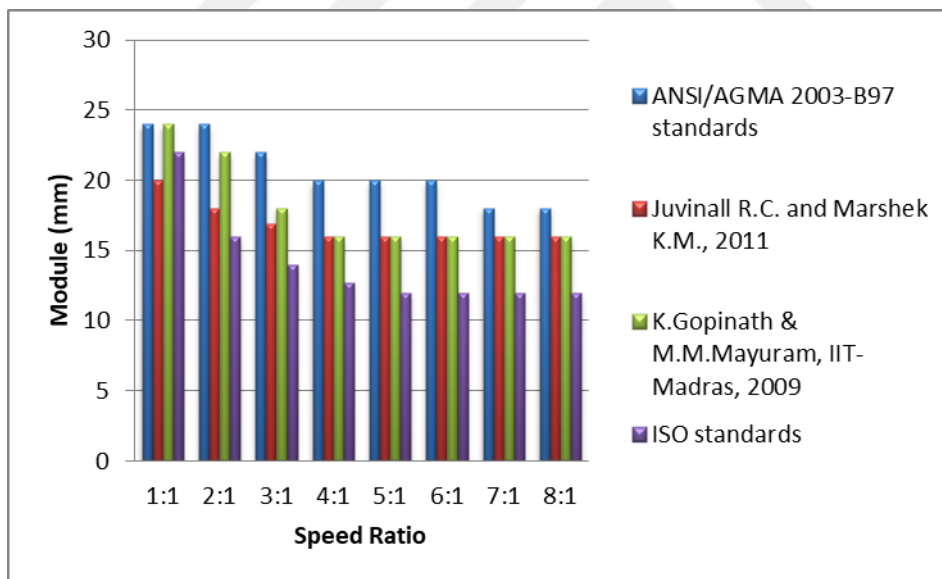
Figure B.20. The effect of speed ratio on module selection based on bending fatigue failure at 500 kW power transmission (for Ø=20°, Material type 3)
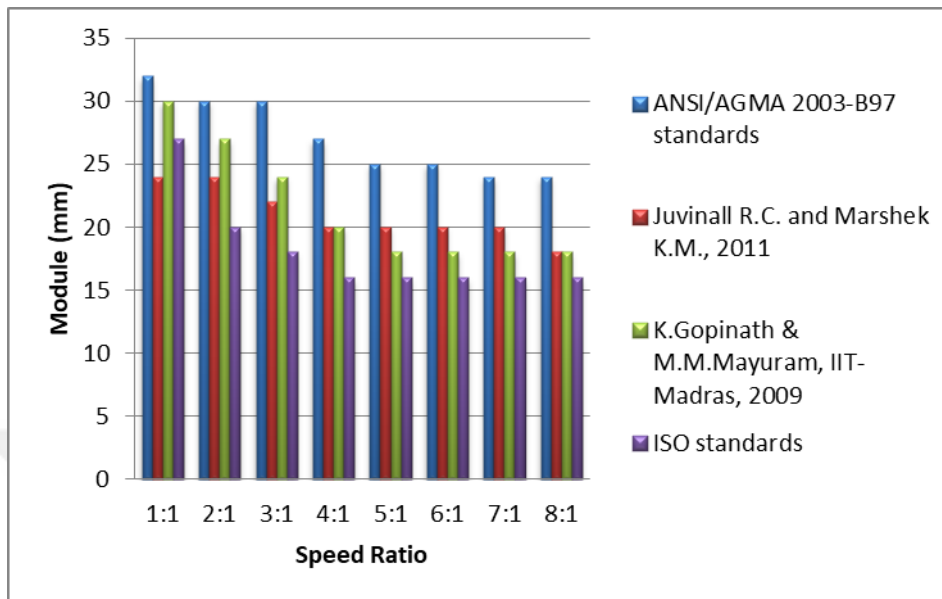
Figure B.21. The effect of speed ratio on module selection based on bending
   fatigue failure at 1000 kW power transmission (for Ø=20°, Material
   type 3)

**B.3. Obtaining Geometric Rating Number (GR$_i$) for Design Approaches for Ø=20°, Material type 3**
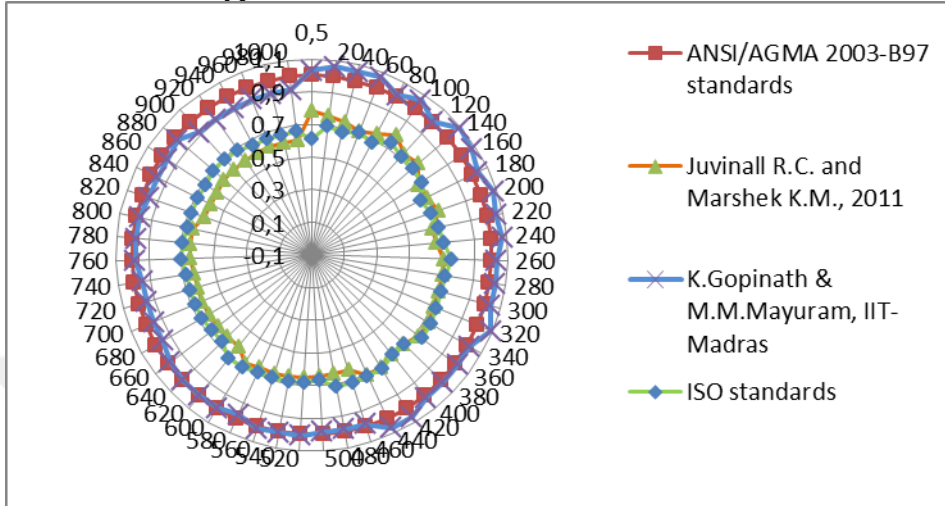
Figure B.22. Comparison of mxF/m$_0$xF$_0$ ratios for the design approaches at 1:1 speed ratio (for Ø=20°, Material type 3)
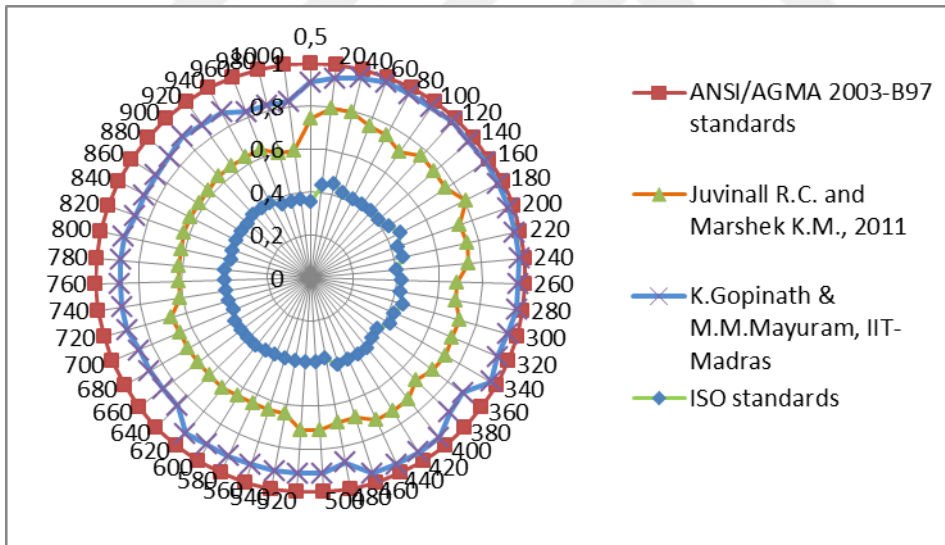
Figure B.23. Comparison of mxF/m$_0$xF$_0$ ratios for the design approaches at 2:1 speed ratio (for Ø=20°, Material type 3)
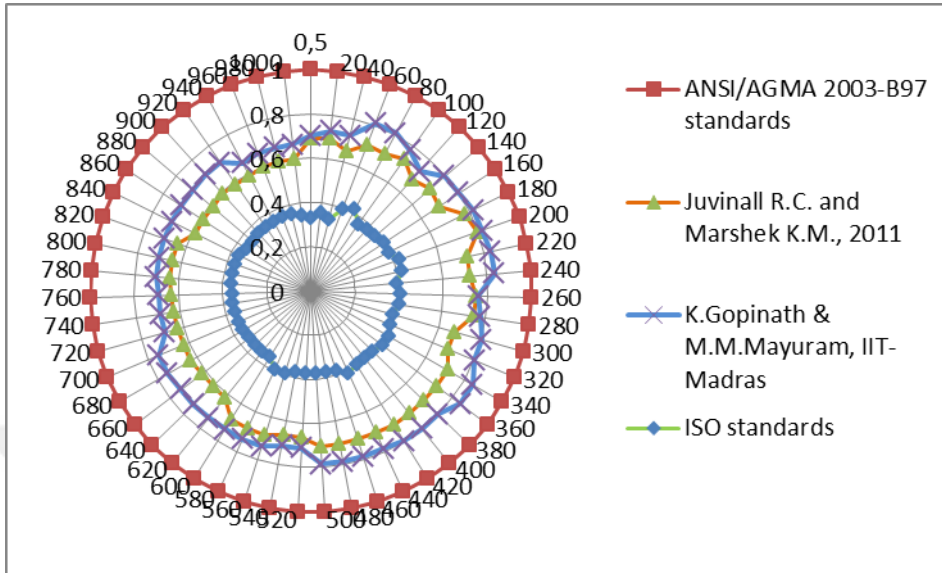
Figure B.24. Comparison of mxF/m₀xF₀ ratios for the design approaches at 3:1 speed ratio (for $\varnothing=20^{\circ}$, Material type 3)
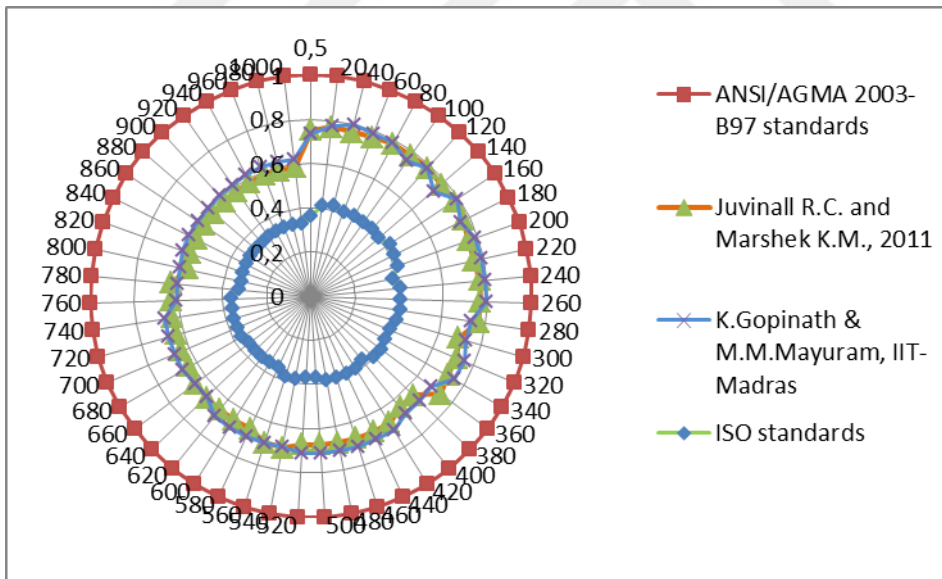
Figure B.25. Comparison of mxF/m₀xF₀ ratios for the design approaches at 4:1 speed ratio (for $\varnothing=20^{\circ}$, Material type 3)

209
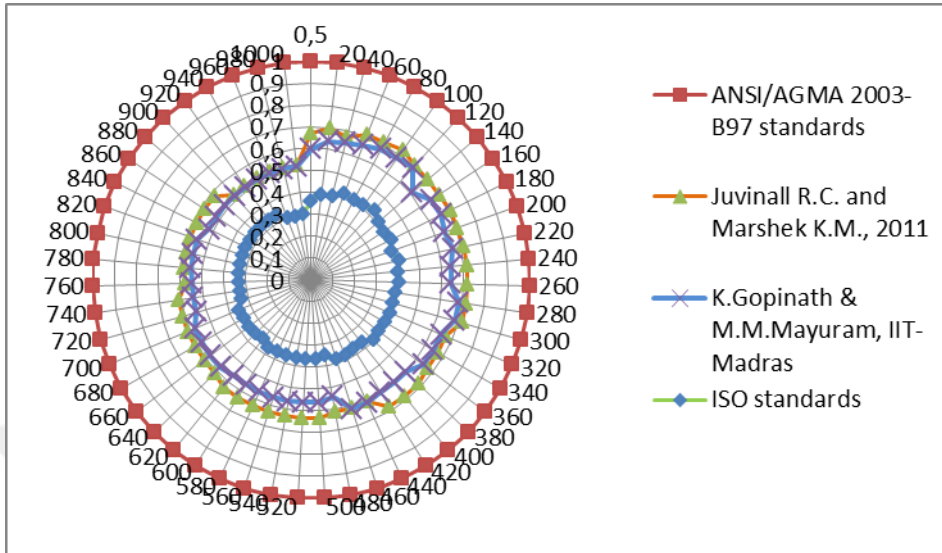
Figure B.26. Comparison of mxF/m_0xF_0 ratios for the design approaches at 5:1 speed ratio (for Ø=20°, Material type 3)
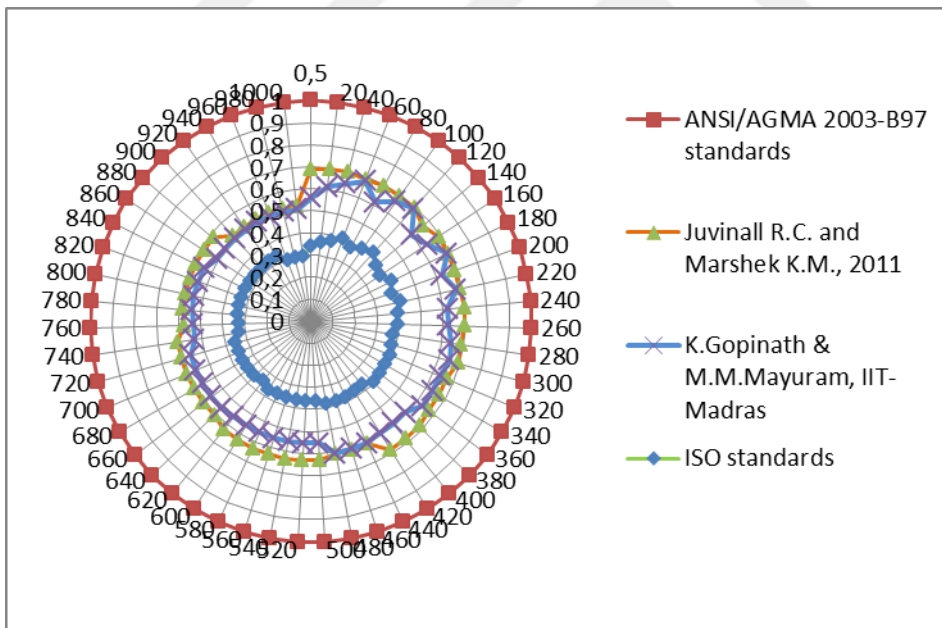
Figure B.27. Comparison of mxF/m_0xF_0 ratios for the design approaches at 6:1 speed ratio (for Ø=20°, Material type 3)
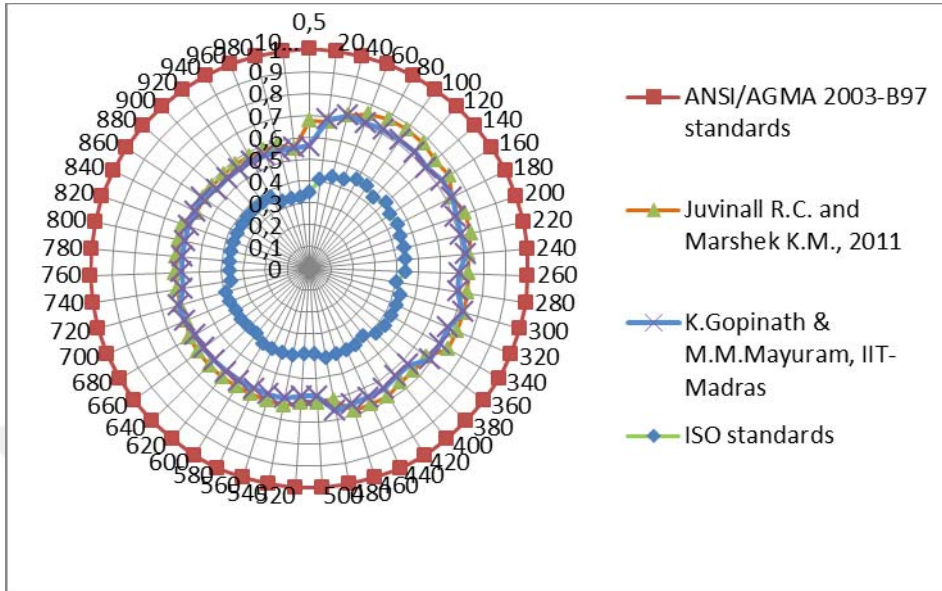
Figure B.28. Comparison of mxF/m$_0$xF$_0$ ratios for the design approaches at 7:1 speed ratio (for Ø=20°, Material type 3)
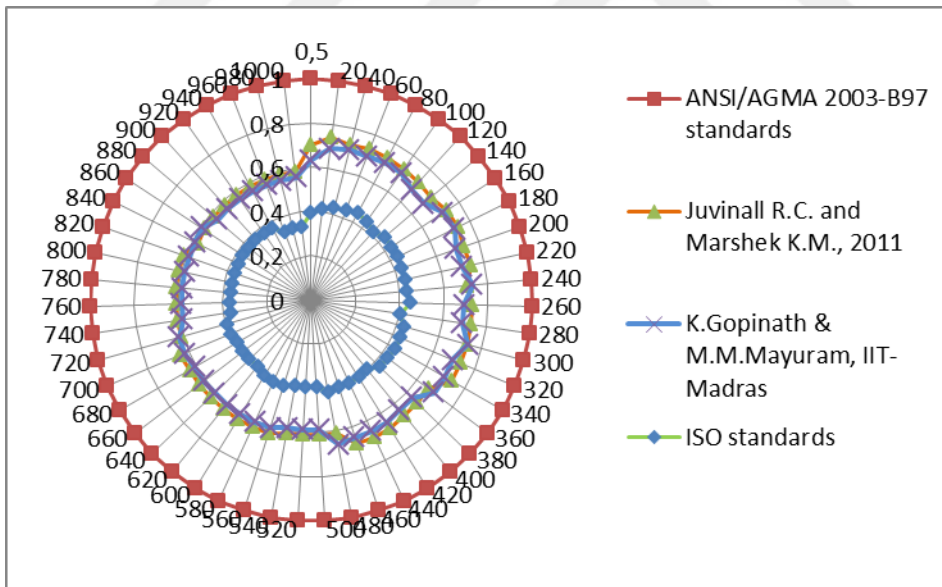
Figure B.29. Comparison of mxF/m$_0$xF$_0$ ratios for the design approaches at 8:1 speed ratio (for Ø=20°, Material type 3)

C.1. Comparison of Module Selection and Face Width Results of the Design Approaches for Ø=25°, Material type 1
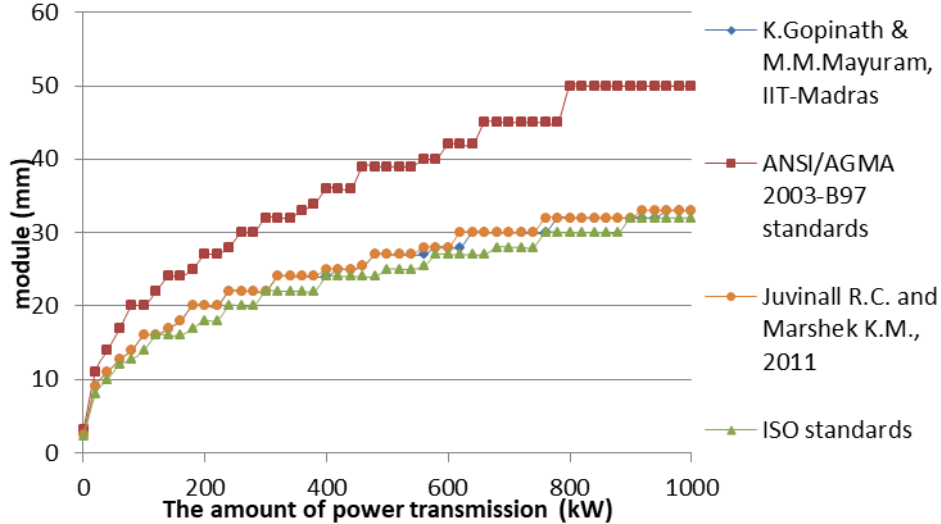
Figure C.1. Module variation considering bending fatigue failure under increasing power at 1:1 speed ratio (for Ø=25°, Material type 1)
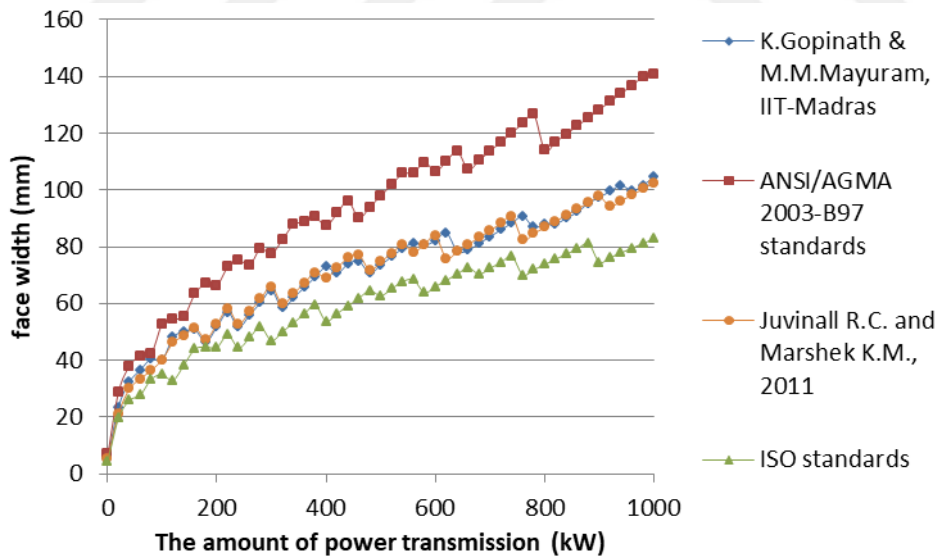
Figure C.2. Face width variation considering bending fatigue failure under increasing power at 1:1 speed ratio (for Ø=25°, Material type 1)
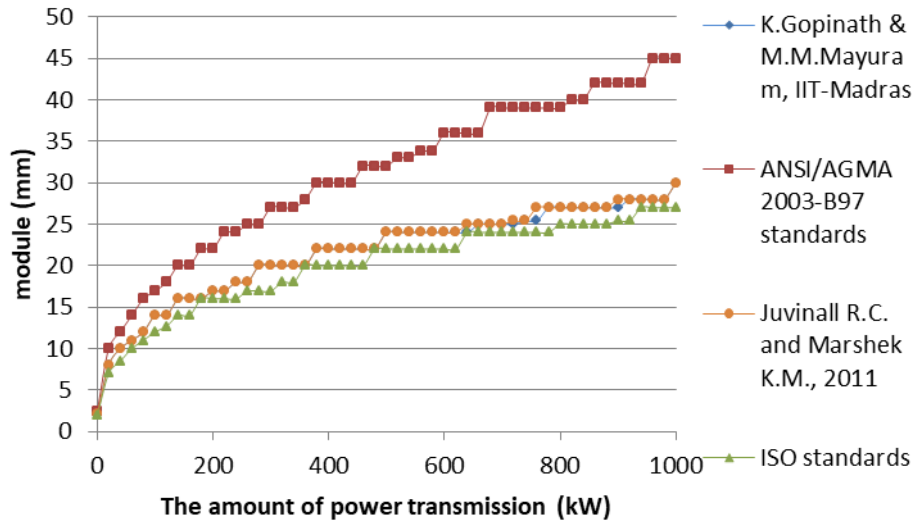
Figure C.3. Module variation considering bending fatigue failure under increasing power at 2:1 speed ratio (for Ø=25°, Material type 1)
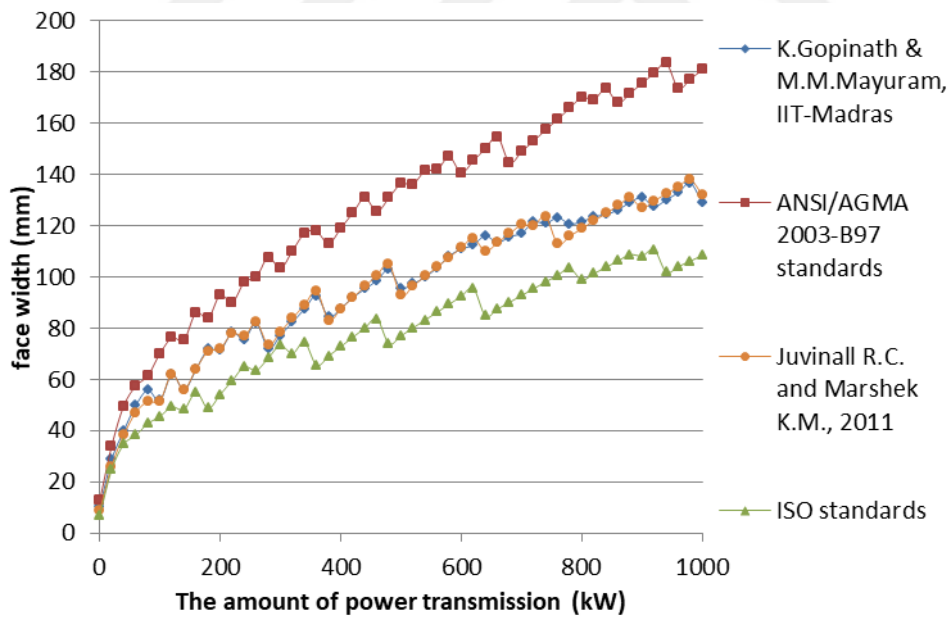
Figure C.4. Face width variation considering bending fatigue failure under increasing power at 2:1 speed ratio (for Ø=25°, Material type 1)
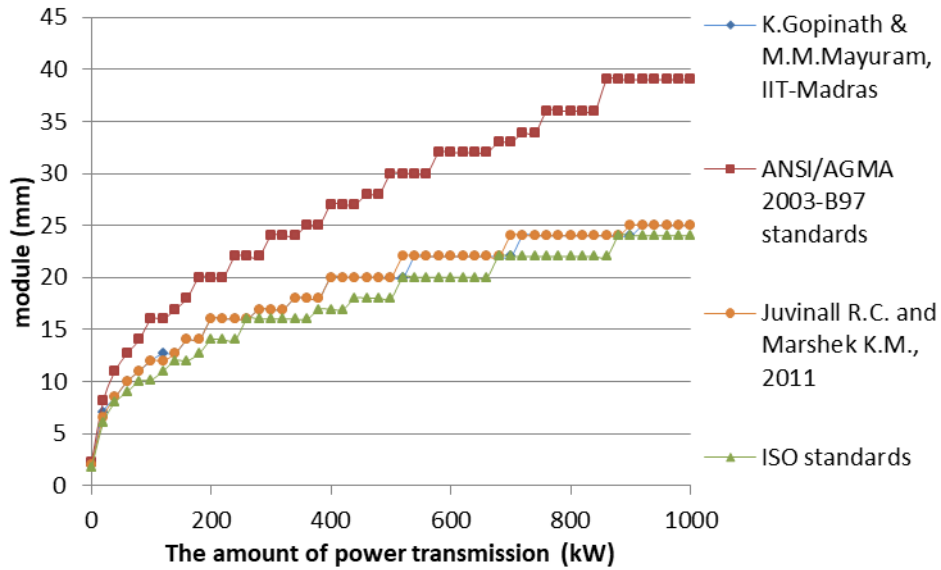
Figure C.5. Module variation considering bending fatigue failure under increasing power at 3:1 speed ratio (for Ø=25°, Material type 1)
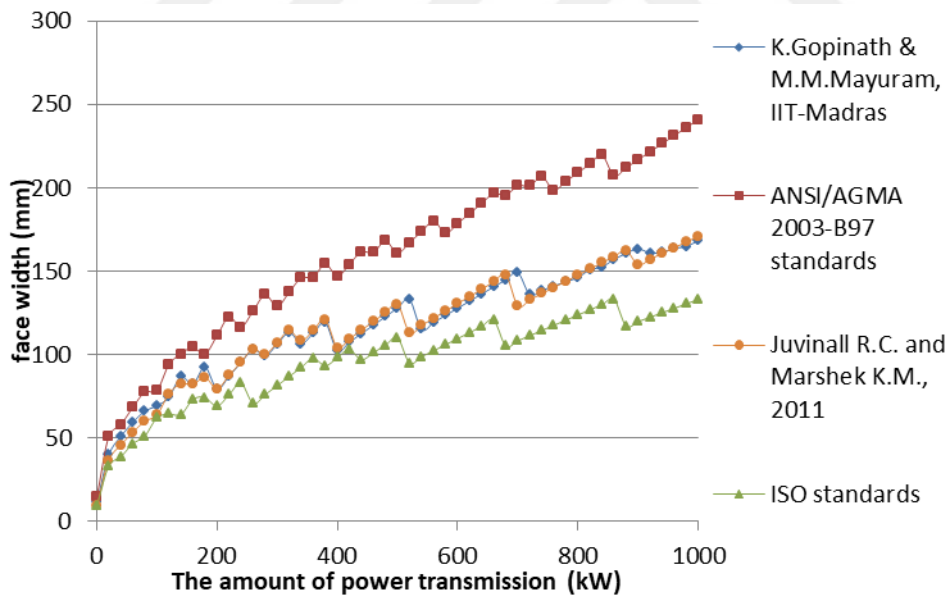

Figure C.6. Face width variation considering bending fatigue failure under increasing power at 3:1 speed ratio (for Ø=25°, Material type 1)
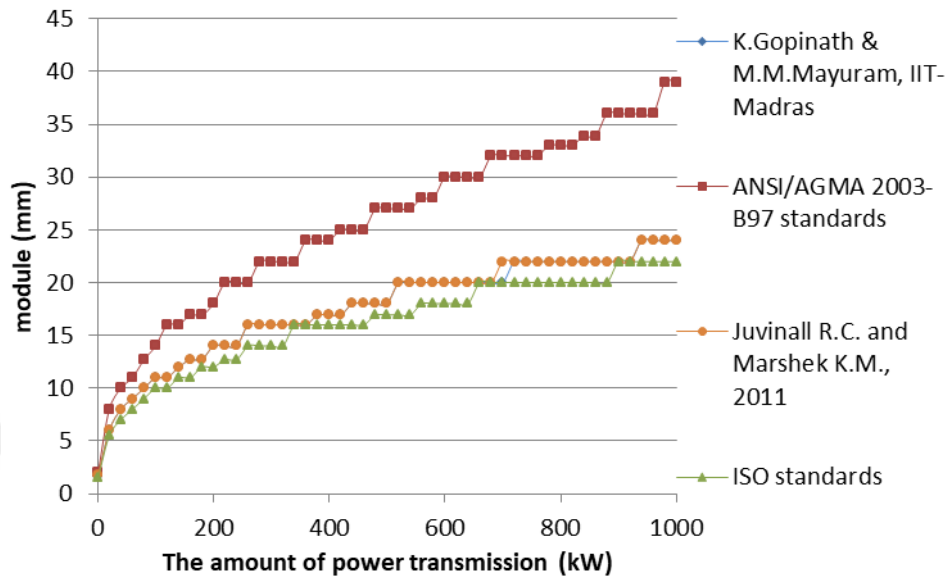
Figure C.7. Module variation considering bending fatigue failure under increasing power at 4:1 speed ratio (for Ø=25°, Material type 1)
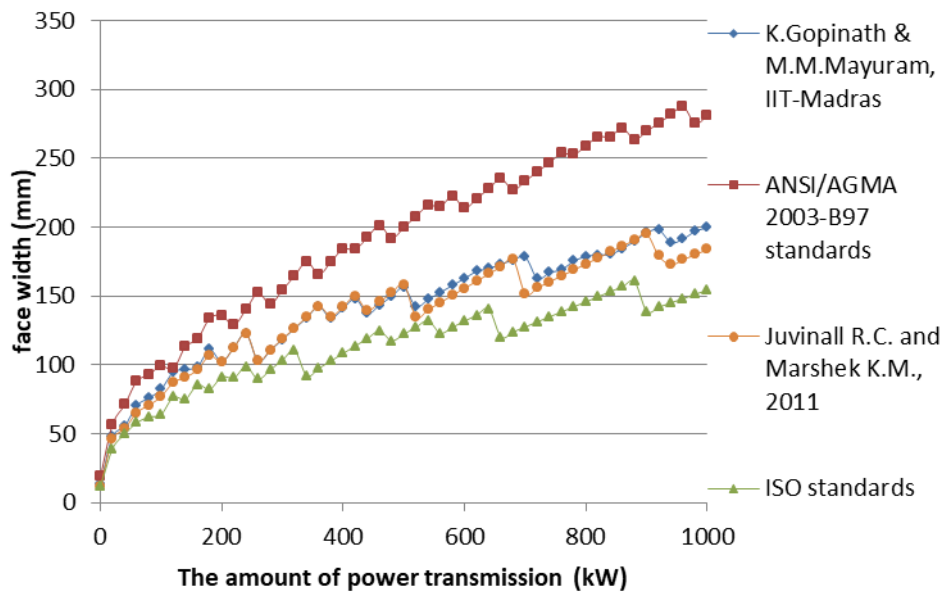

Figure C.8. Face width variation considering bending fatigue failure under increasing power at 4:1 speed ratio (for Ø=25°, Material type 1)
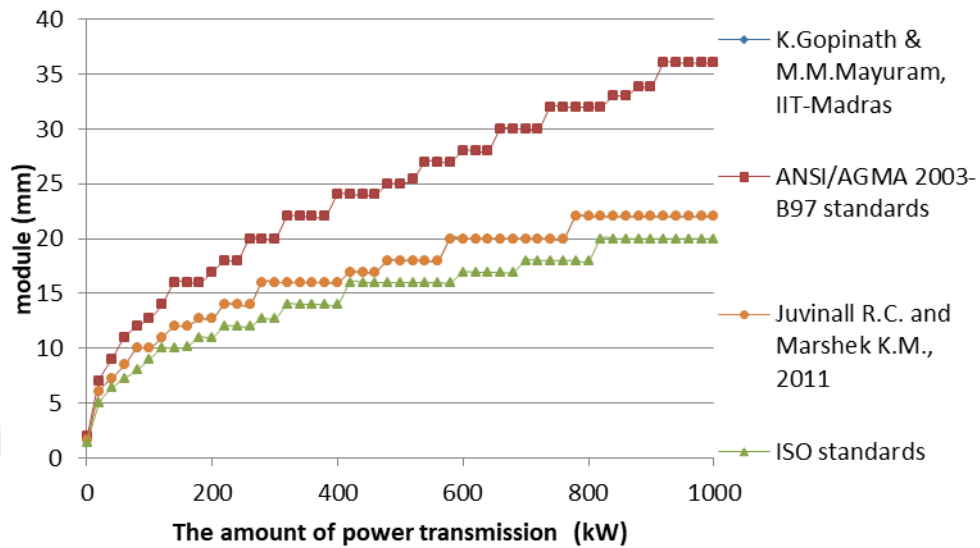
Figure C.9. Module variation considering bending fatigue failure under increasing power at 5:1 speed ratio (for Ø=25°, Material type 1)
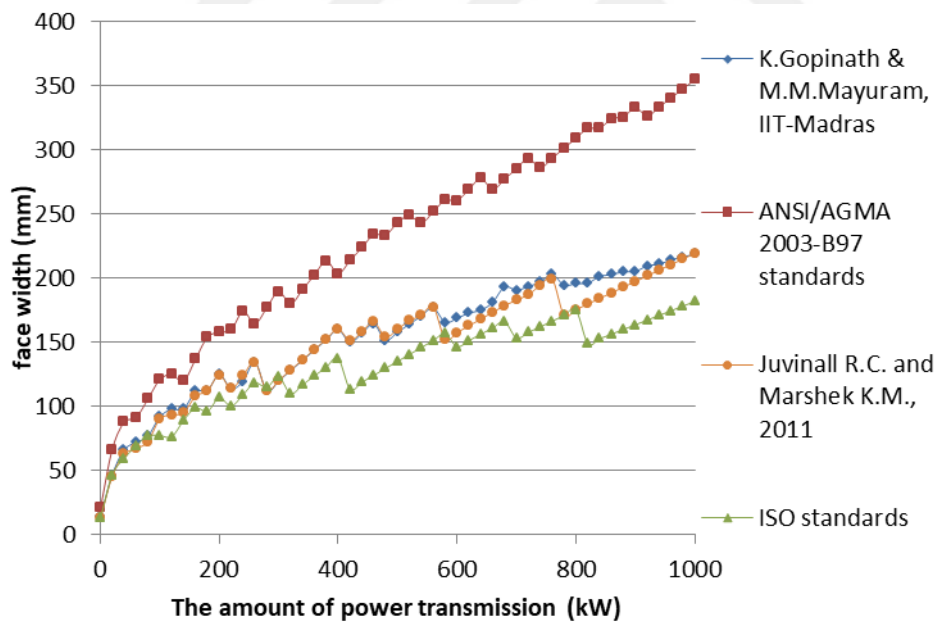
Figure C.10. Face width variation considering bending fatigue failure under increasing power at 5:1 speed ratio (for Ø=25°, Material type 1)
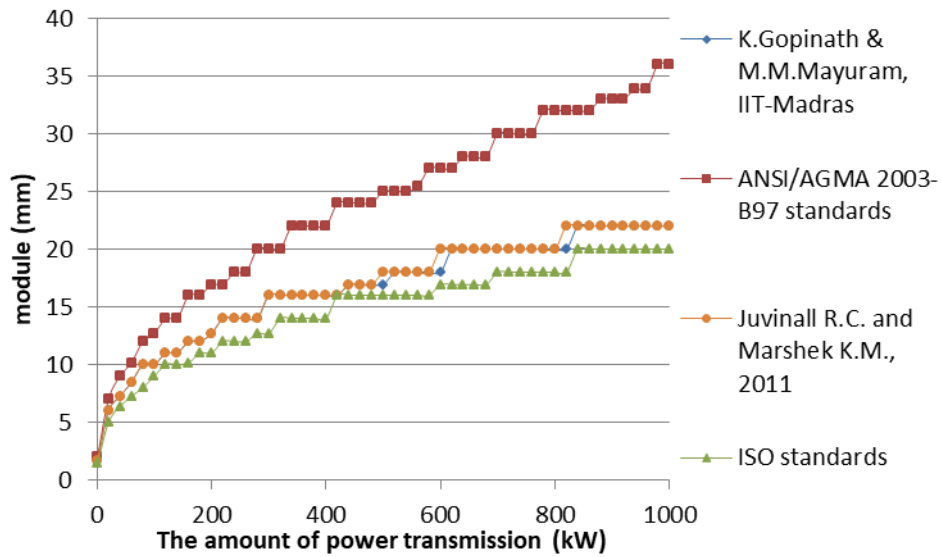
Figure C.11. Module variation considering bending fatigue failure under increasing power at 6:1 speed ratio (for Ø=25°, Material type 1)
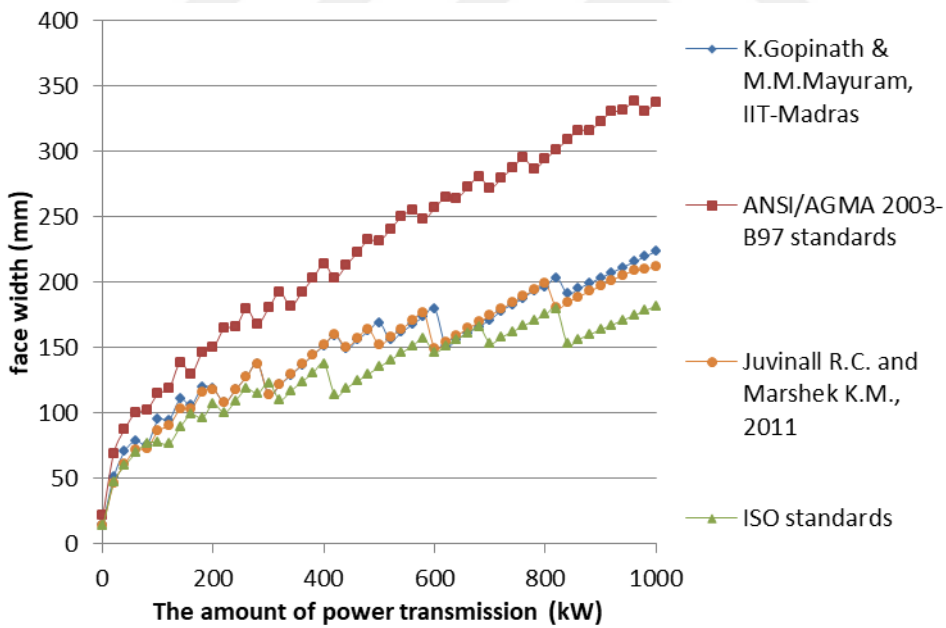
Figure C.12. Face width variation considering bending fatigue failure under increasing power at 6:1 speed ratio (for Ø=25°, Material type 1)
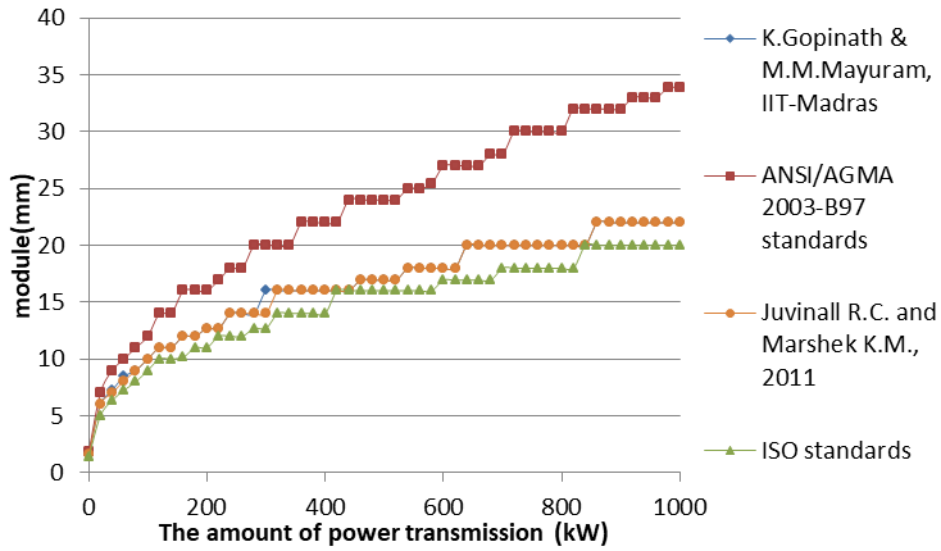
Figure C.13. Module variation considering bending fatigue failure under increasing power at 7:1 speed ratio (for Ø=25°, Material type 1)
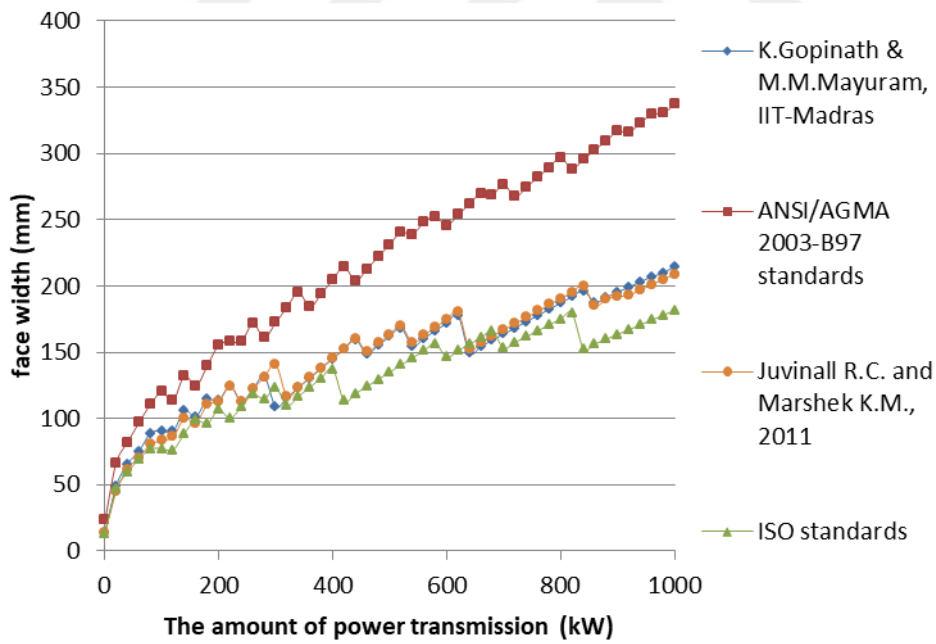
Figure C.14. Face width variation considering bending fatigue failure under increasing power at 7:1 speed ratio (for Ø=25°, Material type 1)

218
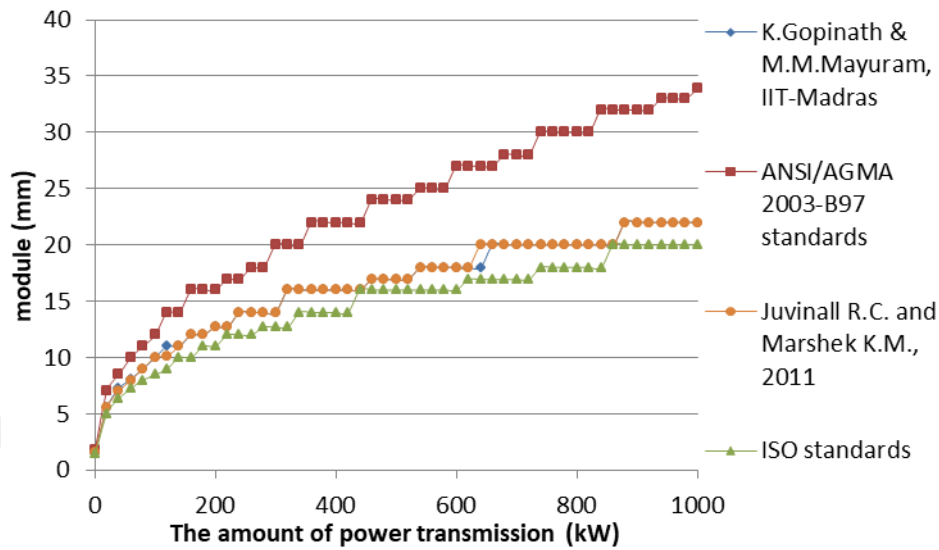
Figure C.15. Module variation considering bending fatigue failure under increasing power at 8:1 speed ratio (for Ø=25°, Material type 1)
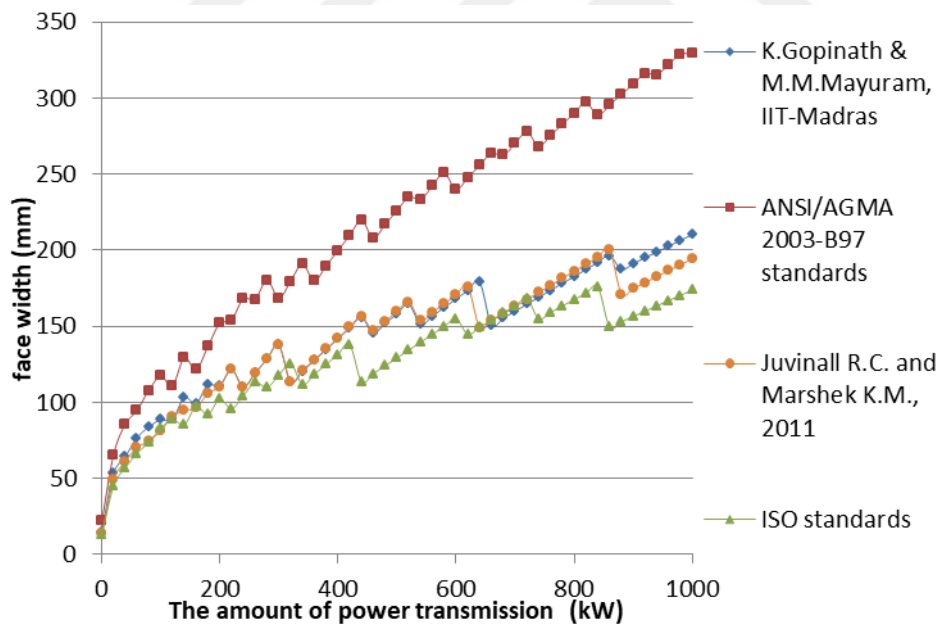
Figure C.16. Face width variation considering bending fatigue failure under increasing power at 8:1 speed ratio (for Ø=25°, Material type 1)

C.2. Comparison of the Results Based on Bending Fatigue Failure Considering Speed Ratio for the Selected Power Transmissions for Ø=25°, Material type 1
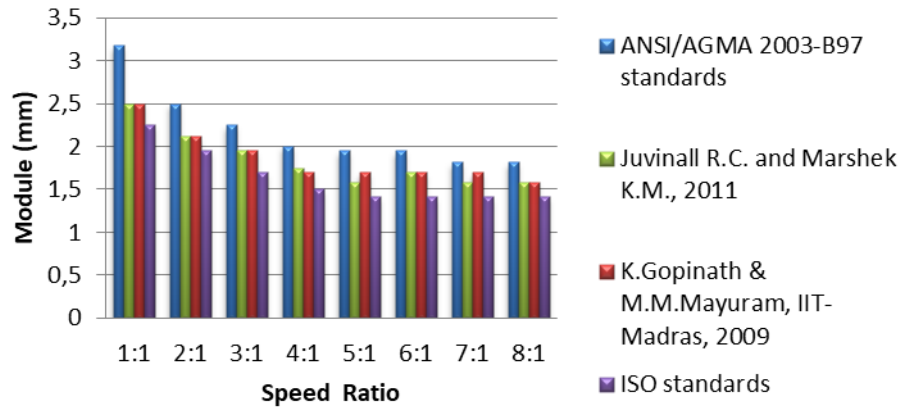
Figure C.17. The effect of speed ratio on module selection based on bending fatigue failure at 0,5 kW power transmission (for Ø=25°, Material type 1)
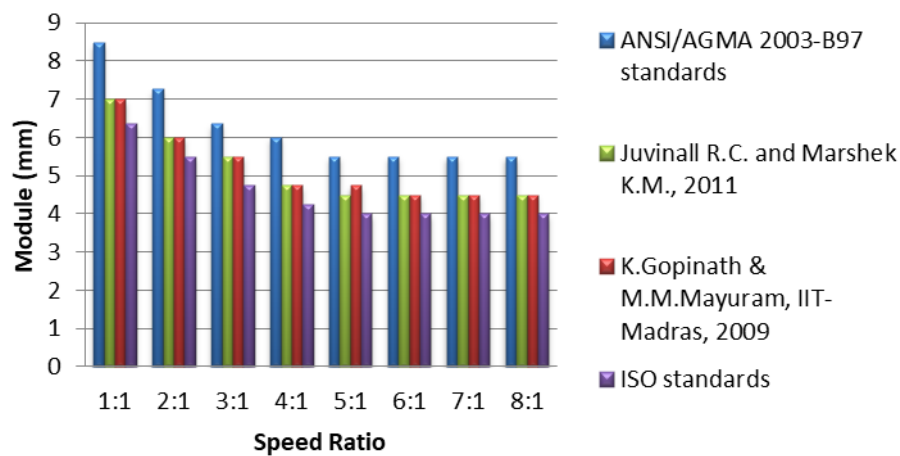
Figure C.18. The effect of speed ratio on module selection based on bending fatigue failure at 10 kW power transmission (for Ø=25°, Material type 1)
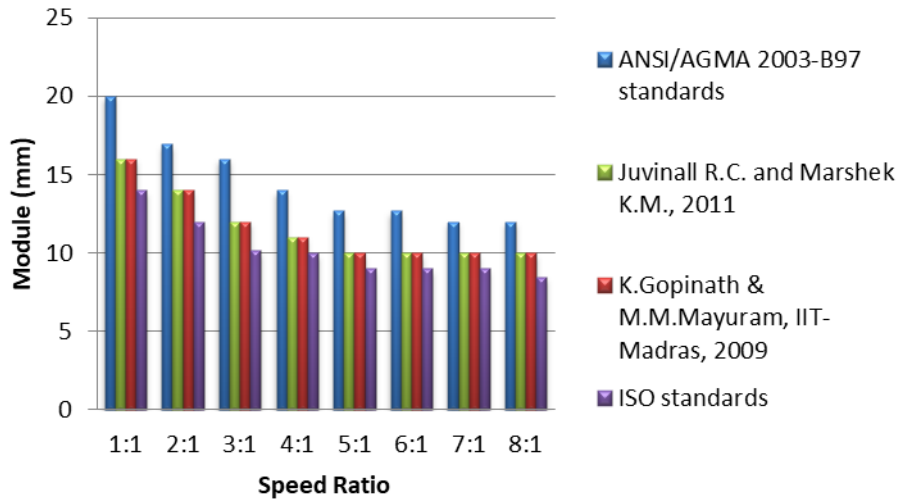
Figure C.19. The effect of speed ratio on module selection based on bending fatigue failure at 100 kW power transmission (for Ø=25°, Material type 1)
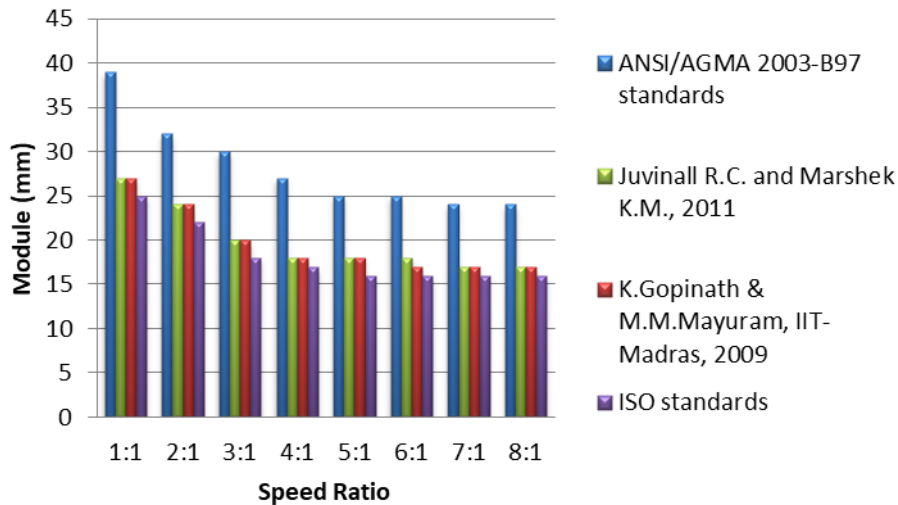
Figure C.20. The effect of speed ratio on module selection based on bending fatigue failure at 500 kW power transmission (for Ø=25°, Material type 1)

221
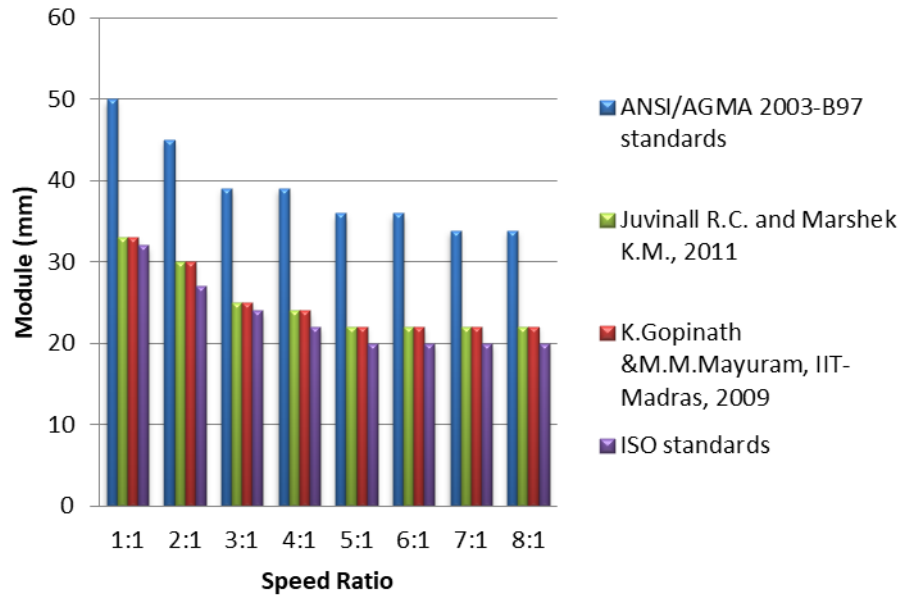
Figure C.21. The effect of speed ratio on module selection based on bending fatigue failure at 1000 kW power transmission (for Ø=25°, Material type 1)

C.3. Obtaining Geometric Rating Number (GR$_i$) for Design Approaches for Ø=25°, Material type 1
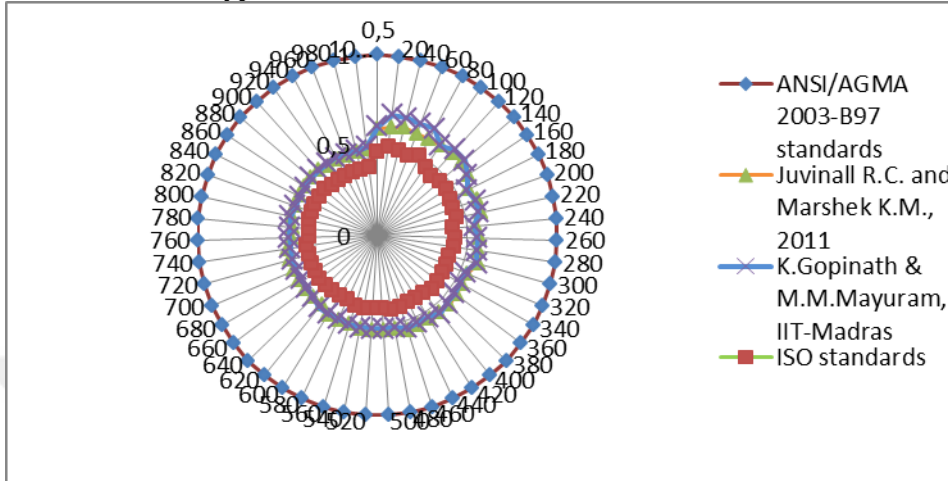
Figure C.22. Comparison of mxF/m$_0$xF$_0$ ratios for the design approaches at 1:1 speed ratio (for Ø=25°, Material type 1)
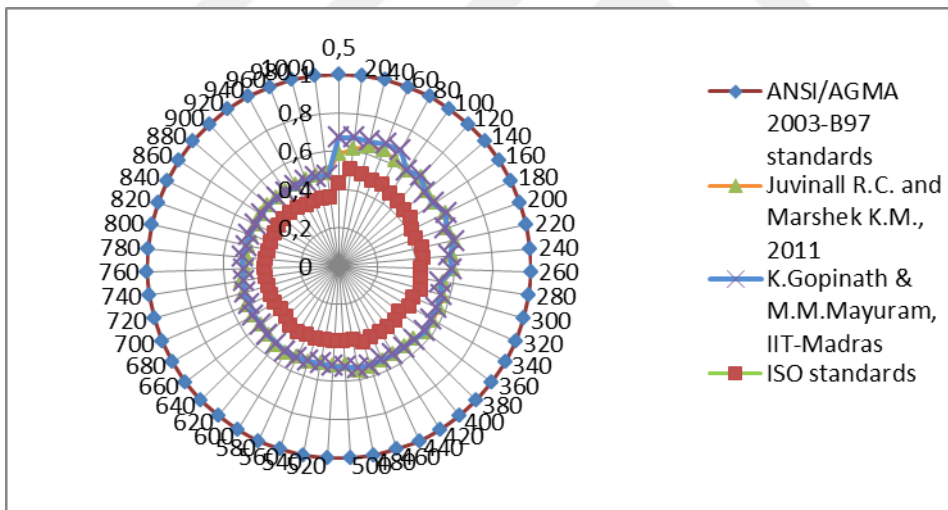
Figure C.23. Comparison of mxF/m$_0$xF$_0$ ratios for the design approaches at 2:1 speed ratio (for Ø=25°, Material type 1)
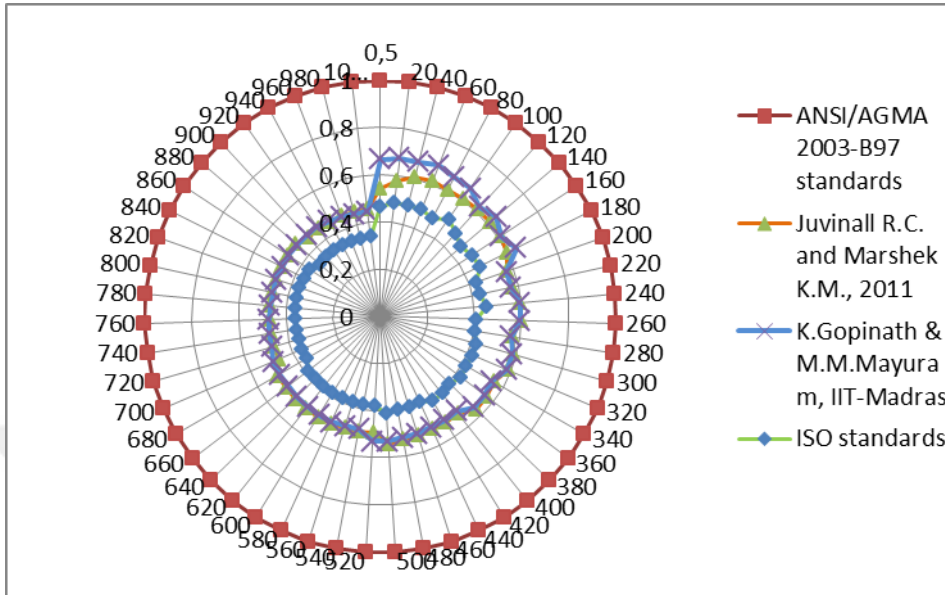
Figure C.24. Comparison of mxF/m_0xF_0 ratios for the design approaches at 3:1 speed ratio (for $\emptyset=25^o$, Material type 1)
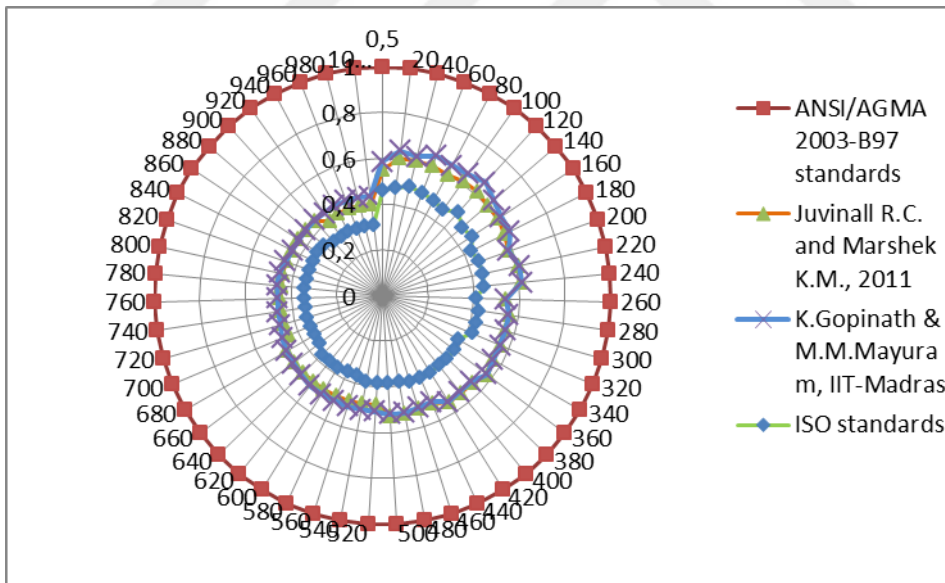
Figure C.25. Comparison of mxF/m_0xF_0 ratios for the design approaches at 4:1 speed ratio (for $\emptyset=25^o$, Material type 1)
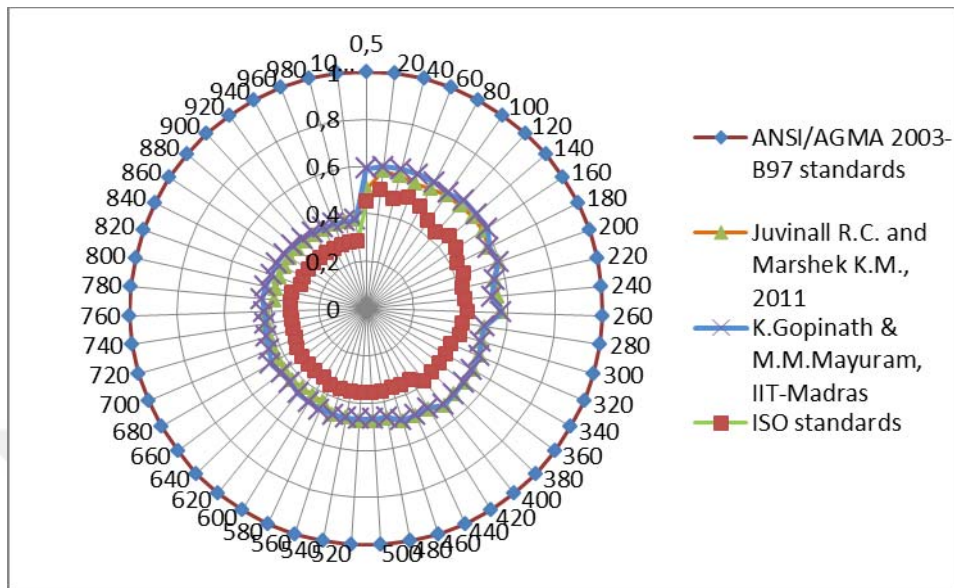
Figure C.26. Comparison of mxF/m_0xF_0 ratios for the design approaches at 5:1 speed ratio (for $\varnothing=25^\circ$, Material type 1)
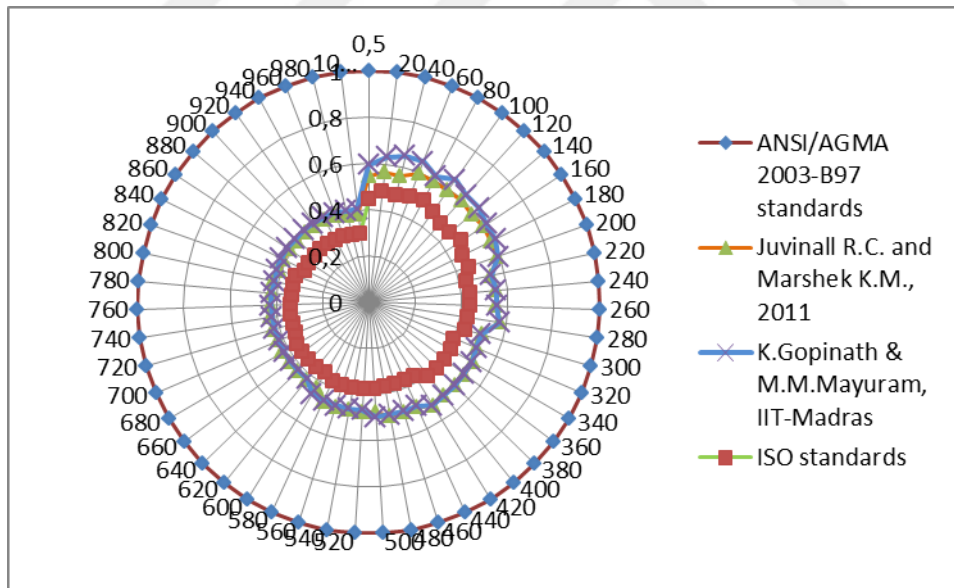
Figure C.27. Comparison of mxF/m_0xF_0 ratios for the design approaches at 6:1 speed ratio (for $\varnothing=25^\circ$, Material type 1)
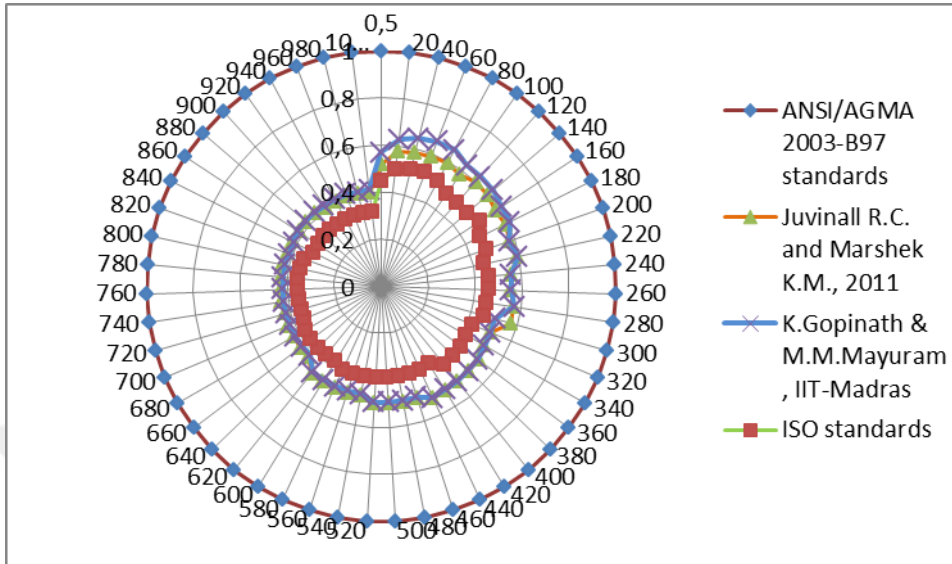
Figure C.28. Comparison of mxF/m_0xF_0 ratios for the design approaches at 7:1 speed ratio (for Ø=25°, Material type 1)
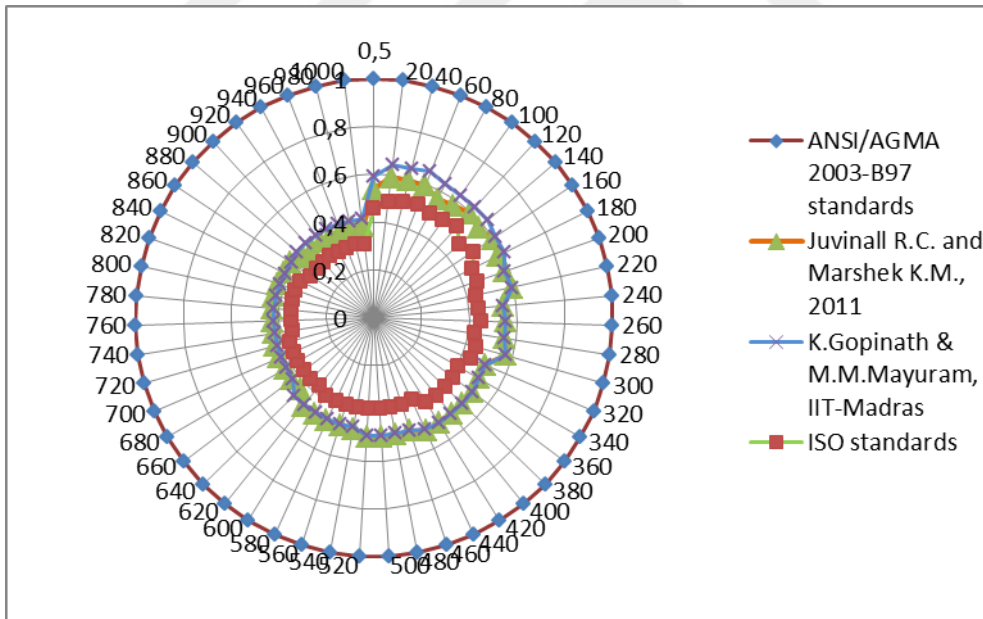
Figure C.29. Comparison of mxF/m_0xF_0 ratios for the design approaches at 8:1 speed ratio (for Ø=25°, Material type 1)

226

APPENDIX D

**D.1. Comparison of Module Selection and Face Width Results of the Design Approaches for Ø=25°, Material type 2**
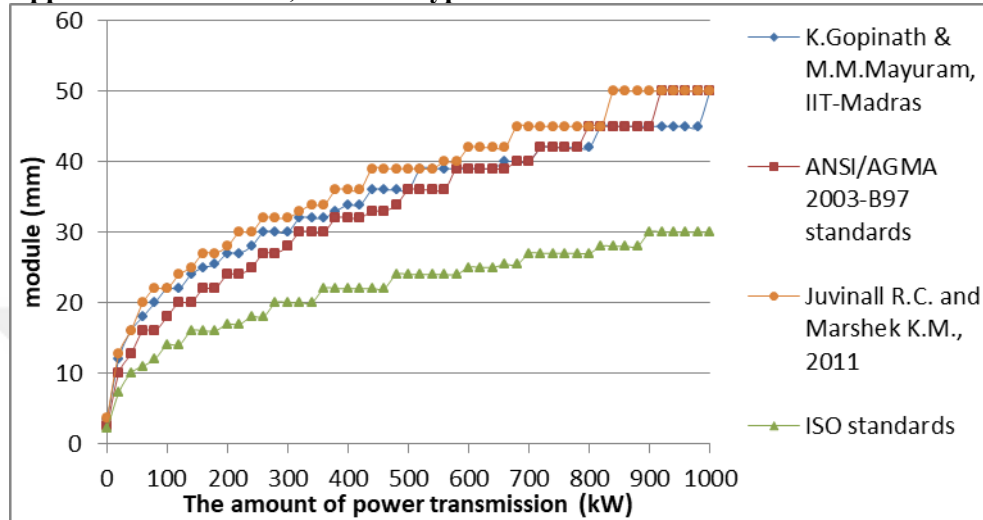
Figure D.1. Module variation considering bending fatigue failure under increasing power at 1:1 speed ratio (for Ø=25°, Material type 2)
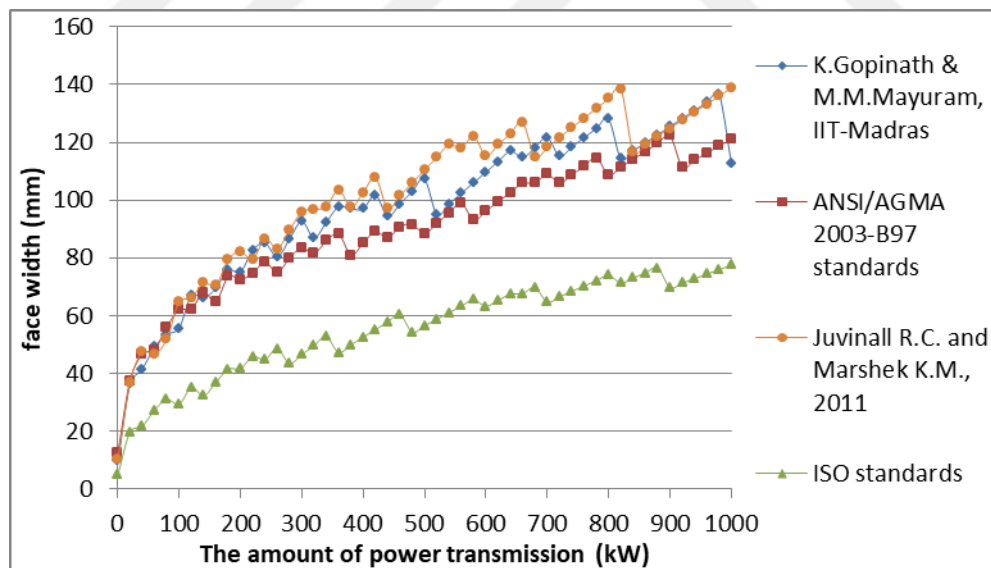
Figure D.2. Face width variation considering bending fatigue failure under increasing power at 1:1 speed ratio (for Ø=25°, Material type 2)
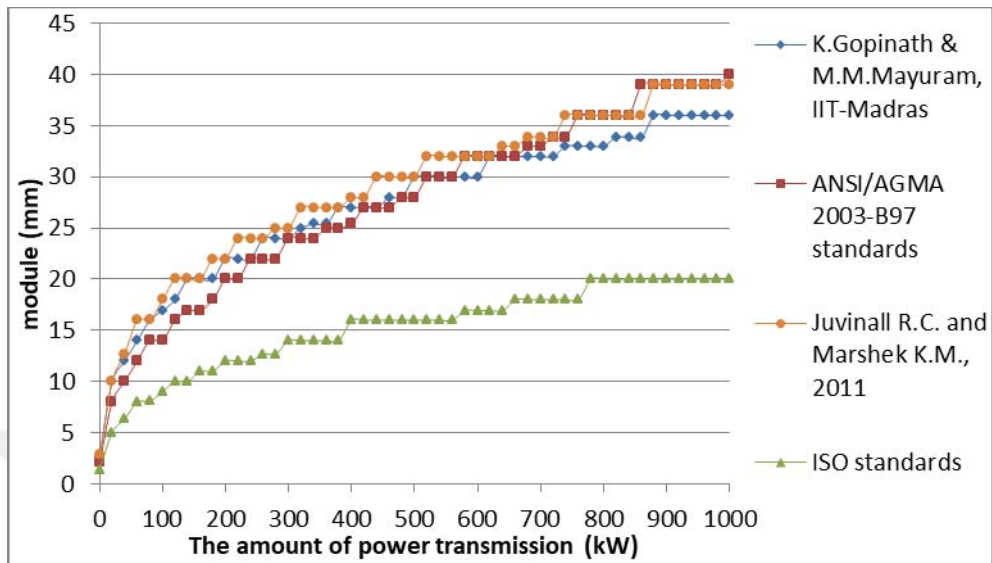
Figure D.3. Module variation considering bending fatigue failure under increasing power at 2:1 speed ratio (for Ø=25°, Material type 2)
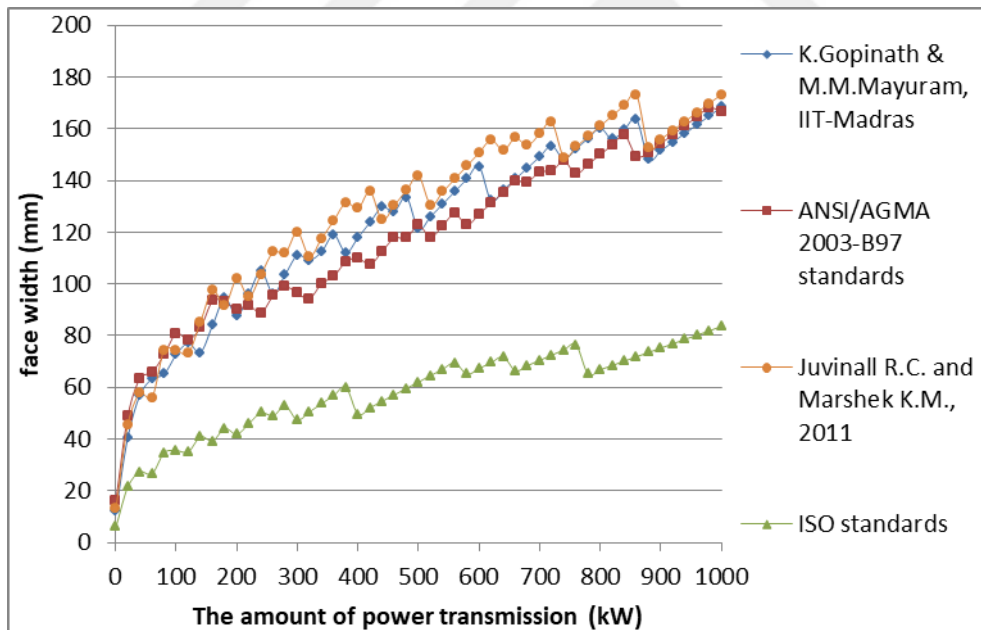
Figure D.4. Face width variation considering bending fatigue failure under increasing power at 2:1 speed ratio (for Ø=25°, Material type 2)
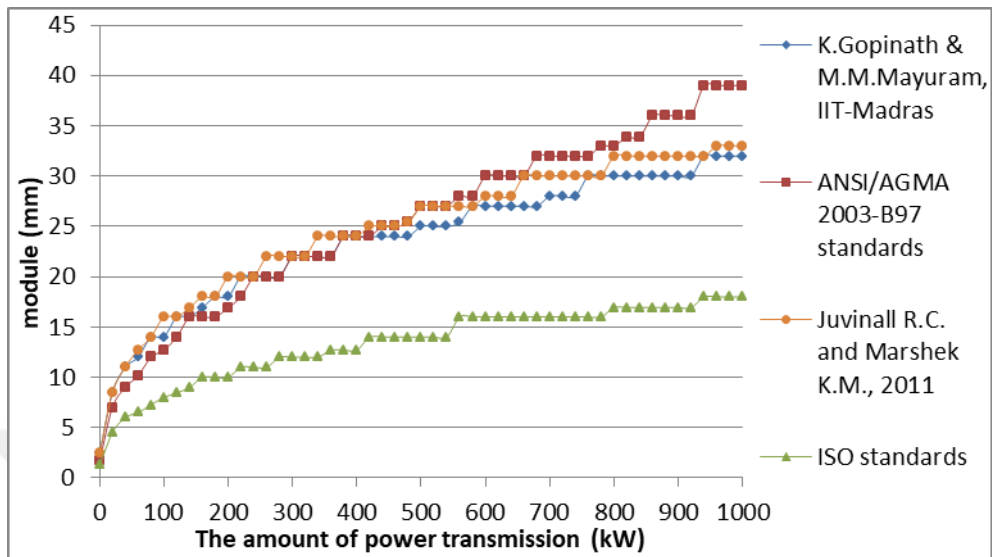
Figure D.5. Module variation considering bending fatigue failure under increasing power at 3:1 speed ratio (for Ø=25°, Material type 2)
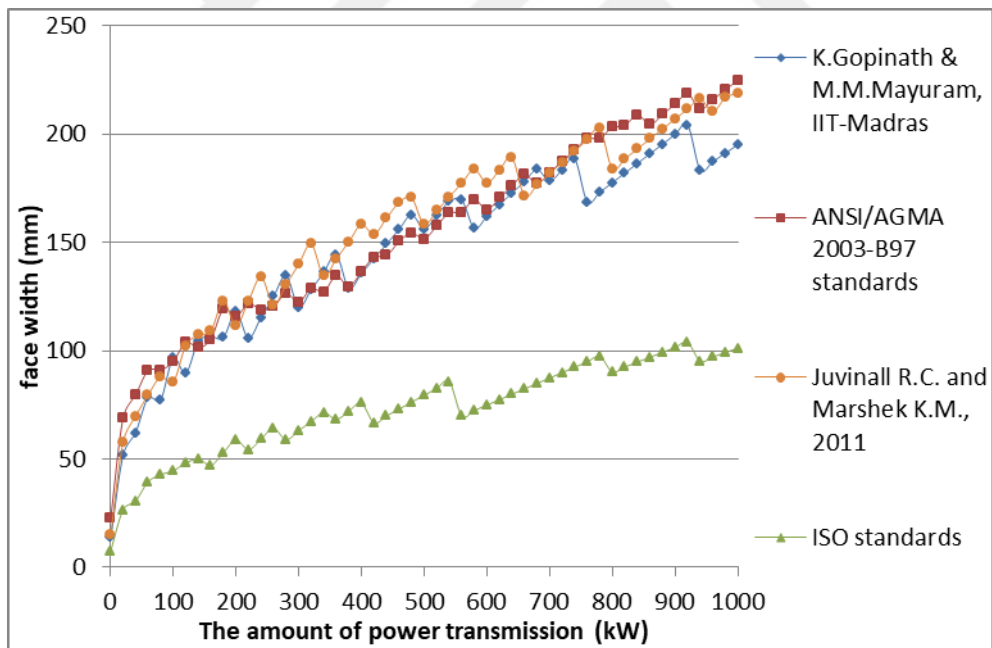
Figure D.6. Face width variation considering bending fatigue failure under increasing power at 3:1 speed ratio (for Ø=25°, Material type 2)
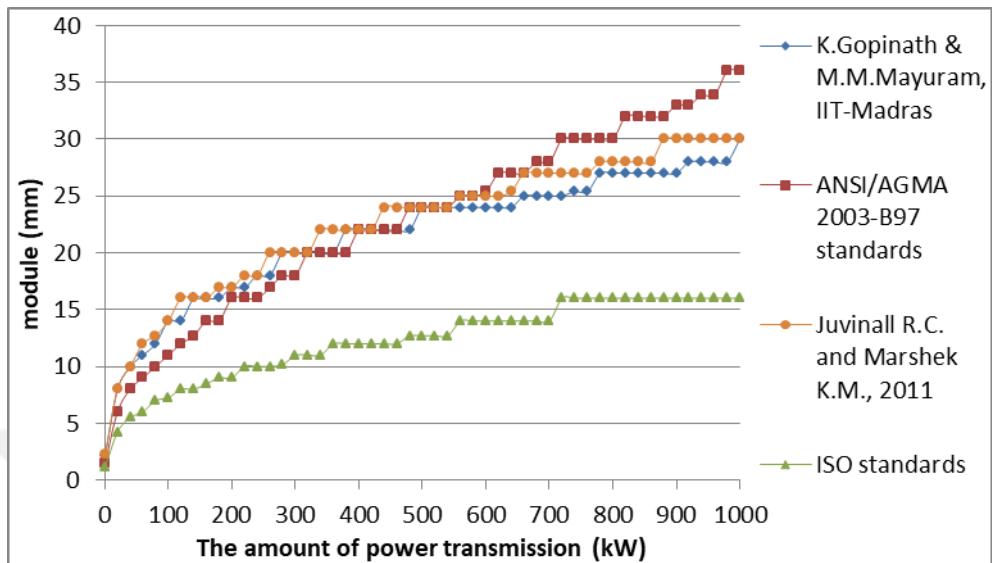
Figure D.7. Module variation considering bending fatigue failure under increasing power at 4:1 speed ratio (for Ø=25°, Material type 2)
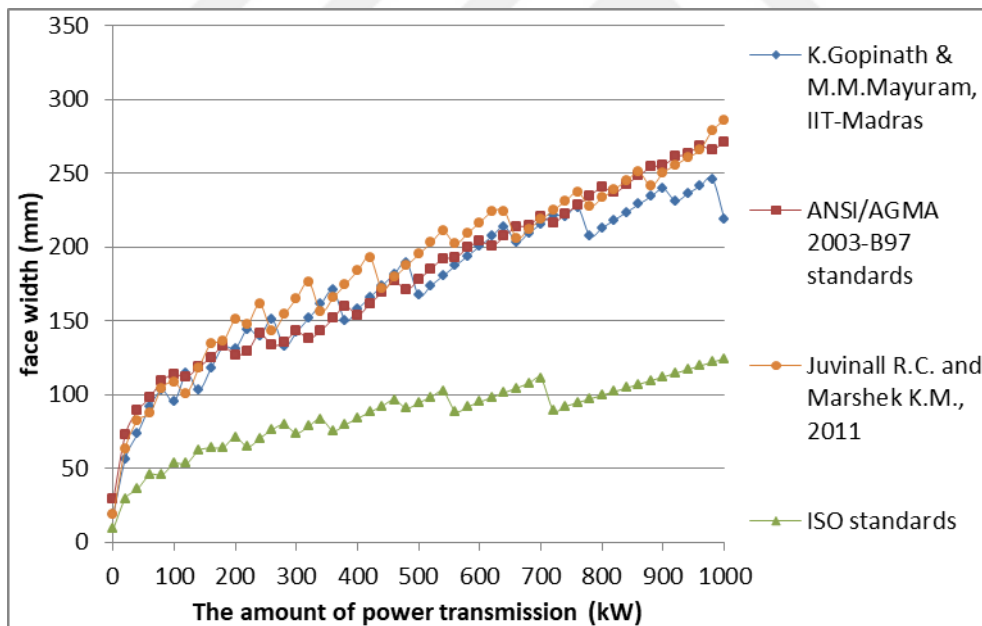
Figure D.8. Face width variation considering bending fatigue failure under increasing power at 4:1 speed ratio (for Ø=25°, Material type 2)
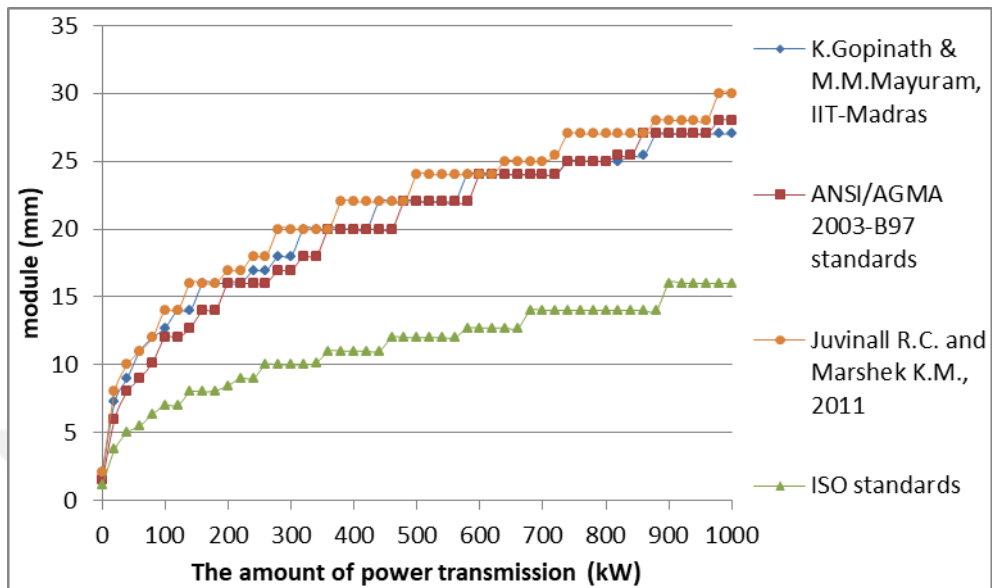
Figure D.9. Module variation considering bending fatigue failure under increasing power at 5:1 speed ratio (for $\varnothing=25^{\circ}$, Material type 2)
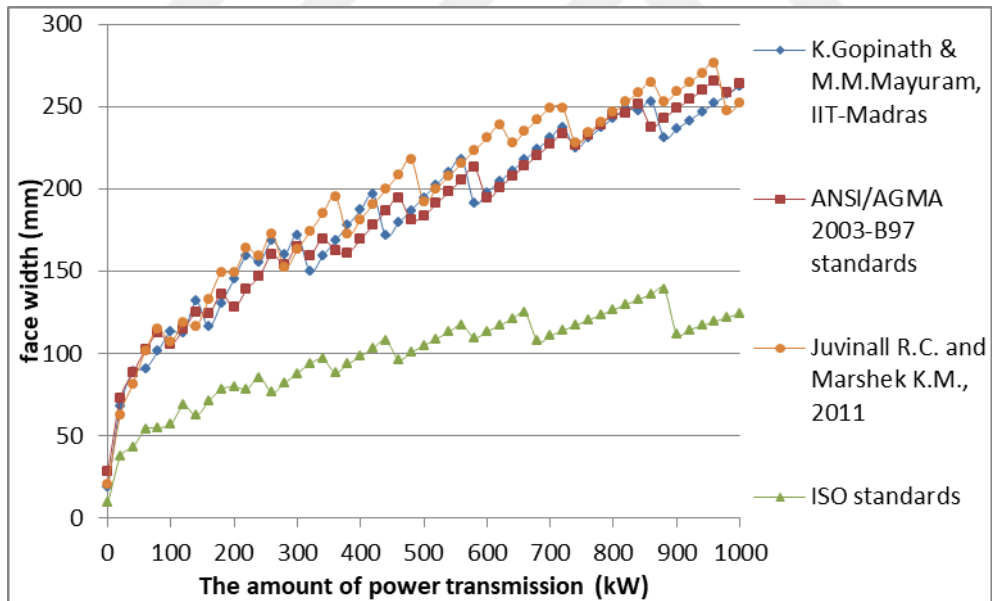
Figure D.10. Face width variation considering bending fatigue failure under increasing power at 5:1 speed ratio (for $\varnothing=25^{\circ}$, Material type 2)
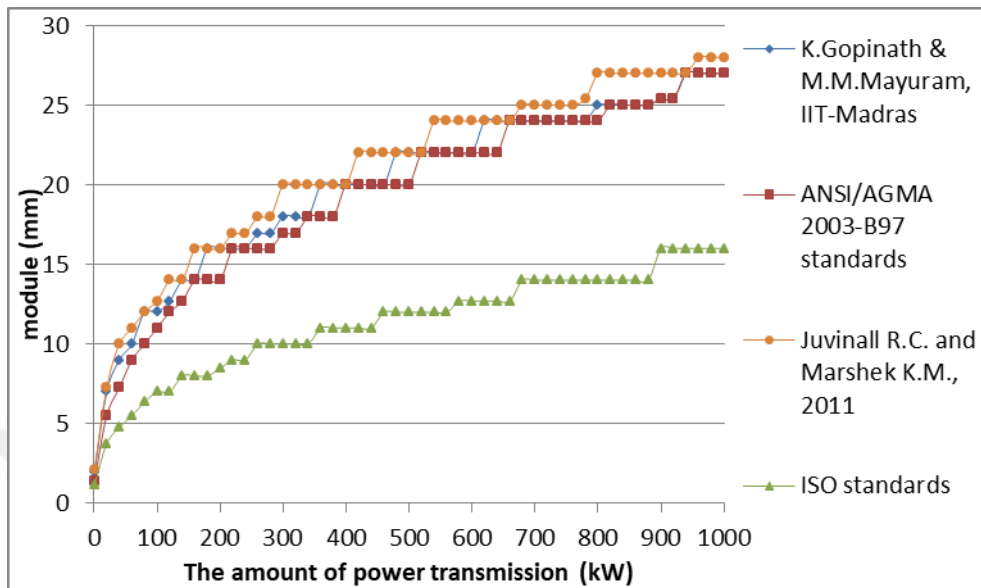
Figure D.11. Module variation considering bending fatigue failure under increasing power at 6:1 speed ratio (for Ø=25°, Material type 2)
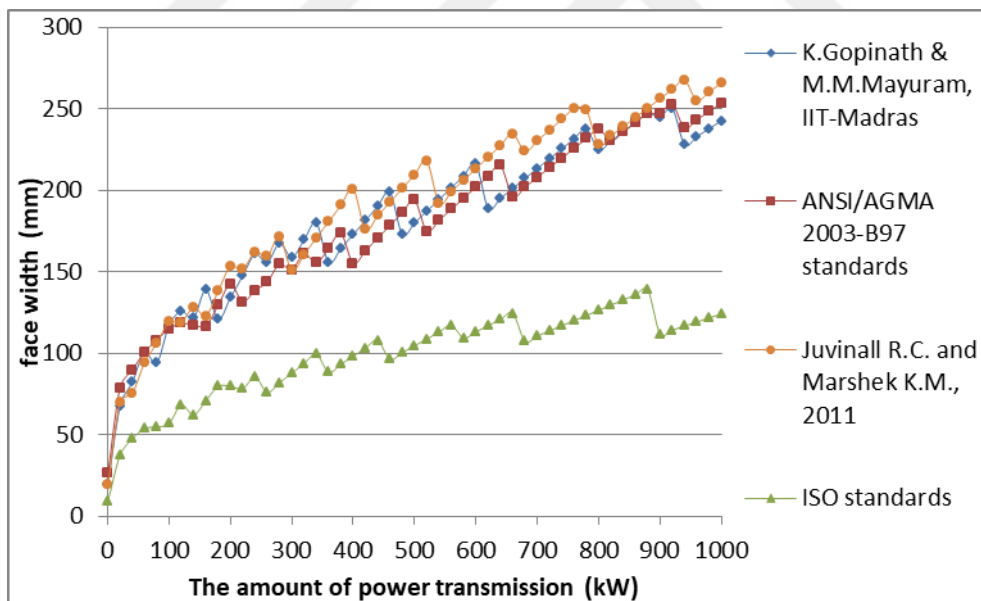
Figure D.12. Face width variation considering bending fatigue failure under increasing power at 6:1 speed ratio (for Ø=25°, Material type 2)
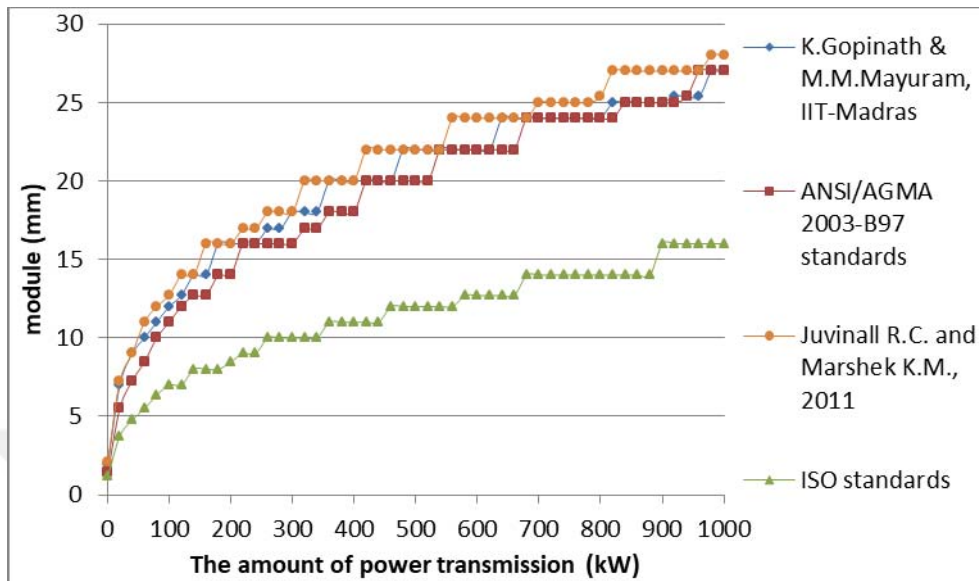
Figure D.13. Module variation considering bending fatigue failure under increasing
power at 7:1 speed ratio (for Ø=25°, Material type 2)
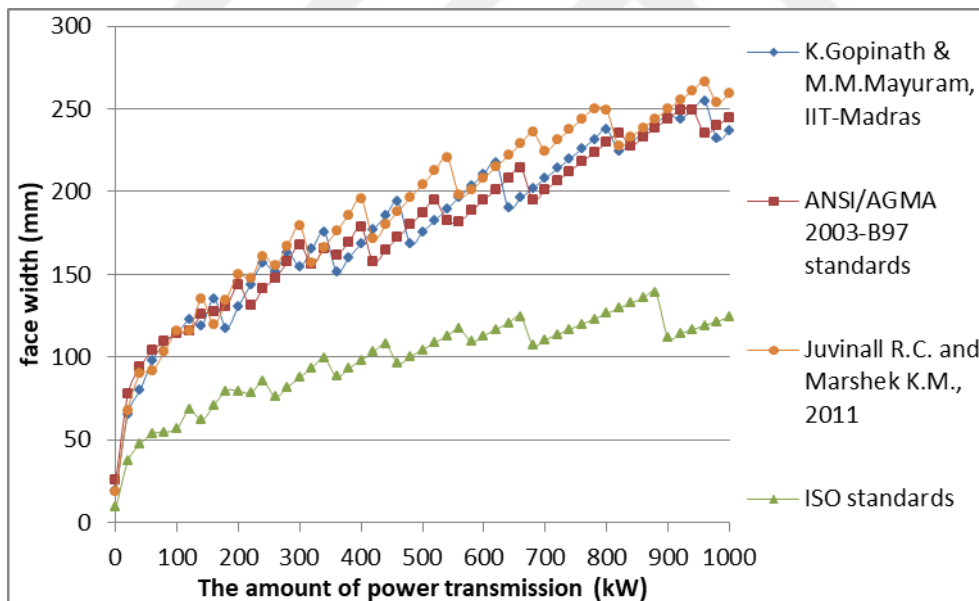
Figure D.14. Face width variation considering bending fatigue failure under
increasing power at 7:1 speed ratio (for Ø=25°, Material type 2)
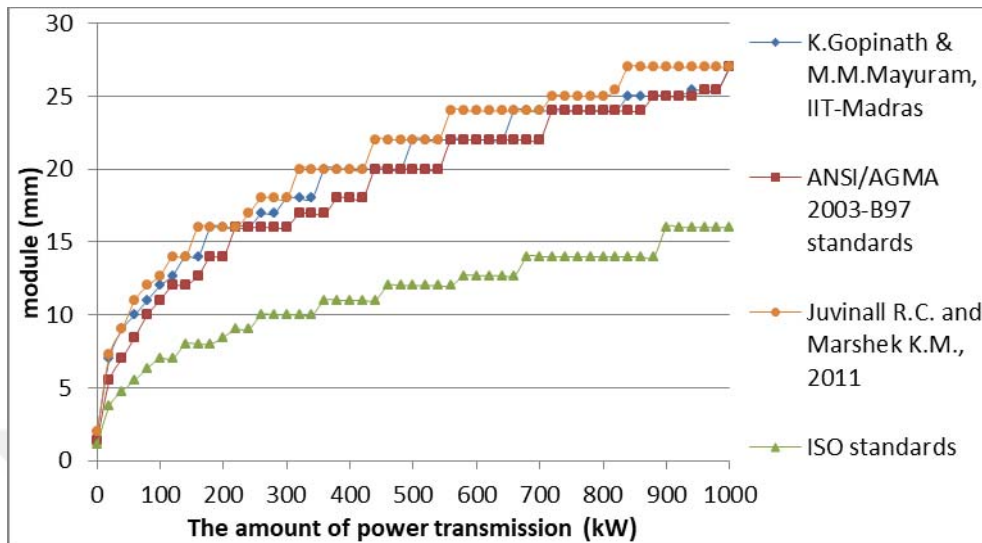
Figure D.15. Module variation considering bending fatigue failure under increasing power at 8:1 speed ratio (for Ø=25°, Material type 2)
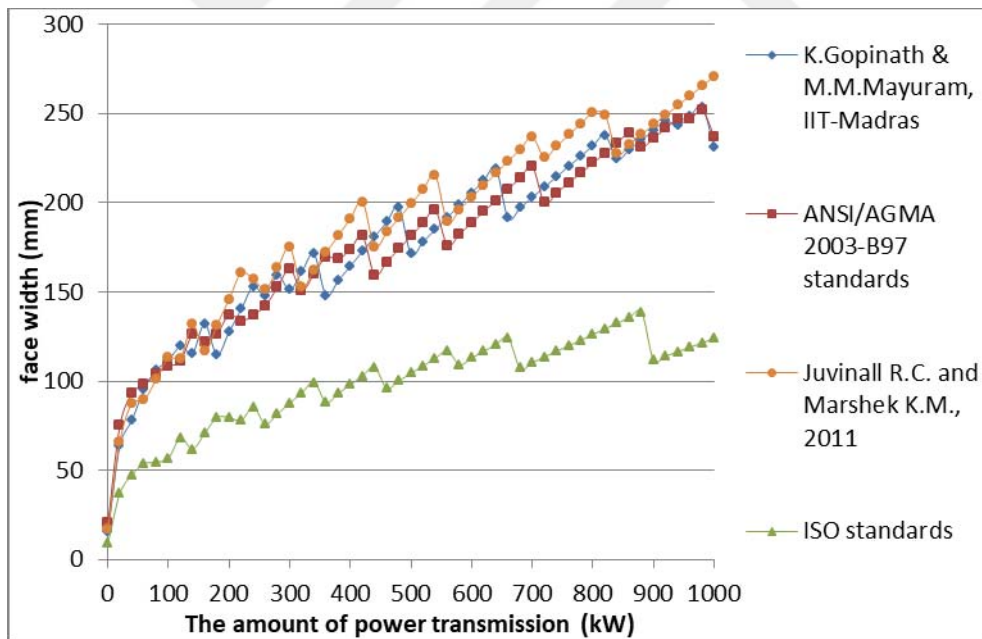
Figure D.16. Face width variation considering bending fatigue failure under increasing power at 8:1 speed ratio (for Ø=25°, Material type 2)

D.2. Comparison of the Results Based on Bending Fatigue Failure Considering Speed Ratio for the Selected Power Transmissions for Ø=25°, Material type 2
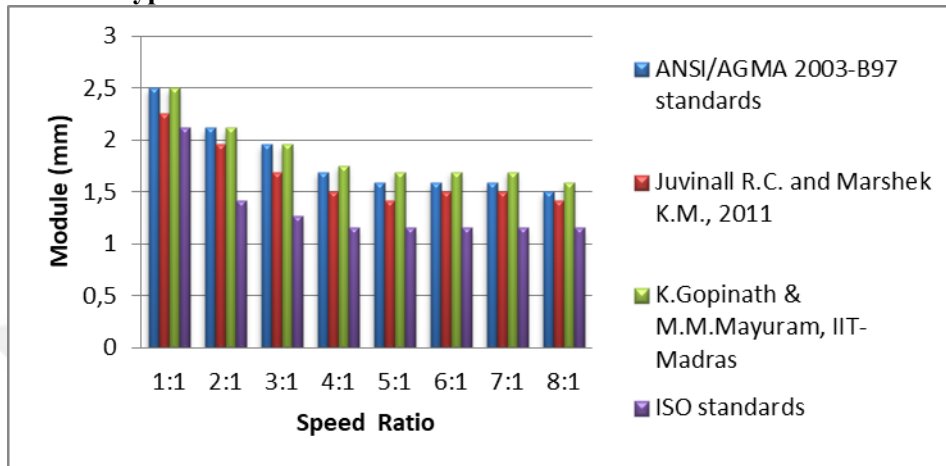
Figure D.17. The effect of speed ratio on module selection based on bending fatigue failure at 0,5 kW power transmission (for Ø=25°, Material type 2)
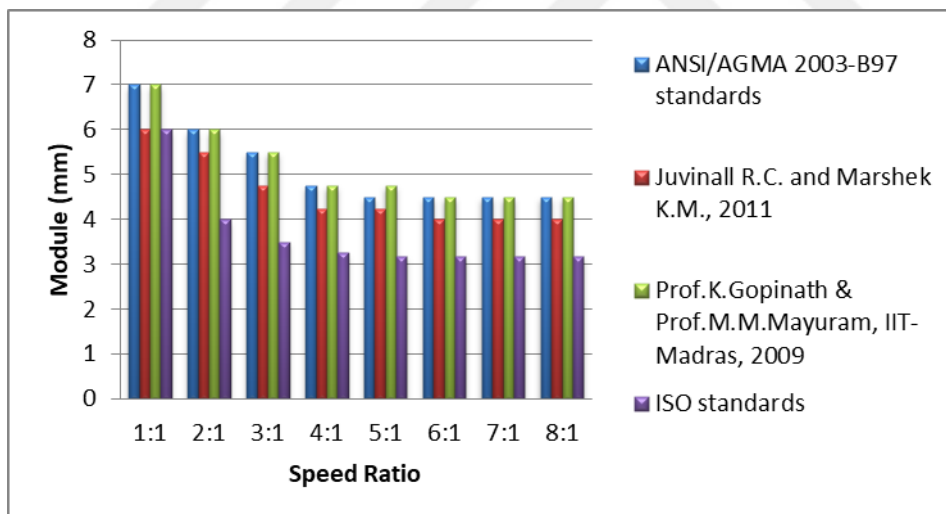
Figure D.18. The effect of speed ratio on module selection based on bending fatigue failure at 10 kW power transmission (for Ø=25°, Material type 2)
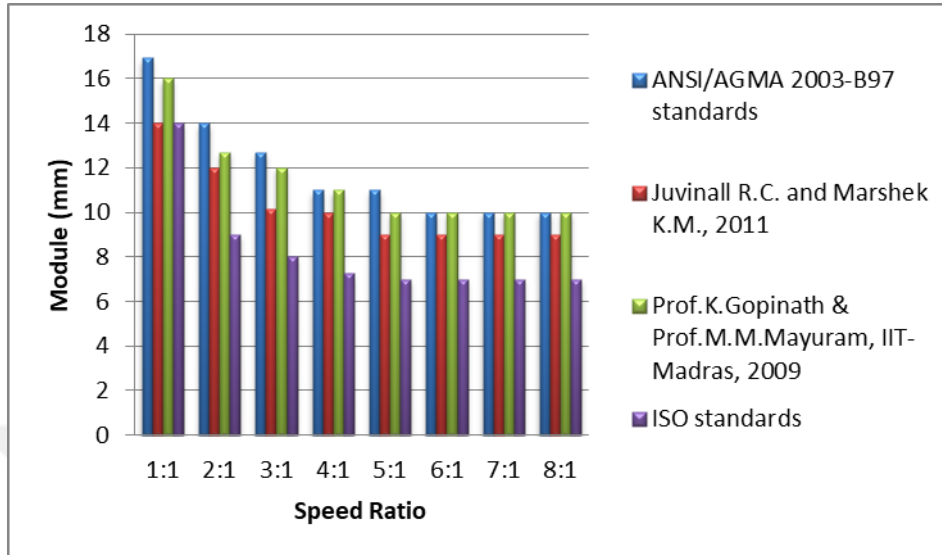
Figure D.19. The effect of speed ratio on module selection based on bending
fatigue failure at 100 kW power transmission (for Ø=25°, Material
type 2)
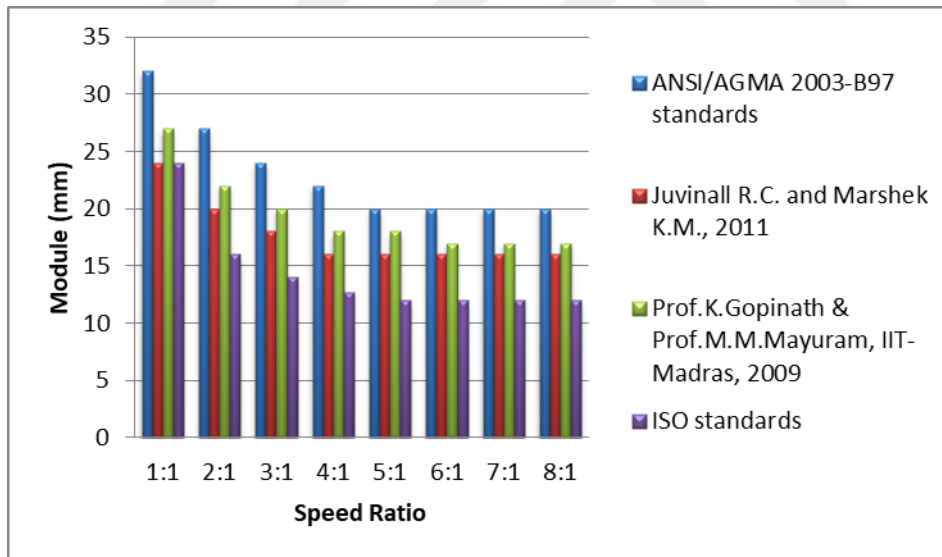
Figure D.20. The effect of speed ratio on module selection based on bending
fatigue failure at 500 kW power transmission (for Ø=25°, Material
type 2)
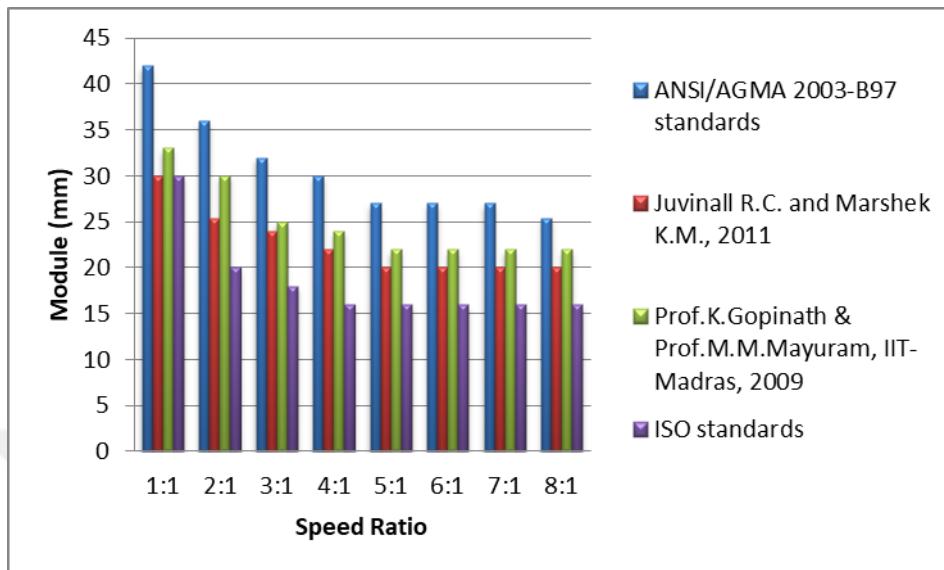
Figure D.21. The effect of speed ratio on module selection based on bending fatigue failure at 1000 kW power transmission (for Ø=25°, Material type 2)

D.3. Obtaining Geometric Rating Number (GR$_i$) for Design Approaches for Ø=25°, Material type 2
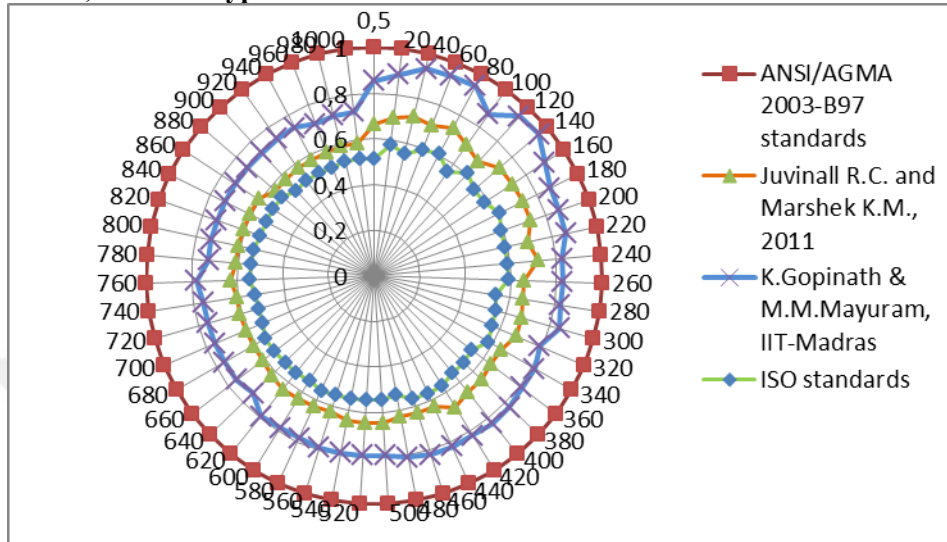
Figure D.22. Comparison of mxF/m$_0$xF$_0$ ratios for the design approaches at 1:1 speed ratio (for Ø=25°, Material type 2)
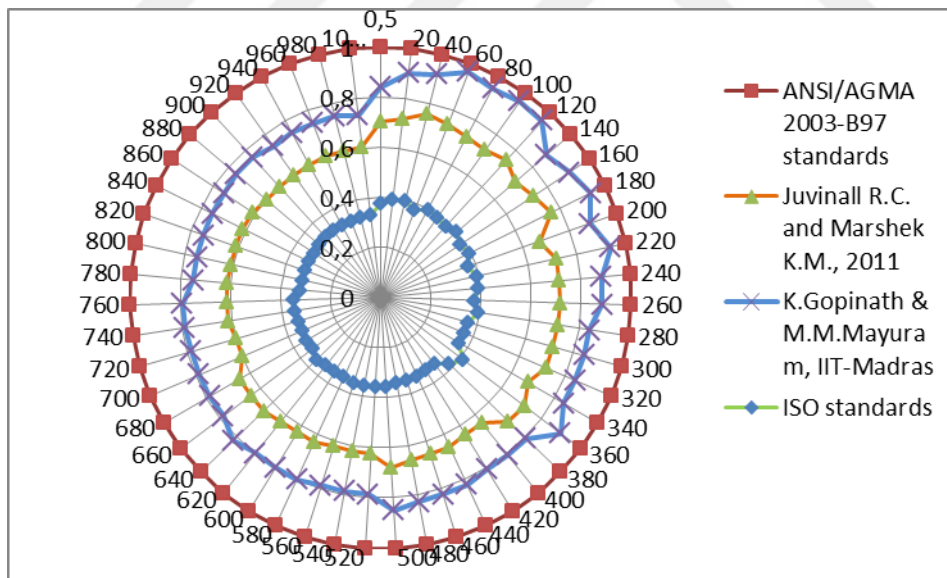
Figure D.23. Comparison of mxF/m$_0$xF$_0$ ratios for the design approaches at 2:1 speed ratio (for Ø=25°, Material type 2)
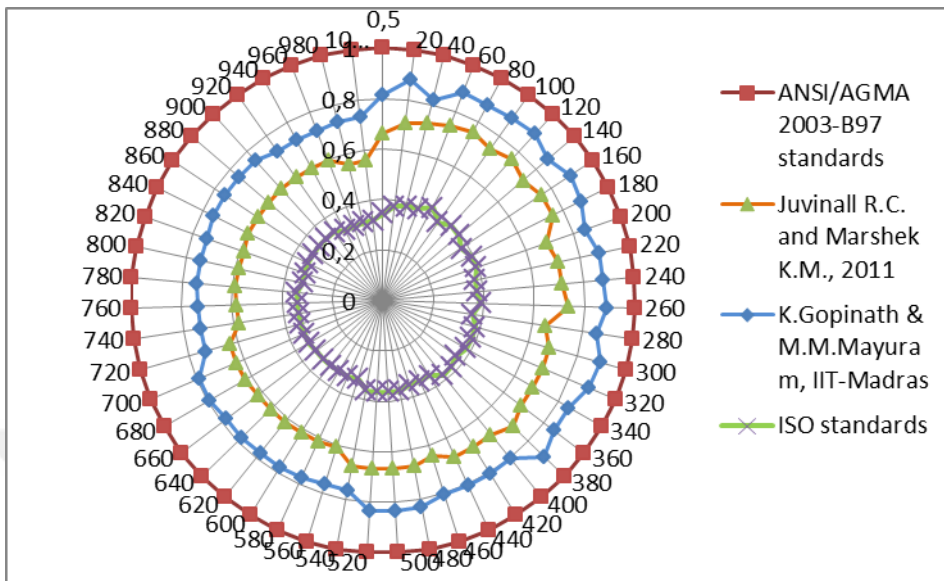
Figure D.24. Comparison of mxF/m_0xF_0 ratios for the design approaches at 3:1 speed ratio (for $\emptyset=25^o$, Material type 2)
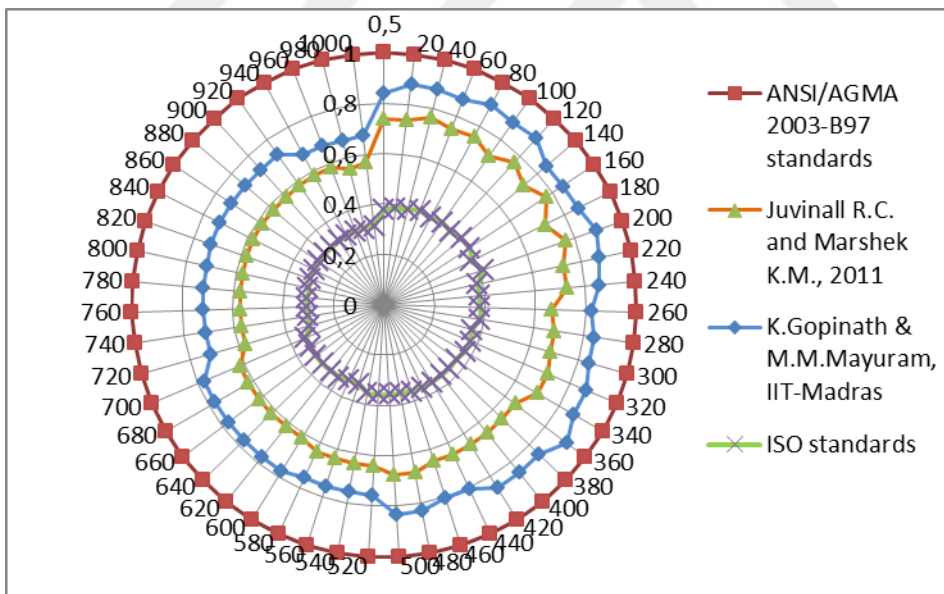
Figure D.25. Comparison of mxF/m_0xF_0 ratios for the design approaches at 4:1 speed ratio (for $\emptyset=25^o$, Material type 2)
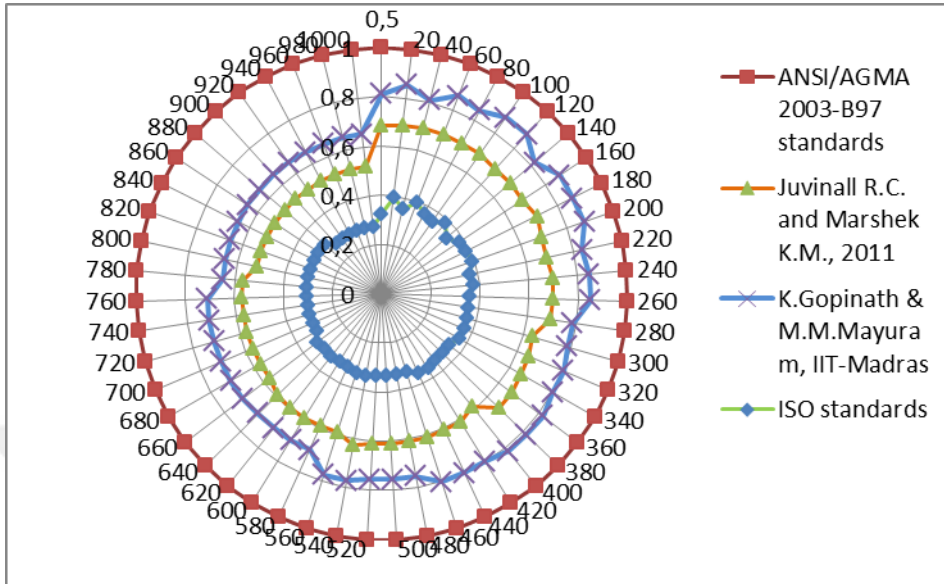
Figure D.26. Comparison of mxF/m₀xF₀ ratios for the design approaches at 5:1 speed ratio (for Ø=25°, Material type 2)
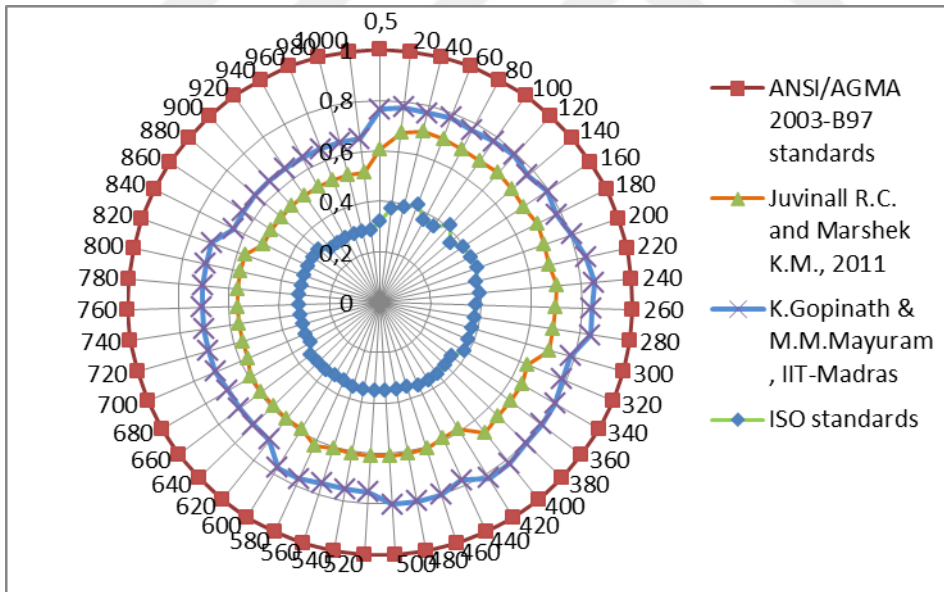
Figure D.27. Comparison of mxF/m₀xF₀ ratios for the design approaches at 6:1 speed ratio (for Ø=25°, Material type 2)
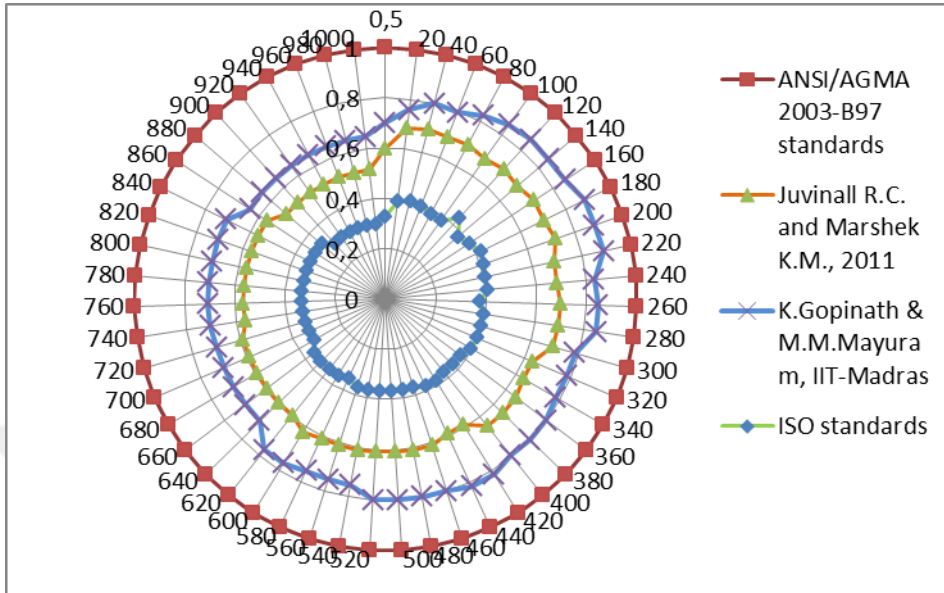
Figure D.28. Comparison of mxF/m$_0$xF$_0$ ratios for the design approaches at 7:1 speed ratio (for Ø=25°, Material type 2)
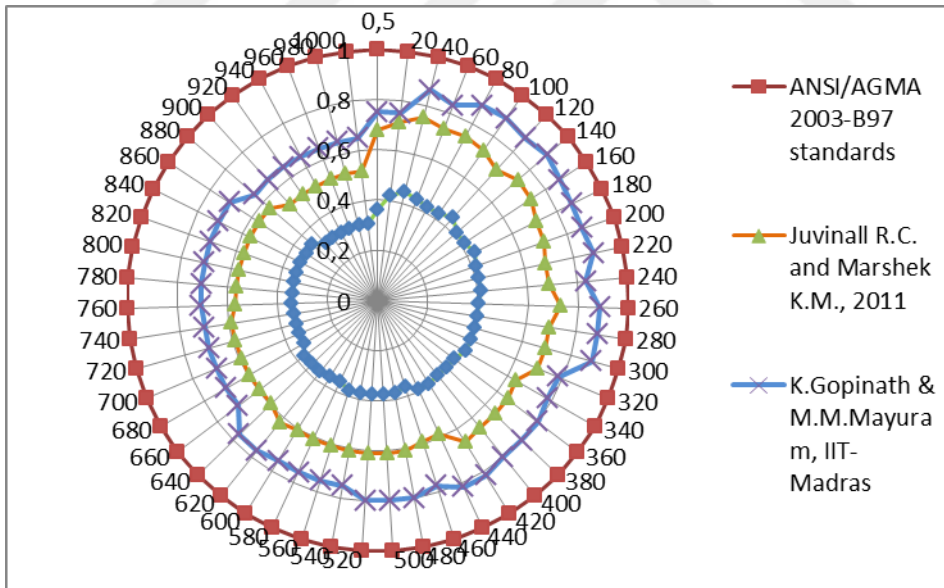
Figure D.29. Comparison of mxF/m$_0$xF$_0$ ratios for the design approaches at 8:1 speed ratio (for Ø=25°, Material type 2)

E.1. Comparison of Module Selection and Face Width Results of the Design Approaches for Ø=25⁰, Material type 3
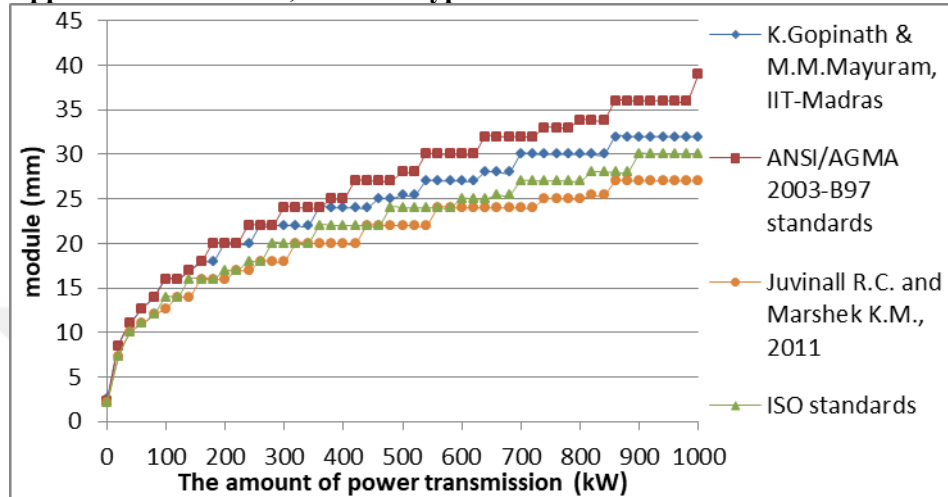
Figure E.1. Module variation considering bending fatigue failure under increasing power at 1:1 speed ratio (for Ø=25°, Material type 3)
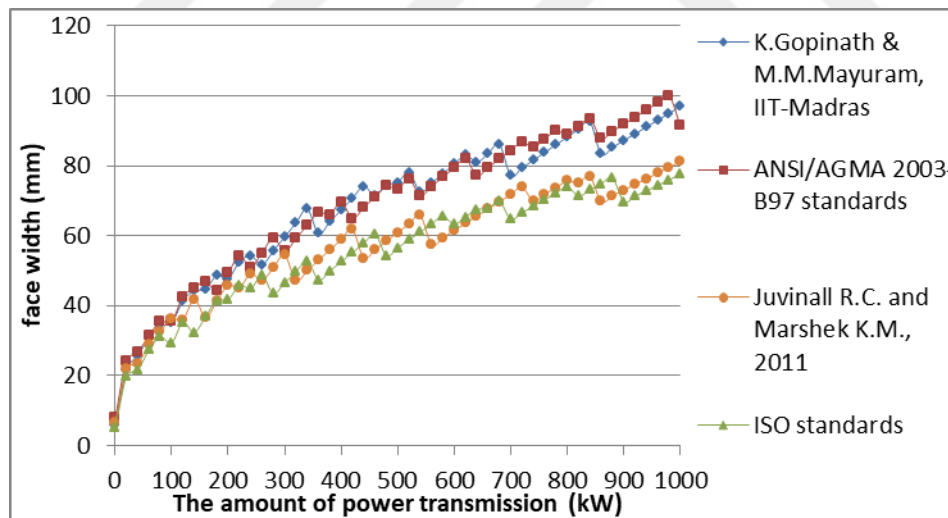
Figure E.2. Face width variation considering bending fatigue failure under increasing power at 1:1 speed ratio (for Ø=25°, Material type 3)
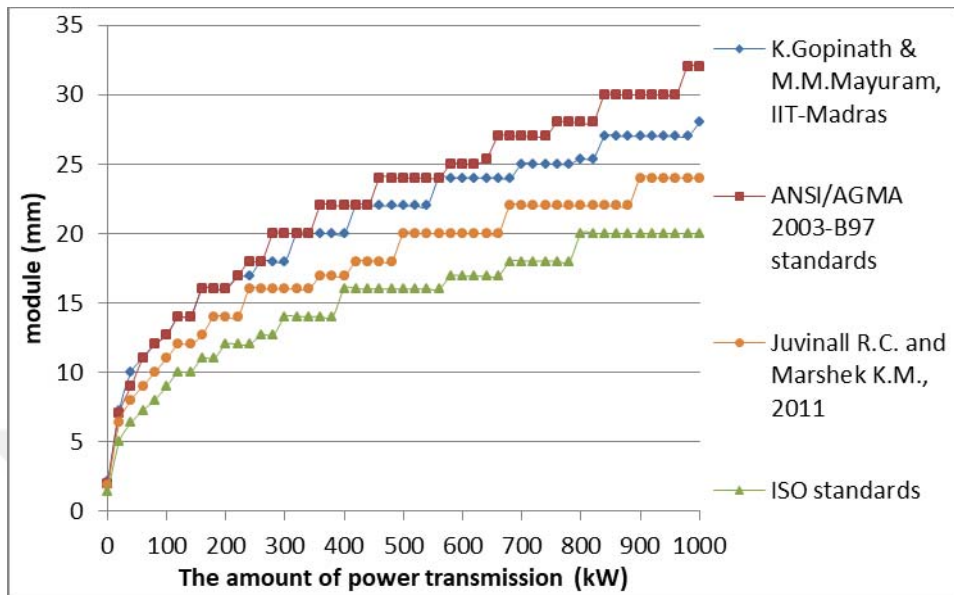
Figure E.3. Module variation considering bending fatigue failure under increasing power at 2:1 speed ratio (for Ø=25°, Material type 3)
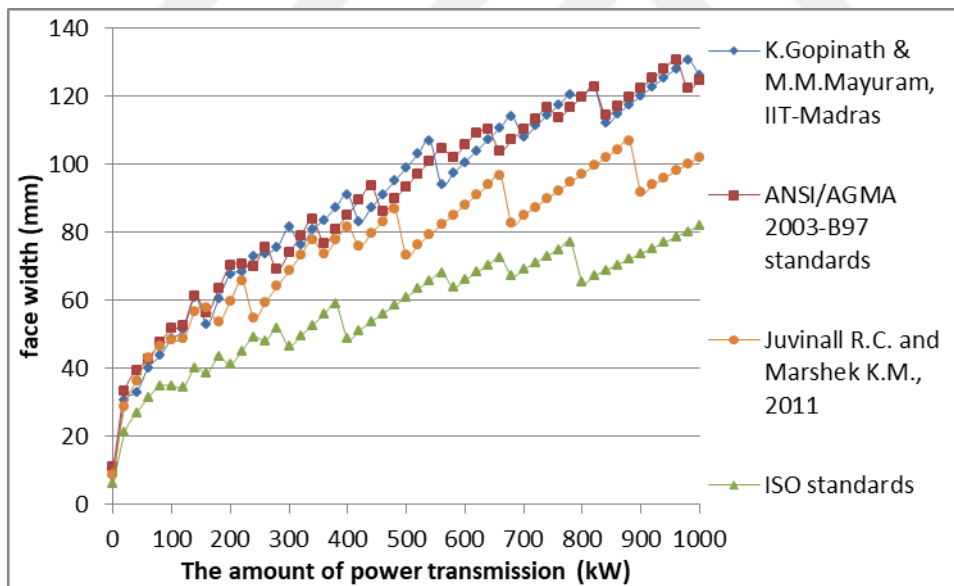
Figure E.4. Face width variation considering bending fatigue failure under increasing power at 2:1 speed ratio (for Ø=25°, Material type 3)
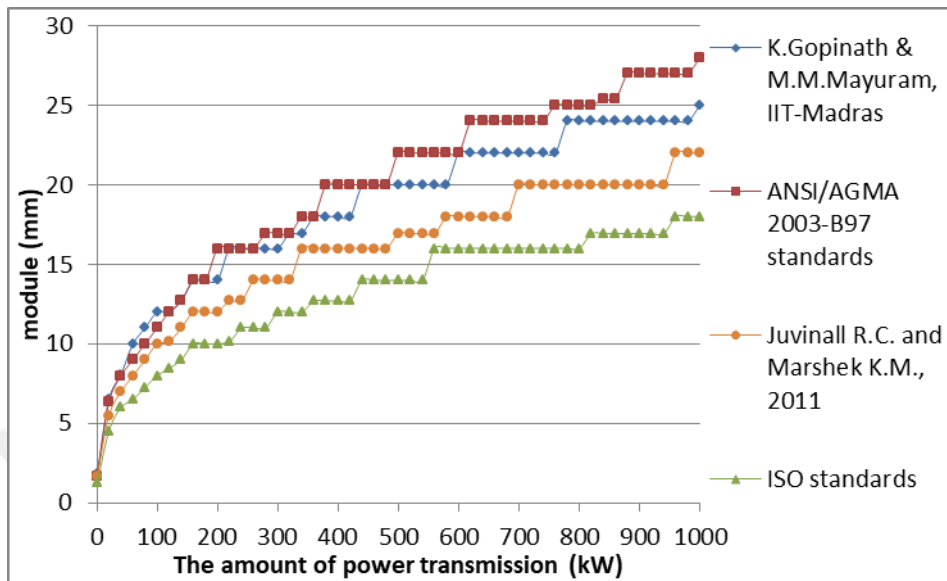
Figure E.5. Module variation considering bending fatigue failure under increasing power at 3:1 speed ratio (for Ø=25°, Material type 3)
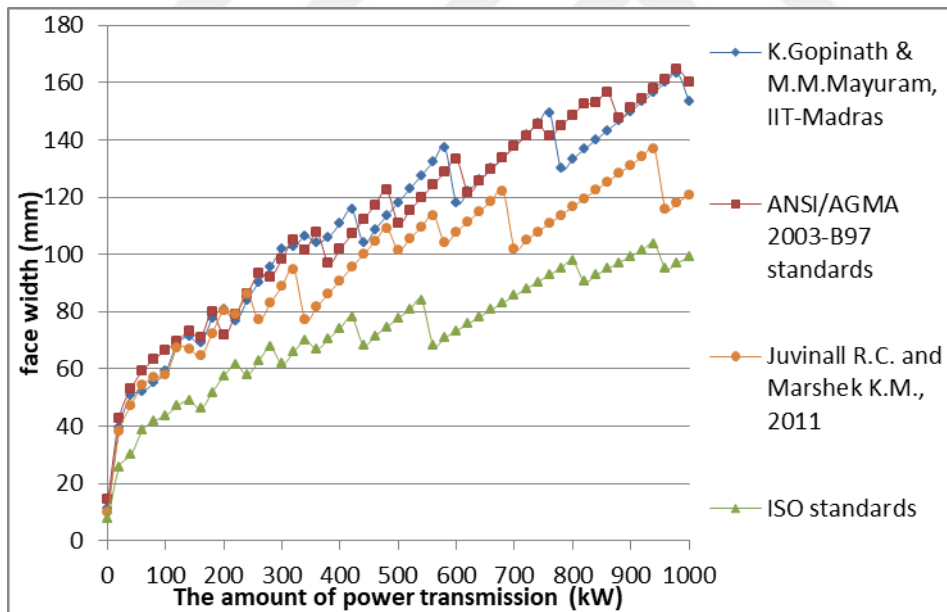
Figure E.6. Face width variation considering bending fatigue failure under increasing power at 3:1 speed ratio (for Ø=25°, Material type 3)
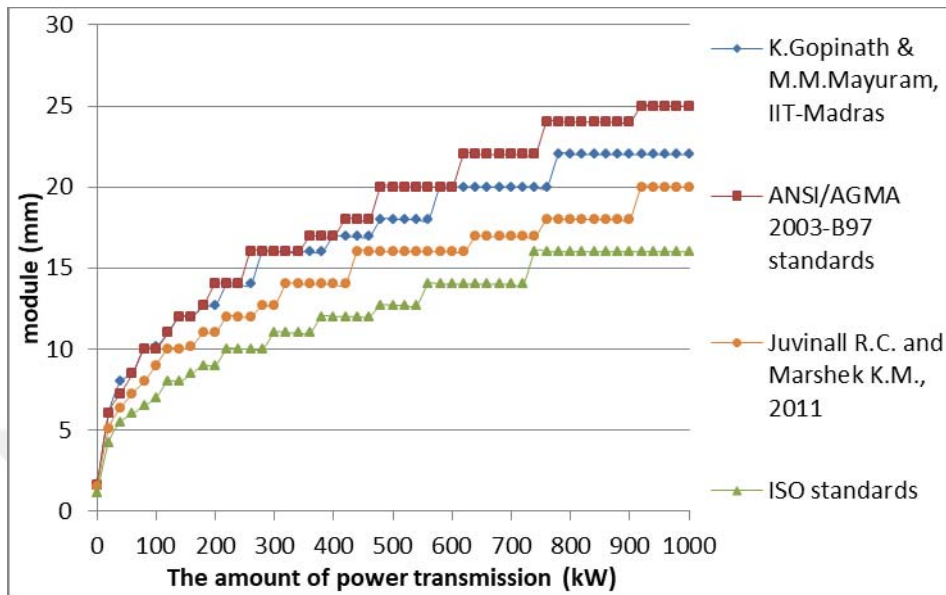
Figure E.7. Module variation considering bending fatigue failure under increasing power at 4:1 speed ratio (for Ø=25°, Material type 3)
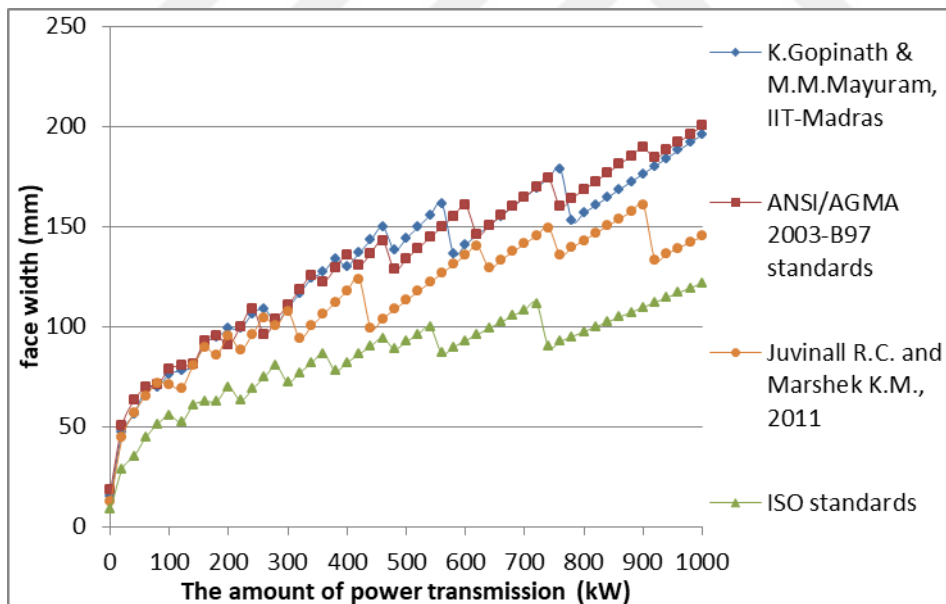

Figure E.8. Face width variation considering bending fatigue failure under increasing power at 4:1 speed ratio (for Ø=25°, Material type 3)

245
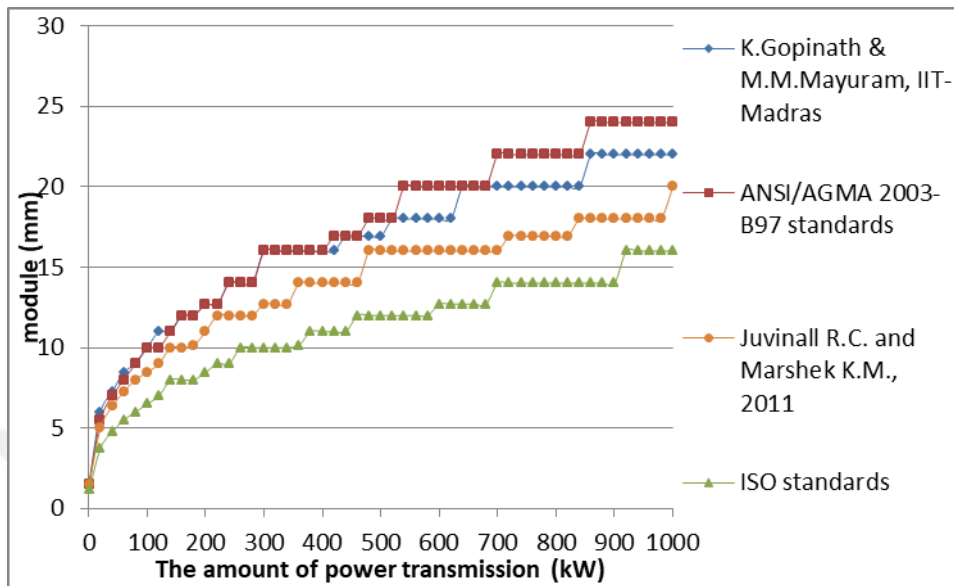
Figure E.9. Module variation considering bending fatigue failure under increasing power at 5:1 speed ratio (for Ø=25°, Material type 3)
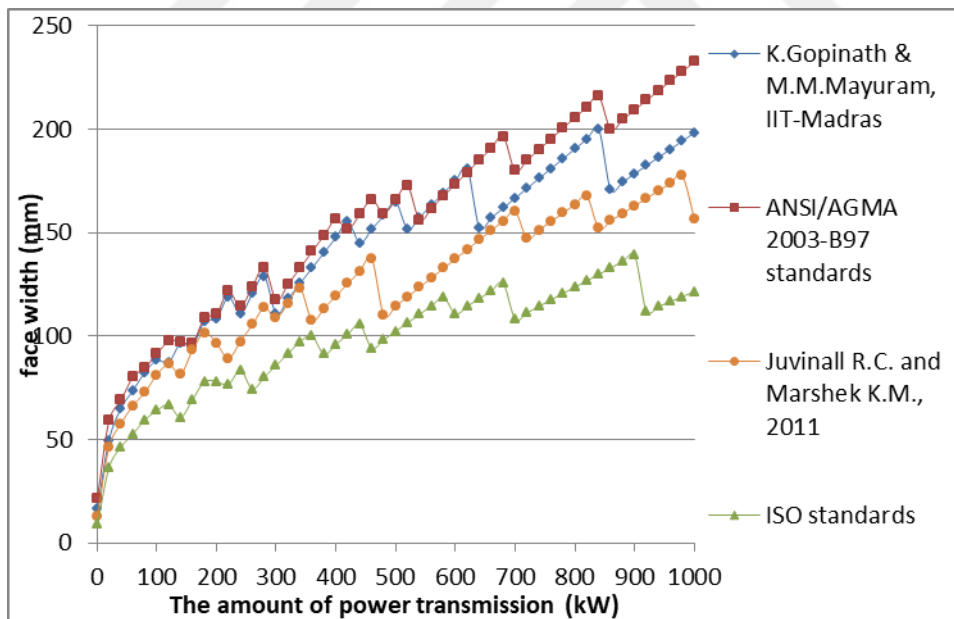
Figure E.10. Face width variation considering bending fatigue failure under increasing power at 5:1 speed ratio (for Ø=25°, Material type 3)
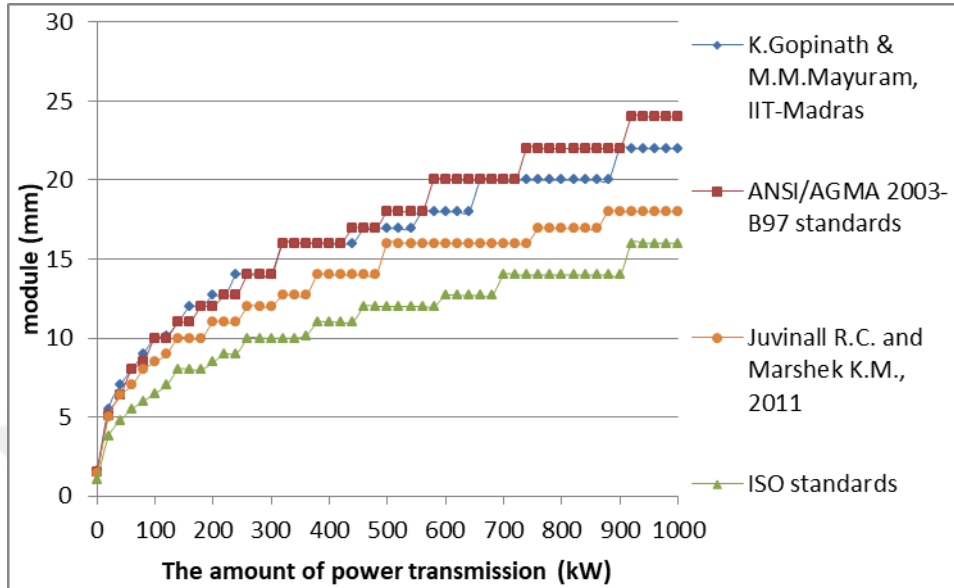
Figure E.11. Module variation considering bending fatigue failure under increasing
power at 6:1 speed ratio (for Ø=25°, Material type 3)
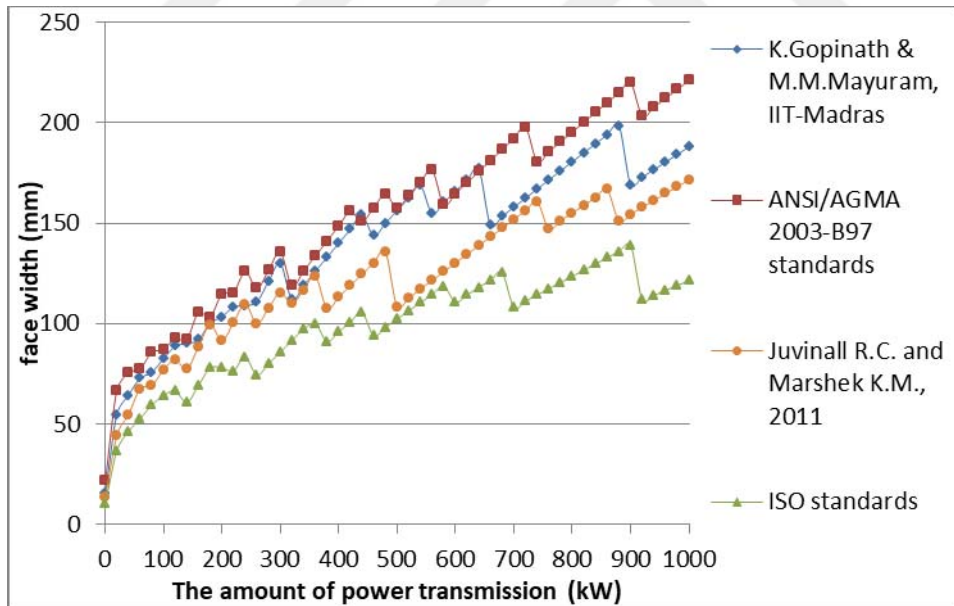


Figure E.12. Face width variation considering bending fatigue failure under
increasing power at 6:1 speed ratio (for Ø=25°, Material type 3)
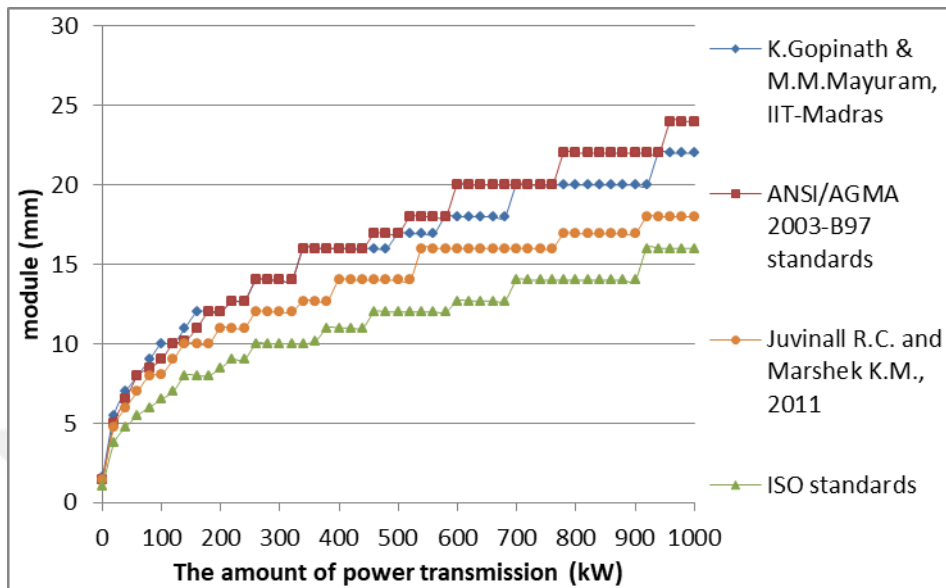
Figure E.13. Module variation considering bending fatigue failure under increasing power at 7:1 speed ratio (for Ø=25°, Material type 3)
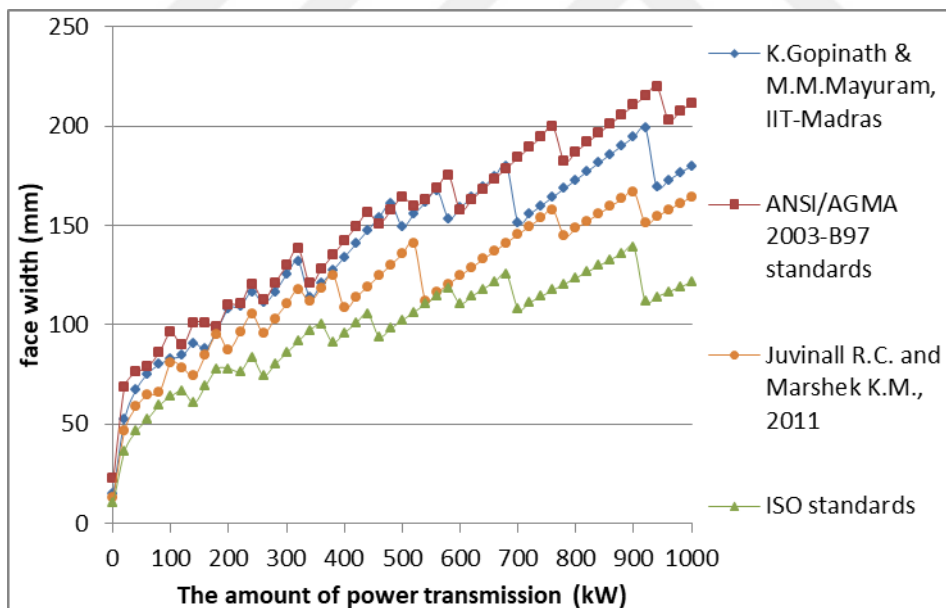
Figure E.14. Face width variation considering bending fatigue failure under increasing power at 7:1 speed ratio (for Ø=25°, Material type 3)
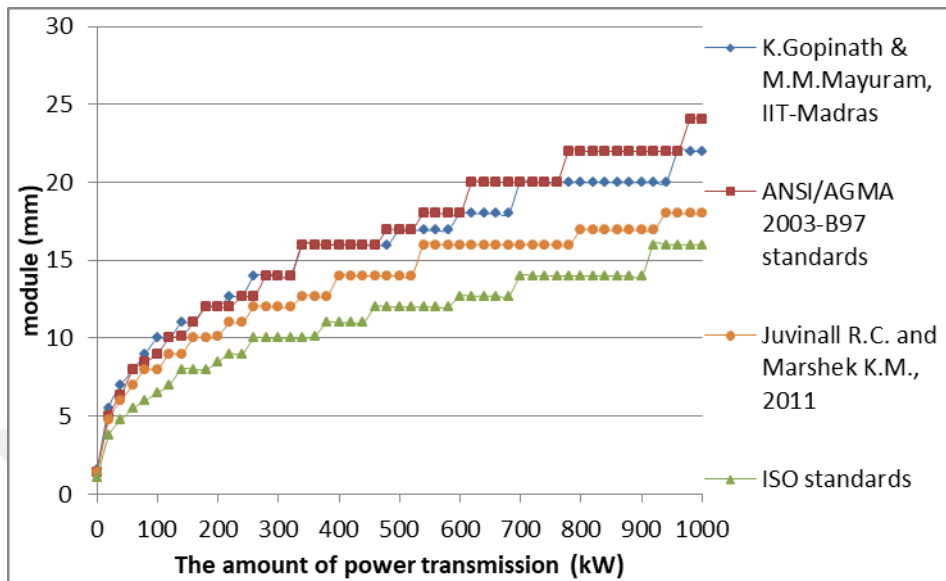
Figure E.15. Module variation considering bending fatigue failure under increasing power at 8:1 speed ratio (for Ø=25°, Material type 3)
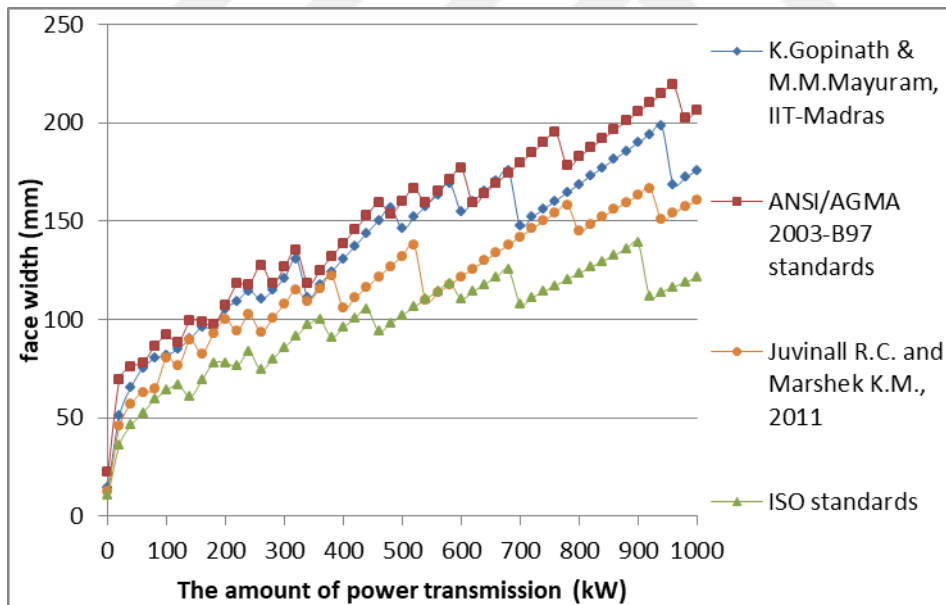
Figure E.16. Face width variation considering bending fatigue failure under increasing power at 8:1 speed ratio (for Ø=25°, Material type 3)

E.2. Comparison of the Results Based on Bending Fatigue Failure Considering Speed Ratio for the Selected Power Transmissions for Ø=25⁰, Material type 3
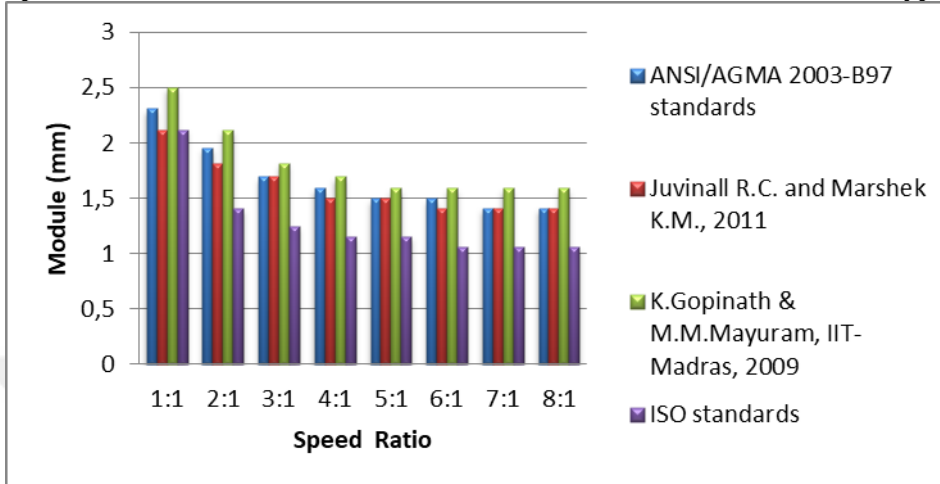

Figure E.17. The effect of speed ratio on module selection based on bending fatigue failure at 0,5 kW power transmission (for Ø=25⁰, Material type 3)
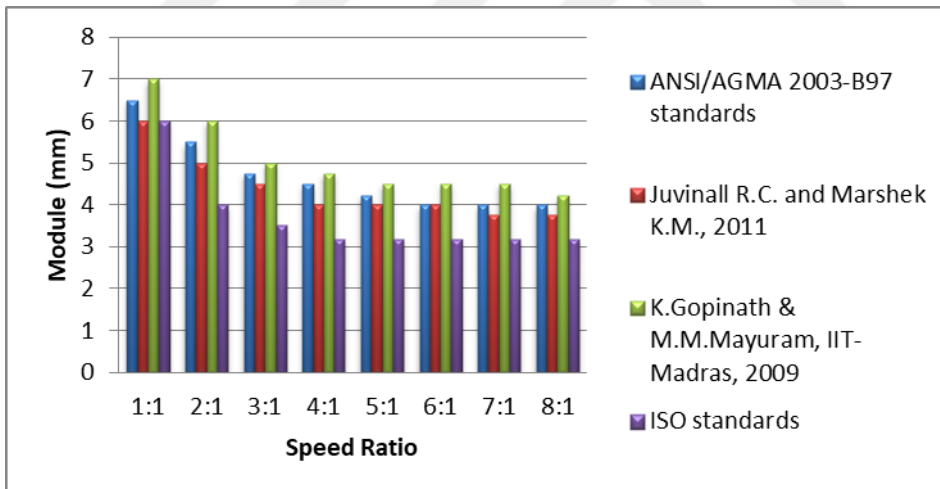

Figure E.18. The effect of speed ratio on module selection based on bending fatigue failure at 10 kW power transmission (for Ø=25⁰, Material type 3)
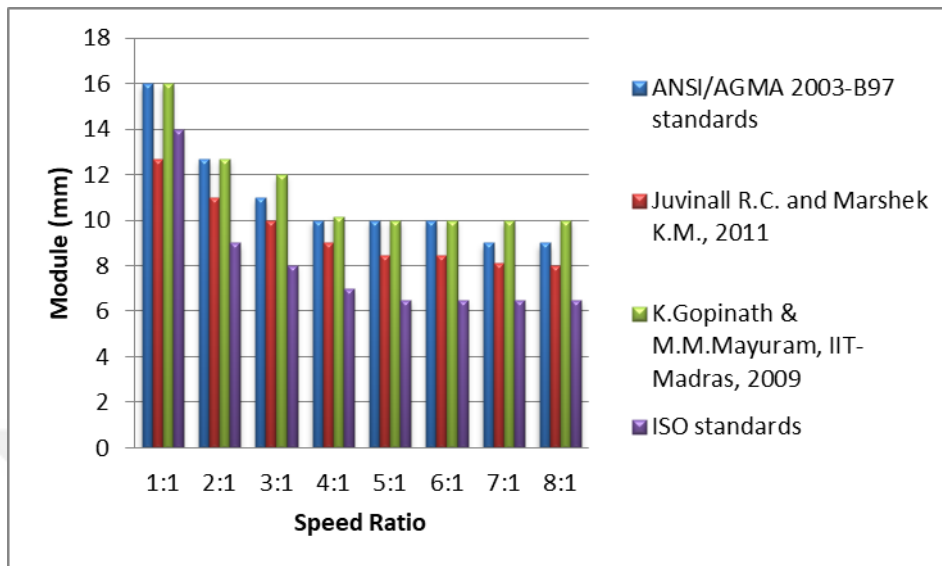
Figure E.19. The effect of speed ratio on module selection based on bending
fatigue failure at 100 kW power transmission (for Ø=25°, Material
type 3)
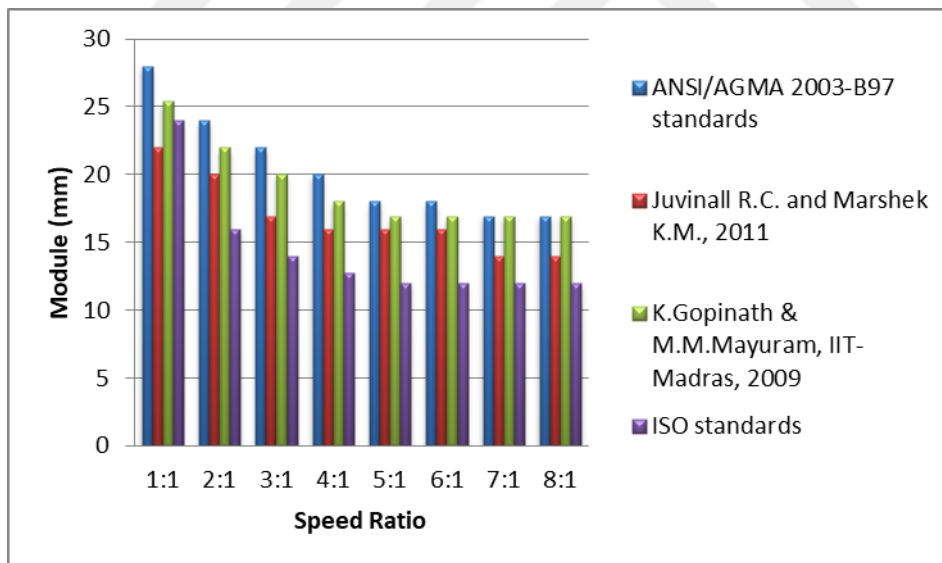
Figure E.20. The effect of speed ratio on module selection based on bending
fatigue failure at 500 kW power transmission (for Ø=25°, Material
type 3)
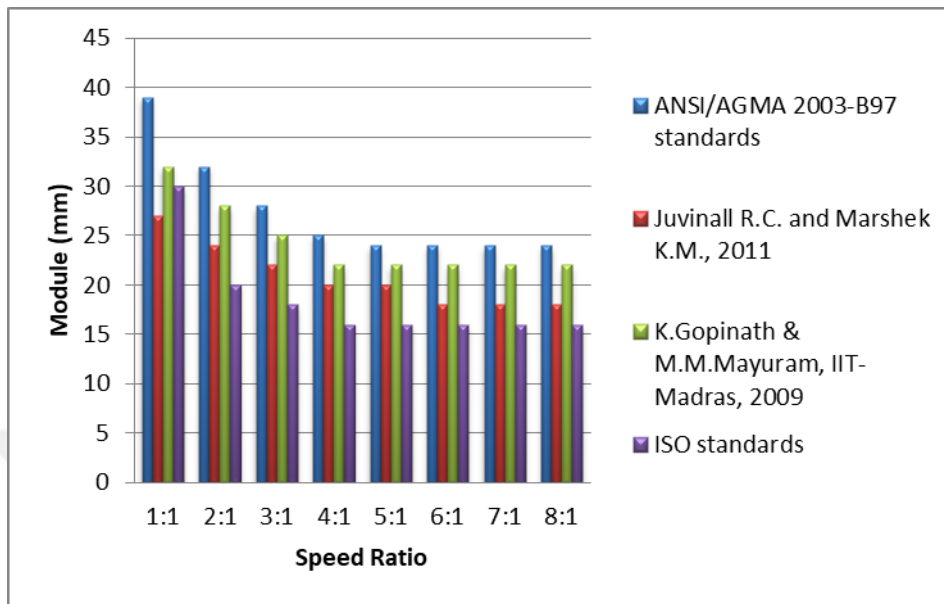
Figure E.21. The effect of speed ratio on module selection based on bending
fatigue failure at 1000 kW power transmission (for Ø=25°, Material
type 3)

**E.3. Obtaining Geometric Rating Number (GRi) for Design Approaches for Ø=25°, Material type 3**
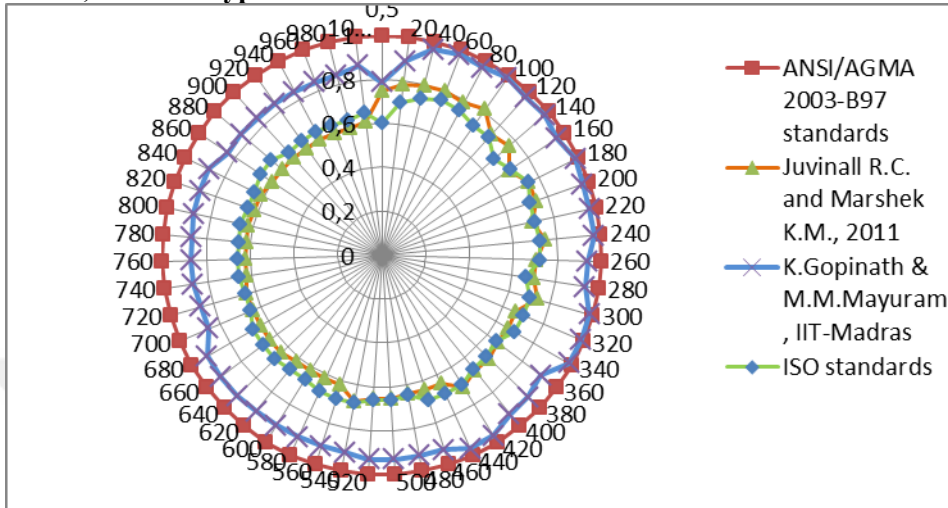
Figure E.22. Comparison of mxF/m_0xF_0 ratios for the design approaches at 1:1 speed ratio (for Ø=25°, Material type 3)
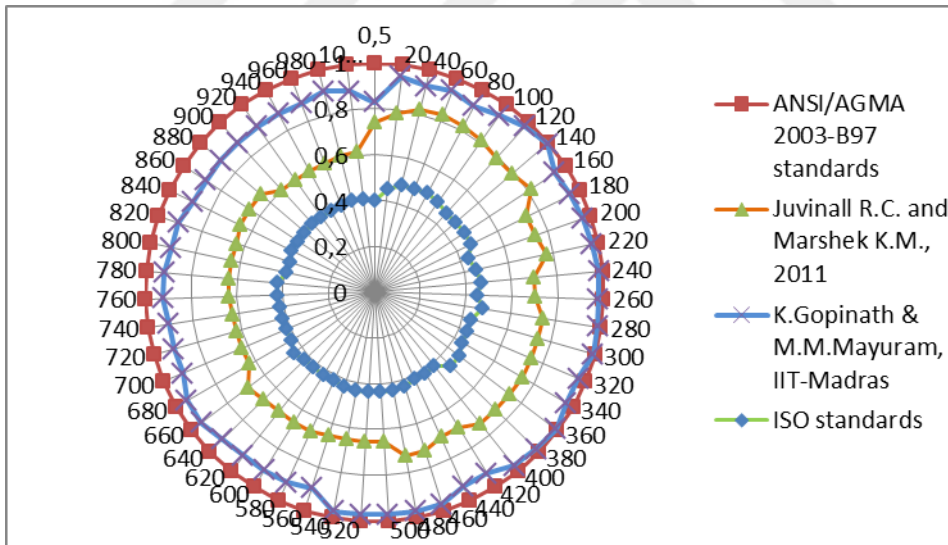

Figure E.23. Comparison of mxF/m_0xF_0 ratios for the design approaches at 2:1 speed ratio (for Ø=25°, Material type 3)
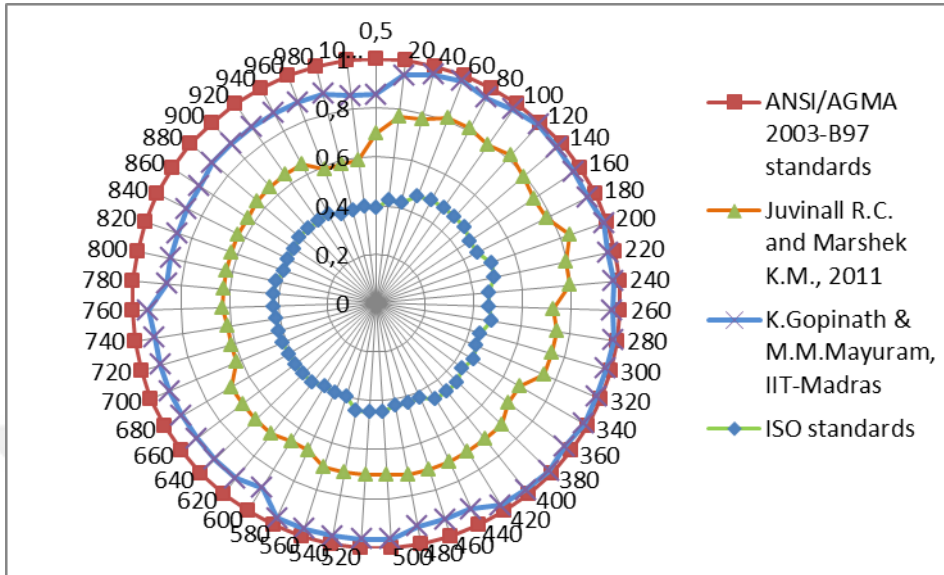
Figure E.24. Comparison of mxF/m_0xF_0 ratios for the design approaches at 3:1 speed ratio (for $\emptyset=25^{\circ}$, Material type 3)
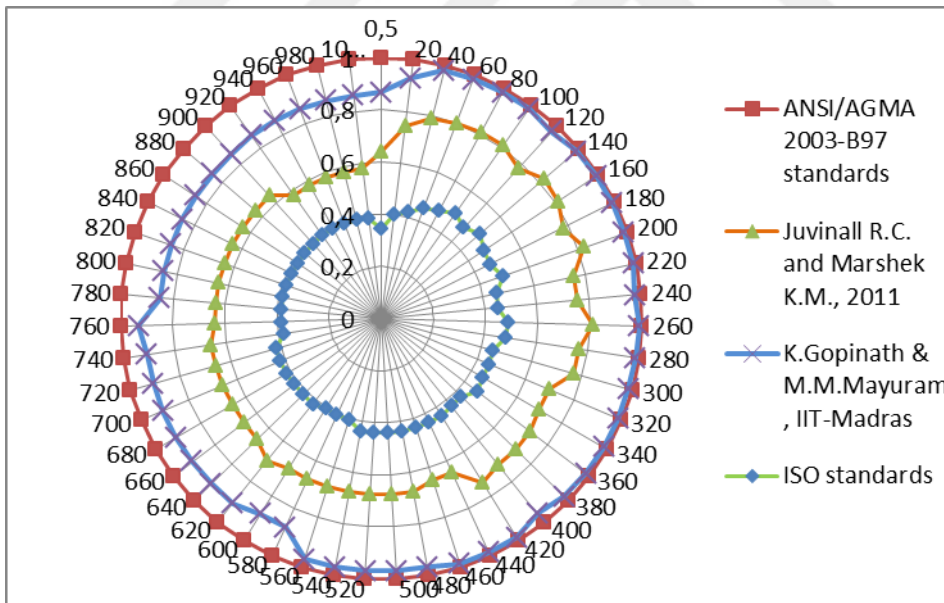
Figure E.25. Comparison of mxF/m_0xF_0 ratios for the design approaches at 4:1 speed ratio (for $\emptyset=25^{\circ}$, Material type 3)
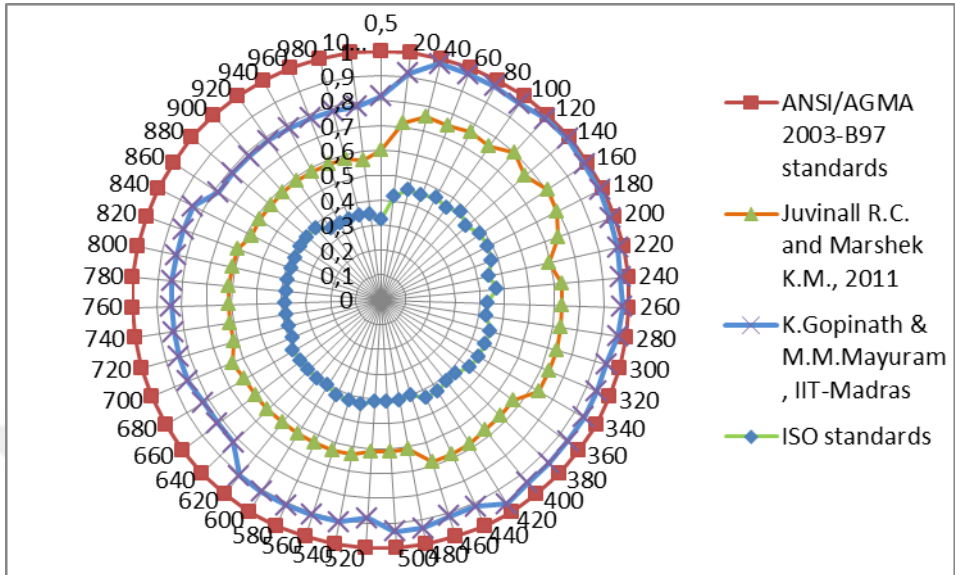
Figure E.26. Comparison of mxF/m_0xF_0 ratios for the design approaches at 5:1 speed ratio (for $\varnothing=25^{o}$, Material type 3)
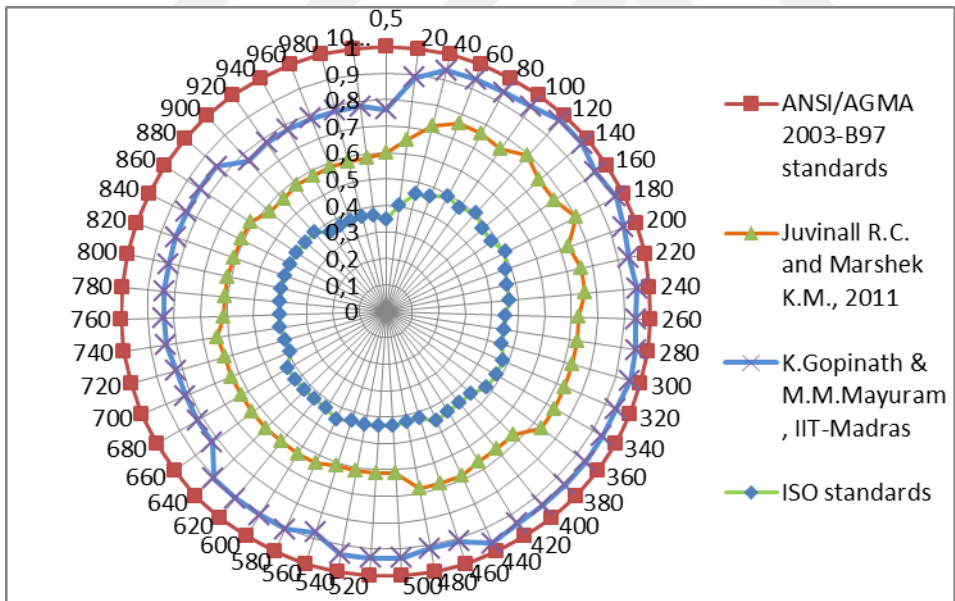

Figure E.27. Comparison of mxF/m_0xF_0 ratios for the design approaches at 6:1 speed ratio (for $\varnothing=25^{o}$, Material type 3)
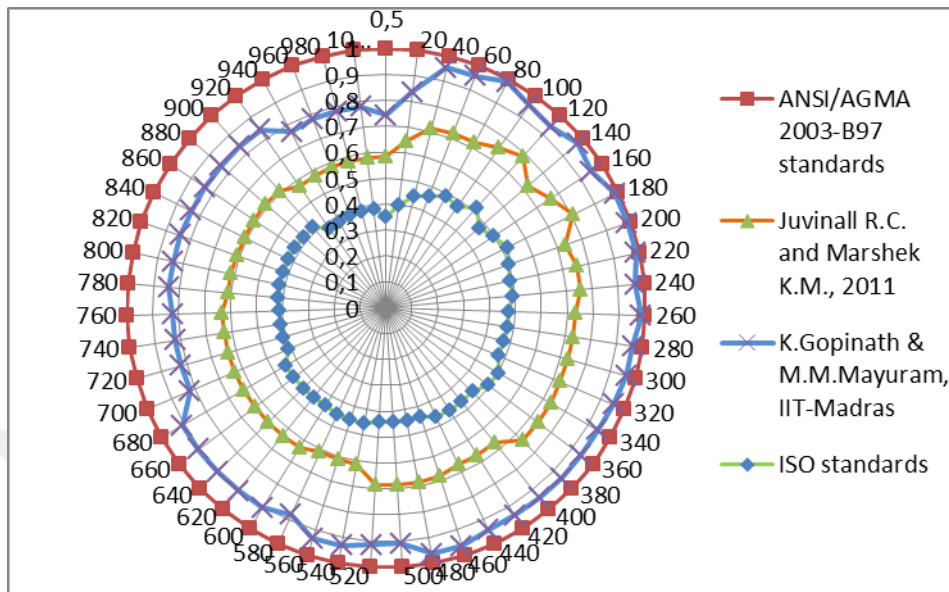
Figure E.28. Comparison of mxF/m_0xF_0 ratios for the design approaches at 7:1 speed ratio (for $\varnothing=25^o$, Material type 3)
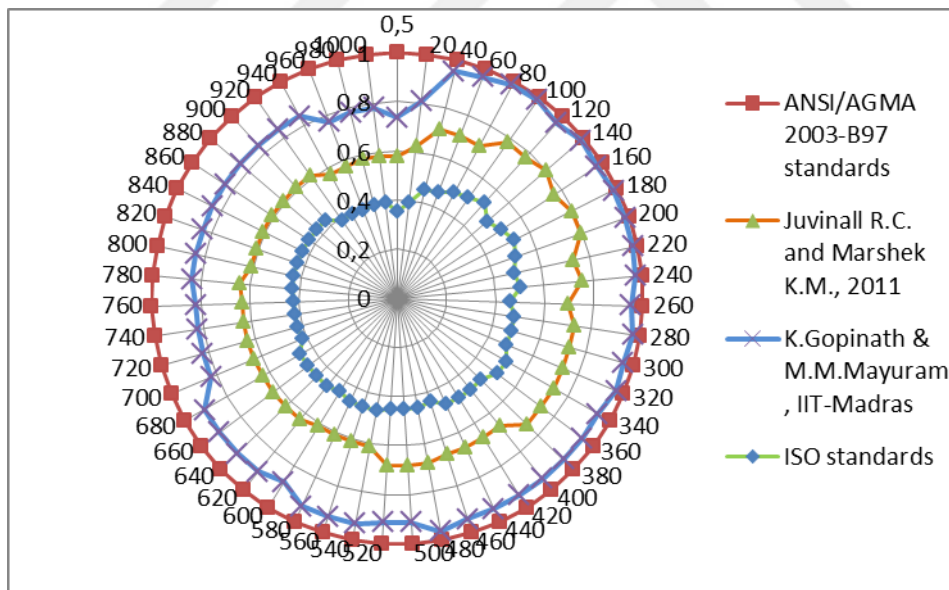

Figure E.29. Comparison of mxF/m_0xF_0 ratios for the design approaches at 8:1 speed ratio (for $\varnothing=25^o$, Material type 3)

APPENDIX F

F.1. Comparison of Module Selection and Face Width Results of the Design Approaches for Ø=20°, Material type 2
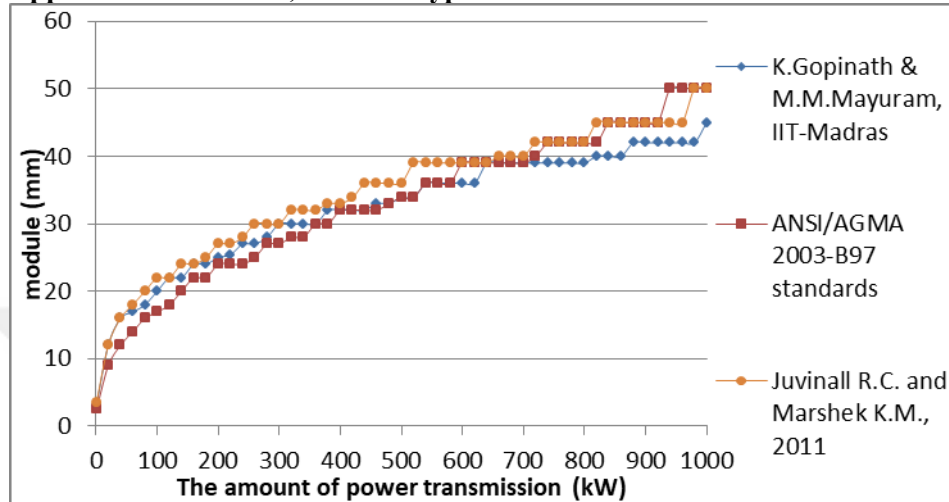
Figure F.1. Module variation considering surface contact fatigue failure under increasing power at 1:1 speed ratio (for Ø=20°, Material type 2)
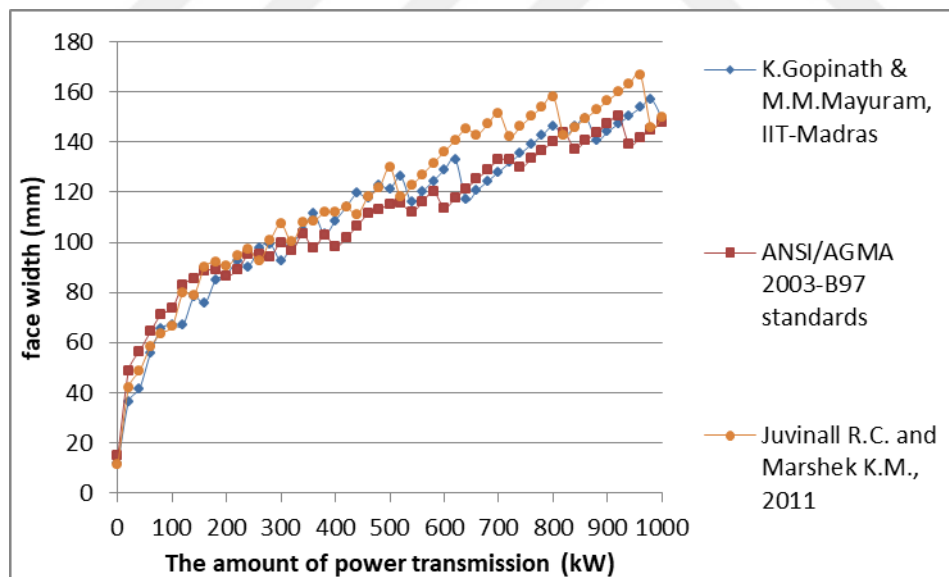
Figure F.2. Face width variation considering surface contact fatigue failure under increasing power at 1:1 speed ratio (for Ø=20°, Material type 2)

257
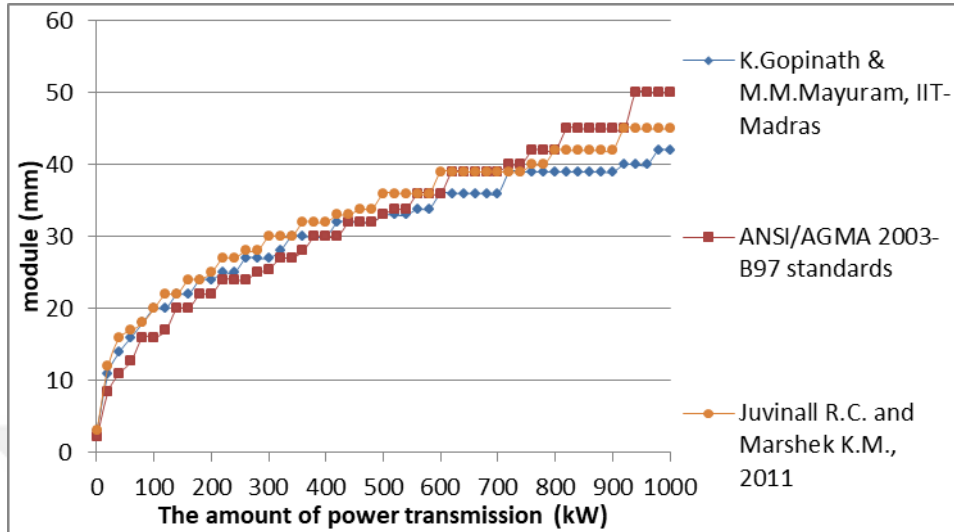
Figure F.3. Module variation considering surface contact fatigue failure under increasing power at 2:1 speed ratio (for Ø=20°, Material type 2)
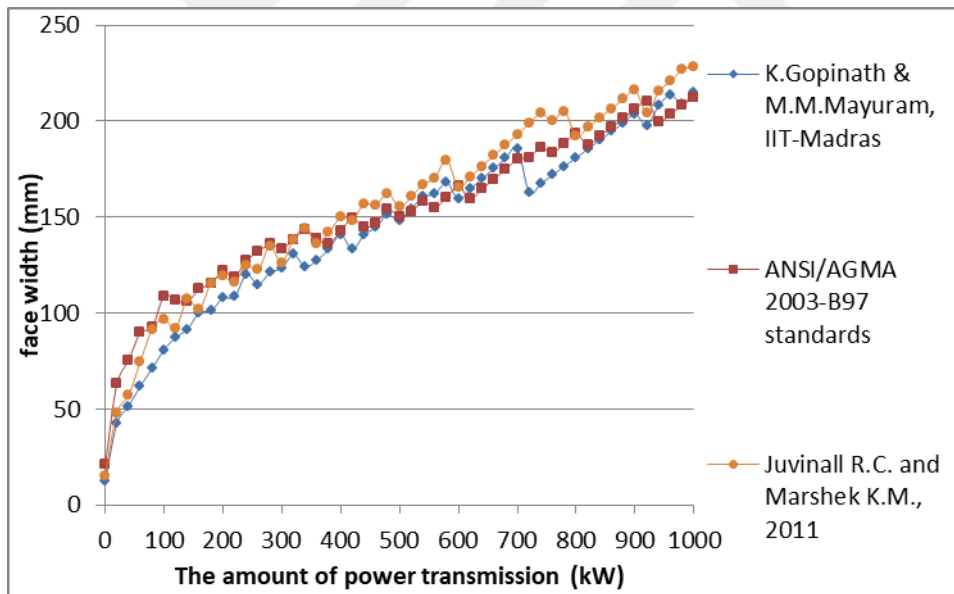
Figure F.4. Face width variation considering surface contact fatigue failure under increasing power at 2:1 speed ratio (for Ø=20°, Material type 2)
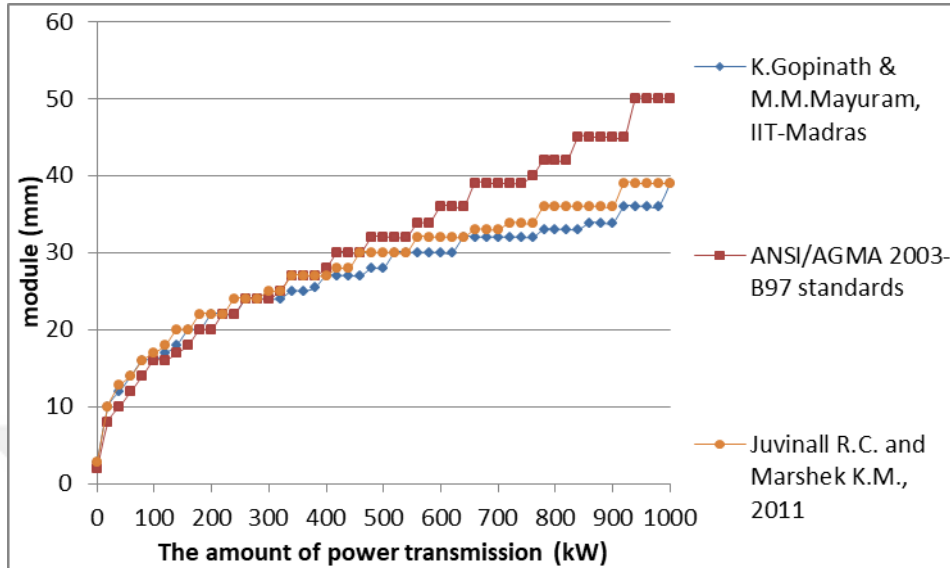
Figure F.5. Module variation considering surface contact fatigue failure under increasing power at 3:1 speed ratio (for Ø=20°, Material type 2)
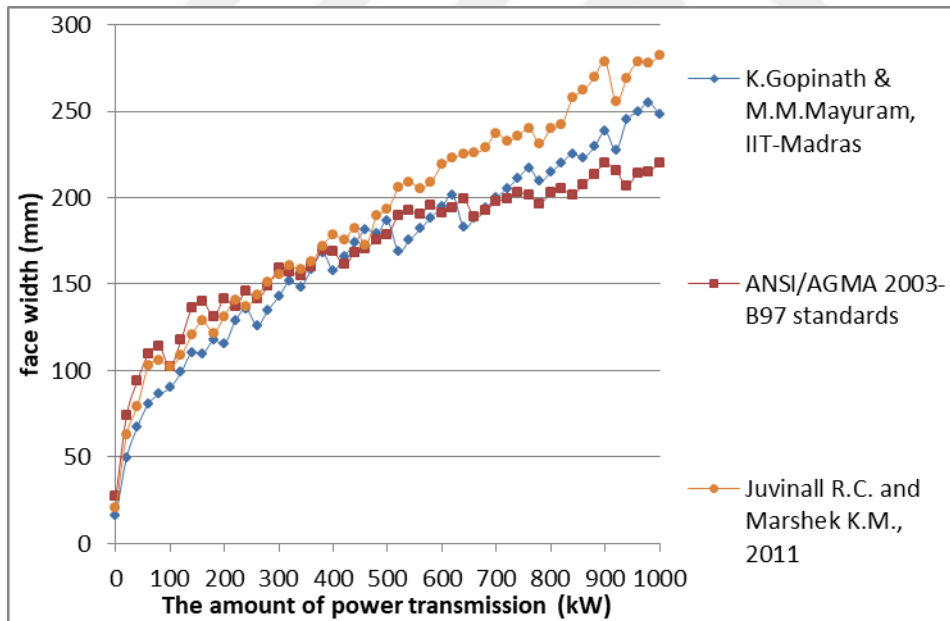
Figure F.6. Face width variation considering surface contact fatigue failure under increasing power at 3:1 speed ratio (for Ø=20°, Material type 2)
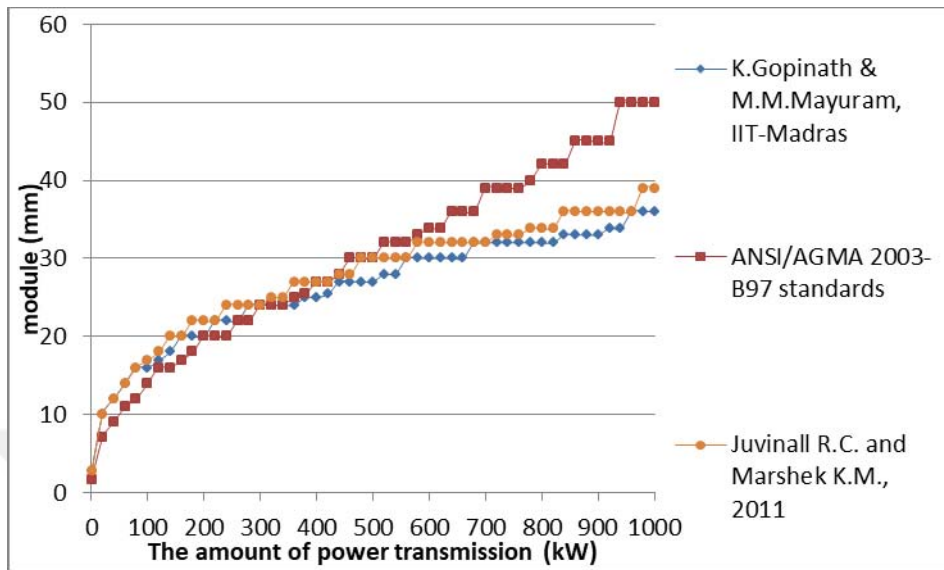
Figure F.7. Module variation considering surface contact fatigue failure under
increasing power at 4:1 speed ratio (for Ø=20°, Material type 2)
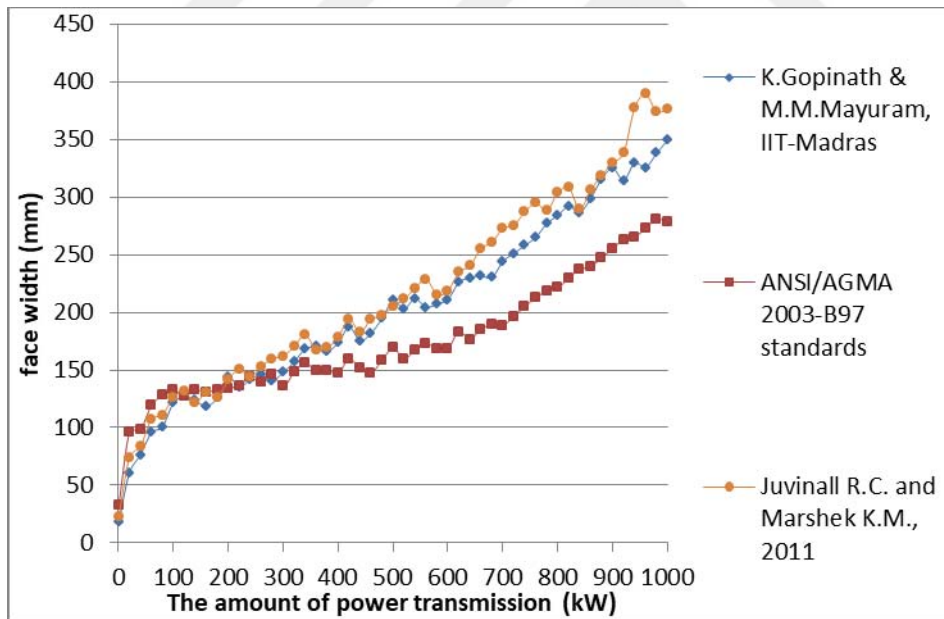

Figure F.8. Face width variation considering surface contact fatigue failure under
increasing power at 4:1 speed ratio (for Ø=20°, Material type 2)
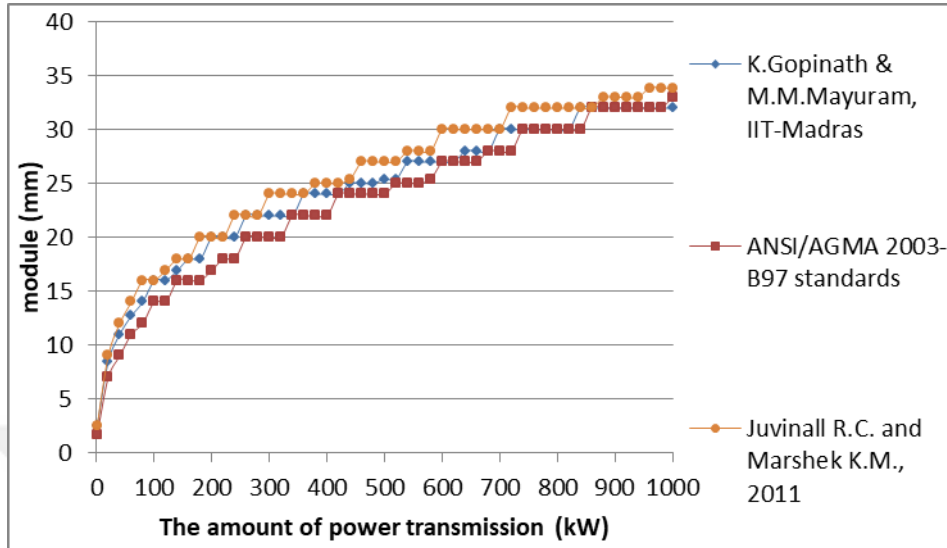
Figure F.9. Module variation considering surface contact fatigue failure under increasing power at 5:1 speed ratio (for Ø=20°, Material type 2)
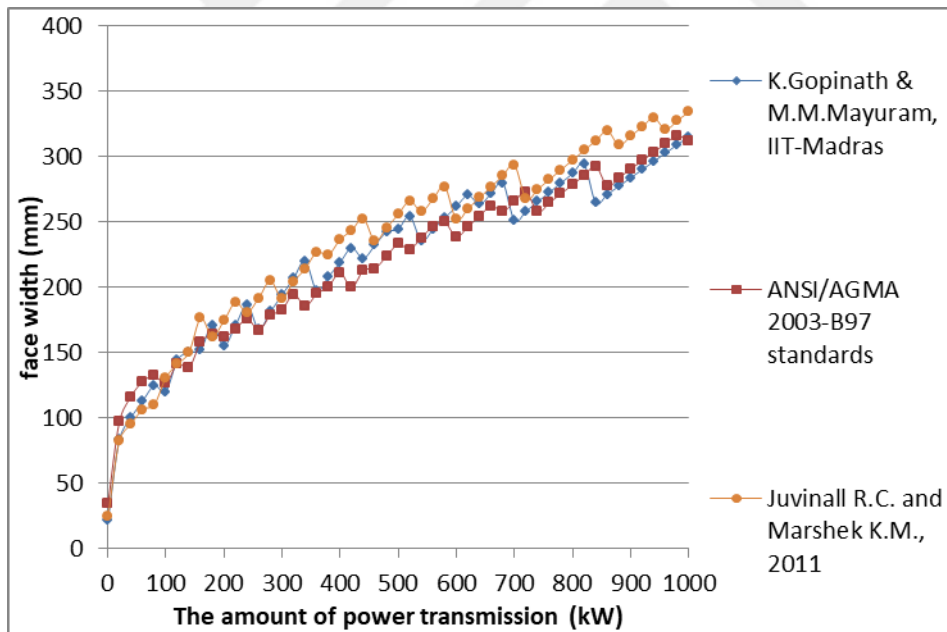
Figure F.10. Face width variation considering surface contact fatigue failure under increasing power at 5:1 speed ratio (for Ø=20°, Material type 2)

261
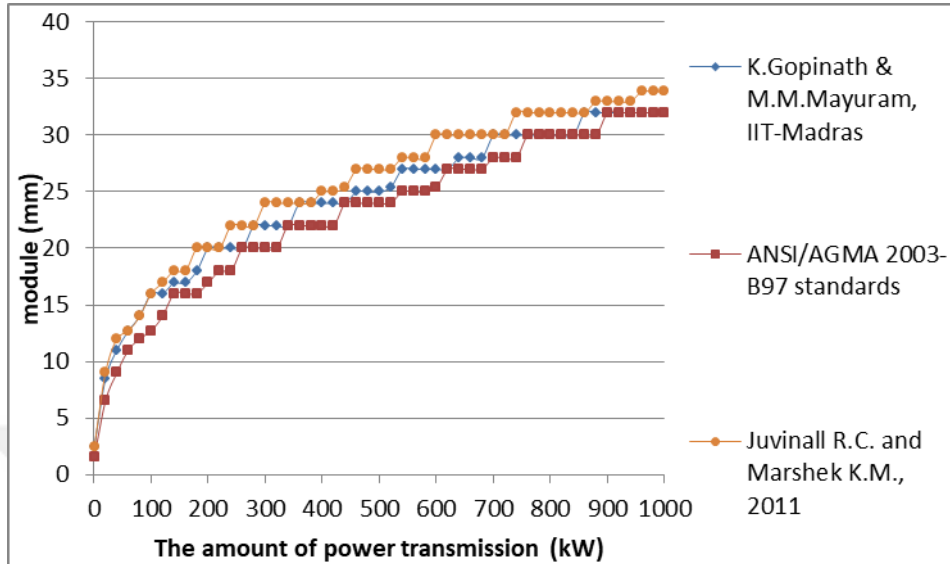
Figure F.11. Module variation considering surface contact fatigue failure under increasing power at 6:1 speed ratio (for Ø=20°, Material type 2)
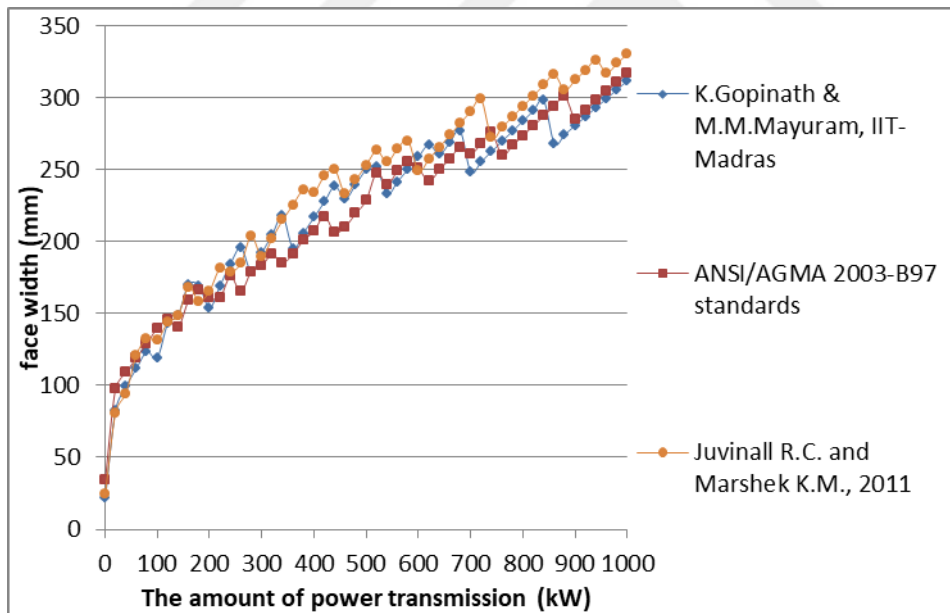

Figure F.12. Face width variation considering surface contact fatigue failure under increasing power at 6:1 speed ratio (for Ø=20°, Material type 2)

262
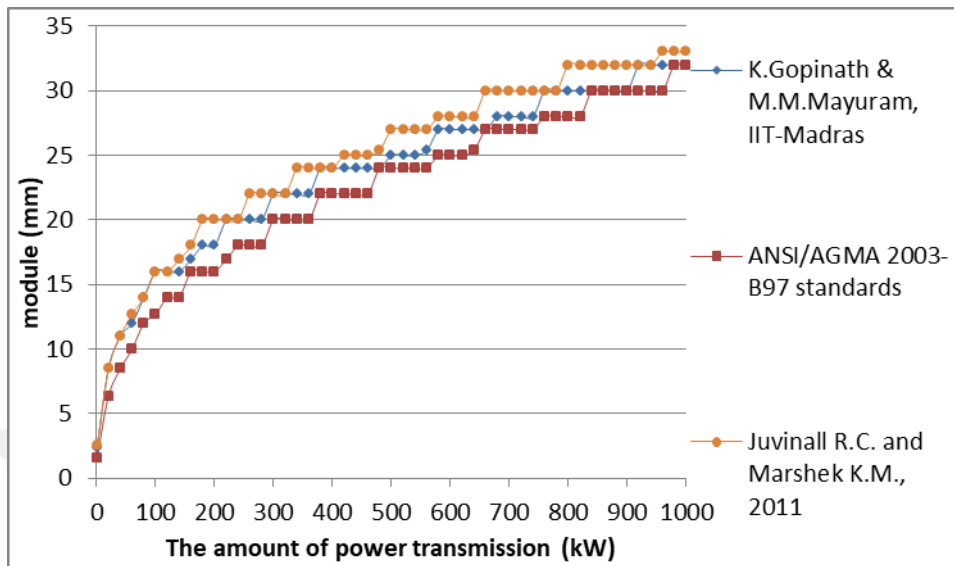
Figure F.13. Module variation considering surface contact fatigue failure under increasing power at 7:1 speed ratio (for Ø=20°, Material type 2)
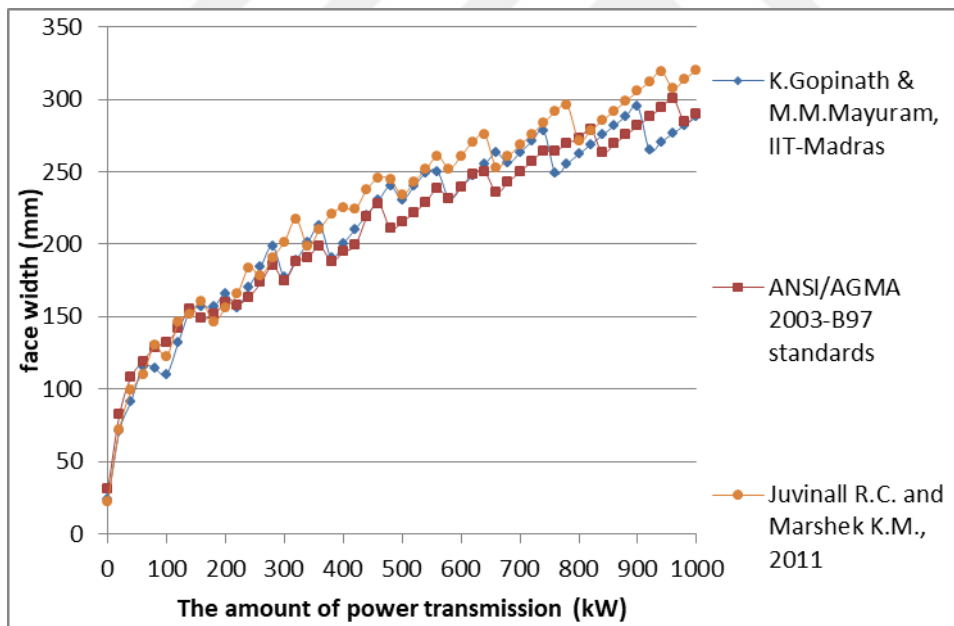
Figure F.14. Face width variation considering surface contact fatigue failure under increasing power at 7:1 speed ratio (for Ø=20°, Material type 2)
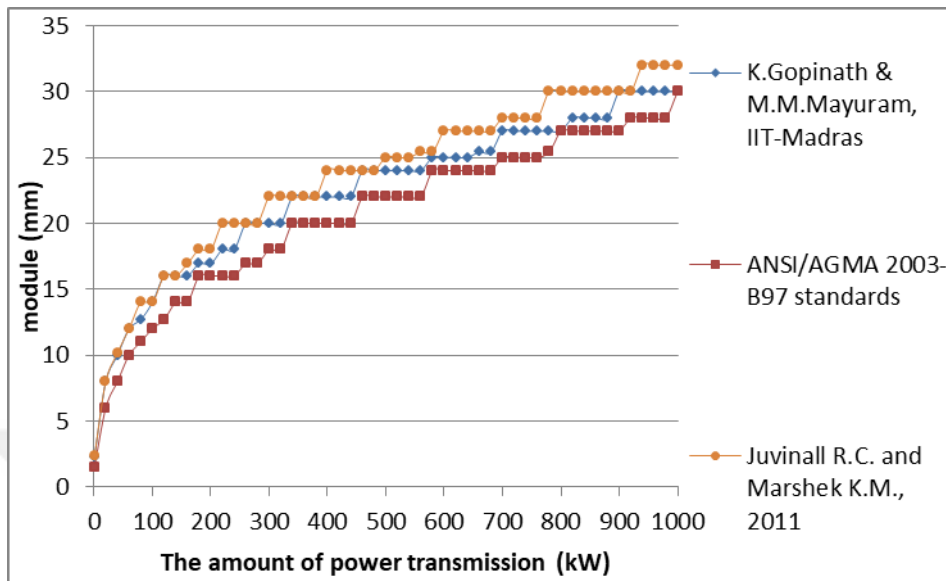
Figure F.15. Module variation considering surface contact fatigue failure under
increasing power at 8:1 speed ratio (for Ø=20°, Material type 2)
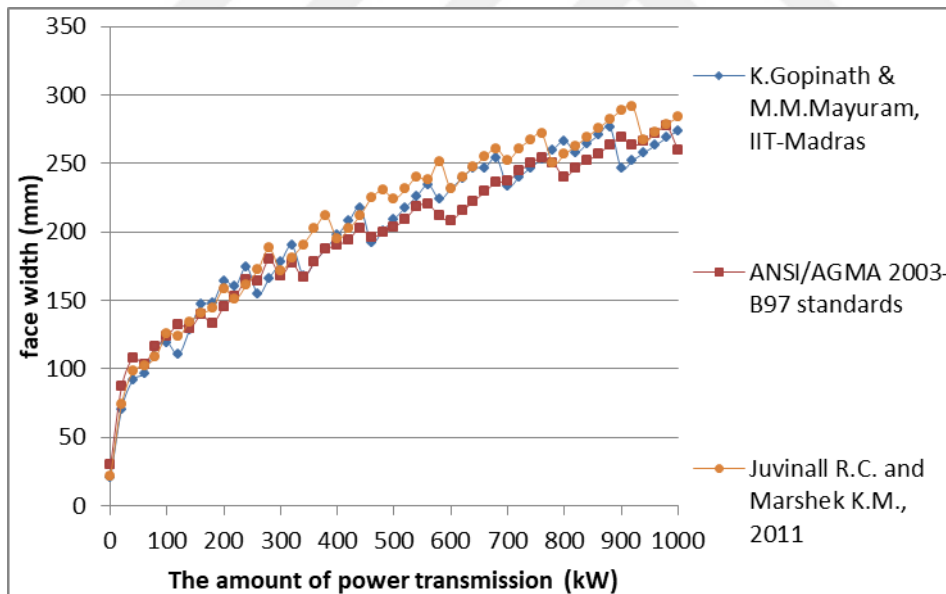
Figure F.16. Face width variation considering surface contact fatigue failure under
increasing power at 8:1 speed ratio (for Ø=20°, Material type 2)

264

F.2. Comparison of the Results Based on Surface Contact Fatigue Failure Considering Speed Ratio for the Selected Power Transmissions for Ø=20°, Material type 2
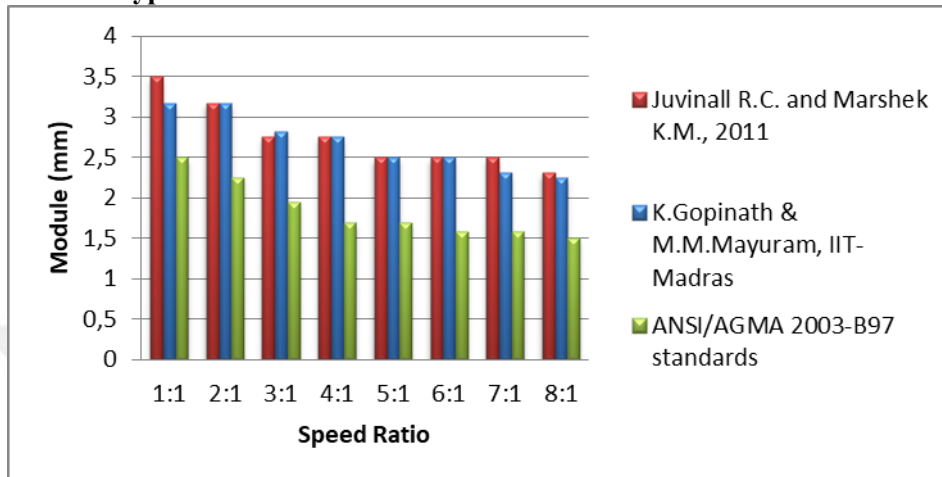
Figure F.17. The effect of speed ratio on module selection based on surface contact fatigue failure at 0,5 kW power transmission (for Ø=20°, Material type 2)
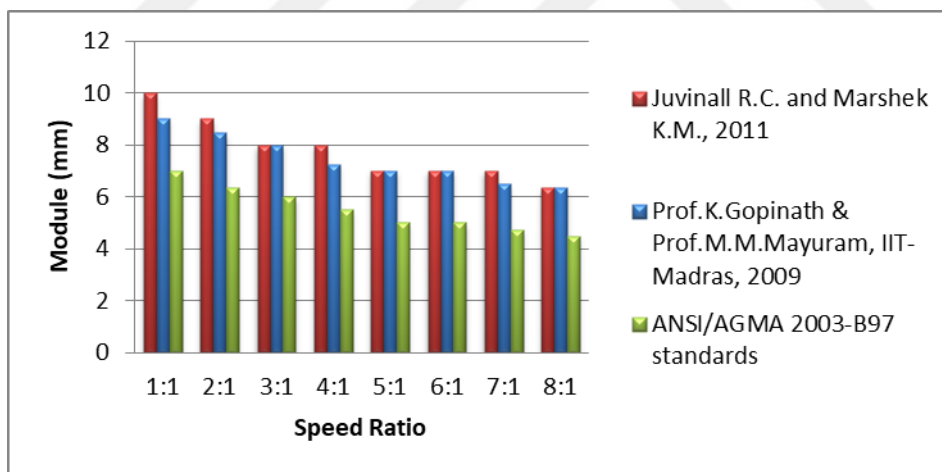
Figure F.18. The effect of speed ratio on module selection based on surface contact fatigue failure at 10 kW power transmission (for Ø=20°, Material type 2)
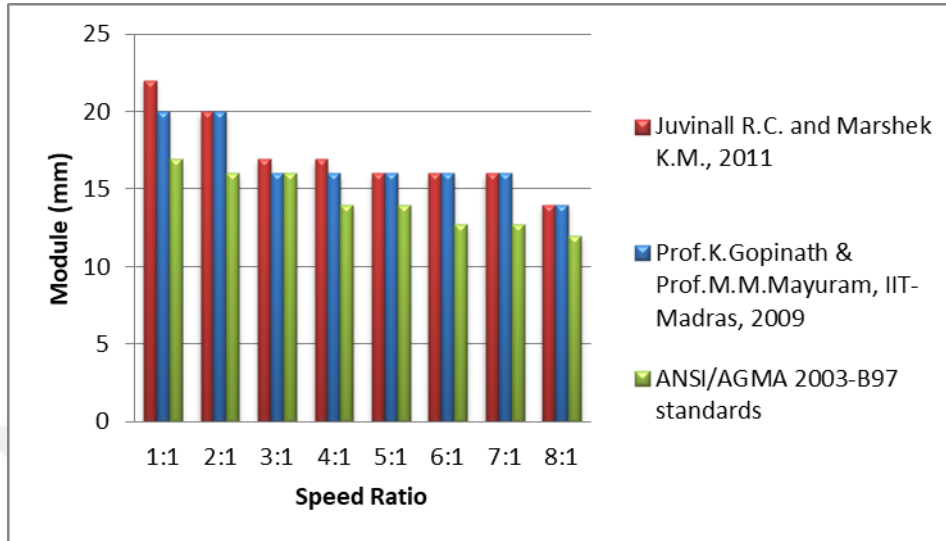
Figure F.19. The effect of speed ratio on module selection based on surface contact fatigue failure at 100 kW power transmission (for Ø=20°, Material type 2)
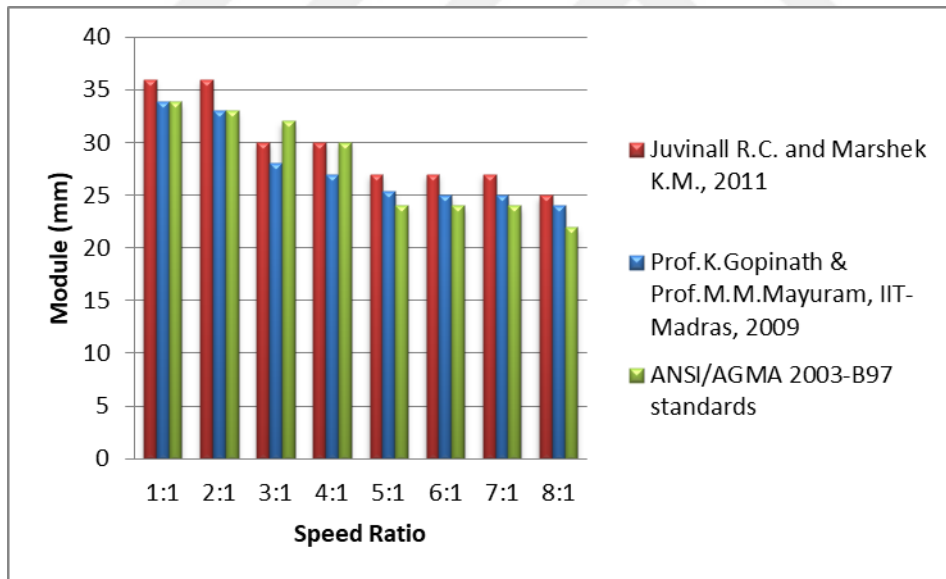
Figure F.20. The effect of speed ratio on module selection based on surface contact fatigue failure at 500 kW power transmission (for Ø=20°, Material type 2)

266
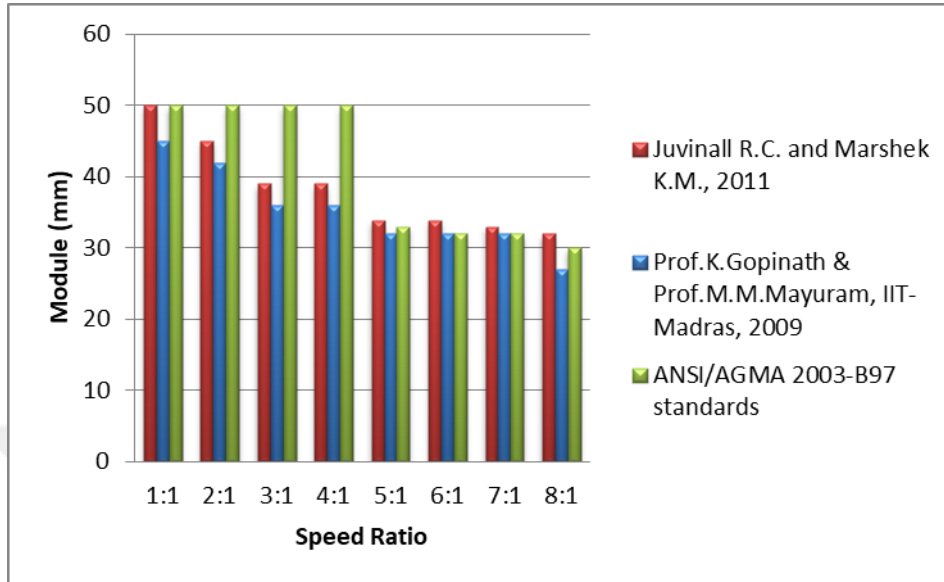
Figure F.21. The effect of speed ratio on module selection based on surface contact fatigue failure at 1000 kW power transmission (for Ø=20°, Material type 2)

F.3. Obtaining Geometric Rating Number (GRi) for Design Approaches for Ø=20°, Material type 2
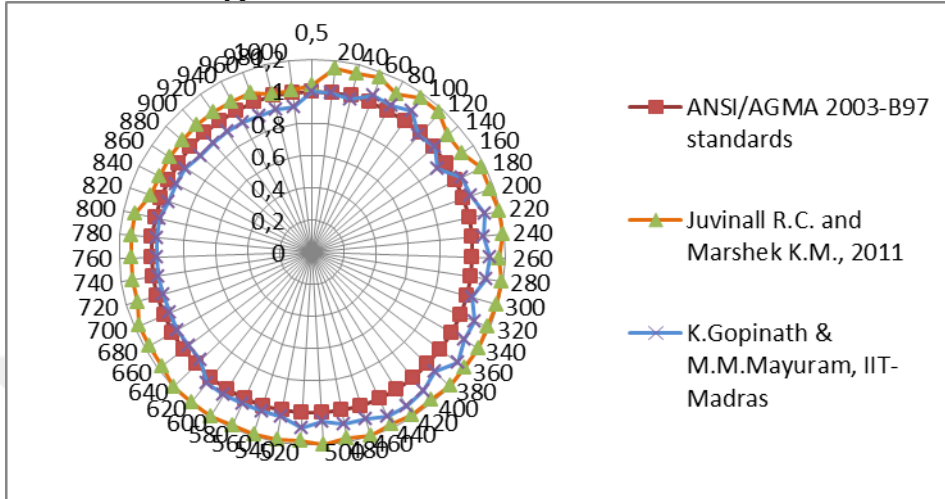
Figure F.22. Comparison of mxF/m₀xF₀ ratios for the design approaches at 1:1 speed ratio (for Ø=20°, Material type 2)
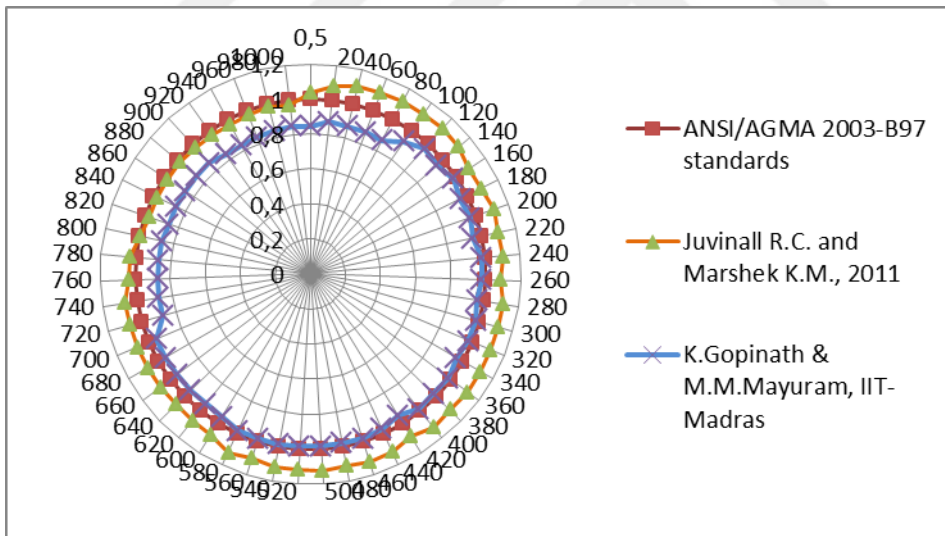
Figure F.23. Comparison of mxF/m₀xF₀ ratios for the design approaches at 2:1 speed ratio (for Ø=20°, Material type 2)
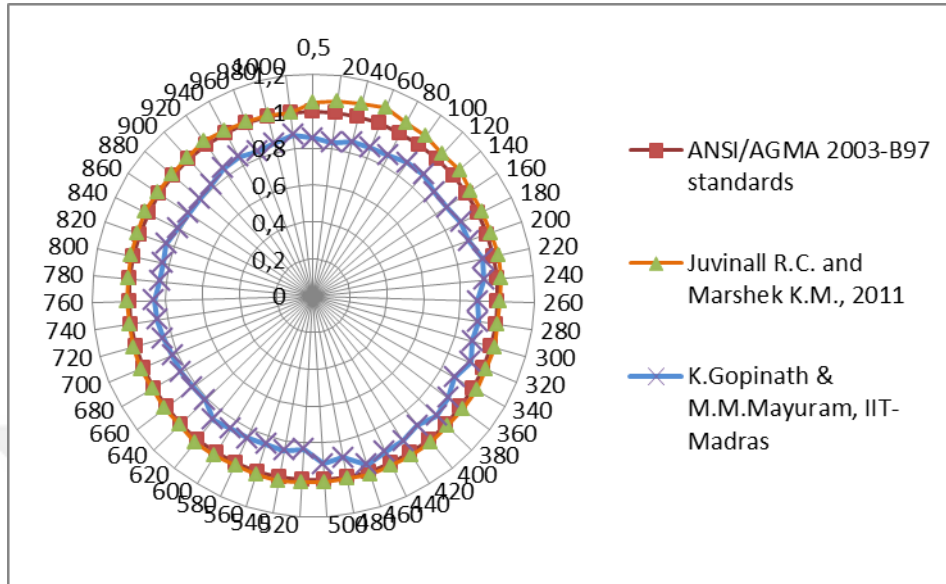
Figure F.24. Comparison of mxF/m_0xF_0 ratios for the design approaches at 3:1 speed ratio (for $\varnothing=20^o$, Material type 2)
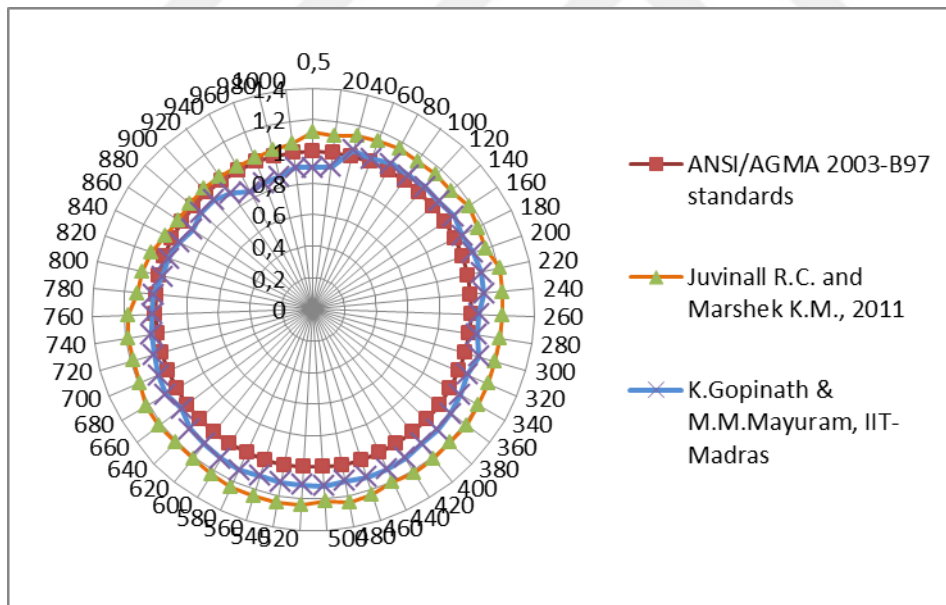
Figure F.25. Comparison of mxF/m_0xF_0 ratios for the design approaches at 4:1 speed ratio (for $\varnothing=20^o$, Material type 2)
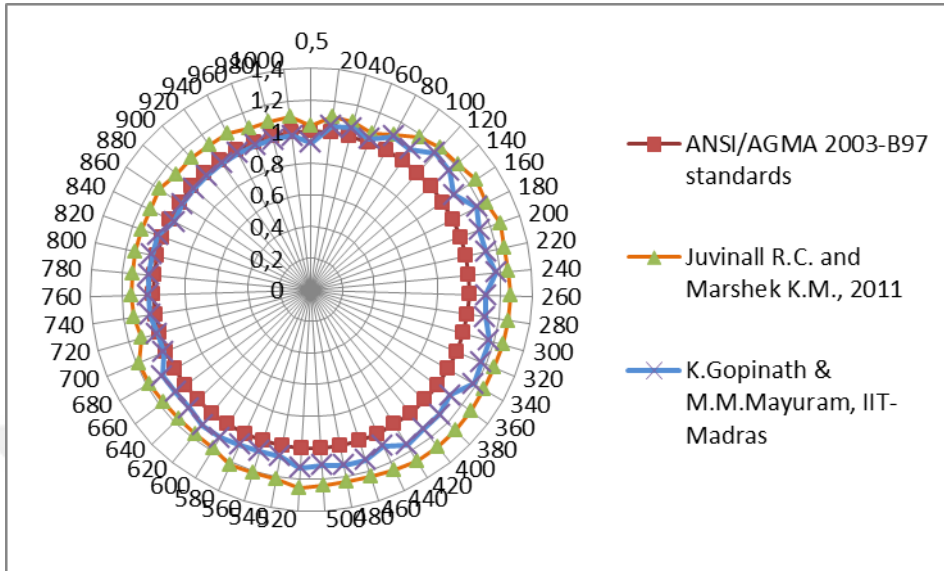
Figure F.26. Comparison of mxF/m$_0$xF$_0$ ratios for the design approaches at 5:1 speed ratio (for Ø=20°, Material type 2)
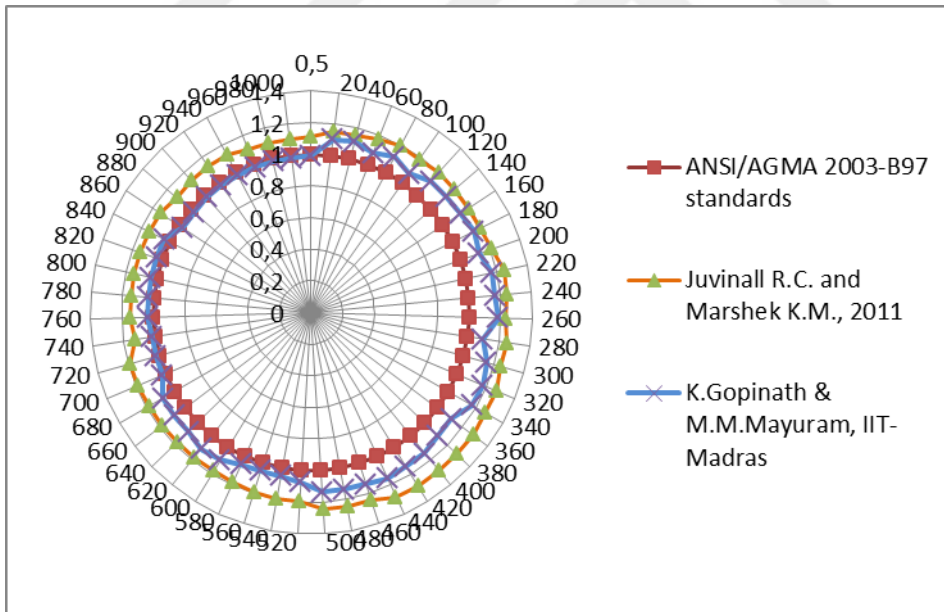
Figure F.27. Comparison of mxF/m$_0$xF$_0$ ratios for the design approaches at 6:1 speed ratio (for Ø=20°, Material type 2)

270
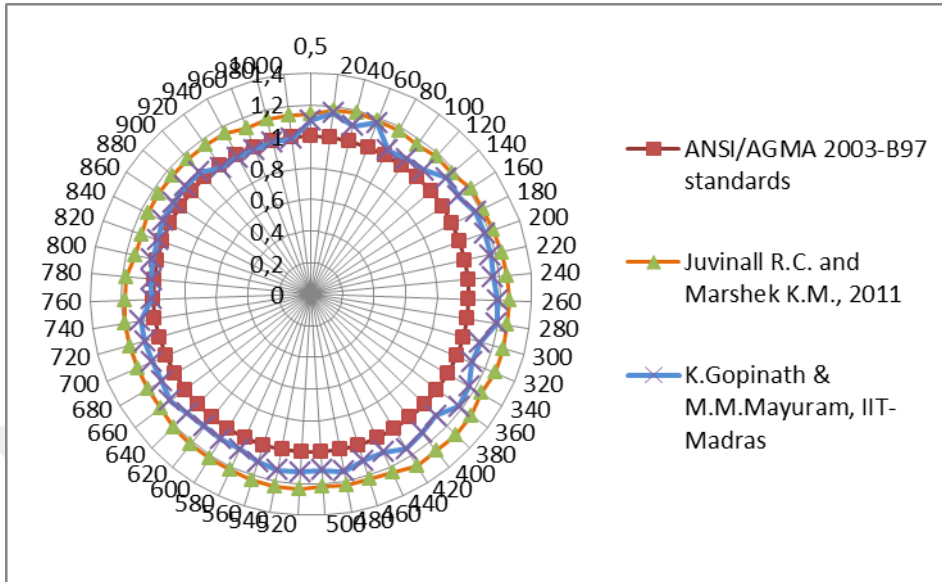
Figure F.28. Comparison of mxF/m$_0$xF$_0$ ratios for the design approaches at 7:1 speed ratio (for Ø=20°, Material type 2)
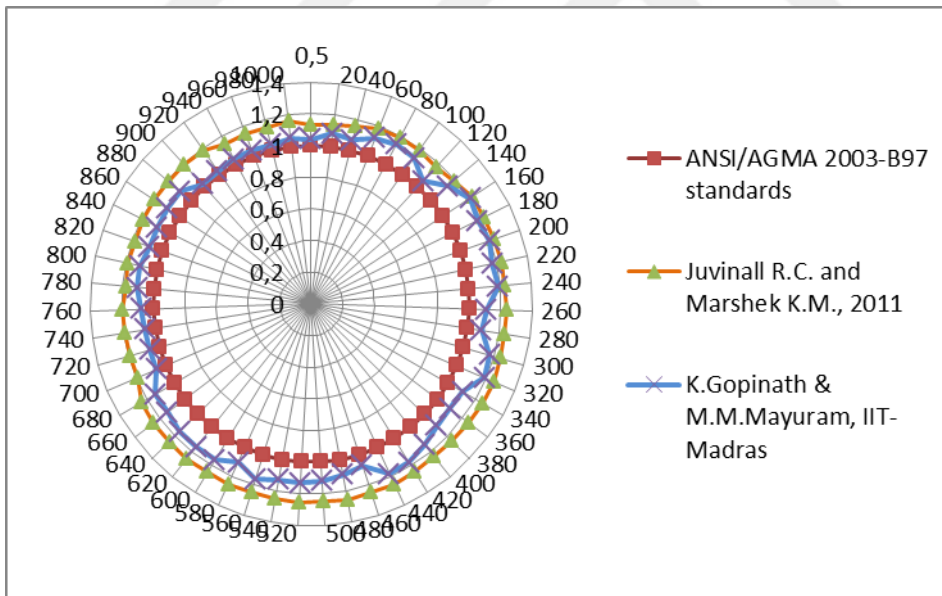
Figure F.29. Comparison of mxF/m$_0$xF$_0$ ratios for the design approaches at 8:1 speed ratio (for Ø=20°, Material type 2)

APPENDIX G

G.1. Comparison of Module Selection and Face Width Results of the Design Approaches for Ø=20°, Material type 3
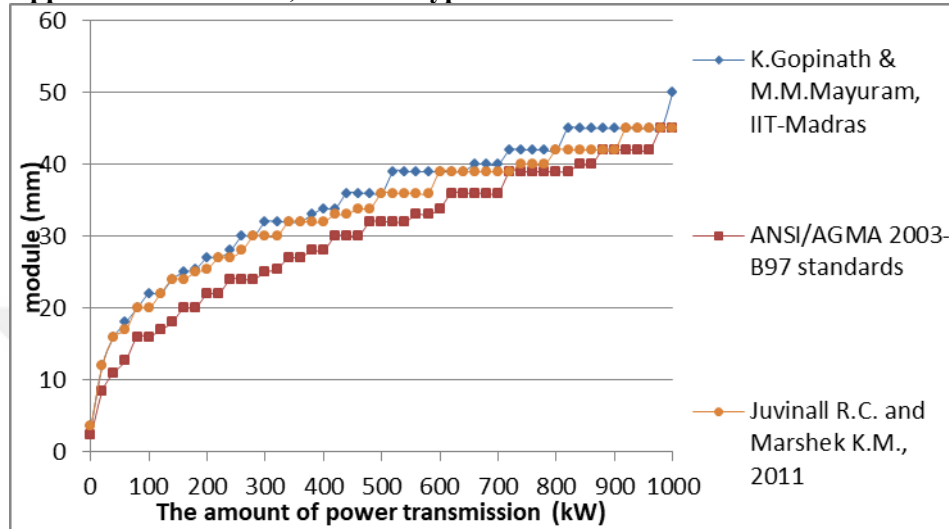
Figure G.1. Module variation considering surface contact fatigue failure under increasing power at 1:1 speed ratio (for Ø=20°, Material type 3)
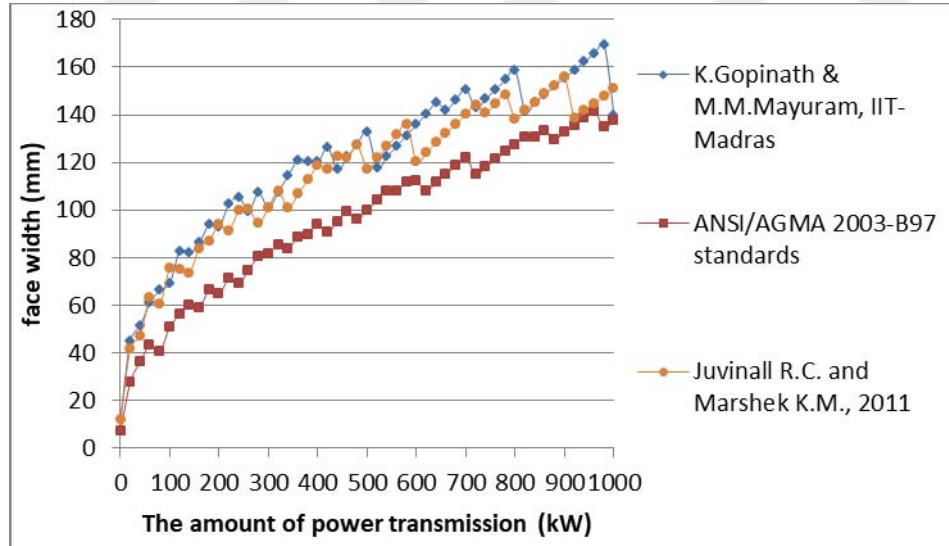

Figure G.2. Face width variation considering surface contact fatigue failure under increasing power at 1:1 speed ratio (for Ø=20°, Material type 3)

272
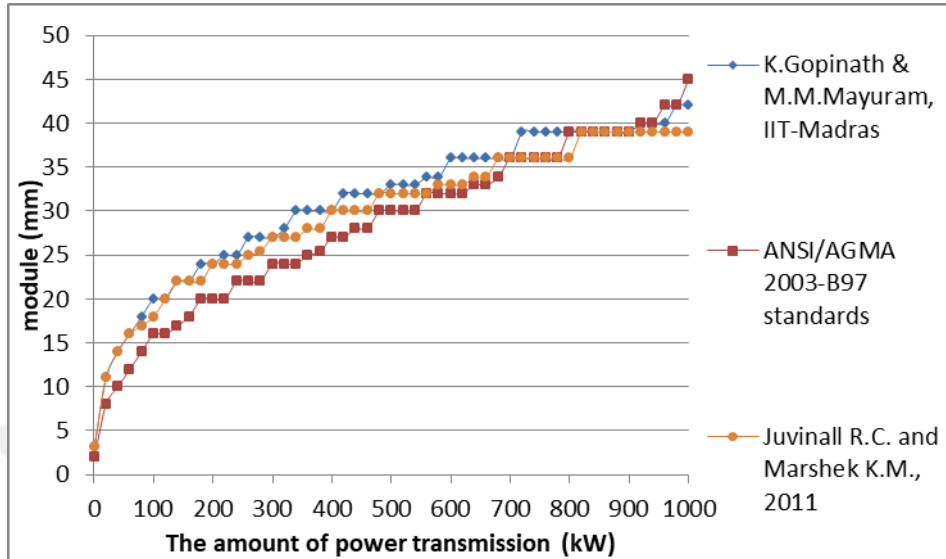
Figure G.3. Module variation considering surface contact fatigue failure under increasing power at 2:1 speed ratio (for Ø=20°, Material type 3)
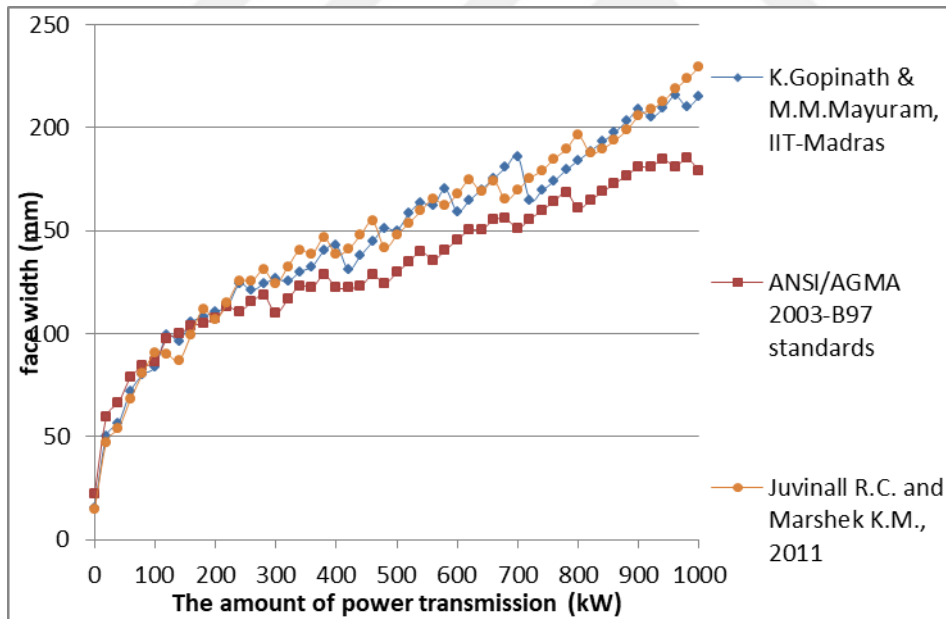
Figure G.4. Face width variation considering surface contact fatigue failure under increasing power at 2:1 speed ratio (for Ø=20°, Material type 3)
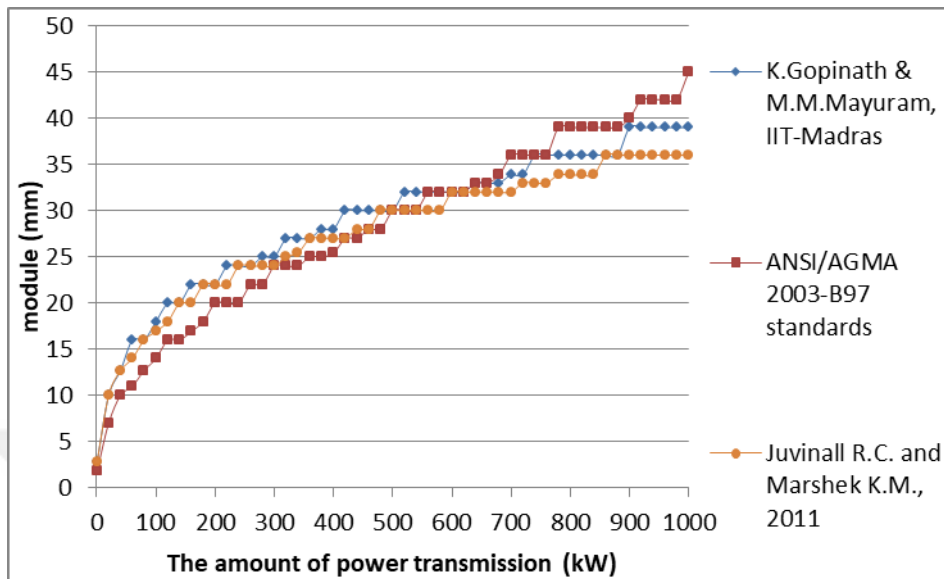
Figure G.5. Module variation considering surface contact fatigue failure under increasing power at 3:1 speed ratio (for Ø=20°, Material type 3)
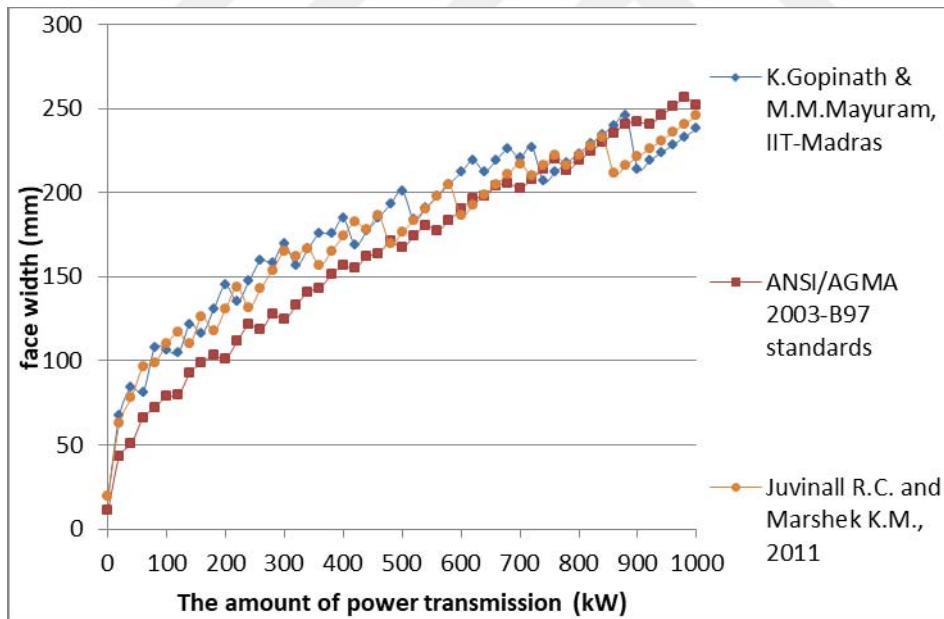
Figure G.6. Face width variation considering surface contact fatigue failure under increasing power at 3:1 speed ratio (for Ø=20°, Material type 3)
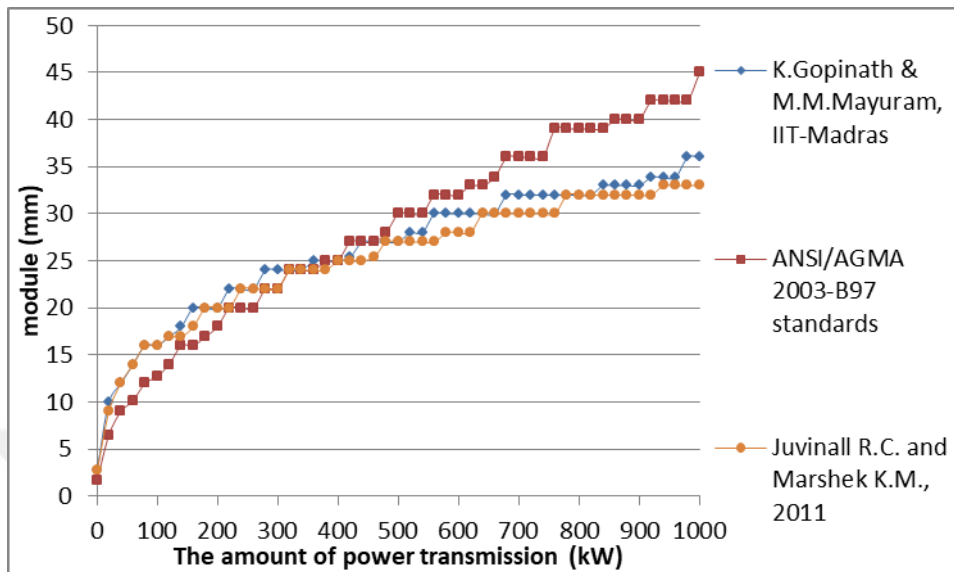
Figure G.7. Module variation considering surface contact fatigue failure under increasing power at 4:1 speed ratio (for Ø=20°, Material type 3)
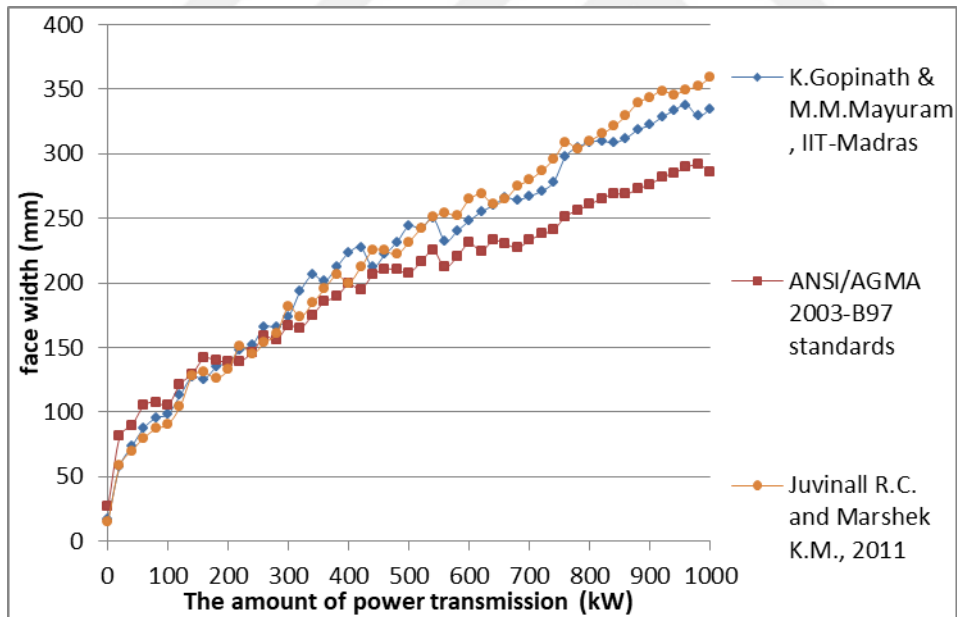
Figure G.8. Face width variation considering surface contact fatigue failure under increasing power at 4:1 speed ratio (for Ø=20°, Material type 3)

275
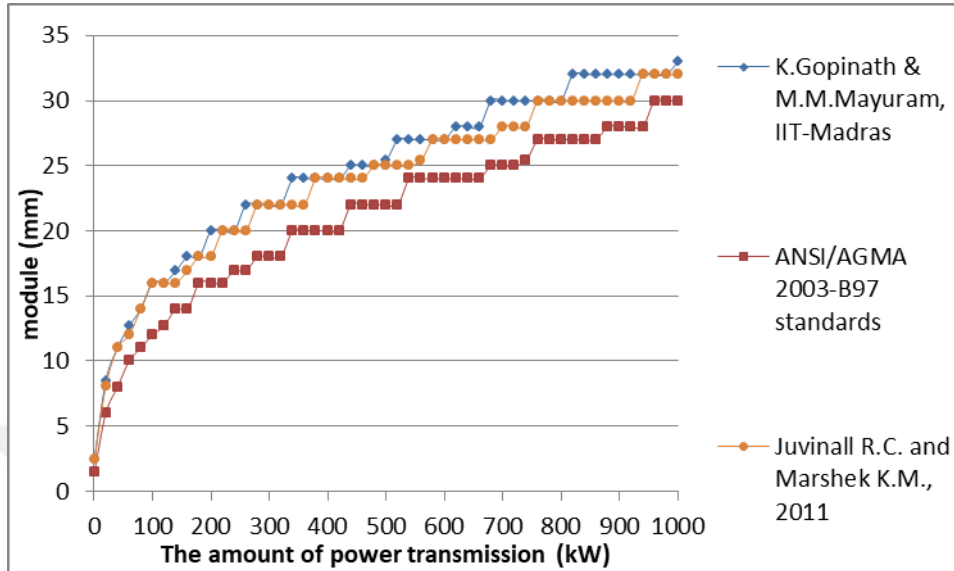
Figure G.9. Module variation considering surface contact fatigue failure under increasing power at 5:1 speed ratio (for Ø=20°, Material type 3)
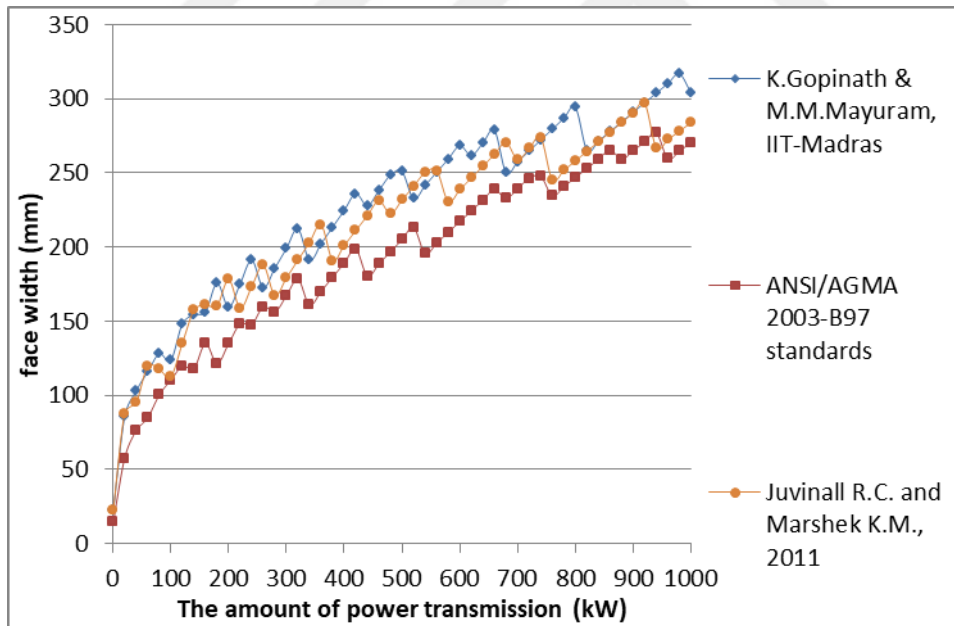
Figure G.10. Face width variation considering surface contact fatigue failure under increasing power at 5:1 speed ratio (for Ø=20°, Material type 3)
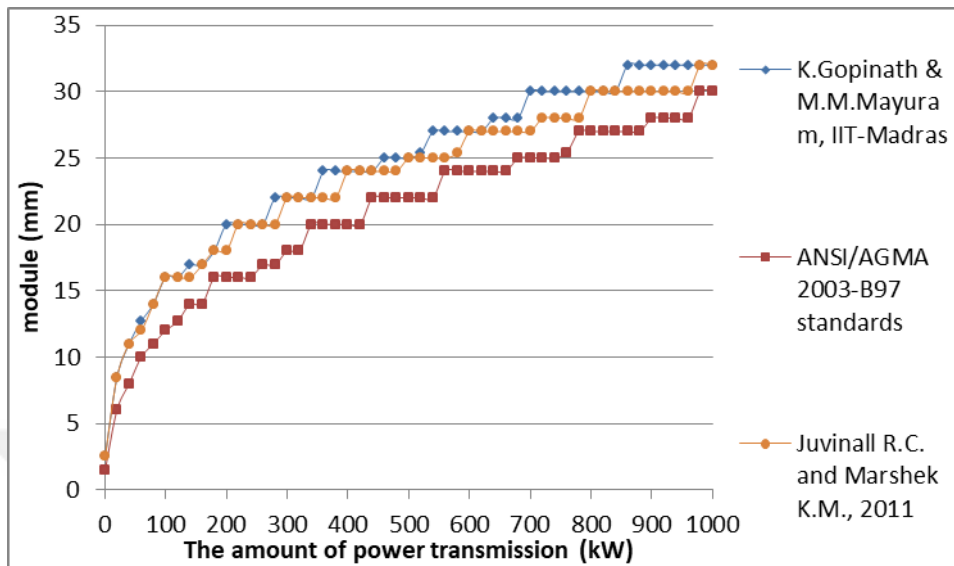
Figure G.11. Module variation considering surface contact fatigue failure under increasing power at 6:1 speed ratio (for Ø=20°, Material type 3)
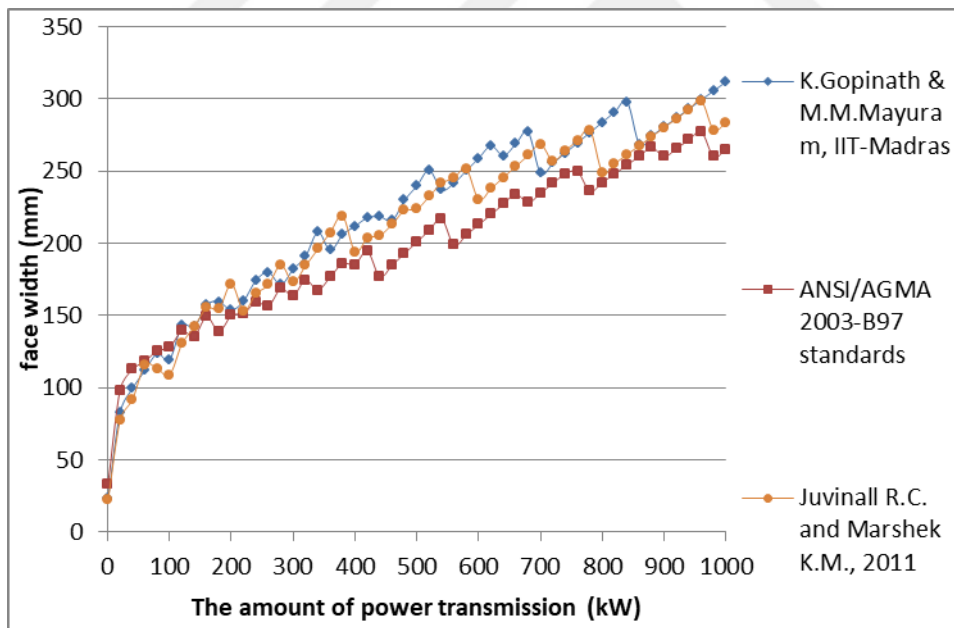
Figure G.12. Face width variation considering surface contact fatigue failure under increasing power at 6:1 speed ratio (for Ø=20°, Material type 3)
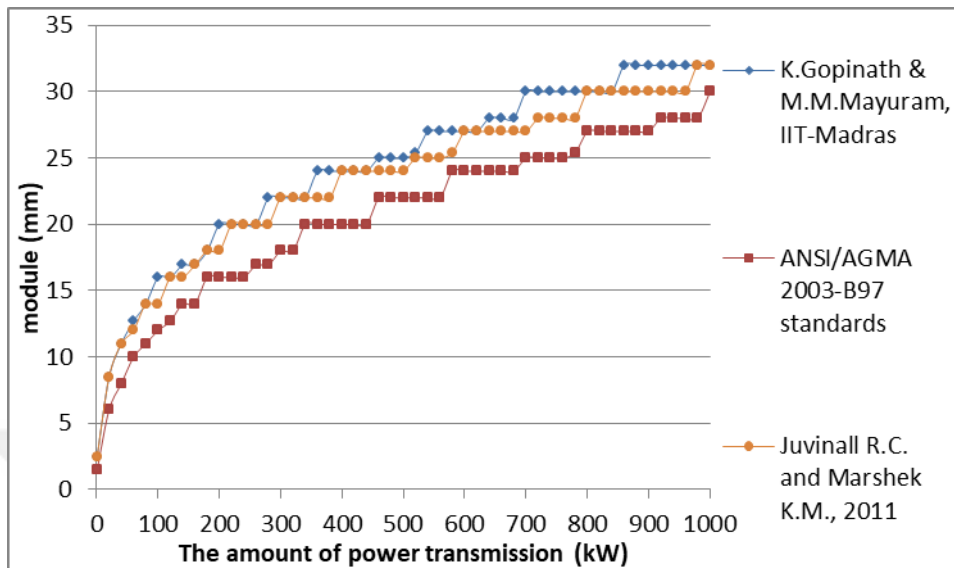
Figure G.13. Module variation considering surface contact g fatigue failure under increasing power at 7:1 speed ratio (for Ø=20°, Material type 3)
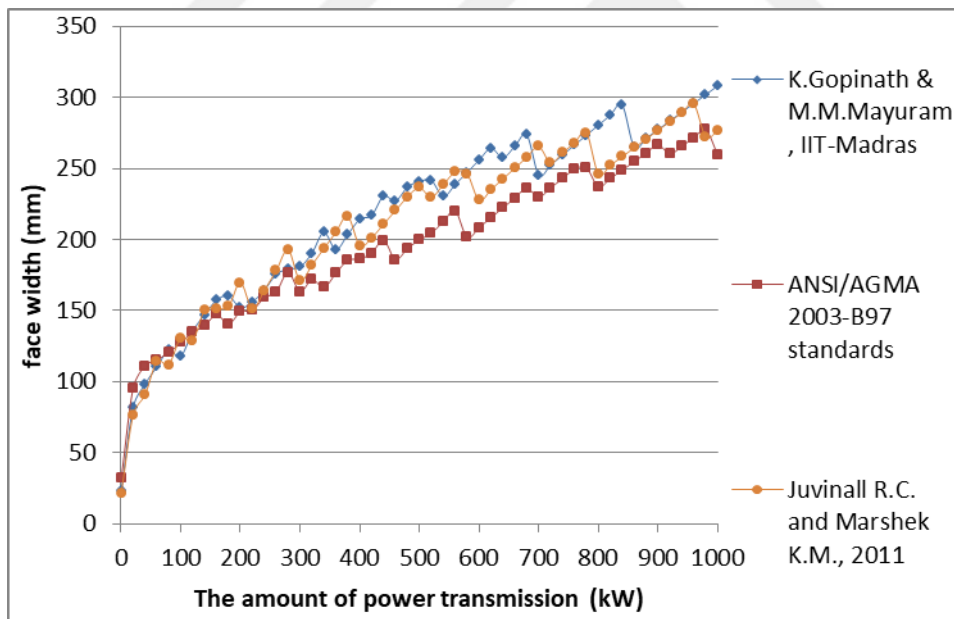
Figure G.14. Face width variation considering surface contact fatigue failure under increasing power at 7:1 speed ratio (for Ø=20°, Material type 3)
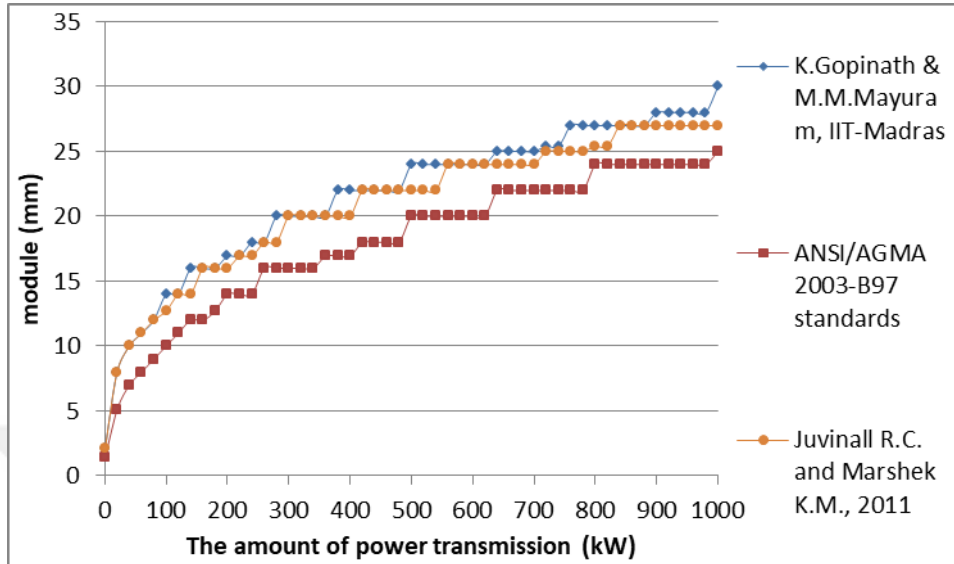
Figure G.15. Module variation considering surface contact fatigue failure under increasing power at 8:1 speed ratio (for Ø=20°, Material type 3)
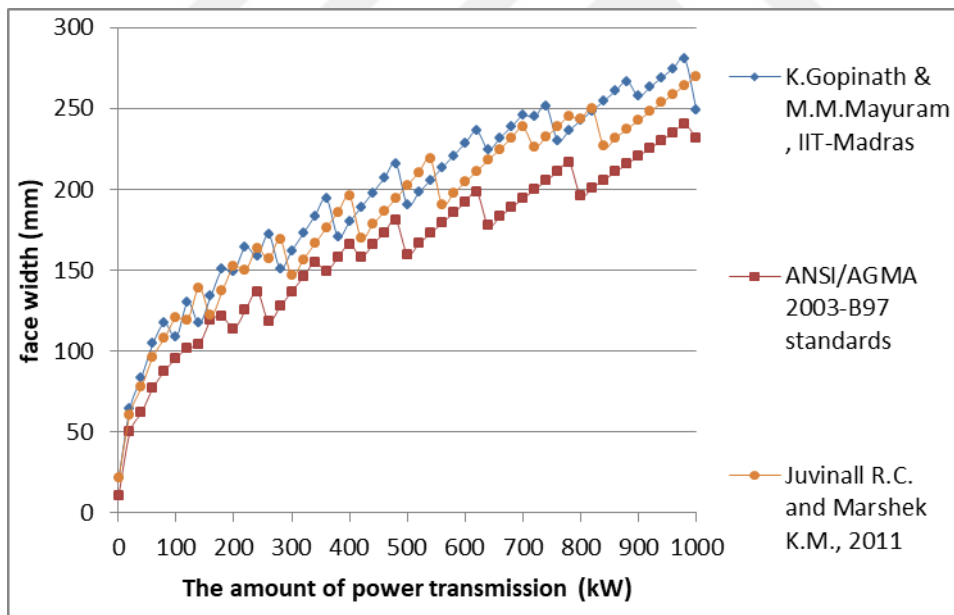
Figure G.16. Face width variation considering surface contact fatigue failure under increasing power at 8:1 speed ratio (for Ø=20°, Material type 3)

279

G.2. Comparison of the Results Based on Surface Contact Fatigue Failure Considering Speed Ratio for the Selected Power Transmissions for Ø=20°, Material type 3
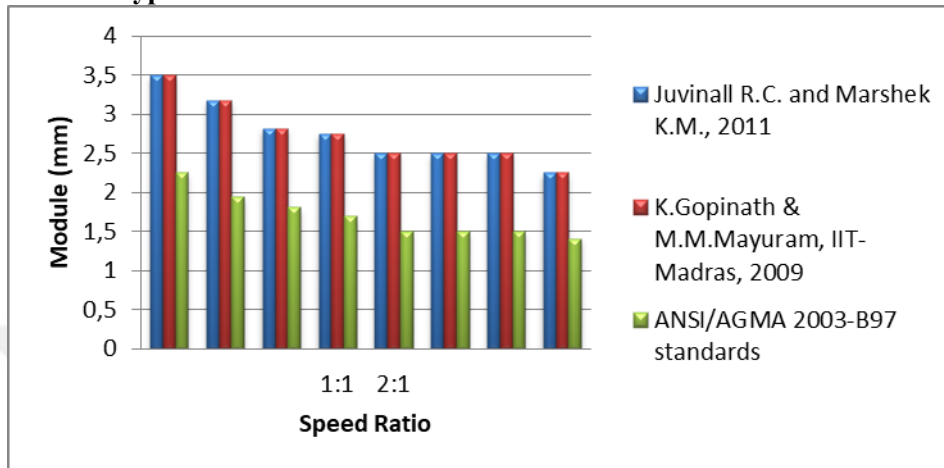
Figure G.17. The effect of speed ratio on module selection based on bending fatigue failure at 0,5 kW power transmission (for Ø=20°, Material type 3)
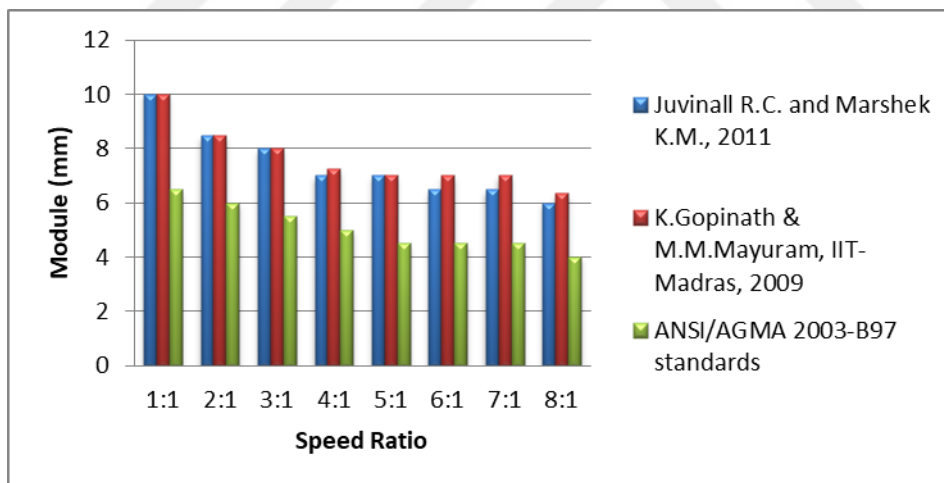
Figure G.18. The effect of speed ratio on module selection based on bending fatigue failure at 10 kW power transmission (for Ø=20°, Material type 3)
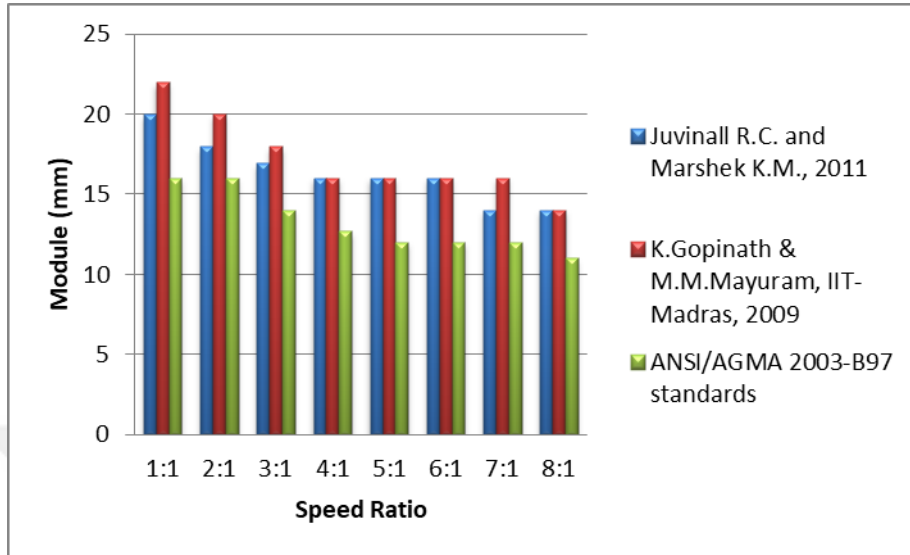
Figure G.19. The effect of speed ratio on module selection based on bending
fatigue failure at 100 kW power transmission (for Ø=20°, Material
type 3)
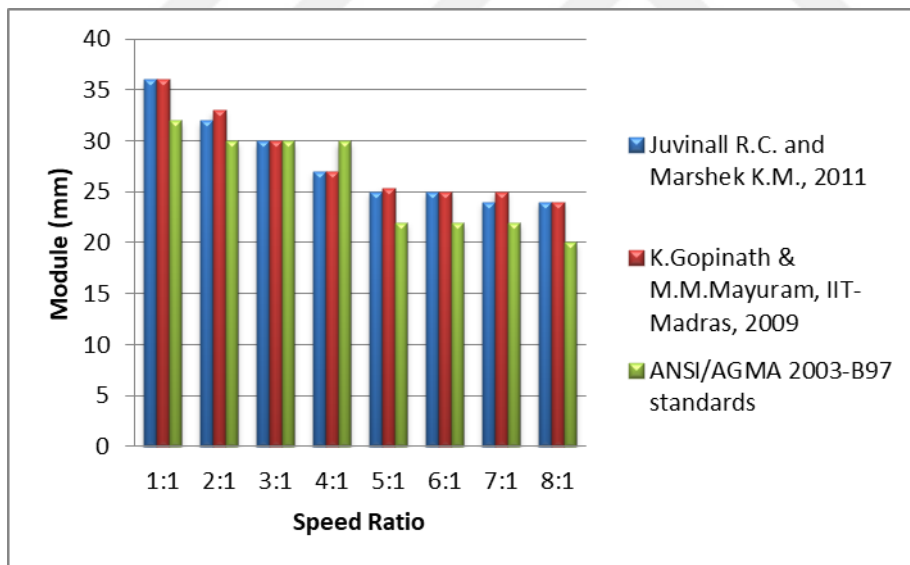
Figure G.20. The effect of speed ratio on module selection based on bending
fatigue failure at 500 kW power transmission (for Ø=20°, Material
type 3)
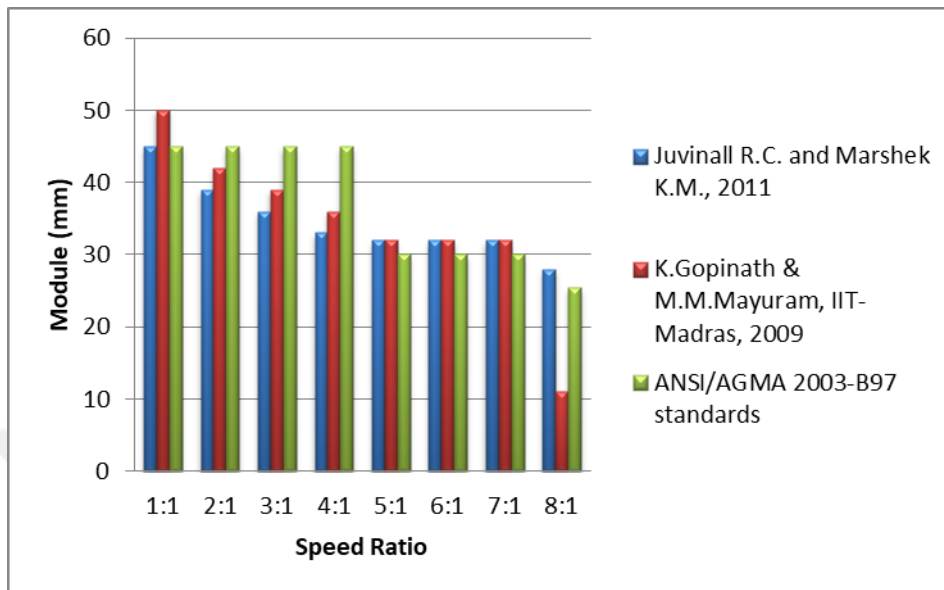
Figure G.21. The effect of speed ratio on module selection based on bending fatigue failure at 1000 kW power transmission (for Ø=20°, Material type 3)

**G.3. Obtaining Geometric Rating Number (GRᵢ) for Design Approaches for Ø=20°, Material type 3**
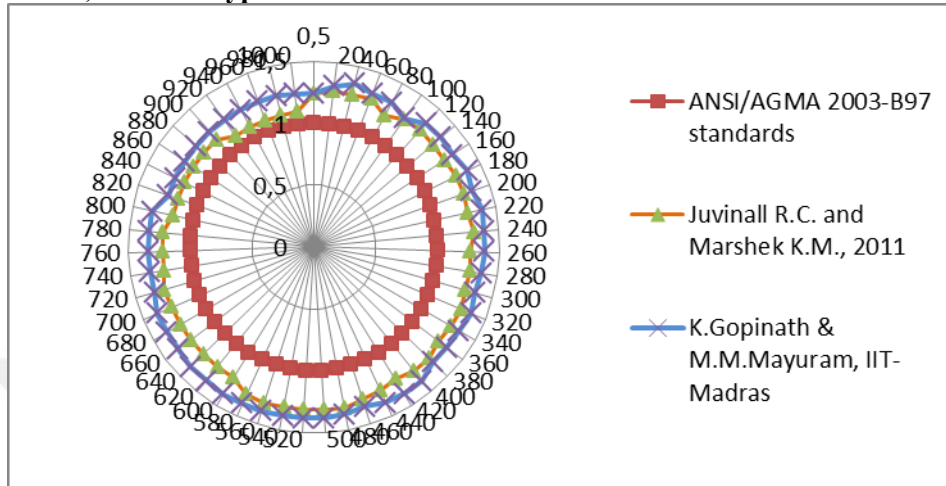
Figure G.22. Comparison of mxF/m_0xF_0 ratios for the design approaches at 1:1 speed ratio (for Ø=20°, Material type 3)
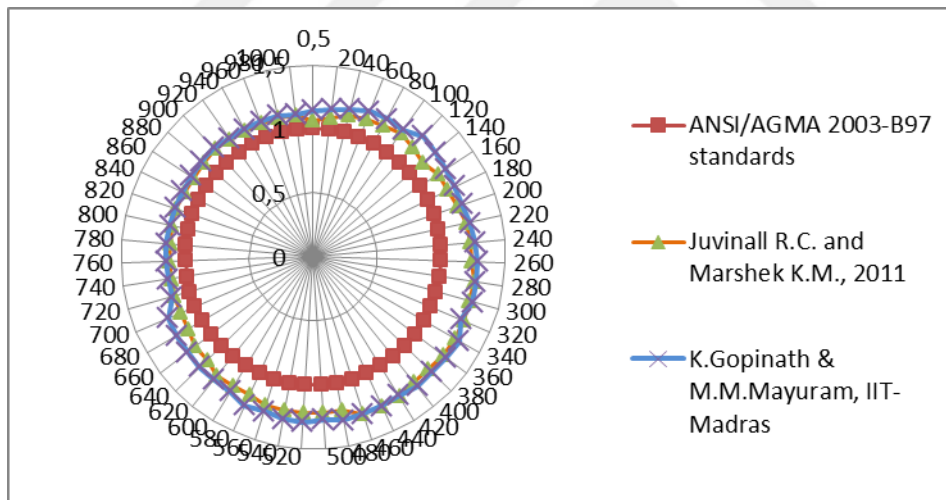
Figure G.23. Comparison of mxF/m_0xF_0 ratios for the design approaches at 2:1 speed ratio (for Ø=20°, Material type 3)
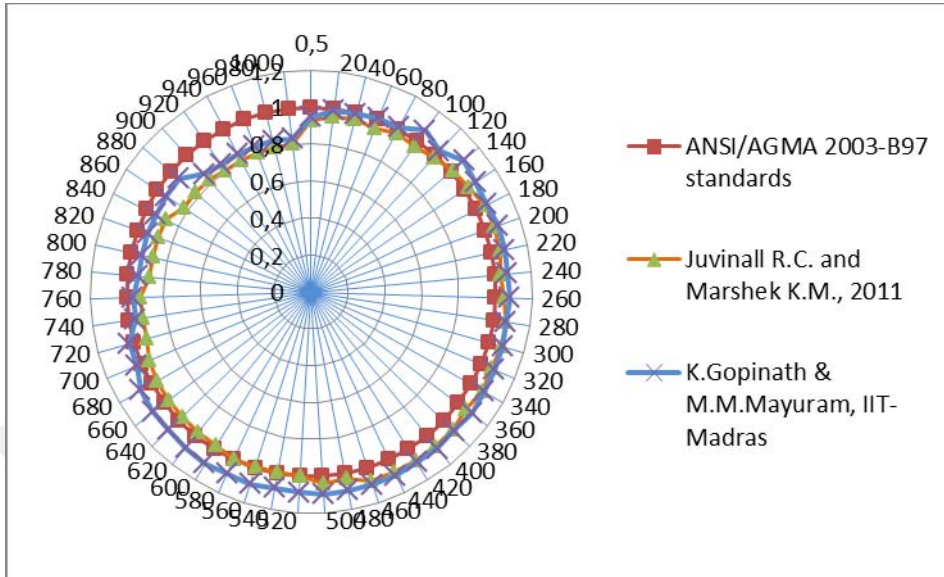
Figure G.24. Comparison of mxF/m$_0$xF$_0$ ratios for the design approaches at 3:1 speed ratio (for Ø=20°, Material type 3)
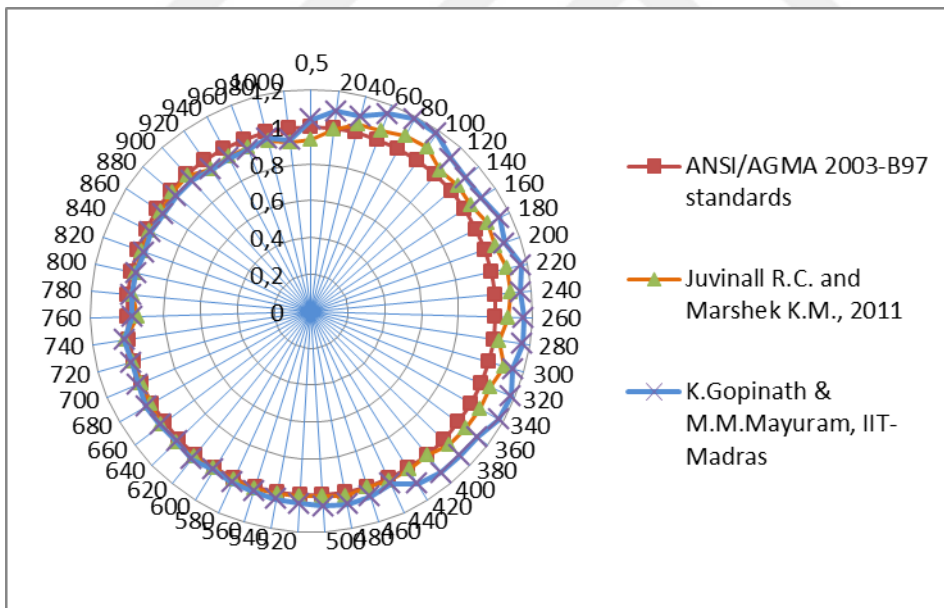
Figure G.25. Comparison of mxF/m$_0$xF$_0$ ratios for the design approaches at 4:1 speed ratio (for Ø=20°, Material type 3)
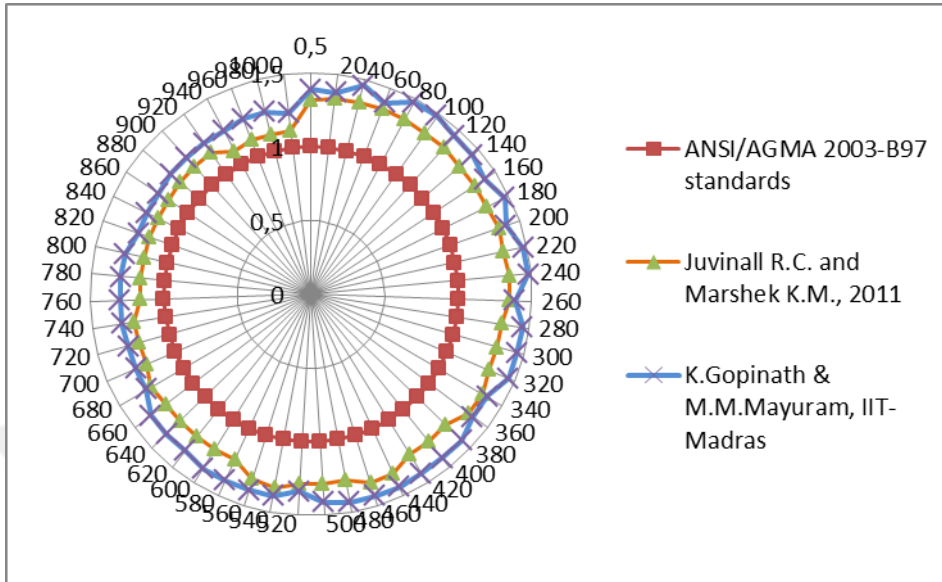
Figure G.26. Comparison of mxF/m_0xF_0 ratios for the design approaches at 5:1 speed ratio (for $\varnothing=20^o$, Material type 3)
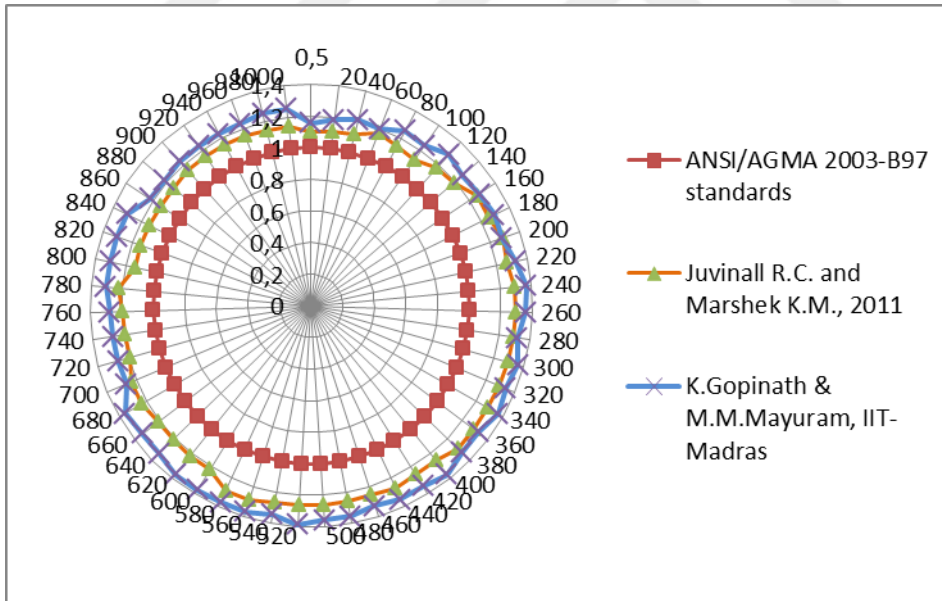
Figure G.27. Comparison of mxF/m_0xF_0 ratios for the design approaches at 6:1 speed ratio (for $\varnothing=20^o$, Material type 3)
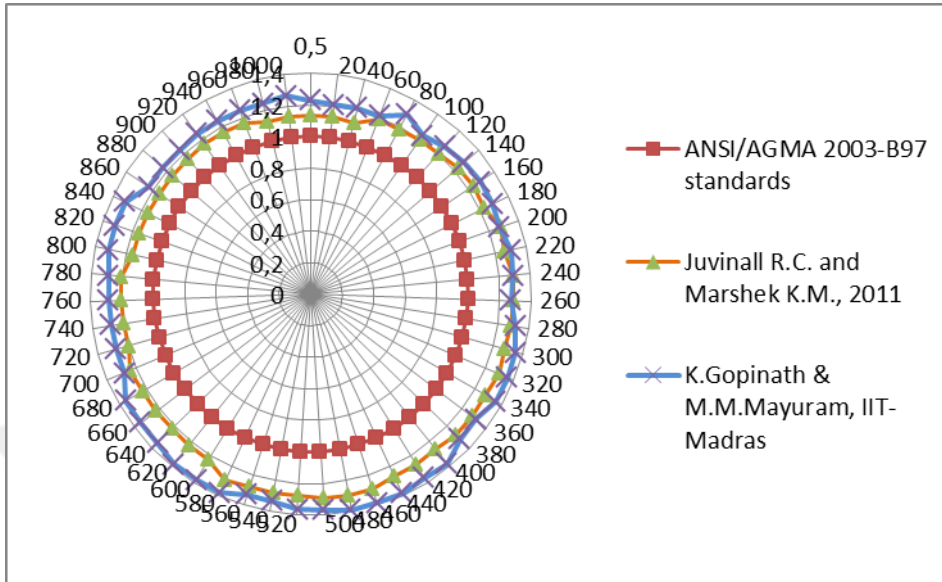
Figure G.28. Comparison of mxF/m_0xF_0 ratios for the design approaches at 7:1 speed ratio (for $\emptyset=20^o$, Material type 3)
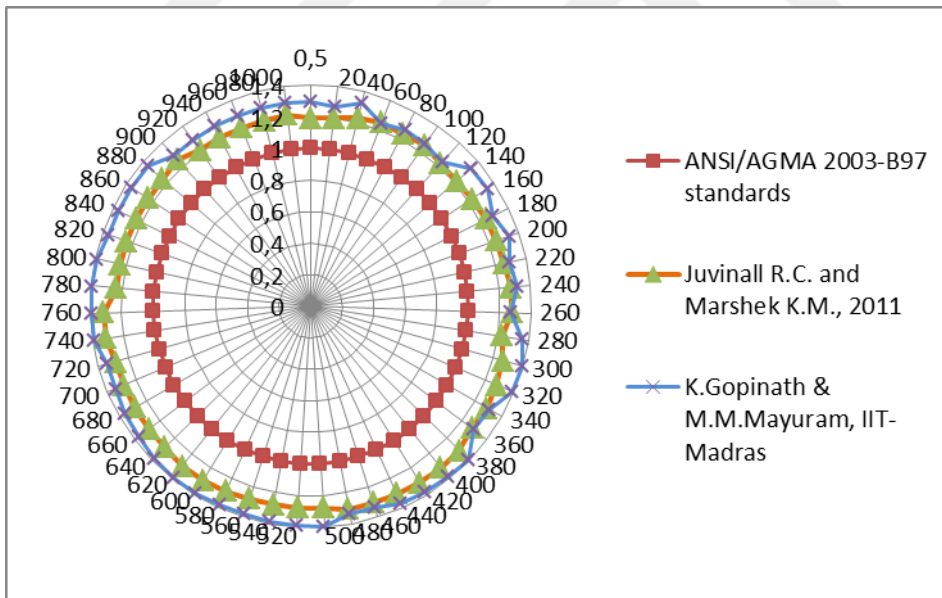
Figure G.29. Comparison of mxF/m_0xF_0 ratios for the design approaches at 8:1 speed ratio (for $\emptyset=20^o$, Material type 3)

APPENDIX H

H.1. Comparison of Module Selection and Face Width Results of the Design Approaches for Ø=25°, Material type 1
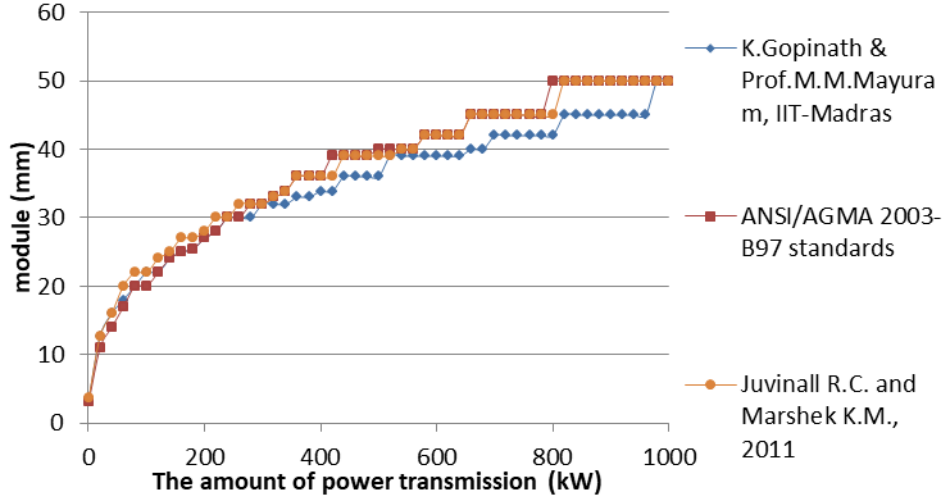
Figure H.1. Module variation considering surface contact fatigue failure under increasing power at 1:1 speed ratio (for Ø=25°, Material type 1)
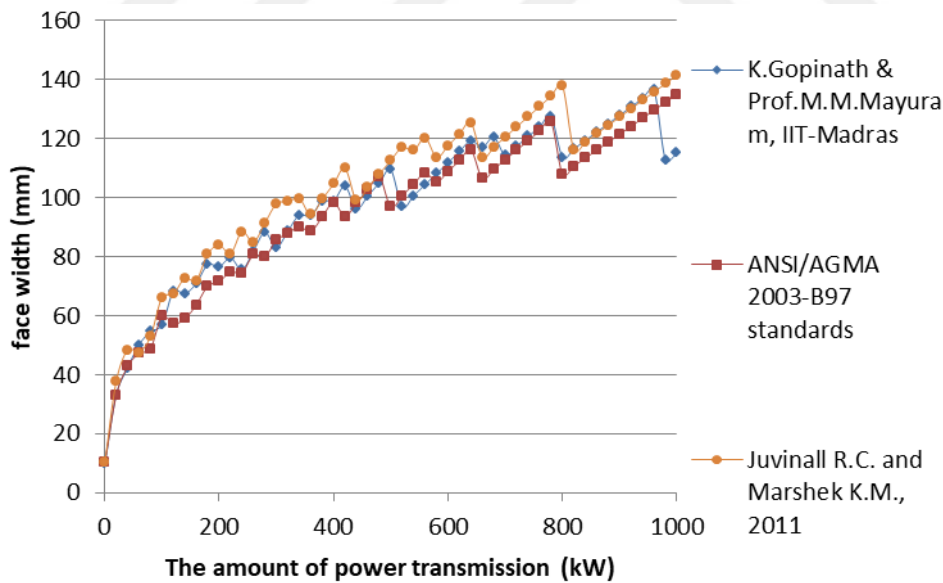

Figure H.2. Face width variation considering surface contact fatigue failure under increasing power at 1:1 speed ratio (for Ø=25°, Material type 1)
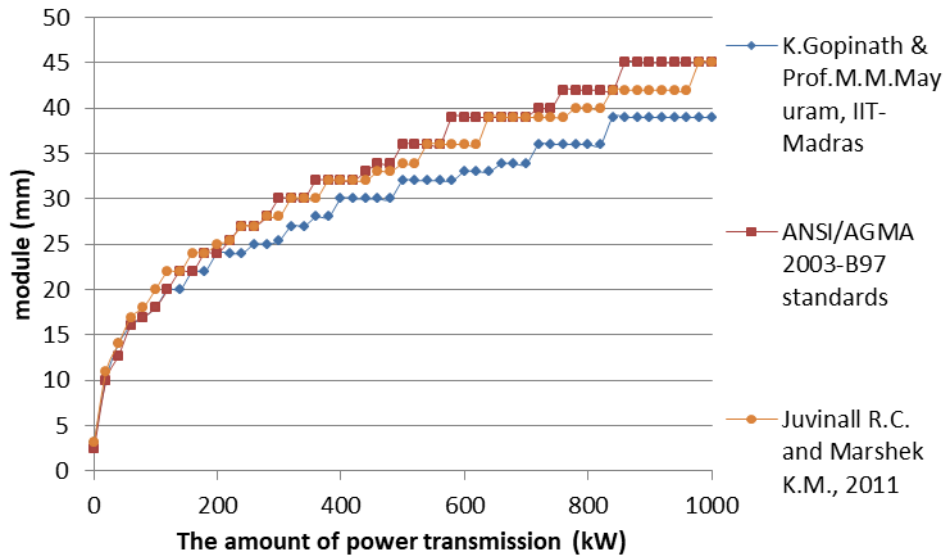
Figure H.3. Module variation considering surface contact fatigue failure under increasing power at 2:1 speed ratio (for Ø=25°, Material type 1)
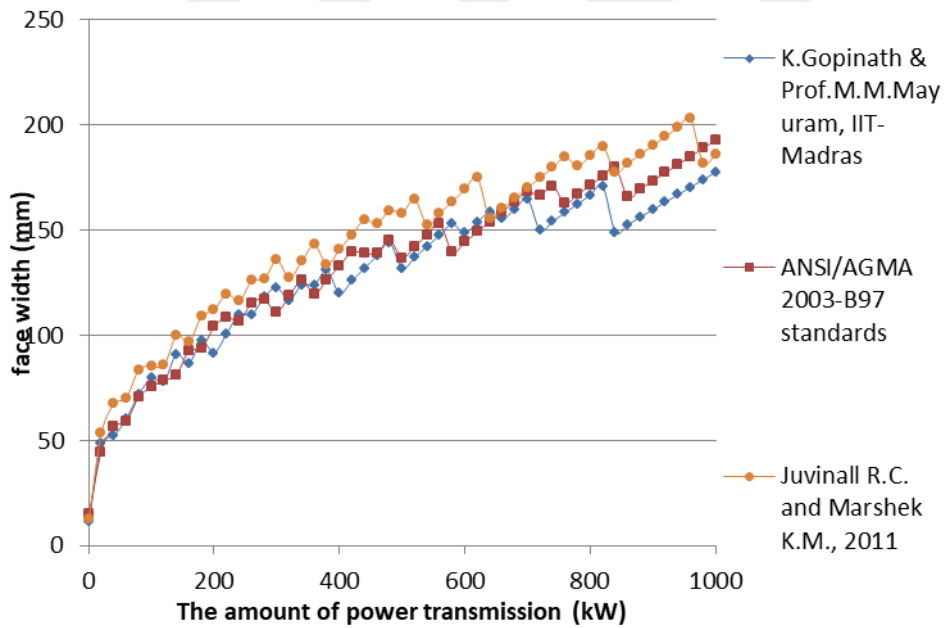
Figure H.4. Face width variation considering surface contact fatigue failure under increasing power at 2:1 speed ratio (for Ø=25°, Material type 1)

288
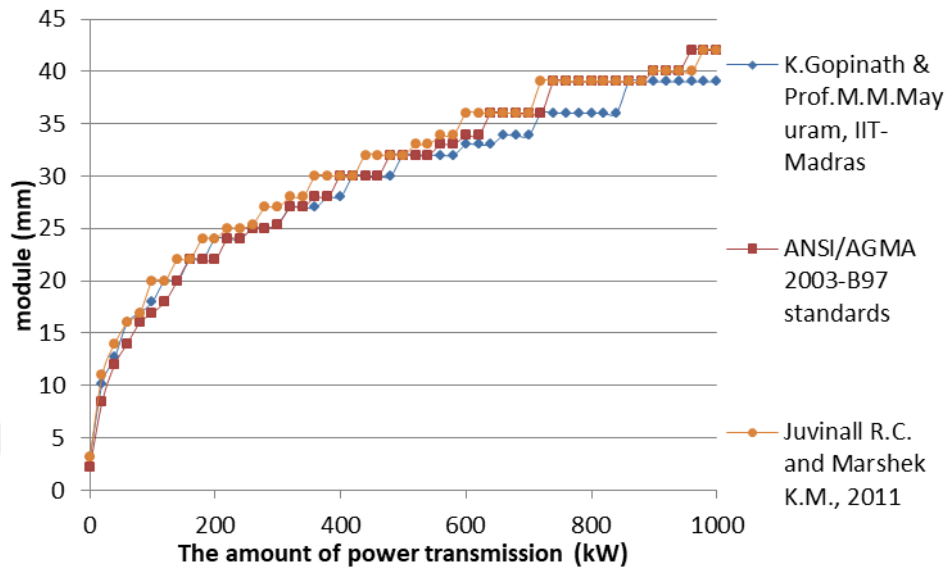
Figure H.5. Module variation considering surface contact fatigue failure under increasing power at 3:1 speed ratio (for Ø=25°, Material type 1)
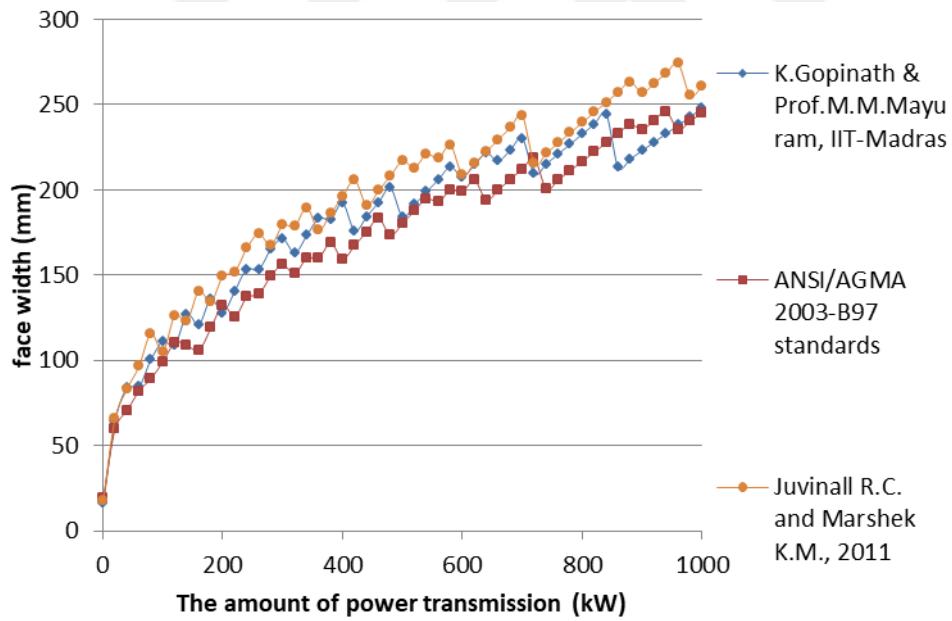

Figure H.6. Face width variation considering surface contact fatigue failure under increasing power at 3:1 speed ratio (for Ø=25°, Material type 1)
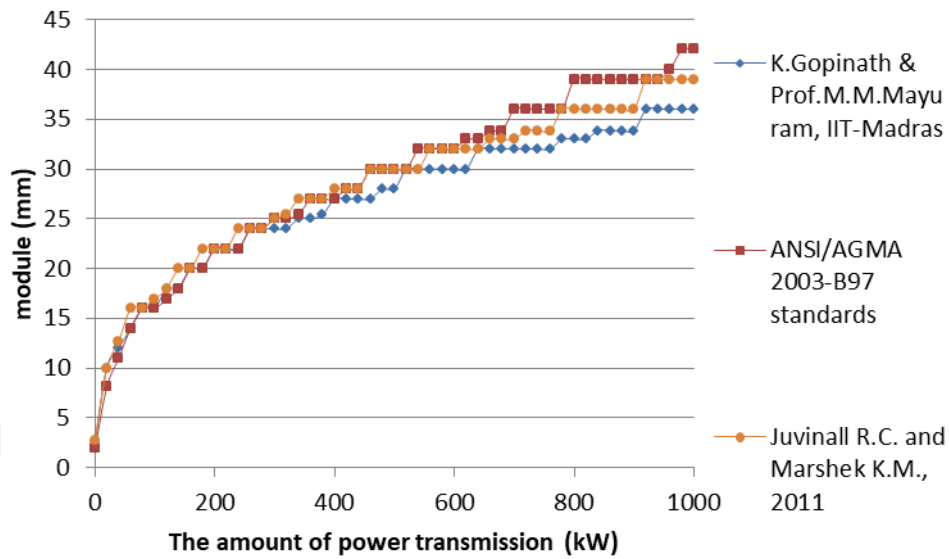
Figure H.7. Module variation considering surface contact fatigue failure under increasing power at 4:1 speed ratio (for Ø=25°, Material type 1)
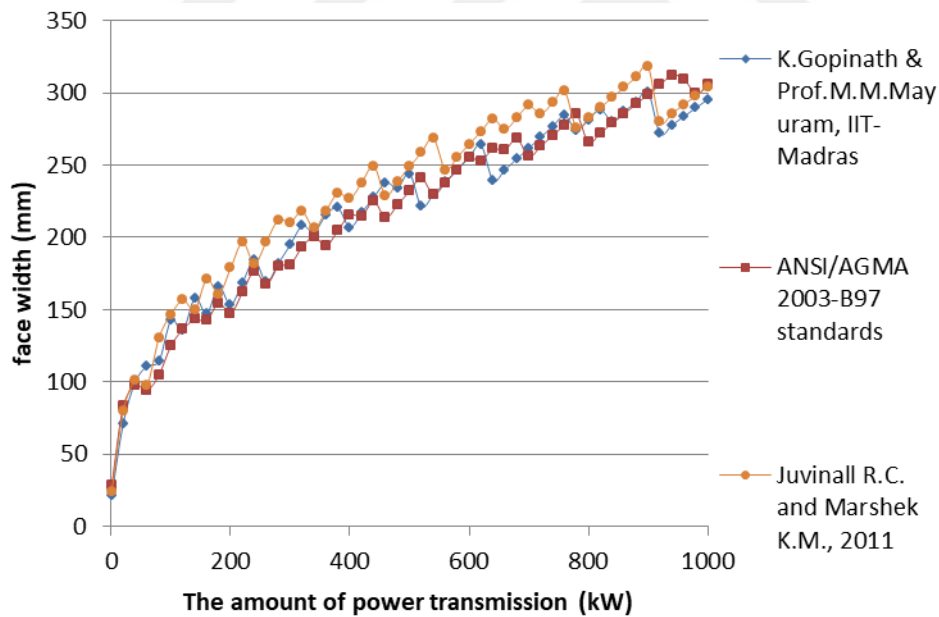
Figure H.8. Face width variation considering surface contact fatigue failure under increasing power at 4:1 speed ratio (for Ø=25°, Material type 1)
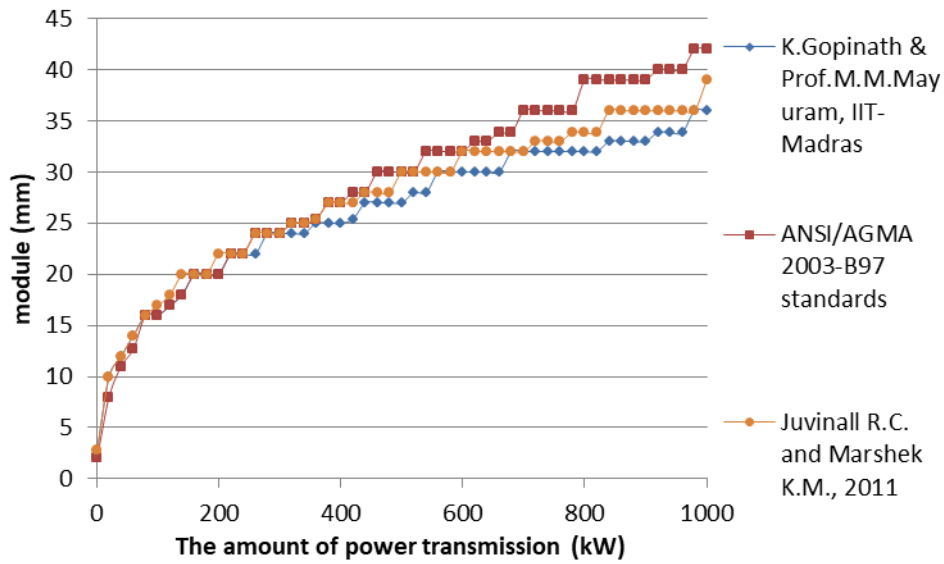
Figure H.9. Module variation considering surface contact fatigue failure under increasing power at 5:1 speed ratio (for Ø=25°, Material type 1)
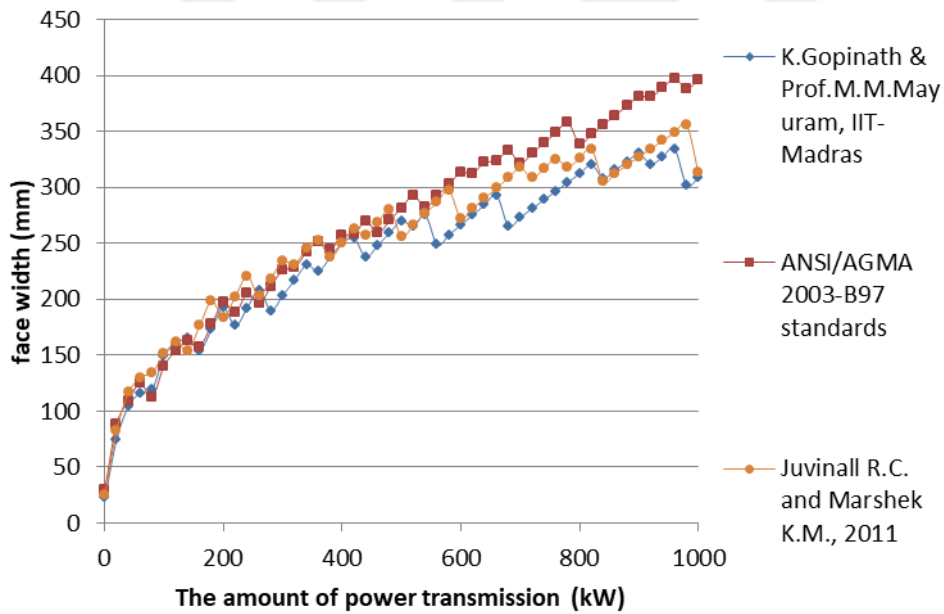

Figure H.10. Face width variation considering surface contact fatigue failure under increasing power at 5:1 speed ratio (for Ø=25°, Material type 1)
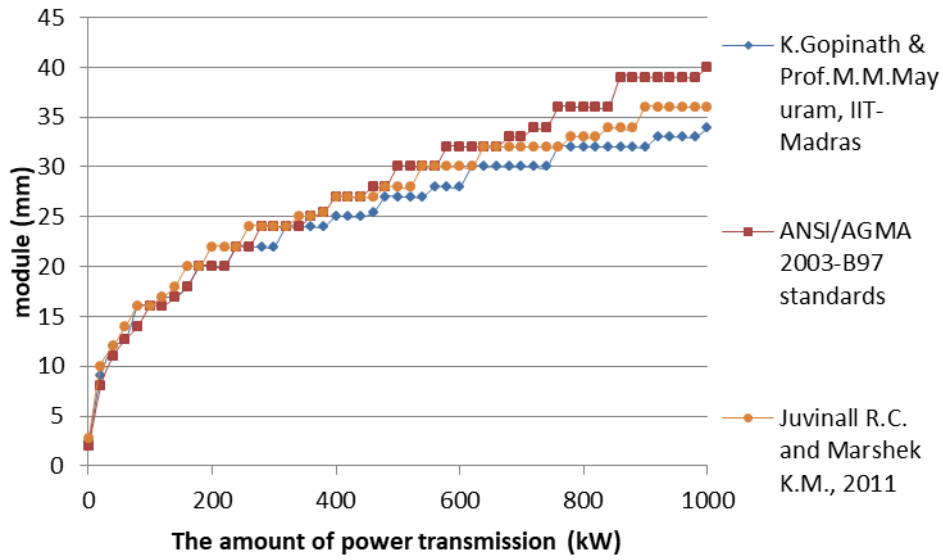
Figure H.11. Module variation considering surface contact fatigue failure under increasing power at 6:1 speed ratio (for Ø=25°, Material type 1)
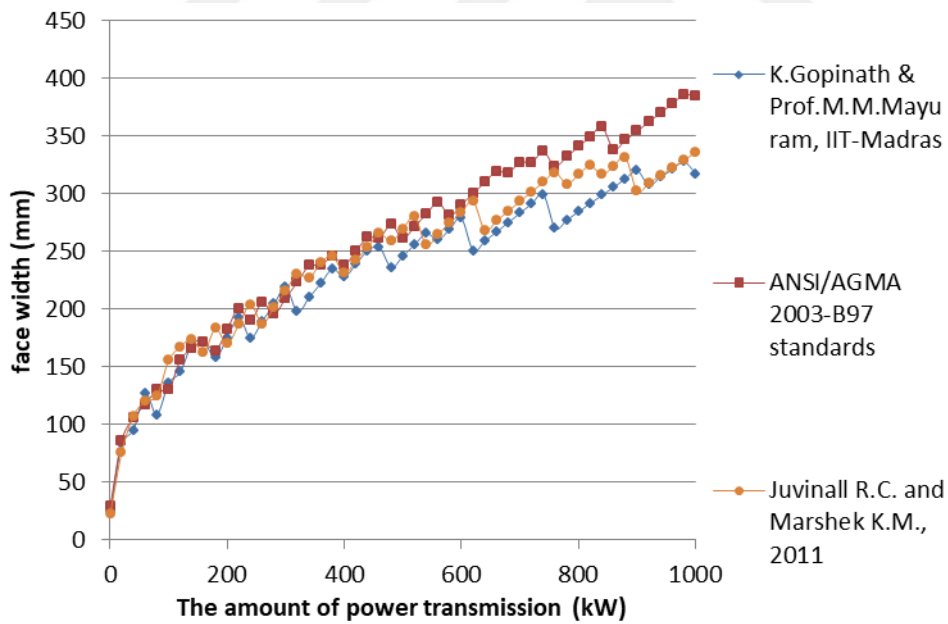

Figure H.12. Face width variation considering surface contact fatigue failure under increasing power at 6:1 speed ratio (for Ø=25°, Material type 1)
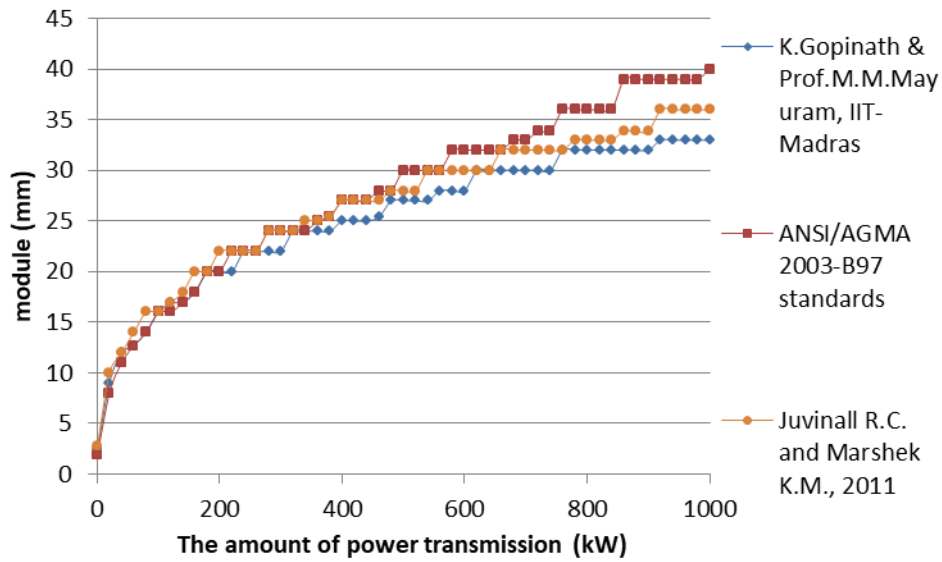
Figure H.13. Module variation considering surface contact fatigue failure under increasing power at 7:1 speed ratio (for Ø=25°, Material type 1)
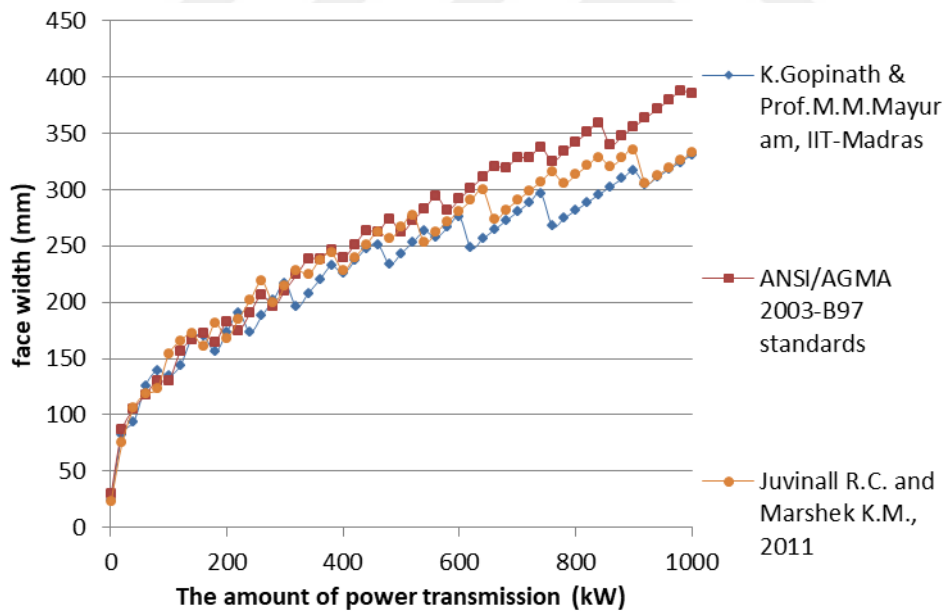
Figure H.14. Face width variation considering surface contact fatigue failure under increasing power at 7:1 speed ratio (for Ø=25°, Material type 1)

293
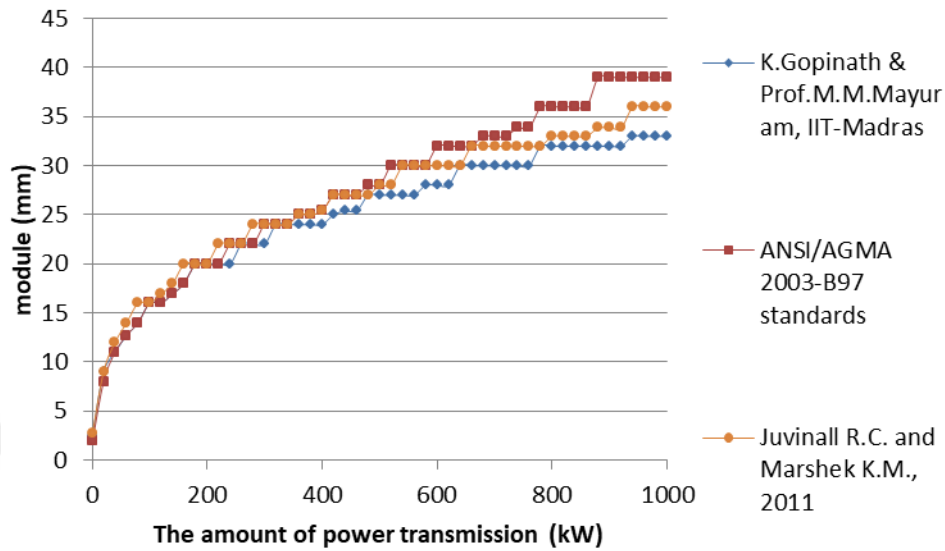
Figure H.15. Module variation considering surface contact fatigue failure under increasing power at 8:1 speed ratio (for Ø=25°, Material type 1)
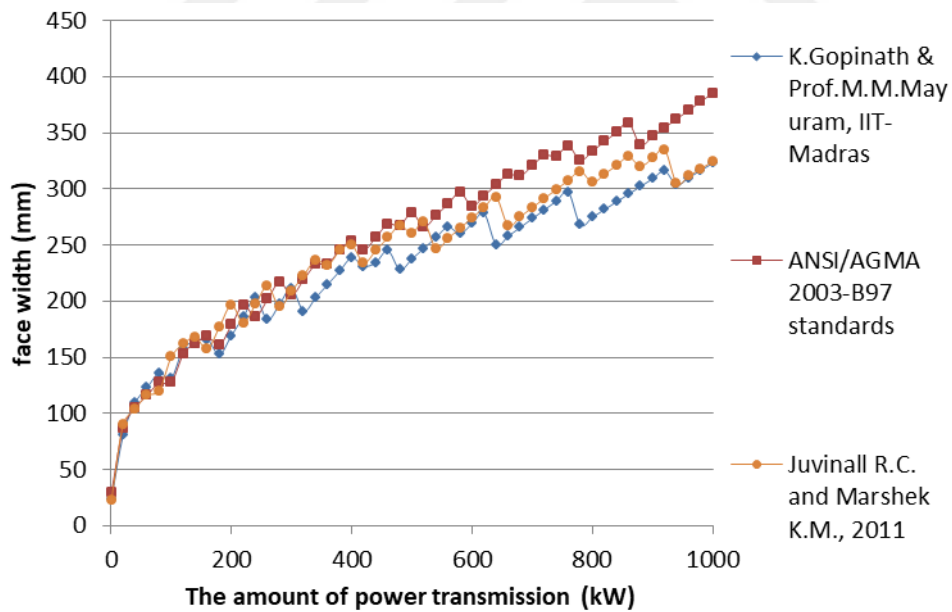

Figure H.16. Face width variation considering surface contact fatigue failure under increasing power at 8:1 speed ratio (for Ø=25°, Material type 1)

H.2. Comparison of the Results Based on Surface Contact Fatigue Failure Considering Speed Ratio for the Selected Power Transmissions for Ø=25°, Material type 1
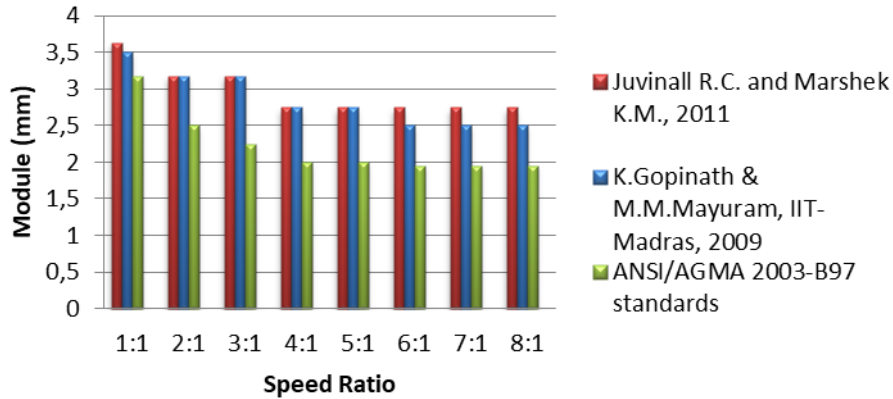
Figure H.17. The effect of speed ratio on module selection based on surface contact fatigue failure at 0,5 kW power transmission (for Ø=25°, Material type 1)
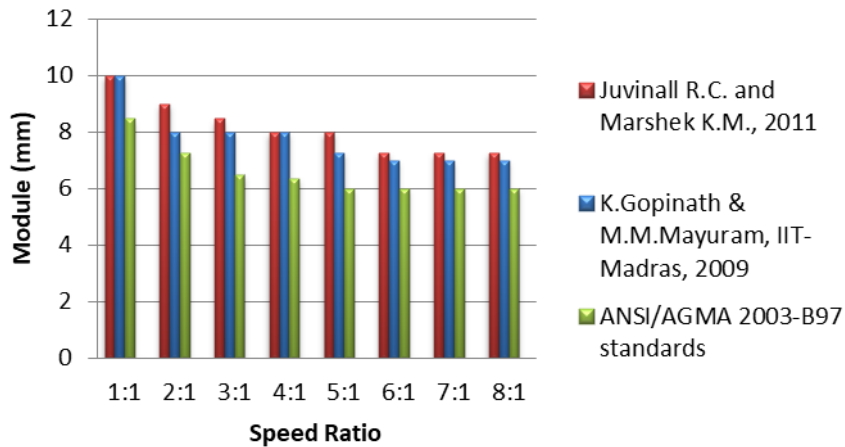
Figure H.18. The effect of speed ratio on module selection based on surface contact fatigue failure at 10 kW power transmission (for Ø=25°, Material type 1)
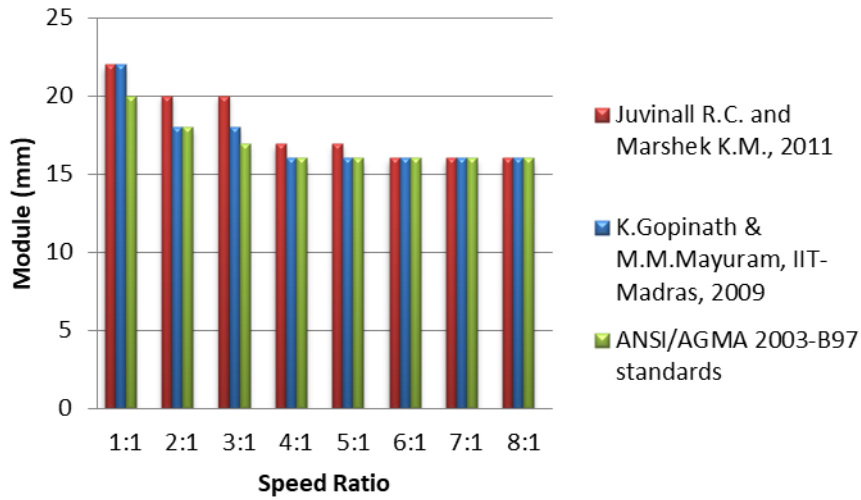
Figure H.19. The effect of speed ratio on module selection based on surface contact fatigue failure at 100 kW power transmission (for Ø=25°, Material type 1)
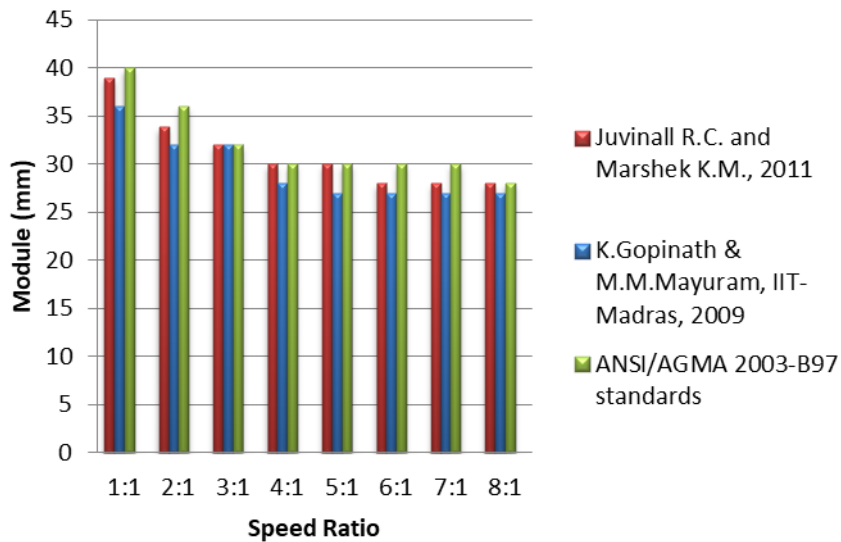
Figure H.20. The effect of speed ratio on module selection based on surface contact fatigue failure at 500 kW power transmission (for Ø=25°, Material type 1)
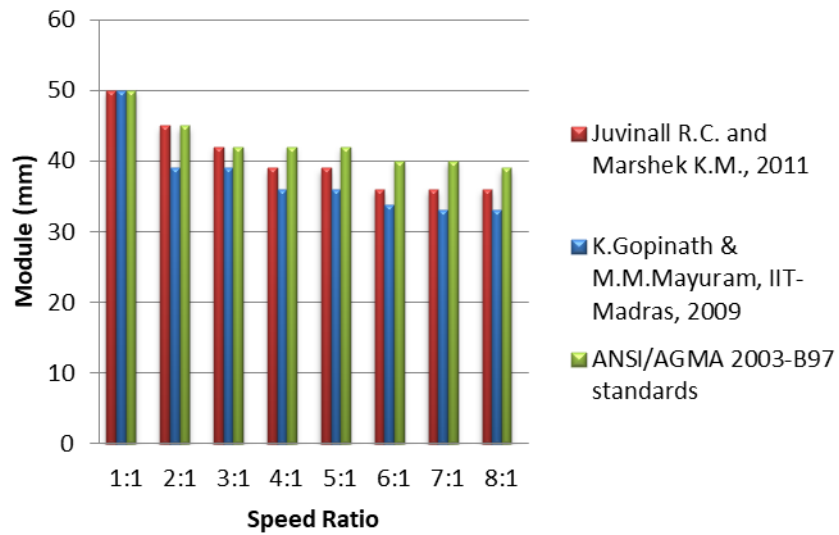
Figure H.21. The effect of speed ratio on module selection based on surface contact fatigue failure at 1000 kW power transmission (for Ø=25°, Material type 1)

**H.3. Obtaining Geometric Rating Number (GR$_i$) for Design Approaches** for Ø=25°, Material type 1
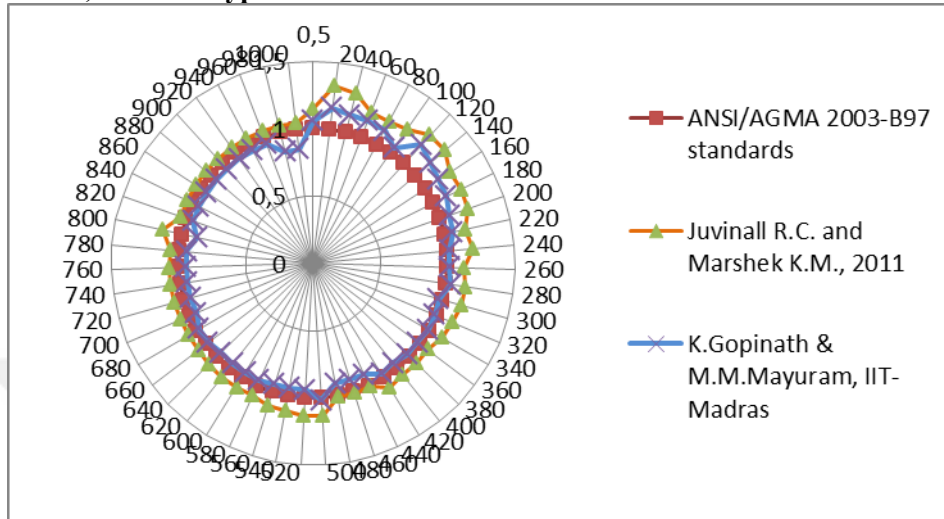
Figure H.22. Comparison of mxF/m$_0$xF$_0$ ratios for the design approaches at 1:1 speed ratio (for Ø=25°, Material type 1)
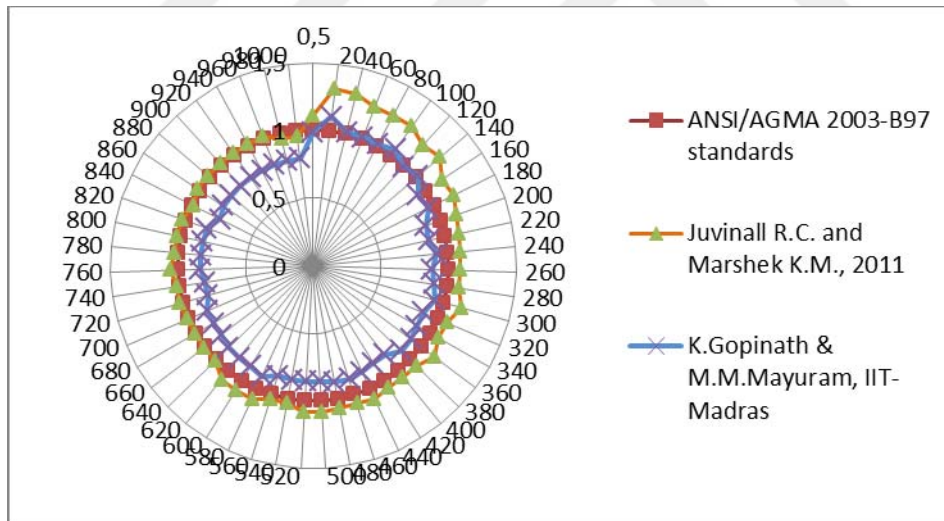
Figure H.23. Comparison of mxF/m$_0$xF$_0$ ratios for the design approaches at 2:1 speed ratio (for Ø=25°, Material type 1)
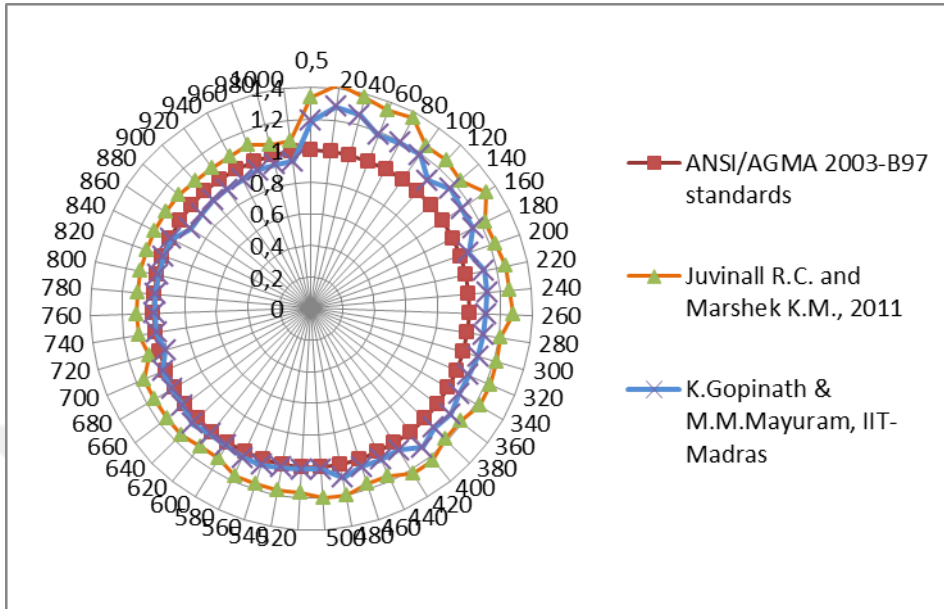
Figure H.24. Comparison of mxF/m_0xF_0 ratios for the design approaches at 3:1 speed ratio (for $\varnothing=25^{\circ}$, Material type 1)
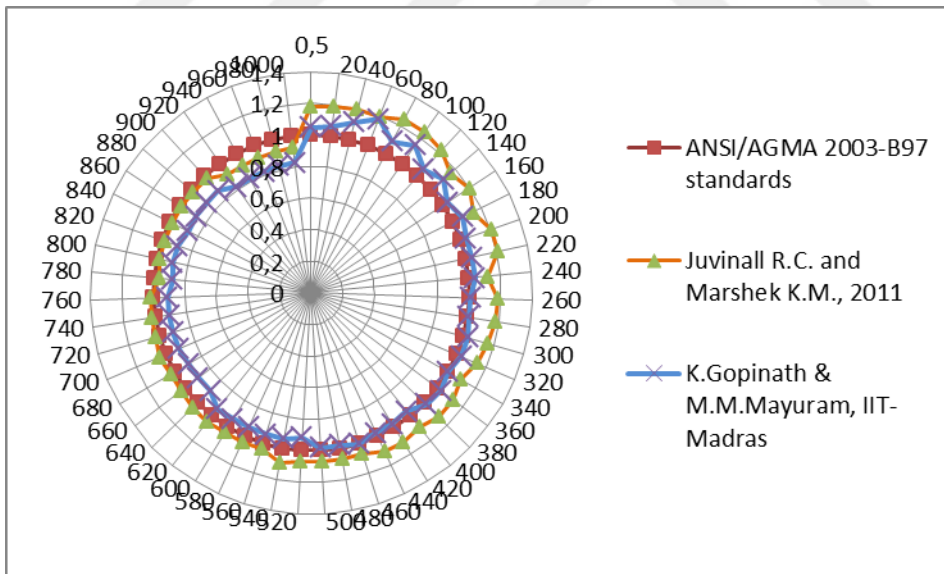
Figure H.25. Comparison of mxF/m_0xF_0 ratios for the design approaches at 4:1 speed ratio (for $\varnothing=25^{\circ}$, Material type 1)
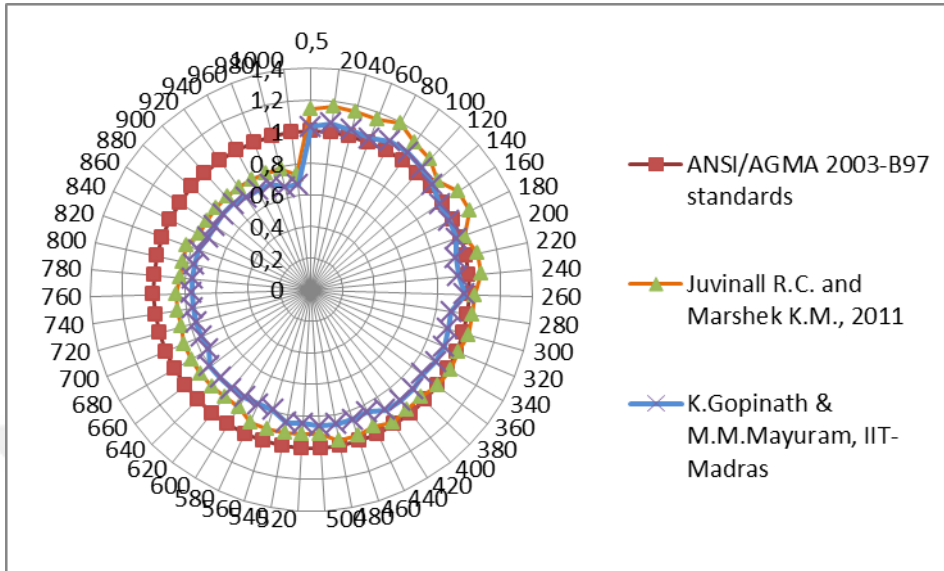
Figure H.26. Comparison of mxF/m$_0$xF$_0$ ratios for the design approaches at 5:1 speed ratio (for Ø=25°, Material type 1)
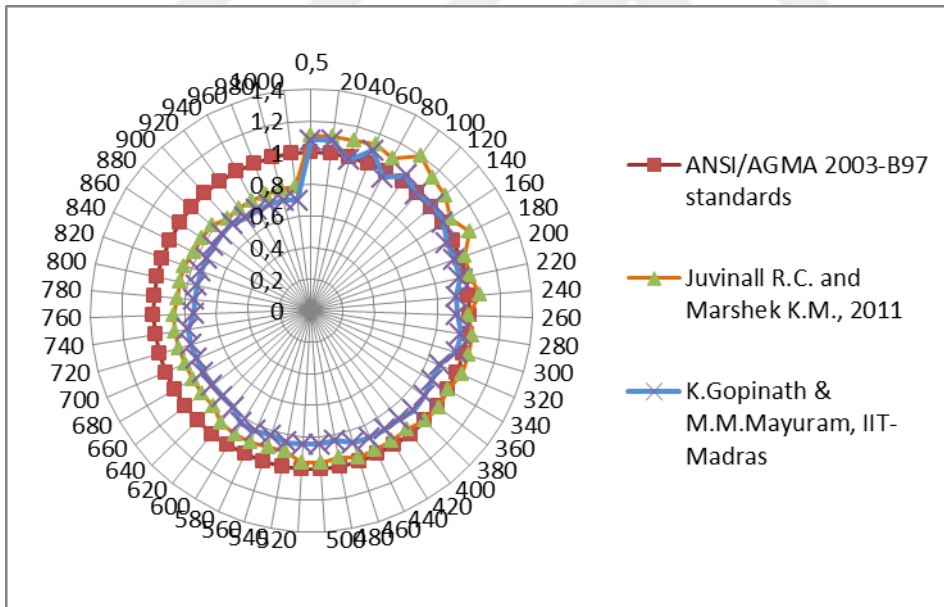

Figure H.27. Comparison of mxF/m$_0$xF$_0$ ratios for the design approaches at 6:1 speed ratio (for Ø=25°, Material type 1)
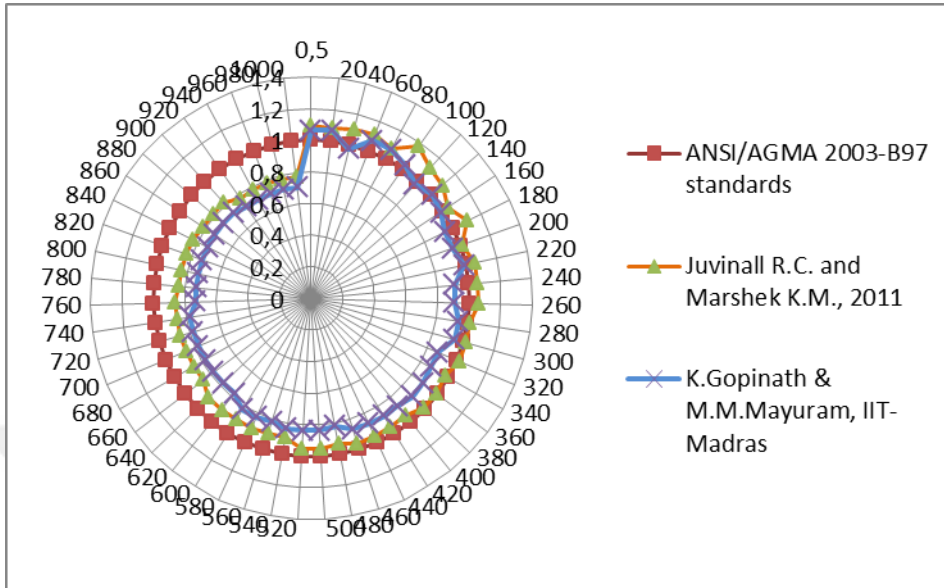
Figure H.28. Comparison of mxF/m$_0$xF$_0$ ratios for the design approaches at 7:1 speed ratio (for Ø=25°, Material type 1)
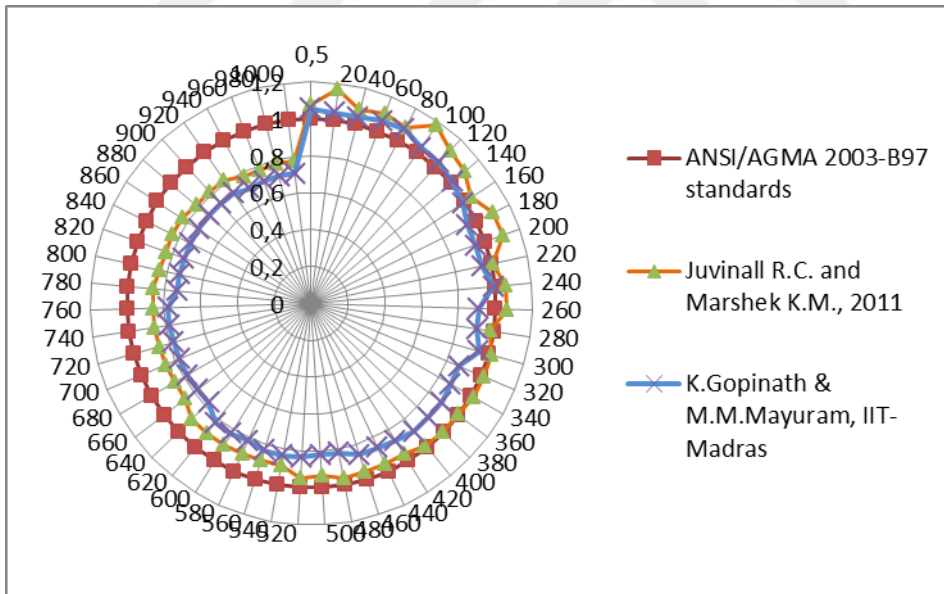
Figure H.29. Comparison of mxF/m$_0$xF$_0$ ratios for the design approaches at 8:1 speed ratio (for Ø=25°, Material type 1)

301

J.1. Comparison of Module Selection and Face Width Results of the Design Approaches for Ø=25⁰, Material type 2
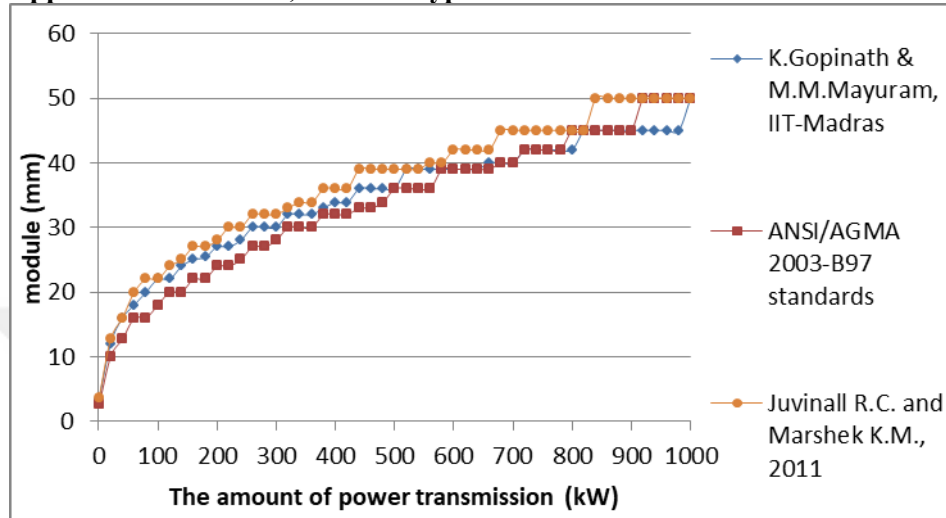
Figure J.1. Module variation considering surface contact fatigue failure under increasing power at 1:1 speed ratio (for Ø=25°, Material type 2)
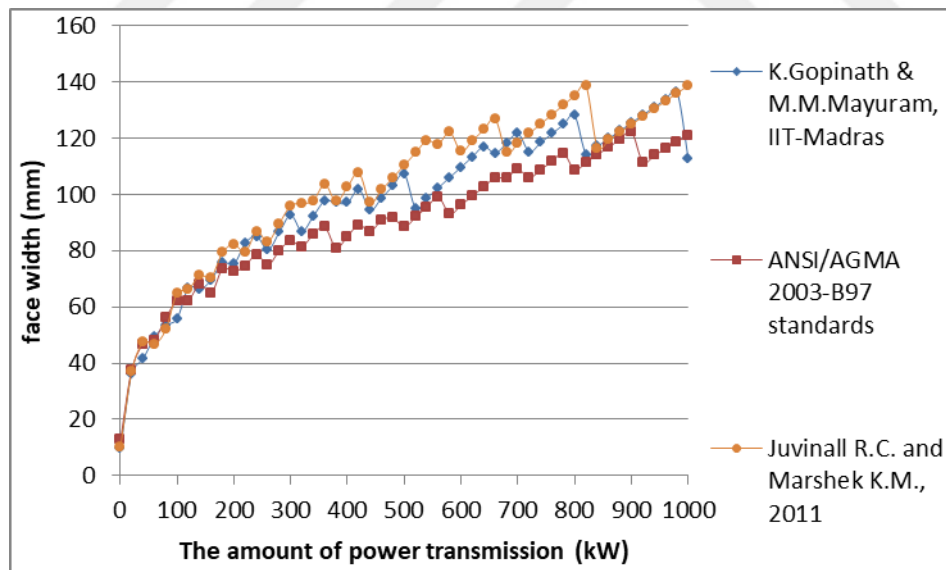
Figure J.2. Face width variation considering surface contact fatigue failure under increasing power at 1:1 speed ratio (for Ø=25°, Material type 2)
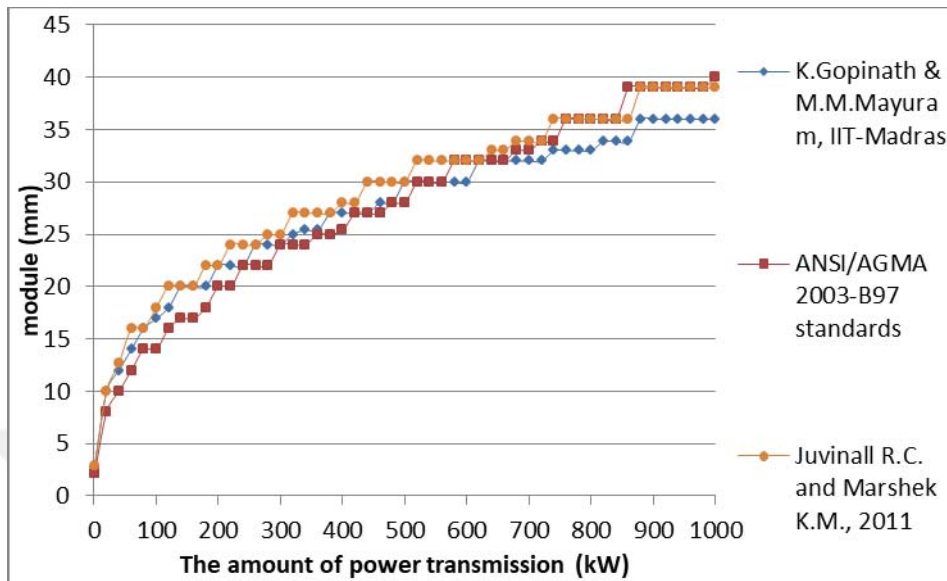
Figure J.3. Module variation considering surface contact fatigue failure under increasing power at 2:1 speed ratio (for Ø=25°, Material type 2)
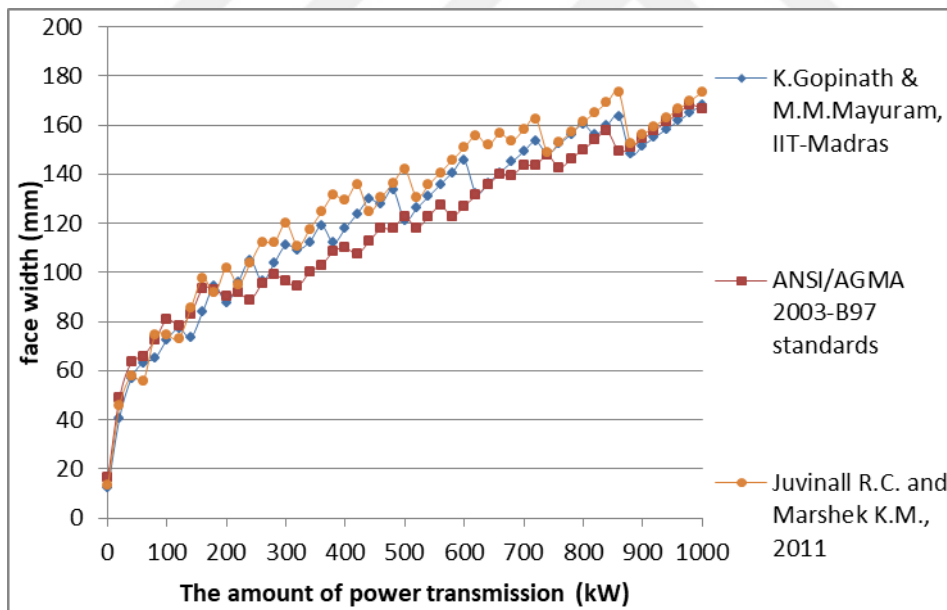
Figure J.4. Face width variation considering surface contact fatigue failure under increasing power at 2:1 speed ratio (for Ø=25°, Material type 2)

303
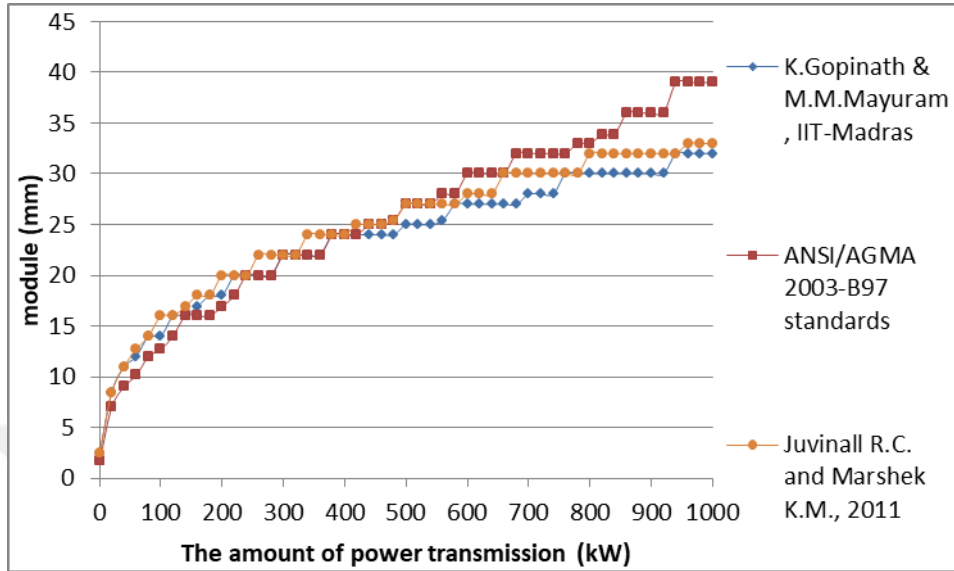
Figure J.5. Module variation considering surface contact fatigue failure under increasing power at 3:1 speed ratio (for Ø=25°, Material type 2)
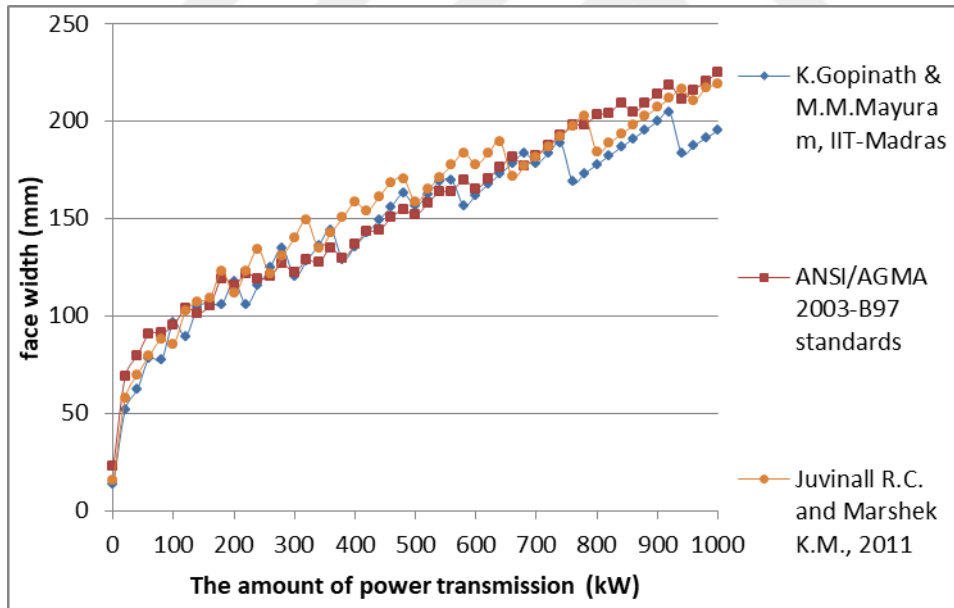
Figure J.6. Face width variation considering surface contact fatigue failure under increasing power at 3:1 speed ratio (for Ø=25°, Material type 2)
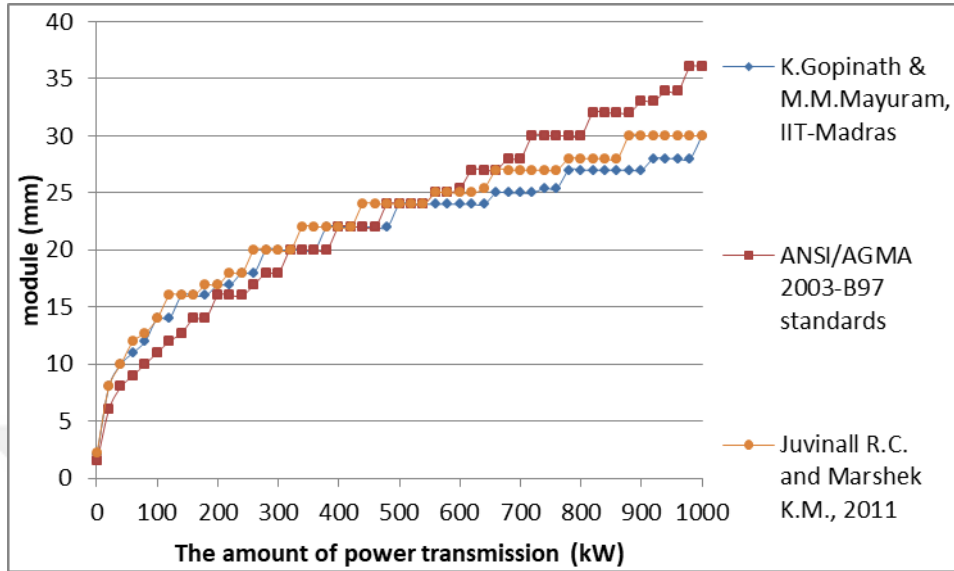
Figure J.7. Module variation considering surface contact fatigue failure under increasing power at 4:1 speed ratio (for Ø=25°, Material type 2)
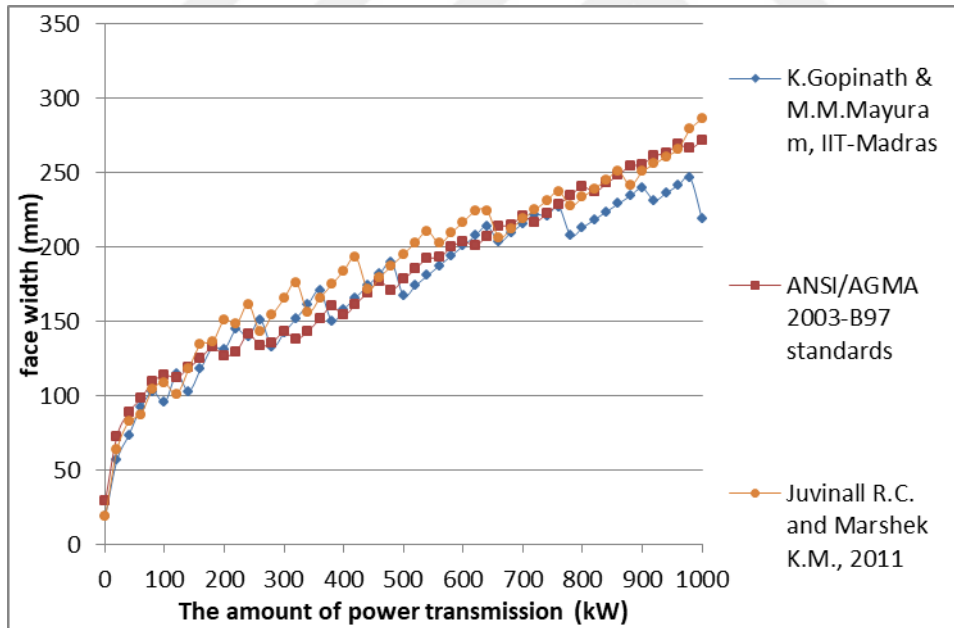
Figure J.8. Face width variation considering surface contact fatigue failure under increasing power at 4:1 speed ratio (for Ø=25°, Material type 2)
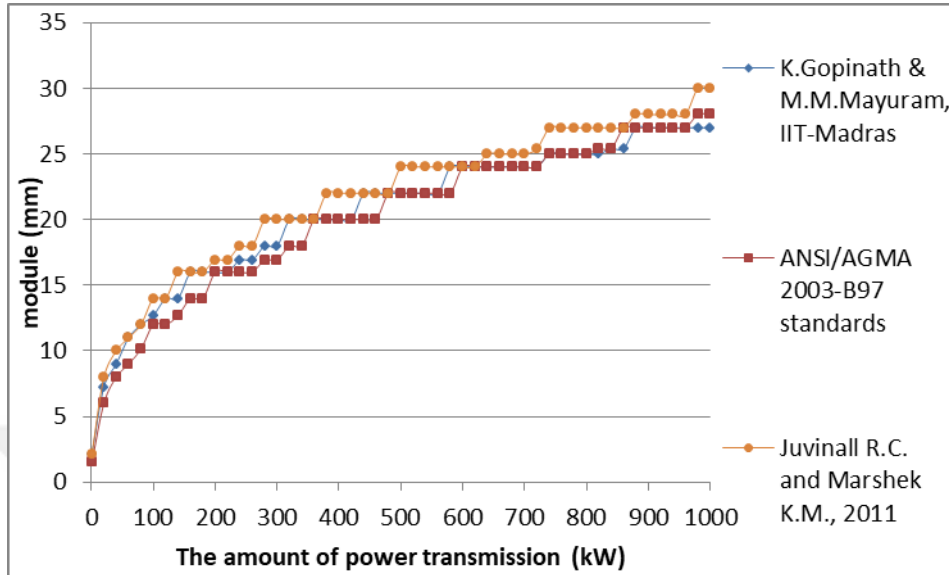
Figure J.9. Module variation considering surface contact fatigue failure under increasing power at 5:1 speed ratio (for Ø=25°, Material type 2)
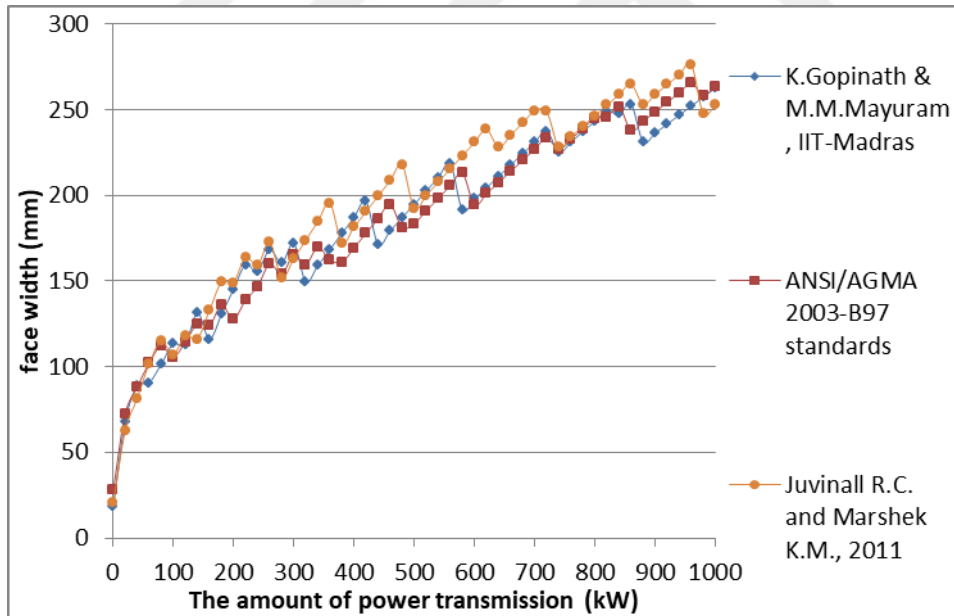
Figure J.10. Face width variation considering surface contact fatigue failure under increasing power at 5:1 speed ratio (for Ø=25°, Material type 2)
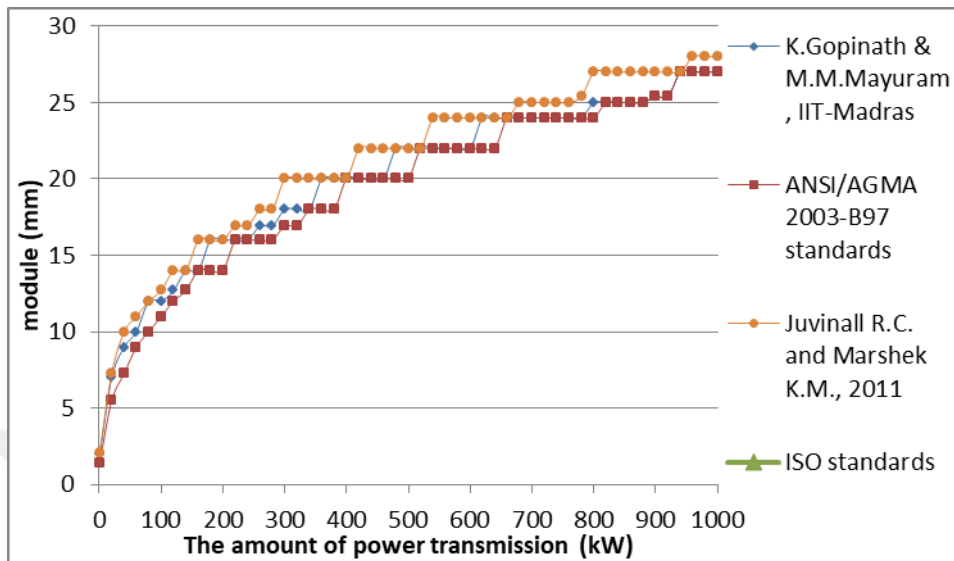
Figure J.11. Module variation considering surface contact fatigue failure under increasing power at 6:1 speed ratio (for Ø=25°, Material type 2)
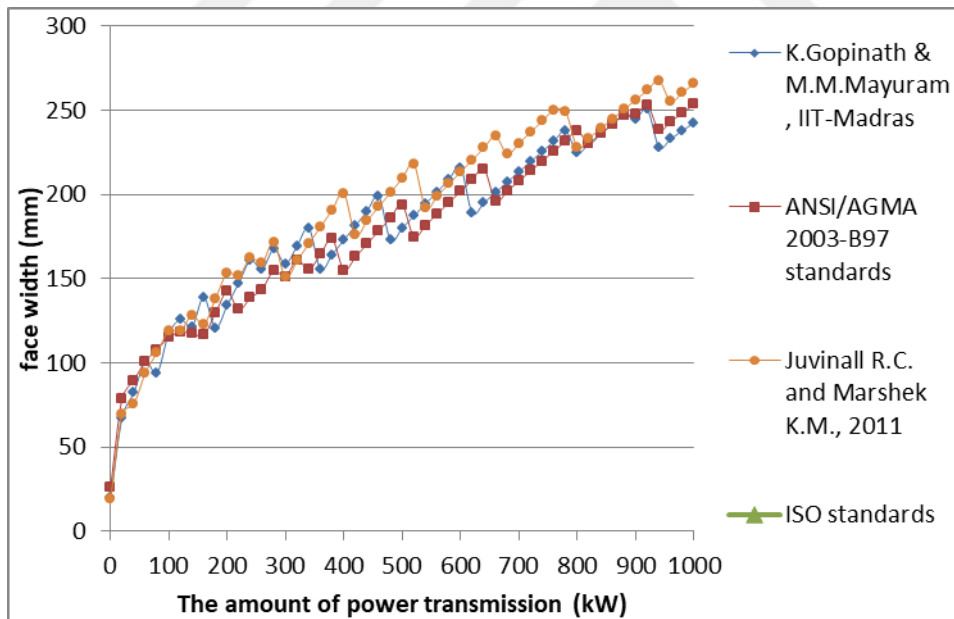
Figure J.12. Face width variation considering surface contact fatigue failure under increasing power at 6:1 speed ratio (for Ø=25°, Material type 2)

307
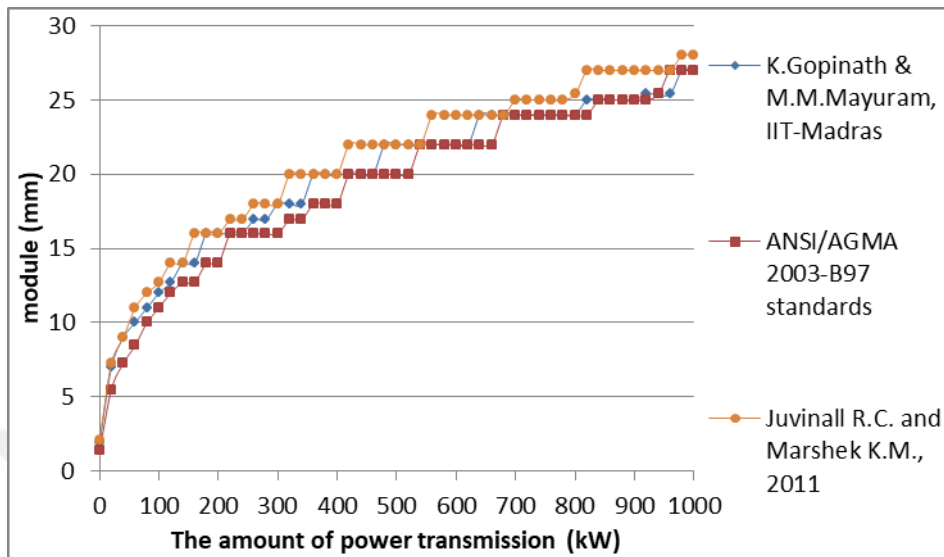
Figure J.13. Module variation considering surface contact fatigue failure under increasing power at 7:1 speed ratio (for Ø=25°, Material type 2)
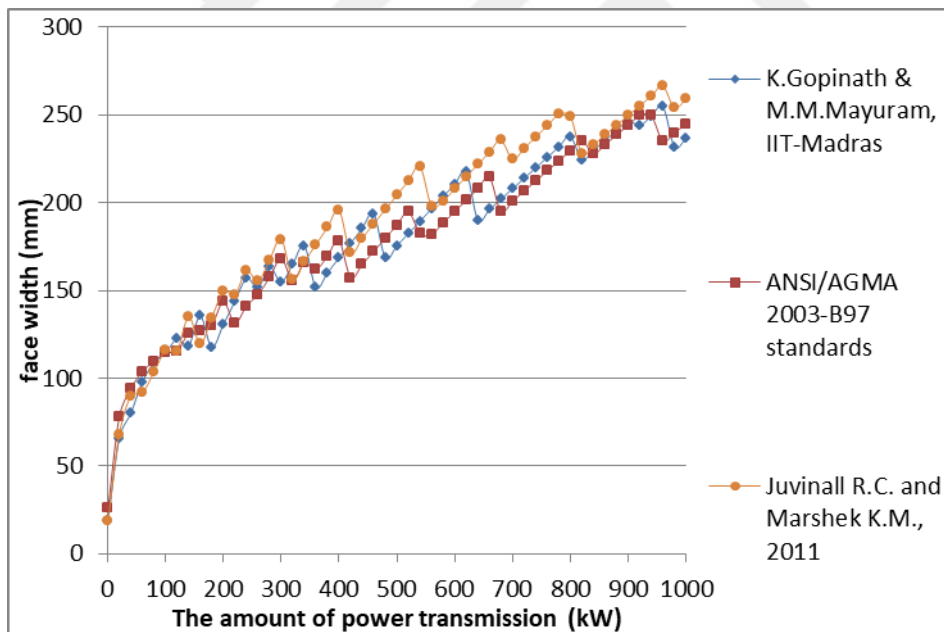
Figure J.14. Face width variation considering surface contact fatigue failure under increasing power at 7:1 speed ratio (for Ø=25°, Material type 2)
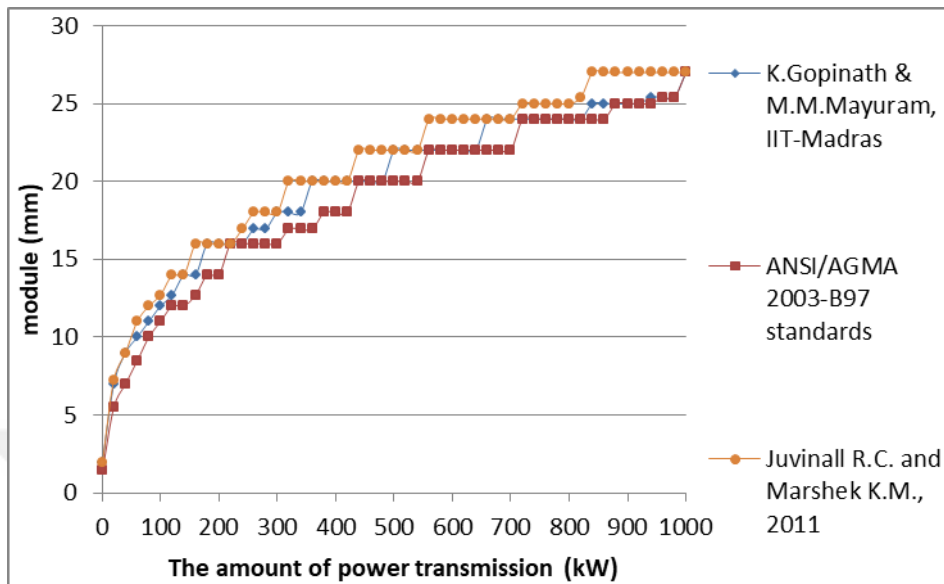
Figure J.15. Module variation considering surface contact fatigue failure under increasing power at 8:1 speed ratio (for Ø=25°, Material type 2)
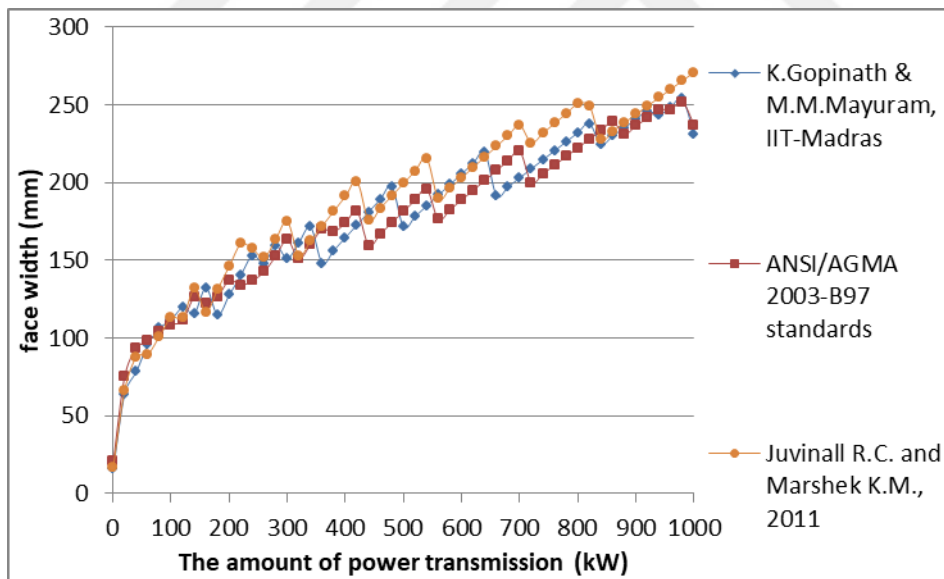

Figure J.16. Face width variation considering surface contact fatigue failure under increasing power at 8:1 speed ratio (for Ø=25°, Material type 2)

J.2. Comparison of the Results Based on Surface Contact Fatigue Failure Considering Speed Ratio for the Selected Power Transmissions for Ø=25°, Material type 2
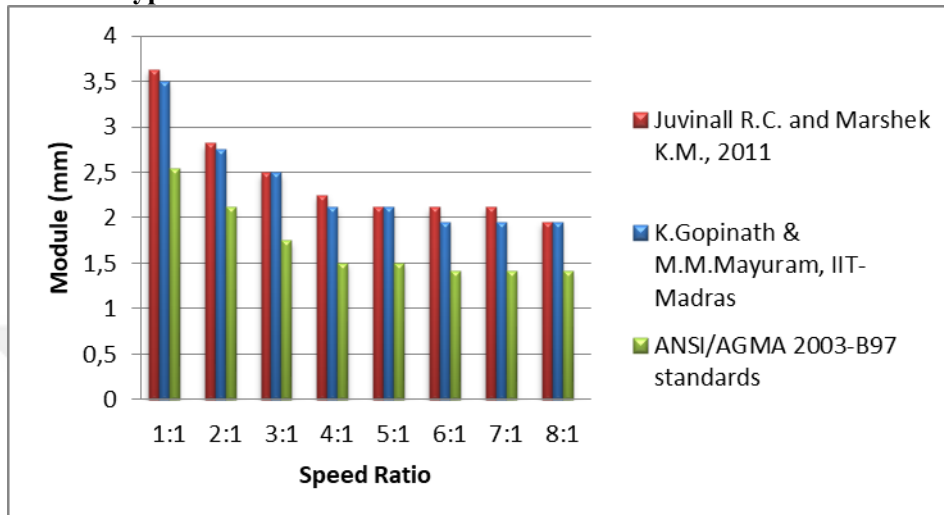
Figure J.17. The effect of speed ratio on module selection based on surface contact fatigue failure at 0,5 kW power transmission (for Ø=25°, Material type 2)
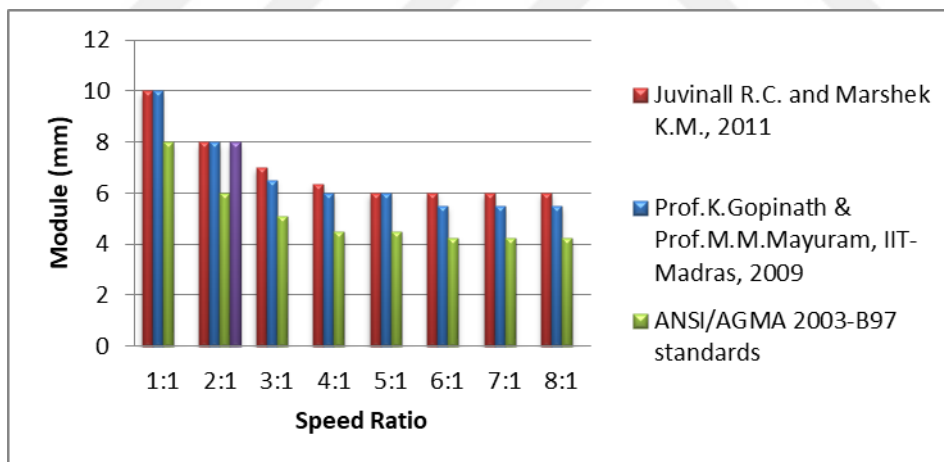
Figure J.18. The effect of speed ratio on module selection based on surface contact fatigue failure at 10 kW power transmission (for Ø=25°, Material type 2)
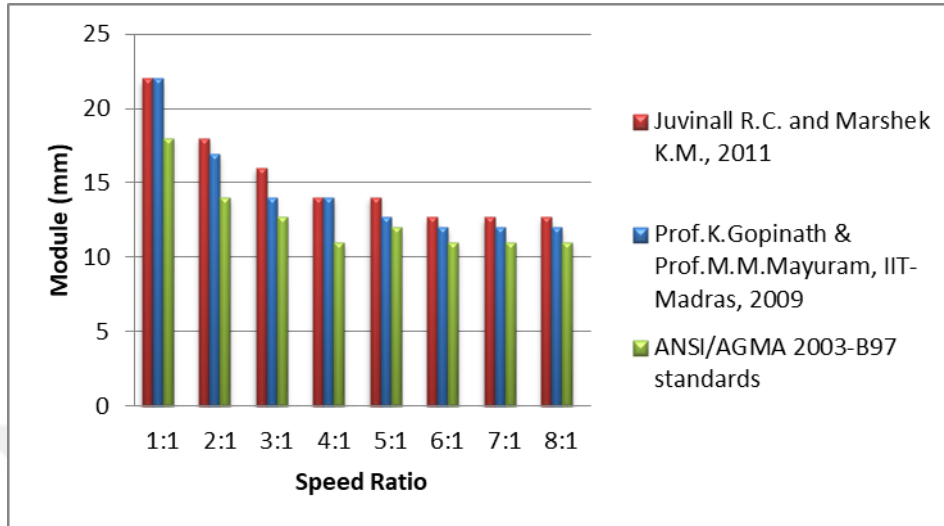
Figure J.19. The effect of speed ratio on module selection based on surface contact fatigue failure at 100 kW power transmission (for Ø=25°, Material type 2)
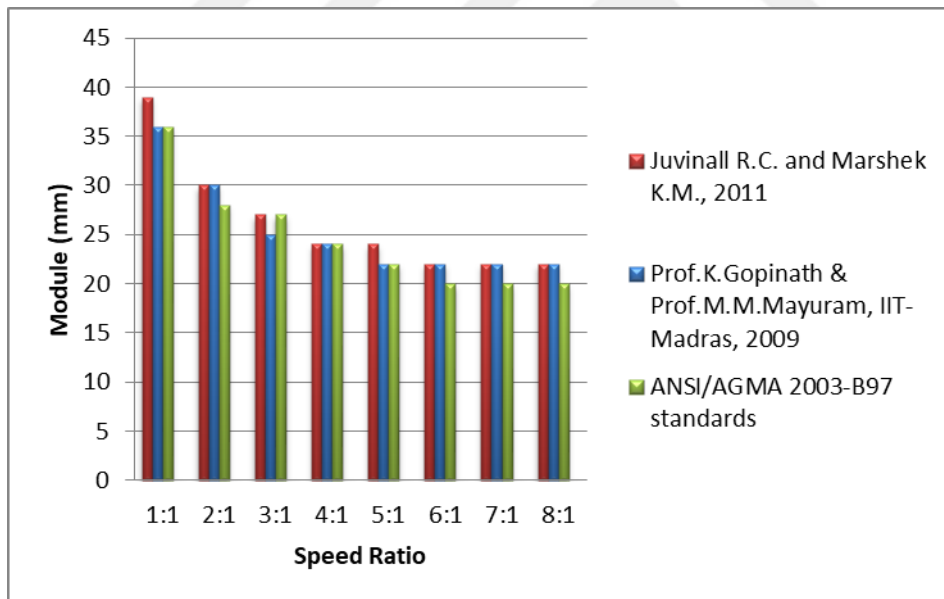
Figure J.20. The effect of speed ratio on module selection based on surface contact fatigue failure at 500 kW power transmission (for Ø=25°, Material type 2)
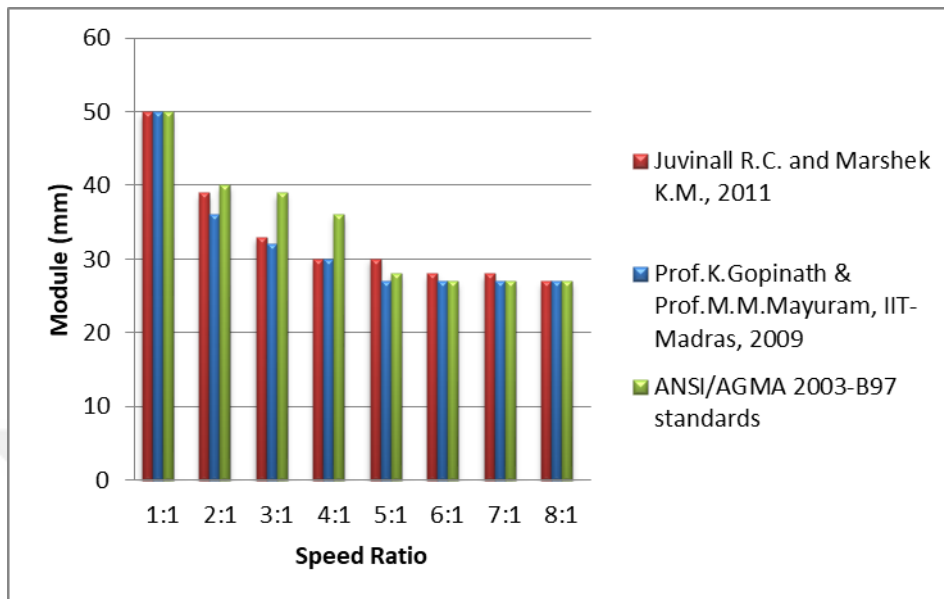
Figure J.21. The effect of speed ratio on module selection based on surface contact fatigue failure at 1000 kW power transmission (for Ø=25°, Material type 2)

J.3. Obtaining Geometric Rating Number (GR$_i$) for Design Approaches for Ø=25°, Material type 2
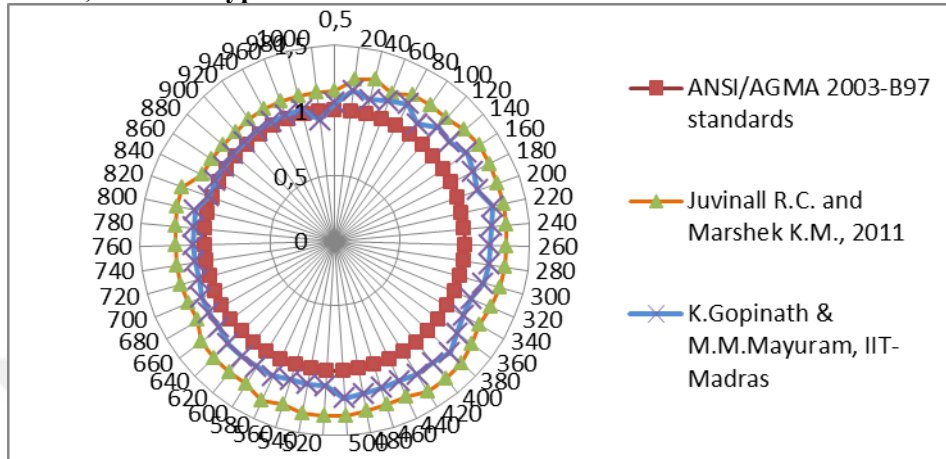
Figure J.22. Comparison of mxF/m$_0$xF$_0$ ratios for the design approaches at 1:1 speed ratio (for Ø=25°, Material type 2)
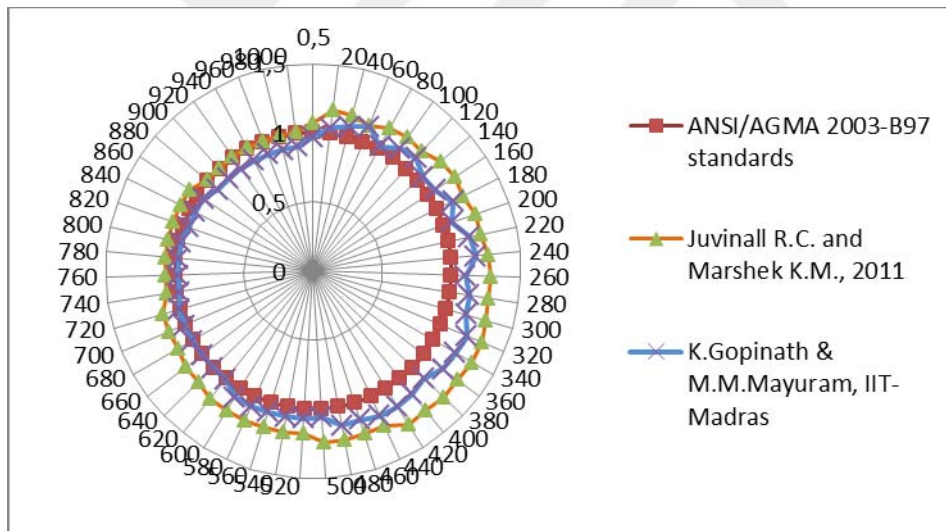
Figure J.23. Comparison of mxF/m$_0$xF$_0$ ratios for the design approaches at 2:1 speed ratio (for Ø=25°, Material type 2)
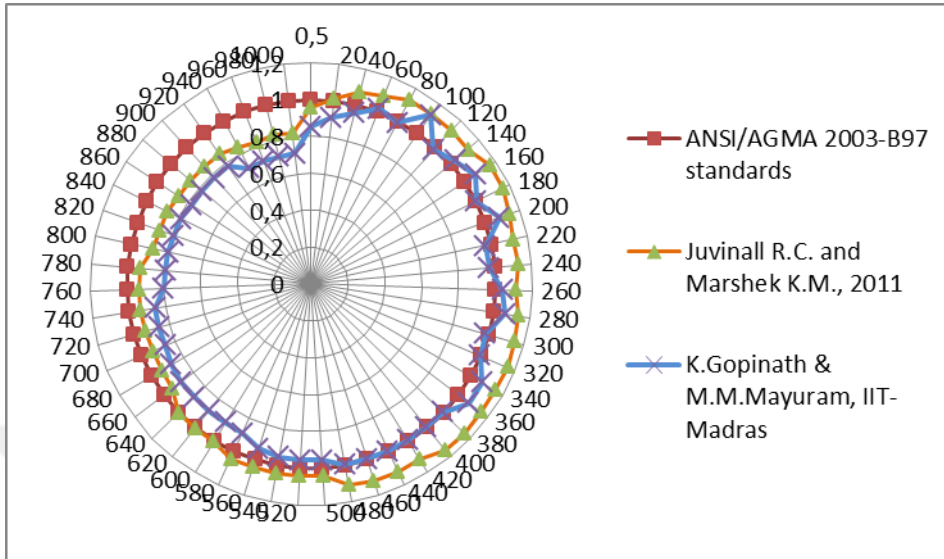
Figure J.24. Comparison of mxF/m₀xF₀ ratios for the design approaches at 3:1 speed ratio (for Ø=25°, Material type 2)
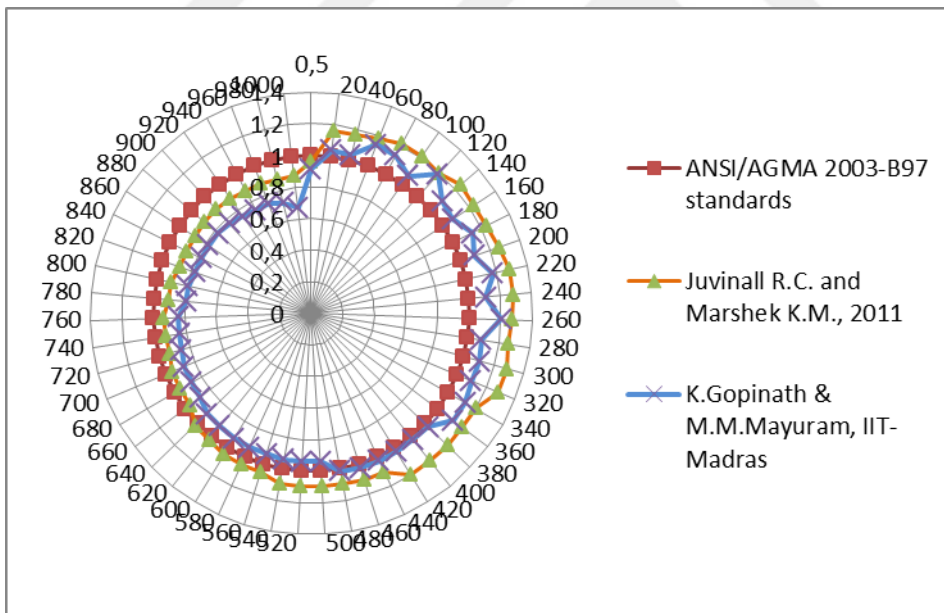
Figure J.25. Comparison of mxF/m₀xF₀ ratios for the design approaches at 4:1 speed ratio (for Ø=25°, Material type 2)

314
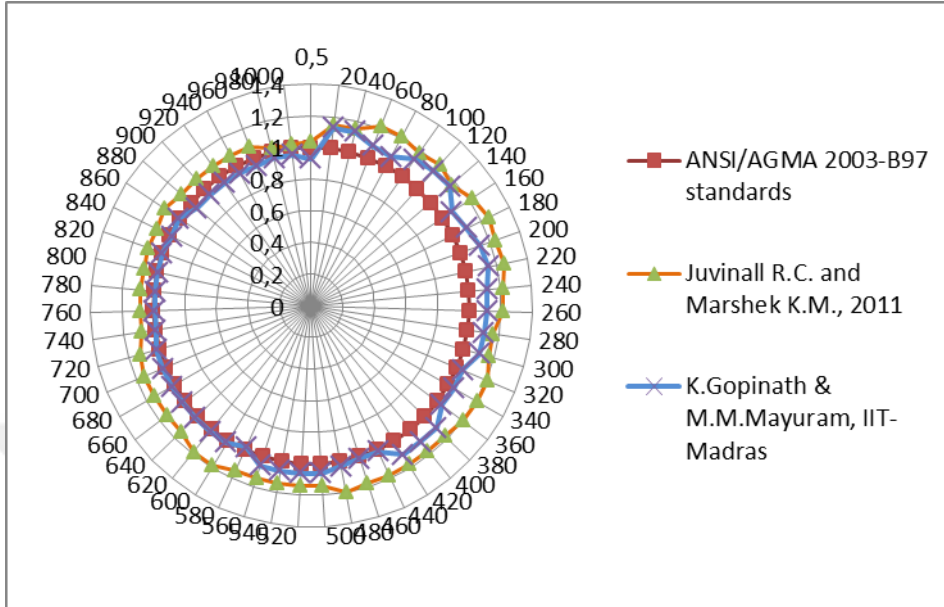
Figure J.26. Comparison of mxF/m_0xF$_0$ ratios for the design approaches at 5:1 speed ratio (for Ø=25°, Material type 2)
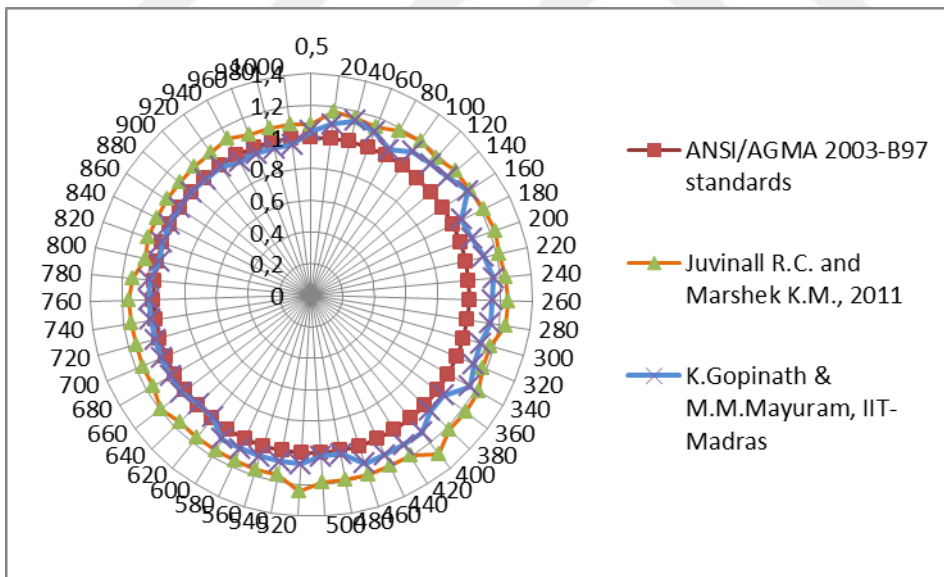
Figure J.27. Comparison of mxF/m_0xF$_0$ ratios for the design approaches at 6:1 speed ratio (for Ø=25°, Material type 2)
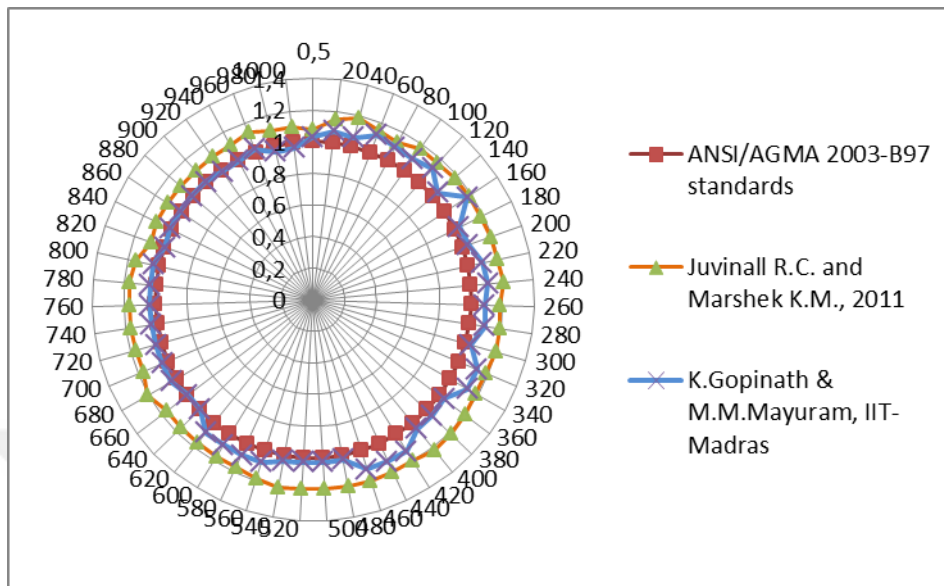
Figure J.28. Comparison of mxF/m$_0$xF$_0$ ratios for the design approaches at 7:1 speed ratio (for Ø=25°, Material type 2)
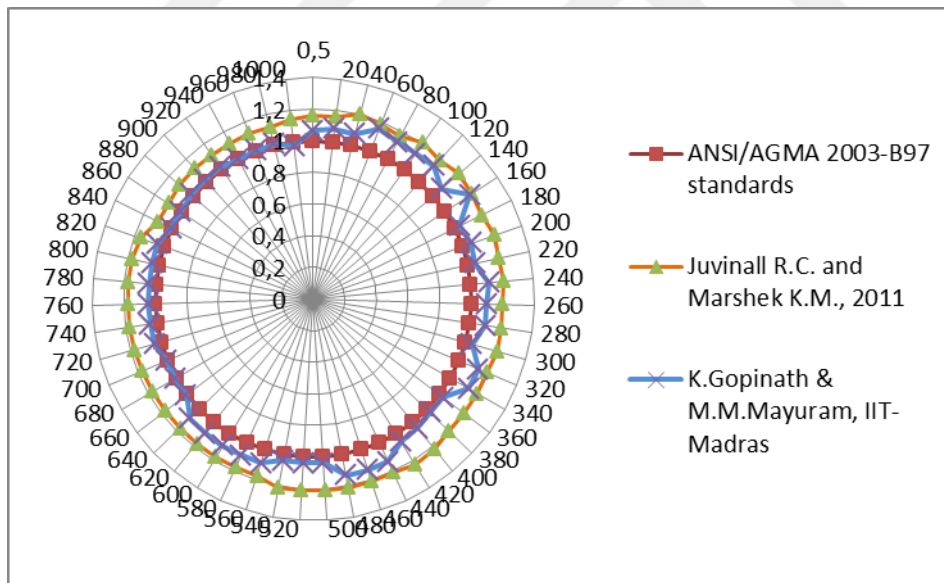
Figure J.29. Comparison of mxF/m$_0$xF$_0$ ratios for the design approaches at 8:1 speed ratio (for Ø=25°, Material type 2)

316

APPENDIX K

## K.1. Comparison of Module Selection and Face Width Results of the Design Approaches for Ø=25°, Material type 3
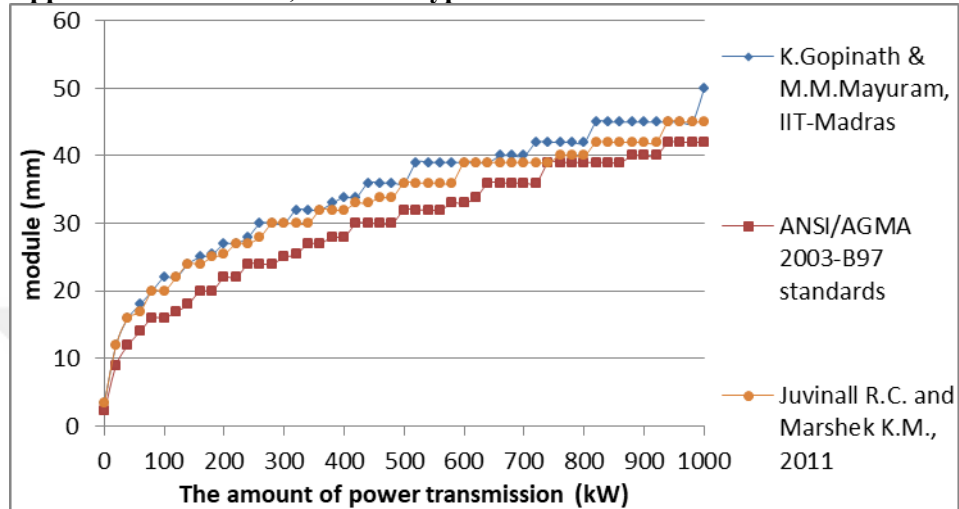
Figure K.1. Module variation considering surface contact fatigue failure under increasing power at 1:1 speed ratio (for Ø=25°, Material type 3)
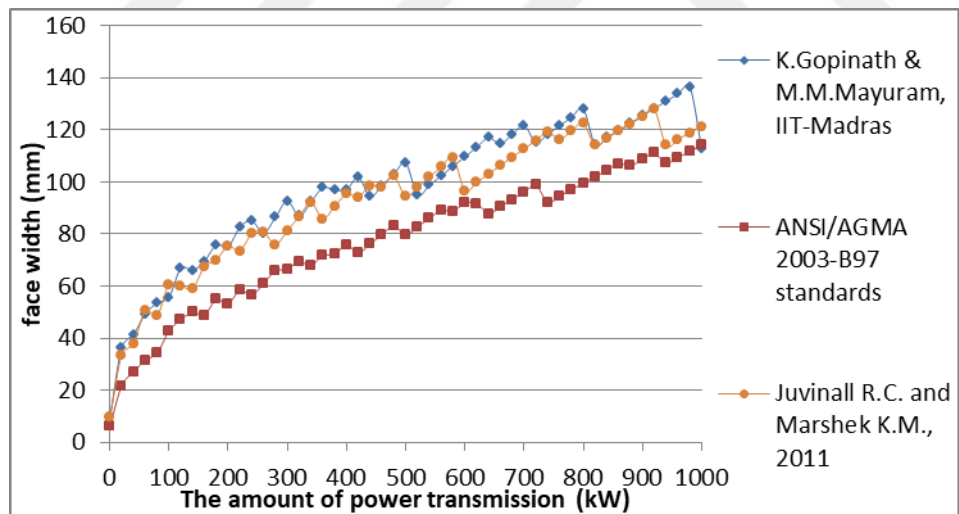

Figure K.2. Face width variation considering surface contact fatigue failure under increasing power at 1:1 speed ratio (for Ø=25°, Material type 3)
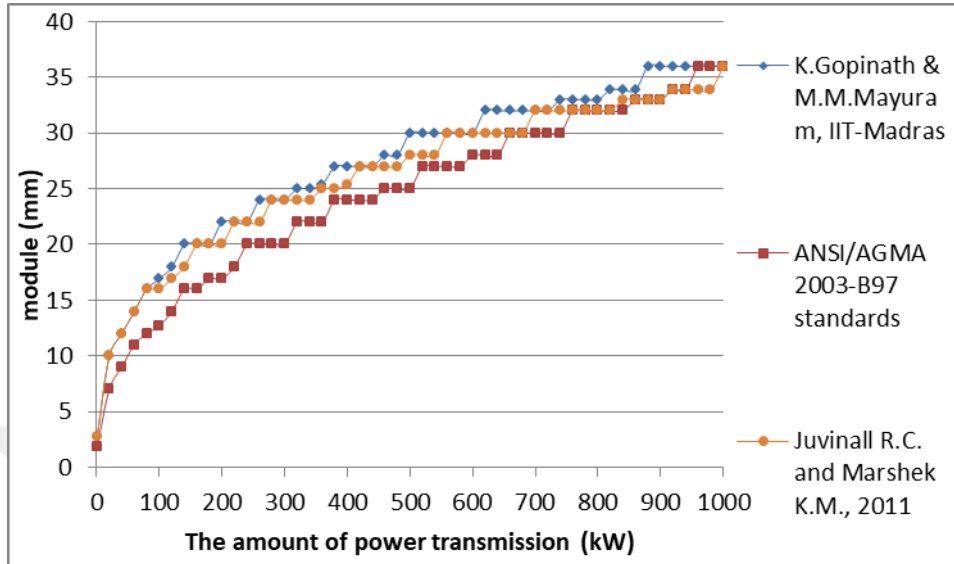
Figure K.3. Module variation considering surface contact fatigue failure under increasing power at 2:1 speed ratio (for Ø=25°, Material type 3)
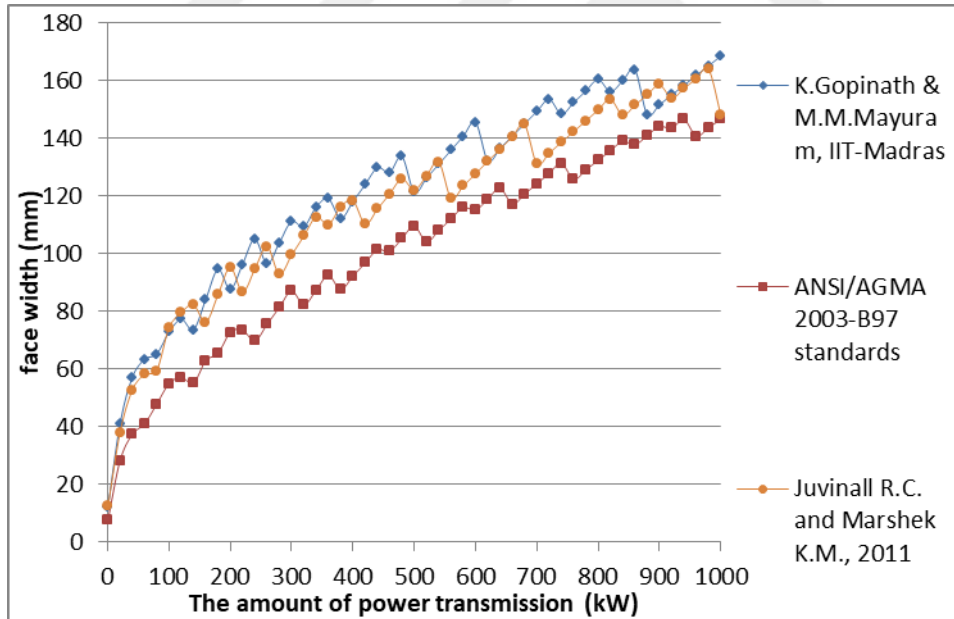

Figure K.4. Face width variation considering surface contact fatigue failure under increasing power at 2:1 speed ratio (for Ø=25°, Material type 3)

318
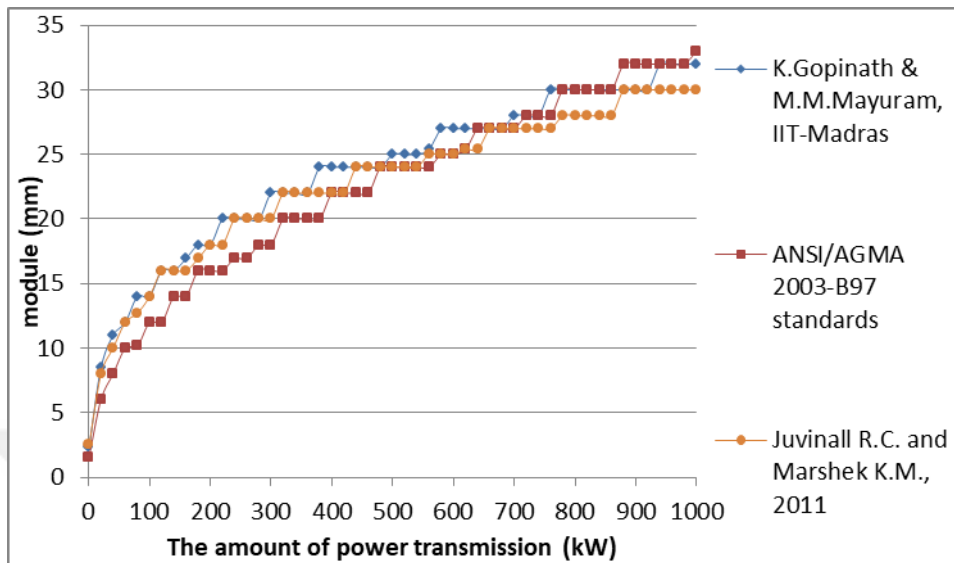
Figure K.5. Module variation considering surface contact fatigue failure under increasing power at 3:1 speed ratio (for Ø=25°, Material type 3)
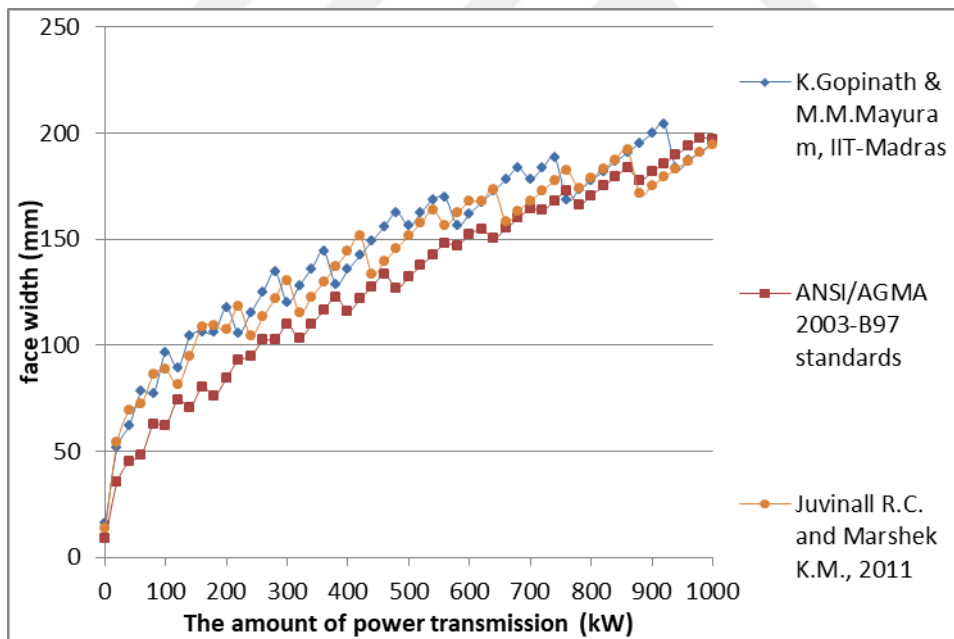
Figure K.6. Face width variation considering surface contact fatigue failure under increasing power at 3:1 speed ratio (for Ø=25°, Material type 3)
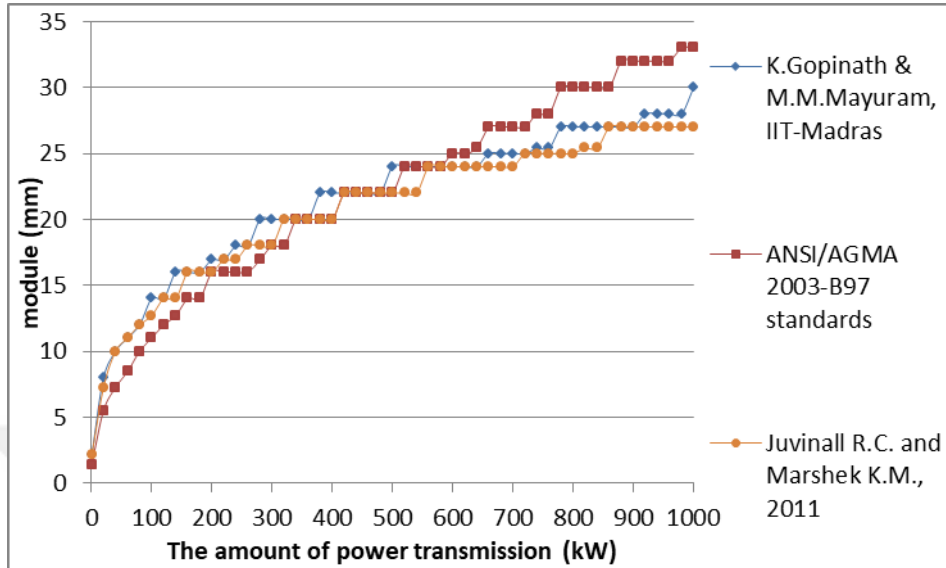
Figure K.7. Module variation considering surface contact fatigue failure under increasing power at 4:1 speed ratio (for Ø=25°, Material type 3)
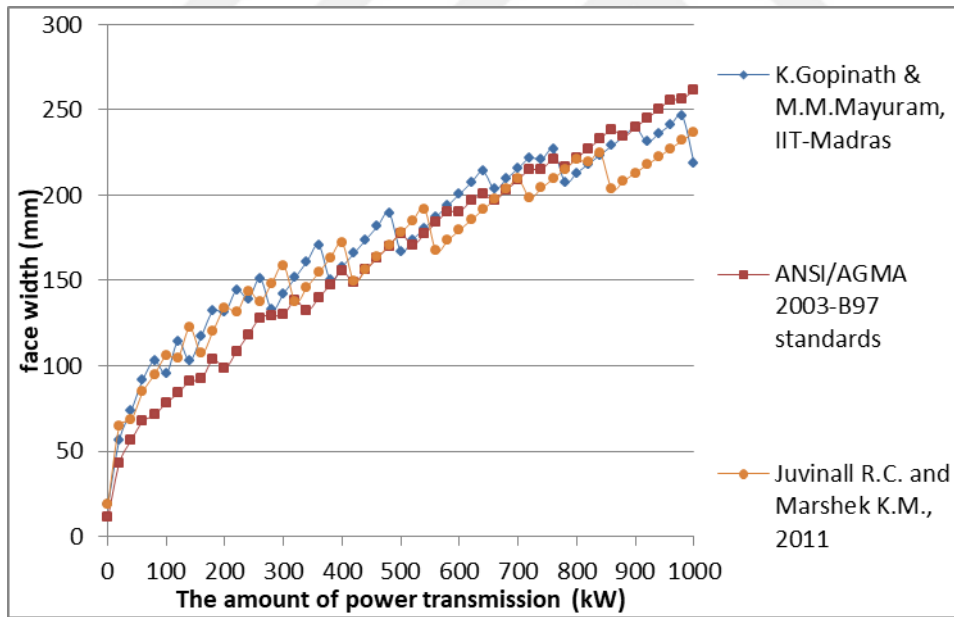

Figure K.8. Face width variation considering surface contact fatigue failure under increasing power at 4:1 speed ratio (for Ø=25°, Material type 3)
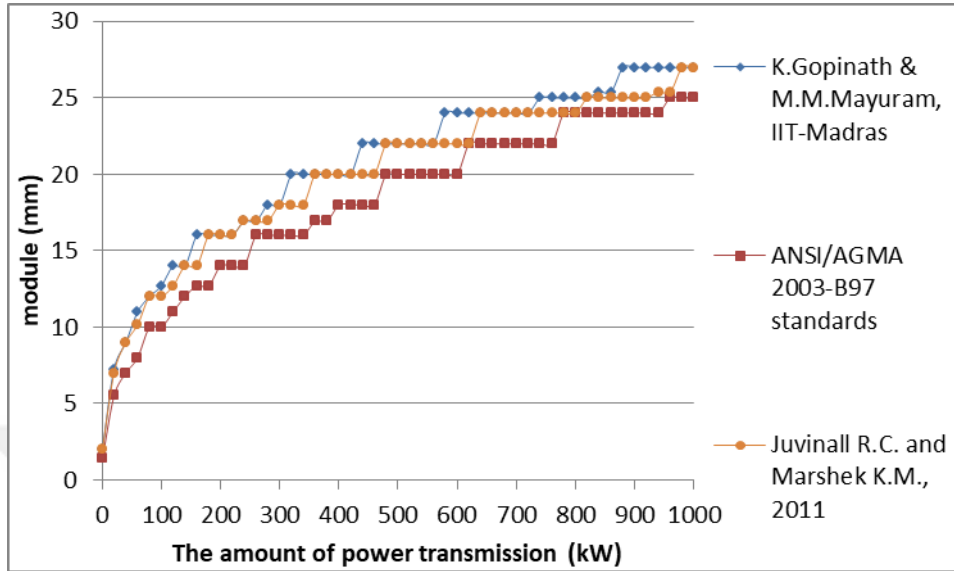
Figure K.9. Module variation considering surface contact fatigue failure under increasing power at 5:1 speed ratio (for Ø=25°, Material type 3)
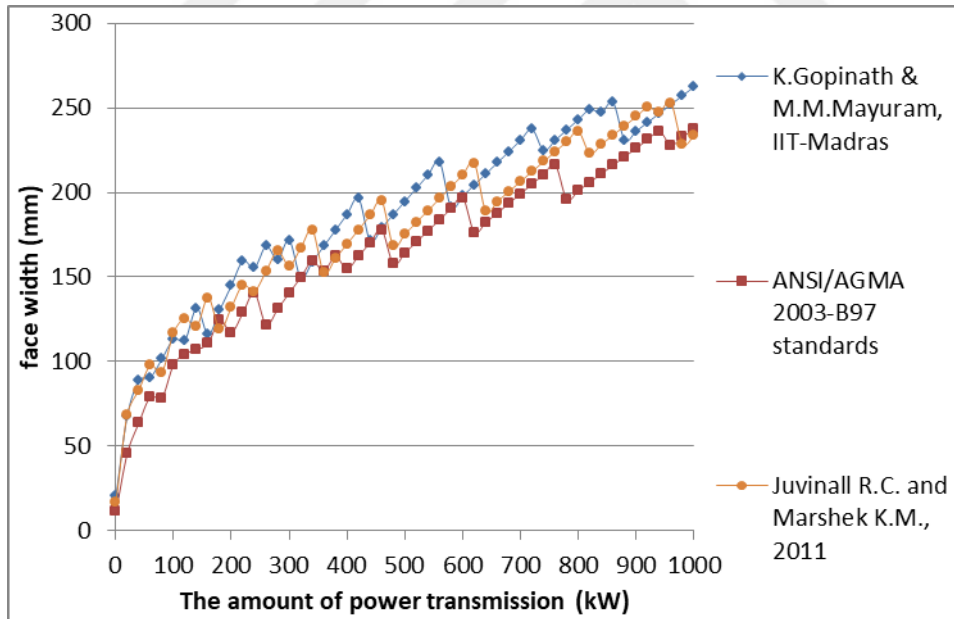
Figure K.10. Face width variation considering surface contact fatigue failure under increasing power at 5:1 speed ratio (for Ø=25°, Material type 3)
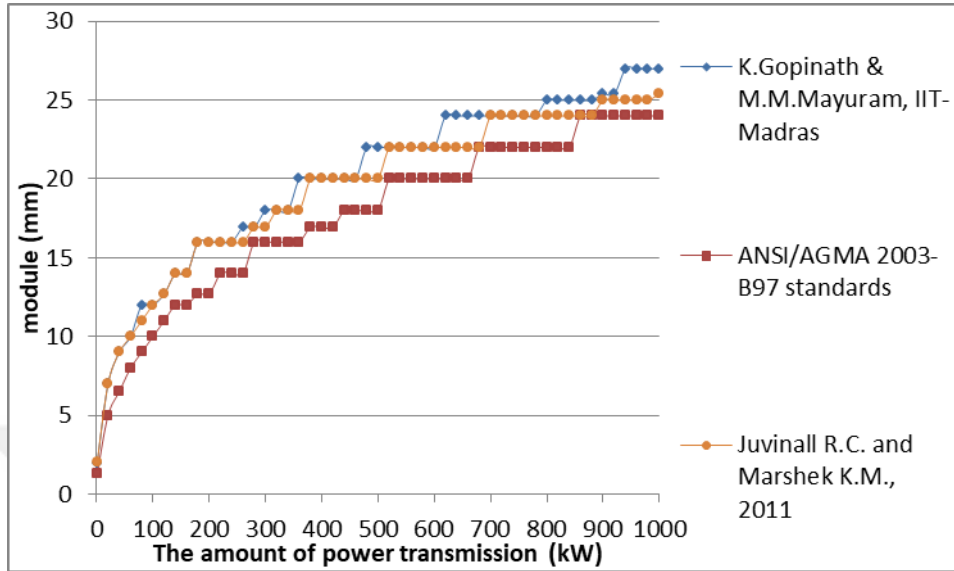
Figure K.11. Module variation considering surface contact fatigue failure under increasing power at 6:1 speed ratio (for Ø=25°, Material type 3)
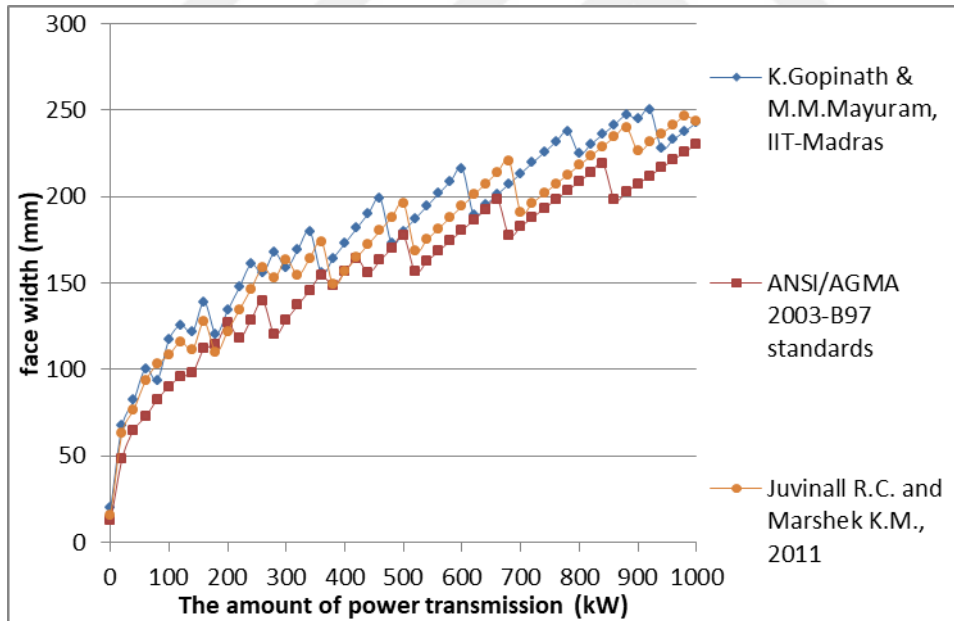
Figure K.12. Face width variation considering surface contact fatigue failure under increasing power at 6:1 speed ratio (for Ø=25°, Material type 3)

322
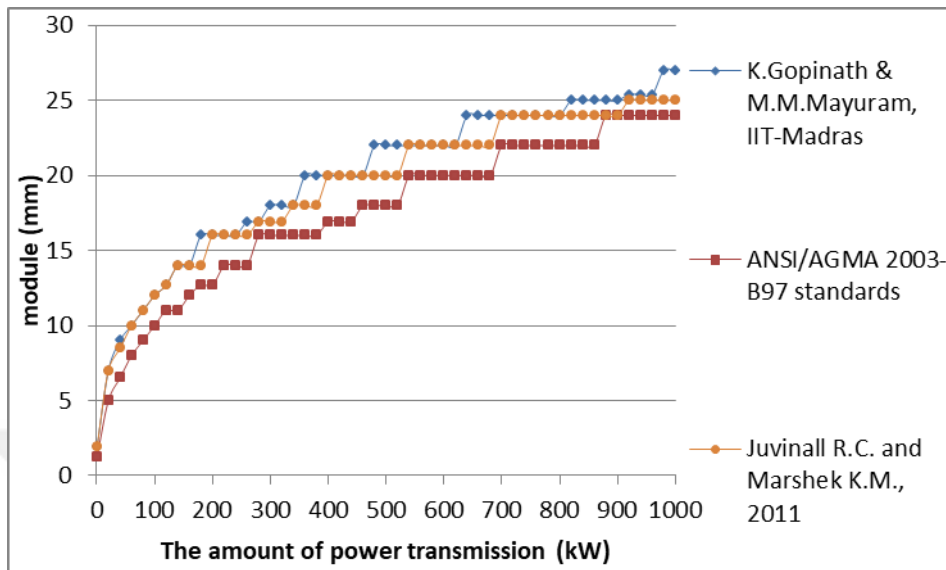
Figure K.13. Module variation considering surface contact fatigue failure under increasing power at 7:1 speed ratio (for Ø=25°, Material type 3)
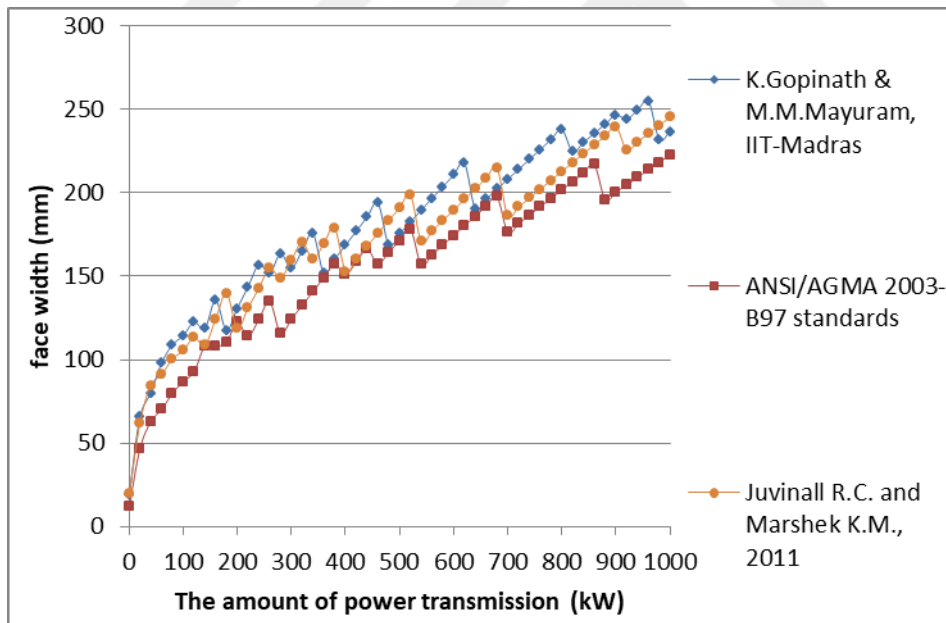
Figure K.14. Face width variation considering surface contact fatigue failure under increasing power at 7:1 speed ratio (for Ø=25°, Material type 3)
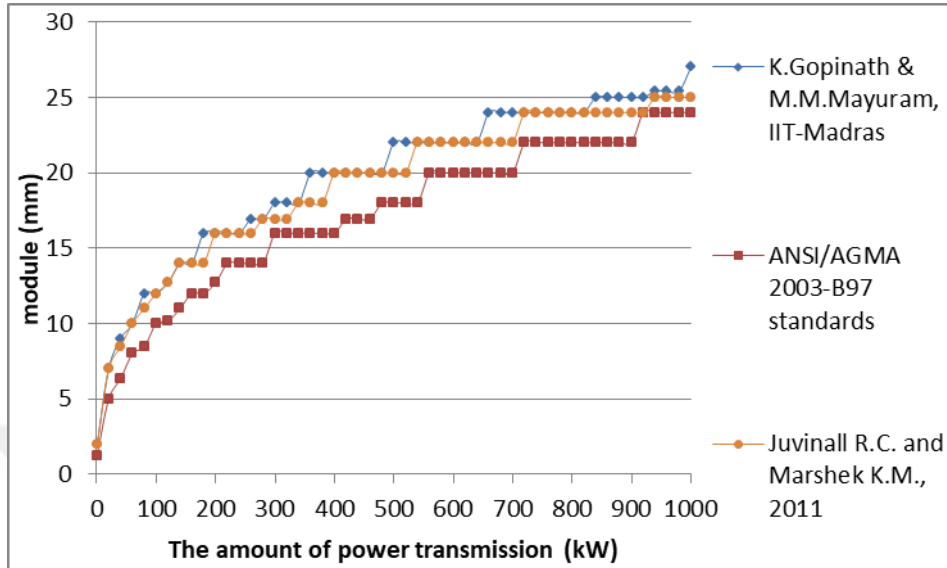
Figure K.15. Module variation considering surface contact fatigue failure under increasing power at 8:1 speed ratio (for Ø=25°, Material type 3)
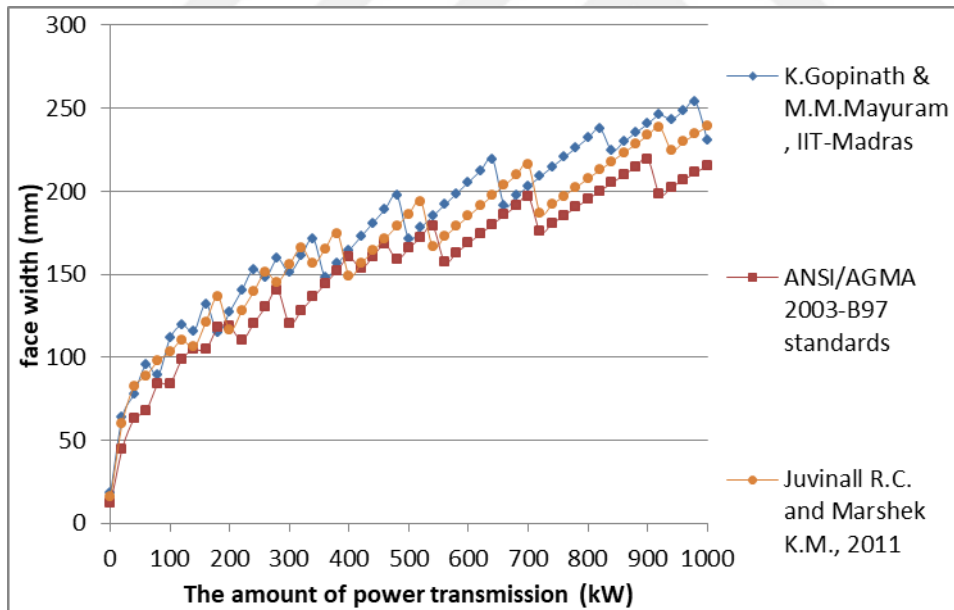
Figure K.16. Face width variation considering surface contact fatigue failure under increasing power at 8:1 speed ratio (for Ø=25°, Material type 3)

K.2. Comparison of the Results Based on Surface Contact Fatigue Failure Considering Speed Ratio for the Selected Power Transmissions for Ø=25°, Material type 3
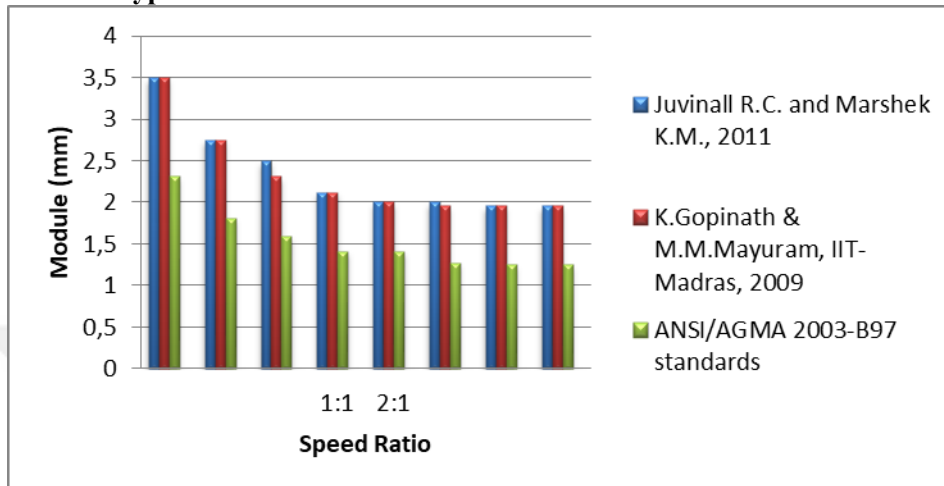
Figure K.17. The effect of speed ratio on module selection based on surface contact fatigue failure at 0,5 kW power transmission (for Ø=25°, Material type 3)
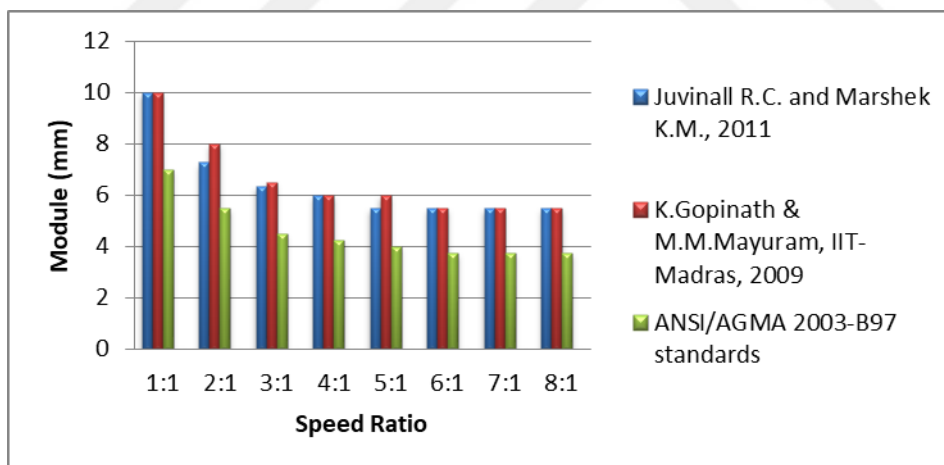

Figure K.18. The effect of speed ratio on module selection based on surface contact fatigue failure at 10 kW power transmission (for Ø=25°, Material type 3)
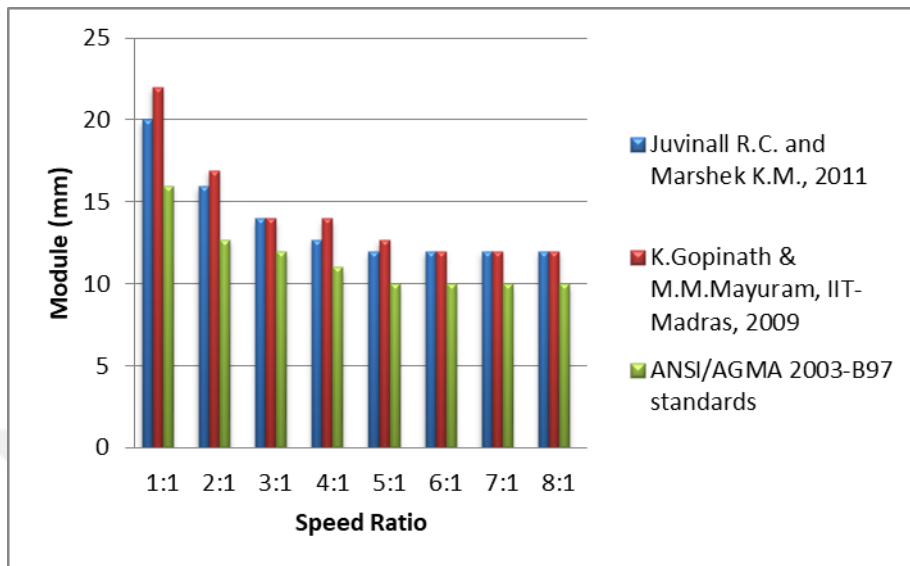
Figure K.19. The effect of speed ratio on module selection based on surface contact fatigue failure at 100 kW power transmission (for Ø=25°, Material type 3)
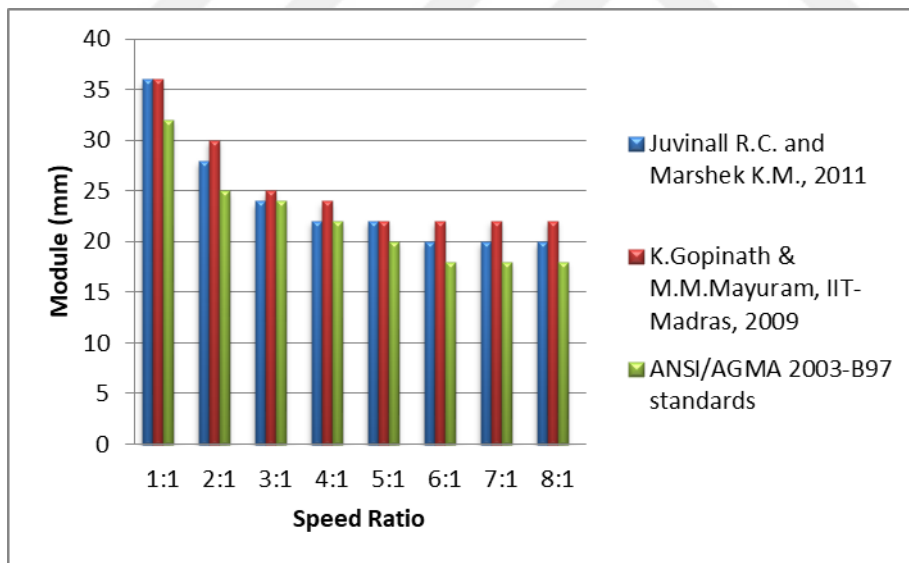
Figure K.20. The effect of speed ratio on module selection based on surface contact fatigue failure at 500 kW power transmission (for Ø=25°, Material type 3)
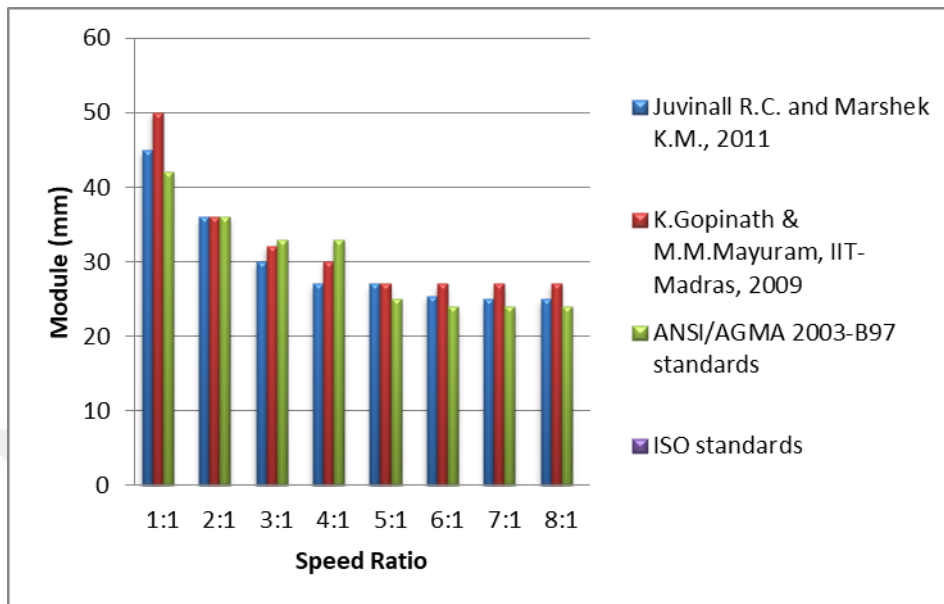
Figure K.21. The effect of speed ratio on module selection based on surface contact fatigue failure at 1000 kW power transmission (for Ø=25°, Material type 3)

K.3. Obtaining Geometric Rating Number (GR$_i$) for Design Approaches for Ø=25°, Material type 3
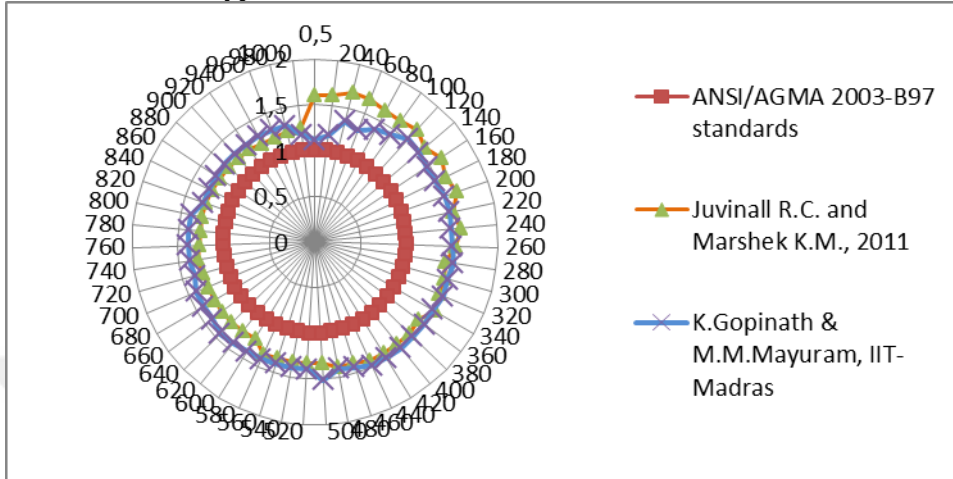
Figure K.22. Comparison of mxF/m$_0$xF$_0$ ratios for the design approaches at 1:1 speed ratio (for Ø=25°, Material type 3)
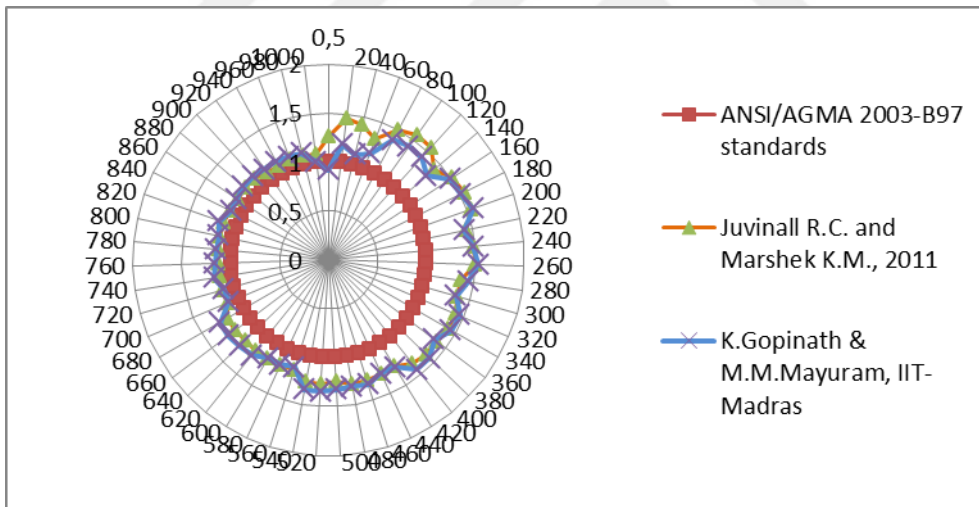

Figure K.23. Comparison of mxF/m$_0$xF$_0$ ratios for the design approaches at 2:1 speed ratio (for Ø=25°, Material type 3)
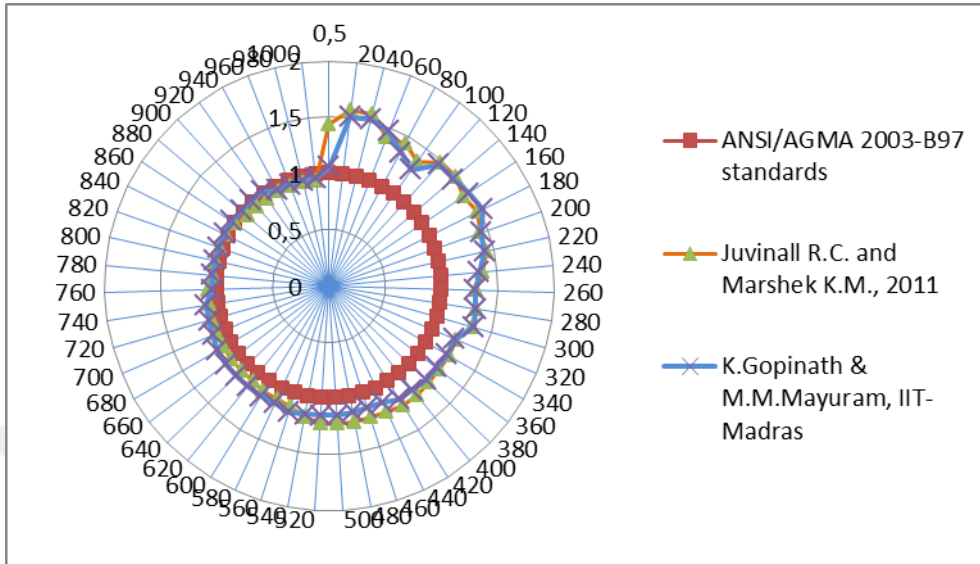
Figure K.24. Comparison of mxF/m$_0$xF$_0$ ratios for the design approaches at 3:1 speed ratio (for Ø=25°, Material type 3)
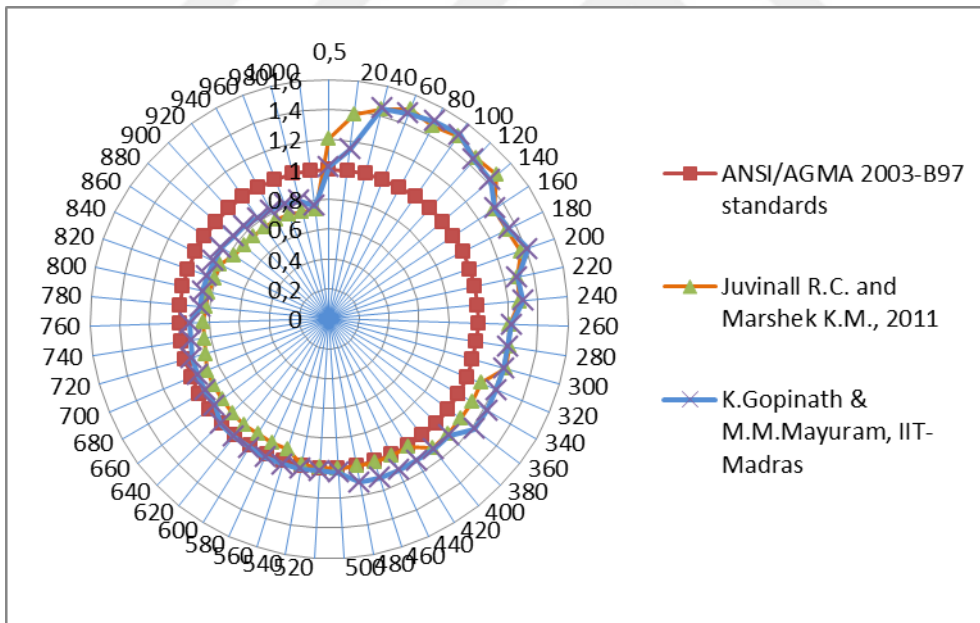
Figure K.25. Comparison of mxF/m$_0$xF$_0$ ratios for the design approaches at 4:1 speed ratio (for Ø=25°, Material type 3)
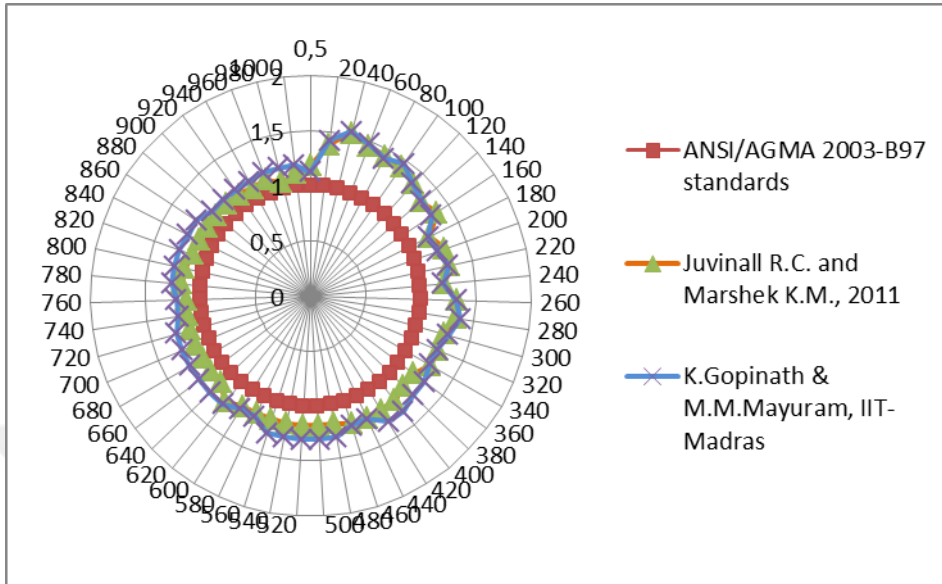
Figure K.26. Comparison of mxF/m$_0$xF$_0$ ratios for the design approaches at 5:1 speed ratio (for Ø=25°, Material type 3)
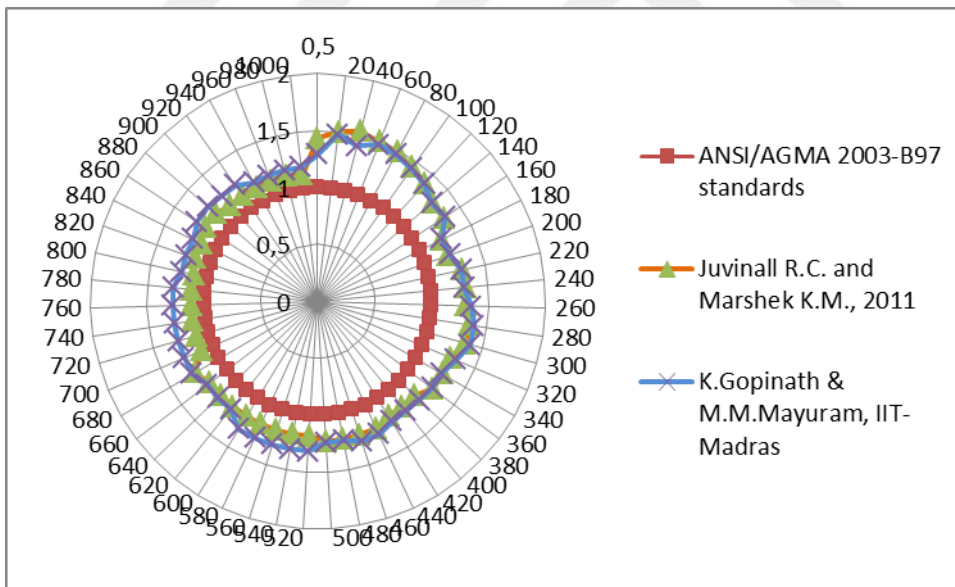

Figure K.27. Comparison of mxF/m$_0$xF$_0$ ratios for the design approaches at 6:1 speed ratio (for Ø=25°, Material type 3)
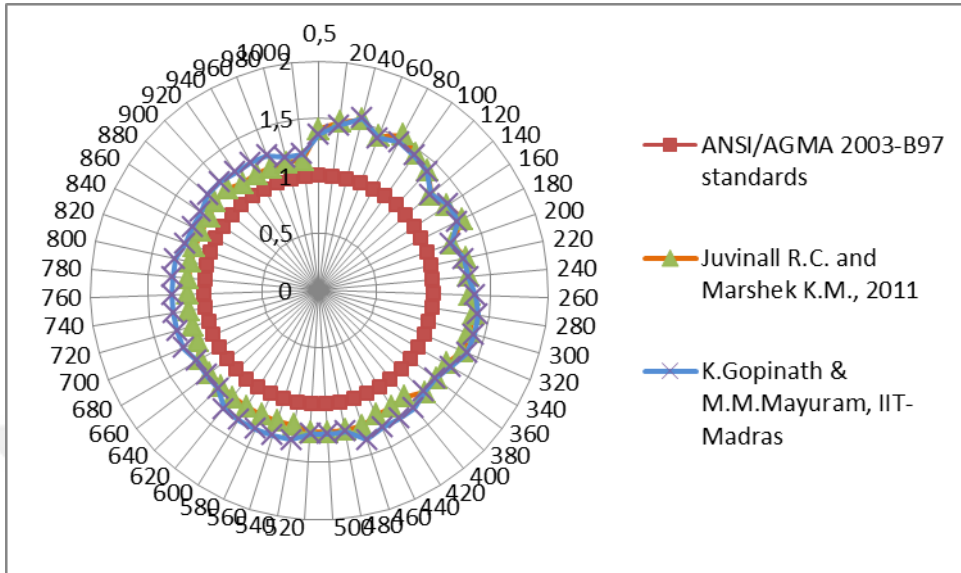
Figure K.28. Comparison of mxF/m$_0$xF$_0$ ratios for the design approaches at 7:1 speed ratio (for Ø=25$^{\text{o}}$, Material type 3)
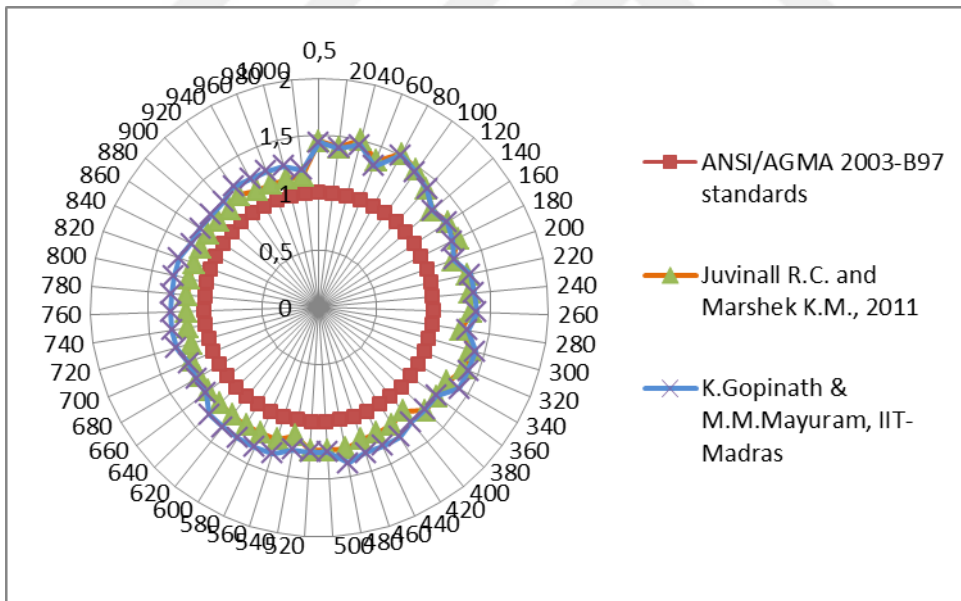
Figure K.29. Comparison of mxF/m$_0$xF$_0$ ratios for the design approaches at 8:1 speed ratio (for Ø=25$^{\text{o}}$, Material type 3)